

Engineering Materials 2

Engineering Materials 2

An Introduction to Microstructures and Processing

Fourth Edition

Michael F. Ashby

Royal Society Research Professor Emeritus
University of Cambridge and Former Visiting
Professor of Design at the Royal College of Art
London

David R. H. Jones

President, Christ's College
Cambridge



AMSTERDAM • BOSTON • HEIDELBERG • LONDON
NEW YORK • OXFORD • PARIS • SAN DIEGO
SAN FRANCISCO • SINGAPORE • SYDNEY • TOKYO

Butterworth-Heinemann is an imprint of Elsevier



Butterworth-Heinemann is an imprint of Elsevier
The Boulevard, Langford Lane, Kidlington, Oxford, OX5 1GB UK
225 Wyman Street, Waltham, MA 02451 USA

First published 1986
Second Edition 1998
Reprinted 1999, 2000, 2001
Third Edition 2006

Copyright © 2013 Michael F. Ashby and David R. H. Jones. Published by Elsevier Ltd. All rights reserved

The right of Michael F. Ashby and David R. H. Jones to be identified as the authors of this work has been asserted in accordance with the Copyright, Designs and Patents Act 1988.

No part of this publication may be reproduced or transmitted in any form or by any means, electronic or mechanical, including photocopying, recording, or any information storage and retrieval system, without permission in writing from the publisher. Details on how to seek permission, further information about the Publisher's permissions policies and our arrangements with organizations such as the Copyright Clearance Center and the Copyright Licensing Agency, can be found at our website: www.elsevier.com/permissions.

This book and the individual contributions contained in it are protected under copyright by the Publisher (other than as may be noted herein).

Notices

Knowledge and best practice in this field are constantly changing. As new research and experience broaden our understanding, changes in research methods, professional practices, or medical treatment may become necessary.

Practitioners and researchers must always rely on their own experience and knowledge in evaluating and using any information, methods, compounds, or experiments described herein. In using such information or methods they should be mindful of their own safety and the safety of others, including parties for whom they have a professional responsibility.

To the fullest extent of the law, neither the Publisher nor the authors, contributors, or editors, assume any liability for any injury and/or damage to persons or property as a matter of products liability, negligence or otherwise, or from any use or operation of any methods, products, instructions, or ideas contained in the material herein.

Library of Congress Cataloging-in-Publication Data

Application submitted.

British Library Cataloguing-in-Publication Data

A catalogue record for this book is available from the British Library

ISBN: 978-0-08-096668-7

For information on all Butterworth-Heinemann publications,
visit our website at www.books.elsevier.com

Printed in the United States of America

12 13 14 15 1 2 3 4 5 6 7 8 9 10

Working together to grow
libraries in developing countries

www.elsevier.com | www.bookaid.org | www.sabre.org

ELSEVIER

BOOK AID
International

Sabre Foundation

Preface to the Fourth Edition

In preparing this fourth edition of *Engineering Materials 2*, I have made significant changes, whilst being careful not to alter the essential character of the book. At the most obvious level, I have added many new photographs to illustrate the basic coursework and the case studies—many taken during my travels around the world investigating materials problems. These days, the Internet is an essential tool of knowledge and communication—to the extent that textbooks should be used alongside web-based sources. I have given frequent references in the text to web pages and video clips—ranging from the accident investigation report on the space shuttle Columbia to the low-expansion glass water gauges on a Ffestiniog Railway steam loco. And when a geographical location is involved—like the Sydney Opera House, or the Roman aqueduct in Segovia—I have given the coordinates (latitude and longitude), which can be plugged into the search window in Google Earth to take you right there. Not only does this give you a feel for the truly global reach of materials and engineering, it also leads you straight to the large number of derivative sources and references, such as photographs and web pages, which can help you follow up your own particular interests.

The section on phase diagrams—which had been an appendix in previous editions—is now moved to its logical place early in the book, as two new chapters (Chapters 3 and 4). (The solutions to the examples in these chapters are retained but are placed together at the end of each chapter.) There is more detail on aspects of phase transformations, including interface kinetics, nucleation and growth, and constitutional undercooling. New material has been added on phases in stainless steels (Schaeffler diagram) and modern improvements to stainless steels. The chapter on processing metals has been expanded to two chapters (Chapters 15 and 16), with increased emphasis on secondary processing, including the use of continuous cooling transformation diagrams in steel heat treatment.

The two chapters on mechanical properties of ceramics have been condensed to one (Chapter 19), as a consequence of moving probabilistic fracture of brittle materials to the 4th edition of *Engineering Materials 1*; however, detail has been added on deriving the Weibull parameters from modulus of rupture data. New sections have been added on calculating thermal stress, and reinforcing cement and concrete.

A new section on composites has been added, so each of the four materials classes (metals, ceramics, polymers, composites) now has its own section.

Many new case studies have been added, and many existing case studies have been replaced. In particular, I have added new chapters of case studies in the sections on ceramics (Chapter 22), polymers (Chapter 27), and composites (Chapter 30).

I have added many worked examples to illustrate, develop, or consolidate a topic without interrupting the flow of the text. Most are directly related to real examples of materials processing, microstructures, properties, and applications, and cover a wide range of subjects, ranging from excessive penetration of brazing alloy into electronic device connection pins, through gluing wings and fuselages together in aircraft, to why wood is such a special material.

The number of examples has been doubled, and many contain case studies or practical examples relevant to processing, microstructures, properties, and applications. I have tried to choose case study topics which are informative and connected to the real world. So the worked example on the Columbia space shuttle disaster—caused by polymer foam detaching from the fuel tank and hitting the shuttle’s ceramic-composite thermal protection system—indicates how easy it is for a large organization to lose the “folk memory” of past mistakes (the loss of the Challenger shuttle, 17 years earlier).

Materials occupy a central place in engineering for without them, nothing can be made, nothing can be done. The challenge is to know how the ways in which materials are processed directly determines their microstructures, which in turn determine their properties; and to know how these properties can be tailored by processing so they best satisfy the demands of real structures, components, or devices. To the materials engineer who is always curious, aware, and vigilant, the world is a fascinating place.

David Jones
Cambridge, July 2012

ACKNOWLEDGEMENTS

Unless otherwise attributed, all photographs were taken by Dr David R. H. Jones.

Figures 10.6, 10.7, 12.7, 12.8, 14.8 and the photograph for Example 14.10 were commissioned by DRHJ.

The photograph for Example 13.7, and Figures 30.8, 30.9, and 30.10 were taken for DRHJ by Mr Alan Heaver, Department of Engineering, University of Cambridge.

We acknowledge with thanks other photographs and diagrams as follows.

Figures 2.2 and 2.6. Dr D. C. Houghton, Dr D. R. H. Jones and Elsevier (*Acta Metallurgica*, 27, 1979, 1013–1039).

Figure 4.9. Professor G. A. Chadwick and Elsevier (*Metallography of Phase Transformations*, 1972).

Figure 4.16. Mr K. J. Pascoe and van Nostrand Reinhold (*An Introduction to the Properties of Engineering Materials*, 3rd edition, 1978).

Figure 10.8. Dr J. H. Cleland.

Figure 21.14. Professors L. Vehovar, V. Kuhar, A. Vehovar and Elsevier (*Engineering Failure Analysis*, 5, 1998, 21–27).

Diagram for Chapter 21 Worked Example. Professor A. Valiente and Elsevier (*Engineering Failure Analysis*, 8, 2001, 245–261).

Figures 27.1–27.5. Dr D. R. H. Jones and Elsevier (*Engineering Failure Analysis*, 11, 2004, 857–872).

Diagrams for Example 30.12. Dr B. Jakobsen and Elsevier (*Engineering Failure Analysis*, 1, 1994, 193–199).

DRHJ is deeply indebted to his wife Siân for correcting the proofs of this book.

General Introduction

TO THE READER

Materials occupy a central place in engineering for without them, nothing can be made, nothing can be done. They are a key *enabling technology*. The characteristics of individual materials (or groups of related materials) very much dictate how they can be processed; in turn, the processing can strongly influence the final microstructure; and this determines the properties of the processed material, and its ability to perform in the intended application. In many cases, there are choices available to the engineer—of different materials or processing routes. Innovation often takes the form of replacing a part made from one material class (a metal, for example) with another (a fiber composite, for example). Radical changes in the material usually involve redesigning the part so the processing, structure, and properties of the replacement material are taken into account fully. In some cases, however, there is literally only one type of material which will do the job at all: without superalloys, we would have to fly around in piston-engine aircraft; without rubber tires, we would have to travel overland by railroad; without cement and concrete, modern construction would not exist; and we could not do without paper—a wonder composite made from a natural material.

This book gives you a broad introduction to the microstructures of materials, the ways in which materials are processed (altering structure), and how structure determines the final properties. It can be used on its own, or alongside our companion text (M. F. Ashby and D. R. H. Jones, *Engineering Materials 1—An Introduction to Properties, Applications and Design*, 4th edition, Elsevier, 2012; referred to as “EM1Ed4” in the following chapters).

You can see from the Contents that the chapters are arranged into four sections—*metals*, *ceramics*, *polymers*, and *composites*—representing the four distinct *generic classes* of materials. (These classes have very distinct characteristics, which determine the ways in which they are processed, and the properties of the processed structure.) Each section of chapters begins by

introducing the distinct *categories* of materials that go to make up the *generic class*. We then look at the defining features of the microstructures, and see how the materials are processed to get the microstructures (and properties) that we need. Each section of chapters ends with a chapter of *case studies*, which show how the scientific principles of material behavior are relevant to the real engineering world.

At the end of chapters, you will find sets of examples. Each is meant to consolidate, develop, illustrate, or apply a point covered in the text. Try to do the examples from each chapter while it is still fresh in your mind. This way, you will gain confidence that you are on top of the subject. To help you in solving problems, the main definitions and formulae are summarized at the end of the book, together with a list of magnitudes of properties for generic materials classes.

TO THE LECTURER

This book is a concise introduction to the *microstructures and processing* of materials (*metals, ceramics, polymers, and composites*) for students of engineering (and other related subjects). It can be used with our other text (M. F. Ashby and D. R. H. Jones, *Engineering Materials 1—An Introduction to Properties, Applications and Design*, 4th edition, Elsevier, 2012) or on its own.

The text is deliberately concise. Each chapter is designed to cover the content of one 50-minute lecture (30 in all), allowing time for demonstrations and graphics. Six chapters are devoted entirely to *case studies*—these illustrate and develop information presented in the preceding groups of chapters, and place it in the context of real engineering applications. Many chapters also contain shorter *worked examples*. Problems (*examples*) for students to solve are given at chapter ends—again, many contain case studies or practical examples.

We have tried to present the material in an uncomplicated way, while establishing the main physical concepts and showing how processing, microstructures, and properties are interrelated. Given the very large number of engineering materials available, and their diversity of structure and behavior, we found that a good way of doing this was to divide materials up into four main generic classes (each with common unifying characteristics)—*metals, ceramics, polymers, and composites*—and then, within each class, to consider the main *categories* of materials in that *class*.

Finally, it is worth emphasizing that materials data are notoriously variable. The data given here (in tables, and elsewhere) is approximate, and should

never be used for final designs (which require reliable and sufficiently accurate data from either suppliers or specially commissioned tests).

ACCOMPANYING RESOURCES

The following web-based resources are available to teachers and lecturers who adopt or recommend this text for class use. For further details and access to these resources, go to <http://www.textbooks.elsevier.com>

Instructor's manual

A full Solutions Manual with worked answers to the exercises in the main text is available for downloading.

Image bank

An image bank of downloadable figures from the book is available for use in lecture slides and class presentations.

Online materials science tutorials

A series of online materials science tutorials accompanies Engineering Materials 1 and 2. These were developed by Alan Crosky, Mark Hoffman, Paul Munroe, and Belinda Allen at the University of New South Wales (UNSW) in Australia; they are based on earlier editions of the books. The group is particularly interested in the effective and innovative use of technology in teaching. They realized the potential of the material for the teaching of Materials Engineering to their students in an online environment and have developed and then used these very popular tutorials for a number of years at UNSW. The results of this work have also been published and presented extensively.

The tutorials are designed for students of materials science as well as for those studying materials as a related or elective subject—for example, mechanical and/or civil engineering students. They are ideal for use as ancillaries to formal teaching programs and also may be used as the basis for quick refresher courses for more advanced materials science students. In addition, by picking selectively from the range of tutorials available, they will make ideal subject primers for students from related faculties.

The software has been developed as a self-paced learning tool, separated into learning modules based around key materials science concepts.

ABOUT THE AUTHORS OF THE TUTORIALS

Alan Crosky is a professor in the School of Materials Science and Engineering, UNSW. His teaching specialties include metallurgy, composites, and fractography.

Belinda Allen is an educational designer and adjunct lecturer in the Curriculum Research, Evaluation and Development team in the Learning and Teaching Unit, UNSW. She contributes to strategic initiatives and professional development programs for curriculum renewal, with a focus on effective integration of learning technologies.

Mark Hoffman is a professor in the School of Materials Science and Engineering, UNSW. His teaching specialties include fracture, numerical modeling, mechanical behavior of materials, and engineering management.

Paul Munroe has a joint appointment as a professor in the School of Materials Science and Engineering and director of the Electron Microscope Unit, UNSW. His teaching specialties are the deformation and strengthening mechanisms of materials and crystallographic and microstructural characterization.

Metals

1.1 INTRODUCTION

This first group of chapters looks at metals. There are so many different metals—literally hundreds of them—that it is impossible to remember them all. It isn't necessary—nearly all have evolved from a few “generic” metals and are tuned-up modifications of the basic recipes. If you know about the generic metals, you know most of what you need.

This chapter introduces the generic metals. But rather than bore you with a catalogue, we introduce them through real engineering examples. They allow us not only to find examples of the uses of the main generic metals but also to introduce the all-important business of how the characteristics of each metal determine how it is used in practice.

1.2 METALS FOR A MODEL STEAM ENGINE

Model making is big business. The testing of scale models provides a cheap way of getting critical design information for things from Olympic yacht hulls to tidal barrages. Architects sell their newest creations with the help of miniature versions correct to the nearest garden shrub. And many people find an outlet for their energies in making models—perhaps putting together a miniature aircraft from a kit of plastic parts or, at the other extreme, building a fully working model of a steam engine from the basic raw materials in their own “garden-shed” machine shop.

Figure 1.1 shows a model of a nineteenth-century steam engine built in a home workshop from plans published in a well-known modelers' magazine. Everything works just as it did in the original—the boiler even burns the same type of coal to raise steam—and the model is capable of towing several people. But what interests us here is the large range of metals that were used in its construction, and the way in which their selection was dictated by the

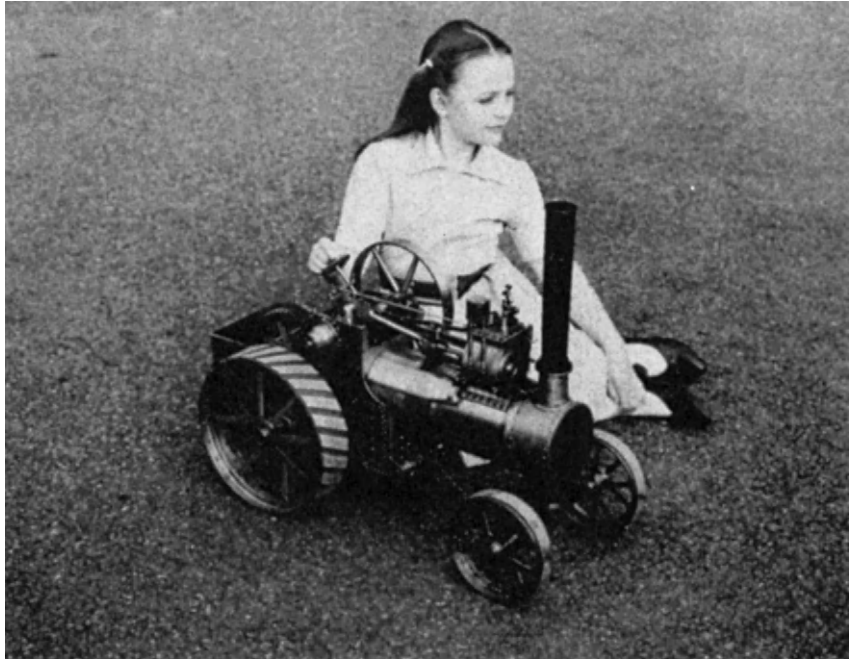


FIGURE 1.1

A fully working model, one-sixth full size, of a steam engine of the type used on many farms a hundred years ago. The model can pull several people on a few liters of water and a handful of coal. But it is also a nice example of materials selection and design.

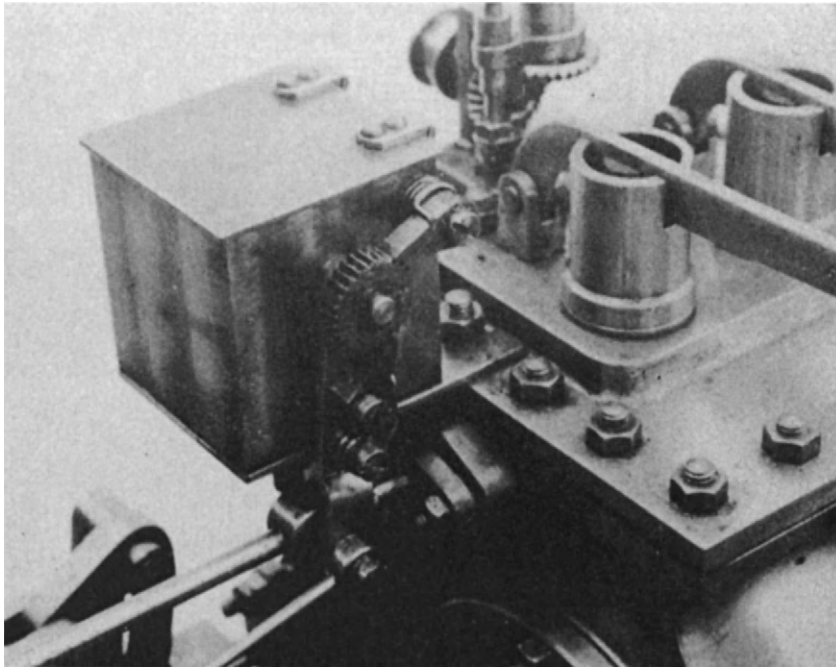
requirements of design. We begin by looking at metals based on *iron* (*ferrous* metals). [Table 1.1](#) lists the generic iron-based metals.

How are these metals used in the engine? The design loads in components like the wheels and frames are sufficiently low that *mild steel*, with a yield strength σ_y of around 220 MN m^{-2} , is more than strong enough. It is also easy to cut, bend, or machine to shape. And last, but not least, it is cheap.

The stresses in the machinery—like the gear-wheel teeth or the drive shafts—are higher, and these parts are made from either *medium-carbon*, *high-carbon*, or *low-alloy steels* to give extra strength. However, there are a few components where even the strength of high-carbon steels as delivered “off the shelf” ($\sigma_y \approx 400 \text{ MN m}^{-2}$) is not enough. We can see a good example in the mechanical lubricator, shown in [Figure 1.2](#), which is essentially a high-pressure oil metering pump. This is driven by a ratchet and pawl. These have sharp teeth which would quickly wear if they were made of a soft alloy. But how do we raise the hardness above that of ordinary high-carbon steel? Well, medium- and high-carbon steels can be hardened to give a yield strength of up to 1000 MN m^{-2} by heating them

Table 1.1 Generic Iron-Based Metals

Metal	Typical Composition (wt%)	Typical Uses
Low-carbon (mild) steel	Fe + 0.04 to 0.3 C (+ ≈ 0.8 Mn)	Low-stress uses: general constructional steel, suitable for welding
Medium-carbon steel	Fe + 0.3 to 0.7 C (+ ≈ 0.8 Mn)	Medium-stress uses: machinery parts—nuts and bolts, shafts, gears
High-carbon steel	Fe + 0.7 to 1.7 C (+ ≈ 0.8 Mn)	High-stress uses: springs, cutting tools, dies
Low-alloy steel	Fe + 0.2 C 0.8 Mn 1 Cr 2 Ni	High-stress uses: pressure vessels, aircraft parts
High-alloy (stainless) steel	Fe + 0.1 C 0.5 Mn 18 Cr 8 Ni	High-temperature or anticorrosion uses: chemical or steam plants
Cast iron	Fe + 1.8 to 4 C (+ ≈ 0.8 Mn 2 Si)	Low-stress uses: cylinder blocks, water pipes

**FIGURE 1.2**

A close-up of the mechanical lubricator on the steam engine. Unless the bore of the steam cylinder is kept oiled, it will become worn and scored. The lubricator pumps small metered quantities of steam oil into the cylinder to stop this happening. The drive is taken from the piston rod by the ratchet and pawl arrangement.

to bright red heat and then quenching them in cold water. Although the quench makes the hardened steel brittle, we can make it tough again (though still hard) by *tempering* it—a process that involves heating the steel again but to a much lower temperature. And so the ratchet and pawls are made from a quenched and tempered high-carbon steel.

Stainless steel is used in several places. Figure 1.3 shows the fire grate—the metal bars which carry the burning coals inside the firebox. When the engine is working hard, the coal is red hot; then, both oxidation and creep are problems. Mild steel bars can burn out in a season, but stainless steel bars last indefinitely.

Finally, what about *cast iron*? Although this is rather brittle, it is fine for low-stressed components like the cylinder block. In fact, because cast iron has a lot of carbon, it has several advantages over mild steel. Complicated components like the cylinder block are best produced by casting. Now cast iron melts much more easily than steel (adding carbon reduces the melting point in just the way that adding antifreeze works with water) and this makes the

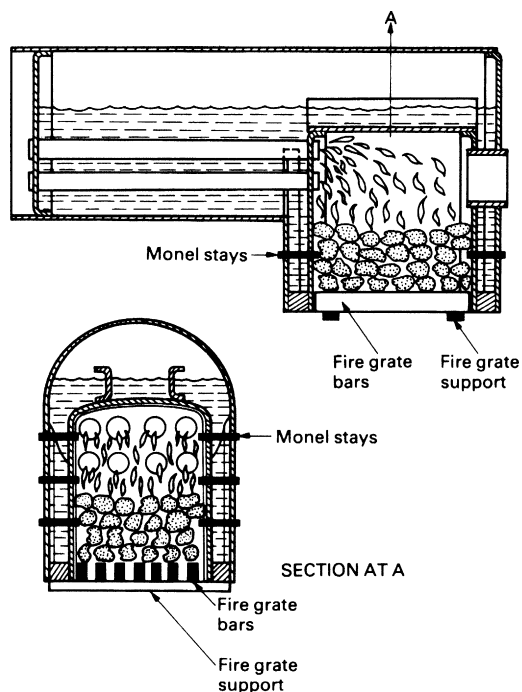


FIGURE 1.3

The fire grate, which carries the red-hot fire inside the firebox, must resist oxidation and creep. Stainless steel is best for this application. Note also the threaded monel stays which hold the firebox sides together against the internal pressure of the steam.

pouring of the castings much easier. During casting, the carbon can be made to separate out as tiny particles of graphite, distributed throughout the iron, which make an ideal boundary lubricant. Cylinders and pistons made from cast iron wear very well; look inside the cylinders of a car engine when the head is taken off, and you will be amazed by the polished, almost glazed look of the bores—and this after perhaps 10^8 piston strokes.

These, then, are the basic classes of ferrous alloys. Their compositions and uses are summarized in [Table 1.1](#), and you will learn more about them in Chapters 12 and 13, but let us now look at the other generic alloy groups.

An important group of alloys are those based on copper ([Table 1.2](#)).

The most notable part of the engine made from copper is the boiler and its firetubes (see [Figure 1.1](#)). In full size, this would have been made from mild steel, and the use of copper in the model is a nice example of how the choice of material can depend on the *scale* of the structure. The boiler plates of the full-size engine are about 10 mm thick, of which perhaps only 6 mm is needed to stand the load from the pressurized steam safely—the other 4 mm is an allowance for corrosion. Although a model steel boiler would stand the pressure with plates only 1 mm thick, it would still need the same corrosion allowance of 4 mm, totaling 5 mm altogether. This would mean a very heavy boiler, and a lot of water space would be taken up by thick plates and firetubes. Because copper hardly corrodes in clean water, this is the obvious material to use. Although weaker than steel, 2.5 mm thick copper plates are strong enough to resist the working pressure, and there is no need for a separate corrosion allowance. Of course, copper is expensive—it would be prohibitive in full size—but this is balanced by its ductility (it is very easy to bend and flange to shape) and by its high thermal conductivity (which means that the boiler steams very freely).

Brass is stronger than copper, is much easier to machine, and is fairly corrosion proof (although it can “dezincify” in water after a long time).

Table 1.2 Generic Copper-Based Metals

Metal	Typical Composition (wt%)	Typical Uses
Copper	100 Cu	Ductile, corrosion resistant, and a good electrical conductor: water pipes, electrical wiring
Brass	Zn	Stronger than copper, machinable, reasonable corrosion resistance: water fittings, screws, electrical components
Bronze	Cu + 10 to 30 Sn	Good corrosion resistance: bearings, ships' propellers, bells
Cupronickel	Cu + 30 Ni	Good corrosion resistance, coinage

A good example of its use in the engine is for steam valves and other boiler fittings (Figure 1.4). These are intricate and must be easy to machine; dezincification is a long-term possibility, so occasional inspection is needed. Alternatively, corrosion can be avoided altogether by using the more expensive *bronzes*, although some are hard to machine.

Nickel and its alloys form another important class of nonferrous metals (Table 1.3). The superb creep resistance of the nickel-based superalloys is a

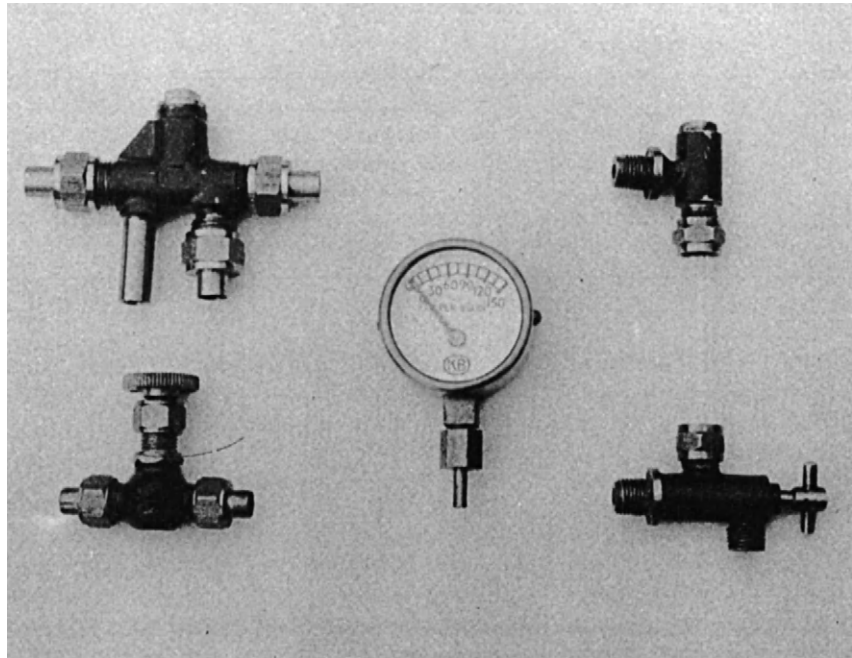


FIGURE 1.4

Miniature boiler fittings made from brass: a water-level gauge, a steam valve, a pressure gauge, and a feed-water injector. Brass is so easy to machine that it is good for intricate parts like these.

Table 1.3 Generic Nickel-Based Metals

Metal	Typical Composition (wt%)	Typical Uses
Monels	Ni + 30 Cu 1 Fe 1 Mn	Strong, corrosion resistant: heat-exchanger tubes
Superalloys	Ni + 30 Cr 30 Fe 0.5 Ti 0.5 Al	Creep and oxidation resistant: furnace parts
	Ni + 10 Co 10 W 9 Cr 5 Al 2 Ti	Highly creep resistant: turbine blades and disks

key factor in designing the modern gas turbine aeroengine. But nickel alloys even appear in a model steam engine. The flat plates in the firebox must be stayed together to resist the internal steam pressure (see Figure 1.3). Some model builders make these stays from pieces of monel rod because it is stronger than copper, takes threads much better and is very corrosion resistant.

1.3 METALS FOR DRINKS CANS

Few people would think that the humble drinks can (Figure 1.5) was anything special. But to a materials engineer, it is high technology. Look at the requirements. As far as possible we want to avoid seams. The can must not leak, should use as little metal as possible, and be recyclable. We have to choose a metal that is ductile to the point that it can be drawn into a single-piece can body from one small slug of metal. It must not corrode in beer or coke and, of course, it must be nontoxic. And it must be light and must cost almost nothing.



FIGURE 1.5

The aluminum drinks can is an innovative product. The body is made from a single slug of a 3000 series aluminum alloy. The can top is a separate pressing which is fastened to the body by a rolled seam once the can has been filled. There are limits to one-piece construction.

Table 1.4 Generic Aluminum-Based Metals		
Metal	Typical Composition (wt%)	Typical Uses
1000 Series unalloyed Al	>99 Al	Weak but ductile and a good electrical conductor: power transmission lines, cooking foil
2000 Series major additive Cu	Al + 4 Cu + Mg, Si, Mn	Strong age-hardening alloy: aircraft skins, spars, forgings, rivets
3000 Series major additive Mn	Al + 1 Mn	Moderate strength, ductile, excellent corrosion resistance: roofing sheet, cooking pans, drinks can bodies
5000 Series major additive Mg	Al + 3 Mg 0.5 Mn	Strong work-hardening weldable plate: pressure vessels, ship superstructures
6000 Series major additives Mg + Si	Al + 0.5 Mg 0.5 Si	Moderate-strength age-hardening alloy: anodized extruded sections, e.g., window frames
7000 Series major additives Zn + Mg	Al + 6 Zn + Mg, Cu, Mn	Strong age-hardening alloy: aircraft forgings, spars, lightweight railway carriage shells
Casting alloys	Al + 11 Si	Sand and die castings
Aluminum–lithium alloys	Al + 3 Li	Low density and good strength: aircraft skins and spars

Aluminum-based metals are the obvious choice (Table 1.4)—they are light and corrosion resistant. But it took several years to develop the process for forming the can and the alloy to go with it. The end product is a big advance from the days when drinks only came in glass bottles and has created a new market for aluminum (now threatened by polymers). Because aluminum is lighter than most other metals, it is also the obvious choice for transportation—aircraft, high-speed trains. Most of the alloys listed in Table 1.4 are designed with these uses in mind. We will discuss the origin of their strength and their uses, in more detail, in Chapter 11.

1.4 METALS FOR HIP JOINTS

As a last example we turn to the world of medicine. Osteoarthritis is an illness that affects many people as they get older. The disease affects the joints between different bones in the body and makes it hard—and painful—to move them. The problem is caused by small lumps of bone which grow on the rubbing surfaces of the joints and which prevent them sliding properly. The problem can only be cured by removing the bad joints and putting artificial joints in their place. The first recorded hip joint replacement was

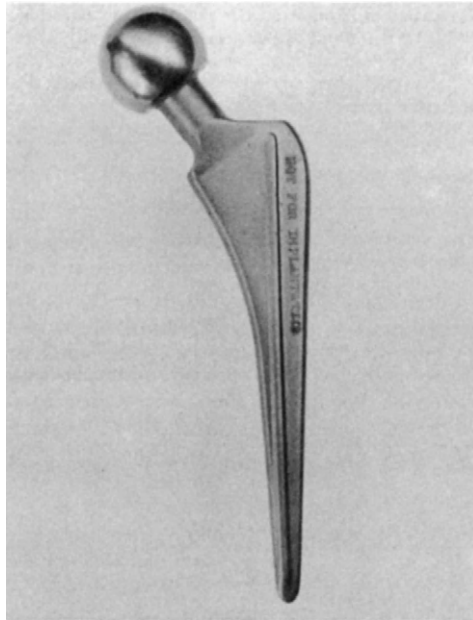


FIGURE 1.6

A titanium alloy implant for a replacement hip joint. The long shank is glued into the top of the femur. The spherical head engages in a high-density polythene socket which is glued into the pelvic socket.

done as far back as 1897—when it must have been a pretty hazardous business—but the operation is now a routine piece of orthopedic surgery. In fact, half a million hip joints are replaced worldwide every year.

Figure 1.6 shows the implant for a replacement hip joint. In the operation, the head of the femur is cut off and the soft marrow is taken out to make a hole down the center of the bone. Into the hole is glued a long metal shank which carries the artificial head. This fits into a high-density polythene socket which in turn is glued into the old bone socket. The requirements of the implant are stringent. It has to take large loads without bending. Every time the joint is used ($\approx 10^6$ times a year), the load on it fluctuates, giving us a high-cycle fatigue problem as well. Body fluids are as corrosive as seawater, so we must design against corrosion, stress corrosion, and corrosion fatigue. The metal must be biocompatible. And, ideally, it should be light as well.

One material which meets these tough requirements is based on *titanium* (although stainless steel and cobalt–chromium alloy are also used). The α – β alloy shown in Table 1.5 is as strong as a hardened and tempered high-carbon steel and is more corrosion resistant in body fluids than stainless

Table 1.5 Generic Titanium-Based Metals		
Metal	Typical Composition (wt%)	Typical Uses
α - β titanium alloy	Ti-6 Al 4 V	Light, very strong, excellent corrosion resistance, high melting point, good creep resistance. The alloy workhorse: turbofans, airframes, chemical plant, surgical implants.

steel but is only half the weight. A disadvantage is that its modulus is only half that of steels, so that it tends to be “whippy” under load. But this can be overcome by using slightly stiffer sections. The same alloy is used in aircraft, both in the airframes and in the compressors of the gas turbine engines.

1.5 DATA FOR METALS

When you select a metal for any design application you need *data* for the properties. Table 1.6 gives you *approximate* property data for the main generic metals, useful for the first phase of a design project. When you have narrowed down your choice, you should turn to more exhaustive published sources of data. Finally, before making final design decisions you should get detailed material specifications from the supplier who will provide the materials you intend to use. And if the component is a critical one (meaning that its failure could precipitate a catastrophe), you should arrange to test it yourself.

There are, of course, many more metals available than those listed here. It is useful to know that some properties depend very little on microstructure: the density, modulus, thermal expansion, and specific heat of *any* steel are pretty close to those listed in Table 1.6. (Look at the table and you will see that the variations in these properties are seldom more than $\pm 5\%$.) These are the “*structure-insensitive*” properties. Other properties, though, vary greatly with the heat treatment and mechanical treatment and the detailed alloy composition. These are the “*structure-sensitive*” properties: yield and tensile strength, ductility, fracture toughness, and creep and fatigue strength. They cannot be guessed from data for other alloys, even when the composition is almost the same. For these it is *essential* to consult manufacturers’ data sheets listing the properties of the alloy you intend to use with the same mechanical and heat treatment.

Table 1.6 Properties of the Generic Metals

Metal	Density (Mg m ⁻³)	Young's Modulus (GN m ⁻²)	Yield Strength (MN m ⁻²)	Tensile Strength (MN m ⁻²)	Ductility	Fracture Toughness (MN m ^{-3/2})	Melting Temperature (K)	Specific Heat (J kg ⁻¹ K ⁻¹)	Thermal Conductivity (W m ⁻¹ K ⁻¹)	Thermal Expansion Coefficient (MK ⁻¹)
Iron	7.9	211	50	200	0.3	80	1809	456	78	12
Mild steel	7.9	210	220	430	0.21	140	1765	482	60	12
High-carbon steel	7.8	210	350–1600	650–2000	0.1–0.2	20–50	1570	460	40	12
Low-alloy steels	7.8	203	290–1600	420–2000	0.1–0.2	50–170	1750	460	40	12
High-alloy steels	7.8	215	170–1600	460–1700	0.1–0.5	50–170	1680	500	12–30	10–18
Cast irons	7.4	152	50–400	10–800	0–0.18	6–20	1403			
Copper	8.9	130	75	220	0.5–0.9	>100	1356	385	397	17
Brasses	8.4	105	200	350	0.5	30–100	1190		121	20
Bronzes	8.4	120	200	350	0.5	30–100	1120		85	19
Nickel	8.9	214	60	300	0.4	>100	1728	450	89	13
Monels	8.9	185	340	680	0.5	>100	1600	420	22	14
Superalloys	7.9	214	800	1300	0.2	>100	1550	450	11	12
Aluminum	2.7	71	25–125	75–135	0.1–0.5	45	933	917	240	24
1000 Series	2.7	71	28–165	75–180	0.1–0.45	45	915			24
2000 Series	2.8	71	200–500	300–600	0.1–0.25	10–50	860		180	24
5000 Series	2.7	71	40–300	120–430	0.1–0.35	30–40	890		130	22
7000 Series	2.8	71	350–600	500–670	0.1–0.17	20–70	890		150	24
Casting alloys	2.7	71	65–350	130–400	0.01–0.15	5–30	860		140	20
Titanium	4.5	120	170	240	0.25		1940	530	22	9
Ti–6 Al4V	4.4	115	800–900	900–1000	0.1–0.2	50–80	1920	610	6	8
Zinc	7.1	105		120	0.4		693	390	120	31
Lead–tin solder	9.4	40					456			
Diecasting alloy	6.7	105		280–330	0.07–0.15		650	420	110	27

EXAMPLES

1.1 Explain what is meant by the following terms:

- a. structure-sensitive property,
- b. structure-insensitive property.

List five different structure-sensitive properties.

List four different structure-insensitive properties.

Answers

Structure-sensitive properties: yield strength, hardness, tensile strength, ductility, fracture toughness, fatigue strength, creep strength, corrosion resistance, wear resistance, thermal conductivity, electrical conductivity. Structure-insensitive properties: elastic moduli, Poisson's ratio, density, thermal expansion coefficient, specific heat.

1.2 Name five generic classes of metals. For each generic class:

- a. give one example of a specific component made from that class,
- b. indicate why that class was selected for the component.

Metal Structures

2.1 INTRODUCTION

At the end of Chapter 1, we noted that structure-sensitive properties like strength, ductility, or toughness depend critically on things like the composition of the metal and on whether it has been heated, quenched, or cold formed. Alloying or heat treating work by controlling the *structure* of the metal. Table 2.1 shows the large range over which a material has structure. The bracketed subset in the table can be controlled to give a wide choice of structure-sensitive properties.

2.2 CRYSTAL AND GLASS STRUCTURES

We begin by looking at the smallest scale of controllable structural feature—the way in which the atoms in the metals are packed together to give either a crystalline or a glassy (amorphous) structure. Table 2.2 lists the crystal structures of the pure metals at room temperature. In nearly every case the metal atoms pack into the simple crystal structures of face-centered cubic (f.c.c.), body-centered cubic (b.c.c.) or close-packed hexagonal (c.p.h.).

Metal atoms tend to behave like miniature ball bearings and tend to pack together as tightly as possible. f.c.c. and c.p.h. give the highest possible packing density with 74% of the volume of the metal taken up by the atomic spheres. However, in some metals, like iron or chromium, the metallic bond has some directionality and this makes the atoms pack into the more open b.c.c. structure with a packing density of 68%.

Some metals have more than one crystal structure. The most important examples are iron and titanium. As Figure 2.1 shows, iron changes from b.c.c. to f.c.c. at 914 °C but goes back to b.c.c. at 1391 °C. Titanium changes from c.p.h. to b.c.c. at 882 °C—you can visualize this phase change directly in Figure 2.2. This multiplicity of crystal structures is called *polymorphism*.

Table 2.1 Size Ranges of Structural Features

Structural Feature	Typical Scale (m)	
Nuclear structure	10^{-15}	
Structure of atom	10^{-10}	
Crystal or glass structure	10^{-9}	} Range that can be controlled to alter properties
Structures of solutions and compounds	10^{-9}	
Structures of grain and phase boundaries	10^{-8}	
Shapes of grains and phases	10^{-7} to 10^{-3}	
Aggregates of grains	10^{-5} to 10^{-2}	
Engineering structures	10^{-3} to 10^3	

It is obviously out of the question to try to control crystal structure simply by changing the temperature (iron is useless as a structural material well below 914°C). Polymorphism can, however, be brought about at room temperature by alloying. Indeed, the “austenitic” stainless steels are f.c.c. rather than b.c.c. and, especially at low temperatures, have much better ductility and toughness than ordinary carbon steels. This is why stainless steel is so good for cryogenic work: the fast fracture of a carbon steel vacuum flask containing liquid nitrogen would be embarrassing, to say the least, but f.c.c. metals such as austenitic stainless and aluminum alloys are essential for the systems needed to cool and superconducting magnets down to liquid helium temperatures, for storing liquid hydrogen, oxygen, or natural gas.

If molten metals (or, more usually, alloys) are cooled sufficiently fast, there is no time for the randomly arranged atoms in the liquid to switch into the orderly arrangement of a solid crystal. Instead, a *glassy* or *amorphous* solid is produced which has essentially a “frozen-in” liquid structure. This structure—which is termed *dense random packing* (d.r.p)—can be modeled very well by pouring ball bearings into a polythene bag and shaking them down to maximize the packing density. It is interesting to see that, although this structure is disordered, it has well-defined characteristics. For example, the packing density is always 64%, which is why corn was always sold in bushels (1 bushel = 8 UK gallons): provided the corn was always shaken down well in the sack a bushel always gave $0.64 \times 8 = 5.12$ gallons of corn material! It has only recently become practicable to make glassy metals in quantity but, because their structure is so different from that of “normal” metals, they have some very unusual and exciting properties.

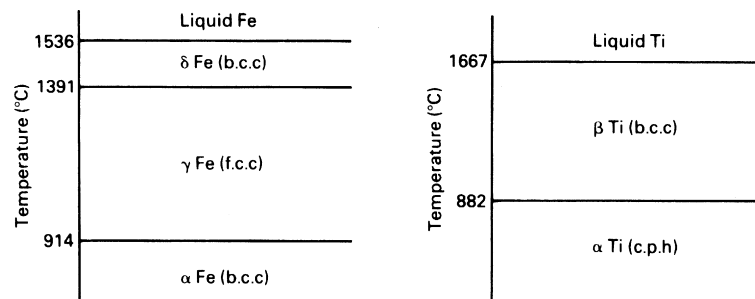
2.3 STRUCTURES OF SOLUTIONS AND COMPOUNDS

As you can see from the tables in Chapter 1, few metals are used in their pure state—they nearly always have other elements added to them which

Table 2.2 Crystal Structures of Pure Metals at Room Temperature

Pure Metal	Structure	Unit Cell Dimensions (nm)	
		<i>a</i>	<i>c</i>
Aluminum	f.c.c.	0.405	
Beryllium	c.p.h.	0.229	0.358
Cadmium	c.p.h.	0.298	0.562
Chromium	b.c.c.	0.289	
Cobalt	c.p.h.	0.251	0.409
Copper	f.c.c.	0.362	
Gold	f.c.c.	0.408	0.506
Hafnium	c.p.h.	0.320	
Indium	Face-centered tetragonal		
Iridium	f.c.c.	0.384	
Iron	b.c.c.	0.287	
Lanthanum	c.p.h.	0.376	0.606
Lead	f.c.c.	0.495	
Magnesium	c.p.h.	0.321	0.521
Manganese	Cubic	0.891	
Molybdenum	b.c.c.	0.315	
Nickel	f.c.c.	0.352	
Niobium	b.c.c.	0.330	
Palladium	f.c.c.	0.389	
Platinum	f.c.c.	0.392	
Rhodium	f.c.c.	0.380	
Silver	f.c.c.	0.409	
Tantalum	b.c.c.	0.331	
Thallium	c.p.h.	0.346	0.553
Tin	Body-centered tetragonal		
Titanium	c.p.h.	0.295	0.468
Tungsten	b.c.c.	0.317	
Vanadium	b.c.c.	0.303	
Yttrium	c.p.h.	0.365	0.573
Zinc	c.p.h.	0.267	0.495
Zirconium	c.p.h.	0.323	0.515

turn them into *alloys* and give them better mechanical properties. The alloying elements will always dissolve in the basic metal to form a *solid solution*, although the solubility can vary between <0.01% and 100% depending on the combinations of elements we choose. As examples, the iron in a carbon steel can only dissolve 0.007% carbon at room temperature; the copper in brass can dissolve more than 30% zinc; and the copper–nickel system—the basis of the monels and the cupronickels—has complete solid solubility.

**FIGURE 2.1**

Some metals have more than one crystal structure. The most important examples of this *polymorphism* are in iron and titanium.

**FIGURE 2.2**

A polished and etched section through a cube of Ti. The top face was heated by a 20 W electron beam for 300 h in a vacuum chamber (to stop the titanium oxidizing). The bottom face was soldered to a water-cooled copper quench block. After 300 h, the beam was switched off, and the cube was quenched before removal and sectioning. In order of decreasing temperature, we can see a cavity V which had been Ti vapor, a dark layer L which had been liquid Ti, recrystallized grains which had been the high-temperature form of Ti (β) and finally the low-temperature form (α). The temperature gradient just below the cavity was $22,000\text{ }^{\circ}\text{C mm}^{-1}$. Magnification $\times 115$.

There are two basic classes of solid solution. In the first, small atoms (like carbon, boron, and most gases) fit between the larger metal atoms to give *interstitial solid solutions* (Figure 2.3(a)). Although this interstitial solubility is usually limited to a few percent, it can have a large effect on properties. Indeed, as we shall see later, interstitial solutions of carbon in iron are largely responsible for the enormous range of strengths that we can get from

carbon steels. It is more common, though, for the dissolved atoms to have a similar size to those of the host metal. Then the dissolved atoms simply replace some of the host atoms to give a *substitutional solid solution* (Figure 2.3(b)). Brass and cupronickel are good examples of the large solubilities that this atomic substitution can give.

Solutions normally tend to be *random* so that one cannot predict which of the sites will be occupied by which atoms (Figure 2.3(c)). But if A atoms prefer to have A neighbors, or B atoms prefer B neighbors, the solution can *cluster* (Figure 2.3(d)); and when A atoms prefer B neighbors the solution can *order* (Figure 2.3(e)).

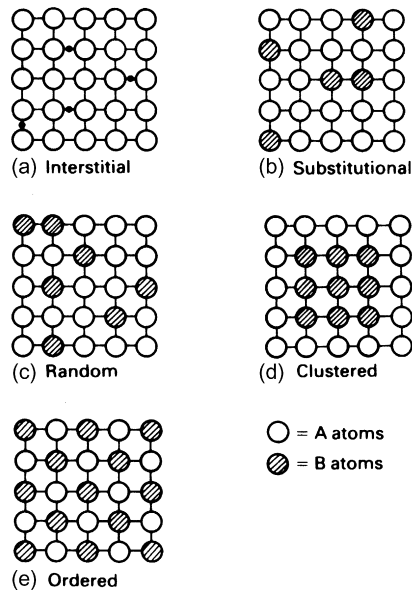
Many alloys contain more of the alloying elements than the host metal can dissolve. Then the surplus must separate out to give regions that have a high concentration of the alloying element. In a few alloys these regions consist of a solid solution based on the *alloying* element. (The lead–tin alloy system, on which most soft solders are based, Table 1.6, is a nice example of this—the lead can only dissolve 2% tin at room temperature and any surplus tin will separate out as regions of *tin* containing 0.3% dissolved lead.) In most alloy systems, however, the surplus atoms of the alloying element separate out as *chemical compounds*. An important example of this is in the aluminum–copper system (the basis of the 2000 series alloys, Table 1.4) where surplus copper separates out as the compound CuAl_2 . CuAl_2 is hard and is not easily cut by dislocations. And when it is finely dispersed throughout the alloy, it can give *very* big increases in strength. Other important compounds are Ni_3Al , Ni_3Ti , Mo_2C , and TaC (in superalloys) and Fe_3C (in carbon steels). Figure 2.4 shows the crystal structure of CuAl_2 . As with most compounds, it is quite complicated.

2.4 PHASES

The things that we have been talking about so far—metal crystals, amorphous metals, solid solutions, and solid compounds—are all *phases*. A phase is a region of material that has uniform physical and chemical properties. Water is a phase—any one drop of water is the same as the next. Ice is another phase—one splinter of ice is the same as any other. But the mixture of ice and water in your glass is not a single phase, because its properties vary as you move from water to ice. Ice + water is a *two-phase* mixture.

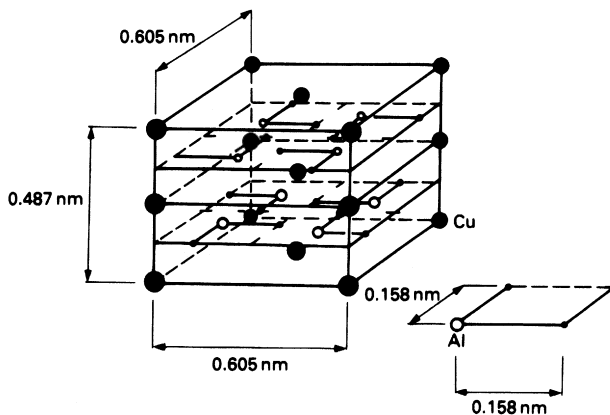
2.5 GRAIN AND PHASE BOUNDARIES

A pure metal, or a solid solution, is single phase. It is certainly possible to make single crystals of metals or alloys, but it is difficult and the expense is only worth it for high-technology applications such as single-crystal turbine

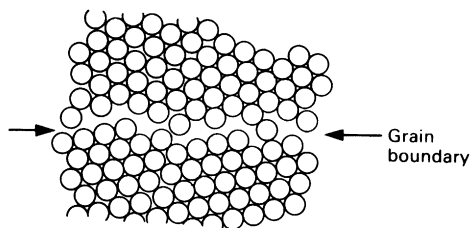
**FIGURE 2.3**

Solid solution structures. In *interstitial* solutions small atoms fit into the spaces between large atoms. In *substitutional* solutions similarly sized atoms replace one another. If A—A, A—B, and B—B bonds have the same strength, then this replacement is *random*. But unequal bond strengths can give *clustering* or *ordering*.

blades or single-crystal silicon for microchips. Normally, any single-phase metal is *polycrystalline*—it is made up of millions of small crystals, or *grains*, “stuck” together by *grain boundaries* (Figure 2.5). Because of their unusual structure, grain boundaries have special properties of their own. First, the lower bond density in the boundary is associated with a boundary surface energy: typically 0.5 Joules per square meter of boundary area (0.5 J m^{-2}). Secondly, the more open structure of the boundary can give much faster diffusion in the boundary plane than in the crystal on either side. And finally, the extra space makes it easier for oversized impurity atoms to dissolve in the boundary. These atoms tend to *segregate* to the boundaries, sometimes very strongly. Then an *average* impurity concentration of a few parts per million can give a *local* concentration of 10% in the boundary with very damaging effects on the fracture toughness. Henry Bessemer, the great Victorian iron-master and the first person to mass-produce mild steel, was nearly bankrupted by this. When he changed his suppliers of iron ore, his steel began to crack in service. The new ore contained phosphorus, which we now know segregates badly to grain boundaries. As a result, modern steels must contain less than $\approx 0.05\%$ phosphorus. Figure 2.6 shows an example of what grain boundaries look like in a metal sample.

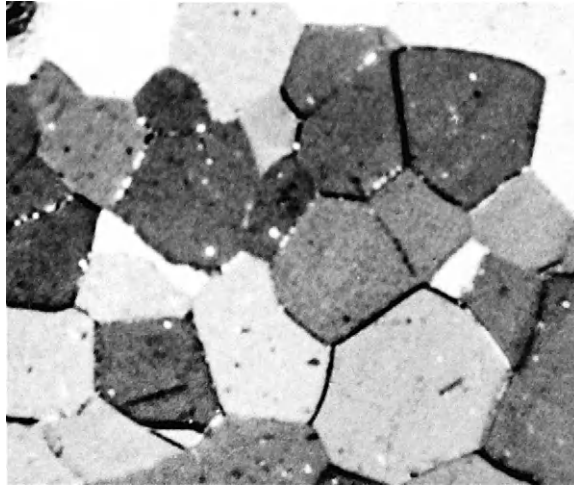
**FIGURE 2.4**

The crystal structure of the “intermetallic” compound CuAl_2 . The structures of compounds are usually more complicated than those of pure metals.

**FIGURE 2.5**

The structure of a typical grain boundary. In order to “bridge the gap” between two crystals of different orientation the atoms in the grain boundary have to be packed in a less ordered way. The packing density in the boundary is then as low as 50%.

As we have already seen, when an alloy contains more of the alloying element than the host metal can dissolve, it will split up into *two* phases. The two phases are “stuck” together by *interphase boundaries* which, again, have special properties of their own. We look first at two phases which have different chemical compositions but the same crystal structure (Figure 2.7(a)). Provided they are oriented in the right way, the crystals can be made to match up at the boundary. Then, although there is a sharp change in chemical composition, there is no structural change, and the energy of this *coherent* boundary is low (typically 0.05 J m^{-2}). If the two crystals have slightly different lattice spacings, the boundary is still coherent but has some strain (and more energy) associated with it (Figure 2.7(b)). The strain obviously gets bigger as the boundary grows sideways: full coherency is usually possible only with small second-phase particles. As the particle grows, the strain

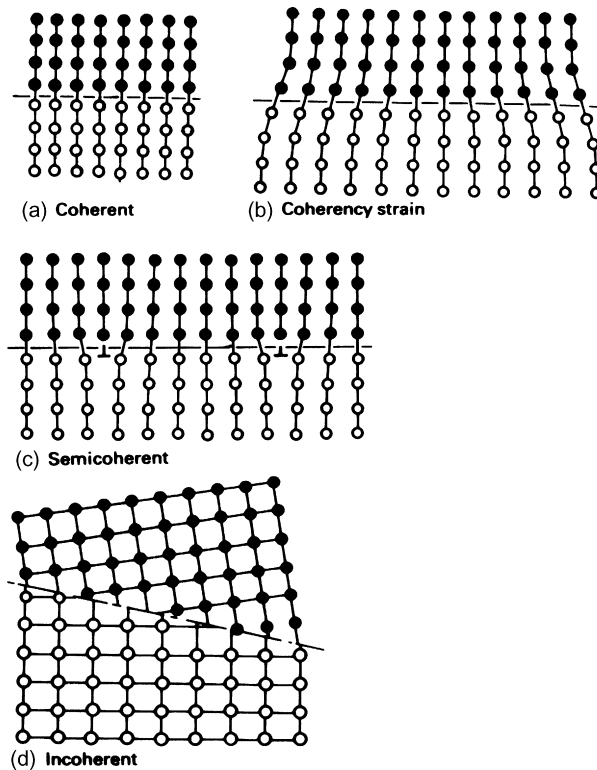
**FIGURE 2.6**

A polished and etched section through a sample of titanium showing the grain boundaries. Magnification $\times 390$.

builds up until it is relieved by the injection of dislocations to give a *semicoherent* boundary (Figure 2.7(c)). Often the two phases which meet at the boundary are large and differ in both chemical composition *and* crystal structure. Then the boundary between them is *incoherent*; it is like a grain boundary across which there is also a change in chemical composition (Figure 2.7(d)). Such a phase boundary has a high energy—comparable with that of a grain boundary—around 0.5 J m^{-2} .

2.6 SHAPES OF GRAINS AND PHASES

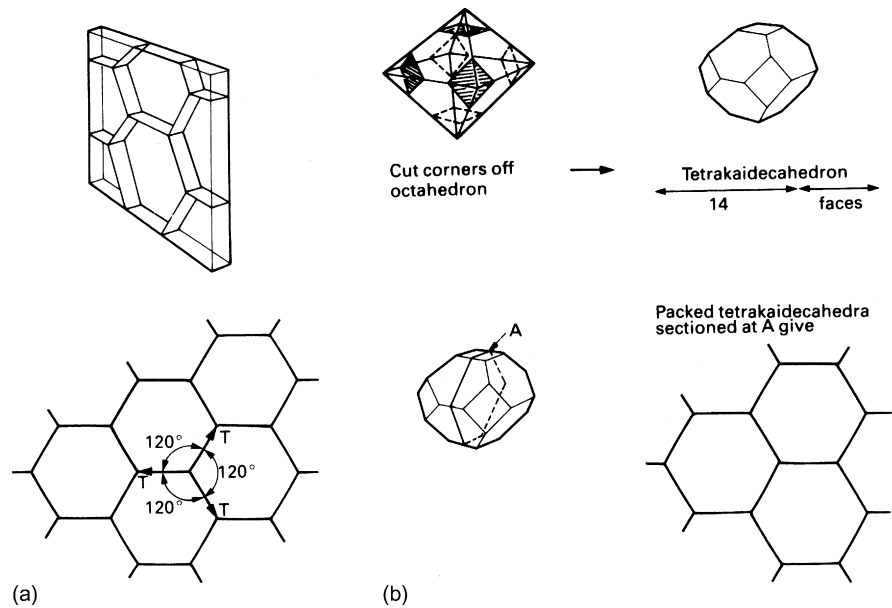
Grains come in all shapes and sizes, and both shape and size can have a big effect on the properties of the polycrystalline metal (a good example is mild steel—its strength can be *doubled* by a 10 times decrease in grain size). Grain shape is strongly affected by the way in which the metal is processed. Rolling or forging, for instance, can give stretched-out (or “textured”) grains; and in casting the solidifying grains are often elongated in the direction of the easiest heat loss. But if there are no external effects like these, then the energy of the grain boundaries is the important thing. This can be illustrated very nicely by looking at a “two-dimensional” array of soap bubbles in a thin glass cell. The soap film minimizes its overall energy by straightening out; and at the corners of the bubbles the films meet at angles of 120° to balance the surface tensions (Figure 2.8(a)). Of course, a polycrystalline metal is three dimensional, but the same principles apply: the grain

**FIGURE 2.7**

Structures of interphase boundaries.

boundaries try to form themselves into flat planes, and these planes always try to meet at 120° . A grain shape does indeed exist which not only satisfies these conditions but also packs together to fill space. It has 14 faces and is therefore called a tetrakaidecahedron (Figure 2.8(b)). This shape is remarkable, not only for the properties just given but because it appears in almost every physical science (the shape of cells in plants, bubbles in foams, grains in metals, and Dirichlet cells in solid-state physics).

If the metal consists of *two* phases, then we can get more shapes. The simplest is when a single-crystal particle of one phase forms inside a grain of another phase. Then, if the energy of the interphase boundary is *isotropic* (the same for all orientations), the second-phase particle will try to be *spherical* in order to minimize the interphase boundary energy (Figure 2.9(a)). Figure 2.10 shows a real example. Naturally, if coherency is possible along some planes, but not along others, the particle will tend to grow as a *plate*, extensive along the low-energy planes but narrow along the high-energy

**FIGURE 2.8**

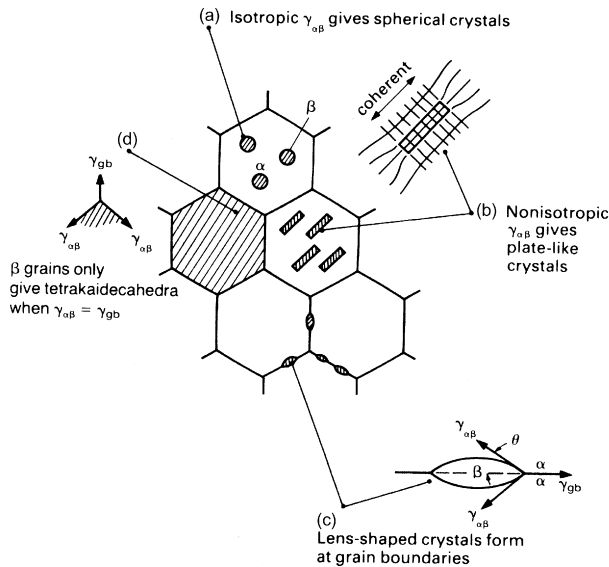
(a) The surface energy of a “two-dimensional” array of soap bubbles is minimized if the soap films straighten out. Where films meet the forces of surface tension must balance. This can only happen if films meet in “120° threes.” (b) In a three-dimensional polycrystal, the grain-boundary energy is minimized if the boundaries flatten out. These flats must meet in 120° threes to balance the grain-boundary tensions. If we fill space with equally sized tetrakaidecahedra, we will satisfy these conditions. Grains in polycrystals therefore tend to be shaped like tetrakaidecahedra when the grain-boundary energy is the dominating influence.

ones (Figure 2.9(b)). Phase shapes get more complicated when interphase boundaries and grain boundaries meet. Figure 2.9(c) shows the shape of a second-phase particle that has formed at a grain boundary. The particle is shaped by two spherical caps which meet the grain boundary at an angle θ . This angle is set by the balance of boundary tensions

$$2\gamma_{\alpha\beta} \cos \theta = \gamma_{gb} \quad (2.1)$$

where $\gamma_{\alpha\beta}$ is the tension (or energy) of the interphase boundary and γ_{gb} is the grain boundary tension (or energy).

In some alloys, $\gamma_{\alpha\beta}$ can be $\leq \gamma_{gb}/2$ in which case $\theta = 0$. The second phase will then spread along the boundary as a thin layer of β . This “wetting” of the grain boundary can be a great nuisance—if the phase is brittle then cracks can spread along the grain boundaries until the metal falls apart completely. A favorite scientific party trick is to put some aluminum sheet in

**FIGURE 2.9**

Many metals are made up of *two* phases. This figure shows some of the shapes that they can have when boundary energies dominate. To keep things simple, we have sectioned the tetrakaidecahedral grains in the way that we did in Figure 2.8(b). Note that Greek letters are often used to indicate phases. We have called the major phase α and the second phase β . But γ is the symbol for the energy (or tension) of grain boundaries (γ_{gb}) and interphase interfaces ($\gamma_{\alpha\beta}$).

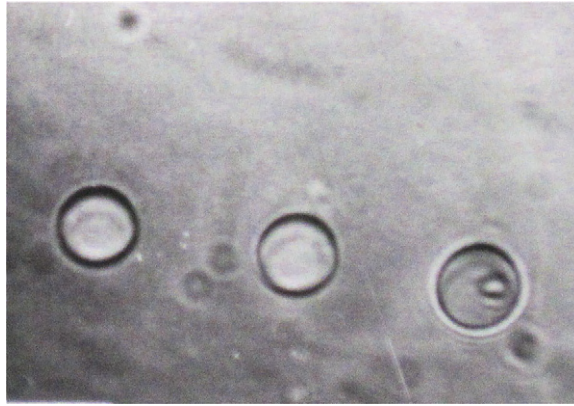
a dish of molten gallium and watch the individual grains of aluminum come apart as the gallium whizzes down the boundary.

The second phase can, of course, form complete grains (Figure 2.9(d)). But only if $\gamma_{\alpha\beta}$ and γ_{gb} are similar will the phases have tetrakaidecahedral shapes where they come together. In general, $\gamma_{\alpha\beta}$ and γ_{gb} may be quite different and the grains then have more complicated shapes.

2.7 SUMMARY—CONSTITUTION AND STRUCTURE

The structure of a metal is defined by two things. The first is the *constitution*:

- The overall composition—the elements (or *components*) that the metal contains and the relative weights of each of them.
 - The number of phases and their relative weights.
 - The composition of each phase.
- The second is the geometric information about *shape and size*:
- The shape of each phase.
 - The sizes and spacings of the phases.

**FIGURE 2.10**

An example of a spherical second phase. The matrix is a transparent organic compound—camphene—which melts at 50 °C. It is held at a temperature just below its melting point. The second phase is actually a *liquid* rich in dissolved impurities. The energy of the *solid–liquid* interface, γ_{SL} , is clearly isotropic. Magnification $\times 470$.

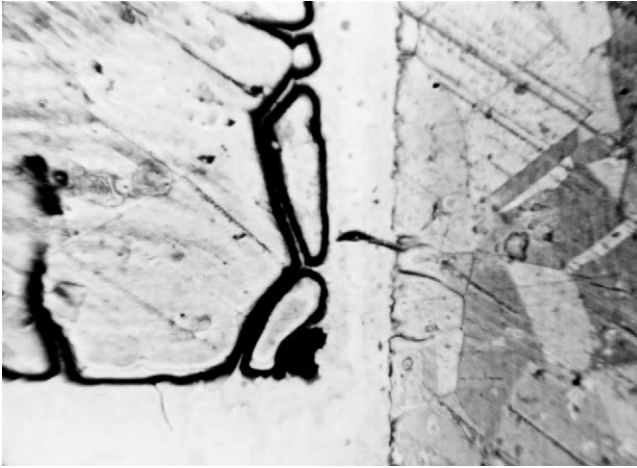
Armed with this information, we are in a strong position to reexamine the mechanical properties, and explain the great differences in strength, or toughness, or corrosion resistance between alloys. But where does this information come from? The *constitution* of an alloy is summarized by its phase diagram—the subject of the next two chapters. The *shape and size* are more difficult, since they depend on the details of how the alloy was made. But, as we shall see from later chapters, a fascinating range of microscopic processes operates when metals are cast, or worked or heat treated into finished products; and by understanding these, shape and size can, to a large extent, be predicted.

WORKED EXAMPLE

The following photograph shows a polished cross section through a brazed joint (magnification $\times 290$). The braze alloy itself appears white—it is “Pallabraz 950”, a proprietary brazing alloy with composition 54%Ag/25%Pd/21%Cu and melting range 901–950 °C.

<http://www.jm-metaljoining.com/applications-pages2.asp?pageid=8&id=120>

The material on both sides of the joint is “Nilo-K” or “Kovar”, a low thermal expansion alloy ($\alpha \approx 6 \times 10^{-6} \text{ } ^\circ\text{C}^{-1}$) with composition 54%Fe/29%Ni/17%Co and melting point 1450 °C.



Cross section through brazed joint. From left to right: (a) material adjacent to hole in Kovar sheet; (b) solidified Pallabraz 950 (white and featureless); and (c) part section of Kovar pin. Magnification $\times 290$.

http://www.alloywire.com/nilo_alloy_K.html

The component on the left of the joint is the lid of a small pot (containing an electronic device) which was press formed from thin Kovar sheet. A number of holes were drilled through the sheet, and the Kovar pins were inserted through the holes before being brazed in place in a furnace at 1000°C . (In other places, the holes were made larger in diameter, and the pins were located in the holes by tiny glass ferrules. The ferrules melted during the heating cycle and fused with the surfaces of both pin and hole. These *glass-metal seals* were intended to insulate the pins from the pot. It was in order to match the α values for the metal and the glass that Kovar was specified.)

http://en.wikipedia.org/wiki/Glass-to-metal_seal

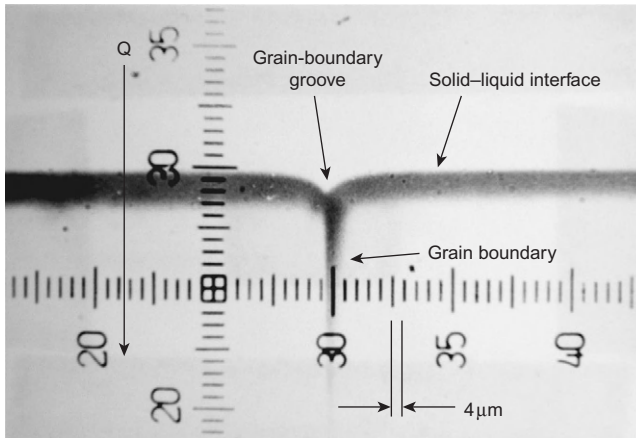
As the above photograph shows, during the time the brazing alloy was liquid in the furnace, it penetrated along the grain boundaries in the Kovar sheet. The depth of penetration was about $45\text{ }\mu\text{m}$. This is comparable to the grain size of the sheet, and in fact two grains have detached completely from the metal next to the hole. This is an excellent example of having $\gamma_{\text{SL}} \leq \gamma_{\text{gb}}/2$. This means that the liquid braze wets the grain boundaries and spreads along them easily. (The pin was attached to a smaller depth—and no grains were detached—because it was plated with a thin layer of nickel before brazing; nickel acts as a partial barrier to diffusion of the brazing alloy.) The main cause of the problem, however, was the long time it took to fuse the

glass, which exposed the Kovar to the liquid braze alloy for longer than was strictly necessary just to braze the pins in place.

EXAMPLES

- 2.1** Describe, in a few words, with an example or sketch where appropriate, what is meant by each of the following:
- polymorphism
 - dense random packing
 - an interstitial solid solution
 - a substitutional solid solution
 - clustering in solid solutions
 - ordering in solid solutions
 - an intermetallic compound
 - a phase in a metal
 - a grain boundary
 - an interphase boundary
 - a coherent interphase boundary
 - a semicoherent interphase boundary
 - an incoherent interphase boundary
 - the constitution of a metal
 - a component in a metal.
- 2.2** Why do impurity atoms segregate to grain boundaries?
- 2.3** A large furnace flue operating at 440 °C was made from a steel containing 0.10% phosphorus as an impurity. After 2 years in service, specimens were removed from the flue and tested for fracture toughness. The value of K_{Ic} was 30 MN m^{-3/2}, compared to 100 MN m^{-3/2} for new steel. Because of this, the flue had to be scrapped for safety reasons. Explain this dramatic drop in toughness.
- 2.4** Indicate the shapes that the following adopt *when boundary energies dominate*:
- a polycrystalline pure metal (isotropic γ_{gb})
 - an intermetallic precipitate inside a grain (isotropic $\gamma_{\alpha\beta}$)
 - an intermetallic precipitate at a grain boundary ($\gamma_{\alpha\beta} > \gamma_{gb}/2$)
 - an intermetallic precipitate at a grain boundary ($\gamma_{\alpha\beta} < \gamma_{gb}/2$).
- 2.5** The photograph which follows shows a solid–liquid interface in the transparent organic compound camphene (which melts at 50 °C). The sample of camphene was held in a temperature gradient until it reached equilibrium. The direction of heat flow was from top to bottom in the photograph, so at the top the material was molten, and at the bottom it was solid. The isotherms are horizontal, and the 50 °C isotherm locates the solid–liquid interface. The solid contains grain boundaries, which have migrated until they are perpendicular to the solid–liquid interface. Where the grain boundary meets the solid–liquid interface, it forms a

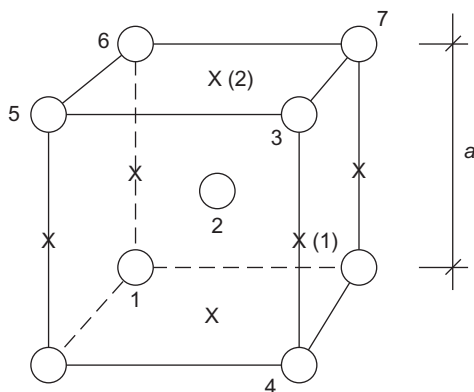
grain-boundary groove. By measuring the angle θ (see Figure 2.9(c)), estimate the ratio of the solid–liquid energy to the grain-boundary energy, $\gamma_{\text{SL}}/\gamma_{\text{gb}}$.



Answer

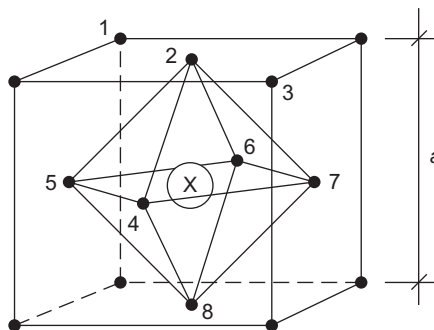
0.7.

- 2.6** A sample of Al + 5 wt%Sn was cooled slowly to 230 °C, at which point the structure consisted of 95 wt% solid Al and 5 wt% liquid Sn as dispersed droplets. The sample was held at 230 °C for a long time, after which it was quenched to room temperature. The liquid Sn solidified as soon as the temperature fell below 228 °C. The sample was sectioned and polished, and the shapes of the quenched Sn droplets observed. The droplets all had circular profiles on the plane of the section. What does this say about the three-dimensional equilibrium shape of the droplets when they were liquid? What does this equilibrium shape say about γ_{SL} for solid Al–liquid Sn?
- 2.7** The diagram which follows shows the unit cell of the b.c.c. crystal structure. The atoms touch along cube diagonals (e.g., atoms 1, 2, 3). Using this information, find the diameter D of each atom in terms of the lattice constant a . The diagram shows the locations (marked “X”) of “octahedral” spaces between the atoms. Calculate the diameter d of the largest dissolved atom which can fit into the octahedral spaces (express d in terms of a). To do this, draw a diagram showing atom 3, location X(1), and atom 4, all in a straight line. Also find the ratio d/D . Without being told how to calculate d , you could have chosen instead to draw a plan looking down on the top of the unit cell, showing atoms 3, 5, 6, 7 and location X(2). What value of d would you have calculated from this plan for a dissolved atom placed at X(2)? Why does the smaller of the two d values determine the diameter of the largest dissolved atom?

**Answers**

$$D = 0.8660a; d = 0.1340a; d/D = 0.155; d = 0.5482a.$$

- 2.8** The diagram which follows shows the unit cell of the f.c.c. crystal structure. The atoms touch along cube face diagonals (e.g., atoms 1, 2, 3). Using this information, find the diameter D of each atom in terms of the lattice constant a . The diagram shows the location (marked “X”) of an “octahedral” space between the atoms. Calculate the diameter d of the largest dissolved atom which can fit into an octahedral space (express d in terms of a). To do this, draw a plan looking down on the plane containing atoms 4, 5, 6, 7 showing the positions of these 4 atoms and X. Also find the ratio d/D . Would your answer have been any different if you had drawn a plan view of atoms 4, 2, 6, 8, and X instead? Explain your conclusion.

**Answers**

$$D = 0.7071a; d = 0.2929a; d/D = 0.4142.$$

- 2.9** a for f.c.c. iron is 0.355 nm; from Example 2.8, calculate the maximum diameter of an interstitial atom in an octahedral space. a for b.c.c. iron is 0.286 nm; from Example 2.7, calculate the maximum diameter of an interstitial atom in an octahedral space. The diameter of a carbon atom is 0.154 nm. f.c.c. iron can dissolve up to 1.7 wt% C (at 1130 °C). b.c.c. iron can dissolve up to 0.035 wt% C

(at 732 °C). Explain the relative solubilities of C in f.c.c. and b.c.c. iron in terms of the relative sizes of the octahedral spaces in the f.c.c. and b.c.c. crystal structures. How does the metal behave so it can accommodate C atoms which are larger than the octahedral spaces?

Answers

0.104 nm; 0.0383 nm.

2.10 The table shows pairs of metals (“metal 1” and “metal 2”) which have complete solid solubility in one another. Taking data from [Table 2.2](#), write down the crystal structure for both metals in each pair. What do you notice about the crystal structures? Why must this always be the case for complete solid solubility? Taking data from [Table 2.2](#), write down the value of the lattice parameter a for both metals in each pair. How do these a values explain the ability of the pairs of metals to form solid solutions over the full range of composition from 100% metal 1 to 100% metal 2?

Metal 1	Metal 2	Structure 1	Structure 2	a_1 (nm)	a_2 (nm)
Ag	Au				
Cr	Mo				
Cu	Ni				
Ir	Pt				
Mo	W				
Ni	Pd				
Ni	Pt				
Pt	Rh				
Ti	Zr				

Phase Diagrams 1

3.1 INTRODUCTION

If you work through the next two chapters, doing the examples, you will get a working knowledge of what a phase diagram (or equilibrium diagram) means and how to use it. To help, we have put the solutions to the examples at the end of each chapter. Don't rush it: learn the definitions and meditate a little over the diagrams themselves, checking yourself as you go. Some parts (the definitions, for instance) are pretty concentrated stuff. Others (some of the examples, perhaps) may strike you as trivial. That is inevitable in a course for students with differing backgrounds. Do them anyway. The whole thing should take you about 4 h. The material given here broadly parallels the introductory part of the excellent text by Hansen and Beiner (see [Section 3.2](#)); if you can read German, and want to learn more, work through this.

Phase diagrams are important. Whenever materials engineers have to report on the properties of a metallic alloy, or a ceramic, the first thing they do is reach for the phase diagram. It tells them what, at equilibrium, the structure of the alloy or ceramic is. The real structure may not be the equilibrium one, but equilibrium structure gives a baseline from which other (nonequilibrium) structures can be inferred.

Some excellent sources of phase diagrams are given below.

3.2 SOURCE BOOKS

ASM. Metals Handbook, 2nd desktop edition. ASM, 1999.

W. Gale and T. Totemeier, Smithells reference book, 8th edition. Elsevier, 2003.

M. Hansen and K. Anderko, *Constitution of Binary Alloys*, McGraw-Hill, 1958; and supplements, by R. P. Elliott, 1965, and F. A. Shunk, 1969.

J. Hansen and F. Beiner, *Heterogeneous Equilibrium*, De Gruyter, 1975.

W. Hume-Rothery, J. W. Christian and W. B. Pearson, *Metallurgical Equilibrium Diagrams*, Institute of Physics, 1952.

E. M. Levin, C. R. Robbins and H. F. McMurdie, *Phase Diagrams for Ceramists*, American Ceramic Society, 1964.

3.3 COMPONENTS, PHASES, AND STRUCTURES

Definitions are enclosed in boxes and signaled by “DEF.” These you have to learn. The rest follows in a logical way.

Alloys

DEF.

A metallic alloy is a mixture of a metal with other metals or nonmetals. Ceramics, too, can be mixed to form alloys.

Copper (Cu) and zinc (Zn), when mixed, form the alloy *brass*. Magnesia (MgO) and alumina (Al₂O₃) when mixed in equal proportions form *spinel*. Iron (Fe) and carbon (C) mix to give *carbon steel*.

Components

Alloys are usually made by melting together and mixing the components.

DEF.

The *components* are the chemical elements which make up the alloy.

In *brass*, the components are Cu and Zn. In *carbon steel*, the components are Fe and C. In *spinel*, they are Mg, Al, and O.

DEF.

A *binary alloy* contains two components. A *ternary alloy* contains three; a *quaternary*, four, etc.

Symbols

Components are given capital letters: A, B, C or the element symbols Cu, Zn, C.

Concentration

An alloy is described by stating the components and their concentrations.

DEF.

The weight % of component A:

$$W_A = \frac{\text{weight of component A}}{\sum \text{weights of all components}} \times 100$$

The atom (or mol) % of component A:

$$X_A = \frac{\text{number of atoms (or mols) of component A}}{\sum \text{number of atoms (or mols) of all components}} \times 100$$

(Weight in g)/(atomic or molecular wt in g mol^{-1}) = number of mols.

(Number of mols) \times (atomic or molecular wt in g mol^{-1}) = weight in g.

EXAMPLES

- 3.1 (a)** Calculate the concentration in wt% of copper in a brass containing 40 wt% zinc.

Concentration of copper, in wt%:

$$W_{\text{Cu}} = \underline{\hspace{2cm}}$$

- (b)** 1 kg of an α -brass contains 0.7 kg of Cu and 0.3 kg of Zn.

The concentration of copper in α -brass, in wt%:

$$W_{\text{Cu}} = \underline{\hspace{2cm}}$$

The concentration of zinc in α -brass, in wt%:

$$W_{\text{Zn}} = \underline{\hspace{2cm}}$$

- (c)** The atomic weight of copper is 63.5 and of zinc 65.4.

The concentration of copper in α -brass, in at%:

$$X_{\text{Cu}} = \underline{\hspace{2cm}}$$

The concentration of zinc in α -brass, in at%:

$$X_{\text{Zn}} = \underline{\hspace{2cm}}$$

- 3.2** A special brazing alloy contains 63 wt% of gold (Au) and 37 wt% of nickel (Ni).

The atomic weight of Au (197.0) is more than three times that of Ni (58.7). At a glance, which of the two compositions, in at%, is likely to be the right one?

- (a)** $X_{\text{Au}} = 0.34$, $X_{\text{Ni}} = 0.66$.

- (b)** $X_{\text{Au}} = 0.66$, $X_{\text{Ni}} = 0.34$.

- 3.3** Your favorite vodka is 100° proof (49 wt% of alcohol). The molecular weight of water is 18; that of ethyl alcohol— $\text{C}_2\text{H}_5\text{OH}$ —is 46. What is the mol% of alcohol in the vodka?

Mol% of alcohol: $X_{\text{C}_2\text{H}_5\text{OH}} = \underline{\hspace{2cm}}$

- 3.4** An alloy consists of X_A at% of A with an atomic weight α_A , and X_B at% of B with an atomic weight of α_B . Derive an equation for the concentration of A in wt%. By symmetry, write down the equation for the concentration of B in wt%.

Structure

Alloys are usually made by melting the components and mixing them together while liquid, though you can make them by depositing the components from the vapor, or by diffusing solids into each other. No matter how you make it, a binary alloy can take one of four forms:

- (a) single solid solution
- (b) two separated, essentially pure, components
- (c) two separated solid solutions
- (d) a chemical compound, together with a solid solution.

How can you tell which form you have got? By examining the *microstructure*. To do this, the alloy is cut to expose a flat surface which is then polished, first with successively finer grades of emery paper, and then with diamond pastes (on rotating felt disks) until it reflects like a mirror. Finally, the polished surface is etched, usually in a weak acid or alkali, to reveal the microstructure—the pattern of grains and phases. Grain boundaries show up because the etch attacks them preferentially. The etch also attacks the crystals, leaving densely packed crystallographic planes exposed; light is reflected from these planes, so some grains appear light and others dark, depending on whether the light is reflected in the direction in which you are looking. Phases can be distinguished, too, because the phase boundaries etch, and because many etches are designed to attack one phase more than another, giving a contrast difference between phases.

The Al–11 wt% Si casting alloy is typical of (b): the Si separates out as fine needles ($\approx 1\ \mu\text{m}$ diameter) of essentially *pure* Si in a matrix of *pure* Al. The Cd–60 wt% Zn alloy typifies (c): it consists of a *zinc-rich phase* of Zn with 0.1 wt% Cd dissolved in it plus a *cadmium-rich phase* of Cd with 0.8 wt% Zn dissolved in it. Finally, slow-cooled Al–4 wt% Cu is typical of (d) (Figure 11.3).

EXAMPLE

- 3.5** List the compositions of the alloy and the phases mentioned above.

	wt% Cd	wt% Zn
Cadmium–zinc alloy		
Zinc-rich phase		
Cadmium-rich phase		

Phases

DEF.

All parts of an alloy with the same physical and chemical properties and the same composition are parts of a *single phase*.

The Al–Si, Cd–Zn, and Al–Cu alloys are all made up of two phases.

EXAMPLES

- 3.6** You heat pure copper. At 1083 °C it starts to melt. While it is melting, solid and liquid copper coexist. Using the definition above, are one or two phases present? _____
Why? _____
- 3.7** Three components A, B, and C of an alloy dissolve completely when liquid but have no mutual solubility when solid. They do not form any chemical compounds. How many phases, and of what compositions, do you think would appear in the solid state?
Phases _____
Compositions _____

The constitution of an alloy

DEF.

The *constitution* of an alloy is described by:

- (a) the phases present
- (b) the weight fraction of each phase
- (c) the composition of each phase.

The properties of an alloy (yield strength, toughness, oxidation resistance, etc.) depend critically on its constitution and on two further features of its structure: the *scale* (nm or μm or mm) and *shape* (round or rod-like or plate-like) of the phases, not described by the constitution. The constitution and the scale and shape of the phases depend on the thermal treatment that the material has had.

WORKED EXAMPLE

The alloy aluminum–4 wt% copper forms the basis of the 2000 series (Duralumin or Dural for short). It melts at about 650 °C. At 500 °C, solid Al

dissolves as much as 4 wt% of Cu completely. At 20 °C its equilibrium solubility is only 0.1 wt% Cu. If the material is slowly cooled from 500 to 20 °C, $4 - 0.1 \text{ wt\%} = 3.9 \text{ wt\%}$ copper separates out from the aluminum as large lumps of a new phase: not pure copper, but of the compound CuAl_2 . If, instead, the material is quenched (cooled very rapidly, often by dropping it into cold water) from 500 to 20 °C, there is no time for the dissolved copper atoms to move together, by diffusion, to form CuAl_2 , and the alloy remains a solid solution.

At room temperature, diffusion is so slow that the alloy just stays like this, frozen as a single phase. But if you heat it up just a little—to 160 °C, for example—and hold it there (“aging”), the copper starts to diffuse together to form an enormous number of very tiny (nm) plate-like particles of composition roughly CuAl_2 . On recooling to room temperature, this new structure is again frozen in.

The yield strength and toughness of Dural differ enormously in these three conditions (slow-cooled, quenched, and quenched and aged); the last gives the highest yield and lowest toughness because the tiny particles obstruct dislocations very effectively.

It is important to be able to describe the constitution and structure of an alloy quickly and accurately. So do the following, even if they seem obvious.

EXAMPLES

3.8 In the example above:

- (a) How many phases are present at 500 °C? _____
- (b) How many phases after slow cooling to 20 °C? _____
- (c) How many phases after quenching to 20 °C? _____
- (d) How many phases after quenching and aging? _____

3.9 An alloy of 120 g of lead (Pb) and 80 g of tin (Sn) is melted and cast. At 100 °C, two phases are found. There is 126.3 g of the lead-rich phase and 73.7 g of the tin-rich phase. It is known that the lead-rich phase contains $W_{\text{Pb}} = 95\%$ of lead. The constitution of the alloy at room temperature is described by:

- (a) Number of phases _____
- (b) Weight% of lead-rich phase _____
Weight% of tin-rich phase _____
- (c) Composition of lead-rich phase, in wt%:
 $W_{\text{Pb}} =$ _____
 $W_{\text{Sn}} =$ _____

(d) Composition of tin-rich phase, in wt%:

$W_{\text{Pb}} =$ _____

$W_{\text{Sn}} =$ _____

Equilibrium constitution

The Al–4 wt% Cu alloy of the example can exist at 20 °C in three different states. Only one—the slowly cooled one—is its equilibrium state, though given enough time the others would ultimately reach the same state. At a given temperature, then, there is an *equilibrium constitution* for an alloy to which it tends.

DEF.

A sample has its *equilibrium constitution* when, at a given, constant temperature T and pressure p , there is no further tendency for its constitution to change with time. This constitution is the stable one.

Alloys can exist in nonequilibrium states—the Al–Cu example was an illustration. But it is always useful to know the equilibrium constitution. It gives a sort of baseline for the constitution of the real alloy, and the likely nonequilibrium constitutions can often be deduced from it.

State variables

Ten different samples with the same composition, held at the same T and p , have the same equilibrium constitution. Ten samples each of different composition, or each held at different T or p values, have ten different equilibrium constitutions.

DEF.

The independent *constitution variables* or *state variables* are T , p , and composition.

WORKED EXAMPLE

The Al–Cu alloy (see Figure 11.3)

Values of the state variables	Equilibrium constitution

$$\begin{array}{ll}
 \text{(a)} & \left. \begin{array}{l} T = 500\text{ }^{\circ}\text{C} \\ p = 1\text{ atm} \\ W_{\text{Al}} = 96\% \\ W_{\text{Cu}} = 4\% \end{array} \right\} \rightarrow \text{Single-phase solid solution of copper in aluminum} \\
 \text{(b)} & \left. \begin{array}{l} T = 20\text{ }^{\circ}\text{C} \\ p = 1\text{ atm} \\ W_{\text{Al}} = 96\% \\ W_{\text{Cu}} = 4\% \end{array} \right\} \rightarrow \text{Two phases: Al containing 0.1 wt\% Cu, and CuAl}_2
 \end{array}$$

They are *equilibrium* constitutions because they are the ones reached by very slow cooling; slow cooling gives time for equilibrium to be reached.

Certain thermodynamic relations exist between the state variables. In general, for a binary alloy, we choose p , T , and X_B (the at% of component B) as the *independent variables*—though presently we shall drop p . The volume V and the composition X_A ($= 1 - X_B$) are then determined: they are the *dependent variables*. Of course, the weight percentages W_A and W_B can be used instead.

Equilibrium constitution (or phase) diagrams

The equilibrium constitution of an alloy can be determined experimentally by metallography and thermal analysis (described later). If the pressure is held constant at 1 atm, then the independent variables which control the constitution of a binary alloy are T and X_B or W_B .

DEF.

An equilibrium constitution diagram or *equilibrium diagram* for short (or, shorter still, *phase diagram*), is a diagram with T and X_B (or W_B) as axes. It shows the results of experiments which measure the equilibrium constitution at each T and X_B (or W_B).

Figure 3.1 shows a phase diagram for the lead–tin system (the range of alloys obtained by mixing lead and tin, which includes soft solders). The horizontal axis is composition X_{Pb} (at%) below and W_{Pb} (wt%) above. The vertical axis is temperature in $^{\circ}\text{C}$. The diagram is divided into *fields*: regions in which the number of phases is constant. In the unshaded fields, the equilibrium constitution is single phase: liquid (above), or tin containing a little dissolved lead (left), or lead containing dissolved tin (right). In the shaded fields, the equilibrium constitution has two phases: liquid plus solid Sn, or liquid plus solid Pb, or solid Pb mixed with solid Sn (each containing a little of the other in solution).

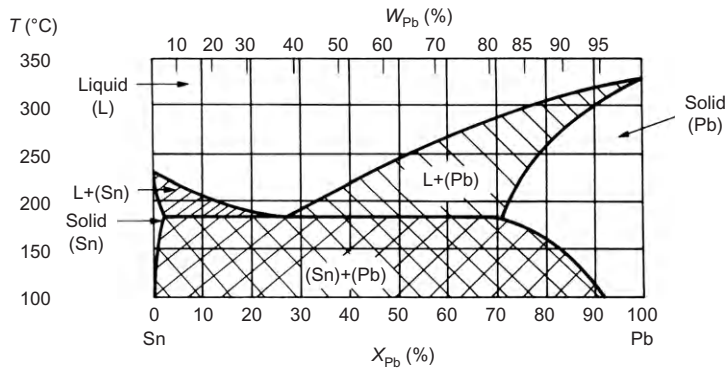


FIGURE 3.1

DEF.

The diagram shows the equilibrium constitution for all the binary alloys that can be made of lead and tin, in all possible proportions, or, in short, for the lead–tin *system*.

A *binary system* is a system with two components.

A *ternary system* is a system with three components.

The constitution point

The state variables define a point on the diagram: the “constitution point”. If this point is given, then the equilibrium number of phases can be read off. So, too, can their composition and the quantity of each phase—but that comes later. So the diagram tells you the entire constitution of any given alloy, at equilibrium. Refer back to the definition of *constitution* (p. 37) and check that this is so.

EXAMPLES

3.10 Figure 3.2 shows the Pb–Sn diagram again but without shading.

- (a) What is the composition and temperature (the state variables) of point 1?
 Composition _____ at% Pb
 and _____ at% Sn
 Temperature _____ °C
- (b) Mark the constitution point for a Pb–70 at% Sn alloy at 250 °C onto Figure 3.2.
 What does the alloy consist of at 250 °C? _____
 How many phases? _____

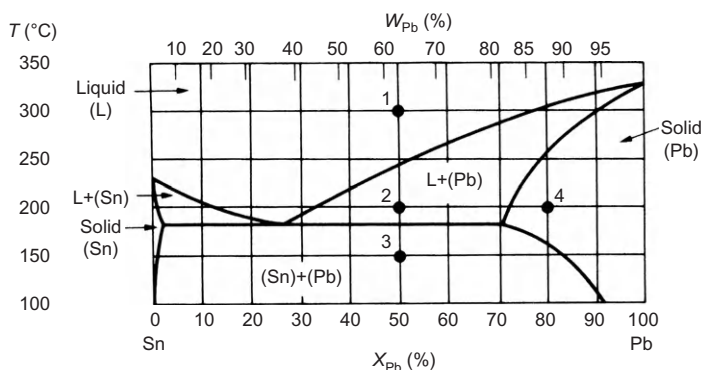


FIGURE 3.2

- (c) Mark the point for a Pb–30 at% Sn at 250 °C.
 What does it consist of? _____
 How many phases? _____
- (d) Describe what happens as the alloy corresponding initially to the constitution point 1 is cooled to room temperature.
 At which temperatures do changes in the number or type of phases occur? _____
 What phases are present at point 2? _____
 What phases are present at point 3? _____
- (e) Describe similarly what happens when the alloy corresponding to the constitution point 4 is cooled to room temperature.
 Initial composition and temperature _____
 Initial number of phases _____
 Identify initial phase(s) _____
 Temperature at which change of phase occurs _____
 Number of phases below this temperature _____
 Identify phases _____

3.11 Is a mixture of a metal and a nonmetal called an alloy?

Yes	No
-----	----

3.12 Pernod is a transparent yellow fluid consisting of water, alcohol, and Evil Esters. The Evil Esters dissolve in strong water–alcohol solutions but precipitate out as tiny whitish droplets if the solution is diluted with more water. It is observed that Pernod turns cloudy at 60 wt% water at 0 °C, at 70 wt% water at 20 °C, and at 85 wt% water at 40 °C. Using axes of T and concentration of water in wt%, sketch an approximate phase diagram (Figure 3.3) for the Pernod–water system, indicating the single- and two-phase fields.

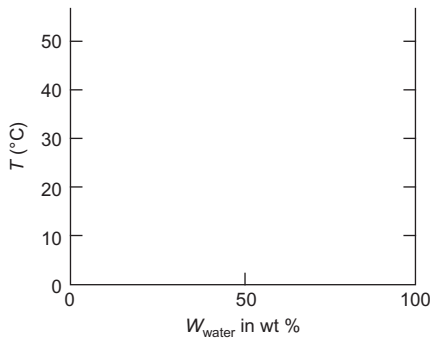


FIGURE 3.3

3.13 A micrograph reveals 10 black-etching needles and 8 globular regions that etch gray, set in a white-etching matrix.

- (a) How many phases would you judge there to be?

- (b) Does the constitution of the alloy depend on the shape of the phases?

- (c) Can the constitution of the alloy depend on its thermal history?

- (d) What do you call the entire range of alloys which can be made of lead and tin? _____

3.4 ONE- AND TWO-COMPONENT SYSTEMS

Phase diagrams are mostly determined by *thermal analysis*. We now discuss one-component systems to show how it works. The more complicated diagrams for binary, ternary, or quaternary alloys are determined by the same method.

Reminder

One-component systems	Independent variables p and T
Binary (A + B) systems	Independent variables p , T , and X_B
Ternary (A + B + C) systems	Independent variables p , T , X_B , and X_C
Quaternary (A + B + C + D) systems	Independent variables p , T , X_B , X_C , and X_D

One-component systems

The equilibrium constitution of a one-component system is fixed by the variables p and T so the equilibrium phases can be shown on a diagram with p

and T axes. The one shown in Figure 3.4 has only one solid phase. Some, like ice or iron, have several.

Single-phase regions are *areas*.

Two phases coexist along *lines*.

Three phases coexist at a *point*: the triple point.

The behavior at constant p is given by a horizontal cut through the diagram. The solid *melts* at T_M and *vaporizes* at T_V . The phase diagram at constant pressure is a line (shown on the right) along which the span of stability of each phase is marked, as shown in Figure 3.5.

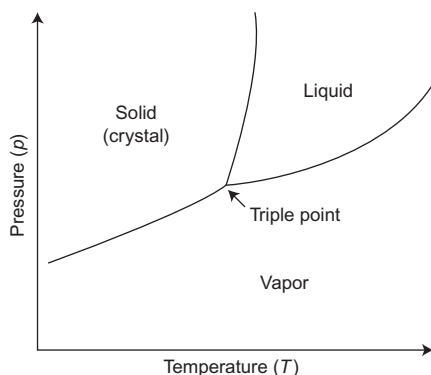


FIGURE 3.4

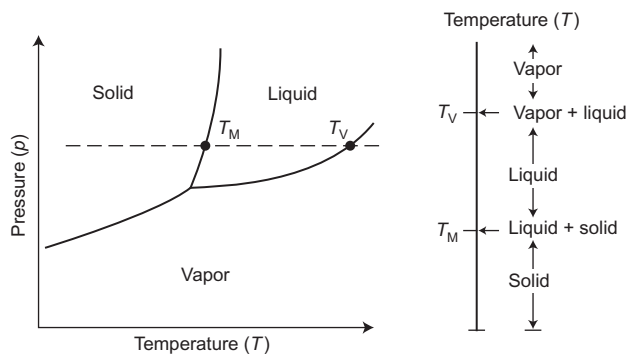


FIGURE 3.5

EXAMPLES

3.14 List the phases shown on the T – p diagram (Figure 3.5)

3.15 If the pressure is increased, does the melting point of the material of the diagram increase, decrease, or stay constant? _____

- 3.16** At 1 atm, iron melts at 1536 °C and boils at 2860 °C. When it solidifies (a phase change), it does so in the b.c.c. crystal structure and is called δ -iron. On cooling further, it undergoes two further phase changes. The first is at 1391 °C when it changes to the f.c.c. crystal structure and is then called γ -iron. The second is at 914 °C when it changes *back* to the b.c.c. crystal structure and is called α -iron.
- Construct the one-dimensional phase diagram at constant pressure (1 atm) for iron (Figure 3.6).
 - Mark on it the regions in which each phase is stable. Label them with the names of the phases.
 - Indicate with arrows the points or regions where two phases coexist in equilibrium.

Cooling curves

If a one-component system is allowed to cool at constant pressure, and the temperature is recorded as a function of time, it looks as shown in Figure 3.7. It shows five regions:

- vapor
- vapor-to-liquid phase change

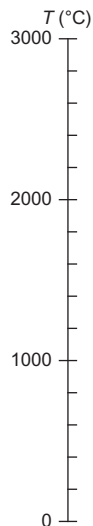


FIGURE 3.6

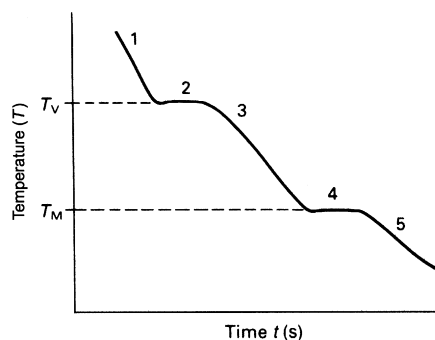


FIGURE 3.7

- 3. liquid
- 4. liquid-to-solid phase change
- 5. solid.

The system is a single phase in regions 1, 3, and 5. Phase changes occur at the temperatures corresponding to regions 2 and 4. When a phase transformation takes place, the *latent heat* of the transformation is released (on cooling) or absorbed (on heating). Because of this the temperature stays almost constant during the transformation, giving shelves 2 and 4; cooling continues only when the transformation is complete.

Phase transformations in the solid state (like those in iron), too, have latent heats. They may be small but with sensitive equipment for measuring cooling curves or heating curves; they are easily detected.

The shelves of the cooling curve are called *arrest points*. The two shown in the picture are at the boiling point and the melting point of the material at the given pressure.

Differential thermal analysis, DTA

Even in complicated, multicomponent alloys, phase changes can be determined by cooling (or heating) a sample, recording temperature as a function of time, and observing the arrest points. Greater accuracy is possible with *differential thermal analysis*. A sample with the same thermal mass as the test sample, but showing no phase transformations, is cooled (or heated) side-by-side with the test sample, and the *difference* ΔT between the cooling (or heating) curves is plotted. Sometimes the difference in power needed to heat the two samples at the *same rate* is measured instead: there is a sudden difference in power at the phase transformation. Both are just sophisticated ways of getting the information shown in the cooling curve.

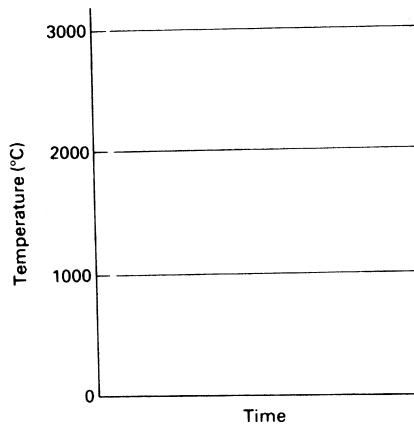


FIGURE 3.8

EXAMPLES

- 3.17** Construct the general shape of a cooling curve for iron, starting at 3000 °C and ending at 0 °C, using the data given in Example 3.16 (Figure 3.8).
- 3.18** Which phases do you expect at each of the following constitution points for the lead–tin system?
- (a) $X_{\text{Pb}} = 40\%$, $T = 175\text{ °C}$
 - (b) $W_{\text{Pb}} = 15\%$, $T = 200\text{ °C}$
 - (c) $W_{\text{Sn}} = 10\%$, $T = 200\text{ °C}$
 - (d) $W_{\text{Pb}} = 35\%$, $T = 200\text{ °C}$
- 3.19** You cool a sample of $X_{\text{Pb}} = 80\%$ from 325 to 125 °C sufficiently slowly that equilibrium is maintained. Mark the two points on Figure 3.9 and join them to show the *cooling path*. In sequence, what phases appear as the alloy is cooled?
- (a) _____
 - (b) _____
 - (c) _____
- 3.20** Figure 3.10 shows the phase diagram for ice. (The pressures are so large that steam appears only at the extreme upper left.) There are eight different solid phases of ice, each with a different crystal structure.

Current ideas of the evolution of the large satellite of Jupiter, Ganymede, assume it to be largely made of ice. The pressure caused by gravitational forces rises about linearly from the surface to the center, reaching a peak of around 2 GN m^{-2} . Radioactive decay causes the center to have a temperature of about 30 °C but at the surface the temperature is below—100 °C. Assuming a linear temperature gradient from the surface to the center, which phases of ice would be found in Ganymede?

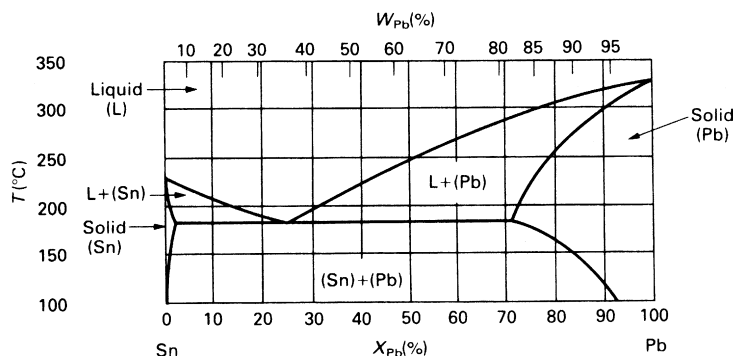


FIGURE 3.9

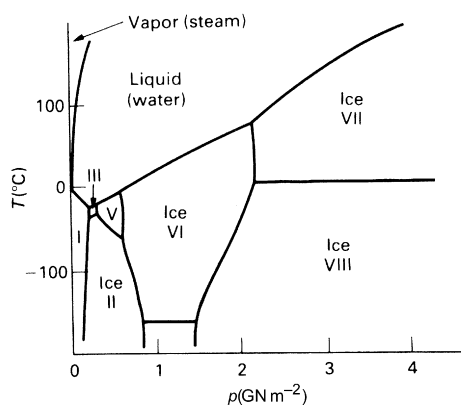


FIGURE 3.10

Binary systems

What defines the *constitution* of an alloy? If you can't remember, refer back to the definition on p. 37 and revise. The phase diagram gives all three pieces of information. The first you know already. This section explains how to get the other two.

At first sight, there is a problem in drawing phase diagrams for binary systems: there are three state variables (p , T , and X_B).

The pressures on the ice phase diagram (above) are enormous, and when they are this large they do affect phase equilibrium. But, almost always, we are interested only in pressures near atmospheric (maybe up to 100 atm), and such small pressures have almost no effect on phase diagrams for solids

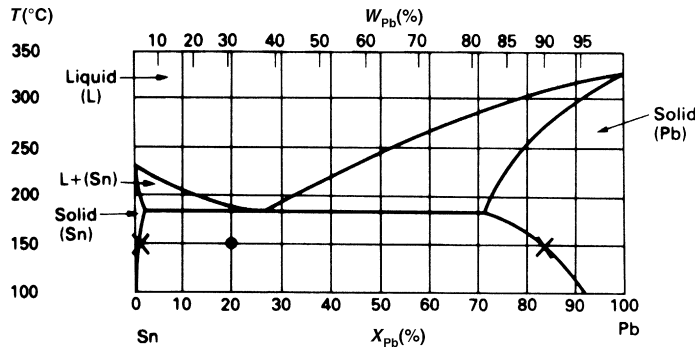


FIGURE 3.11

and liquids. So, we can drop p as a variable and plot the phase diagram in two dimensions, with T and X_B as axes. For ternary (or higher) systems, there is no way out—even after dropping p there are three (or more) variables. Then, we can only show *sections* through the phase diagram of constant T or of constant X_C , for example.

Composition of the phases

The phase diagram for a binary alloy (Figure 3.11) shows *single-phase fields* (e.g., liquid) and *two-phase fields* (e.g., liquid plus A). The fields are separated by *phase boundaries*. When a phase boundary is crossed, a phase change starts, or finishes, or both.

DEF.

When the constitution point lies in a single-phase region, the alloy consists of a single, homogeneous phase. Its composition must (obviously) be that of the alloy. The *phase composition* and the *alloy composition* coincide in single-phase fields.

When the constitution point lies in a two-phase region, the alloy breaks up into two phases which do not have the same composition as the alloy (though a properly weighted *mean* of the two compositions must equal that of the alloy).

What are these compositions? Well, if the alloy is at a temperature T , the two phases (obviously) are at this temperature. Consider a Sn–20 at% Pb alloy, at 150 °C. Figure 3.11 shows that, at this temperature, tin dissolves 1 at% of lead and lead dissolves 17 at% of tin. The compositions are shown as X_s on the 150 °C isotherm (horizontal line): they are the *equilibrium phases* at 150 °C. The line joining them is called a *tie line*.

DEF.

When the constitution point for an alloy lies in the two-phase field, the alloy breaks up into a mixture of two phases. The composition of each phase is obtained by constructing the *tie line* (the isotherm spanning the two-phase region, terminating at the nearest phase boundary on either side). The *composition of each phase* is defined by the ends of the tie line.

Any alloy which lies on the tie line breaks up into the same two phases at its ends. The *proportions* of each phase, of course, depend on the alloy composition.

EXAMPLES

- 3.21 (a)** The constitution point for a Sn–60 at% Pb alloy at 250 °C lies in a two-phase field. Construct a tie line on Figure 3.12 and read off the two phases and their compositions.

The phases are _____

The composition of phase 1 is _____

The composition of phase 2 is _____

- (b)** The alloy is slowly cooled to 200 °C. At 200 °C:
The phases are _____

The composition of phase 1 is _____

The composition of phase 2 is _____

- (c)** The alloy is cooled further to 150 °C. At this temperature:

The phases are _____

The composition of phase 1 is _____

The composition of phase 2 is _____

- (d)** Indicate with arrows on the figure the lines along which:

1. The composition of phase 1 moves
2. The composition of phase 2 moves

The overall composition of the alloy stays the same, of course. How can the compositions of the phases change?

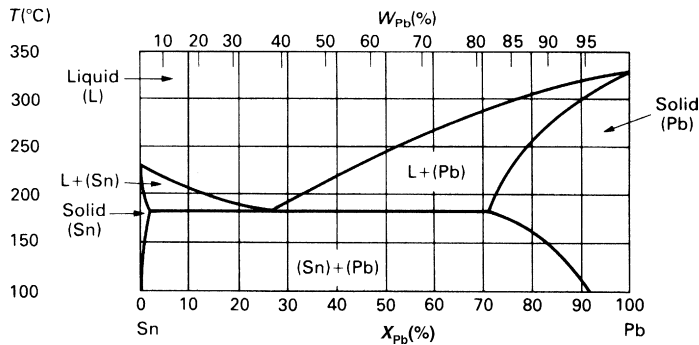


FIGURE 3.12

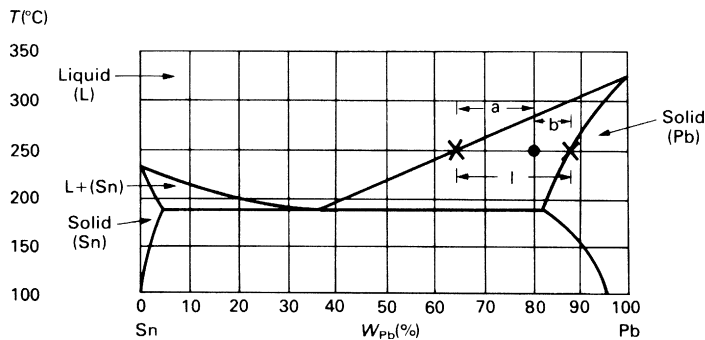


FIGURE 3.13

Proportions of phases in two-phase alloys

You can get the *relative amounts* of each phase in a two-phase alloy from the phase diagram.

DEF.

The weight fraction of phase α is designated W_{α} .

That of phase β is W_{β} . In a binary alloy, $W_{\alpha} + W_{\beta} = 1$.

Prove this result to yourself. Notice that, for the first time, we have not given a parallel result for atomic (or mol) fraction. You cannot have an atom fraction of a *phase* because a phase (as distinct from a pure element or a chemical compound of a *specific* composition) does not have an atomic weight. Its composition can vary within the limits given by the phase diagram.

To find the relative amounts of each phase, start off by constructing a tie line through the constitution point and read off the compositions of the phases (Figure 3.13).

WORKED EXAMPLE

At 250 °C, the Sn–Pb alloy with $W_{\text{Pb}} = 80\%$ consists of two phases:

Liquid with $W_{\text{Pb}}^{\text{LIQ}} = 65\%$

Solid with $W_{\text{Pb}}^{\text{SOL}} = 87\%$.

The *weight fractions* of each phase, W_{LIQ} and W_{SOL} , are fixed by the requirement that matter is conserved. Then:

$$\left. \begin{array}{l} \text{The weight fraction of solid in the alloy is} \\ W_{\text{SOL}} = \frac{a}{l} \\ \text{and the weight fraction of liquid is} \\ W_{\text{LIQ}} = \frac{b}{l} \end{array} \right\} \text{the "lever" rule}$$

and $W_{\text{SOL}} + W_{\text{LIQ}} = 1$ as they obviously must.

The easiest way to understand this result is to notice that, if the constitution point coincides with the left-hand X (the left-hand end of the tie line), the alloy is all liquid; and when it coincides with the right-hand X, it is all solid;

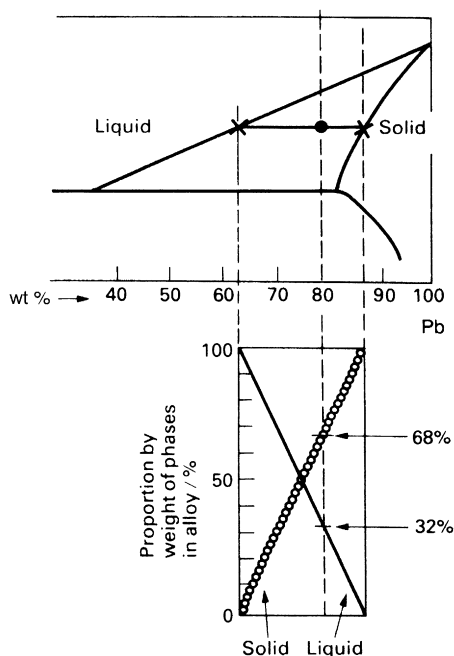


FIGURE 3.14

provided the phase diagram has a linear wt% scale, the weight fraction of each phase is proportional to distance measured along the tie line. Figure 3.14 shows how this relates to our example of an 80 wt% Pb alloy. The weight percentages of other alloys along the tie line can be found in exactly the same way: the results can be calculated using the lever rule or, more approximately, can be read straight off the linear graphs in the figure.

When the wt% scale is *not* linear (often it is not), you get the weight fractions by writing

$$\begin{aligned} l &= W_{\text{Pb}}^{\text{SOL}} - W_{\text{Pb}}^{\text{LIQ}} \\ a &= W_{\text{Pb}} - W_{\text{Pb}}^{\text{LIQ}} \\ b &= W_{\text{Pb}}^{\text{SOL}} - W_{\text{Pb}} \end{aligned}$$

where $W_{\text{Pb}}^{\text{LIQ}}$ is the percentage of lead in the liquid and $W_{\text{Pb}}^{\text{SOL}}$ is that in the solid (as before). These can be read off the (nonlinear) wt% scale, and the results used in the lever rule.

EXAMPLES

3.22 A lead–tin alloy with composition $W_{\text{Pb}} = 80\%$ is held at a temperature T .

- (a) At $T = 280^\circ\text{C}$ which is the dominant phase?
- (b) At $T = 200^\circ\text{C}$ which is the dominant phase?

Indicate by arrows on Figure 3.15 the changes in the compositions of the liquid phase and the solid phase as the alloy is cooled from 280 to 200 °C.

3.23 The alloy is cooled to 150 °C.

- (a) How many phases are present? _____
- (b) List the approximate composition of the phase(s) _____
- (c) Which is the dominant phase? _____
- (d) What (roughly) are the proportions by weight of each phase? _____

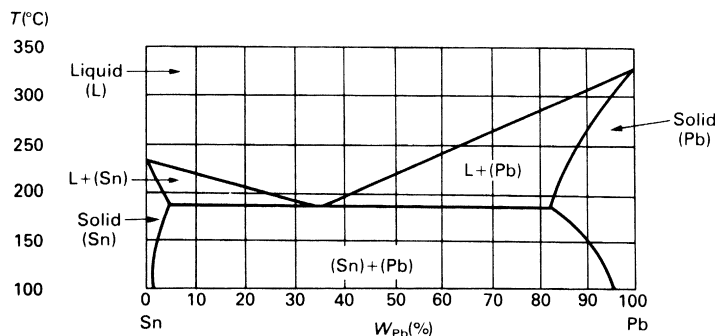


FIGURE 3.15

Gibbs phase rule

DEF.

The number of phases P which coexist in equilibrium is given by the phase rule

$$F = C - P + 2$$

where C is the number of *components* (p. 34) and F is the number of free *independent state variables* (p. 39) or “degrees of freedom” of the system. If the pressure p is held constant (as it usually is for solid systems), then the rule becomes $F = C - P + 1$.

A one-component system ($C = 1$) has two independent state variables (T and p). At the triple point, three phases (solid, liquid, vapor) coexist in equilibrium, so $P = 3$. From the phase rule $F = 0$, so that at the triple point, T and p are fixed—neither is free but both are uniquely determined. If T is free but p depends on T (a sloping *line* on the phase diagram), then $F = 1$ and $P = 2$ that is, two phases, solid and liquid say, coexist at equilibrium. If both p and T are free (an *area* on the phase diagram) $F = 2$ and $P = 1$; only one phase exists at equilibrium (Figure 3.16).

EXAMPLES

3.24 For a binary A–B alloy:

- (a) The number of components $C =$ _____
- (b) The independent state variables are _____
- (c) If pressure is held fixed at atmospheric pressure, there are at most _____ degrees of freedom.
- (d) If $F = 0$, how many phases can coexist in equilibrium at constant p ? _____
- (e) If $F = 1$, how many phases coexist at constant p ? _____

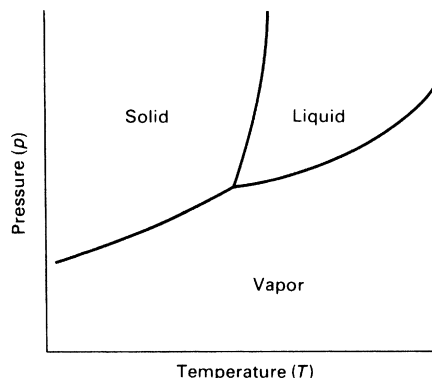


FIGURE 3.16

(f) If $F = 2$, how many phases coexist at constant p ? _____

(g) In a single-phase field, how many degrees of freedom are there at constant p ? _____

(h) In a two-phase field, how many degrees of freedom are there at constant p ? _____

3.25 Figure 3.17 shows the phase diagram for the copper–zinc system. It is more complicated than you have seen so far, but all the same rules apply. The Greek letters (conventionally) identify the single-phase fields.

(a) Shade in the two-phase fields. Note that single-phase fields are always separated by two-phase fields except at points.

(b) The two common commercial brasses are:

70/30 brass: $W_{\text{Cu}} = 70\%$;

60/40 brass: $W_{\text{Cu}} = 60\%$

Mark their constitution points onto the diagram at 200 °C (not much happens between 200 °C and room temperature).

What distinguishes the two alloys? _____

(c) What, roughly, is the melting point of 70/30 brass? _____

(d) What are the phase(s) in 60/40 brass at 200 °C? _____

What are the phase(s) in 60/40 brass at 800 °C? _____

What has happened to the other phase? _____

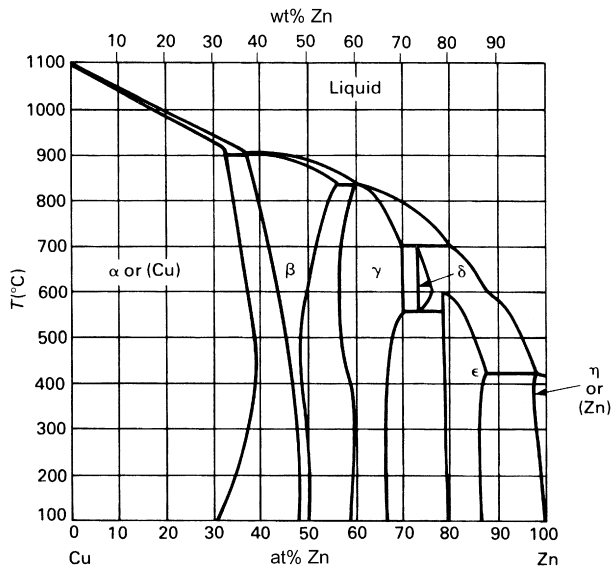


FIGURE 3.17

3.5 SOLUTIONS TO EXAMPLES

- 3.1 (a) $W_{\text{Cu}} = 60\%$.
 (b) $W_{\text{Cu}} = 70\%$, $W_{\text{Zn}} = 30\%$.
 (c) $X_{\text{Cu}} = 71\%$, $X_{\text{Zn}} = 29\%$.
 3.2 (a) is the correct composition.
 3.3 Your vodka contains 27 mol% of alcohol.
 3.4

$$W_A = \frac{a_A X_A}{a_A X_A + a_B X_B}.$$

$$W_B = \frac{a_B X_B}{a_A X_A + a_B X_B}.$$

3.5

	wt% Cd	wt% Zn
Cadmium–zinc alloy	40	60
Zinc-rich phase	0.1	99.9
Cadmium-rich phase	99.2	0.8

- 3.6 Two phases: liquid and solid. Although they have the same chemical composition, they differ in *physical* properties.
 3.7 Three phases: pure A, pure B, and pure C.
 3.8 (a) 1.
 (b) 2.
 (c) 1.
 (d) 2.
 3.9 (a) 2.
 (b) 63%, 37%.
 (c) 95%, 5%.
 (d) 0%, 100%.
 3.10 (a) 50%, 50%, 300 °C.
 (Figure 3.18)
 (b) Liquid; 1.
 (c) Liquid plus lead-rich solid; 2.
 (d) 240 °C, 183 °C.
 At point 2: liquid plus solid (Pb).
 At point 3: two solids, (Sn) and (Pb).
 (e) $X_{\text{Pb}} = 80\%$, $T = 200$ °C.
 1 phase.

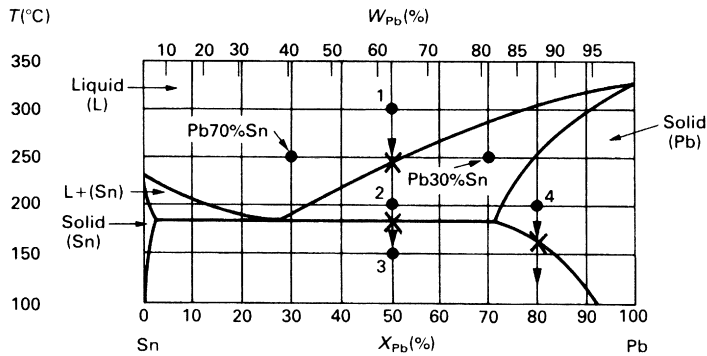


FIGURE 3.18

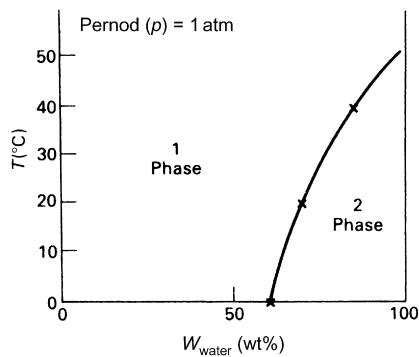


FIGURE 3.19

Lead-rich solid.

155 °C.

Two phases: lead-rich solid (Pb) and tin-rich solid (Sn).

3.11 Yes (see definition, on p. 34).

3.12 (Figure 3.19)

3.13 (a) 3.

(b) Not at all.

(c) Yes (see example of Dural on p. 37).

(d) The lead–tin alloy system.

3.14 Crystalline solid, liquid, and vapor.

3.15 It increases.

3.16 (Figure 3.20)

3.17 (Figure 3.21).

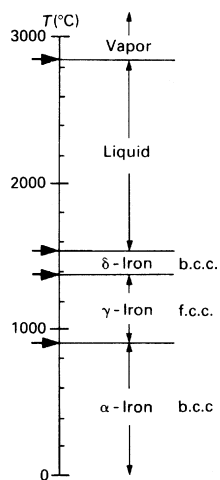


FIGURE 3.20

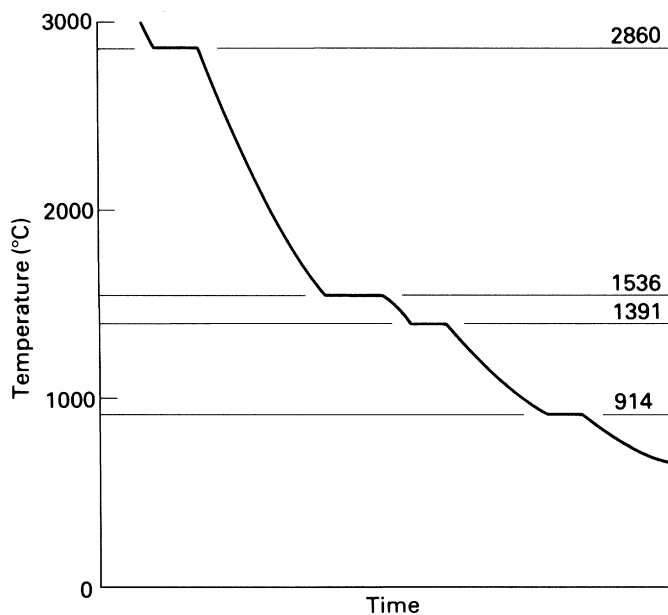


FIGURE 3.21

- 3.18 (a) Tin-rich solid plus lead-rich solid.
 (b) Liquid plus tin-rich solid.
 (c) Lead-rich solid only.
 (d) Liquid only.

- 3.19** (a) Liquid plus lead-rich solid between 1 and 2.
 (b) Lead-rich solid between 2 and 3.
 (c) Lead-rich solid plus tin-rich solid below 3 (Figure 3.22).
- 3.20** Ice VI at the core, ice II nearer the surface, ice I at the surface, possibly a thin shell of ice V between ice II and ice VI.
- 3.21** (a) Liquid plus lead-rich solid at 250 °C
 $X_{\text{Pb}} = 53\%$ in the liquid
 $X_{\text{Pb}} = 79\%$ in the solid.
 (b) Liquid plus lead-rich solid at 200 °C
 $X_{\text{Pb}} = 33\%$ in the liquid
 $X_{\text{Pb}} = 73\%$ in the solid.
 (c) Tin-rich solid plus lead-rich solid at 150 °C
 $X_{\text{Pb}} = 1\%$ in the tin-rich solid
 $X_{\text{Pb}} = 83\%$ in the lead-rich solid.
 (d) (Figure 3.23)

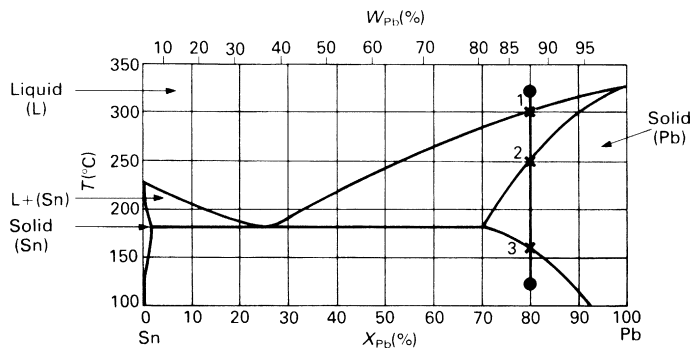


FIGURE 3.22

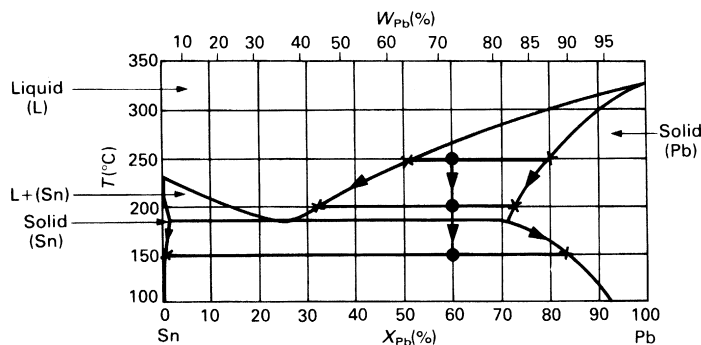


FIGURE 3.23

The compositions of the phases can change provided that their relative proportions change so as to lead to the same overall alloy composition. In practice, changes in phase composition occur by diffusion.

3.22 (a) Liquid.

(b) Solid.

Figure 3.24.

3.23 (a) 2.

(b) $W_{\text{Pb}} = 2\%$, $W_{\text{Pb}} = 90\%$.

(c) The lead-rich solid.

(d) Tin-rich solid 11% of total weight.

Lead-rich solid 89% of total weight (see Figure 3.24).

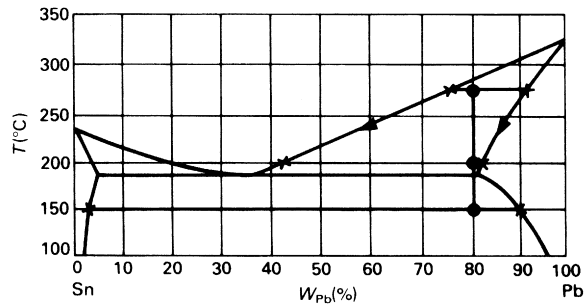


FIGURE 3.24

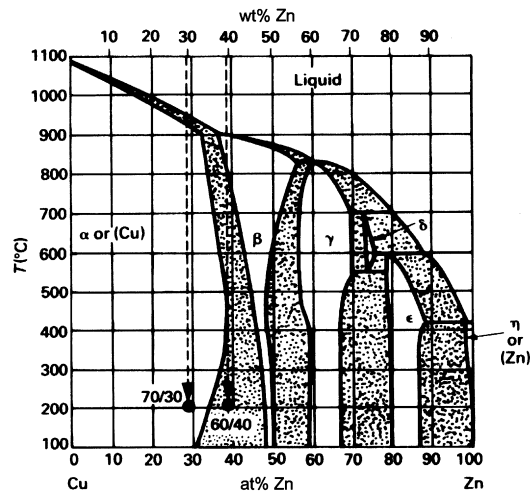


FIGURE 3.25

- 3.24** (a) $C = 2$.
 (b) Intensive variables p , T , X_B , or X_A .
 (c) 2.
 (d) 3.
 (e) 2.
 (f) 1.
 (g) 2.
 (h) Only 1. The compositions of the phases are given by the ends of the tie lines so that T and X_B (or X_A) are dependent on one another.
- 3.25** (a) Figure 3.25.
 (b) 70/30 brass is single phase, but 60/40 brass is two phase.
 (c) 70/30 brass starts to melt at 920°C and is completely liquid at 950°C .
 60/40 brass starts to melt at 895°C and is completely liquid at 898°C .
 (d) At 200°C : α (copper-rich solid) and β (roughly CuZn).
 At 800°C : β .
 The α has dissolved in the β .

Phase Diagrams 2

4.1 EUTECTICS, EUTECTOIDS, AND PERITECTICS

Eutectics and eutectoids are important. They are common in engineering alloys and allow the production of special, strong, microstructures. Peritectics are less important. But you should know what they are and what they look like to avoid confusing them with other features of phase diagrams.

Eutectics

The Pb–Sn system has a *eutectic*. Look at the Pb–Sn phase diagram (Figure 4.1). Above 327 °C, liquid lead and liquid tin are *completely miscible*, that is, the one dissolves in the other completely. On cooling, solid first starts to appear when the lines (or boundaries) which limit the bottom of the liquid field are reached.

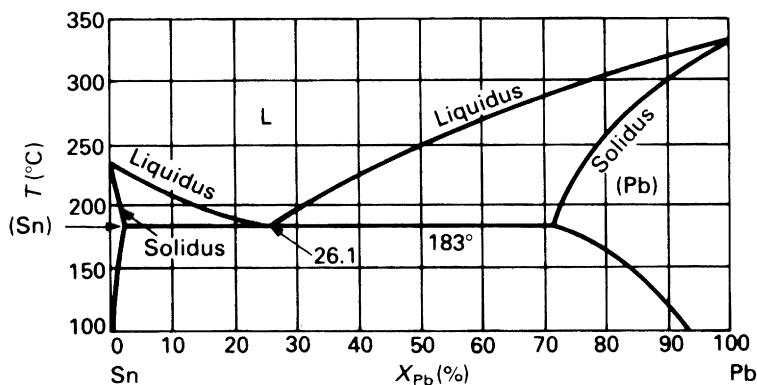


FIGURE 4.1

DEF.

The phase boundary which limits the bottom of the liquid field is called the *liquidus line*. The other boundary of the two-phase liquid–solid field is called the *solidus line*.

The liquidus lines start from the melting points of the pure components. Almost always, alloying lowers the melting point, so the liquidus lines *descend* from the melting points of the pure components, forming a shallow V.

DEF.

The bottom point of the V formed by two liquidus lines is the *eutectic point*.

In the lead–tin system, it is the point $X_{\text{Pb}} = 26.1 \text{ wt\%}$, $T = 183 \text{ }^\circ\text{C}$.

Most alloy systems are more complicated than the lead–tin system and show *intermediate phases*: compounds which form between components, like CuAl_2 or Al_3Ni or Fe_3C . Their melting points are, usually, lowered by alloying also, so eutectics can form between CuAl_2 and Al (for example) or between Al_3Ni and Al. The eutectic point is always the apex of the more or less shallow V formed by the liquidus lines.

Figure 4.2 shows the unusual silver–strontium phase diagram. It has four intermetallic compounds. Note that it is just five simple phase diagrams, like the Pb–Sn diagram, stuck together. The first is the Ag– SrAg_5 diagram, the second is the SrAg_5 – Sr_3Ag_5 diagram, and so on. Each has a eutectic. You can always dissect complicated diagrams in this way.

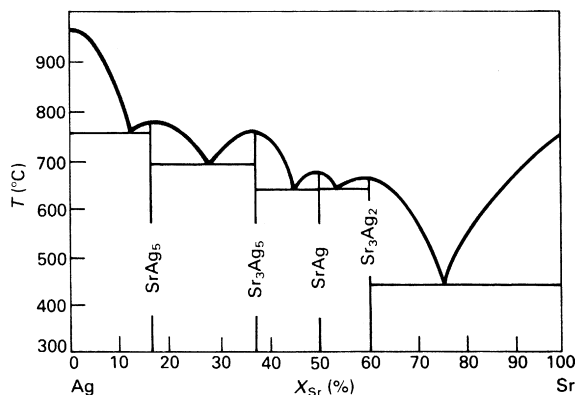


FIGURE 4.2

EXAMPLE

- 4.1** The three-phase diagrams, or parts of diagrams, shown in Figure 4.3, all have a eutectic point. Mark the point with an arrow and list the eutectic temperature and composition in wt% (the coordinates of the point).

Phase reactions

When an alloy is cooled, the constitution point for the alloy drops vertically on the phase diagram. In a single-phase field, the composition of the phase is, of course, that of the alloy. In a two-phase region, the compositions of the two phases are related by the tie line through the constitution point (p. 50: check it if you've forgotten); the phase compositions are given by the

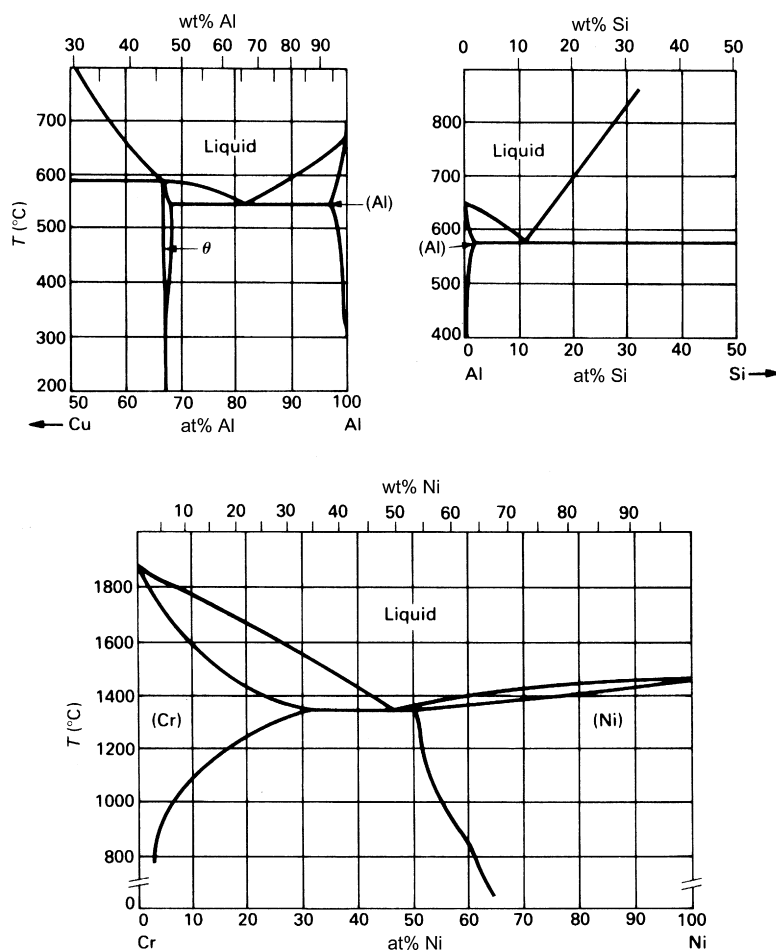


FIGURE 4.3

two ends of the tie line. These do *not* (in general) fall vertically; instead, they run along the phase boundaries. The compositions of the two phases then change with temperature.

DEF.

When the compositions of the phases change with temperature, we say that a *phase reaction* takes place.

Cooling *without* a phase reaction occurs:

- (a) in a single-phase field,
- (b) when both phase boundaries on either side of the constitution point are vertical.

Cooling *with* a phase reaction occurs when the constitution point lies in a two-phase region and at least one of the phase boundaries is not vertical.

Figure 4.4 shows the cooling of a lead–tin alloy with $X_{\text{Pb}} = 80\%$. On cooling from 350°C , the following regimes appear.

1. From 350 to 305°C . Single-phase liquid; no phase reaction.
2. From 305 to 255°C . The liquidus line is reached at 305°C ; the reaction liquid \rightarrow solid (Pb-rich solid solution) starts. The solid contains less tin than the liquid (see first tie line), so the liquid becomes richer in tin and the composition of the liquid moves down the liquidus line as shown by the arrow. The composition of the solid in equilibrium with this liquid also changes, becoming richer in tin also, as shown by the arrow on the solidus line: a *phase reaction* is taking place. The *proportion* of liquid changes from 100% (first tie line) to 0% (second tie line).
3. From 255 to 160°C . Single-phase solid with composition identical to that of the alloy. No phase reaction.

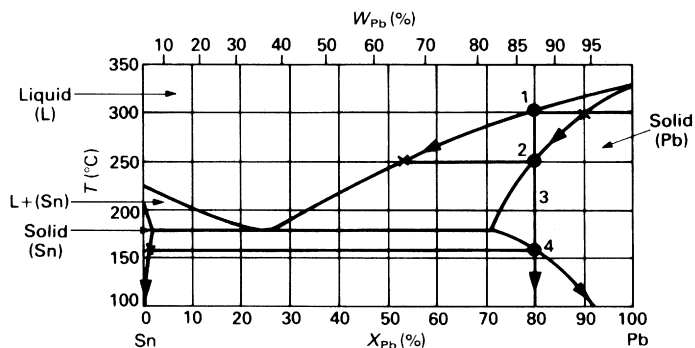


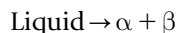
FIGURE 4.4

4. From 160 °C to room temperature. The lead-rich phase becomes unstable when the phase boundary at 160 °C is crossed. It breaks down into *two solid phases*, with compositions given by the ends of the tie line through point 4. On further cooling, the composition of the two solid phases changes as shown by the arrows: each dissolves less of the other. A phase reaction takes place. The *proportion* of each phase is given by the lever rule. The *compositions* of each are read directly from the diagram (the ends of the tie lines).

The eutectic reaction

Consider now the cooling of an alloy with 50 at% lead. Starting from 300 °C, the regions are shown in Figure 4.5.

1. From 300 to 245 °C. Single-phase liquid; no phase reactions.
2. From 245 to 183 °C. The liquidus is reached at 245 °C, and solid (a lead-rich solid solution) first appears. The composition of the liquid moves along the liquidus line, that of the solid along the solidus line. This regime ends when the temperature reaches 183 °C. Note that the alloy composition in *weight %* (64) is roughly half-way between that of the solid (81 wt%) and liquid (38 wt%), so the alloy is about half liquid, half solid, by weight.
3. At 183 °C. The liquid composition has reached the *eutectic point* (the bottom of the V). This is the lowest temperature at which liquid is stable. At this temperature all the remaining liquid transforms to two solid phases: a tin-rich α phase, composition $X_{\text{Pb}} = 1.45\%$ and a lead-rich β phase, composition $X_{\text{Pb}} = 71\%$. This reaction:



at constant temperature is called a *eutectic reaction*.

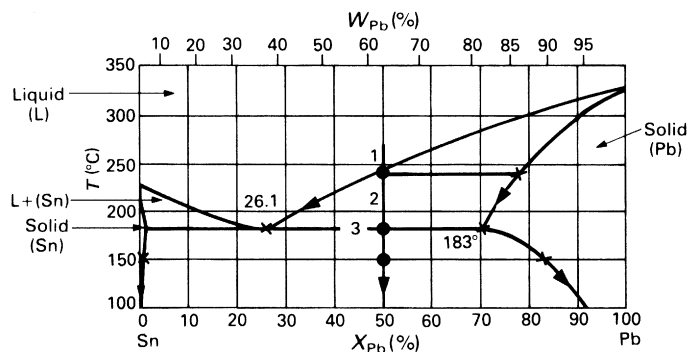


FIGURE 4.5

DEF.

A *eutectic reaction* is a three-phase reaction, by which, on cooling, a liquid transforms into two solid phases at the same time. It is a phase reaction, of course, but a special one. If the bottom of a liquid-phase field closes with a V, the bottom of the V is a eutectic point.

At the eutectic point, the three phases are in equilibrium. The compositions of the two new phases are given by the ends of the line through the eutectic point.

4. From 183 °C to room temperature. In this two-phase region, the compositions and proportions of the two solid phases are given by constructing the tie line and applying the lever rule, as illustrated. The compositions of the two phases change, following the phase boundaries, as the temperature decreases, that is, a further phase reaction takes place.

EXAMPLES

- 4.2 Check, using the phase rule, that three phases can coexist only at a point (the eutectic point) in the lead–tin system at constant pressure. If you have trouble, revise the Phase Rule on p. 54.
- 4.3 Not all alloys in the lead–tin system show a eutectic: pure lead, for example, does not. Examine the Pb–Sn phase diagram and list the composition range for which a eutectic reaction is possible.
- 4.4 We defined a eutectic reaction (e.g., that of the lead–tin system) as a three-phase reaction by which, on cooling, a liquid transforms into two solids. In general:



What happens on heating?

Eutectic structure

The aluminum *casting alloys* are mostly based on the Al–Si system (phase diagram Figure 4.6). It is a classic eutectic system with a eutectic point at about 11% Si and 577 °C. Consider the cooling of a Al–6% Si casting alloy. The liquidus is reached at about 635 °C, when solid (Al) starts to separate out (top of Figure 4.7). As the temperature falls further, the liquid composition moves along the liquidus line, and the amount of solid (Al) increases. When the eutectic temperature (577 °C) is reached, about half the liquid has solidified (middle of Figure 4.7). The solid that appears in this way is called *primary solid*, primary (Al) in this case.

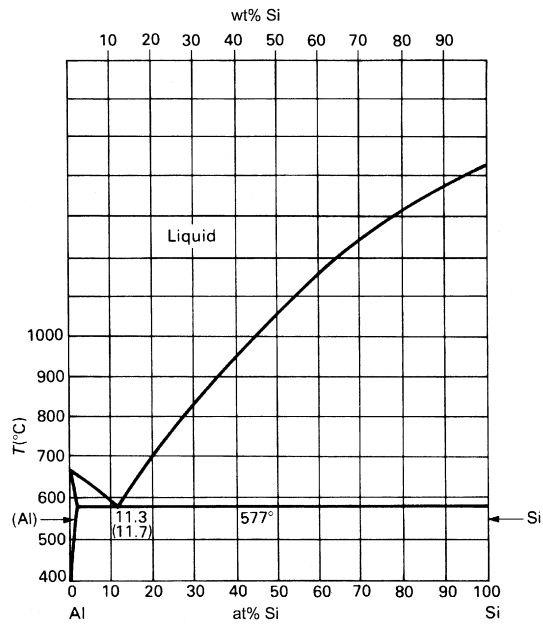


FIGURE 4.6

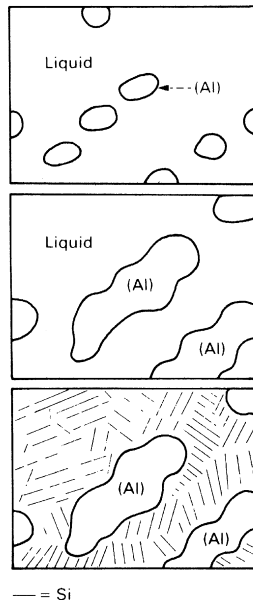


FIGURE 4.7

At 577 °C, the eutectic reaction takes place: the liquid decomposes into solid (Al) mixed with solid Si but on a finer scale than before (bottom of Figure 4.7). This intimate mixture of *secondary* (Al) with *secondary* Si is the eutectic structure.

On further cooling to room temperature, the composition of the (Al) changes—it dissolves less silicon at the lower temperature. So silicon must diffuse out of the (Al), and the amount of Si must increase a little. But the final structure still looks like the bottom of Figure 4.7.

Dendrites

When a metal is cast, heat is conducted out of it through the walls of the mold. The mold walls are the coldest part of the system, so solidification starts there. In the Al–Si casting alloy, for example, primary (Al) crystals form on the mold wall and grow inward. Their composition differs from that of the liquid: it is purer and contains less silicon. This means that silicon is *rejected* at the surface of the growing crystals, and the liquid grows richer in silicon: that is why the liquid composition moves along the liquidus line.

The rejected silicon accumulates in a layer just ahead of the growing crystals, and *lowers* the melting point of the liquid there. That slows down the solidification, because more heat has to be removed to get the liquid in this layer to freeze. But suppose a protrusion or bump on the solid (Al) pokes through the layer (Figure 4.8), it finds itself in liquid which is *not* enriched with silicon and *can* solidify. So the bump, if it forms, is unstable and grows rapidly. Then the (Al) will grow, not as a sphere, but in a branched shape called a *dendrite*. Many alloys show *primary dendrites* (Figure 4.9); and the eutectic, if it forms, fills in the gaps between the branches.

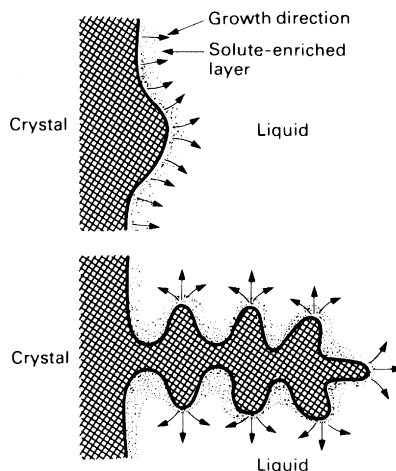


FIGURE 4.8

Segregation

If an 80 at% Pb alloy is cooled, the first solid appears at 305 °C and is primary (Pb) with a composition of about 90% Pb (Figure 4.10). From 305 to 255 °C the amount of primary (Pb) increases, and its composition, which (at equilibrium) follows the solidus line, changes: it becomes richer in tin. This means that lead must diffuse *out* of the solid (Pb), and tin must diffuse *in*.

This diffusion takes time. If cooling is slow, time is available and equilibrium is maintained. But if cooling is rapid, there is insufficient time for diffusion, and, although the new primary (Pb), on the outside of the solid, has the proper composition, the inside (which solidified first) does not. The inside is purer than the outside; there is a *composition gradient* in each

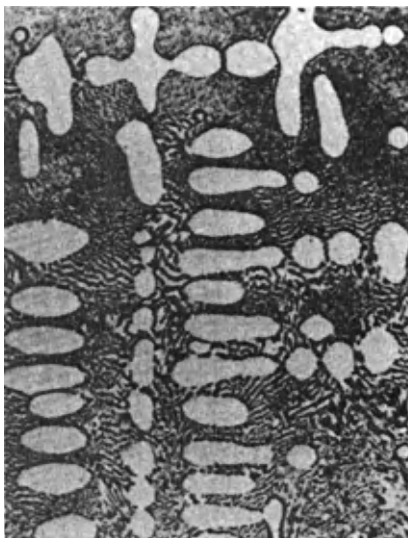


FIGURE 4.9
Dendrites of silver in a copper—silver eutectic matrix, $\times 280$.

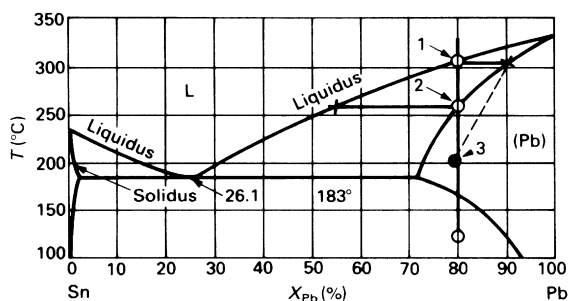


FIGURE 4.10

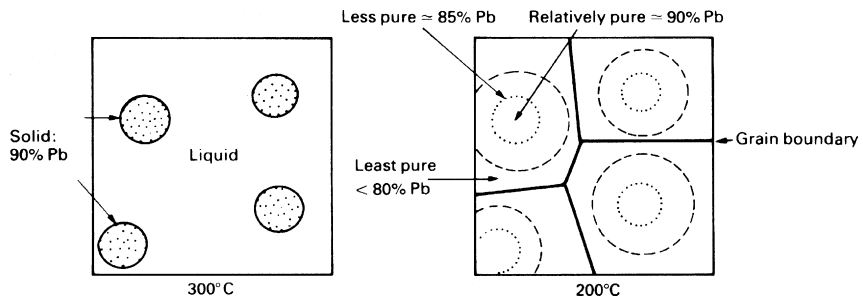


FIGURE 4.11

(Pb) grain, from the middle to the outside. This gradient is called *segregation* and is found in almost all alloys (Figure 4.11).

The phase diagram describes the equilibrium constitution of the alloy—the one given by very slow cooling. In the last example, all the liquid should have solidified at the point marked 2 on Figure 4.10, when all the solid has moved to the composition $X_{\text{Pb}} = 80\%$ and the temperature is 255°C . Rapid cooling prevents this; the solid has not had time to move to a composition $X_{\text{Pb}} = 80\%$. Instead, it has an average composition about half-way between that of the first solid to appear ($X_{\text{Pb}} = 90\%$) and the last ($X_{\text{Pb}} = 80\%$), that is, an average composition of about $X_{\text{Pb}} = 85\%$. This “rapid cooling” solidus lies to the right of the “equilibrium” solidus; it is shown as a broken line on Figure 4.10. If this is so, the alloy is *not* all solid at 260°C . The rule for calculating the amounts of each phase still applies, using the “rapid cooling” solidus as one end of the tie line: it shows that the alloy is completely solid only when point 3 is reached. Because of this, the liquid composition overshoots the point marked X and may even reach the eutectic point—so eutectic may appear in a rapidly cooled alloy even though the equilibrium phase diagram says it shouldn’t.

Eutectoids

Figure 4.12 shows the iron–carbon phase diagram up to 6.7 wt% carbon (to the first intermetallic compound, Fe_3C). Of all the phase diagrams you, as an engineer, will encounter, this is the most important. So much so that you simply have to learn the names of the phases, and the approximate regimes of composition and temperature they occupy. The phases are:

Ferrite: α (b.c.c) iron with up to 0.035 wt% C dissolved in solid solution.

Austenite: γ (f.c.c.) iron with up to 1.7 wt% C dissolved in solid solution.

δ -iron: δ (b.c.c) with up to 0.08 wt% C dissolved in solid solution.

Cementite: Fe_3C , a compound, at the right of the diagram.

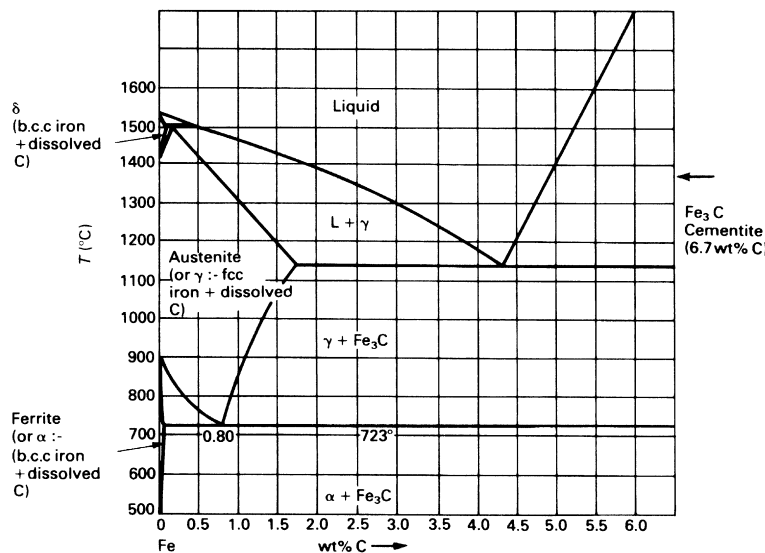
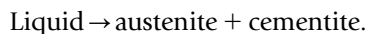


FIGURE 4.12

Ferrite (or α) is the low-temperature form of iron. On heating, it changes to austenite (or γ) at 914 °C when it is pure, and this form remains stable until it reaches 1391 °C when it changes to δ -iron (if you have forgotten this, check back to p. 18). The phase diagram shows that carbon changes the temperatures of these transitions, stabilizing γ over a wider temperature interval.

The iron–carbon system has a eutectic: find it and mark it on the diagram (Figure 4.12). At the eutectic point, the phase reaction, on cooling, is



But the diagram shows another feature which looks like a eutectic: it is the V at the bottom of the austenite field. The transformation which occurs there is very like the eutectic transformation, but this time it is a *solid*, austenite, which transforms on cooling to two other solids. The point at the base of the V is called a *eutectoid point*.

DEF.

A *eutectoid reaction* is a three-phase reaction by which, on cooling, a solid transforms into two other solid phases at the same time. If the bottom of a single-phase solid field closes (and provided the adjacent two-phase fields are solid also), it does so with a eutectoid point.

The compositions of the two new phases are given by the ends of the tie line through the eutectoid point.

EXAMPLES

- 4.5** The copper–zinc system (which includes brasses) has one eutectoid reaction. Mark the eutectoid point on the phase diagram (Figure 4.13).
- 4.6** The copper–tin system (which includes *bronzes*) has four eutectoids (Figure 4.14). One is obvious; the other three take a little hunting for. Remember that, if the bottom of the single-phase field for a solid closes, then it does so with a eutectoid. Try to locate (and ring carefully) the four eutectoid points on the copper–tin phase diagram.

Eutectoid structures

Eutectoid structures are like eutectic structures but much finer in scale. The original solid decomposes into two others, both with compositions which differ from the original, and in the form (usually) of fine, parallel plates. To allow this, atoms of *B* must diffuse away from the A-rich plates and A atoms must diffuse in the opposite direction, as shown in Figure 4.15. Taking the eutectoid decomposition of iron as an example, carbon must diffuse to the carbon-rich Fe_3C plates and away from the (carbon-poor) α -plates, just ahead of the interface. The colony of plates then grows to the right, consuming the austenite (γ). The eutectoid structure in iron has a special name: it is called *pearlite* (because it has a pearly look). The micrograph (Figure 4.16) shows pearlite.

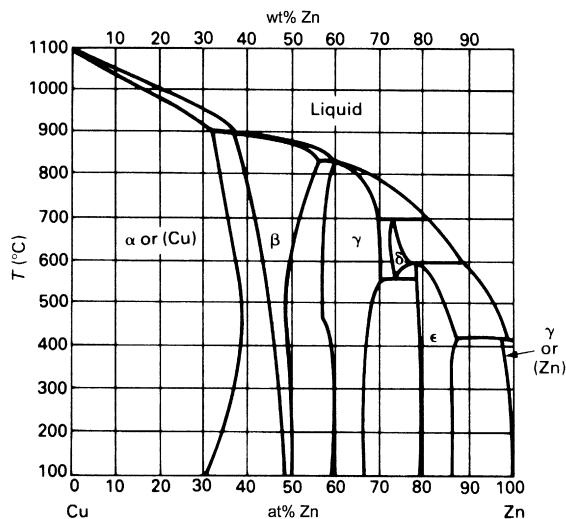


FIGURE 4.13

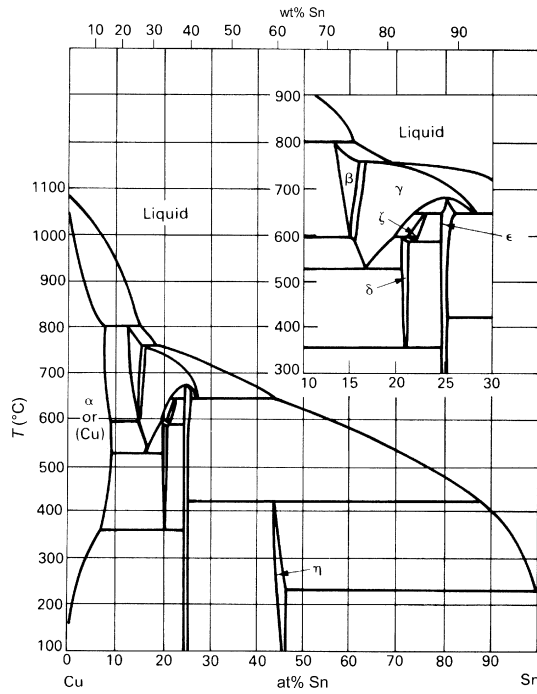


FIGURE 4.14

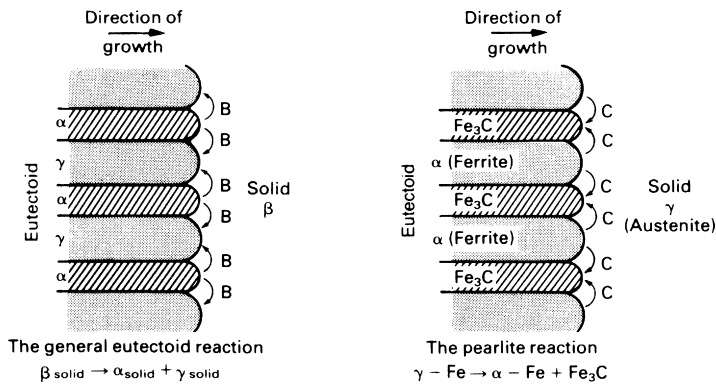
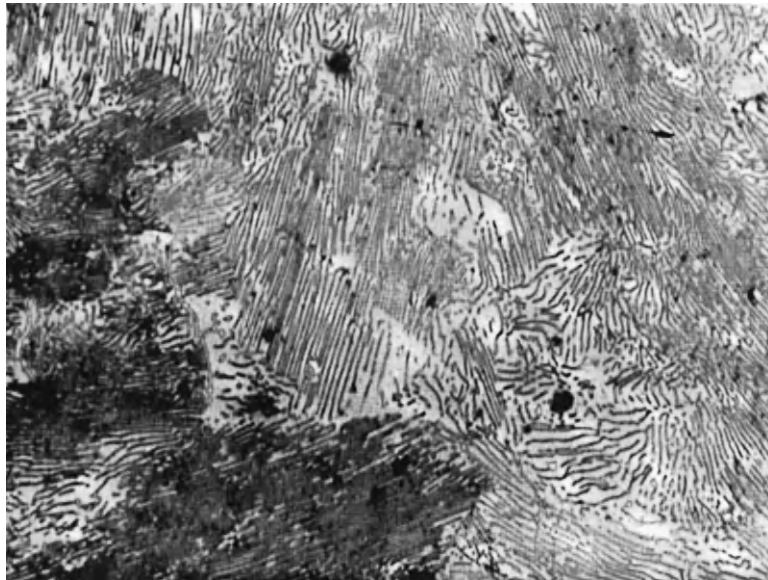
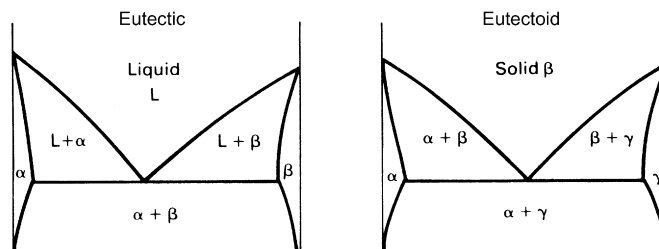


FIGURE 4.15

**FIGURE 4.16**

Pearlite in a eutectoid-composition plain-carbon steel, $\times 500$.

**FIGURE 4.17**

Peritectics

Eutectics and eutectoids are common features of engineering alloys. At their simplest, they look like a V resting on a horizontal line (Figure 4.17). The phase reactions, on cooling, are

Liquid $L \rightarrow \alpha + \beta$ (eutectic)

Solid $\beta \rightarrow \alpha + \gamma$ (eutectoid).

Many phase diagrams show another feature. It looks like an upside-down V (i.e., a \wedge) touching a horizontal line. It is a *peritectic reaction*, and the tip of the \wedge is a *peritectic point* (Figure 4.18).

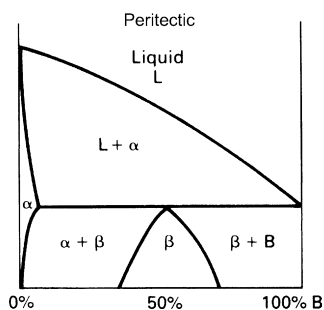
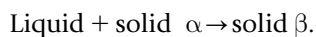


FIGURE 4.18

DEF.

A *peritectic reaction* is a three-phase reaction by which, on cooling, two phases (one of them liquid) react to give a single new solid phase.

On Figure 4.18, the peritectic reaction is



The composition of the β which forms (in this example) is 50 at% B.

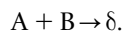
EXAMPLES

- 4.7 The iron–carbon diagram (Figure 4.12) has a peritectic point. Ring it on the diagram.
- 4.8 The copper–zinc system shown in Figure 4.13 has no fewer than five peritectic reactions. Locate them and ring the peritectic points. (Remember that when a single-phase field closes above at a point, the point is a peritectic point.)

Peritectoids**DEF.**

A *peritectoid* is a three-phase reaction by which, on cooling, two *solid* phases react to give a single new solid phase.

On Figure 4.19, the peritectoid reaction is



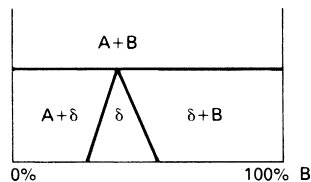


FIGURE 4.19

4.2 TEST EXAMPLES

This last section allows you to test your understanding of the use of phase diagrams.

EXAMPLES

- 4.9** When the temperature or pressure is decreased very rapidly, high-temperature or high-pressure phases can be “trapped,” and are observed at atmospheric temperature and pressure. (diamond, for instance, is a high-pressure form of carbon. It is only metastable at atmospheric pressure: the stable form is graphite.)

A roughly spherical meteorite of pure iron passes through the Earth’s atmosphere, causing surface heating, and impacts in the Mill pond creating a (uniform) pressure wave, and a certain amount of consternation. The meteorite is recovered and sectioned. It shows signs of having melted externally and of having had an outer shell of γ -iron, an inner shell of ϵ -iron, and a core of α -iron. Use the p – T phase diagram for iron to deduce the approximate magnitude of the pressure wave. Express the result in atmospheres (Figure 4.20).

- 4.10** Your ancient granny dies and leaves you her most prized possession: an urn of pure gold. One afternoon, while mixing paint remover in the urn, you are disturbed to note that it has turned an evil green in color. Whipping out your magnifying glass, you observe that the paint remover, in attacking the urn, has also etched it, clearly revealing the presence of two phases. This (of course) raises in your mind certain nagging doubts as to the purity of the gold. Your friend with an electron microprobe analyzer performs a quick chemical analysis for you, with the distressing result:

Copper	60 at%;
Zinc	40 at%;
Gold	< 0.001 at%;

Figure 4.21 shows the appropriate phase diagram. Assuming the urn to be at equilibrium (though Granny might not have been):

- (a) Mark the constitution point onto the diagram (assume that the constitution at room temperature is the same as at 200 °C).

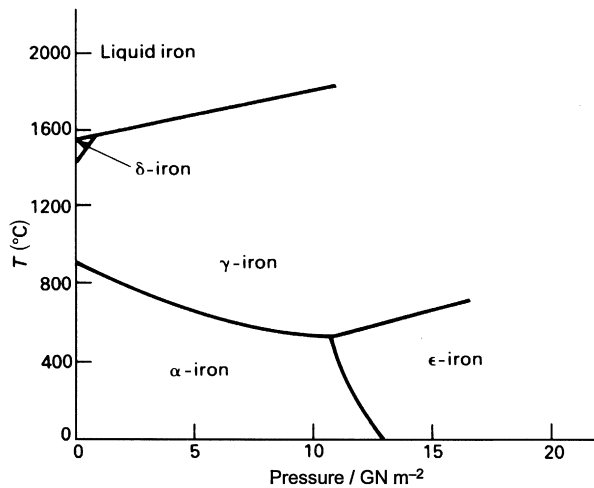


FIGURE 4.20

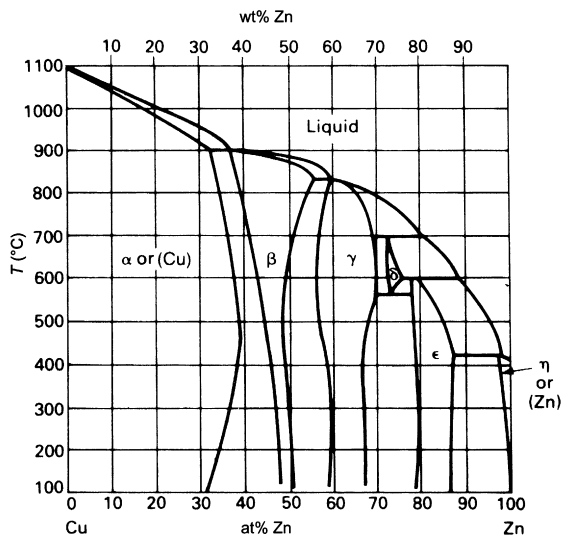


FIGURE 4.21

- (b) Is it in a single- or two-phase region? _____
- (c) What phase(s) are present? _____
- (d) List the approximate phase composition(s) _____
- (e) Calculate approximately the proportions of each phase _____

Well done! You have determined the constitution of granny's urn.

- 4.11** Figure 4.22 shows a system with *complete solid solubility*. How many phases are present in an alloy of 60 wt% Ni and 40 wt% Cu at:
- 1400 °C
 - 1300 °C
 - 1000 °C.
- 4.12** Figure 4.23 shows the Ti–Al phase diagram (important for the standard commercial alloy Ti–6% Al–4% V). It shows two *peritectic reactions*, at each of which liquid reacts with a solid phase to give an intermetallic compound.
- Ring the peritectics and give the (approximate) chemical formula for the two compounds.
 - Shade all two-phase fields.
 - At what temperature does a Ti–6 wt% Al alloy start to melt?
 - Over what temperature range does it change from the α (c.p.h.) to the β (b.c.c.) structure?
- 4.13** Figure 4.24 shows the aluminum–silicon system, basis of most aluminum casting alloys.
- What is the eutectic composition and temperature?
 - How many phases are present in an alloy of eutectic composition at 1000 °C and 400 °C?
 - Describe the solidification of an alloy of eutectic composition and the resulting structure.
 - Compare and contrast this with the formation of a eutectoid structure.
- 4.14** A hypothetical equilibrium diagram between two elements A and B shows the following features:
- A has three solid allotropic forms with change temperatures of 800 °C and 1150 °C and melts at 1980 °C. These form solid solutions α , β , and γ containing B, α being the low-temperature one.

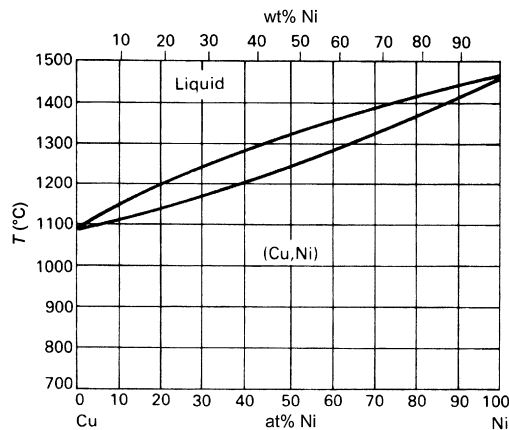


FIGURE 4.22

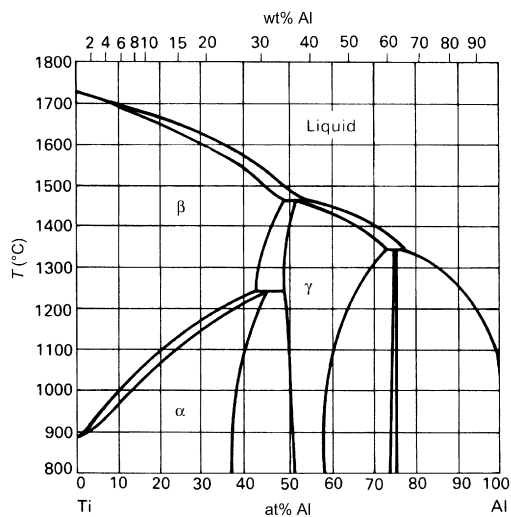


FIGURE 4.23

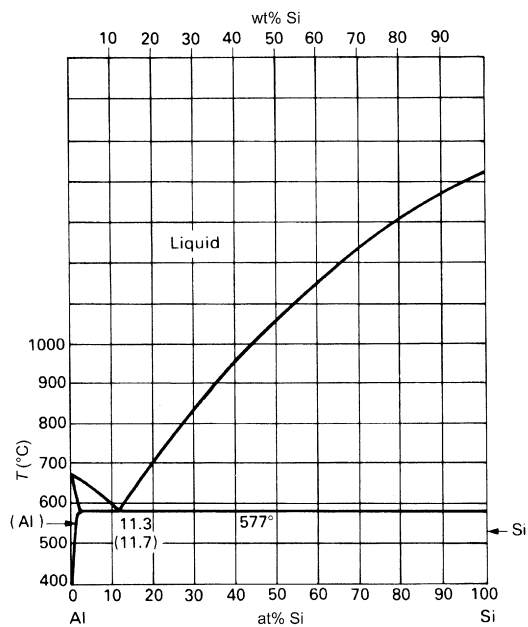


FIGURE 4.24

An intermediate compound A_2B_3 melts at 1230°C . It has a limited solid solubility for A forming solid solution ϵ and no solid solubility for B.

B melts at 800°C and has negligible solid solubility for A.

Eutectic reactions:

at 1000°C , liquid (55% B) $\rightarrow \beta$ (25% B) + ϵ (60% B)

at 650°C , liquid (90% B) $\rightarrow A_2B_3 + B$.

Peritectic reaction at 1300°C :

γ (8% B) + liquid (35% B) $\rightarrow \beta$ (15% B).

Eutectoid reaction at 600°C :

β (12% B) $\rightarrow \alpha$ (5% B) + ϵ (65% B).

Peritectoid reaction at 300°C :

α (3% B) + ϵ (69% B) $\rightarrow \delta$ (40% B).

At 0°C the solubilities of B in A and A in A_2B_3 are negligible and the δ phase extends from 35% to 45% B.

All percentages given are by weight. The atomic weight of B is twice that of A. Draw the equilibrium diagram assuming all phase boundaries are straight lines. For an alloy containing 30% B, describe the changes that occur as it is cooled from 1600 to 0°C . Give the proportions of phases present immediately above and immediately below each temperature at which a reaction occurs.

4.3 SOLUTIONS TO EXAMPLES

4.1 (See Figure 4.25) 550°C , 67%; 580°C , 11%; 1350°C , 49%.

4.2 The reduced (constant pressure) phase rule is

$$F = C - P + 1.$$

There are two components; the three phases (two solids and one liquid) coexist. So $F = 0$, that is, the three phases can coexist only at a point (the eutectic point).

4.3 From $X_{\text{Pb}} = 1.45\%$ to $X_{\text{Pb}} = 71\%$.

4.4 Remember that this is an *equilibrium* diagram. Any point on the diagram corresponds to a unique constitution. So, on heating, the reaction simply goes in reverse. The two solids “react” to give a single liquid. In general:

or, for the lead – tin system $\left. \begin{array}{l} \alpha + \beta \rightarrow \text{Liquid} \\ (\text{Pb}) + (\text{Sn}) \rightarrow \text{Liquid}(\text{Pb} - \text{Sn}) \end{array} \right\} \text{on heating}$

4.5 (Also 4.8) (Figure 4.26)

4.6 Eutectoids ringed with solid circles (Figure 4.27).

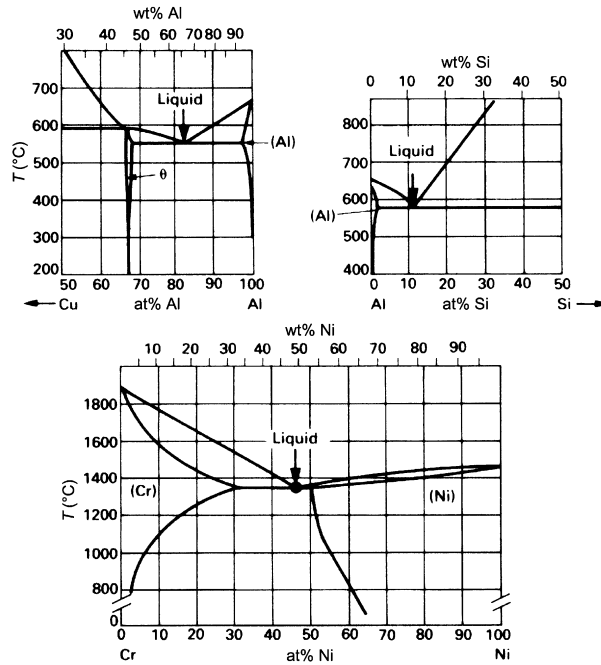


FIGURE 4.25

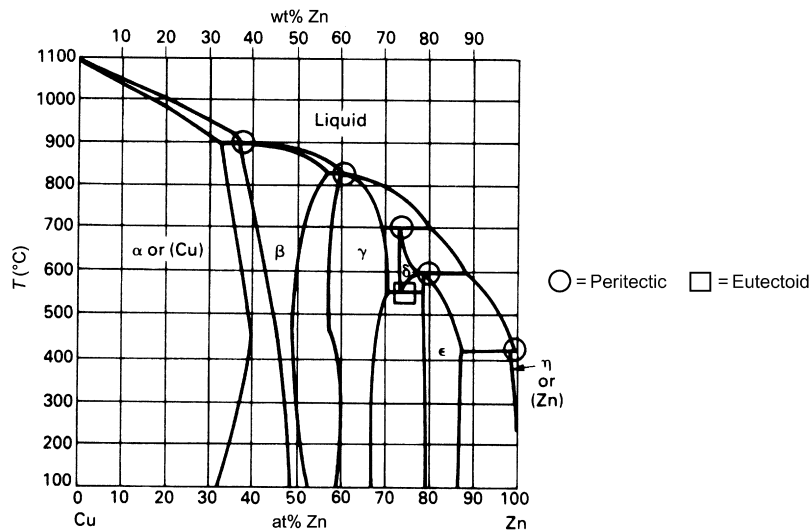


FIGURE 4.26

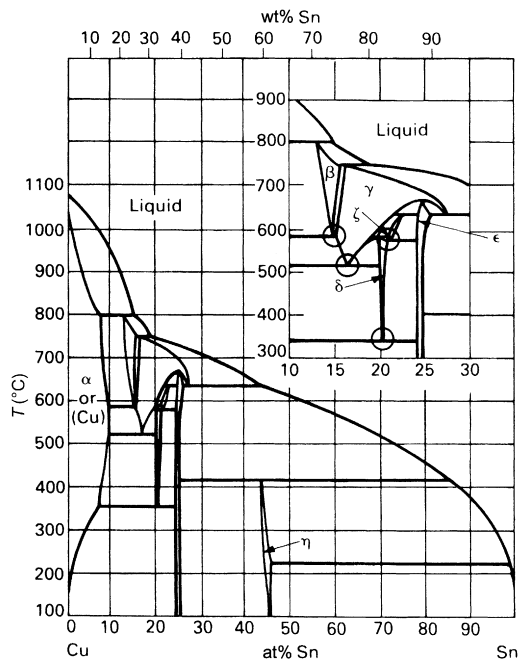


FIGURE 4.27

- 4.7 (See Figure 4.28)
- 4.8 (See Figure 4.26)
- 4.9 Between about 11.5 and 13.0 GN m⁻² or $1.14 \times 10^5 - 1.28 \times 10^5$ atm.
- 4.10 (a) See Figure 4.29.
- (b) Two-phase region.
- (c) α (copper-rich solid) and β (the compound Cu₃Sn).
- (d) $W_{\text{Zn}} \approx 33\%$, $W_{\text{Zn}} \approx 48\%$.
- (e) Very roughly, 50–50; more precisely:

$$\frac{\text{wt\% of } \alpha}{\text{wt\% of } \beta} = \frac{48 - 40}{40 - 33} = \frac{8}{7}.$$

- 4.11 (a) 1.
- (b) 2.
- (c) 1.
- 4.12 (a) AlTi, Al₃Ti.
- (b) See Figure 4.30.
- (c) 1680 °C.
- (d) 980–1010 °C.

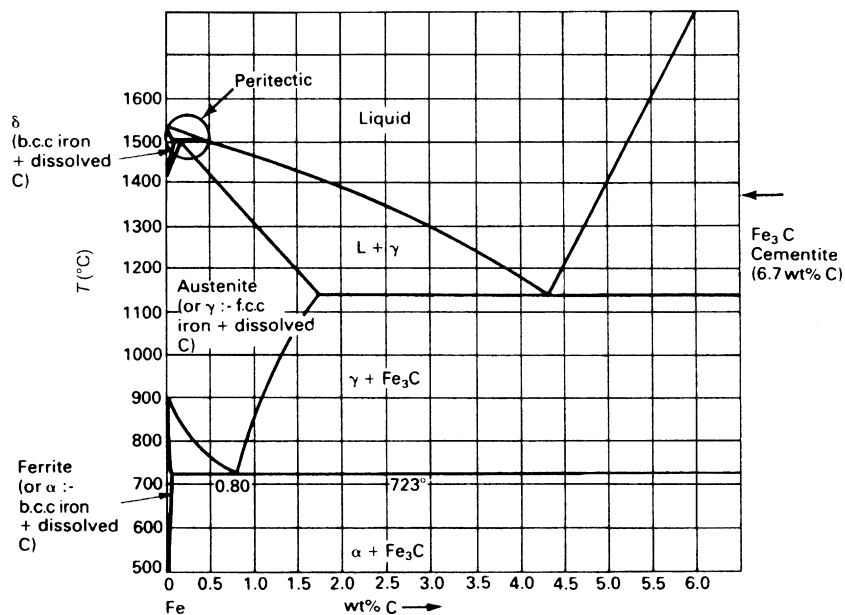


FIGURE 4.28

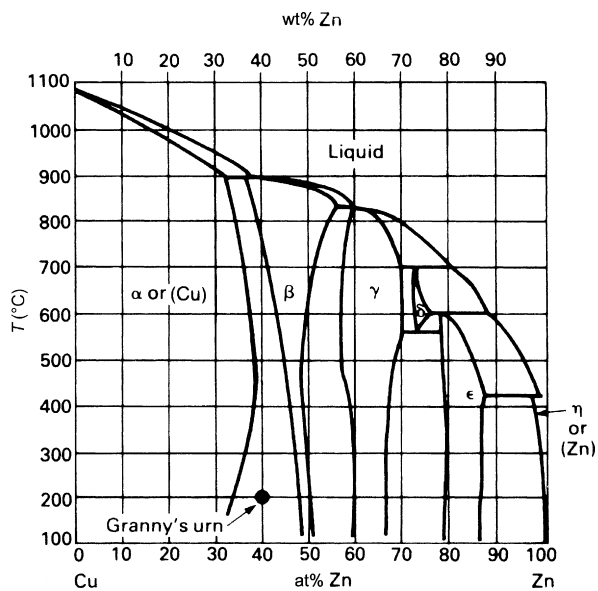


FIGURE 4.29

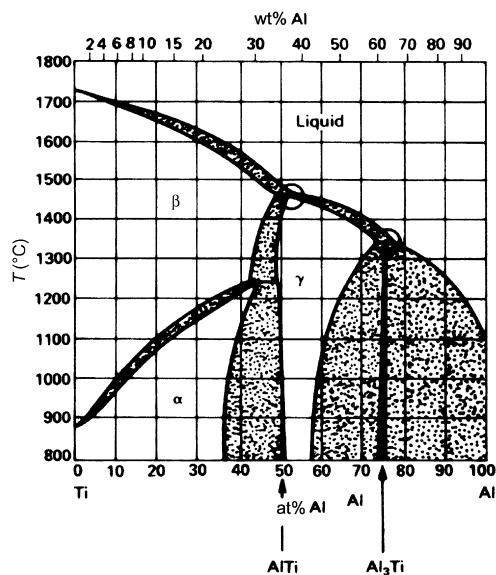


FIGURE 4.30

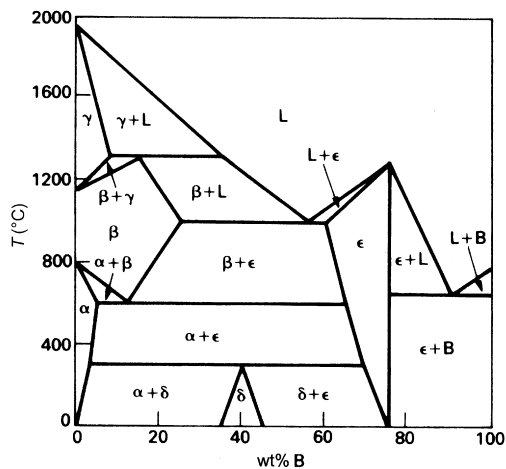


FIGURE 4.31

- 4.13** (a) 11.7 wt% Si, 577 $^{\circ}\text{C}$.
 (b) One phase at 1000 $^{\circ}\text{C}$, two phases at 400 $^{\circ}\text{C}$.
 (c) See pp. 68–70.
 (d) Eutectoid structure produced by the decomposition of a solid phase not a liquid.

4.14 A_2B_3 contains $3 \times 2 / (2 \times 1 + 3 \times 2) = 75\%$ B by weight. Hence, equilibrium diagram is as given in Figure 4.31. On cooling, 30% B mixture from 1600 °C: at 1397 °C, solidification commences by separation of γ crystals. Just above 1300 °C 22/27 (=81.5%) liquid (35% B) + 5/27 (=18.5%) γ (8% B). At 1300 °C, all γ + some liquid form β in peritectic reaction. Just below 1300 °C 15/20 (=75%) liquid (35% B) + 5/20 (=25%) β (15% B). 1300 °C \rightarrow 1000 °C, more β separates. Just above 1000 °C 5/30 (=17%) liquid (55% B) + 25/30 (=83%) β (25% B). At 1000 °C all liquid forms β and ϵ in eutectic reaction. Just below 1000 °C 5/35 (=14.3%) ϵ (60% B) + 30/35 (=85.7%) β (25% B). 1000 °C \rightarrow 600 °C, β precipitates ϵ and ϵ precipitates β . Just above 600 °C 18/53 (=34%) ϵ (65% B) + 35/53 (=66%) β (12% B). At 600 °C all β forms α and ϵ in eutectoid reaction. Just below 600 °C 25/60 (=42%) ϵ (65% B) + 35/60 (=58%) α (5% B). 600 °C \rightarrow 300 °C, α precipitates ϵ and ϵ precipitates α . Just above 300 °C 27/66 (=41%) ϵ (69% B) + 39/66 (=59%) α (3% B). At 300 °C all ϵ and some α form δ in peritectoid reaction. Just below 300 °C 27/37 (=73%) δ (40% B) + 10/37 (=27%) α (3% B). 300 °C \rightarrow 0 °C, amount of α decreases and δ increases. At 0 °C 30/35 (=86%) δ (35% B) + 5/35 (=14%) α (0% B).

Case Studies in Phase Diagrams

5.1 INTRODUCTION

We now look at some practical examples of how phase diagrams are used. In the first, a typical design problem, we find out how solders are chosen for different uses. In the second, we look at the high-technology area of microchip fabrication and study the production, by zone refining, of ultrapure silicon. And lastly, for some lighthearted relief, we find out how bubble-free ice is made for upmarket cocktails.

5.2 CHOOSING SOFT SOLDERS

Most soft solders are based on the lead–tin system (Table 5.1). Soft solders are called “soft” because they are just that—soft mechanically and soft in the sense that they melt easily. Even so, thin soldered joints can be very strong in shear. And the “thermal” softness of the solder can be a positive advantage. A good example of this is in the soldering of electronic components—like transistors, resistors, or integrated circuits—into printed circuit boards. Because the components will be damaged if they get too hot, we want a solder with a low melting point. The phase diagram (Figure 5.1) shows at a glance that the alloy we want is tin + 38% lead. Now that you are familiar with phase diagrams, you will know that the three-phase horizontal where

$$L \rightleftharpoons \alpha + \beta$$

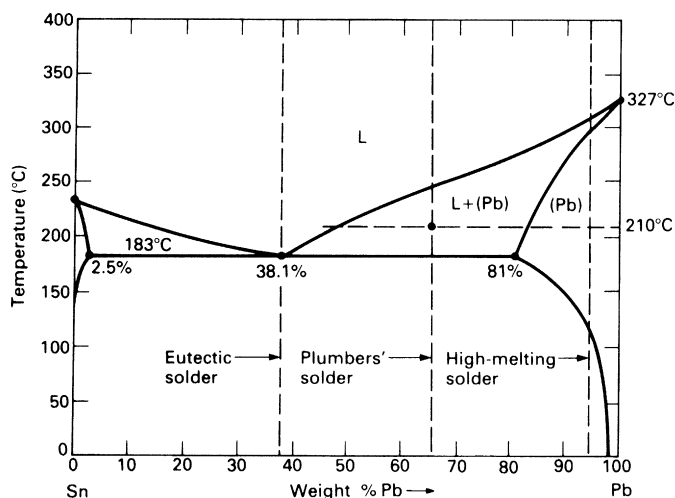
or, in our case,

$$L \rightleftharpoons (\text{Sn}) + (\text{Pb})$$

is called a *eutectic*, from the Greek for “easy melting.” And electronic solders are, appropriately enough, marketed under trade names like “Eutectic.” But eutectic solders have another property. They become completely molten as soon as they are heated up past 183 °C; and they flow nicely into the joints,

Table 5.1 Properties of Common Solders

Type	Composition (wt%)	Melting Range ($^{\circ}\text{C}$)	Typical Uses
Soft; eutectic (free flowing)	62 Sn + 38 Pb	183	Electronic assemblies
Soft; general purpose (moderately pasty)	50 Sn + 50 Pb	183–212	Joints in copper water systems; sheet metal work
Soft; plumbers (pasty)	35 Sn + 65 Pb	183–244	Wiped joints; car body filling
Soft; high melting (free flowing)	5 Sn + 1.5 Ag	296–301	Higher temperatures
	+ 93.5 Pb		
Silver; eutectic (free flowing)	42 Ag + 19 Cu	610–620	High-strength; high-temperature
	+ 16 Zn + 25 Cd		
Silver; general purpose (pasty)	38 Ag + 20 Cu	605–650	High-strength; high-temperature
	+ 22 Zn + 20 Cd		

**FIGURE 5.1**

The lead–tin phase diagram showing the compositions of the three main soft solders. The diagram tells us that, as soon as *eutectic solder* reaches 183 $^{\circ}\text{C}$, it melts completely and flows easily into joints. *Plumbers' solder*, on the other hand, has a *melting range*—although it starts to melt at 183 $^{\circ}\text{C}$ it doesn't become completely molten until it gets up to 244 $^{\circ}\text{C}$. At a middling temperature like 210 $^{\circ}\text{C}$, it is a half-solid–half-liquid paste. *High melting point soft solders* are nearly pure lead. They have a small melting range and, like eutectic solders, flow easily into joints.

leaving small tidy fillets of solder around each connection. You can imagine the number of faults that you could get on a crowded circuit board if the solder did *not* flow easily and had to be “put on with a trowel.”

There are times, however, when soft solder *is*—almost literally—put on with a trowel. Lead was widely used by the Romans for piping water; and it is only within the past 50 years that copper—and more recently polymers—have replaced lead as the major plumbing material. A vital part of the plumber’s craft was joining lengths of lead pipe together. This was done by bringing the ends of the pipes up to one another and gradually building a deposit of solder around the joint. The joint was “wiped” by hand with a moleskin pad as fresh solder was added, producing the very fine wiped joints as shown in [Figure 5.2](#).

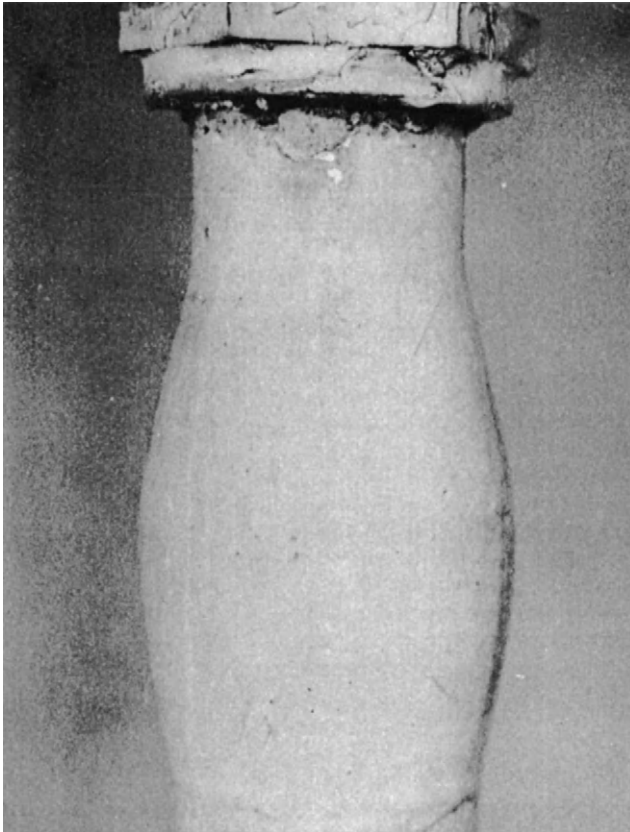


FIGURE 5.2

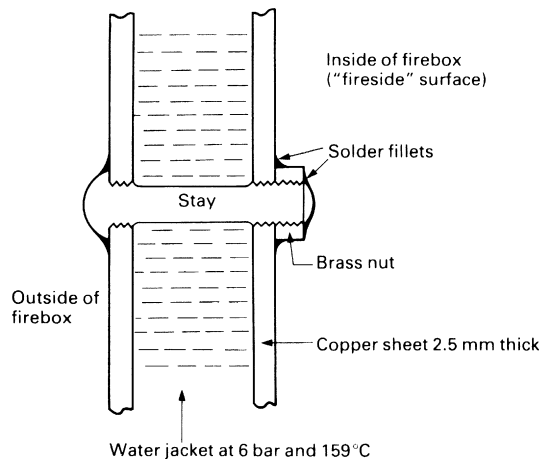
When we heat plumbers’ solder to about 210 °C and make it “pasty”, we can “wipe” it into elegantly curved shapes. Lead pipes have been joined in this way for centuries.

Eutectic solder would be useless for this purpose. It would either be fully molten and run all over the place or it would go solid and stick on the job in unsightly lumps. What is wanted is a *pasty* solder which can be gradually molded to the shape of the joint. If we look at an alloy of tin + 65% lead on the phase diagram, we can see that, at around 210 °C, the alloy will be a half-molten, half-solid slurry. This will work very nicely to shape without the temperature being too critical. And there is also little chance of melting the lead pipes by accident. So this is the sort of composition that plumbers' solders have (Table 5.1). Actually, lead–tin alloys with a freezing range like this (called “mushy freezers” in the foundry world) are still used quite widely for things like filling-in dents in car body panels and soldering car radiators together. But in many cases, they are used not so much because they are mushy freezers, but because they contain less tin than eutectic solders and are therefore cheaper.

One of the interesting things about the lead–tin diagram (Figure 5.1) is that all alloys containing between 2.5% and 81% of added lead *start* to melt at 183 °C even though some—as we have just seen—don't become completely molten until they are quite a bit hotter. This is obviously a problem when we want to use soft solders in hot surroundings, because they will rapidly lose their strength as they get near to 183 °C.

There is a nice illustration of this problem in the model steam engine that we looked at in the first case study in Chapter 1. If you look back, you will see that the most critical component in the engine is the copper boiler (Figure 1.1). The main parts of the boiler are soldered together with a “silver solder” which melts between 610 and 620 °C (Table 5.1). This is an extremely strong and ductile alloy which loses little of its structural strength at boiler operating temperatures. But the screwed stays that tie the flat fire-box sides together (Figures 1.3, 5.3) present a problem. To make them pressure tight, they need to be sealed with solder. Now, it is easy enough to silver solder the stays where they come out through the outside of the fire-box; but it is difficult to do this *inside* the firebox because the gas blow torches that we normally use for silver soldering copper will not burn properly in a confined space (an oxyacetylene torch will, but it has a very localized flame that can easily burn a hole in thin copper). Will soft solder—which of course melts much more easily than silver solder—be adequate for sealing stays inside the firebox?

Model boilers typically work at a gauge pressure of 6 bar. At this pressure, the temperature of the saturated water and steam in the boiler is 159 °C, only 24 °C below the temperature at which lead–tin solders start to melt. Worse, the inner surface of the firebox is hotter even than the water because it is next to the fire. In fact, ordinary soft solders have been used successfully

**FIGURE 5.3**

The flat plates that make up the firebox of a model steam boiler are tied together with screwed *stays*. To make the threads pressure tight, they must be sealed with solder.

for many years inside model fireboxes, probably because the copper is very good at conducting away the heat of the fire. But there is little room for variation—if you habitually run the boiler on hard scale-forming water or accidentally let the water level down too far when steaming hard or increase the boiler pressure and thus temperature to get better performance, you are likely to blow leaks big enough to put the fire out. The solution is to use the high melting point soft solder in Table 5.1 which is very close to being pure lead, and this is recommended by the leading designers of miniature steam engines.

5.3 PURE SILICON FOR MICROCHIPS

The semiconductor industry would have been impossible had not the process of *zone refining* been invented first. It is the standard way of producing ultrapure materials, both for research and for making silicon and germanium-based devices.

Zone refining works like this. We start with a bar of silicon containing a small uniform concentration C_0 of impurity (Figure 5.4(a)). A small tubular electric furnace is put over the left-hand end of the bar, and this is used to melt a short length (Figure 5.4(b)). Obviously, the concentration of impurity in this molten section must still be C_0 as no impurity has either left it or come into it. But before we can go any further, we must look at the phase diagram (Figure 5.5). To have equilibrium between the

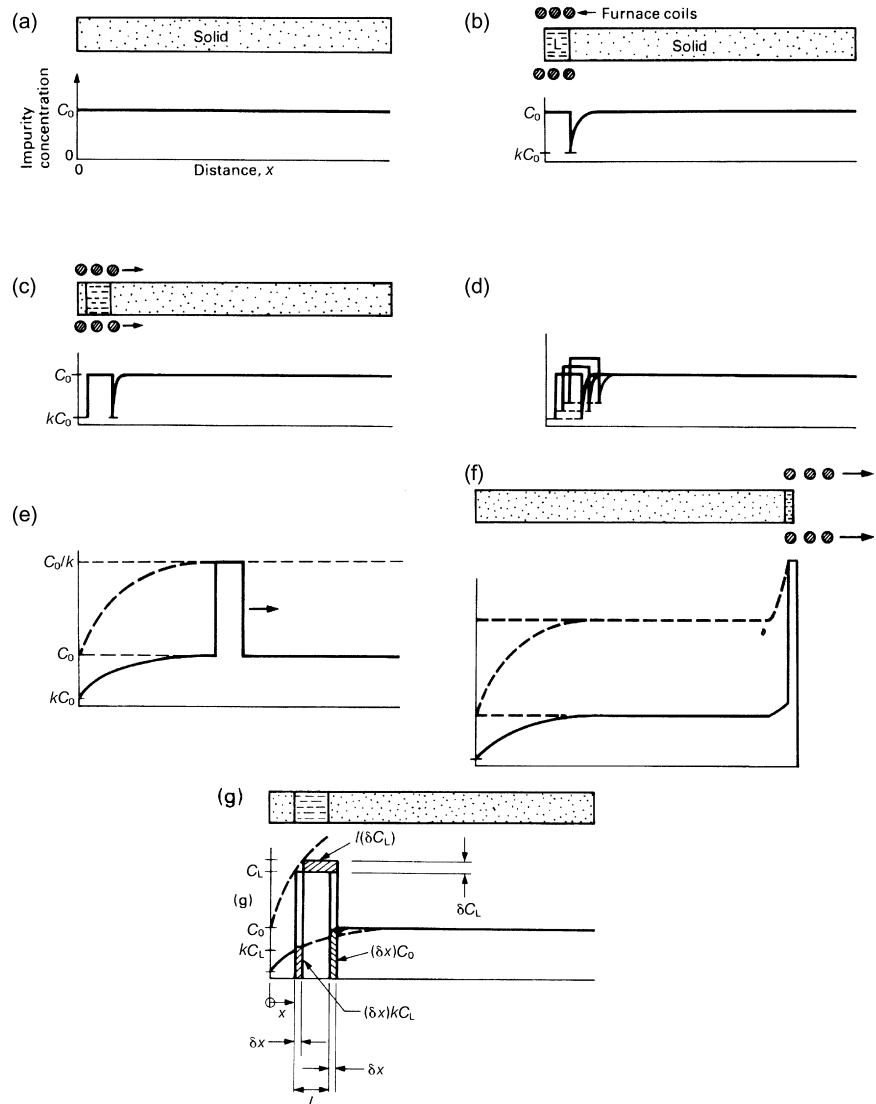
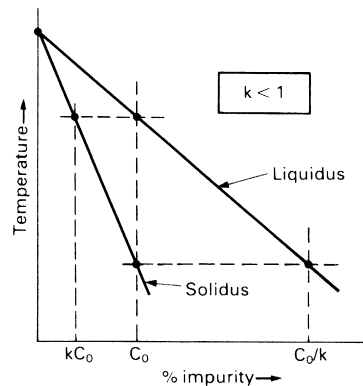


FIGURE 5.4

Stages in zone refining a bar of impure silicon: (a) we start with a bar that has a uniform concentration of impurity, C_0 . (b) The left-hand end of the bar is melted by a small electric tube furnace, making a liquid zone. The bar is encapsulated in a ceramic tube to stop the liquid running away. (c) The furnace is moved off to the right, pulling the zone with it. (d) As the zone moves, it takes in more impurity from the melted solid on the right than it leaves behind in the freshly frozen solid on the left. The surplus pushes up the concentration of impurity in the zone, which in turn pushes up the concentration of impurity in the next layer of solid frozen from it. (e) Eventually, we reach steady state, (f) when the zone gets to the end of the bar the concentrations in both solid and liquid increase rapidly. (g) How we set up Equation (5.1)?

**FIGURE 5.5**

Schematic of top left corner of the “silicon-impurity” phase diagram. To make things simple, we assume that the liquidus and solidus lines are straight. The impurity concentration in the solid is then always less than that in the liquid by the factor k (called the *distribution coefficient*).

new liquid of composition C_0 and the existing solid in the bar, the solid must be of composition kC_0 . And yet the solid already has a composition of C_0 , $(1/k)$ times too big. In fact, the situation is rescued because a *local* equilibrium forms between liquid and solid at the interface where they touch. The solid next to this interface loses a small amount of impurity into the liquid by diffusion, and this lowers the composition of the solid to kC_0 . Naturally, a gradient is produced in the composition of the solid (Figure 5.4(b)), but because solid-state diffusion is relatively sluggish, we can neglect the atomic flux that the gradient causes in the present situation.

The next stage in the zone-refining process is to move the furnace slowly and steadily to the right. The left-hand end of the bar will then cool and refreeze but with the equilibrium composition kC_0 (Figure 5.4(c)). As the furnace continues to move to the right, the freezing solid, because it contains much less impurity than the liquid, rejects the surplus impurity *into* the liquid zone. This has the effect of *increasing* the impurity concentration in the zone, which in turn then increases the impurity concentration in the next layer of freshly frozen solid, and so on (Figure 5.4(d)). Eventually, the concentrations ramp themselves up to the situation shown in Figure 5.4(e). Here, the solid ahead of the zone has exactly the same composition as the newly frozen solid behind the zone. This means that we have a *steady state* where as much impurity is removed *from* the zone in the form of freshly frozen solid as is taken *into* the zone by melting old solid ahead of it; the composition of the zone itself therefore stays constant.

The final stage takes place when the furnace runs up to the end of the bar (Figure 5.4(f)). The freshly frozen solid behind the zone continues to pump surplus impurity into an ever-shortening zone, and the compositions of the liquid and the solid frozen from it ramp themselves up again, eventually reaching in theory (but not in practice) infinite values.

Figure 5.4(f) shows what moving the molten zone along the bar has done to it: we have removed impurity from the left-hand end of the bar and dumped it at the right-hand end; that is, we have *zone refined* the left-hand part of the bar.

Because we need to know how long the refined section of the bar is, it is important to describe the ramping up of the compositions in a quantitative way. We can do this by writing a differential equation which describes what happens as the zone moves from some general position x to a new position $x + \delta x$ (Figure 5.4(g)). For a bar of unit cross section, we can write the mass conservation equation

$$\begin{array}{lll}
 (\delta x)C_0 & - & (\delta x)kC_L \\
 \text{impurity taken} & \text{impurity lost from} & \text{surplus impurity left in} \\
 \text{into zone by} & \text{zone in slice off} & \text{fixed-volume zone which} \\
 \text{melting slice of bar} & \text{freshly frozen solid} & \text{increases concentration of} \\
 \text{of thickness } \delta x & \text{of thickness } \delta x & \text{impurity in liquid by } \delta C_L
 \end{array} = l(\delta C_L).$$

(5.1)

Here C_L is the concentration of impurity in the liquid and l is the zone length. All concentrations are given in units of impurity atoms per unit volume.

Developing Equation (5.1), we get

$$l(dC_L) = (C_0 - kC_L)dx, \quad (5.2)$$

and

$$\frac{ldC_L}{(C_0 - kC_L)} = dx, \quad (5.3)$$

which we can integrate to give

$$-\frac{l}{k} \ln(C_0 - kC_L) = x + \text{constant}. \quad (5.4)$$

Now the boundary condition is that, when $x = 0$, $C_L = C_0$. Substituting this into Equation (5.4) allows us to work out what the constant of integration is and gives the solution

$$-\frac{l}{k} \ln\left(\frac{C_0 - kC_L}{C_0 - kC_0}\right) = x. \quad (5.5)$$

What we really want is the impurity concentration in the solid, C_S . To get this, we manipulate Equation (5.5) as follows.

$$\ln\left(\frac{C_0 - kC_L}{C_0 - kC_0}\right) = -\frac{kx}{l}, \quad (5.6)$$

which we can invert to give

$$C_0 - kC_L = (C_0 - kC_0)\exp\left\{-\frac{kx}{l}\right\}. \quad (5.7)$$

Substituting $C_S = kC_L$ in Equation (5.7) produces

$$C_0 - C_S = C_0(1 - k)\exp\left\{-\frac{kx}{l}\right\}. \quad (5.8)$$

This gives, at last,

$$C_S = C_0\left\{1 - (1 - k)\exp\left\{-\frac{kx}{l}\right\}\right\}, \quad (5.9)$$

which we have plotted schematically in Figure 5.6.

Figure 5.6 is interesting because it shows that for the best refining performance we need both a long zone and an impurity that is relatively insoluble in the solid (low k). Unfortunately, long liquid zones can be destabilized by

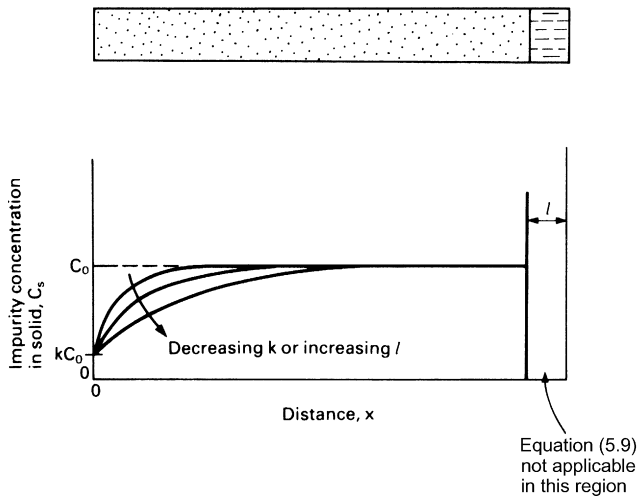
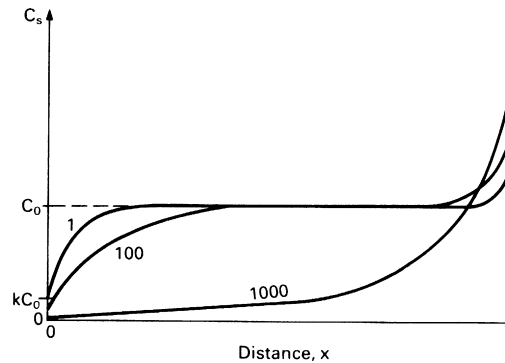
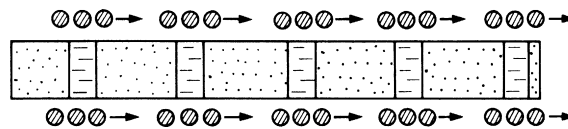


FIGURE 5.6

Schematic plot of Equation (5.9) showing how small k and long l give the best zone-refining performance.

**FIGURE 5.7**

If the bar is repeatedly zone refined from left to right, then more and more of the impurity will be swept to the right-hand end of the bar. A large number of zone-refining passes may be needed to make the left-hand half of the bar as pure as we need. The right-hand half is cut off and recycled. Note that Equation (5.9) can only be used to calculate the impurity distribution produced by the *first* pass. A computer program has to be written to handle each subsequent pass.

**FIGURE 5.8**

A multiheater arrangement gives much faster zone refining.

convection, and impurities with a low k do not come to order! Commercial zone-refining processes may therefore involve a large number of passes done one after the other (Figure 5.7). This obviously adds a lot to the cost of the pure material, but the process can be speeded up considerably by using the multiheater arrangement shown in Figure 5.8.

5.4 MAKING BUBBLE-FREE ICE

People who go in for expensive cocktails like to cool them with ice cubes which are crystal clear—it adds to the aura of bejeweled, refreshing purity. Unfortunately, ice cubes grown in an ordinary fridge are cloudy. So establishments which cater for upmarket clients install special machines to make clear ice.

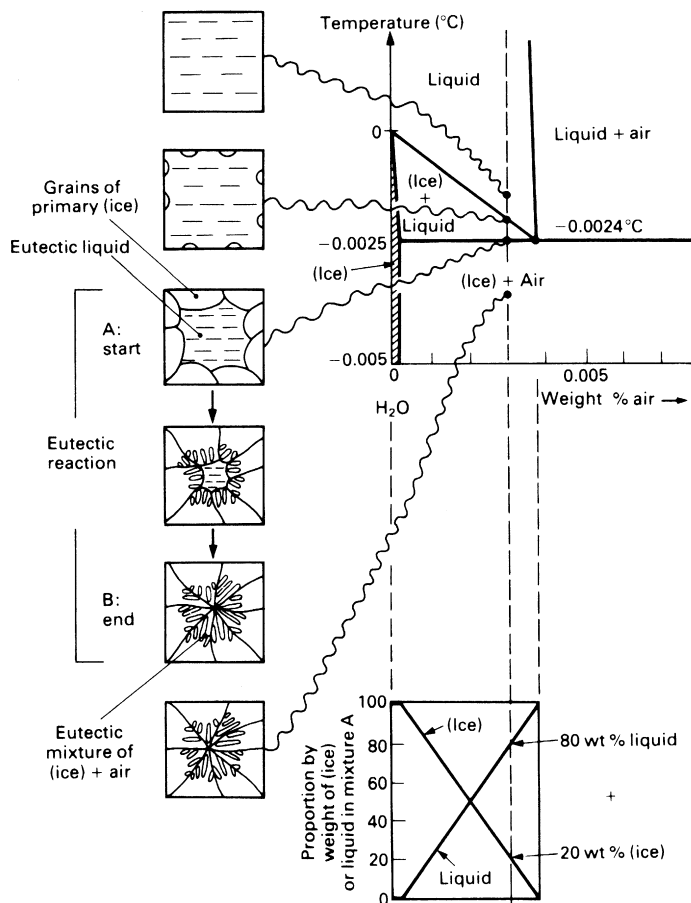


FIGURE 5.9

Stages in freezing an “ordinary” ice cube can be inferred from the phase diagram for the H₂O + air system.

The cloudiness of ordinary ice cubes is caused by thousands of tiny air bubbles. Air dissolves in water, and tap water at 10 °C can—and usually *does*—contain 0.0030 wt% of air. In order to follow what this air does when we make an ice cube, we need to look at the phase diagram for the H₂O–air system (Figure 5.9). As we cool our liquid solution of water + air, the first change takes place at about –0.002 °C when the composition line hits the liquidus line. At this temperature ice crystals will begin to form and, as the temperature is lowered still further, they will grow. By the time we reach the eutectic three-phase horizontal at –0.0024 °C, we will have 20 wt% ice (called *primary* ice) in our two-phase mixture, leaving 80 wt% liquid

(Figure 5.9). This liquid will contain the maximum possible amount of dissolved air (0.0038 wt%). As latent heat of freezing is removed at -0.0024°C , the three-phase eutectic reaction of

Eutectic liquid ($\text{H}_2\text{O} + 0.0038 \text{ wt\% air}$) \rightarrow eutectic mixture of (ice) + air

will take place. Finally, when all the eutectic liquid has frozen to ice, we will be left with a two-phase mixture of eutectic [(ice) + air] which we can then cool down below the eutectic temperature of -0.0024°C . In fact, because the solubility of air in ice is so small (Figure 5.9), almost all the air that *was* dissolved in the eutectic liquid separates out into bubbles of air as soon as we get below the three-phase horizontal. And although this air accounts for only 0.0038% by *weight* of the eutectic mixture, it takes up 2.92% by *volume*. This is why ordinary ice looks cloudy—it contains a network of air bubbles which scatter light very effectively.

Having understood why ordinary ice cubes are cloudy, could we devise a way of making bubble-free ice? Since air bubbles can only form from liquid

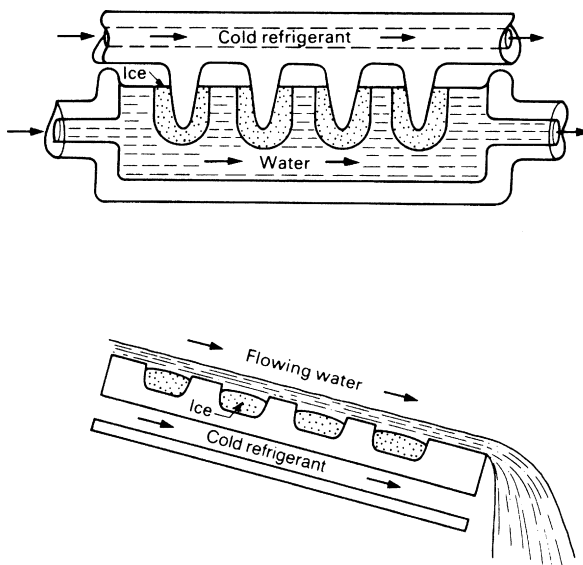


FIGURE 5.10

Two types of clear-ice machine. In the top one, the ice grows on the outside of a set of aluminum cold fingers. In the bottom one, the cubes grow in aluminum trays. Cubes are removed when they are big enough by stopping the flow of refrigerant and heating the aluminum electrically. This melts the surface of the ice so that it can fall away from the metal (remember that the easiest way to take the wrapper off an ice lolly is to warm the outside with your hands for a minute!)

having the eutectic composition, one obvious way would be to make sure that the liquid into which the ice grains are growing never reaches the eutectic composition. This is in fact the approach used in the standard ice-making machines (Figure 5.10). Here, tap water continually flows across the growing ice grains so that the composition of the liquid is always kept at about 0.0030 wt% air. This is safely below the eutectic composition of 0.0038 wt%, and the bubble-free ice thus made is, apparently, to the entire satisfaction of the customers!

Of course, because all liquids dissolve gases, bubbles tend to form not just in ice but in any frozen solid. And this *casting porosity* is a major worry to foundry staff. The approach used in the ice-cube machines is useless for dealing with an enclosed casting and we have to find other ways. When making high-strength castings, the metal is usually melted in a vacuum chamber so that the dissolved gas will diffuse out of the liquid and be pumped away. And for ordinary castings, “degassing” chemicals are added which react with the dissolved gases to form gaseous compounds that bubble out of the liquid or solid compounds that remain in the metal as harmless inclusions.

WORKED EXAMPLE

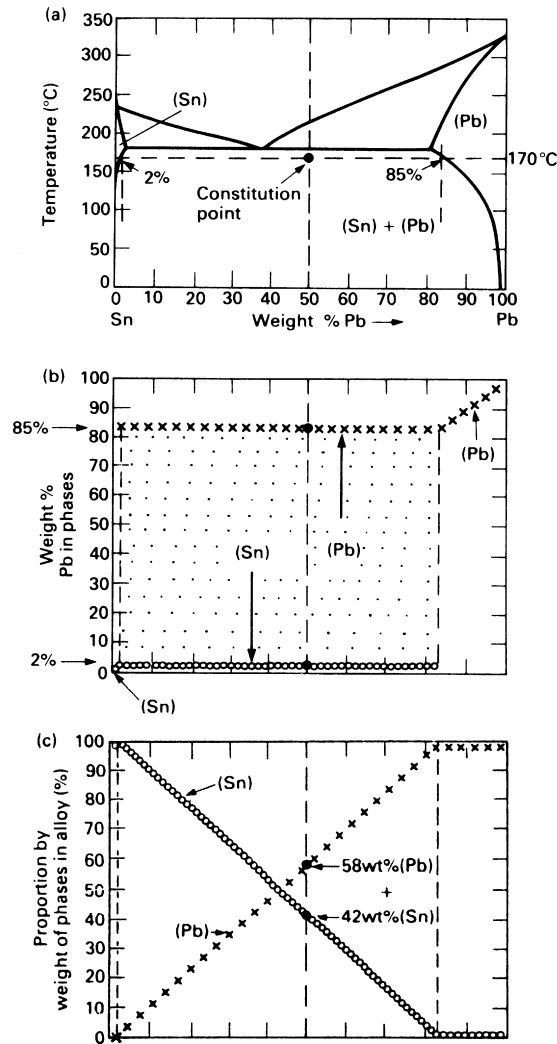
The phase diagram for any alloy is simply a map compiled from experimental data on its make-up (“constitution”) *when the system is in equilibrium*. If we know the overall composition of the alloy, we can use the phase diagram to tell us what the equilibrium *constitution* of the alloy is at any given temperature. By now, you will have some experience of doing this in Chapters 3 and 4. In this Worked Example, we look at additional charts which may help you to look up details of the constitution directly.

Take as an example, an alloy of lead and tin with an overall composition of 50 wt% lead + 50 wt% tin at a temperature of 170 °C. The diagram shows how details of the constitution can be read off directly. We write down the full constitution as:

- (a) the overall composition (50 wt% lead + 50 wt% tin),
- (b) the number of phases (two),
- (c) the composition of each phase (2 wt% lead, 85 wt% lead),
- (d) the proportion of each phase (58 wt% (Pb), 42 wt% (Sn)).

In particular, check that you can read (d) directly from diagram (c)— this is a direct lookup instead of having to do a calculation using the “lever rule.”

We give some more examples below (still at 170 °C) for you to check from the diagrams.



(a) A 50—50 lead—tin alloy at 170 °C has a constitution point that puts it in the (Sn) + (Pb) two-phase field. The compositions of the (Sn) and (Pb) phases in the two-phase mixture are 2 wt% lead and 85 wt% lead. Remember that in any overall composition, or in any phase, wt% tin + wt% lead = 100%. So the compositions of the (Sn) and (Pb) phases could just as well have been written as 98 wt% tin and 15 wt% tin. (b) This diagram only duplicates information that is already contained in the phase diagram, but it helps to emphasize how the compositions of the phases depend on the overall composition of the alloy. (c) The 50—50 alloy at 170 °C consists of 58 wt% of the (Pb) phase and 42 wt% of the (Sn) phase. The straight-line relations in the diagram are a simple consequence of the following requirements: (i) mass (Pb) phase + mass (Sn) phase = mass alloy; (ii) mass lead in (Pb) + mass lead in (Sn) = mass lead in alloy; (iii) mass tin in (Pb) + mass tin in (Sn) = mass tin in alloy.

- (a) 25 wt% lead + 75 wt% tin,
- (b) two phases,
- (c) 2 wt% lead, 85 wt% lead,
- (d) 30 wt% (Pb), 70 wt% (Sn).

- (a) 75 wt% lead + 25 wt% tin,
- (b) two phases,
- (c) 2 wt% lead, 85 wt% lead,
- (d) 87 wt% (Pb), 13 wt% (Sn).

- (a) 85 wt% lead + 15 wt% tin,
- (b) one phase (just),
- (c) 85 wt% lead,
- (d) 100 wt% (Pb).

- (a) 95 wt% lead + 5 wt% tin,
- (b) one phase,
- (c) 95 wt% lead,
- (d) 100 wt% (Pb).

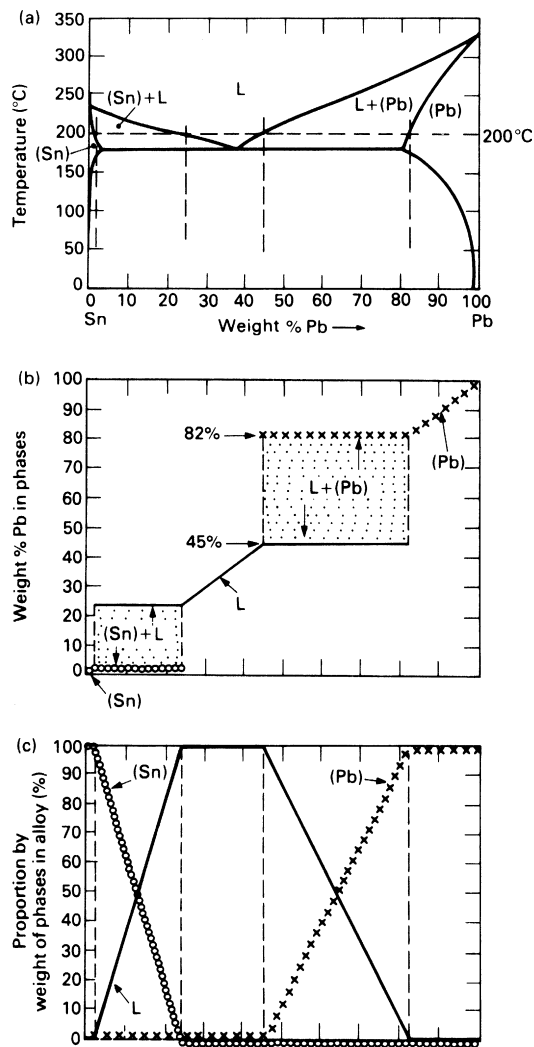
- (a) 2 wt% lead + 98 wt% tin,
- (b) one phase (just),
- (c) 2 wt% lead,
- (d) 100 wt% (Sn).

- (a) 1 wt% lead + 99 wt% tin,
- (b) one phase,
- (c) 1 wt% lead,
- (d) 100 wt% (Sn).

Let us now look at lead–tin alloys at 200 °C. We can use the same method, as the next diagram shows. A typical constitution at 200 °C would be:

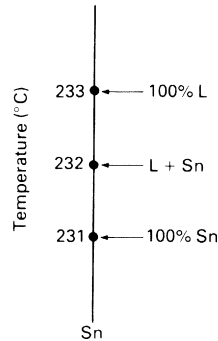
- (a) 50 wt% lead + 50 wt% tin,
- (b) two phases,
- (c) 45 wt% lead, 82 wt% lead,
- (d) 87 wt% (L), 13 wt% (Pb).

You should be able to write down many others for yourself.

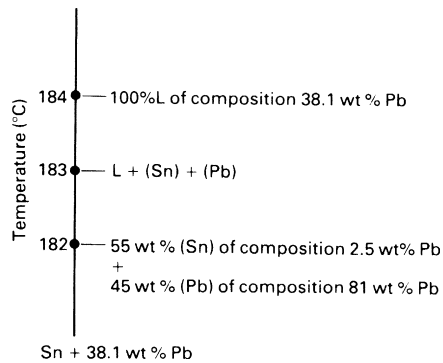


Diagrams showing how you can find the equilibrium constitution of any lead—tin alloy at 200 °C. Once you have had a little practice you will be able to write down constitutions directly from the phase diagram without using diagrams like (b) or (c).

Finally, there are places in the phase diagram where the constitution cannot be defined fully. These are the melting points of pure lead and pure tin and the horizontal line of the eutectic reaction. The diagrams below explain why.



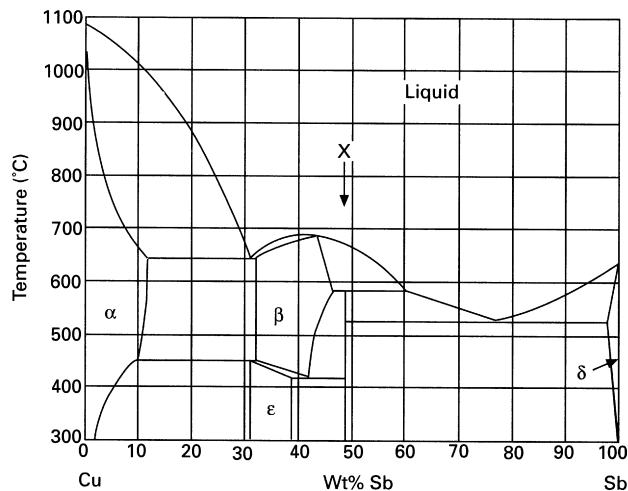
At 232 °C, the melting point of pure tin, we have a L + Sn two-phase mixture. But, without more information, we can't say what the relative weights of L and Sn *are*.



At 183 °C, we have a *three-phase mixture* of L + (Sn) + (Pb). Their relative weights can't be found from the phase diagram.

EXAMPLES

- 5.1 Explain briefly what is meant by the following terms:
 - (a) a eutectic reaction,
 - (b) a eutectoid reaction.
- 5.2 The phase diagram for the copper–antimony system is shown below. The phase diagram contains the intermetallic compound marked “X” on the diagram. Determine the chemical formula of this compound. The atomic weights of copper and antimony are 63.54 and 121.75, respectively.

**Answer**

Cu_2Sb .

5.3 The copper–antimony phase diagram contains two eutectic reactions and one eutectoid reaction. For each reaction:

- (a) identify the phases involved,
- (b) give the compositions of the phases,
- (c) give the temperature of the reaction.

Answers

Eutectic at 650 °C: $\text{L}(31\% \text{ Sb}) = \alpha(12\% \text{ Sb}) + \beta(32\% \text{ Sb})$.

Eutectic at 520 °C: $\text{L}(77\% \text{ Sb}) = \text{Cu}_2\text{Sb} + \delta(98\% \text{ Sb})$

Eutectoid at 420 °C: $\beta(42\% \text{ Sb}) = \epsilon(38\% \text{ Sb}) + \text{Cu}_2\text{Sb}$.

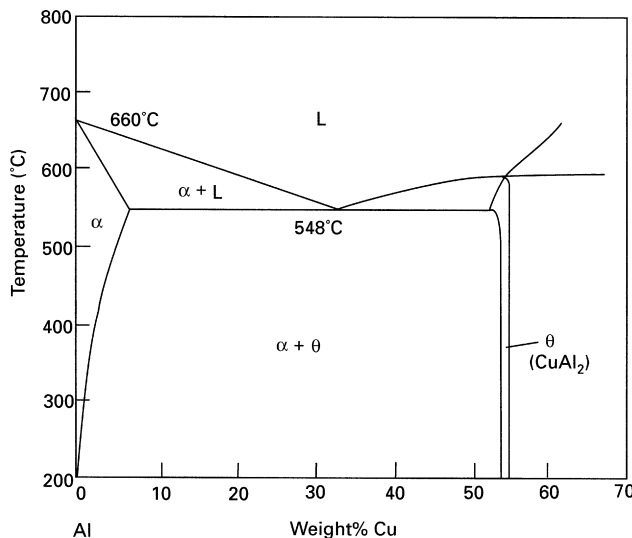
- 5.4** A copper–antimony alloy containing 95 wt% antimony is allowed to cool from 650 °C to room temperature. Describe the different phase changes which take place as the alloy is cooled and make labeled sketches of the microstructure to illustrate your answer.
- 5.5** Sketch a graph of temperature against time for a copper–antimony alloy containing 95 wt% antimony over the range 650–500 °C and account for the shape of your plot.
- 5.6** What composition of lead–tin solder is the best choice for joining electronic components? Why is this composition chosen?
- 5.7** A single-pass zone-refining operation is to be carried out on a uniform bar 2000 mm long. The zone is 2 mm long. Setting the initial impurity concentration $C_0 = 1$ unit of concentration, plot C_S as a function of x for $0 < x < 1000$ mm (a) when $k = 0.01$, (b) when $k = 0.1$.
[Hint: use Equation (5.9).]

- 5.8** A single-pass zone-refining operation is to be carried out on a long uniform bar of aluminum containing an even concentration C_0 of copper as a dissolved impurity. The left-hand end of the bar is first melted to produce a short liquid zone of length/and concentration C_L . The zone is then moved along the bar so that fresh solid deposits at the left of the zone and existing solid at the right of the zone melts. The length of the zone remains unchanged. Show that the concentration C_S of the fresh solid is related to the concentration C_L of the liquid from which it forms by the relation

$$C_S = 0.15 C_L.$$

At the end of the zone-refining operation the zone reaches the right-hand end of the bar. The liquid at the left of the zone then begins to solidify so that in time the length of the zone decreases to zero. Derive expressions for the variations of both C_S and C_L with distance x in this final stage. Explain whether or not these expressions are likely to remain valid as the zone length tends to zero.

The aluminum–copper phase diagram is shown below.



Answer

$$C_L = \frac{C_0}{0.15} \left(\frac{l}{l-x} \right)^{0.85} ; \quad C_S = C_0 \left(\frac{l}{l-x} \right)^{0.85}.$$

- 5.9** Upmarket radiators for central heating systems are built up from modules having an internal water space and external heat-transfer fins (typically 2 mm thick and 40 mm deep). They are cast to shape from Al–12 wt% Si alloy (see Figure 4.6) for the phase diagram). What makes this alloy a good choice for casting such thin sections? Why would Al–6 wt% Si not be such a good choice?

Driving Force for Structural Change

6.1 INTRODUCTION

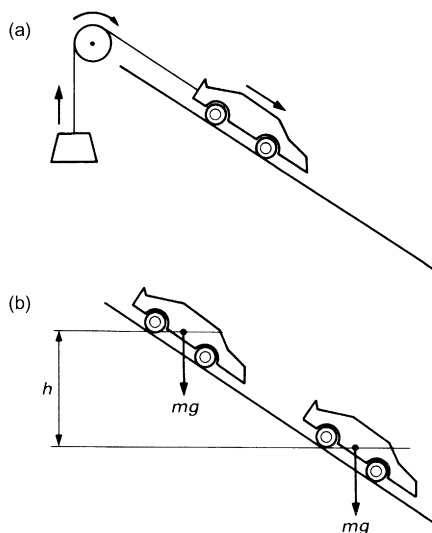
When the structure of a metal changes, it is because there is a *driving force* for the change. When iron goes from b.c.c. to f.c.c. as it is heated, or when a boron dopant diffuses into a silicon semiconductor, or when a powdered superalloy sinters together, it is because each process is pushed along by a driving force.

The mere fact of having a driving force does not guarantee that a change *will* occur. There must also be a *route* that the process can follow. For example, even though boron will *want* to mix with silicon, it can only do this if the route for the process—atomic diffusion—is fast enough. At high temperature, with plenty of thermal energy for diffusion, the doping process *will* be fast; but at low temperature, it will be immeasurably slow. The rate at which a structural change actually takes place is then a function of both the *driving force* and the speed or *kinetics* of the route; and both must have finite values if we are to get a change.

We will be looking at kinetics in Chapter 7. But before we can do this, we need to know what we mean by driving forces and how we calculate them. In this chapter, we show that driving forces can be expressed in terms of simple thermodynamic quantities, and we illustrate this by calculating driving forces for some typical processes like solidification, changes in crystal structure, and precipitate coarsening.

6.2 DRIVING FORCES

A familiar example of a change is what takes place when an automobile is allowed to move off down a hill (Figure 6.1). As the car moves downhill, it can be made to do work—perhaps by raising a weight (Figure 6.1) or driving a machine. This work is called *the free work*, W_f . It is the free work that drives the change of the car going downhill and provides what we term the “driving

**FIGURE 6.1**

(a) An automobile moving downhill can do work. It is this *free work* that drives the process. (b) In the simplest situation, the free work can be calculated from the change in potential energy, mgh , that takes place during the process.

force” for the change. (The traditional term driving force is rather unfortunate because we don’t mean “force,” with units of N, but *work*, with units of J).

How can we calculate the free work? The simplest case is when the free work is produced by the decrease of *potential energy*, with

$$W_f = mgh. \quad (6.1)$$

This equation does, of course, assume that all the potential energy is converted into useful work. This is impossible in practice because some work will be done against friction—in wheel bearings, tires, and air resistance—and the free work must really be written as

$$W_f \leq mgh. \quad (6.2)$$

What do we do when there are other ways of doing free work? As an example, if our car were initially moving downhill with velocity v but ended up stationary at the bottom of the hill, we would have

$$W_f \leq mgh + \frac{1}{2}mv^2 \quad (6.3)$$

instead. And we could get even more free work by putting a giant magnet at the bottom of the hill! In order to cover all these possibilities, we usually write

$$W_f \leq -\Delta N, \quad (6.4)$$

where ΔN is the change in the *external energy*. The minus sign comes in because a decrease in external energy (e.g., a decrease in potential energy) gives us a positive output of work W . *External energy* simply means all sources of work that are due solely to directed (i.e., nonrandom) movements (as in mgh , $\frac{1}{2}mv^2$ and so on).

A quite different source of work is the *internal energy*. This is characteristic of the intrinsic nature of the materials themselves, whether they are moving nonrandomly or not. Examples in our present illustration are the chemical energy that could be released by burning the fuel, the elastic strain energy stored in the suspension springs, and the thermal energy stored in the random vibrations of all the atoms. Obviously, burning the fuel in the engine will give us an extra amount of free work given by

$$W_f \leq -\Delta U_b, \quad (6.5)$$

where ΔU_b is the change in internal energy produced by burning the fuel.

Finally, *heat* can be turned into work. If our car were steam powered, for example, we could produce work by exchanging heat with the boiler and the condenser.

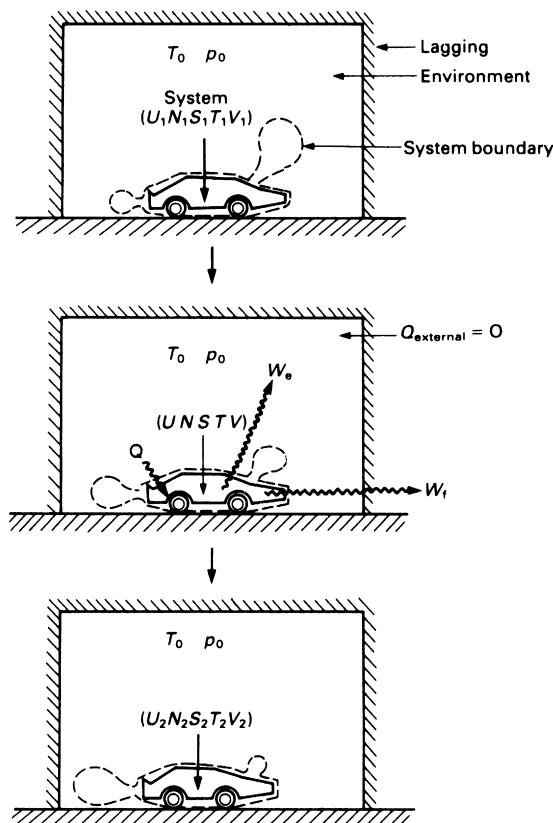
The first law of thermodynamics—which is just a statement of energy conservation—allows us to find out how much work is produced by *all* the changes in N , all the changes in U , and all the heat flows, from the equation

$$W = Q - \Delta U - \Delta N. \quad (6.6)$$

The nice thing about this result is that the inequalities have all vanished. This is because any energy lost in one way (e.g., potential energy lost in friction) must appear somewhere else (e.g., as heat flowing out of the bearings). But [Equation \(6.6\)](#) gives us the *total* work produced by Q , ΔU , and ΔN ; and this is not necessarily the *free* work available to drive the change.

In order to see why, we need to look at our car in a bit more detail ([Figure 6.2](#)). We start by assuming that it is surrounded by a large and thermally insulated environment kept at constant thermodynamic temperature T_0 and absolute pressure p_0 (assumptions that are valid for most structural changes in the earth's atmosphere). We define our *system* as: (the automobile + the air needed for burning the fuel + the exhaust gases given out at the back). The system starts off with internal energy U_1 , external energy N_1 , and volume V_1 . As the car travels to the right U , N and V change until, at the end of the change, they end up as U_2 , N_2 , and V_2 . Obviously, the total work produced will be

$$W = Q - (U_2 - U_1) - (N_2 - N_1). \quad (6.7)$$

**FIGURE 6.2**

Changes that take place when an automobile moves in a thermally insulated environment at constant temperature T_0 and pressure p_0 . The environment is taken to be large enough that the change in system volume $V_2 - V_1$ does not increase p_0 ; and the flow of heat Q across the system boundary does not affect T_0 .

However, the volume of gas put out through the exhaust pipe will be greater than the volume of air drawn in through the air filter and V_2 will be greater than V_1 . We thus have to do work W_e in pushing back the environment, given by

$$W_e = p_0(V_2 - V_1). \quad (6.8)$$

The free work, W_f , is thus given by $W_f = W - W_e$, or

$$W_f = Q - (U_2 - U_1) - p_0(V_2 - V_1) - (N_2 - N_1). \quad (6.9)$$

6.3 REVERSIBILITY

A thermodynamic change can take place in two ways—either *reversibly* or *irreversibly*. In a reversible change, all the processes take place as efficiently as the second law of thermodynamics will allow them to. In this case, the second law tells us that

$$dS = dQ/T. \quad (6.10)$$

This means that, if we put a small amount of heat dQ into the system when it is at thermodynamic temperature T , we will increase the system entropy by a small amount dS which can be calculated from Equation (6.10). If our car operates reversibly, we can then write

$$S_2 - S_1 = \int_Q \frac{dQ(T)}{T}. \quad (6.11)$$

However, we have a problem in working out this integral: unless we continuously monitor the movements of the car, we will not know just how much heat dQ will be put into the system in each temperature interval of T to $T + dT$ over the range $T_1 - T_2$. The way out of the problem lies in seeing that, because $Q_{\text{external}} = 0$ (see Figure 6.2), there is no change in the entropy of the (system + environment) during the movement of the car. In other words, the increase of system entropy $S_2 - S_1$ must be balanced by an equal *decrease* in the entropy of the environment. Since the environment is always at T_0 , we do not have to integrate and can just write

$$(S_2 - S_1)_{\text{environment}} = \frac{-Q}{T_0} \quad (6.12)$$

so that

$$(S_2 - S_1) = -(S_2 - S_1)_{\text{environment}} = \frac{Q}{T_0}. \quad (6.13)$$

This can then be substituted into Equation (6.9) to give us

$$W_f = -(U_2 - U_1) - p_0(V_2 - V_1) + T_0(S_2 - S_1) - (N_2 - N_1), \quad (6.14)$$

or, in more compact notation,

$$W_f = -\Delta U - p_0\Delta V + T_0\Delta S - \Delta N. \quad (6.15)$$

To summarize, Equation (6.15) allows us to find how much *free work* is available for driving a reversible process as a function of the thermodynamic properties of the system (U, V, S, N) and its surroundings (p_0, T_0).

Equation (6.15) was originally derived so that engineers could find out how much work they could get from machines like steam generators or

petrol engines. Changes in external energy cannot give continuous outputs of work, and engineers therefore distinguish between ΔN and $-\Delta U - p_0 V + T_0 \Delta S$. They define a function A , called the *availability*, as

$$A \equiv U + p_0 V - T_0 S. \quad (6.16)$$

The free, or available, work can then be expressed in terms of changes in *availability* and *external energy* using the final result

$$W_f = -\Delta A - \Delta N. \quad (6.17)$$

Of course, real changes can never be ideally efficient, and some work will be lost in *irreversibilities* (e.g., friction). Equation (6.17) then gives us an overestimate of W_f . But it is very difficult to calculate irreversible effects in materials processes. We will therefore stick to Equation (6.17) as the best we can do!

6.4 STABILITY, INSTABILITY, AND METASTABILITY

The stability of a static mechanical system can, as we know, be tested very easily by looking at how the potential energy is affected by any changes in the orientation or position of the system (Figure 6.3). The stability of more complex systems can be tested in exactly the same sort of way using W_f (Figure 6.4).

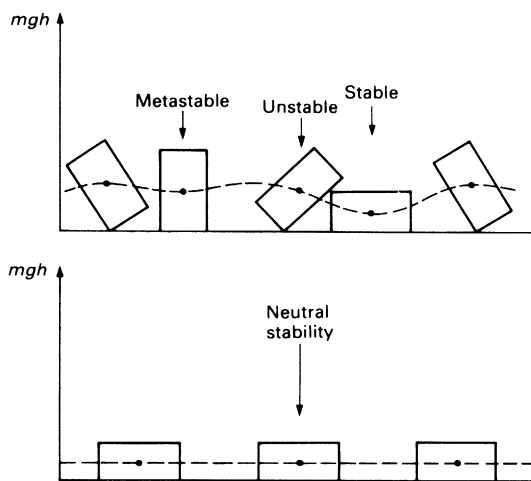


FIGURE 6.3

Changes in the potential energy of a static mechanical system tell us whether it is in a stable, unstable, or metastable state.

6.5 DRIVING FORCE FOR SOLIDIFICATION

How do we actually use Equation (6.17) to calculate driving forces in materials processes? A good example to begin with is solidification—most metals are melted or solidified during manufacture, and we have already looked at two case studies involving solidification (zone refining and making bubble-free ice). Let us therefore look at the thermodynamics involved when water solidifies to ice.

We assume (Figure 6.5) that all parts of the system and of the environment are at the same constant temperature T and pressure p . Let's start with a mixture of ice and water at the melting point T_M (if $p = 1$ atm then $T_M = 273$ K of course). At the melting point, the ice–water system is in a state of *neutral equilibrium*: no free work can be extracted if some of the remaining water is frozen to ice or if some of the ice is melted to water. If we neglect changes in external energy (freezing ponds don't get up and walk away!), then Equation (6.17) tells us that $\Delta A = 0$, or

$$(U + pV - T_M S)_{\text{ice}} = (U + pV - T_M S)_{\text{water}}. \quad (6.18)$$

We know from thermodynamics that the enthalpy H is defined by $H \equiv U + pV$, so Equation (6.18) becomes

$$(H - T_M S)_{\text{ice}} = (H - T_M S)_{\text{water}}. \quad (6.19)$$

Thus, for the ice–water change, $\Delta H = T_M \Delta S$, or

$$\Delta S = \frac{\Delta H}{T_M}. \quad (6.20)$$

This is of exactly the same form as Equation (6.10) and ΔH is simply the “latent heat of melting” that generations of schoolchildren have measured in

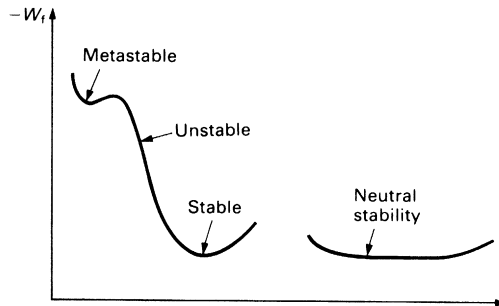
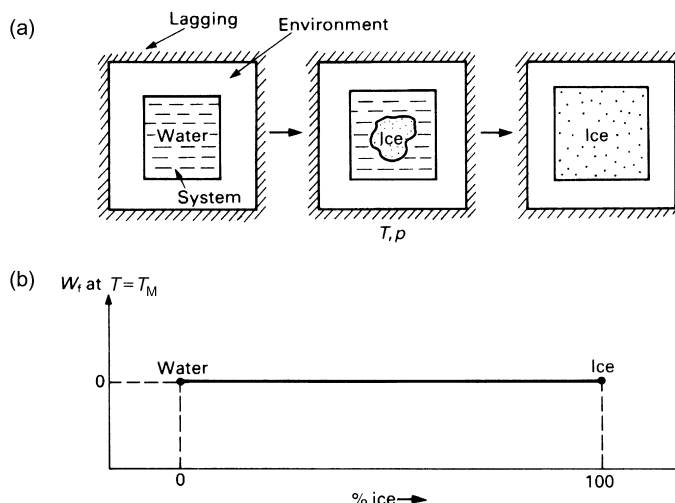


FIGURE 6.4

The stability of complex systems is determined by changes in the free work W_f . Note the minus sign—systems try to move so that they *produce* the *maximum* work.

**FIGURE 6.5**

(a) Stages in the freezing of ice. All parts of the system and of the environment are at the same constant temperature T and pressure p . (b) An ice–water system at the melting point T_M is in neutral equilibrium.

school physics laboratories. To melt ice, we have to put heat into the system. This increases the system entropy via Equation (6.20). Physically, entropy represents *disorder*; and Equation (6.20) tells us that water is more disordered than ice. We would expect this anyway because the atoms in a liquid are arranged much more chaotically than they are in a crystalline solid. When water freezes, of course, heat *leaves* the system and the entropy *decreases*.

We now take some water at a temperature $T < T_M$. We know that this will have a definite tendency to freeze, so W_f is positive. To calculate W_f , we have $W_f = -\Delta A$ and $H \equiv U + pV$ to give us

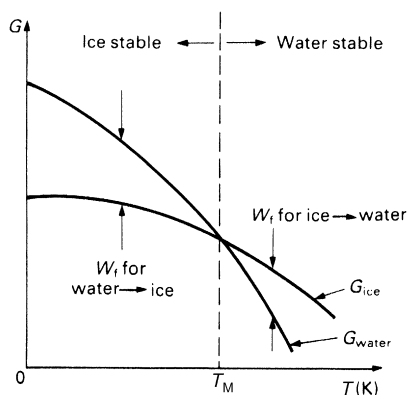
$$W_f = -[(H - TS)_{\text{ice}} - (H - TS)_{\text{water}}], \quad (6.21)$$

or

$$W_f = -\Delta H + T\Delta S. \quad (6.22)$$

If we assume that neither ΔH nor ΔS change much with temperature (which is reasonable for small $T_M - T$), then substituting Equation (6.20) in Equation (6.22) gives us

$$W_f(T) = -\Delta H + T\left(\frac{\Delta H}{T_M}\right), \quad (6.23)$$

**FIGURE 6.6**

Plot of the Gibbs functions for ice and water as functions of temperature. Below the melting point T_M , $G_{\text{water}} > G_{\text{ice}}$ and ice is the stable state of H_2O ; above T_M , $G_{\text{ice}} > G_{\text{water}}$ and water is the stable state.

or

$$W_f(T) = \frac{-\Delta H}{T_M} (T_M - T). \quad (6.24)$$

We can now put some numbers into the equation. Calorimetry experiments tell us that $\Delta H = -334 \text{ kJ kg}^{-1}$. For water at 272 K, with $T_M - T = 1 \text{ K}$, we find that $W_f = 1.22 \text{ kJ kg}^{-1}$ (or 22 J mol^{-1}). 1 kg of water at 272 K thus has 1.22 kJ of free work available to make it turn into ice. The reverse is true at 274 K, of course, where each kilogram of ice has 1.22 kJ of free work available to make it *melt*.

For large departures from T_M , we have to fall back on Equation (6.21) in order to work out W_f . Thermodynamics people soon got fed up with writing $H - TS$ all the time and invented a new term, the Gibbs function G , defined by

$$G \equiv H - TS. \quad (6.25)$$

Then, for any reversible structural change at constant uniform temperature and pressure

$$W_f = -(G_2 - G_1) = -\Delta G. \quad (6.26)$$

We have plotted G_{ice} and G_{water} in Figure 6.6 as a function of temperature in a way that clearly shows how the regions of stability of ice and water are determined by the “driving force,” $-\Delta G$.

6.6 SOLID-STATE PHASE CHANGES

We can use exactly the same approach for phase changes in the solid state, like the α - γ transformation in iron or the α - β transformation in titanium. And, in line with Equation (6.24), we can write

$$W_f(T) = -\frac{\Delta H}{T_e}(T_e - T), \quad (6.27)$$

where ΔH is now the latent heat of the *phase transformation* and T_e is the temperature at which the two *solid phases* are in equilibrium. For example, the α and β phases in titanium are in equilibrium at 882 °C or 1155 K. ΔH for the α - β reaction is $-3.48 \text{ kJ mol}^{-1}$, so that a departure of 1 K from T_e gives us a W_f of 3.0 J mol^{-1} .

Driving forces for solid-state phase transformations are about one-third of those for solidification. This is just what we would expect: the difference in order between two crystalline phases will be less than the difference in order between a *liquid* and a crystal; the entropy change in the solid-state transformation will be less than in solidification; and $\Delta H/T_e$ will be less than $\Delta H/T_M$.

6.7 PRECIPITATE COARSENING

Many metals—like nickel-based superalloys or age-hardened aluminum alloys—depend for their strength on a dispersion of fine second-phase particles. But if the alloys get too hot during manufacture or in service, the particles can *coarsen*, and the strength will fall off badly. During coarsening, small precipitates shrink, and eventually vanish altogether, whereas large precipitates grow at their expense. Matter is transferred between the precipitates by solid-state diffusion. Figure 6.7 summarizes the process. But how do we work out the driving force?

As before, we start with our basic static-system equation

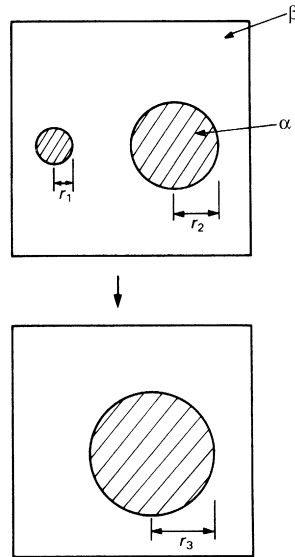
$$W_f = -\Delta A. \quad (6.28)$$

Now the only way in which the system can do free work is by reducing the total energy of α - β interface. Thus

$$\Delta A = 4\pi r_3^2\gamma - 4\pi r_1^2\gamma - 4\pi r_2^2\gamma \quad (6.29)$$

where γ is the energy of the α - β interface per unit area. Conservation of volume gives

$$\frac{4}{3}\pi r_3^3 = \frac{4}{3}\pi r_1^3 + \frac{4}{3}\pi r_2^3. \quad (6.30)$$

**FIGURE 6.7**

Schematic of precipitate coarsening. The small precipitate is shrinking, and the large precipitate is growing at its expense. Material travels between the two by solid-state diffusion.

Combining Equations (6.29) and (6.30) gives

$$\Delta A = 4\pi\gamma \left[(r_1^3 + r_2^3)^{2/3} - (r_1^2 + r_2^2) \right]. \quad (6.31)$$

For r_1/r_2 in the range 0–1, this result is negative. $W_f = -\Delta A$ is therefore positive, and this is what drives the coarsening process.

How large is the driving force for a typical coarsening process? If we put $r_1 = r_2/2$ in Equation (6.31), we get $\Delta A = -4\pi\gamma(-0.17r_2^2)$. If $\gamma = 0.5 \text{ J m}^{-2}$ and $r_2 = 10^{-7} \text{ m}$, our two precipitates give us a free work of 10^{-14} J or about 7 J mol^{-1} . And this is large enough to make coarsening quite a problem. One way of getting over this is to choose alloying elements that give us *coherent* precipitates. γ is then only about 0.05 J m^{-2} (see Chapter 2), and this brings W_f down to only 0.7 J mol^{-1} .

6.8 GRAIN GROWTH

The grain boundary energy tied up in a polycrystalline metal works in the same sort of way to give us a driving force for *grain* coarsening. As we shall see in Chapter 14, grain coarsening can cause us problems when we try to

weld high-strength steels together. A typical γ_{gb} (0.5 J m^{-2}) and grain size ($100 \text{ }\mu\text{m}$) give us W_f of about $2 \times 10^{-2} \text{ J mol}^{-1}$.

6.9 RECRYSTALLIZATION

When metals are deformed plastically at room temperature, the dislocation density goes up enormously (to $\approx 10^{15} \text{ m}^{-2}$). Each dislocation has a strain energy of about $Gb^2/2$ per unit length and the total dislocation strain energy in a cubic meter of deformed metal is about 2 MJ, equivalent to 15 J mol^{-1} . When cold-worked metals are heated to about $0.6T_M$, new strain-free grains nucleate and grow to consume all the cold-worked metal. This is called—for obvious reasons—*recrystallization*. Metals are much softer when they have been recrystallized (or “annealed”). And provided metals are annealed often enough they can be deformed almost indefinitely.

6.10 SIZES OF DRIVING FORCES

In Table 6.1, we have listed typical driving forces for structural changes. These range from 10^6 J mol^{-1} for oxidation to $2 \times 10^{-2} \text{ J mol}^{-1}$ for grain growth.

With such a huge range of driving force, we would expect structural changes in materials to take place over a very wide range of timescales. However, as we shall see in the next three chapters, kinetic effects are just as important as driving forces in deciding how fast a structural change will go.

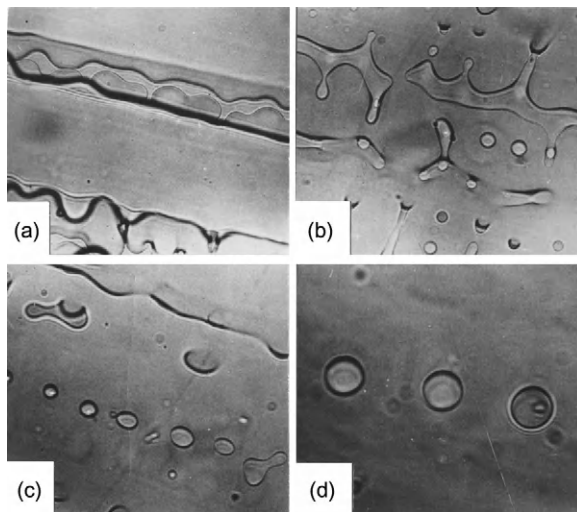
Table 6.1 Driving Forces for Structural Change

Change	$-\Delta G$ (J mol^{-1})
Chemical reaction—oxidation	$0-10^6$
Chemical reaction—formation of intermetallic compounds	$300-5 \times 10^4$
Diffusion in solid solutions (dilute ideal solutions: between solute concentrations $2c$ and c at 1000 K)	6×10^3
Solidification or melting (1°C departure from T_M)	8–22
Polymorphic transformations (1°C departure from T_θ)	1–8
Recrystallization (caused by cold working)	≈ 15
Precipitate coarsening	0.7–7
Grain growth	2×10^{-2}

WORKED EXAMPLE

The photograph which follows shows a sample of the transparent organic compound camphene (which melts at 50°C). Solidification has recently taken place by the growth of dendrites from left to right, and the sample has then been held at a temperature just below its melting point. The second phase is liquid containing segregated impurities. In (a) (magnification $\times 135$), you can see the dendrite arms with liquid spaces in between them. In (b) (magnification $\times 135$), you can see the liquid spaces separating and starting to break down into discrete droplets. This process is more advanced in (c) (magnification $\times 135$), and in (d) (magnification $\times 235$), all the liquid is in the form of spherical droplets.

The driving force for this sequence is the energy of the solid–liquid interface, γ_{SL} . As the sequence progresses, the total area of solid–liquid interface in the sample decreases, because accommodating a fixed volume of liquid as spheres is more efficient in terms of surface area than accommodating the volume as long channels or tubes.



EXAMPLES

- 6.1** Calculate the free work available to drive the following processes *per kilogram of material*.
- (a) Solidification of molten copper at 1080°C . (For copper, $T_{\text{M}} = 1083^\circ\text{C}$, $\Delta H = 13.02 \text{ kJ mol}^{-1}$, atomic weight = 63.54).
 - (b) Transformation from $\beta\text{-Ti}$ to $\alpha\text{-Ti}$ at 800°C . (For titanium, $T_{\text{e}} = 882^\circ\text{C}$, $\Delta H = 3.48 \text{ kJ mol}^{-1}$, atomic weight = 47.90).

- (c) Recrystallization of cold-worked aluminum with a dislocation density of 10^{15} m^{-2} . (For aluminum, $G = 26 \text{ GN m}^{-2}$, $b = 0.286 \text{ nm}$, density = 2700 kg m^{-3}).

Hint—write the units out in all the steps of your working.

Answers

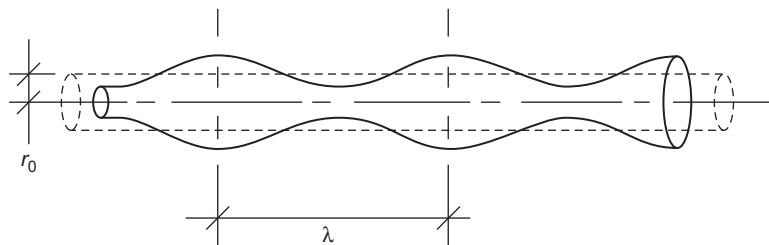
(a) 453 J; (b) 5157 J; (c) 393 J.

- 6.2** The microstructure of normalized carbon steels contains colonies of “pearlite.” Pearlite consists of thin, alternating parallel plates of α -Fe and iron carbide, Fe_3C . When carbon steels containing pearlite are heated at about 700°C for several hours, it is observed that the plates of Fe_3C start to change shape, and eventually become “spheroidized” (each plate turns into a large number of small spheres of Fe_3C). What provides the driving force for this shape change?
- 6.3** When manufacturing components by the process of *powder metallurgy*, the metal is first converted into a fine powder (by atomizing liquid metal and solidifying the droplets). Powder is then compacted into the shape of the finished component and heated at a high temperature. After several hours, the particles of the powder fuse (“sinter”) together to form a polycrystalline solid with mechanical strength. What provides the driving force for the sintering process?
- 6.4** In a die-casting operation 0.1 kg charges of molten zinc alloy at 410°C are injected at a rate of 120 charges per hour. The liquid metal has a specific heat of $480 \text{ J kg}^{-1} \text{ K}^{-1}$ and a freezing temperature of 400°C . The latent heat of solidification of the alloy is $110,000 \text{ J kg}^{-1}$. The casting is ejected from the die as soon as it is solid. The insulated die is water cooled at a rate $C(T_d - T_0)$, where T_d is the die temperature, $T_0 = 20^\circ\text{C}$ is the ambient temperature, and C has the value $5 \text{ J s}^{-1} \text{ K}^{-1}$. Estimate the average die temperature after a long period of steady operation.

Answer

97°C .

- 6.5** The diagram which follows shows a cylindrical cavity of liquid containing segregated impurities in a sample of solid material held just below its melting point. The radius of the cylinder is r_0 . This shape is unstable and over time the cylinder develops sinusoidal perturbations which grow until the cylinder breaks up into a row of spheres spaced a distance λ apart.



The theoretical analysis for this situation predicts that $\lambda = 9r_0$. Assuming that volume is conserved, derive an expression for the radius of the spheres r_S in terms of (a) r_0 , and (b) λ . Hence, find the ratio of sphere diameter to wavelength, $2r_S/\lambda$. Referring to photograph (d) in the Worked Example, take measurements of $2r_S$ and λ , and from them find the ratio $2r_S/\lambda$. How well does this experimental ratio compare with the predicted ratio?

Answers

(a) $r_S = 1.89r_0$; (b) $r_S = 0.21\lambda$; $2r_S/\lambda = 0.42$; measured ratio ≈ 0.43 , good agreement.

- 6.6** Using results from Example 6.5, derive an expression for the free work produced when the cylinder breaks down into spheres. Is the sign of W_f consistent with the cylinder being unstable? Derive an expression for the free work *per unit volume of liquid*.

Estimate the free work per unit volume of liquid for the camphene system (use the value of $\gamma_{SL} = 5.3 \text{ mJ m}^{-2}$ for camphene, and find r_0 from the measurements taken of photograph (d) in Example 6.5). The free work per unit volume varies inversely with the radius of the cylinder. Comment on the practical significance of this scaling law.

Answers

$W_f = 3.7\pi r_0^2 \gamma_{SL}$; yes; $0.41\gamma_{SL}/r_0$; 4 J m^{-3} .

- 6.7** When ice freezes from water in a system at uniform temperature T_M and pressure p_0 , heat must be removed from the system in the form of latent heat, ΔH (per kilogram or per mole). Assuming all processes take place reversibly, write down an expression for the change in entropy of the system, ΔS . Does the entropy decrease or increase as freezing continues? How can the change in entropy (and the sign of the change) be explained by the way in which the H_2O molecules are arranged in the liquid and solid phases?
- 6.8** It is found that the ratio $\Delta S/R$ (where ΔS is the entropy of fusion and R is the gas constant) is less than about 4 for metals (and organic compounds which have essentially spherical molecules), whereas it is much greater than 4 for organic compounds which have elongated molecules. What does this tell us about the relative states of order in the liquid and solid phases? How and why is that affected by the molecular shape?
- 6.9** State whether the following systems are (i) stable, (ii) unstable, (iii) in neutral equilibrium, with respect to small departures from the initial state.
- (a) A mixture of ice and water at T_M and p_0 in an environment at T_M and p_0 .
 - (b) The system shown in the photograph of Example 2.5.
 - (c) An alloy sample containing a dispersion of spherical precipitates (all of the same diameter) at a temperature high enough to permit diffusion.

Explain your answer in each case.

Answers

(a) neutral equilibrium; (b) stable; (c) unstable.

Kinetics 1—Diffusive Transformations

7.1 INTRODUCTION

The speed of a structural change is important. Some changes occur in fractions of a second; others are so slow that they become a problem to the engineer only when a component is held at a high temperature for some years. To a geologist, the timescale is even wider: during volcanic eruptions, phase changes (such as the formation of glasses) may occur in seconds; but deep in the Earth's crust other changes (such as the formation of mineral deposits or the growth of large natural diamonds) occur at rates which can be measured in terms of millennia.

Predicting the speed of a structural change is rather like predicting the speed of an automobile. The driving force alone tells us nothing about the speed—it is like knowing the energy content of the petrol. To get at the speed, we need to understand the details of how the petrol is converted into movement by the engine, transmission, and road gear. In other words, we need to know about the *mechanism* of the change.

Structural changes have two types of mechanism: *diffusive* and *displacive*. Diffusive changes require the diffusion of atoms (or molecules) through the material. Displacive changes, on the other hand, involve only the minor “shuffling” of atoms about their original positions and are limited by the propagation of shear waves through the solid at the speed of sound. Most structural changes occur by a diffusive mechanism. But one displacive change is important: the quench hardening of carbon steels is only possible because a displacive transformation occurs during the quench. This chapter and the next concentrate on diffusive transformations; we will look at displacive transformations in Chapter 9.

7.2 SOLIDIFICATION

Most metals are melted or solidified at some stage during their manufacture, and solidification provides an important as well as an interesting example of

a diffusive change. We saw in Chapter 6 that the driving force for solidification was given by

$$W_f = -\Delta G. \quad (7.1)$$

For small $(T_M - T)$, ΔG was found from the relation

$$\Delta G \approx \frac{\Delta H}{T_M} (T_M - T). \quad (7.2)$$

In order to predict the speed of the process, we must find out how quickly individual atoms or molecules diffuse under the influence of this driving force.

We begin by examining the solidification behavior of a rather unlikely material—phenyl salicylate, commonly called “salol.” Although organic compounds like salol are of more interest to chemical engineers, they provide excellent laboratory demonstrations of the processes which underlie solidification. Salol is a colorless, transparent material which melts at about 43 °C. Its solidification behavior can be followed very easily in the following way. First, a thin glass cell is made up by gluing two microscope slides together as shown in Figure 7.1. Salol crystals are put into a shallow glass dish which is heated to about 60 °C on a hot plate. At the same time, the cell is warmed up on the hot plate and is filled with molten salol by putting it into the dish. (Trapped air can be released from the cell by lifting the open end with a pair of tweezers.) The filled cell is taken out of the dish and the contents are frozen by holding the cell under the cold-water tap. The cell is then put on to a temperature-gradient microscope stage (Figure 7.2). The salol above the cold block stays solid, but the solid above the hot block melts. A stationary solid–liquid interface soon forms at the position where $T = T_M$ and can be seen in the microscope.

To get a driving force, the cell is pushed toward the cold block, which cools the interface below T_M . The solid then starts to grow into the liquid

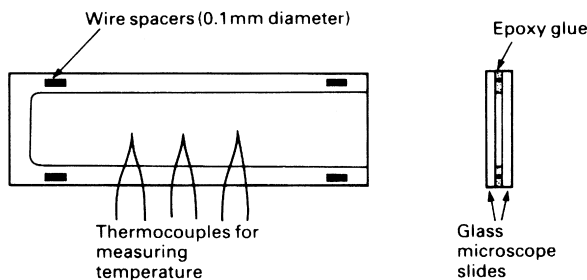


FIGURE 7.1

A glass cell for solidification experiments.

and the growth speed can be measured against a calibrated scale in the microscope eyepiece. When the interface is cooled to 35°C , the speed is about 0.6 mm min^{-1} . At 30°C , the speed is 2.3 mm min^{-1} . And the maximum growth speed, of 3.7 mm min^{-1} , is obtained at an interface temperature of 24°C (Figure 7.3). At still lower temperatures, the speed decreases. Indeed, if the interface is cooled to -30°C , there is hardly any growth at all.

Equation (7.2) shows that the driving force increases almost linearly with decreasing temperature; and we might well expect the growth speed to do the same. The decrease in growth rate below 24°C is therefore quite unexpected; but it can be accounted for perfectly well in terms of the movements of molecules at the solid–liquid interface. We begin by looking at solid and liquid salol in equilibrium at T_M . Then $\Delta G = 0$ from Equation (7.2). In other words, if a molecule is taken from the liquid and added to the solid, then the change in Gibbs free energy, ΔG , is zero (Figure 7.4). However, in order to move from positions in the liquid to positions in the solid, each molecule must first free itself from the attractions of the neighboring liquid molecules: specifically, it must be capable of overcoming the energy barrier q in Figure 7.4. Due to thermal agitation, the molecules vibrate, oscillating about their mean positions with a frequency ν (typically about 10^{13} s^{-1}). The average thermal energy of each molecule is $3kT_M$, where k is Boltzmann's constant. But as the molecules vibrate, they collide and energy

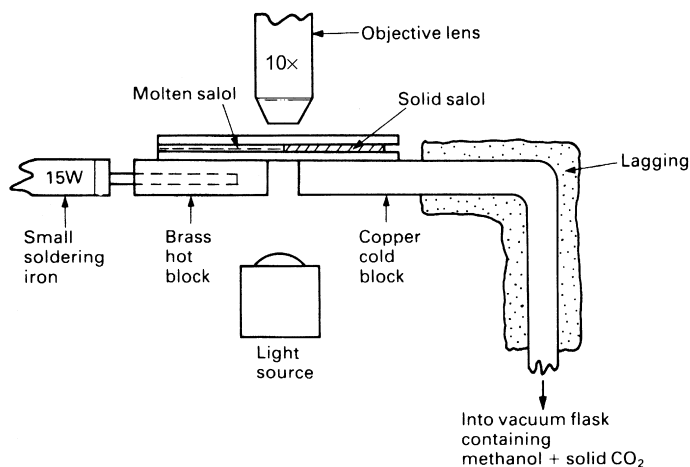
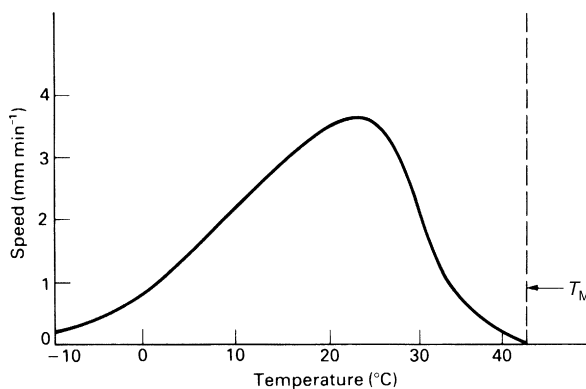
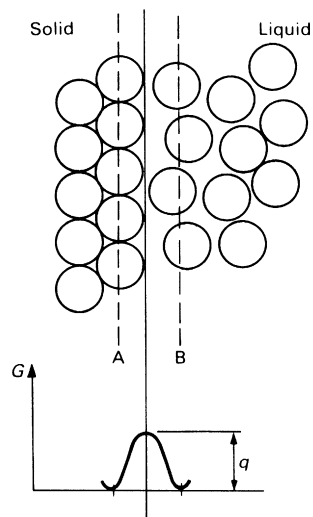


FIGURE 7.2

The solidification of salol can be followed very easily on a temperature-gradient microscope stage. This can be made up from standard laboratory equipment and is mounted on an ordinary transmission light microscope.

**FIGURE 7.3**

The solidification speed of salol at different temperatures.

**FIGURE 7.4**

Solid and liquid in equilibrium at T_M .

is continually transferred from one molecule to another. Thus, at any instant, there is a certain probability that a particular molecule has more or less than the average energy $3kT_M$. Statistical mechanics then shows that the probability, p , that a molecule will, at any instant, have an energy $\geq q$ is

$$p = e^{-q/kT_M}. \quad (7.3)$$

We now apply this result to the layer of liquid molecules immediately next to the solid–liquid interface (layer B in [Figure 7.4](#)). The number of liquid molecules that have enough energy to climb over the energy barrier at any instant is

$$n_B p = n_B e^{-q/kT_M}. \quad (7.4)$$

In order for these molecules to jump from liquid positions to solid positions, they must be moving in the correct direction. The number of times each liquid molecule oscillates toward the solid is $\nu/6$ per second (there are six possible directions in which a molecule can move in three dimensions, only one of which is from liquid to solid). Thus, the number of molecules that jump from liquid to solid per second is

$$\frac{\nu}{6} n_B e^{-q/kT_M}. \quad (7.5)$$

In the same way, the number of molecules that jump in the reverse direction from solid to liquid per second is

$$\frac{\nu}{6} n_A e^{-q/kT_M}. \quad (7.6)$$

The net number of molecules jumping from liquid to solid per second is therefore

$$n_{\text{net}} = \frac{\nu}{6} (n_B - n_A) e^{-q/kT_M}. \quad (7.7)$$

In fact, because $n_B \approx n_A$, n_{net} is zero at T_M , and the solid–liquid interface is in a state of *dynamic equilibrium*.

Let us now cool the interface down to a temperature $T(< T_M)$, producing a driving force for solidification. This will bias the energies of the A and B molecules in the way shown in [Figure 7.5](#). Then the number of molecules jumping from liquid to solid per second is

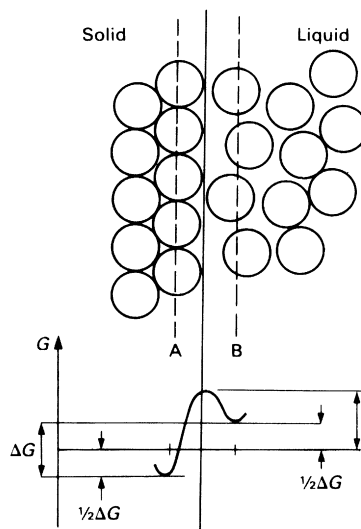
$$\frac{\nu}{6} n_B e^{-\{q+(1/2)\Delta G\}/kT}. \quad (7.8)$$

and the number jumping from solid to liquid is

$$\frac{\nu}{6} n_A e^{-\{q+(1/2)\Delta G\}/kT}. \quad (7.9)$$

The net number jumping from liquid to solid is therefore

$$n_{\text{net}} = \frac{\nu}{6} n_B e^{-\{q-(1/2)\Delta G\}/kT} - \frac{\nu}{6} n_A e^{-\{q+(1/2)\Delta G\}/kT}. \quad (7.10)$$

**FIGURE 7.5**

A solid–liquid interface at temperature T ($< T_M$). ΔG is the free work done when one atom or molecule moves from B to A.

Taking $n_A = n_B = n$ gives

$$n_{\text{net}} = \frac{\nu}{6} n e^{-q/kT} (e^{\Delta G/2kT} - e^{-\Delta G/2kT}). \quad (7.11)$$

Now ΔG is usually much less than $2kT$, so we can use the approximation $e^x \approx 1 + x$ for small x . Equation (7.11) then becomes

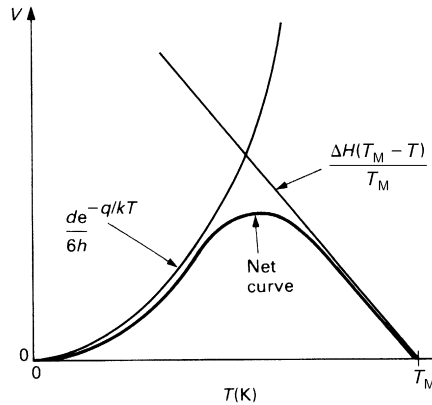
$$n_{\text{net}} = \frac{\nu}{6} n e^{-q/kT} \frac{\Delta G}{kT}. \quad (7.12)$$

Finally, we can replace ΔG by $\Delta H(T_M - T)/T_M$; and the theory of atomic vibrations tells us that $\nu \approx kT/h$, where h is Planck's constant. The equation for n_{net} thus reduces to

$$n_{\text{net}} = \frac{n}{6h} e^{-q/kT} \frac{\Delta H(T_M - T)}{T_M}. \quad (7.13)$$

The distance moved by the solid–liquid interface in 1 s is given by

$$v \approx d \frac{n_{\text{net}}}{n}, \quad (7.14)$$

**FIGURE 7.6**

How the solidification rate should vary with temperature.

where d is the molecular diameter. So the solidification rate is given by

$$v \approx \frac{d}{6h} e^{-q/kT} \frac{\Delta H(T_M - T)}{T_M}. \quad (7.15)$$

This function is plotted out schematically in Figure 7.6. Its shape corresponds well with that of the experimental plot in Figure 7.3. Physically, the solidification rate increases below T_M because the driving force increases as $T_M - T$. But at a low enough temperature, the $e^{-q/kT}$ term starts to become important: there is less thermal energy available to help molecules jump from liquid to solid and the rate begins to decrease. At absolute zero, there is no thermal energy at all; and even though the driving force is enormous, the interface is quite unable to move in response to it.

7.3 HEAT-FLOW EFFECTS

When crystals grow, they give out latent heat. If this is not removed from the interface, then the interface will warm up to T_M and solidification will stop. In practice, latent heat will be removed from the interface by conduction through the solid and convection in the liquid; and the extent to which the interface warms up will depend on how fast heat is generated there, and how fast that heat is removed.

In chemicals like salol, the molecules are elongated (nonspherical) and a lot of energy is needed to rotate the randomly arranged liquid molecules into the specific orientations that they take up in the crystalline solid. Then q is

large, $e^{-q/kT}$ is small, and the interface is very sluggish. There is plenty of time for latent heat to flow away from the interface, and its temperature is hardly affected. The solidification of salol is therefore *interface controlled*: the process is governed almost entirely by the kinetics of molecular diffusion at the interface.

In metals, the situation is quite the opposite. The spherical atoms move easily from liquid to solid and the interface moves quickly in response to very small undercoolings. Latent heat is generated rapidly and the interface is warmed up almost to T_M . The solidification of metals therefore tends to be *heat-flow controlled* rather than interface controlled.

In spite of this dominance of heat flow, the solidification speed of pure metals still obeys Equation (7.15) and depends on temperature as shown in Figure 7.6. But measurements of $v(T)$ are almost impossible for metals. When the undercooling at the interface is big enough to measure easily ($T_M - T \approx 1^\circ\text{C}$), then the velocity of the interface is so large (as much as 1 ms^{-1}) that one does not have enough time to measure its temperature. However, as we shall see later, the kinetics of Equation (7.15) have allowed the development of a range of *glassy metals* with new and exciting properties.

7.4 SOLID-STATE PHASE CHANGES

We can use the same sort of approach to look at phase changes in solids, like the α – γ transformation in iron. Then, as we saw in Chapter 6, the driving force is given by

$$\Delta G \approx \frac{\Delta H}{T_e}(T_e - T). \quad (7.16)$$

And the speed with which the α – γ interface moves is given by

$$v \approx \frac{d}{6h} e^{-q/kT} \frac{\Delta H(T_e - T)}{T_e} \quad (7.17)$$

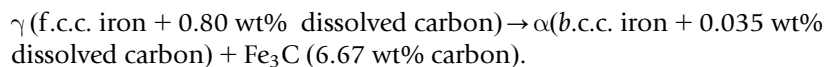
where q is the energy barrier at the α – γ interface and ΔH is the latent heat of the α – γ phase change.

7.5 DIFFUSION-CONTROLLED KINETICS

Most metals in commercial use contain quite large quantities of impurity (e.g., as alloying elements or in contaminated scrap). Solid-state transformations in

impure metals are usually limited by the diffusion of these impurities through the bulk of the material.

We can find a good example of this *diffusion-controlled* growth in plain carbon steels. As we saw in Chapter 4, when steel is cooled below 723 °C, there is a driving force for the eutectoid reaction of



Provided the driving force is not too large, the α and Fe_3C grow alongside one another to give the layered structure called “pearlite” (Figure 7.7). Because the α contains 0.765 wt% carbon less than the γ , it must reject this excess carbon into the γ as it grows. The rejected carbon is then transferred to the $\text{Fe}_3\text{C} - \gamma$ interface, providing the extra 5.87 wt% carbon that the Fe_3C needs to grow. The transformation is controlled by the rate at which the carbon atoms can diffuse through the γ from α to Fe_3C ; and the driving

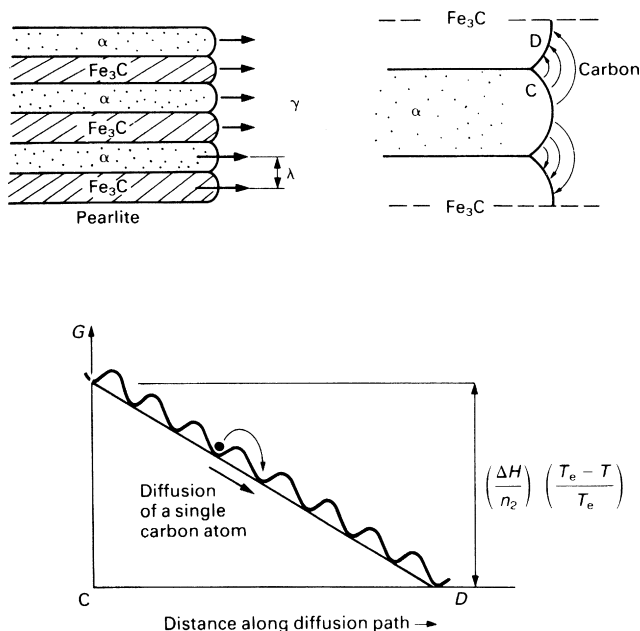


FIGURE 7.7

How pearlite grows from undercooled γ during the eutectoid reaction. The transformation is limited by diffusion of carbon in the γ and driving force must be shared between all the diffusional energy barriers. Note that ΔH is in units of J kg^{-1} ; n_2 is the number of carbon atoms that diffuse from α to Fe_3C when 1 kg of γ is transformed. $(\Delta H/n_2)((T_e - T)/T_e)$ is therefore the free work done when a *single* carbon atom goes from α to Fe_3C .

force must be shared between all the energy barriers crossed by the diffusing carbon atoms (see Figure 7.7).

The driving force applied across any one energy barrier is thus

$$\left(\frac{1}{n_1}\right)\left(\frac{\Delta H}{n_2}\right)\left(\frac{T_e - T}{T_e}\right)$$

where n_1 is the number of barriers crossed by a typical carbon atom when it diffuses from α to Fe_3C . The speed at which the pearlite grows is then given by

$$v \propto e^{-q/kT} \frac{\Delta H(T_e - T)}{n_1 n_2 T_e}, \quad (7.18)$$

which has the same form as Equation (7.15).

7.6 SHAPES OF GRAINS AND PHASES

We saw in Chapter 2 that when boundary energies were the dominant factor, we could easily predict the shapes of the grains or phases in a material. Isotropic energies gave tetrakaidecahedral grains and spherical (or lens shaped) second-phase particles. Now boundary energies can only dominate when the material has been allowed to come quite close to equilibrium. If a structural change is taking place, the material will *not* be close to equilibrium and the mechanism of the transformation will affect the shapes of the phases produced.

The eutectoid reaction in steel is a good example of this. If we look at the layered structure of pearlite, we can see that the flat Fe_3C – α interfaces contain a large amount of boundary energy. The total boundary energy in the steel would be much less if the Fe_3C were accommodated as spheres of Fe_3C rather than extended plates (a sphere gives the minimum surface-to-volume ratio). The high energy of pearlite is “paid for” because it allows the eutectoid reaction to go much more quickly than it would if spherical phases were involved. Specifically, the “cooperative” growth of the Fe_3C and α plates shown in Figure 7.7 gives a small diffusion distance CD; and, because the transformation is diffusion limited, this gives a high growth speed. Even more fascinating is the fact that the bigger the driving force, the finer is the structure of the pearlite (i.e., the smaller is the *interlamellar spacing* λ —see Figure 7.7). The smaller diffusion distance allows the speed of the reaction to keep pace with the bigger driving force; and this pays for the still higher boundary energy of the structure (as $\lambda \rightarrow 0$ the total boundary energy $\rightarrow \infty$).

We can see very similar effects during solidification. You may have noticed long rod-shaped crystals of ice growing on the surface of a puddle of water during the winter. These crystals often have side branches as well and are therefore called “dendrites” after the Greek word meaning “tree.” Nearly all metals solidify with a dendritic structure (Figure 7.8), as do some organic compounds. Although a dendritic shape gives a large surface-to-volume ratio, it also encourages latent heat to flow away from the solid–liquid interface (for the same sort of reason that your hands lose heat much more rapidly if you wear gloves than if you wear mittens). And the faster solidification that we get as a consequence “pays for” the high boundary energy. Large driving forces produce fine dendrites—which explains why one can hardly see the dendrites in an iced lollipop grown in a freezer (-10°C); but they are obvious on a freezing pond (-1°C).

To summarize, the shapes of the grains and phases produced during transformations reflect a balance between the need to minimize the total boundary energy and the need to maximize the speed of transformation. Close to equilibrium, when the driving force for the transformation is small, the grains and phases are primarily shaped by the boundary energies.

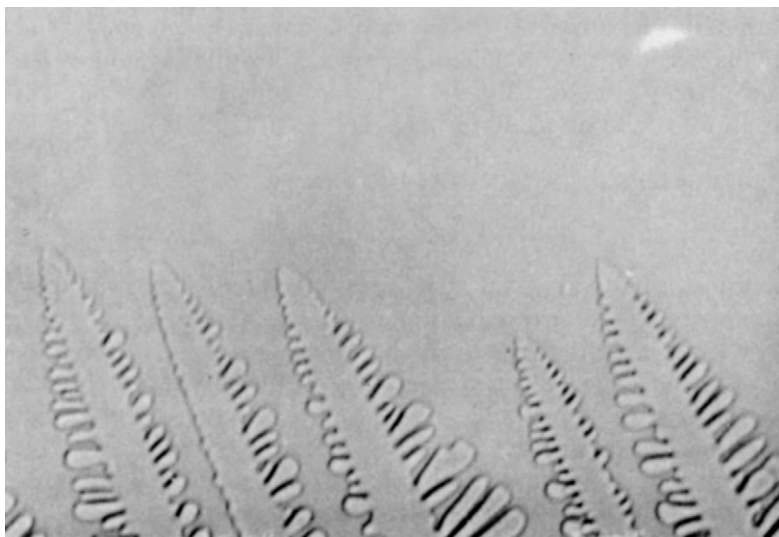


FIGURE 7.8

Most metals solidify with a dendritic structure. It is hard to see dendrites growing in metals but they can be seen very easily in transparent organic compounds like camphene which—because they have spherical molecules—solidify just like metals.

Far from equilibrium, when the driving force for the transformation is large, the structure depends strongly on the *mechanism* of the transformation. Further, even the *scale* of the structure depends on the driving force—the larger the driving force the finer the structure.

WORKED EXAMPLE

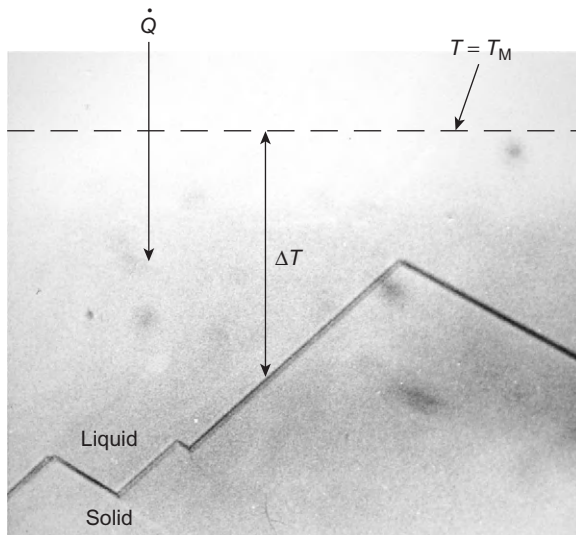
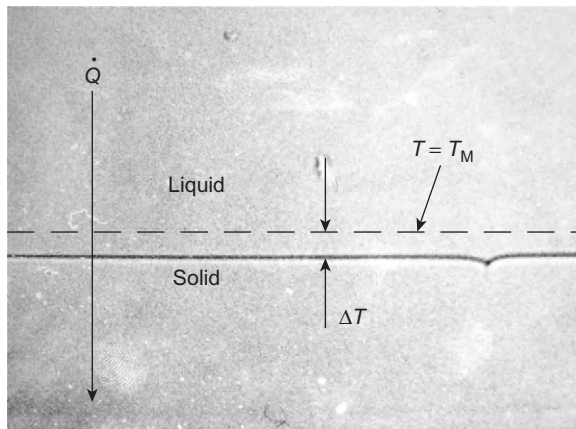
The first photograph (magnification $\times 120$) shows a sample of camphene solidifying in the set-up of Figure 7.2 (except the cold block is cooled with iced water). The glass cell is being moved slowly toward the cold block, so the solid–liquid interface appears stationary in the microscope (although the solid phase is growing). The position of the equilibrium melting temperature isotherm T_M is shown schematically, as is the undercooling $\Delta T \equiv T_M - T$ needed to drive the solidification process. The value of ΔT is extremely small, because camphene (chemical formula $C_{10}H_{16}$) has molecules which are essentially spherical—the three-dimensional structure is shown in: <http://en.wikipedia.org/wiki/Camphene>. The spherical molecules move easily from liquid to solid, and can attach themselves to the solid anywhere on the interface. That is why the interface is located everywhere at the solidification isotherm T . The molecular-scale structure at the interface is as shown in Figure 7.5 (except solid camphene has a b.c.c. structure).

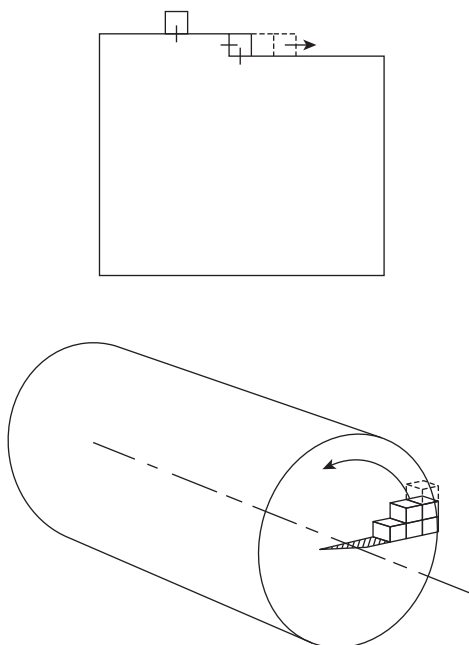
The second photograph (magnification $\times 120$) shows a sample of salol solidifying in the set-up of Figure 7.2. The value of ΔT is now large, because salol (chemical formula $C_{13}H_{10}O_3$) has molecules which are elongated—the three-dimensional structure is shown in: http://en.wikipedia.org/wiki/Phenyl_salicylate. It is difficult for the elongated molecules to move from liquid to solid, and they have to attach themselves to a small number of preferential sites on the interface. That is why the interface is not located at an isotherm—in fact, the interface consists of a number of crystallographic planes (or “growth facets”), and the undercooling ΔT varies considerably from place to place. The molecular-scale structure at the interface is significantly different to that shown in Figure 7.5.

As shown in the diagram, the surface step at the edge of a crystal plane is a good place for attracting an atom from the liquid. The liquid atom is guided into the right position (and orientation) by the geometry of the step. Essentially, the energy barrier q is much less when a liquid atom is attached to a step than when it is attached to a flat surface. (You can imagine that the liquid atom is pulled into position by the atomic bonds at the edge of the step *in addition* to those in the main surface—in other words, having a step

effectively *doubles* the number of atomic bonds which can attract a liquid atom.)

However, the problem with simple surface steps is that they rapidly grow to the edge of the crystal, which gets rid of the step! In order for growth to continue, it is necessary to have a self-renewing source of surface steps. A famous paper published in 1951 by Burton, Cabrera, and Frank gave the answer—screw dislocations in the crystal (see EM1Ed4, p. 141, Figure 9.7). The diagram shows how a screw dislocation provides an “eternal” step, and this allows the crystal to keep on growing as long the growing facet intersects one or more screw dislocations.





EXAMPLES

- 7.1** The solidification speed of salol is about 2.3 mm min^{-1} at 10°C . Using Equation (7.15), estimate the energy barrier q that must be crossed by molecules moving from liquid sites to solid sites. The melting point of salol is 43°C and its latent heat of fusion is $3.2 \times 10^{-20} \text{ J mol}^{-1}$. Assume that the molecular diameter is about 1 nm .

Answer

$6.61 \times 10^{-20} \text{ J}$, equivalent to 39.8 kJ mol^{-1} .

- 7.2** Glass ceramics are a new class of high-technology crystalline ceramic. They are made by taking complex amorphous glasses (like $\text{SiO}_2\text{--Al}_2\text{O}_3\text{--Li}_2\text{O}$) and making them devitrify (crystallize). For a particular glass, it is found that: (a) no devitrification occurs above a temperature of 1000°C ; (b) the rate of devitrification is a maximum at 950°C ; (c) the rate of devitrification is negligible below 700°C . Give reasons for this behavior.
- 7.3** Samples cut from a length of work-hardened mild steel tube were annealed for various times at three different temperatures. The samples were then cooled to room temperature and tested for hardness. The results are given below.

Annealing Temperature (°C)	Vickers Hardness	Time at Annealing Temperature (min)
600	180	0
	160	10
	135	20
	115	30
	115	60
620	180	0
	160	4
	135	9
	115	13
	115	26
645	180	0
	160	1.5
	135	3.5
	115	5
	115	10

Estimate the time that it takes for recrystallization to be completed at each of the three temperatures.

Estimate the time that it would take for recrystallization to be completed at an annealing temperature of 700 °C. Because the new strain-free grains grow by diffusion, you may assume that the rate of recrystallization follows Arrhenius' law, that is, the *time* for recrystallization, t_r , is given by

$$t_r = Ae^{Q/RT},$$

where A is a constant, Q is the activation energy for self-diffusion in the ferrite lattice, R is the gas constant, and T is the temperature in kelvin.

Answers

30, 13, 5 min, respectively; 0.8 min.

7.4 Explain the following:

- (a) metals usually solidify by the growth of dendrites into the liquid;
- (b) the dimensions and spacing of the dendrites decrease as the growth rate increases.

7.5 Explain the following:

- (a) the eutectoid reaction in steel produces pearlite, even though this increases the interfacial energy per unit volume;
- (b) the dimensions and spacing of the plates in pearlite decrease as the growth rate increases.

7.6 A thin glass cell (like the one shown in [Figure 7.1](#), but without any thermocouples) is filled with melted yellow sulfur ("flowers of sulfur"). The cell is then transferred to the glass plate of an overhead projector (OHP) and allowed

to cool naturally. The image of the cell and its contents are projected onto the OHP screen so they can be seen at large magnification. Sulfur crystals soon form and grow rapidly into the liquid. The edges of the growing crystals can be seen clearly on the screen. As growth progresses, however, the rate of solidification decreases noticeably. Explain this observation.

- 7.7 Explain why materials with spherical atoms or molecules (like most metals or organic compounds like camphene) solidify by the transfer of atoms/molecules from the liquid state to random atomic/molecular sites on the surface of the growing crystal. How does this growth mechanism govern the shape of the solid–liquid interface?
- 7.8 Explain why materials with nonspherical molecules (e.g., organic compounds like salol) solidify by the transfer of molecules from the liquid state to molecular sites at steps on the surface of the growing crystal. How does this growth mechanism govern the shape of the solid–liquid interface?
- 7.9 Explain how screw dislocations can provide an “eternal” source of steps for crystal growth in materials with nonspherical molecules. How should the growth rate depend on the density of such dislocations?
- 7.10 For a material which solidifies from steps (i.e., shows faceted growth), why is the rate of *melting* of an isolated crystal usually faster (by several orders of magnitude) than the rate of *solidification* for the same $|\Delta T|$?

Kinetics 2—Nucleation

8.1 INTRODUCTION

We saw in Chapter 7 that diffusive transformations (like the growth of metal crystals from the liquid during solidification or the growth of one solid phase from another during a polymorphic change) involve a mechanism in which atoms are attached to the surfaces of the growing crystals. This means that diffusive transformations can only take place if crystals of the new phase are already present. But how do these crystals—or *nuclei*—form in the first place?

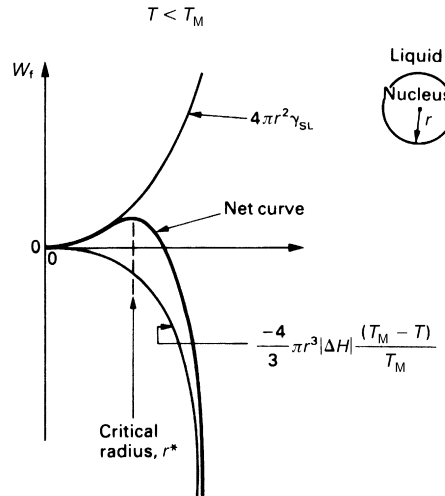
8.2 NUCLEATION IN LIQUIDS

We begin by looking at how crystals nucleate in liquids. Because of thermal agitation the atoms in the liquid are in a state of continual movement. From time to time a small group of atoms will, purely by chance, come together to form a tiny crystal. If the liquid is above T_M the crystal will, after a very short time, shake itself apart again. But if the liquid is below T_M , there is a chance that the crystal will be thermodynamically stable and will continue to grow. How do we calculate the probability of finding stable nuclei below T_M ?

There are two work terms to consider when a nucleus forms from the liquid. Equations (7.1) and (7.2) show that work of the type $|\Delta H|(T_M - T)/T_M$ is available to help the nucleus form. If ΔH is expressed as the latent heat given out when *unit volume* of the solid forms, then the total available energy is $(4/3)\pi r^3 |\Delta H|(T_M - T)/T_M$. But this is offset by the work $4\pi r^2 \gamma_{SL}$ needed to create the solid–liquid interface around the crystal. The net work needed to form the crystal is then

$$W_f = 4\pi r^2 \gamma_{SL} - \frac{4}{3}\pi r^3 |\Delta H| \frac{(T_M - T)}{T_M}. \quad (8.1)$$

This result has been plotted out in [Figure 8.1](#). It shows that there is a maximum value for W_f corresponding to a critical radius r^* . For $r < r^*$, (dW_f/dr)

**FIGURE 8.1**

The work needed to make a spherical nucleus.

is positive, whereas for $r > r^*$ it is negative. This means that if a random fluctuation produces a nucleus of size $r < r^*$, it will be unstable: the system can do free work if the nucleus loses atoms and r decreases. The opposite is true when a fluctuation gives a nucleus with $r > r^*$. Then, free work is done when the nucleus *gains* atoms, and it will tend to grow. To summarize, if random fluctuations in the liquid give crystals with $r > r^*$, then stable nuclei will form and solidification can begin.

To calculate r^* , we differentiate Equation (8.1) to give

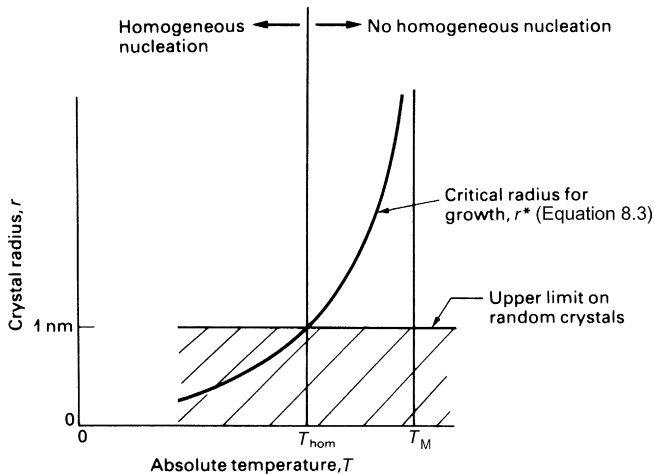
$$\frac{dW_f}{dr} = 8\pi r \gamma_{SL} - 4\pi r^2 |\Delta H| \frac{(T_M - T)}{T_M}. \quad (8.2)$$

We can then use the condition that $dW_f/dr = 0$ at $r = r^*$ to give

$$r^* = \frac{2\gamma_{SL}T_M}{|\Delta H|(T_M - T)} \quad (8.3)$$

for the critical radius.

We are now in a position to go back and look at what is happening in the liquid in more detail. As we said earlier, small groups of liquid atoms are continually shaking themselves together to make tiny crystals which, after a short life, shake themselves apart again. There is a high probability of finding small crystals, but a small probability of finding large crystals. And the probability of finding crystals containing more than 10^2 atoms ($r \gtrsim 1$ nm) is negligible. As Figure 8.2 shows, we can estimate the temperature T_{hom} at which nucleation will first occur by setting $r^* = 1$ nm in Equation (8.3).

**FIGURE 8.2**

Homogeneous nucleation will take place when the random crystals can grow, i.e., when $r > r^*$.

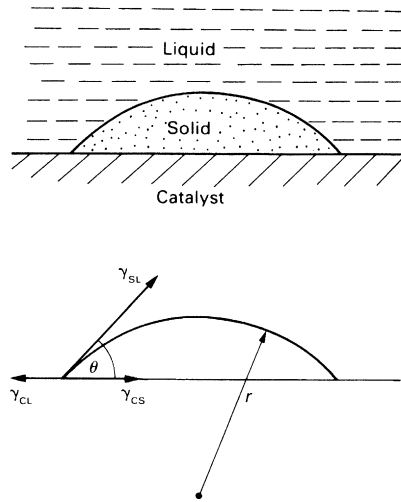
For typical values of γ_{SL} , T_M , and ΔH , we then find that $T_M - T_{\text{hom}} \approx 100 \text{ K}$, so a large undercooling is needed to make nucleation happen.

This sort of nucleation—where the only atoms involved are those of the material itself—is called *homogeneous nucleation*. It cannot be the way materials usually solidify because often an undercooling of 1°C or even less is all that is needed. Homogeneous nucleation has been observed in ultra-clean laboratory samples. But it is the exception, not the rule.

8.3 HETEROGENEOUS NUCLEATION

Normally, when a pond of water freezes over or when a metal casting starts to solidify, nucleation occurs at a temperature only a few degrees below T_M . How do we explain this easy nucleation? Well, liquids like pond water or foundry melts inevitably contain solid particles of dirt. These act as catalysts for nucleation: they give a random crystal a “foothold,” and allow it to grow more easily. It is this *heterogeneous* nucleation which is responsible for solidification in all practical materials situations.

Heterogeneous nucleation is most likely to occur when there is a strong tendency for the crystal to stick to the surface of the catalyst. This sticking tendency can be described by the angle of contact, θ , shown in Figure 8.3: the smaller θ , the better the adhesion. Anyone who has tried to get electronic solder to stick to a strip of copper will understand this well. If the copper is tarnished, the solder will just roll around as a

**FIGURE 8.3**

Heterogeneous nucleation takes place on the surface of a solid catalyst. For the catalyst to be effective, there must be a strong tendency for it to be “wetted” by the crystal, i.e., θ must be small.

molten blob with $\theta = 180^\circ$ and will not stick to the surface at all. If the tarnished copper is fluxed, then θ may decrease to 90° : the molten solder will stay put on the copper but it will not spread. Only when the copper is both clean and fluxed will θ be zero, allowing the solder to “wet” the copper.

If we know the contact angle, we can work out r^* quite easily. We assume that the nucleus is a spherical cap of radius r and use standard mathematical formulae for the area of the solid–liquid interface, the area of the catalyst–solid interface, and the volume of the nucleus. For $0 \leq \theta \leq 90^\circ$, these are:

$$\text{solid – liquid area} = 2\pi r^2(1 - \cos \theta); \quad (8.4)$$

$$\text{catalyst – solid area} = \pi r^2(1 - \cos^2 \theta); \quad (8.5)$$

$$\text{nucleus volume} = \frac{2\pi r^3}{3} \left\{ 1 - \frac{3}{2} \cos \theta + \frac{1}{2} \cos^3 \theta \right\}. \quad (8.6)$$

Then, by analogy with Equation (8.1), we can write

$$W_f = 2\pi r^2(1 - \cos \theta)\gamma_{SL} + \pi r^2(1 - \cos^2 \theta)\gamma_{CS} - \pi r^2(1 - \cos^2 \theta)\gamma_{CL} - \frac{2\pi r^3}{3} \left\{ 1 - \frac{3}{2} \cos \theta + \frac{1}{2} \cos^3 \theta \right\} |\Delta H| \frac{(T_M - T)}{T_M}. \quad (8.7)$$

Note that this equation has two energy terms that did not appear in Equation (8.1). The first, $\pi r^2(1 - \cos^2 \theta)\gamma_{CS}$, is the energy needed to create the new interface between the catalyst and the solid. The second, $-\pi r^2(1 - \cos^2 \theta)\gamma_{CL}$, is the energy released because the area of the catalyst–liquid interface is smaller after nucleation than it was before.

As it stands, Equation (8.7) contains too many unknowns. But there is one additional piece of information that we can use. The interfacial energies, γ_{SL} , γ_{CS} , and γ_{CL} act as surface tensions in just the way that a soap film has both a surface energy and a surface tension. This means that the mechanical equilibrium around the edge of the nucleus can be described by the triangle of forces

$$\gamma_{CL} = \gamma_{CS} + \gamma_{SL} \cos \theta. \quad (8.8)$$

If we substitute this result into Equation (8.7), the interfacial energy terms reduce to

$$2\pi r^2(1 - \cos \theta)\gamma_{SL} + \pi r^2(1 - \cos^2 \theta)(-\gamma_{SL} \cos \theta),$$

or

$$2\pi r^2 \left\{ 1 - \frac{3}{2} \cos \theta + \frac{1}{2} \cos^3 \theta \right\} \gamma_{SL}. \quad (8.9)$$

The complete result for W_f then becomes

$$W_f = \left\{ 1 - \frac{3}{2} \cos \theta + \frac{1}{2} \cos^3 \theta \right\} \left\{ 2\pi r^2 \gamma_{SL} - \frac{2\pi r^3}{3} |\Delta H| \frac{(T_M - T)}{T_M} \right\}. \quad (8.10)$$

Finally, if we use the condition that $dW_f/dr = 0$ at $r = r^*$, we get

$$r^* = \frac{2\gamma_{SL}T_M}{|\Delta H|(T_M - T)} \quad (8.11)$$

for the critical radius in heterogeneous nucleation.

If we compare Equations (8.11) and (8.3), we see that the expressions for the critical radius are identical for both homogeneous and heterogeneous nucleation. But the expressions for the *volume* of the critical nucleus are not. For homogeneous nucleation, the critical volume is

$$V_{\text{hom}}^* = \frac{4}{3} \pi (r_{\text{hom}}^*)^3 \quad (8.12)$$

whereas for heterogeneous nucleation it is

$$V_{\text{het}}^* = \frac{2}{3} \pi (r_{\text{het}}^*)^3 \left\{ 1 - \frac{3}{2} \cos \theta + \frac{1}{2} \cos^3 \theta \right\}. \quad (8.13)$$

The maximum statistical fluctuation of 10^2 atoms is the same in both homogeneous and heterogeneous nucleation. If Ω is the volume occupied by one atom in the nucleus, then we can easily see that

$$V_{\text{hom}}^* = 10^2 \Omega = V_{\text{het}}^*. \quad (8.14)$$

Equating the right-hand terms of Equations (8.12) and (8.13), then tells us that

$$r_{\text{het}}^* = \frac{r_{\text{hom}}^*}{\left(\frac{1}{2} \left\{ 1 - \frac{3}{2} \cos \theta + \frac{1}{2} \cos^3 \theta \right\}\right)^{1/3}}. \quad (8.15)$$

If the nucleus wets the catalyst well, with $\theta = 10^\circ$, say, then Equation (8.15) tells us that $r_{\text{het}}^* = 18 r_{\text{hom}}^*$. In other words, if we arrange our 10^2 atoms as a spherical cap on a good catalyst, we get a much bigger crystal radius than if we arrange them as a sphere. And, as Figure 8.4 explains, this means that heterogeneous nucleation always “wins” over homogeneous nucleation.

It is easy to estimate the undercooling that we would need to get heterogeneous nucleation with a 10° contact angle. From Equations (8.11) and (8.3), we have

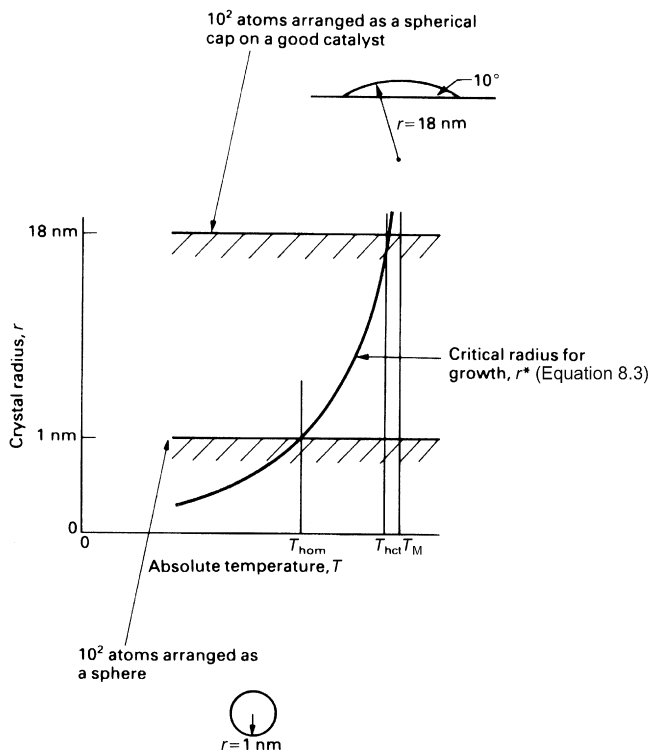
$$\frac{2\gamma_{\text{SL}} T_{\text{M}}}{|\Delta H|(T_{\text{M}} - T_{\text{het}})} = 18 \times \frac{2\gamma_{\text{SL}} T_{\text{M}}}{|\Delta H|(T_{\text{M}} - T_{\text{hom}})}, \quad (8.16)$$

which gives

$$T_{\text{M}} - T_{\text{het}} = \frac{T_{\text{M}} - T_{\text{hom}}}{18} \approx \frac{10^2 \text{ K}}{18} \approx 5 \text{ K}. \quad (8.17)$$

It is nice to see that this result is consistent with the small undercoolings that we often see in practice.

You can observe heterogeneous nucleation easily in carbonated drinks like “fizzy” lemonade. These contain carbon dioxide which is dissolved in the drink under pressure. When a new bottle is opened, the pressure on the liquid immediately drops to that of the atmosphere. The liquid becomes supersaturated with gas, and a driving force exists for the gas to come out of solution in the form of bubbles. The materials used for lemonade bottles—glass or plastic—are poor catalysts for the heterogeneous nucleation of gas bubbles and are usually very clean, so you can swallow the drink before it loses its “fizz.” But ordinary board chalk (for example) is an

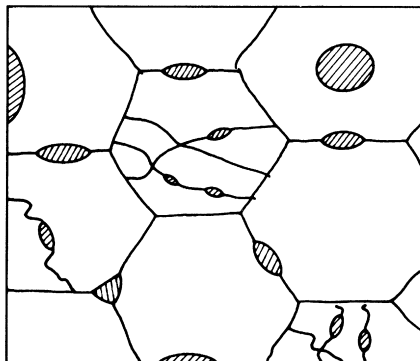
**FIGURE 8.4**

Heterogeneous nucleation takes place at higher temperatures because the maximum random fluctuation of 10^2 atoms gives a bigger crystal radius if the atoms are arranged as a spherical cap.

excellent former of bubbles. If you drop such a catalyst into a newly opened bottle of carbonated beverage, spectacular heterogeneous nucleation ensues. Chalk makes lemonade fizz.

8.4 NUCLEATION IN SOLIDS

Nucleation in solids is very similar to nucleation in liquids. Because solids usually contain high-energy defects (like dislocations, grain boundaries, interphase interfaces, and free surfaces) new phases usually nucleate heterogeneously; homogeneous nucleation, which occurs in defect-free regions, requires a large undercooling. Figure 8.5 summarizes the various ways in which heterogeneous nucleation can take place in a typical polycrystalline solid; and Examples 8.2 and 8.3 illustrate how nucleation theory can be applied to a solid-state situation.

**FIGURE 8.5**

Nucleation in solids. Heterogeneous nucleation can take place at defects like dislocations, grain boundaries, interphase interfaces, and free surfaces. Homogeneous nucleation in defect-free regions requires a large undercooling, $T_M - T$.

8.5 SUMMARY

In this chapter, we have shown that diffusive transformations can only take place if *nuclei* of the new phase can form to begin with. Nuclei form because random atomic vibrations are continually making tiny crystals of the new phase; and if the temperature is low enough these tiny crystals are thermodynamically stable and will grow. In *homogeneous* nucleation, the nuclei form as spheres within the bulk of the material. In *heterogeneous* nucleation, the nuclei form as spherical caps on defects like solid surfaces, grain boundaries, interphase interfaces, or dislocations. Heterogeneous nucleation occurs at much smaller undercoolings than homogeneous nucleation because the defects give the new crystal a good “foothold.” Homogeneous nucleation is unusual because materials almost always contain defects.

8.6 NUCLEATION EVERYWHERE

Nucleation—of one sort or another—crops up almost everywhere. During winter, plants die and people get frostbitten because ice nucleates heterogeneously inside cells. But many plants have adapted themselves to prevent heterogeneous nucleation; they can survive down to the homogeneous nucleation temperature of -40°C . The “contrails” left by aircraft consist of tiny droplets of water that have nucleated and grown from the water vapor produced by combustion. Subatomic particles can be tracked during high-energy physics experiments by firing them through superheated liquid in a “bubble chamber”: the particles trigger the nucleation of gas bubbles which show where the particles have been. And the food industry is plagued by

nucleation problems. Sucrose (sugar) has a big molecule and it is difficult to get it to crystallize from aqueous solutions. That is fine if you want to make caramel—this clear, brown, tooth-breaking substance is just amorphous sucrose. But the sugar refiners have big problems making granulated sugar and will go to great lengths to get adequate nucleation in their sugar solutions. We give examples of how nucleation applies specifically to materials in a set of case studies on phase transformations in Chapter 10.

WORKED EXAMPLE

We saw in [Section 8.2](#) that the critical radius for homogeneous nucleation in an undercooled liquid was given by

$$r^* = \frac{2\gamma_{\text{SL}}T_{\text{M}}}{|\Delta H|(T_{\text{M}} - T)}.$$

When the radius of the nucleus is equal to r^* , it is in equilibrium with the surrounding liquid. However, this is an unstable equilibrium (see Figure 6.3). If the nucleus loses just one or two atoms, $r < r^*$, and it will continue to melt away until it vanishes. If the nucleus gains just one or two atoms, $r > r^*$, and it will continue to grow until it runs out of undercooled liquid.

We can cross-multiply the equation to show the equilibrium temperature when a solid sphere of radius r is in contact with its own liquid.

$$T_{\text{M}} - T_r \equiv \Delta T = \frac{T_{\text{M}}}{|\Delta H|} \times \frac{2\gamma_{\text{SL}}}{r}.$$

Because this equation is derived from first principles using thermodynamics, it can be applied to any size of sphere from a cluster of atoms large enough to define the crystal structure (and the structure of the solid–liquid interface) up to say 1 mm—at which point the use of the equation is limited by the accuracy of temperature measurement. The table gives representative values of ΔT and r over this range *for the ice–water system* as an example.

Now there are some geometries for a convex solid–liquid interface which *are* stable with respect to changes in r . You have already seen one in Chapter 2, Example 2.5. The photograph from Example 2.5 is given again here. The main solid–liquid interface in the sample of camphene is planar, but where it curves down to meet the grain boundary it develops a decreasing radius of curvature r (in one dimension, not two as in a sphere). Because the sample is subjected to a temperature gradient parallel to the grain

boundary, the liquid in the groove is undercooled, and this compensates for the convex curvature of the solid–liquid interface.

Data for ice–water

ΔT (°C)	r
40 (homogeneous nucleation of ice in water)	1 nm
5	10 nm
1	50 nm
10^{-1}	$0.5\ \mu\text{m}$
10^{-2}	$5\ \mu\text{m}$
10^{-3}	$50\ \mu\text{m}$
10^{-4}	$0.5\ \text{mm}$

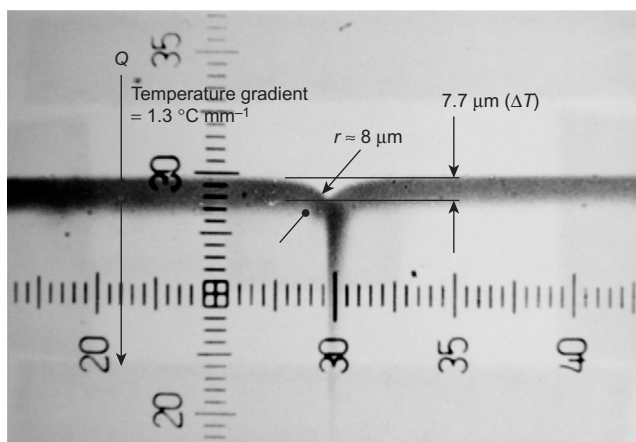
In fact, this is the standard method for measuring solid–liquid interfacial energies. In the case of the photograph, the temperature gradient is $1.3\ ^\circ\text{C mm}^{-1}$, so $\Delta T = 1.3\ ^\circ\text{C mm}^{-1} \times 7.7 \times 10^{-3}\ \text{mm} = 10 \times 10^{-3}\ ^\circ\text{C}$. The radius of curvature at the bottom of the groove, $r \approx 8\ \mu\text{m}$. For camphene, $|\Delta H|/T_M = 61\ \text{kJ m}^{-3}\ \text{K}^{-1}$. Putting numbers in the equation then gives

$$10 \times 10^{-3}\ \text{K} \approx \frac{1}{61\ \text{kJ m}^{-3}\ \text{K}^{-1}} \times \frac{\gamma_{\text{SL}}}{8 \times 10^{-6}\ \text{m}}.$$

Note that because the interface is only curved in one dimension, there is no factor of 2 in front of γ_{SL} . The equation gives

$$\gamma_{\text{SL}} \approx 10 \times 10^{-3}\ \text{K} \times 61\ \text{kJ m}^{-3}\ \text{K}^{-1} \times 8 \times 10^{-6}\ \text{m} \approx 5\ \text{mJ m}^{-2},$$

which is very close to the value obtained from more accurate and extensive experiments.



EXAMPLES

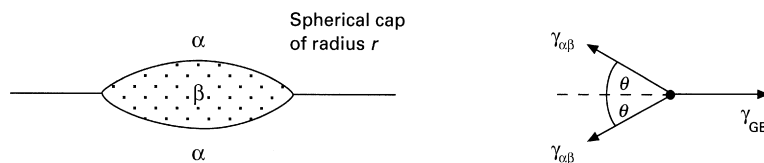
- 8.1** The temperature at which ice nuclei form homogeneously from undercooled water is $-40\text{ }^{\circ}\text{C}$. Find r^* given that $\gamma_i = 25\text{ mJ m}^{-2}$, $|\Delta H| = 335\text{ kJ kg}^{-1}$, and $T_M = 273\text{ K}$. Estimate the number of H_2O molecules needed to make a critical-sized nucleus. Why do ponds freeze over when the temperature falls below $0\text{ }^{\circ}\text{C}$ by only a few degrees?

(The density of ice is 0.92 Mg m^{-3} . The atomic weights of hydrogen and oxygen are 1.01 and 16.00, respectively.)

Answers

$r^* = 1.11\text{ nm}$; 176 molecules.

- 8.2** An alloy is cooled from a temperature at which it has a single-phase structure (α) to a temperature at which the equilibrium structure is two-phase ($\alpha + \beta$). During cooling, small precipitates of the β phase nucleate heterogeneously at α grain boundaries. The nuclei are lens shaped as shown below.



Show that the free work needed to produce a nucleus is given by

$$W_i = \left\{ 1 - \frac{3}{2} \cos \theta + \frac{1}{2} \cos^3 \theta \right\} \left\{ 4\pi r^2 \gamma_{\alpha\beta} - \frac{4}{3} \pi r^3 |\Delta G| \right\}$$

where $|\Delta G|$ is the free work produced when unit volume of β forms from α . You may assume that mechanical equilibrium at the edge of the lens requires that

$$\gamma_{GB} = 2\gamma_{\alpha\beta} \cos \theta.$$

Hence, show that the critical radius is given by

$$r^* = 2\gamma_{\alpha\beta} / |\Delta G|.$$

- 8.3** Pure titanium is cooled from a temperature at which the b.c.c. phase is stable to a temperature at which the c.p.h. phase is stable. As a result, lens-shaped nuclei of the c.p.h. phase form at the grain boundaries. Estimate the number of atoms needed to make a critical-sized nucleus given the following data:
 $\Delta H = 3.48\text{ kJ mol}^{-1}$; atomic weight = 47.90; $T_e - T = 30\text{ K}$; $T_e = 882\text{ }^{\circ}\text{C}$;
 $\gamma = 0.1\text{ J m}^{-2}$; density of the c.p.h. phase = 4.5 Mg m^{-3} ; $\theta = 5^{\circ}$.

Answer

67 atoms.

- 8.4** Adapt Equations (8.1), (8.2), and (8.3) to give the equation for the equilibrium undercooling $\Delta T = T_M - T_r$ for a *cylindrical* crystal of radius r in contact with its own liquid. Hence, verify that your equation does not have the factor of 2 in front of γ_{SL} . (A cylindrical crystal cannot form during homogeneous nucleation, but it *is* the correct representation for the one-dimensional curvature of the solid–liquid interface at a grain-boundary groove—see the Worked Example.)
- 8.5** A classic set of experiments on homogeneous nucleation was published by the brilliant scientist David Turnbull (GE R&D Labs, NY) in 1952. Turnbull used mercury ($T_M = 234.33 \text{ K}$, -38.87°C) as the sample material. 5 cm^3 of liquid Hg was mixed with 150 cm^3 of silicone oil using a food blender (“health and safety” would not like that these days!), which broke the Hg up into a large number of isolated droplets having a mean diameter of $3.27 \mu\text{m}$. The sample was then quenched to various temperatures below T_M , and the solidification of the liquid Hg droplets was followed over time by measuring the contraction in volume of the sample (solid Hg is more dense than liquid Hg). At a temperature of 155.45 K ($\Delta T = 78.88 \text{ K}$), 80% of the droplets had solidified after 650 min. You can assume that it takes much longer for a nucleus to form in each droplet than for the droplet to solidify once the nucleus has formed. Using the information given above, calculate the nucleation rate, I , per second per centimeter cube of undercooled liquid Hg. (Hint: first calculate the number of droplets in the sample.)

Answer

$$1.12 \times 10^6 \text{ s}^{-1} \text{ cm}^{-3}.$$

- 8.6** Turnbull repeated his experiments at lower temperatures (greater ΔT) and obtained the results shown in the table. Nucleation theory gives the following equation for the variation in nucleation rate with temperature.

$$I = A \exp\left(-K \times \frac{1}{T(\Delta T)^2}\right),$$

where A and K are constants.

$T \text{ (K)}$	$\Delta T \text{ (K)}$	$I \text{ (s}^{-1} \text{ cm}^{-3}\text{)}$
155.45	78.88	1.12×10^6
155.17	79.16	1.66×10^6
154.96	79.37	2.60×10^6
154.69	79.64	3.67×10^6
154.41	79.92	5.77×10^6
154.20	80.13	8.37×10^6

Plot values of $\ln I$ versus $1/T(\Delta T)^2$ and determine the value of K from the slope of the plot. K is given by the equation

$$K = \frac{16\pi\gamma_{\text{SL}}^3}{3k} \left(\frac{T_{\text{M}}}{|\Delta H|} \right)^2.$$

$k = 1.381 \times 10^{-23} \text{ J K}^{-1}$ is Boltzmann's constant. Using your value of K , estimate the value of γ_{SL} . $\Delta H = 2.324 \text{ kJ mol}^{-1}$, atomic weight of Hg = 200 g mol^{-1} , and density of solid Hg = 14.1 g cm^{-3} . Because you are using mixed units, write out all the units in your equations! Note that ΔH must be expressed per unit volume of solid Hg.

Answers

$$K = 8.40 \times 10^7 \text{ K}^3; \gamma_{\text{SL}} = 32 \text{ mJ m}^{-2}.$$

- 8.7** At the largest undercooling of 80.13 K, Turnbull measured a nucleation rate of $8.37 \times 10^6 \text{ s}^{-1} \text{ cm}^{-3}$. Following the method you used in Example 8.5, back-calculate the time it would take for 80% of the droplets to nucleate at this temperature. Using the equation

$$I = A \exp\left(-K \times \frac{1}{T(\Delta T)^2}\right),$$

with $K = 8.40 \times 10^7 \text{ K}^3$, estimate the time for 80% nucleation at an undercooling of (a) 85 K and (b) 90 K. Sketch a graph of \log (80% nucleation time) versus ΔT over the range 78.88 – 90 K.

Answers

87 min; (a) 5 s; (b) $1 \times 10^{-2} \text{ s}$.

- 8.8** Using Equation (8.3), and relevant data from Examples 8.5 and 8.6, estimate the critical nucleus radius r^* for ΔT values of (a) 79 K and (b) 90 K. Estimate the number of Hg atoms in the critical nucleus. Calculate the volume occupied by one Hg atom, and hence estimate the number of atoms in the surface of the nucleus (the surface area of a sphere is $4\pi r^2$). Hence verify that the nucleus is large enough to define the structure of the solid–liquid interface.

Answers

1.16 nm; 1.02 nm; 278 atoms; 0.0235 nm^3 , 207 atoms (i.e., 14 atoms by 14 atoms).

- 8.9** Turnbull carried out further experiments where an oxidizing agent (acetyl peroxide) was added to the silicone oil. This reacted with the Hg on the surfaces of the droplets to form a monolayer of crystalline oxide. It was found that nucleation occurred at an undercooling of $\approx 47 \text{ K}$, compared to $\approx 80 \text{ K}$ for homogeneous nucleation. Given that the ratio $\Delta T_{\text{hom}}/\Delta T_{\text{het}} = 80/47 = 1.70$,

use Equations (8.15) and (8.16) to calculate the value of the contact angle θ between the solid nucleus and the oxide catalyst. Why is your value of θ consistent with a large value of ΔT_{het} ?

Answer

$\theta = 65^\circ$ (Turnbull obtained 72° with a more detailed analysis).

- 8.10** Explain why a sample of liquid Hg which has been divided into a large number of separate droplets can be cooled to the homogeneous nucleation temperature, but a single undivided sample cannot.

Kinetics 3—Displacive Transformations

9.1 INTRODUCTION

So far we have only looked at transformations which take place by diffusion: the so-called *diffusive* transformations. But there is one very important class of transformation—the *displacive* transformation—which can occur without any diffusion at all.

The most important displacive transformation is the one that happens in carbon steels. If you take a piece of 0.8% carbon steel “off the shelf” and measure its mechanical properties, you will find, roughly, the values of hardness, tensile strength, and ductility given in [Table 9.1](#). But if you test a piece that has been heated to red heat and then quenched into cold water, you will find a dramatic increase in hardness (4 times or more), and a big decrease in ductility (it is practically zero) ([Table 9.1](#)).

The two samples have such divergent mechanical properties because they have radically different structures: the structure of the as-received steel is shaped by a diffusive transformation, but the structure of the quenched steel is shaped by a displacive change. But what are displacive changes? And why do they take place?

In order to answer these questions, we begin by looking at diffusive and displacive transformations in *pure iron* (once we understand how pure iron transforms we will have no problem in generalizing to iron–carbon alloys).

Table 9.1 Mechanical Properties of 0.8% Carbon Steel

Property	As-Received	Heated to Red Heat and Water Quenched
H (GN m ⁻²)	2	9
σ_{TS} (MN m ⁻²)	600	Limited by brittleness
ϵ_f %	10	≈ 0

Now, as we saw in Chapter 2, iron has different crystal structures at different temperatures. Below 914 °C the stable structure is b.c.c., but above 914 °C it is f.c.c. If f.c.c. iron is cooled below 914 °C, the structure becomes thermodynamically unstable, and it tries to change back to b.c.c. This f.c.c. → b.c.c. transformation usually takes place by a diffusive mechanism.

But under certain conditions, it can occur by a displacive mechanism instead. To understand how iron can transform displacively, we must first look at the details of how it transforms by diffusion.

9.2 DIFFUSIVE F.C.C. TO B.C.C. TRANSFORMATION IN PURE IRON

We saw in Chapter 7 that the speed of a diffusive transformation depends strongly on temperature (see Figure 7.6). The diffusive f.c.c. → b.c.c. transformation in iron shows the same dependence, with a maximum speed at maybe 700 °C (Figure 9.1). We must be careful not to jump to conclusions about Figure 9.1. This plots the *speed* of an individual b.c.c.–f.c.c. interface, measured in millimeter per second. If we want to know the *rate* of the transformation (the *volume* transformed per second), then we need to know the *area* of the b.c.c.–f.c.c. interface as well.

The total area of b.c.c.–f.c.c. interface is obviously related to the number of b.c.c. nuclei. Fewer nuclei mean a smaller interfacial area and a smaller

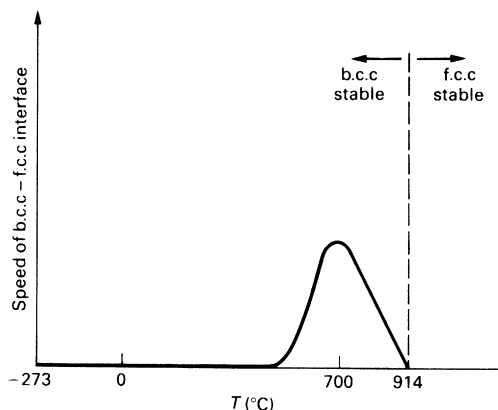


FIGURE 9.1

The diffusive f.c.c. → b.c.c. transformation in iron. The vertical axis shows the speed of the b.c.c.–f.c.c. interface at different temperatures. Note that the transformation can take place extremely rapidly, making it very difficult to measure the interface speeds. The curve is therefore only semischematic.

volume transforming per second. Indeed, if there are no nuclei at all, then the rate of transformation is zero. The rate of transformation is given by

$$\text{Rate (volume s}^{-1}\text{)} = \text{interface area} \times \text{interface speed} \quad (9.1)$$

The nucleation rate is critically dependent on temperature, as [Figure 9.2](#) shows. To see why, let us look at the heterogeneous nucleation of b.c.c. crystals at grain boundaries. By analogy with Equation (8.11) the critical radius for grain-boundary nucleation is given by

$$r^* = \frac{2\gamma_{\alpha\beta}}{|\Delta H|} \frac{T_e}{(T_e - T)}. \quad (9.2)$$

Grain-boundary nucleation will not occur in iron unless it is cooled below perhaps 910 °C. At 910 °C the critical radius is

$$r_{910}^* = \frac{2\gamma_{\alpha\beta}}{|\Delta H|} \frac{(914 + 273)}{(914 - 910)} = \frac{2\gamma_{\alpha\beta}}{|\Delta H|} \times 297. \quad (9.3)$$

But at 908 °C, the critical radius is

$$r_{908}^* = \frac{2\gamma_{\alpha\beta}}{|\Delta H|} \frac{(914 + 273)}{(914 - 908)} = \frac{2\gamma_{\alpha\beta}}{|\Delta H|} \times 198. \quad (9.4)$$

Thus

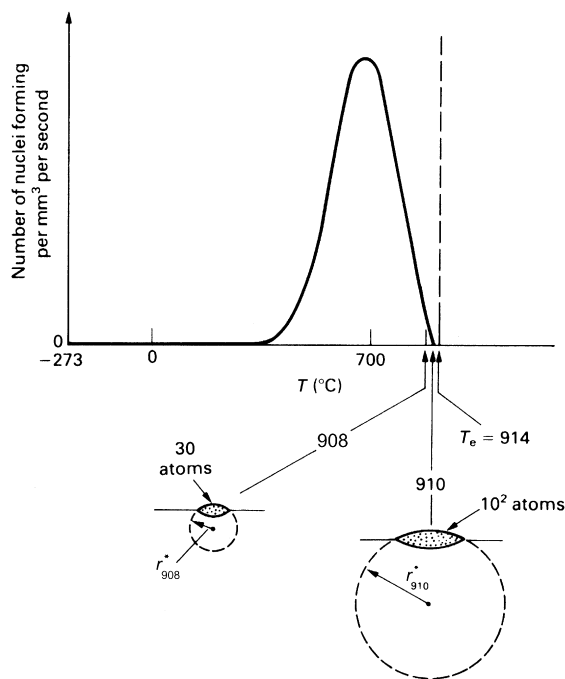
$$(r_{910}^*/r_{908}^*) = (297/198) = 1.5. \quad (9.5)$$

As [Figure 9.2](#) shows, grain-boundary nuclei will be geometrically similar at all temperatures. The *volume* V^* of the lens-shaped nucleus will therefore scale as $(r^*)^3$, i.e.,

$$(V_{910}^*/V_{908}^*) = 1.5^3 = 3.4. \quad (9.6)$$

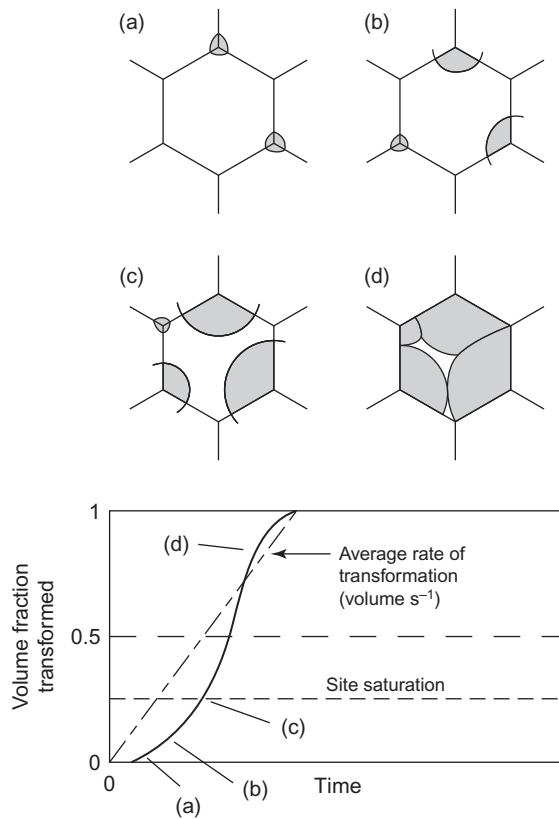
Now, nucleation at 910 °C will only take place if we get a random fluctuation of about 10^2 atoms (which is the maximum fluctuation that we can expect in practice). Nucleation at 908 °C, however, requires a random fluctuation of only $(10^2/3.4) = 30$ atoms. The chances of assembling this small number of atoms are obviously far greater than the chances of assembling 10^2 atoms and grain-boundary nucleation is thus much more rapid at 908 °C than at 910 °C.

[Figure 9.3](#) shows a schematic sequence of the nucleation and growth of b.c.c. iron from f.c.c. iron at our temperature of ≈ 908 °C. After an

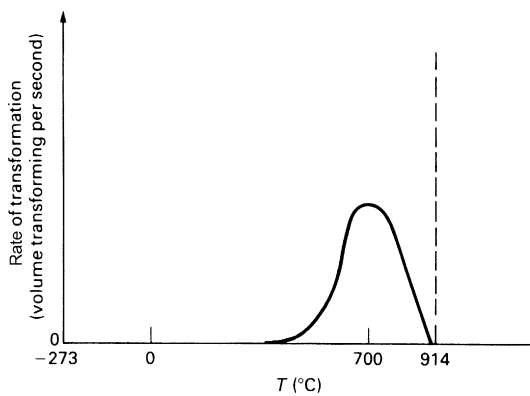
**FIGURE 9.2**

The diffusive f.c.c. \rightarrow b.c.c. transformation in iron: how the nucleation rate depends on temperature (semischematic only).

incubation period, nuclei of b.c.c. iron start to form at the most favorable sites (usually grain corners). These nuclei then grow at the interface speed shown in Figure 9.1 (at the temperature of ≈ 908 °C). With time, more nuclei form and grow. The volume transforming per second increases rapidly as (a) more nuclei form and (b) the total area of the b.c.c.–f.c.c. interface increases. However, nucleation may well stop at ≈ 20 – 30% transformation owing to “site saturation”—all the available sites for nucleation at this particular temperature have been used up. Further growth then takes place only at existing interfaces. The total interface area continues to increase for a while because of the increasing size of the b.c.c. grains, so the volume rate increases as well. Eventually, though, the interface area begins to decrease because grains start to impinge on one another, and the volume rate decreases until all the f.c.c. has transformed (when it becomes zero). This sequence of nucleation and growth leads to the characteristic “S-” shaped curve shown in Figure 9.3. Figure 9.3 also shows how we can define an average volume rate from the S-curve. Figure 9.4 shows this average volume rate plotted

**FIGURE 9.3**

Schematic sequence (a) to (d) of nucleation and growth of b.c.c. iron from f.c.c. iron. Site saturation occurs at (c). The four nuclei lead to four separate grains of b.c.c. iron.

**FIGURE 9.4**

The diffusive f.c.c. \rightarrow b.c.c. transformation in iron: rate of transformation as a function of temperature (semischematic).

against temperature. This has the same form as Figure 9.1, because of the dominant effect of the interface speed.

9.3 TIME—TEMPERATURE—TRANSFORMATION DIAGRAM

It is standard practice to plot the rates of diffusive transformations in the form of time—temperature—transformation (TTT) diagrams or “C-curves”. Figure 9.5 shows the TTT diagram for the diffusive f.c.c. \rightarrow b.c.c. transformation in pure iron. The general shape of the C-curves directly reflects the form of Figure 9.4. In order to see why, let us start with the “1% transformed” curve on the diagram. This gives the time required for 1% of the f.c.c. to transform to b.c.c. at various temperatures. Because the transformation rate is zero at both 910 and -273°C (Figure 9.4), the time required to give 1% transformation must be infinite at these temperatures. This is why the 1% curve tends to infinity as it approaches both 910 and -273°C . And because the transformation rate is a maximum at say 700°C (Figure 9.4), the time for 1% transformation must be a minimum at 700°C , which is why the 1% curve has a

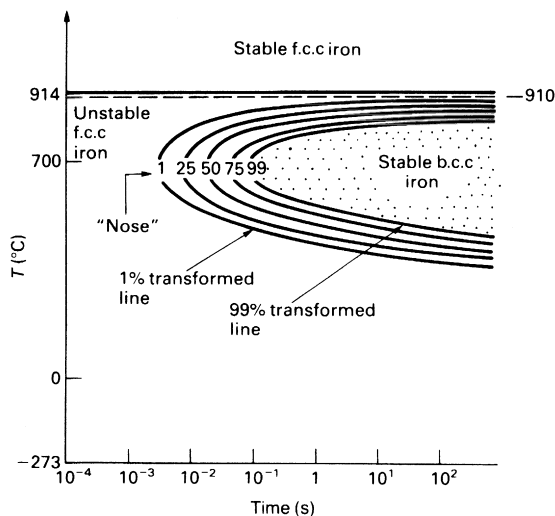


FIGURE 9.5

The diffusive f.c.c. \rightarrow b.c.c. transformation in iron: the time—temperature—transformation (TTT) diagram or “C-curve”. The 1% and 99% curves represent, for all practical purposes, the *start* and *end* of the transformation. Semischematic only.

“nose” there. The same arguments apply, of course, to the 25%, 50%, 75%, and 99% curves.

9.4 DISPLACIVE F.C.C. TO B.C.C. TRANSFORMATION

In order to get the iron to transform *displacively*, we proceed as follows. We start with f.c.c. iron at 914 °C which we then cool to room temperature at a rate of about $10^5\text{ }^\circ\text{C s}^{-1}$. As Figure 9.6 shows, we will miss the nose of the 1% curve, and we would expect to end up with f.c.c. iron at room temperature. f.c.c. iron at room temperature would be undercooled by nearly 900 °C, and there would be a huge driving force for the f.c.c. \rightarrow b.c.c. transformation. Even so, the TTT diagram tells us that we might expect f.c.c. iron to survive for years at room temperature before the diffusive transformation could get under way.

In reality, below 550 °C the driving force becomes so large that it cannot be contained; and the iron transforms from f.c.c. to b.c.c. by the *displacive* mechanism. Small lens-shaped grains of b.c.c. nucleate at f.c.c.

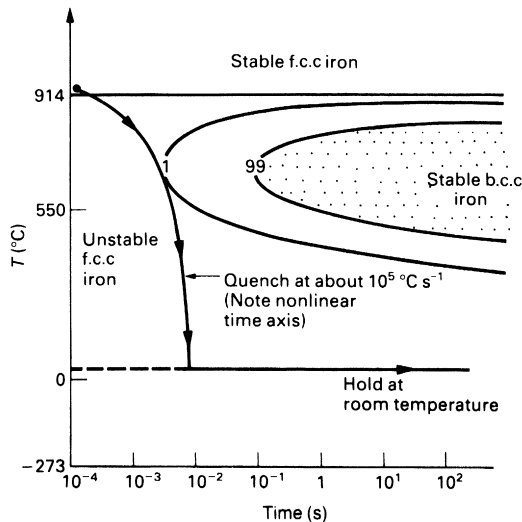


FIGURE 9.6

If we quench f.c.c. iron from 914 °C to room temperature at a rate of about $10^5\text{ }^\circ\text{C s}^{-1}$ we expect to prevent the diffusive f.c.c. \rightarrow b.c.c. transformation from taking place. In reality, below 550 °C, the iron will transform to b.c.c. by a *displacive* transformation instead.

grain boundaries and move across the grains at *speeds approaching the speed of sound in iron* (Figure 9.7). In the “switch zone,” atomic bonds are broken and remade in such a way that the structure “switches” from f.c.c. to b.c.c.. This is very similar to the breaking and remaking of bonds that goes on when a *dislocation* moves through a crystal. In fact there are strong parallels between *displacive transformations* and *plastic deformation*. Both happen almost instantaneously at speeds that are limited by the propagation of lattice vibrations through the crystal. Both happen at low as well as at high temperatures. And both happen by the precisely sequenced switching of one atom after another. As Table 9.2 shows, most characteristics of displacive transformations are quite different from those of diffusive transformations.

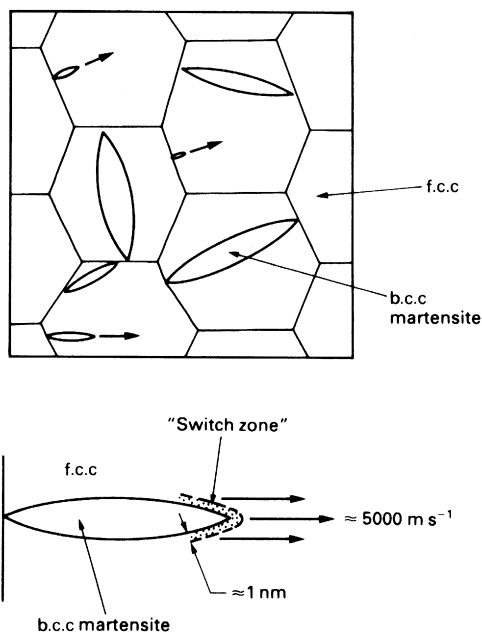
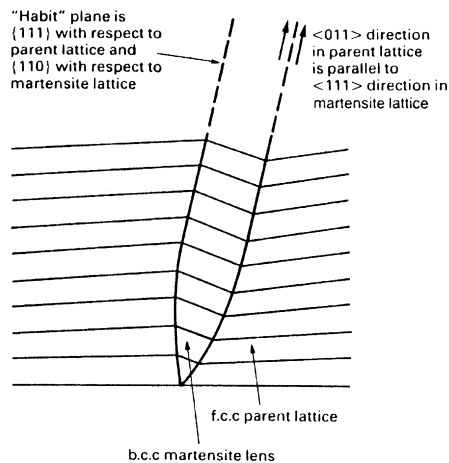


FIGURE 9.7

The *displacive* f.c.c. \rightarrow b.c.c. transformation in iron. b.c.c. lenses nucleate at f.c.c. grain boundaries and grow almost instantaneously. The lenses stop growing when they hit the next grain boundary. Note that when a new phase in *any* material is produced by a displacive transformation, it is always referred to as “martensite.” Displacive transformations are often called “martensitic” transformations as a result.

Table 9.2 Characteristics of Transformations

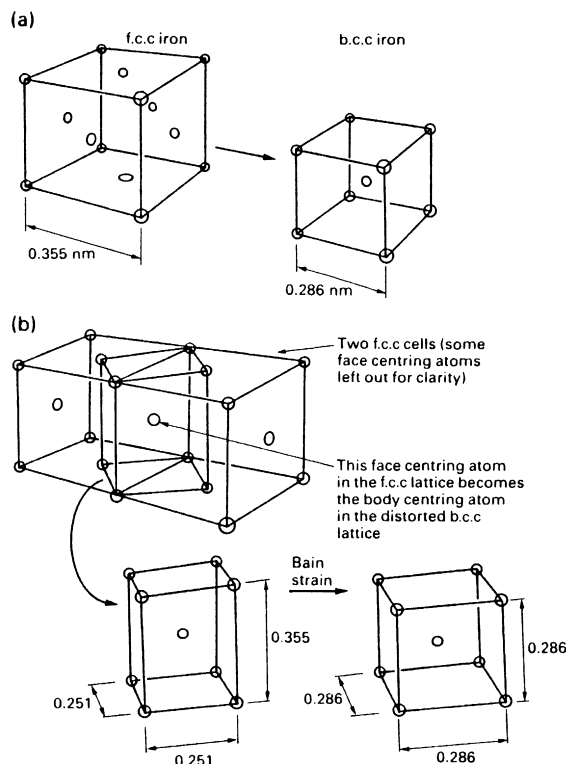
Displacive (also called Diffusionless, Shear, or Martensitic)	Diffusive
Atoms move over distances \leq interatomic spacing.	Atoms move over distances of $1-10^6$ interatomic spacings.
Atoms move by making and breaking interatomic bonds and by minor "shuffling".	Atoms move by thermally activated diffusion from site to site.
Atoms move one after another in precise sequence ("military" transformation).	Atoms hop randomly from site to site (although more hop "forward" than "backward") ("civilian" transformation).
Speed of transformation \approx velocity of lattice vibrations through crystal (essentially independent of temperature); transformation can occur at temperatures as low as 4 K.	Speed of transformation depends strongly on temperature; transformation does not occur below $0.3-0.4 T_M$.
Extent of transformation (volume transformed) depends on temperature only.	Extent of transformation depends on time as well as temperature.
Composition cannot change (because atoms have no time to diffuse, they stay where they are).	Diffusion allows compositions of individual phases to change in alloyed systems.
Always specific crystallographic relationship between martensite and parent lattice.	Sometimes have crystallographic relationships between phases.

**FIGURE 9.8**

Martensites are always coherent with the parent lattice. They grow as thin lenses on preferred planes and in preferred directions in order to cause the least distortion of the lattice. The crystallographic relationships shown here are for pure iron.

9.5 DETAILS OF MARTENSITE FORMATION

As [Figure 9.8](#) shows, the martensite lenses are coherent with the parent lattice. [Figure 9.9](#) shows how the b.c.c. lattice is produced by atomic

**FIGURE 9.9**

(a) The unit cells of f.c.c. and b.c.c. iron. (b) Two adjacent f.c.c. cells make a distorted b.c.c. cell. If this is subjected to the “Bain strain,” it becomes an undistorted b.c.c. cell. This atomic “switching” involves the least shuffling of atoms. As it stands, the new lattice is not coherent with the old one. But we can get coherency by *rotating* the b.c.c. lattice planes as well (Figure 9.8).

movements of the f.c.c. atoms in the “switch zone.” As we have already said, at $\approx 550^\circ\text{C}$ martensite lenses form and grow almost instantaneously. As the lenses grow, the lattice planes distort (see Figure 9.8), and some of the driving force for the f.c.c. \rightarrow b.c.c. transformation is removed as strain energy. Fewer lenses nucleate and grow, and eventually the transformation stops. In other words, provided we keep the temperature constant, the displacive transformation is self-stabilizing (Figure 9.10). To get more martensite, we must cool the iron down to a lower temperature (which gives more driving force). Even at this lower temperature, the displacive transformation will stop when the extra driving force has been used up in straining the lattice. In fact, to get 100% martensite, we have to cool the iron down to $\approx 350^\circ\text{C}$ (Figure 9.10).

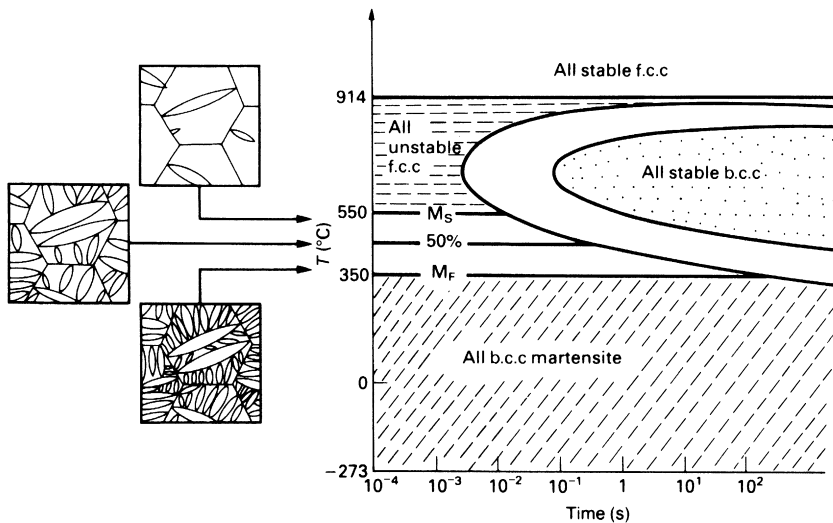


FIGURE 9.10

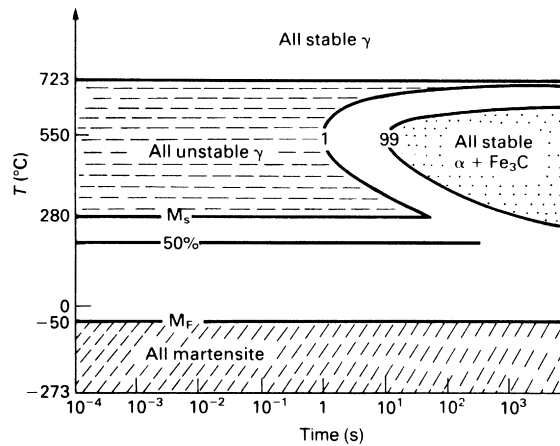
The displacive f.c.c. \rightarrow b.c.c. transformation in iron: the volume of martensite produced is a function of temperature only, and does not depend on time. Note that the temperature at which martensite starts to form is labeled M_s (martensite start); the temperature at which the martensite transformation finishes is labeled M_f (martensite finish).

9.6 MARTENSITE TRANSFORMATION IN STEELS

To make martensite in pure iron, it has to be cooled very fast: at about $10^5 \text{ }^\circ\text{C s}^{-1}$. Metals can only be cooled at such large rates if they are in the form of thin foils. How, then, can martensite be made in sizeable pieces of 0.8% carbon steel? As we saw in Chapter 4, a 0.8% carbon steel is a “eutectoid” steel: when it is cooled relatively slowly it transforms by diffusion into pearlite (the eutectoid mixture of $\alpha + \text{Fe}_3\text{C}$).

The eutectoid reaction can only start when the steel has been cooled below $723 \text{ }^\circ\text{C}$. The nose of the C-curve occurs at $\approx 525 \text{ }^\circ\text{C}$ (Figure 9.11), about $175 \text{ }^\circ\text{C}$ lower than the nose temperature of perhaps $700 \text{ }^\circ\text{C}$ for pure iron (Figure 9.5). Diffusion is much slower at $525 \text{ }^\circ\text{C}$ than it is at $700 \text{ }^\circ\text{C}$. As a result, a cooling rate of $\approx 200 \text{ }^\circ\text{C s}^{-1}$ misses the nose of the 1% curve and produces martensite.

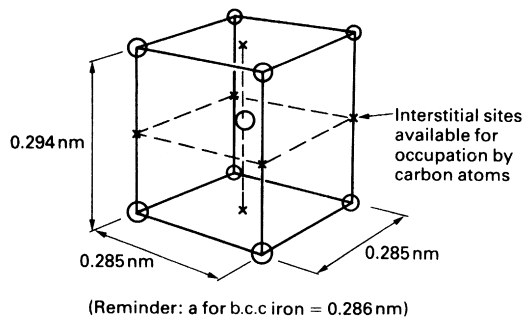
Pure iron martensite has a lattice which is identical to that of ordinary b.c.c. iron. But the displacive and diffusive transformations produce different *large-scale* structures: myriad tiny lenses of martensite instead of large equiaxed grains of b.c.c. iron. Fine-grained materials are harder than coarse-grained ones because grain boundaries get in the way of dislocations (see Chapter 2). For this reason, pure iron martensite is about twice as hard as

**FIGURE 9.11**

The TTT diagram for a 0.8% carbon (eutectoid) steel. We will miss the nose of the 1% curve, if we quench the steel at $\approx 200\text{ }^{\circ}\text{C s}^{-1}$. Note that if the steel is quenched into cold water, then not all the γ will transform to martensite. The steel will contain some “retained” γ which can only be turned into martensite if the steel is cooled below the M_F temperature of $-50\text{ }^{\circ}\text{C}$.

ordinary b.c.c. iron. The grain size argument cannot, however, be applied to the 0.8% carbon steel because pearlite not only has a very fine grain size but also contains a large volume fraction of the hard iron carbide phase. Yet 0.8% carbon martensite is 5 times harder than pearlite. The explanation lies with the 0.8% carbon. Above $723\text{ }^{\circ}\text{C}$, the carbon dissolves in the f.c.c. iron to form a random solid solution. The carbon atoms are about 40% smaller in diameter than the iron atoms, and they are able to squeeze into the space between the iron atoms to form an interstitial solution. When the steel is quenched, the iron atoms transform displacively to martensite. It all happens so fast that the carbon atoms are frozen in place and remain in their original positions. Under normal conditions, b.c.c. iron can only dissolve 0.035% carbon. The martensite is thus grossly oversaturated with carbon and something must give. Figure 9.12 shows what happens. The carbon atoms make room for themselves by stretching the lattice along one of the cube directions to make a *body-centered tetragonal* unit cell. Dislocations find it very difficult to move through such a highly strained structure, and the martensite is very hard as a result.

Martensite transformations are not limited just to metals. Some ceramics, like zirconia, have them; and even the obscure system of (argon + 40 at% nitrogen) forms martensite when it is cooled below 30 K. Helical protein crystals in some bacteria undergo a martensitic transformation and the shape change helps the bacteria to burrow into the skins of animals and people!

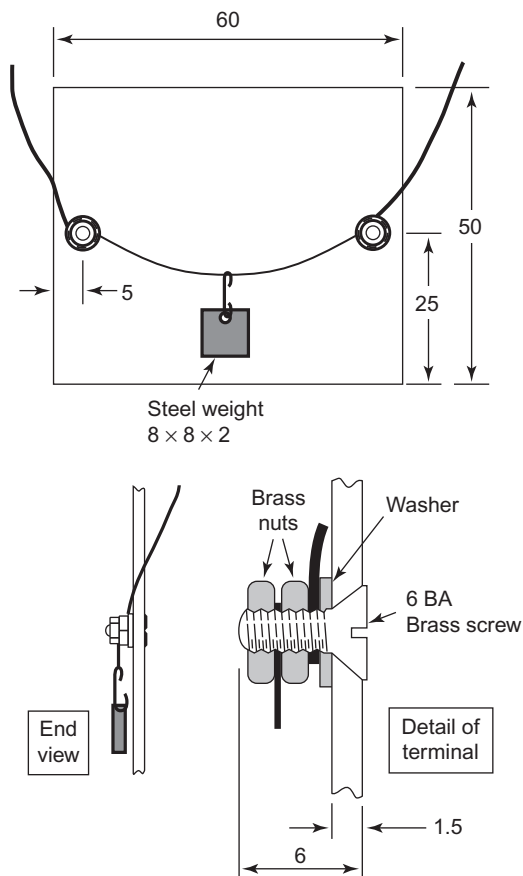
**FIGURE 9.12**

The structure of 0.8% carbon martensite. During the transformation, the carbon atoms put themselves into the interstitial sites shown. To make room for them, the lattice stretches along one cube direction (and contracts slightly along the other two). This produces what is called a *face-centered tetragonal* unit cell. Note that only a small proportion of the labeled sites actually contain a carbon atom.

WORKED EXAMPLE

When undercooled austenite transforms to martensite, the volume of the material increases. This can be used to show martensite actually forming in real time. The diagram shows the demonstration set-up. This consists of a perspex plate measuring $60 \times 50 \times 1.5$ mm. Two electrical terminals are bolted to the plate, and a length of carbon steel piano wire (0.2 mm diameter) is strung between them. A 1 g weight is hooked into the wire at its midpoint. A variable d.c. source (0–12 V) is wired to the terminals and switched on. As the voltage is increased, the wire gets hot and sags with the thermal expansion. The setting required to get the wire to bright red heat (and to transform it to γ) is noted, and the voltage is decreased again to zero. The assembly is then placed in front of a video camera, so the wire can be observed close-up. The voltage is increased to the hot setting, and the power is then abruptly cut. As the wire cools (and the γ contracts), it will move upward. But below the M_s temperature the γ will transform almost instantaneously to martensite—the wire will move down sharply and can be seen to “rock” quite noticeably as the shear waves propagate. If the experiment is carried out with a microphone placed next to it, a tinkling sound can be heard through the signal amplifier/loudspeaker. This is the acoustic signal of the shear waves traveling along the wire. If the wire is pulled sideways with a pair of tweezers once it has cooled down, it will break into several pieces—showing that carbon martensite is brittle. (If you don’t have a video camera and monitor/image projector to hand, the rig will fit into a top-loading slide projector. But remember that the image seen on the projector screen will be upside down, so the movements of the wire will be

inverted. After the test, the rig can be transferred to an overhead projector to demonstrate the brittle behavior of the wire.)



EXAMPLES

- 9.1 Compare and contrast the main features of
 - (a) diffusive transformations,
 - (b) displacive transformations.
- 9.2 Describe the structure of 0.8% carbon martensite
 - (a) at the nanometer-scale level,
 - (b) at the micrometer-scale level.

Why is 0.8% carbon martensite approximately 5 times harder than pearlite?

- 9.3 Sketch the time–temperature–transformation (TTT) diagram for a plain carbon steel of eutectoid composition which exhibits the following features:

- (i) At 650 °C, transformation of the austenite (f.c.c. phase) is 1% complete after 10 s and is 99% complete after 100 s.
- (ii) The fastest rate of transformation occurs at 550 °C. At this temperature, transformation of the austenite is 1% complete after 1 s and is 99% complete after 10 s.
- (iii) At 360 °C, transformation of the austenite is 1% complete after 10 s and is 99% complete after 300 s.
- (iv) The martensite start temperature is 240 °C. 90% of the austenite has transformed to martensite at 100 °C. The martensite finish temperature is 50 °C.

Explain briefly the shape of the lines drawn on the TTT diagram.

- 9.4** Calculate the percentage change in volume when f.c.c. iron changes to b.c.c. iron by a diffusive transformation. Does the volume decrease or increase in going from f.c.c. to b.c.c.? The lattice parameters for f.c.c. and b.c.c. iron are given in Figure 9.9 (a for b.c.c. iron is measured at 20 °C, and a for f.c.c. iron is extrapolated down to 20 °C from high-temperature measurements). (You will need to calculate how many atoms there are in each of the two different unit cells.)

Answer

4.58%.

- 9.5** The following is an empirical equation (from experimental dilatometry data) for the percentage volume change when going from austenite (the γ phase, i.e., f.c.c. iron with carbon in solid solution) to martensite (M) (obviously by a *displacive* transformation):

$$\% \text{ volume change on transformation} = 4.64 - 0.53 \times \text{wt\% carbon}$$

Why should this equation give the correct volume change for the *diffusive* transformation of pure f.c.c. iron to b.c.c. iron? How does the value obtained from this equation at zero wt% carbon compare with the answer to Example 9.4?

- 9.6** The lattice parameters for 0.8% carbon M at 20 °C are given in Figure 9.12. The lattice parameter for 0.8% carbon γ (extrapolated to 20 °C) is 0.3585 nm. Calculate the percentage change in volume when the γ transforms to M. How does your answer compare with the prediction of the equation in Example 9.5?

Answer

4.01%.

- 9.7** Referring to Figure 9.3, explain briefly why the graph of (volume fraction transformed) versus (time) has an “S” shape. How does the number and spatial distribution of the nuclei affect the shapes and sizes of the grains in the new phase?

- 9.8** Referring to Figure 9.5, TTT curves usually show the start of the transformation as occurring at $>0\%$ (e.g., 1%, as in Figure 9.5, or maybe 10%), and the end as occurring at $<100\%$ (e.g., 99%, as in Figure 9.5, or maybe 90%). Explain briefly why this is a consequence of the shape of the S-curve shown in Figure 9.3.
- 9.9** Referring to Figure 9.6, explain why the shape of the cooling curve as drawn on the TTT diagram is nonlinear, even though it relates to a constant cooling rate of $\approx 10^5\text{ }^\circ\text{C s}^{-1}$. How can such a high cooling rate be achieved in practice?
- 9.10** Referring to the Worked Example, why will the demonstration only work when the diameter of the wire is small enough?

Case Studies in Phase Transformations

10.1 INTRODUCTION

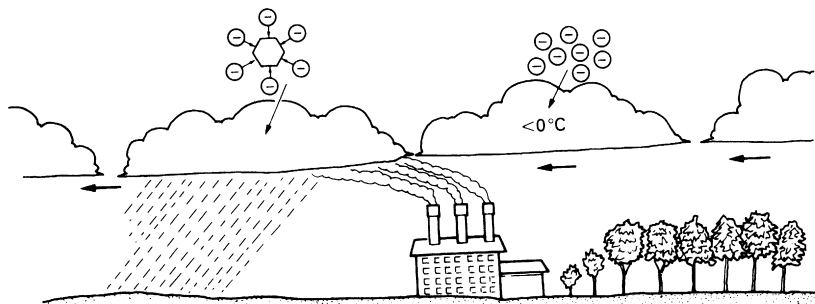
We now apply the thermodynamic and kinetic theory of Chapters 6–9 to four problems: making rain, getting fine-grained castings, growing crystals for semiconductors, and making amorphous metals.

10.2 MAKING RAIN

Often, during periods of drought, there is enough moisture in the atmosphere to give clouds, but rain does not fall. The problem is one of heterogeneous nucleation. A cloud is cloudy because it is a suspension of vast numbers of minute, spherical water droplets. The droplets are too small and light to fall under gravity.

Rain falls when (surprisingly) the droplets freeze to ice. If a droplet freezes, it becomes a stable ice nucleus which then grows by attracting water vapor from the surrounding droplets. The ice particle quickly grows to a size at which gravity can pull it down, and it falls. On cold days, it falls as hail or snow; but in warmer weather, it remelts in the warmer air near the ground and falls as rain. The difficult stage in making rain is getting the ice to nucleate in the first place. If the water droplets are clean, then they will not contain any heterogeneous nucleation catalysts. Ice can then only form if the cloud is cooled to the homogeneous nucleation temperature and that is a very low temperature (-40°C). Clouds rarely get this cold. So the ice must nucleate on something, heterogeneously. Industrial pollution will do: the smoke of a steel works contains so much dirt that the rainfall downwind of it is significantly increased (Figure 10.1). But there are cheaper ways.

The crystal structure of ice is hexagonal, with lattice constants of $a = 0.452\text{ nm}$ and $c = 0.736\text{ nm}$. The inorganic compound silver iodide also has a hexagonal structure, with lattice constants ($a = 0.458\text{ nm}$, $c = 0.749\text{ nm}$) that are

**FIGURE 10.1**

Rain falls when the water droplets in clouds turn to ice. This can only happen if the clouds are below 0°C to begin with. If the droplets are clean, ice can form only in the unlikely event that the clouds cool down to the homogeneous nucleation temperature of -40°C . When dust particles are present they can catalyze nucleation at temperatures quite close to 0°C . This is why there is often heavy rainfall downwind of factory chimneys.

almost identical to those of ice. So if you put a crystal of silver iodide into supercooled water, it is almost as good as putting in a crystal of ice: more ice can grow on it easily, at a low undercooling (Figure 10.2).

This is an example of heterogeneous nucleation. The good matching between ice and silver iodide means that the interface between them has a low energy: the contact angle is very small and the undercooling needed to nucleate ice decreases from 40 to 4°C . In artificial rainmaking silver iodide, in the form of a very fine powder of crystals, is either dusted into the cloud from a plane flying above it or is shot into it with a rocket from below. The powder “seeds” ice crystals which grow and start to fall, taking the silver iodide with them. But if the ice, as it grows, takes on snow-flake forms and the tips of the snow flakes break off as they fall, then the process (once started) is self-catalyzing: each old generation of falling ice crystals leaves behind a new generation of tiny ice fragments to seed the next lot of crystals, and so on.

There are even better catalysts for ice nucleation than silver iodide. The most celebrated ice nucleating catalyst, produced by the microorganism *Pseudomonas syringae*, is capable of forming nuclei at undetectably small undercoolings. The organism is commonly found on plant leaves and, in this situation, it is a great nuisance: the slightest frost can cause the leaves to freeze and die. A mutant of the organism has been produced which lacks the ability to nucleate ice (the so-called “ice-minus” mutant). American bioengineers have proposed that the ice-minus organism should be released into the wild, in the hope that it will displace the natural organism and solve the frost-damage problem; but environmentalists have threatened law suits if this goes ahead.

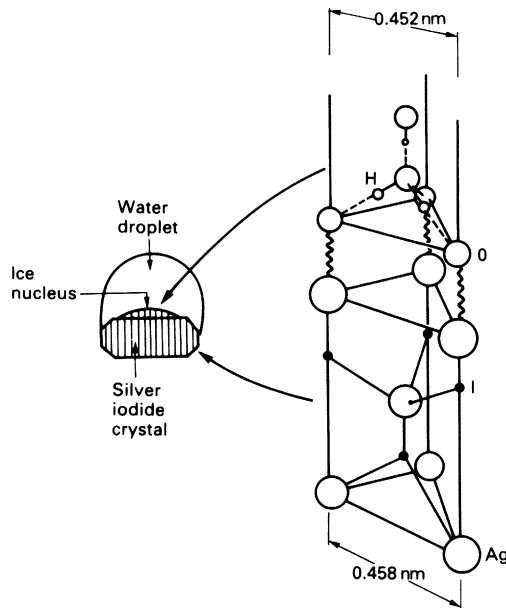


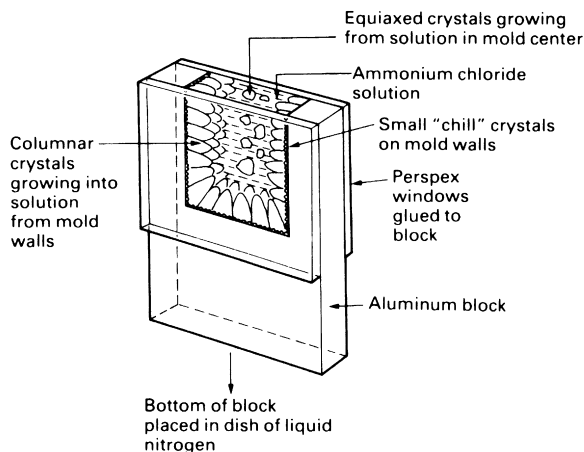
FIGURE 10.2

The excellent crystallographic matching between silver iodide and ice makes silver iodide a very potent nucleating agent for ice crystals. When clouds at subzero temperatures are seeded with AgI dust, spectacular rainfall occurs.

Interestingly, ice nucleation in organisms is not always a bad thing. Take the example of the alpine plant *Lobelia teleki*, which grows on the slopes of Mount Kenya. The ambient temperature fluctuates daily over the range -10 to $+10$ °C and subjects the plant to considerable physiological stress. It has developed a cunning response to cope with these temperature changes. The plant manufactures a potent biogenic nucleating catalyst: when the outside temperature falls through 0 °C some of the water in the plant freezes, and the latent heat evolved stops the plant cooling any further. When the outside temperature goes back up through 0 °C, of course, some ice melts back to water; and the latent heat absorbed now helps keep the plant cool. By removing the barrier to nucleation, the plant has developed a thermal buffering mechanism which keeps it at an even temperature in spite of quite large variations in the temperature of the environment.

10.3 FINE-GRAINED CASTINGS

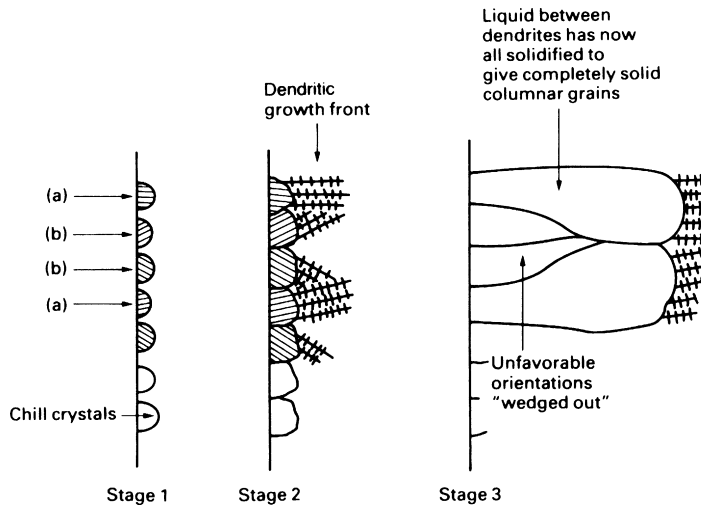
Many engineering components—from cast-iron drain covers to aluminum alloy cylinder heads—are *castings* made by pouring molten metal into a mold of the right shape and allowing it to go solid. The casting process can

**FIGURE 10.3**

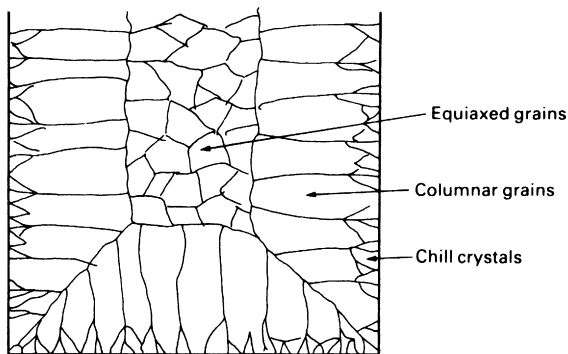
A simple laboratory set-up for observing the casting process directly. The mold volume measures about $50 \times 50 \times 6$ mm. The walls are cooled by putting the bottom of the block into a dish of liquid nitrogen. The windows are kept free of frost by squirting them with alcohol from a wash bottle every 5 min.

be modeled using the set-up shown in [Figure 10.3](#). The mold is made from aluminum but has Perspex side windows to allow the solidification behavior to be watched. The casting “material” used is ammonium chloride solution made up by heating water to 50°C and adding ammonium chloride crystals until the solution just becomes saturated. The solution is then warmed up to 75°C and poured into the cold mold. When the solution touches the cold metal, it cools very rapidly and becomes highly supersaturated. Ammonium chloride nuclei form heterogeneously on the aluminum and a thin layer of tiny *chill* crystals forms all over the mold walls. The chill crystals grow competitively until they give way to the much bigger *columnar* crystals ([Figures 10.3 and 10.4](#)). After a while the top surface of the solution cools below the saturation temperature of 50°C and crystal nuclei form heterogeneously on floating particles of dirt. The nuclei grow to give *equiaxed* (spherical) crystals which settle down into the bulk of the solution. When the casting is completely solid, it will have the grain structure shown in [Figure 10.5](#). This is the classic casting structure found in any cast-metal ingot. [Figures 10.6, 10.7, and 10.8](#) show typical examples of the columnar and dendritic microstructures observed in solidified metals.

This structure is far from ideal. The first problem is one of *segregation*: as the long columnar grains grow they push impurities ahead of them. If, as is usually the case, we are casting *alloys*, this segregation can give big differences in composition—and therefore in properties—between the outside and the inside of the casting. The second problem is one of *grain size*. As we

**FIGURE 10.4**

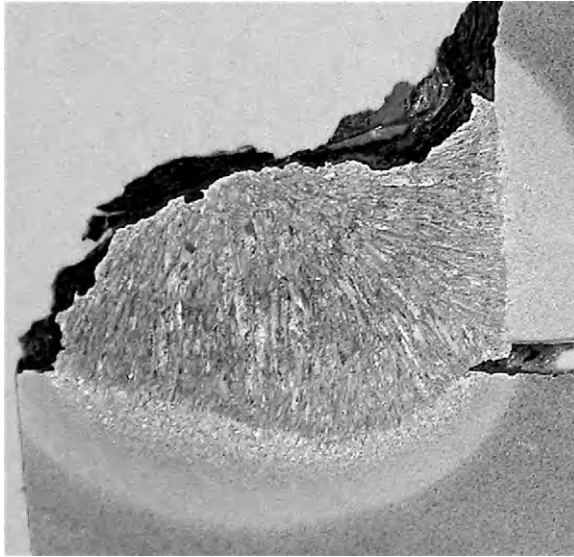
Chill crystals nucleate with random crystal orientations. They grow in the form of *dendrites*. Dendrites always lie along specific crystallographic directions. Crystals oriented like (a) will grow further into the liquid in a given time than crystals oriented like (b); (b)-type crystals will get “wedged out” and (a)-type crystals will dominate, eventually becoming columnar grains.

**FIGURE 10.5**

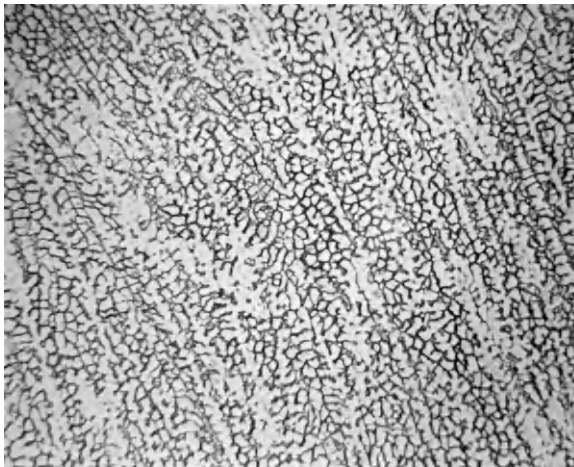
The grain structure of the solid casting.

mentioned in Chapter 9, fine-grained materials are harder than coarse-grained ones. Indeed, the yield strength of steel can be doubled by a 10 times decrease in grain size. Obviously, the big columnar grains in a typical casting are a source of weakness. But how do we get rid of them?

One cure is to cast *at* the equilibrium temperature. If, instead of using under-saturated ammonium chloride solution, we pour *saturated* solution into the

**FIGURE 10.6**

Polished and etched cross section through a weld between two low-carbon steel plates. Magnification $\times 5$. The molten weld pool solidified like a small casting. The photograph clearly shows a columnar structure in the solidified weld metal.

**FIGURE 10.7**

Polished and etched cross section through a 304 L stainless steel weld, showing the microstructure produced by dendritic solidification. Magnification $\times 100$.

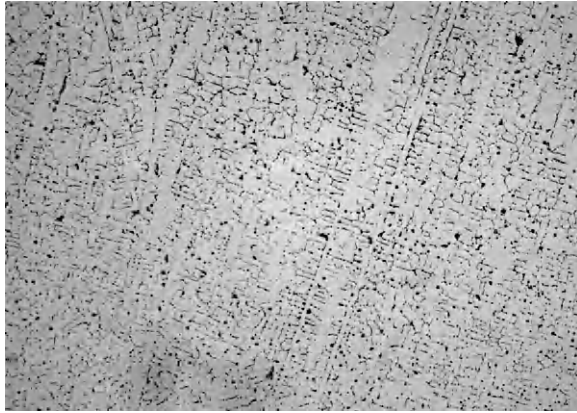
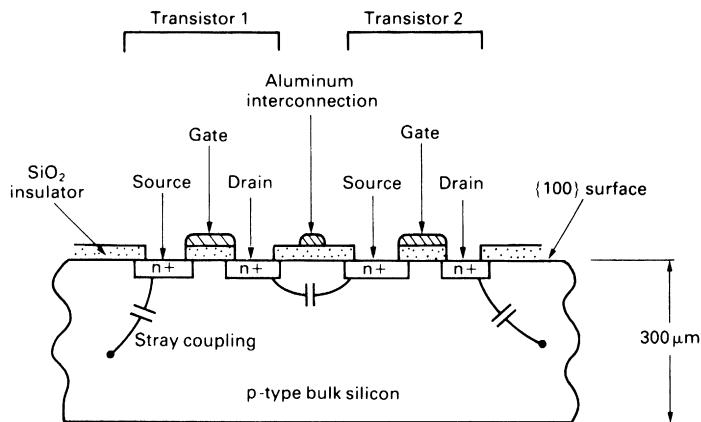


FIGURE 10.8

Polished and etched cross section through a 50 Fe–50 Ni weld, showing the microstructure produced by dendritic solidification. Magnification $\times 35$.

mold, we get what is called “big-bang” nucleation. As the freshly poured solution swirls past the cold walls, heterogeneous nuclei form in large numbers. These nuclei are then swept back into the bulk of the solution where they act as growth centers for equiaxed grains. The final structure is then almost entirely equiaxed with only a small columnar region. For some alloys, this technique (or a modification of it called “rheocasting”) works well. But for most it is found that, if the molten metal is not superheated to begin with, then parts of the casting will freeze prematurely, and this may prevent metal reaching all parts of the mold.

The traditional cure is to use *inoculants*. Small catalyst particles are added to the melt just before pouring (or even poured into the mold *with* the melt) in order to nucleate as many crystals as possible. This gets rid of the columnar region altogether and produces a fine-grained equiaxed structure throughout the casting. This important application of heterogeneous nucleation sounds straightforward, but a great deal of trial and error is needed to find effective catalysts. The choice of AgI for seeding ice crystals was an unusually simple one; finding successful inoculants for metals is still largely empirical. Factors other than straightforward crystallographic matching are important: surface defects, for instance, can be crucial in attracting atoms to the catalyst; and even the smallest quantities of impurity can be adsorbed on the surface to give monolayers which may poison the catalyst. A notorious example of erratic surface nucleation is in the field of electroplating: electroplaters often have difficulty in getting their platings to “take” properly. It is well known (among experienced electroplaters) that pouring condensed milk into the plating bath can help.

**FIGURE 10.9**

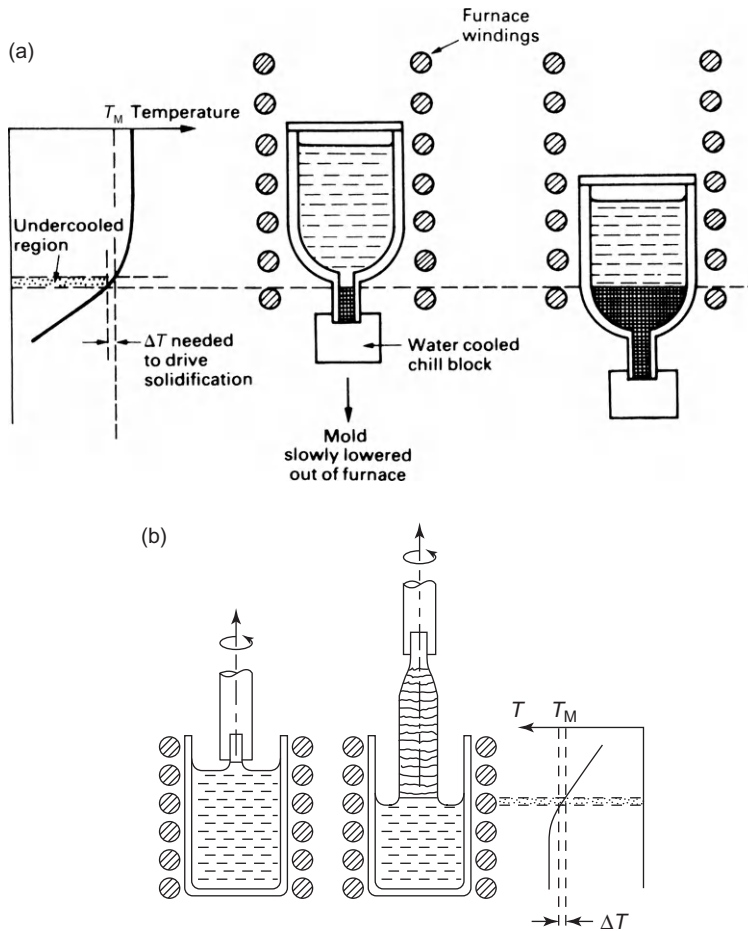
A typical integrated circuit. The silicon wafer is cut from a large single crystal using a chemical saw—mechanical sawing would introduce too many dislocations.

10.4 SINGLE CRYSTALS FOR SEMICONDUCTORS

Materials for semiconductors have to satisfy formidable standards. Their electrical properties are badly affected by the scattering of carriers which occurs at impurity atoms or at dislocations, grain boundaries, and free surfaces. We have already seen (in Chapter 5) how zone refining is used to produce the ultrapure starting materials. The next stage in semiconductor processing is to grow large single crystals under carefully controlled conditions: grain boundaries are eliminated and a very low dislocation density is achieved.

Figure 10.9 shows part of a typical integrated circuit. It is built on a single-crystal wafer of silicon, usually about 300 μm thick. The wafer is doped with an impurity such as boron, which turns it into a p-type semiconductor (bulk doping is usually done after the initial zone refining stage in a process known as zone leveling). The localized n-type regions are formed by firing pentavalent impurities (e.g., phosphorus) into the surface using an ion gun. The circuit is completed by the vapor-phase deposition of silica insulators and aluminum interconnections.

Growing single crystals is the very opposite of pouring fine-grained castings. In castings, we want to undercool as much of the liquid as possible so that nuclei can form everywhere. In crystal growing, we need to start with a single seed crystal of the right orientation and the last thing that we want is for stray nuclei to form. Single crystals are grown using the arrangements shown in Figure 10.10. The only region where the liquid silicon is undercooled is right next to the interface and even there the undercooling is small. So there is little chance of stray nuclei forming and nearly all runs produce single crystals.

**FIGURE 10.10**

Growing single crystals for semiconductor devices, starting from a small “seed” single crystal of the correct crystallographic orientation. (a) Bridgman–Stockbarger method. (b) Czochralski method.

10.5 AMORPHOUS METALS

In Chapter 9, we saw that when carbon steels were quenched from the austenite region to room temperature, the austenite could not transform to the equilibrium low-temperature phases of ferrite and iron carbide. There was no time for diffusion, and the austenite could only transform by a diffusionless (shear) transformation to give the metastable martensite phase. The martensite transformation can give enormously altered mechanical properties and is largely responsible for the great versatility of carbon and low-alloy steels. Unfortunately, few alloys undergo such useful shear transformations. But are there other ways in which we could change the properties of alloys by quenching?

An idea of the possibilities is given by the old high-school chemistry experiment with sulfur crystals (“flowers of sulfur”). A 10 ml beaker is warmed up on a hot plate and some sulfur is added to it. As soon as the sulfur has melted, the beaker is removed from the heater and allowed to cool slowly on the bench. The sulfur will solidify to give a disk of polycrystalline sulfur which breaks easily if pressed or bent. Polycrystalline sulfur is obviously very brittle.

Now take another batch of sulfur flowers, but this time heat it well past its melting point. The liquid sulfur gets darker in color and becomes more and more viscous. Just before the liquid becomes completely unpourable, it is decanted into a dish of cold water, quenching it. When we test the properties of this *quenched* sulfur, we find that we have produced a tough and rubbery substance. We have, in fact, produced an *amorphous* form of sulfur with radically altered properties.

This principle has been used for thousands of years to make glasses. When silicates are cooled from the molten state, they often end up being amorphous, and many polymers are amorphous too. What makes it easy to produce amorphous sulfur, glasses, and polymers is that their high viscosity stops crystallization taking place. Liquid sulfur becomes unpourable at 180 °C because the sulfur polymerizes into long cross-linked chains of sulfur atoms. When this polymerized liquid is cooled below the solidification temperature, it is very difficult to get the atoms to regroup themselves into crystals. The C-curve for the liquid-to-crystal transformation (Figure 10.11)

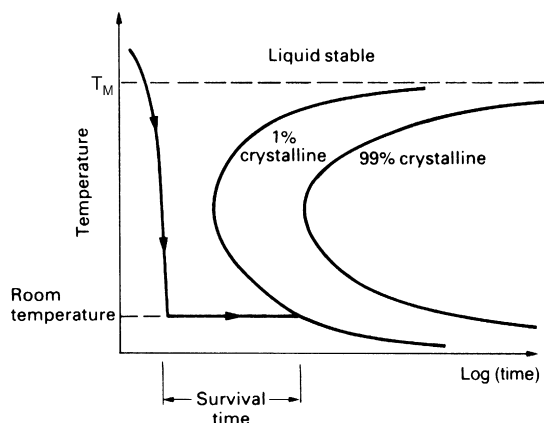


FIGURE 10.11

Sulfur, glasses, and polymers turn into viscous liquids at high temperature. The atoms in the liquid are arranged in long polymerized chains. The liquids are viscous because it is difficult to get these bulky chains to slide over one another. It is also hard to get the atoms to regroup themselves into crystals, and the kinetics of crystallization are very slow. The liquid can easily be cooled past the nose of the C-curve to give a metastable supercooled liquid which can survive for long times at room temperature.

lies well to the right, and it is easy to cool the melt past the nose of the C-curve to give a supercooled liquid at room temperature.

There are formidable problems in applying these techniques to metals. Liquid metals do not polymerize, and it is very hard to stop them crystallizing when they are undercooled. In fact, cooling rates in excess of $10^{10} \text{ }^{\circ}\text{C s}^{-1}$ are needed to make pure metals amorphous. But current rapid-quenching technology has made it possible to make amorphous *alloys*, though their compositions are a bit daunting ($\text{Fe}_{40}\text{Ni}_{40}\text{P}_{14}\text{B}_6$, for instance). This is so heavily alloyed that it crystallizes to give compounds; and in order for these compounds to grow, the atoms must add on from the liquid in a particular sequence. This slows down the crystallization process, and it is possible to make amorphous $\text{Fe}_{40}\text{Ni}_{40}\text{P}_{14}\text{B}_6$ using cooling rates of only $10^5 \text{ }^{\circ}\text{C s}^{-1}$.

Amorphous alloys have been made commercially for the past 40 years by the process known as melt spinning (Figure 10.12). They have some remarkable and attractive properties. Many of the iron-based alloys are ferromagnetic. Because they are amorphous, and literally without structure, they are excellent soft magnets: there is nothing to pin the magnetic domain walls, which move easily at low fields and give a very small coercive force.

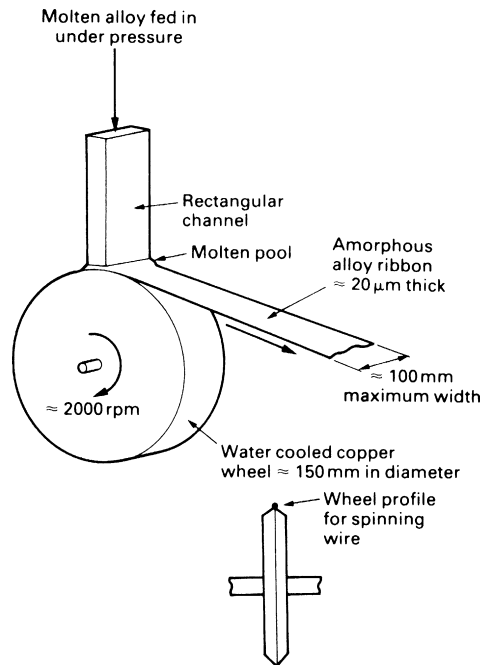


FIGURE 10.12

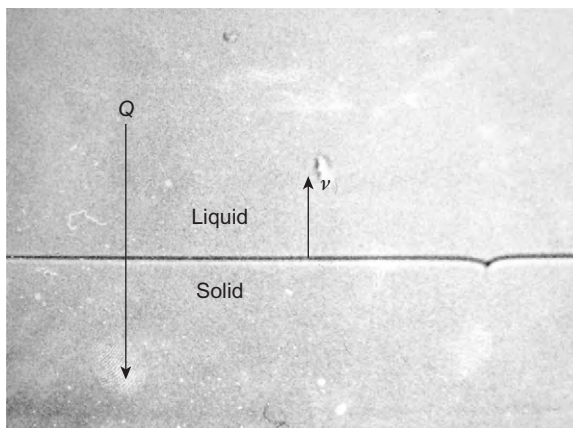
Ribbons or wires of amorphous metal can be made by melt spinning. There is an upper limit on the thickness of the ribbon: if it is too thick it will not cool quickly enough and the liquid will crystallize.

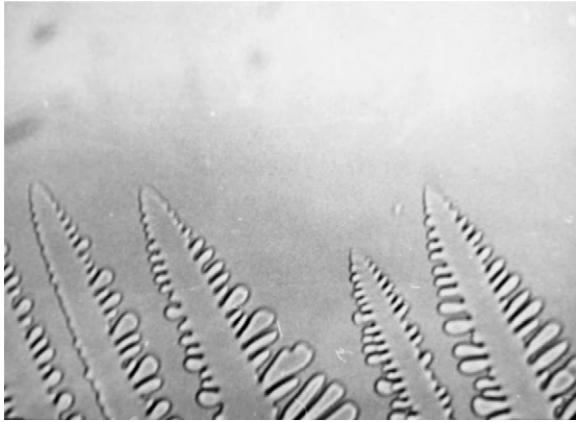
These alloys are now being used for the cores of small transformers and relays. Amorphous alloys have no dislocations (you can only have dislocations in *crystals*), and they are therefore very hard. But, unexpectedly, they are ductile too; ductile enough to be cut using a pair of scissors. Finally, more recent alloy developments have allowed us to make amorphous metals in sections up to 5 mm thick. The absence of dislocations makes for very low mechanical damping, so amorphous alloys are even being used for the striking faces of golf clubs!

WORKED EXAMPLE

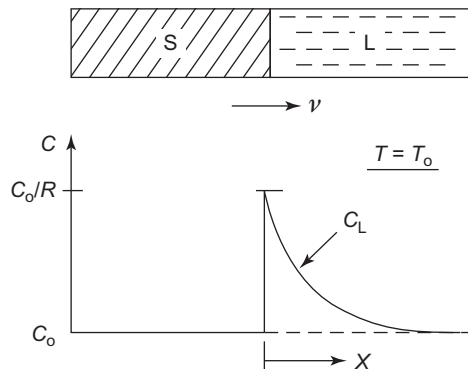
The first photograph (magnification $\times 120$) shows camphene growing slowly (at velocity v) into a positive temperature gradient. (Camphene has a spherical molecule, so its solidification behavior is like that of most metals.) This is the situation in zone refining a bar of metal to sweep it clear of dissolved impurity (see the zone refining case study in Chapter 5). The solid–liquid interface is flat, as it must be if it is to push the impurity-rich liquid away.

The second photograph (magnification $\times 120$) shows camphene growing rapidly into the positive temperature gradient. The flat interface has broken down into dendrites. This is a situation we certainly do not want in zone refining, because a lot of impurity gets trapped between the dendrites (we saw a photograph of this in the Chapter 6 Worked Example). We already have looked in a simple way at how this happens (see Chapter 4). We now do the quantitative analysis—needed to define the processing conditions for stable, planar growth of the solid–liquid interface.

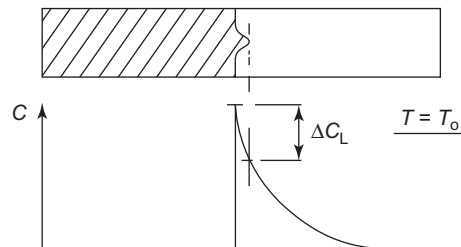




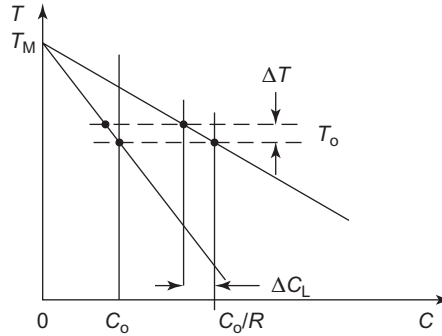
As shown in the first diagram, to get equilibrium at the solid–liquid interface, the concentration of impurity in the liquid must be equal to C_0/k (k is the distribution coefficient). This can only happen if there is a gradient in C_L ahead of the interface. This gradient is supplied by diffusion—as the interface advances into the liquid, impurity is rejected, and this provides the flux needed to produce the concentration gradient.



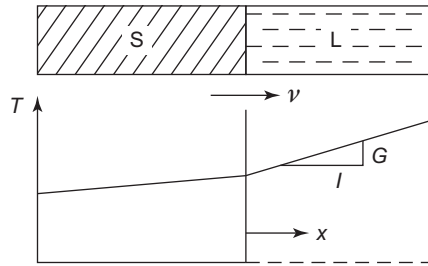
The second diagram shows a local random fluctuation in the growth rate, giving rise to a small protrusion. The solid at the tip of the protrusion will be in contact with liquid having a C_L less than the equilibrium value by amount ΔC_L .



The phase diagram shows that the solid–liquid interface at the tip of the protrusion will be in equilibrium at a temperature $T = T_0 + \Delta T$, in other words at a *higher temperature than the actual temperature*. The interface at the tip of the protrusion is therefore *undercooled* by ΔT , so it wants to keep on growing. This phenomenon is called *constitutional undercooling* (CU) (because the undercooling is caused by a change in concentration, not temperature). This is what eventually leads to the formation of dendrites.



CU can only be prevented if there is a balancing increase in the *actual* temperature at the tip of the protrusion of amount ΔT . This requires a sufficiently large and positive temperature gradient, G , ahead of the growth front, as shown in the diagram.

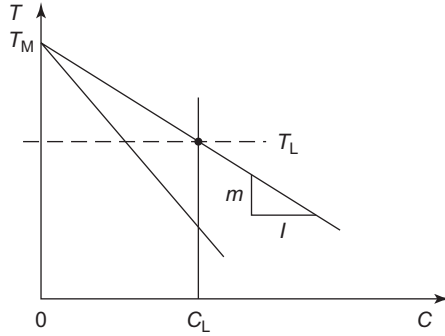


The diffusion of impurity into the liquid is described by Fick's second law,

$$D \frac{\partial^2 C}{\partial x^2} = \frac{\partial C}{\partial t}.$$

Using a frame of reference moving with the growth front at the solidification velocity v , the solution to the diffusion equation is

$$C_L(x) = C_0 \left\{ 1 + \left(\frac{1-k}{k} \right) \exp\left(-\frac{xv}{D}\right) \right\}.$$



The phase diagram shows that $T_L = T_M - mC_L$, where m is the slope of the liquidus line. Thus,

$$T_L = T_M - mC_0 \left\{ 1 + \left(\frac{1-k}{k} \right) \exp\left(-\frac{xv}{D}\right) \right\},$$

$$\frac{dT_L}{dx} = mC_0 \left(\frac{1-k}{k} \right) \left(\frac{v}{D} \right) \exp\left(-\frac{xv}{D}\right),$$

$$\left(\frac{dT_L}{dx} \right)_{x=0} = mC_0 \left(\frac{1-k}{k} \right) \frac{v}{D}.$$

To stop protrusions forming, we need

$$\frac{dT}{dx} \equiv G > mC_0 \left(\frac{1-k}{k} \right) \frac{v}{D}.$$

The CU equation is usually written in the form

$$\frac{G}{v} > \frac{mC_0}{D} \left(\frac{1-k}{k} \right),$$

with the processing variables on the left, and the intrinsic parameters of the alloy system on the right.

When zone refining, both v and C_0 are small, so a small temperature gradient is enough to prevent CU. The required temperature gradient is generated automatically where the bar leaves the end of the tube furnace. The same considerations apply when growing high-purity single crystals—it is important to avoid CU, because dendrites will segregate impurities, and will also create crystal defects. When growing single crystals of semiconductors, for example (see the case study in Section 10.4), both v and C_0 are small, so a small temperature gradient is adequate. When growing single-crystal (SX) turbine blades, v is kept small, but because C_0 is large (it is dictated by the high alloy content of the nickel), large values of G must be

used. Even so, the growth front consists of dendrites; but because these are all parallel (and have the same crystallographic orientation), the resulting solid is a single crystal (it is like one single large columnar grain in a casting). When casting an alloy in the conventional way, v is not small, and G is not large (it may even be zero), so CU is inevitable.

EXAMPLES

- 10.1** Why is it undesirable to have a columnar grain structure in castings? Why is a fine equiaxed grain structure the most desirable option? What factors determine the extent to which the grain structure is columnar or equiaxed?
- 10.2** Why is it easy to produce amorphous polymers and glasses, but difficult to produce amorphous metals?
- 10.3** A cast ingot of pure aluminum has a structure which consists mainly of large columnar grains, whereas a cast ingot of aluminum containing Al–Ti inoculant powder consists of small equiaxed grains. Explain this difference in structure.
- 10.4** Explain what is meant by constitutional undercooling, and indicate how it is relevant to zone refining.
- 10.5** A bar of silver containing 0.1 wt% copper as an impurity is to be zone refined. The zone refining rig moves the bar through the tube furnace at 20 mm h^{-1} . Use the CU equation in the form

$$G > mC_0 \left(\frac{1-k}{k} \right) \frac{v}{D}$$

to calculate the minimum temperature gradient, G , which must be applied in front of the solid–liquid interface to keep it planar. The value of D , the diffusion coefficient in liquid silver at the melting temperature, is $2.55 \times 10^{-3} \text{ mm}^2 \text{ s}^{-1}$. Silver and copper form a simple eutectic system, with the eutectic at 779°C and 28.5 wt% Cu. Pure silver melts at 960.8°C . The Ag-rich phase has a maximum solubility for Cu of 8.8 wt% (at the eutectic temperature). Assume both the liquidus and solidus lines are straight.

Answer

30°C cm^{-1} .

- 10.6** You are now told to zone refine silver containing 1 wt% copper. How would you specify a zone refining set-up to achieve a planar interface in this case? What measures could you take in order to maximize G ? How might your process specification be affected by the requirement to achieve maximum throughput?
- 10.7** By looking at the shape of the impurity concentration profile ahead of a moving solid–liquid interface you guess it has the form

$$C = Ae^{-Bx} + E.$$

Find the constants A and E from the boundary conditions at (i) $x = 0$ and (ii) $x = \infty$. By considering how the concentration profile would change as you altered (i) the growth velocity v and (ii) the diffusion coefficient D , find a functional form for the constant B . Check the units of B to confirm your result. Compare your final equation for C with the one given in the worked example.

- 10.8** With reference to Example 10.7, show that the amount of impurity rejected at the moving solid–liquid interface per second per unit area is given by

$$J_{x=0} = vC_0 \left(\frac{1-k}{k} \right).$$

Fick's first law may therefore be written as

$$-D \frac{dC}{dx} \Big|_{x=0} = vC_0 \left(\frac{1-k}{k} \right).$$

Apply this result to your equation for the concentration profile,

$$C = Ae^{-Bx} + E,$$

and thus find B (use the value of A you calculated in Example 10.7).

- 10.9** Look at the concentration profile ahead of the moving solid–liquid interface in the Worked Example. Imagine that your own position is fixed in the frame of reference of the laboratory, and the interface is approaching you from the left. This means that the impurity concentration C where you are located is increasing with time (at a rate dC/dt). Show that dC/dt is given by $v(dC/dx)$. As a result, Fick's second law may be written as

$$D \frac{d^2C}{dx^2} = v \frac{dC}{dx}.$$

Apply this result to your equation for the concentration profile

$$C = Ae^{-Bx} + E,$$

and confirm that it represents a solution of Fick's second law. Check that applying Fick's second law gives the same result for B that you obtained in Example 10.8.

- 10.10** We have seen previously that solids near their melting point can contain small liquid droplets of segregated impurities (see Chapter 6 Worked Example or Figure 2.10). However, if the solid is held in a *temperature gradient*, the droplets tend to *migrate* in the direction of increasing temperature. Explain the origin of this phenomenon, and show that the velocity of a droplet is given by

$$v = \frac{GD}{(1-k)(T_M - T)},$$

where G is the temperature gradient, D is the diffusion coefficient for impurity in liquid, and T is the temperature of the droplet. (Use Fick's first law to relate the impurity rejected at the solidifying interface to the concentration gradient

in the liquid.) Assume that the liquidus line of the phase diagram is straight. What happens to the *diameter* of the droplets as they move up the temperature gradient?

- 10.11** Using the equation from Example 10.10, estimate the liquid diffusion coefficient using the following data for the temperature gradient migration of droplets in camphene. $G = 8 \text{ K mm}^{-1}$, $v = 0.8 \times 10^{-3} \text{ mm s}^{-1}$, $T_M = 322 \text{ K}$, $T = 314 \text{ K}$. Assume that $k = 0$.

Answer

$$0.8 \times 10^{-3} \text{ mm}^2 \text{ s}^{-1}.$$

Light Alloys

11.1 INTRODUCTION

No fewer than 14 pure metals have densities $\leq 4.5 \text{ Mg m}^{-3}$ (Table 11.1). Of these, titanium, aluminum, and magnesium are in common use as structural materials. Beryllium is difficult to work and is toxic, but it is used in moderate quantities for heat shields and structural members in rockets. Lithium is used as an alloying element in aluminum to lower its density and save weight on airframes. Yttrium has an excellent set of properties and, although scarce, may eventually find applications in advanced aerospace projects. But many are unsuitable for structural use because they are chemically reactive or have low melting points.

Table 11.1 The Light Metals

Metal	Density (Mg m^{-3})	T_M ($^{\circ}\text{C}$)	Comments
Titanium	4.50	1667	High T_M —excellent creep resistance.
Yttrium	4.47	1510	Good strength and ductility; scarce.
Barium	3.50	729	
Scandium	2.99	1538	Scarce.
Aluminum	2.70	660	
Strontium	2.60	770	Reactive in air/water.
Cesium	1.87	28.5	Creeps/melts; very reactive in air/water.
Beryllium	1.85	1287	Difficult to process; very toxic.
Magnesium	1.74	649	
Calcium	1.54	839	Reactive in air/water.
Rubidium	1.53	39	} Creep/melt; very reactive in air/water.
Sodium	0.97	98	
Potassium	0.86	63	
Lithium	0.53	181	

Table 11.2 Mechanical Properties of Structural Light Alloys

Alloy	Density ρ (Mg m^{-3})	Youngs Modulus E (GN m^{-2})	Yield Strength σ_y (MN m^{-2})	E/ρ	$E^{1/2}/\rho$	$E^{1/3}/\rho$	σ_y/ρ	Creep Temperature ($^{\circ}\text{C}$)
Al alloys	2.7	71	25–600	26	3.1	1.5	9–220	150–250
Mg alloys	1.7	45	70–270	25	4.0	2.1	41–160	150–250
Ti alloys	4.5	120	170–1280	27	2.4	1.1	38–280	400–600
(Steels)	(7.9)	(210)	(220–1600)	27	1.8	0.75	28–200	(400–600)

Table 11.2 shows that alloys based on aluminum, magnesium, and titanium may have better stiffness/weight and strength/weight ratios than steel. Not only that: they are also corrosion resistant (with titanium exceptionally so); they are nontoxic; and titanium has good creep properties. So although the light alloys were originally developed for use in the aerospace industry, they are now much more widely used. The dominant use of aluminum alloys is in building and construction: panels, roofs, and frames. The second-largest consumer is the container and packaging industry; after that come transportation systems (the fastest-growing sector, with aluminum replacing steel and cast iron in cars and mass-transit systems); and the use of aluminum as an electrical conductor. Magnesium is lighter but more expensive. Titanium alloys are mostly used in aerospace applications where the temperatures are too high for aluminum or magnesium; but its corrosion resistance makes it attractive in chemical engineering, food processing, and bioengineering.

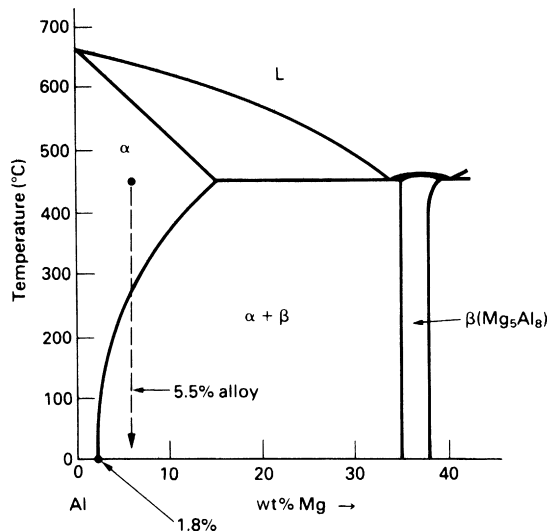
The light alloys derive their strength from *solid solution hardening*, *age* (or *precipitation*) *hardening*, and *work hardening*. We now examine the principles behind each hardening mechanism and illustrate them by drawing examples from our range of generic alloys.

11.2 SOLID SOLUTION HARDENING

When other elements dissolve in a metal to form a solid solution they make the metal harder. The solute atoms differ in size, stiffness, and charge from the solvent atoms. Because of this, the randomly distributed solute atoms interact with dislocations and make it harder for them to move. The theory of solution hardening is rather complicated, but it predicts the following result for the yield strength

$$\sigma_y \propto \varepsilon_s^{3/2} C^{1/2}, \quad (11.1)$$

where C is the solute concentration. ε_s is a term which represents the “mismatch” between solute and solvent atoms. The form of this result is just

**FIGURE 11.1**

The aluminum end of the Al–Mg phase diagram.

what we would expect: badly matched atoms will make it harder for dislocations to move than well-matched atoms; and a large population of solute atoms will obstruct dislocations more than a sparse population.

Of the generic aluminum alloys (see Chapter 1, Table 1.4), the 5000 series derives most of its strength from solution hardening. The Al–Mg phase diagram (Figure 11.1) shows why: at room temperature aluminum can dissolve up to 1.8 wt% magnesium at equilibrium. In practice, Al–Mg alloys can contain as much as 5.5 wt% Mg in solid solution at room temperature—a supersaturation of $5.5 - 1.8 = 3.7$ wt%. In order to get this supersaturation, the alloy is given the following schedule of heat treatments.

(a) Hold at 450 °C (“solution heat treat”)

This puts the 5.5% alloy into the single phase (α) field and all the Mg will dissolve in the Al to give a random substitutional solid solution.

(b) Cool moderately quickly to room temperature

The phase diagram tells us that, below 275 °C, the 5.5% alloy has an *equilibrium* structure that is two phase, $\alpha + \text{Mg}_5\text{Al}_8$. If, then, we cool the alloy *slowly* down through 275 °C, Al and Mg atoms will diffuse together to form precipitates of the intermetallic compound Mg_5Al_8 . However, below 275 °C, diffusion is slow and the C-curve for the precipitation reaction is well over to the right (Figure 11.2). So if we cool the 5.5% alloy moderately quickly, we will miss the nose of the C-curve. None of the Mg will be taken out of solution as Mg_5Al_8 , and we will end up with a supersaturated solid solution

at room temperature. As Table 11.3 shows, this supersaturated Mg gives a substantial increase in yield strength.

Solution hardening is not confined to 5000 series aluminum alloys. The other alloy series all have elements dissolved in solid solution; and they are all solution strengthened to some degree. But most aluminum alloys owe their strength to fine precipitates of intermetallic compounds, and solution strengthening is not dominant as it is in the 5000 series. Turning to the other light alloys, the most widely used titanium alloy (Ti–6Al 4V) is dominated by solution hardening (Ti effectively dissolves about 7 wt% Al and has complete solubility for V). Finally, magnesium alloys can be solution strengthened with Li, Al, Ag, and Zn, which dissolve in Mg between 2 and 5 wt%.

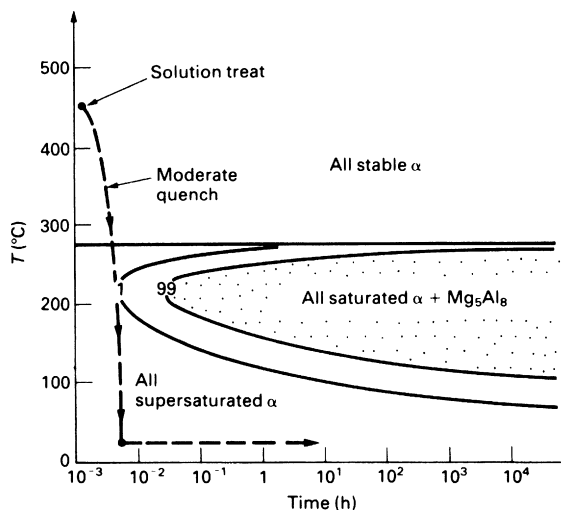


FIGURE 11.2 Semischematic TTT diagram for the precipitation of Mg_5Al_8 from the Al–5.5 wt% Mg solid solution.

Table 11.3 Yield Strengths of 5000 Series (Al–Mg) Alloys

Alloy	(wt% Mg)	σ_y (MN m^{-2}) (Annealed Condition)
5005	0.8	40
5050	1.5	55
5052	2.5	90
5454	2.7	120
5083	4.5	145
5456	5.1	160

} supersaturated

11.3 AGE (PRECIPITATION) HARDENING

When the phase diagram for an alloy has the shape shown in [Figure 11.3](#) (a solid solubility that decreases markedly as the temperature falls), then the potential for *age* (or *precipitation*) *hardening* exists. The classic example is the Duralumins, or 2000 series aluminum alloys, which contain about 4% copper.

The Al–Cu phase diagram tells us that, between 500 and 580 °C, the 4% Cu alloy is single phase: the Cu dissolves in the Al to give the random substitutional solid solution α . Below 500 °C, the alloy enters the two-phase field of $\alpha + \text{CuAl}_2$. As the temperature decreases the amount of CuAl_2 increases, and at room temperature the equilibrium mixture is 93 wt% α + 7 wt% CuAl_2 . [Figure 11.4\(a\)](#) shows the microstructure that we would get by cooling a Al–4 wt% Cu alloy *slowly* down through 500 °C to room temperature. In slow cooling, the temperature is high and the nucleation rate is low (see [Figure 9.3](#)). In order to accommodate the equilibrium amount of CuAl_2 , the few nuclei that do form grow into large precipitates of CuAl_2 spaced well apart. Moving dislocations find it easy to avoid the precipitates and the alloy is rather soft. If, on the other hand, we cool the alloy rather *quickly*, we produce a much finer structure ([Figure 11.4\(b\)](#)). Because the temperature is low, the nucleation rate is high (see [Figure 9.3](#)). The precipitates, although small, are closely spaced: they get in the way of moving dislocations and make the alloy harder.

There are limits to the precipitation hardening that can be produced by direct cooling: if the cooling rate is too high, we will miss the nose of the

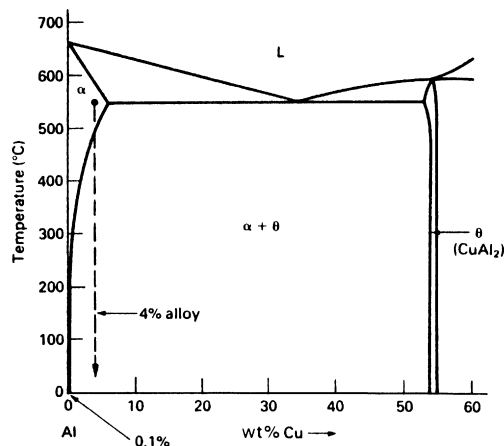
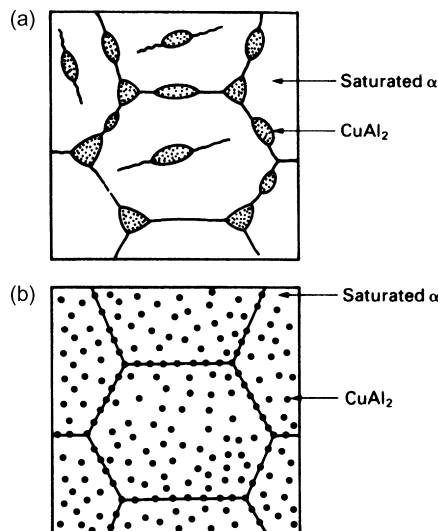


FIGURE 11.3

The aluminum end of the Al–Cu phase diagram.

**FIGURE 11.4**

Room temperature microstructures in the Al + 4 wt% Cu alloy. (a) Produced by slow cooling from 550 °C. (b) Produced by moderately fast cooling from 550 °C. The precipitates in (a) are large and far apart. The precipitates in (b) are small and close together.

C-curve for the precipitation reaction and will not get any precipitates at all! But large increases in yield strength *are* possible if we *age harden* the alloy.

To age harden our Al–4 wt% Cu alloy, we use the following schedule of heat treatments.

- (a) Solution heat treat at 550 °C. This gets all the Cu into solid solution.
- (b) Cool rapidly to room temperature by quenching into water or oil (“quench”). We will miss the nose of the C-curve and will end up with a highly supersaturated solid solution at room temperature (Figure 11.5).
- (c) Hold at 150 °C for 100 h (“age”). As Figure 11.5 shows, the supersaturated α will transform to the equilibrium mixture of saturated α + CuAl_2 . But it will do so at a low temperature and will give a very fine (and very strong) structure.

Figure 11.5, as we have drawn it, is oversimplified. Because the transformation is taking place at a low temperature, where the atoms are not very mobile, it is not easy for the CuAl_2 to separate out in one go. Instead, the transformation takes place in four distinct stages. These are shown in Figure 11.6(a)–(e). The progression may appear rather involved, but it is a good illustration of much of the material in the earlier chapters. More importantly, each stage of the transformation has a direct effect on the yield strength.

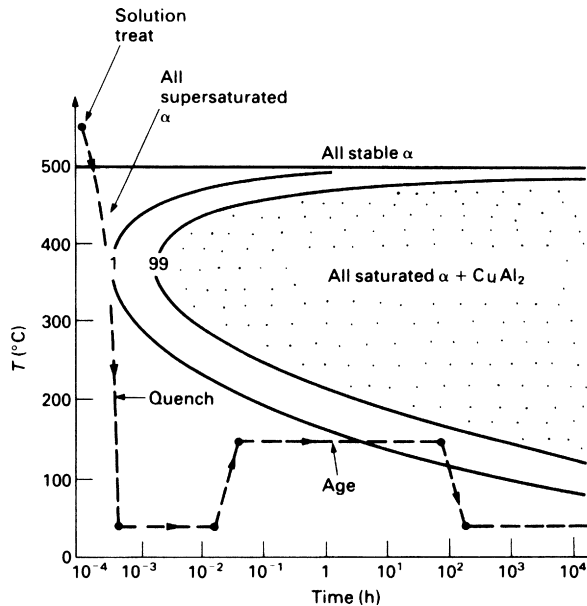


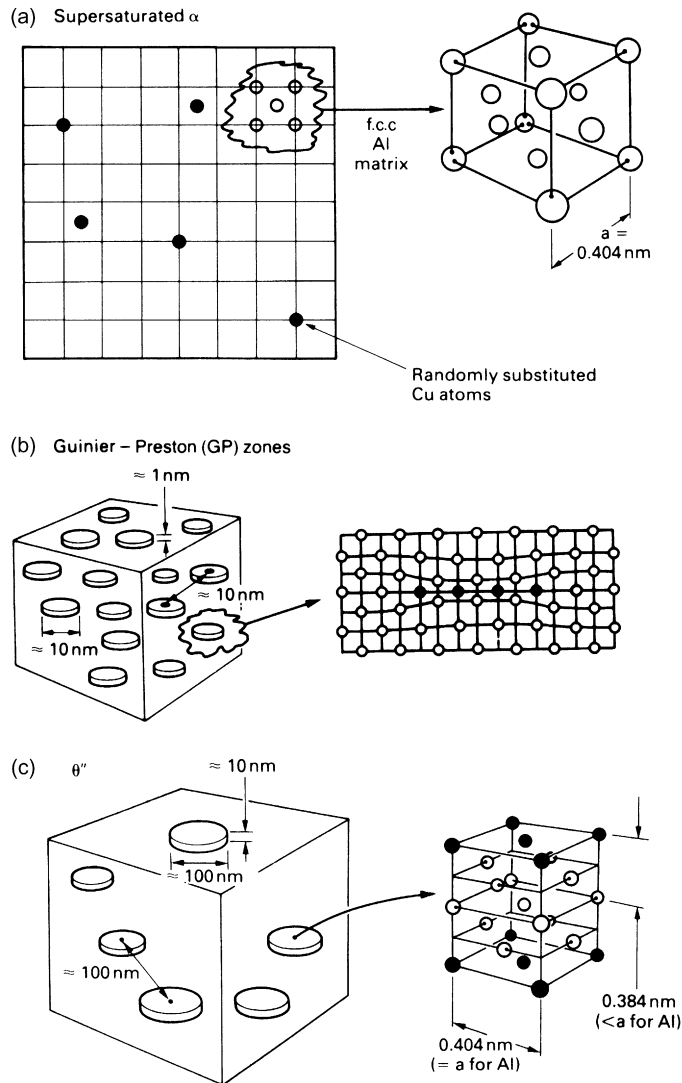
FIGURE 11.5

TTT diagram for the precipitation of CuAl_2 from the Al + 4 wt% Cu solid solution. Note that the equilibrium solubility of Cu in Al at room temperature is only 0.1 wt% (see Figure 11.3). The quenched solution is therefore carrying $4/0.1 = 40$ times as much Cu as it wants to.

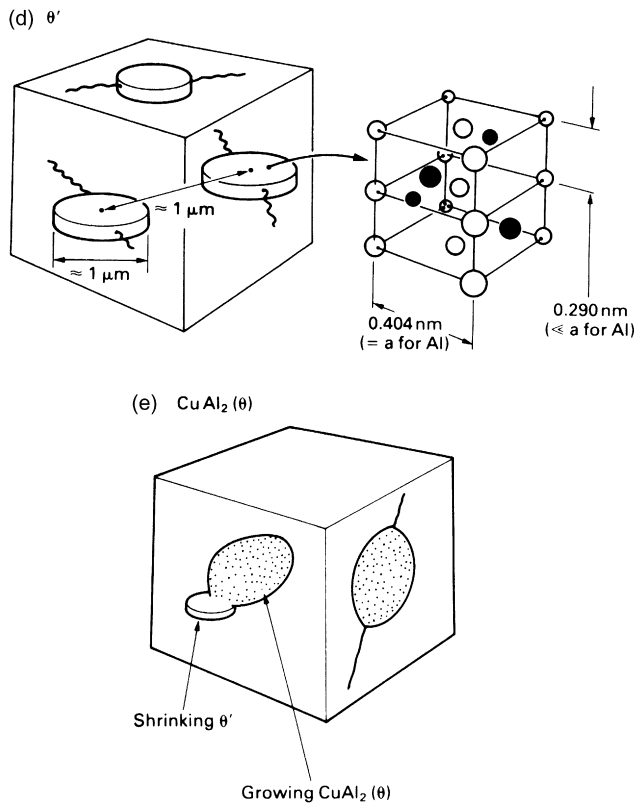
Four separate hardening mechanisms are at work during the aging process:

- (a) Solid solution hardening
At the start of aging, the alloy is mostly strengthened by the 4 wt% of copper that is trapped in the supersaturated α . But when the GP zones form, almost all of the Cu is removed from solution and the solution strengthening virtually disappears (Figure 11.7).
- (b) Coherency stress hardening
The coherency strains around the GP zones and θ'' precipitates generate stresses that help prevent dislocation movement. The GP zones give the larger hardening effect (Figure 11.7).
- (c) Precipitation hardening
The precipitates can obstruct the dislocations directly. But their effectiveness is limited by two things: dislocations can either *cut through* the precipitates or they can *bow around* them (Figure 11.8).

Resistance to cutting depends on a number of factors of which the shearing resistance of the precipitate lattice is only one. In fact, the cutting stress *increases* with aging time (Figure 11.7).

**FIGURE 11.6**

Stages in the precipitation of CuAl_2 . Disk-shaped GP zones (b) nucleate homogeneously from supersaturated solid solution (a). The disk faces are perfectly coherent with the matrix. The disk edges are also coherent but with a large *coherency strain*. (c) Some of the GP zones grow to form precipitates called θ' . (The remaining GP zones dissolve and transfer Cu to the growing θ' by diffusion through the matrix.) Disk faces are perfectly coherent. Disk edges are coherent, but the mismatch of lattice parameters between the θ' and the Al matrix generates coherency strain. (d) Precipitates called θ' nucleate at matrix dislocations. The θ' precipitates all dissolve and transfer Cu to the growing θ' . Disk faces are still perfectly coherent with the matrix. But disk edges are now *incoherent*. Neither faces nor edges show coherency strain but for different reasons. (e) Equilibrium CuAl_2 (θ) nucleates at grain boundaries and at θ' -matrix interfaces. The θ' precipitates all dissolve and transfer Cu to the growing θ . The CuAl_2 is completely *incoherent* with the matrix (see structure in Figure 2.3). Because of this, it grows as *rounded* rather than disk-shaped particles.

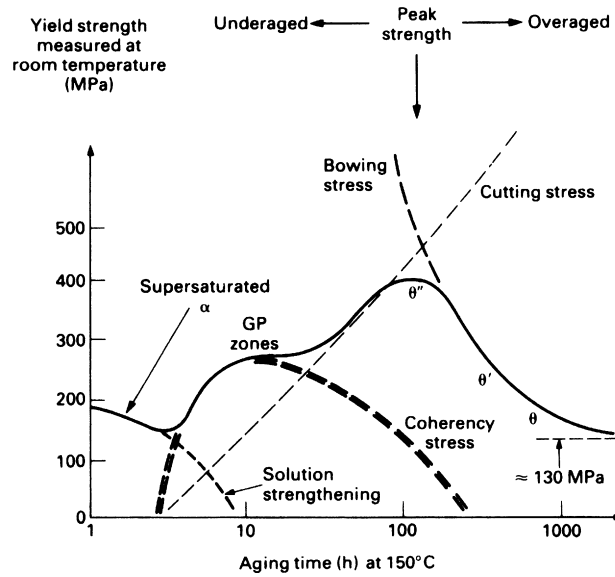
**FIGURE 11.6**

Continued.

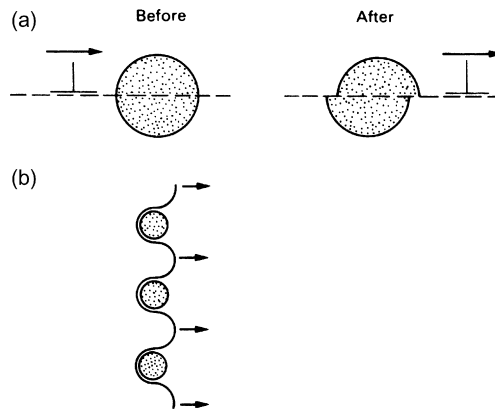
Bowing is easier when the precipitates are far apart. During aging, the precipitate spacing increases from 10 nm to 1 μm and beyond (Figure 11.9). The bowing stress therefore decreases with aging time (Figure 11.7).

The four hardening mechanisms add up to give the overall variation of yield strength as shown in Figure 11.7. *Peak strength is reached if the transformation is stopped at θ' .* If the alloy is aged some more the strength will *decrease*; and the only way of recovering the strength of an overaged alloy is to solution treat it at 550 °C, quench, and start again! If the alloy is not aged for long enough, then it will not reach peak strength; but this can be put right by more aging.

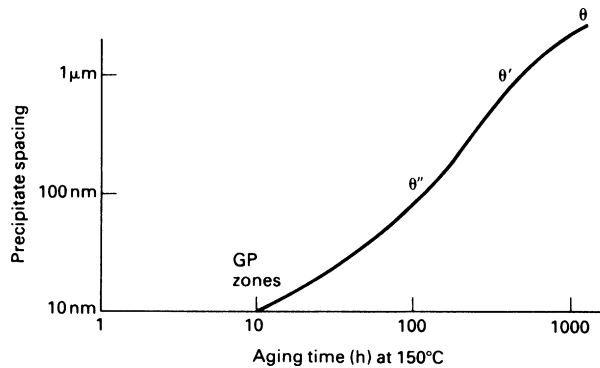
Although we have chosen to age our alloy at 150 °C, we could, in fact, have aged it at any temperature below 180 °C (Figure 11.10). The lower the aging temperature, the longer the time required to get peak hardness. In practice, the aging time should be long enough to give good

**FIGURE 11.7**

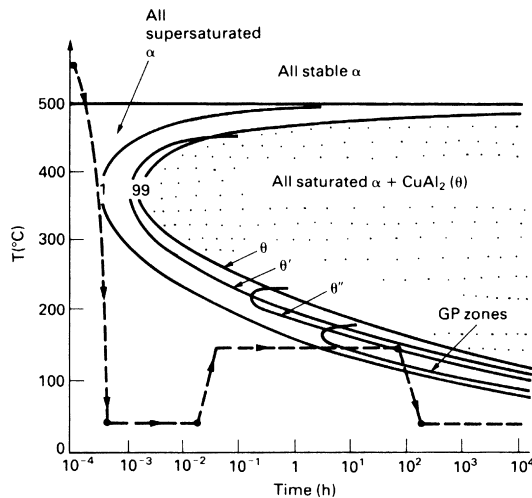
The yield strength of quenched Al–4 wt% Cu changes dramatically during aging at 150 °C.

**FIGURE 11.8**

Dislocations can get past precipitates by (a) cutting or (b) bowing.

**FIGURE 11.9**

The gradual increase of particle spacing with aging time.

**FIGURE 11.10**

Detailed TTT diagram for the Al–4 wt% Cu alloy. We get peak strength by aging to give θ'' . The lower the aging temperature, the longer the aging time. Note that GP zones do not form above 180 °C; if we age above this temperature we will fail to get the peak value of yield strength.

control of the heat treatment operation without being too long (and expensive).

Finally, Table 11.4 shows that copper is not the only alloying element that can age harden aluminum. Magnesium and titanium can be age hardened too, but not as much as aluminum.

Table 11.4 Yield Strengths of Heat Treatable Alloys

Alloy Series	Typical Composition (wt%)	σ_y (MN m ⁻²)	
		Slowly Cooled	Quenched and Aged
2000	Al + 4 Cu + Mg, Si, Mn	130	465
6000	Al + 0.5 Mg 0.5 Si	85	210
7000	Al + 6 Zn + Mg, Cu, Mn	300	570

Table 11.5 Yield Strengths of Work Hardened Aluminum Alloys

Alloy Number	σ_y (MN m ⁻²)		
	Annealed	Half Hard	Hard
1100	35	115	145
3005	65	140	185
5456	140	300	370

11.4 WORK HARDENING

Commercially pure aluminum (1000 series) and the non heat-treatable aluminum alloys (3000 and 5000 series) are usually work hardened. The work hardening superimposes on any solution hardening to give considerable extra strength (Table 11.5).

Work hardening is usually achieved by extrusion or cold rolling. The yield strength increases with strain (reduction in thickness) according to

$$\sigma_y = A\varepsilon^n, \tag{11.2}$$

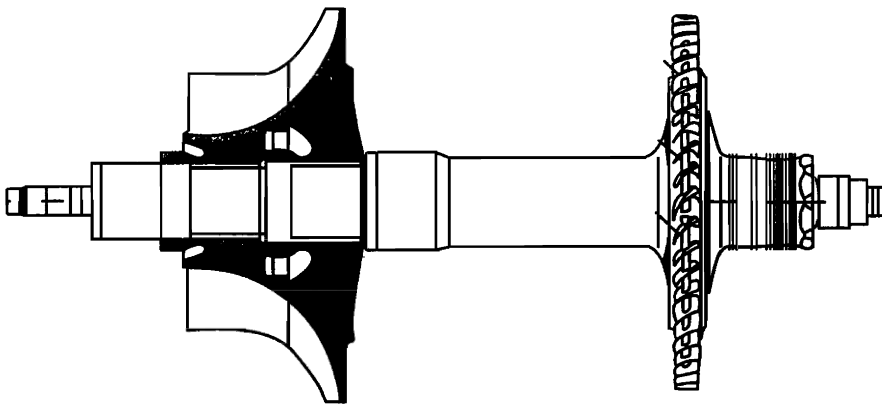
where A and n are constants. For aluminum alloys, n lies between 1/6 and 1/3.

WORKED EXAMPLE

We saw from Figure 11.10 that the Al–4% Cu alloy is age hardened to get peak strength by quenching the solution treated alloy to room temperature, and then holding it at 150 °C for 100 h. However, the aging time depends strongly on temperature—at 100 °C, for example, the time required to

achieve peak strength is much greater—about 10,000 h; and at 180 °C (above this temperature the GP zones no longer form), the time is about 1 h. This tells us that diffusion of Cu and Al in the alloy increases rapidly as the temperature goes above 100–120 °C. This is not surprising when we consider that the alloy starts to melt at around 855 K—after all, 120 °C is $0.46 T_M$.

This also means that if we use age hardened alloys at temperatures much above 100 °C, they will continue to age—and will lose strength. Not only this, but creep becomes a problem too. (We saw in EM1Ed4, p. 312 that metals start to creep when the temperature exceeds approximately $0.3\text{--}0.4 T_M$.) However, there are applications where we do use age hardened aluminum alloys at temperatures of the order of 150 °C. An important example is in the compressor wheels of turbochargers for diesel engines in ships and railway locomotives (see the diagram which follows).



The compressor wheel is manufactured as a forging, which is then machined to shape by a computer controlled 5-axis milling machine. It is then solution treated, quenched, and aged to obtain peak strength. When the engine is operating at full load, the maximum temperature at the outlet end of the compressor can be as high as 175 °C, although most of the time the outlet temperature is “only” about 140–160 °C. (In order to compress the air, the turbine must do work on it, and most of this work goes into heating the air up.)

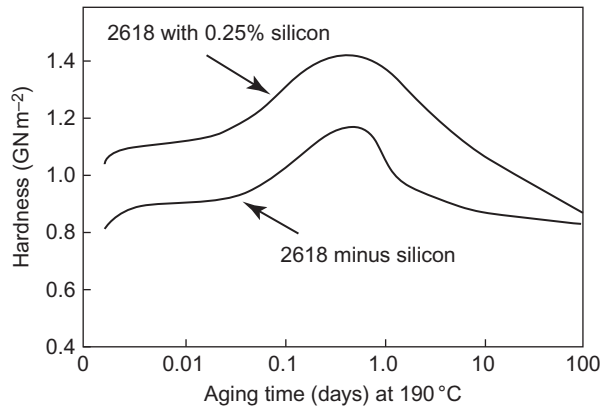
Because the wheels usually rotate at around 15,000 rpm, there is a large centrifugal force acting on them, which tends to make the wheel (especially toward the hot end of the compressor) expand by creep. This is not a good thing, because significant creep will allow the wheel to go out of true (and wobble at the high speed), and also the vanes may start to touch the compressor casing (at best, this will slow down the compressor; at worst it may break off vanes—with disastrous results). However, we want compressor

wheels to last for a long time (maybe 50,000 h) without significant loss in strength or creep strain. (When old compressor wheels are removed from service, they do in fact show a drop in hardness of around 10%.)

Ordinary Al–4% Cu alloy would not do this job—it overages completely after only 1000 h (see Figure 11.9), and in that state it creeps far too rapidly. Not surprisingly, developing a suitable alloy took a great deal of effort. The alloy of choice for this type of application is alloy 2618, in which the Al contains the following major alloying additions: 1.9–2.7 Cu/1.3–1.8 Mg/0.9–1.2 Ni/0.9–1.3 Fe/0.10–0.25 Si. The equilibrium precipitate is not CuAl_2 , but CuAl_2Mg , and the intermediate precipitates which give peak hardness have a different structure to θ'' (they are called S'). (The Ni and Fe are added to give another precipitate— FeNiAl_9 ; this forms large widely spaced particles which do not add to the strength and are there simply to control the grain size—we can forget them here.)

The diagram which follows shows the age hardening curve for alloy 2618 at 190 °C—peak hardness is reached after 0.6 days (14 h). Figure 11.10 shows that Al–4% Cu would reach peak hardness after only about 1 h at this temperature. Alloy 2618 obviously has much better thermal stability than Al–4% Cu. It is also interesting to see that the comparatively small addition of silicon (0.25%) increases peak strength by about 20%. In fact, the silicon makes the S' precipitates smaller, closer together, and more uniformly distributed. The smaller gaps between the precipitates, of course, make the alloy stronger.

Alloy 2618 is also used for things like pistons in diesel engines, which “see” temperatures of about 150 °C. The skin of the supersonic passenger aircraft Concorde was made from a variant of 2618, called RR58, in order to stand the service temperature of 150 °C caused by friction from the high-speed airflow.



Hardness of alloy 2618 measured at room temperature after aging for various times at 190 °C. Note how adding 0.25% silicon increases the hardness.

EXAMPLES

- 11.1** An alloy of Al–4 wt% Cu was heated to 550 °C for a few minutes and was then quenched into water. Samples of the quenched alloy were aged at 150 °C for various times before being quenched again. Hardness measurements taken from the requenched samples gave the following data:

Aging Time (h)	0	10	100	200	1000
Hardness (MN m ⁻²)	650	950	1200	1150	1000

Account briefly for this behavior.

Peak hardness is obtained after 100 h at 150 °C. Estimate how long it would take to get peak hardness at (a) 130 °C, (b) 170 °C.

[Hint: use [Figure 11.10](#).]

Answers

(a) 10³ h; (b) 10 h.

- 11.2** A batch of 7000 series aluminum alloy rivets for an aircraft wing was inadvertently overaged. What steps can be taken to reclaim this batch of rivets?
- 11.3** Two pieces of work hardened 5000 series aluminum alloy plate were butt welded together by arc welding. After the weld had cooled to room temperature, a series of hardness measurements was made on the surface of the fabrication. Sketch the variation in hardness as the position of the hardness indenter passes across the weld from one plate to the other. Account for the form of the hardness profile and indicate its practical consequences.
- 11.4** One of the major uses of aluminum is for making beverage cans. The body is cold drawn from a single slug of 3000 series non heat-treatable alloy, because this has the large ductility required for the drawing operation. However, the top of the can must have a much lower ductility in order to allow the ring-pull to work (the top must tear easily). Which alloy would you select for the top from [Table 11.5](#)? Explain the reasoning behind your choice. Why are non heat-treatable alloys used for can manufacture?
- 11.5** A sample of Al–4 wt% Cu was cooled slowly from 550 °C to room temperature. The yield strength of the slowly cooled sample was 130 MN m⁻². A second sample of the alloy was quenched into cold water from 550 °C and was then aged at 150 °C for 100 h. The yield strength of the quenched-and-aged sample was 450 MN m⁻². Explain the difference in yield strength. (Both yield strengths were measured at 20 °C.)
- 11.6** [Figures 11.2 and 11.5](#) show the TTT diagrams for the precipitation reactions in Al–5.5% Mg and Al–4% Cu. When solution hardening the Al–Mg alloy, it is only necessary to cool the metal moderately quickly (≈ 180 s from the solution treatment temperature to room temperature). However, when quenching the

Al–Cu alloy prior to age hardening, it is necessary to quench the metal very rapidly into cold water or oil (≈ 15 s from the solution treatment temperature to room temperature). Explain why one needs to have this large difference in cooling rate.

- 11.7** In solid solution hardened Al–Mg alloys, the yield strength σ_y is related to the concentration C of Mg in solid solution by the equation

$$\sigma_y = kC^n,$$

where k and n are constants. Use the data given in Table 11.3 to estimate the value of n .

Answer

0.7.

- 11.8** How does adding 0.25% Si to alloy 2618 affect the maximum hardness obtained after age hardening at 190 °C? How does silicon alter the size and spacing of the S' precipitates? How does this explain the effect of silicon on the maximum hardness?
- 11.9** During the age hardening of Al–4% Cu alloy, why are the θ'' precipitates disk shaped whereas the θ precipitates have rounded shapes?
- 11.10** During the age hardening of Al–4% Cu alloy, the GP zones nucleate homogeneously. Why is homogeneous nucleation possible under these conditions?

Steels 1—Carbon Steels

12.1 INTRODUCTION

Iron is one of the oldest known metals. Methods of extracting and working it have been practised for 3000–4000 years, although the large-scale production of carbon steels is a development of the nineteenth century. From these carbon steels (which account for 90% of steel production), a range of alloy steels has evolved: the low alloy steels (containing up to 6% of chromium, nickel, etc.); the stainless steels (containing typically 18% chromium and 8% nickel), and the tool steels (alloyed with chromium, molybdenum, tungsten, vanadium, and cobalt).

We already know something about the transformations that take place in steels and the microstructures that they produce. In this chapter, we draw these features together and go on to show how they are vital in determining the mechanical properties of steels. We restrict ourselves to carbon steels; alloy steels are covered in Chapter 13.

Carbon is the cheapest and the most effective alloying element for hardening iron. We have already seen in Chapter 1 (Table 1.1) that carbon is added to iron in quantities ranging from 0.04 to 1.7 wt% to make low-, medium-, and high-carbon steels. The mechanical properties are strongly dependent on both the carbon content and the type of heat treatment. Steels can therefore be used in a wide range of applications (see Table 1.1).

12.2 MICROSTRUCTURES AFTER SLOW COOLING (NORMALIZING)

Carbon steels as delivered have usually been worked at high temperature by rolling and have then been cooled slowly to room temperature (“normalized”). The room temperature microstructure should then be close to equilibrium and can be inferred from the Fe–C phase diagram (Figure 12.1) which we have already come across in Chapter 4. Table 12.1 lists the *phases*

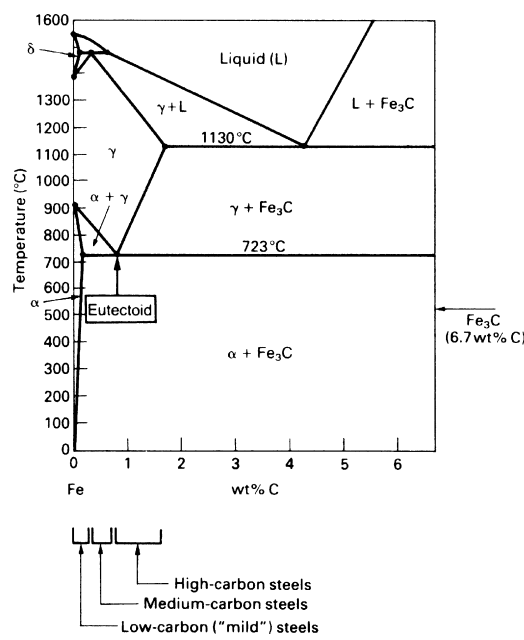


FIGURE 12.1 The left-hand part of the iron–carbon phase diagram. There are five phases in the Fe–Fe₃C system: L, δ, γ, α, and Fe₃C (see Table 12.1).

Table 12.1 Phases in the Fe–Fe ₃ C System		
Phase	Atomic Packing	Description and Comments
Liquid	d.r.p.	Liquid solution of C in Fe.
δ	b.c.c.	Random interstitial solid solution of C in b.c. c. Fe. Maximum solubility of 0.08 wt% C occurs at 1492 °C. Pure δ Fe is the stable polymorph between 1391 and 1536 °C (see Figure 2.1).
γ (also called austenite)	f.c.c.	Random interstitial solid solution of C in f.c.c. Fe. Maximum solubility of 1.7 wt% C occurs at 1130 °C. Pure γ Fe is the stable polymorph between 914 and 1391 °C (see Figure 2.1).
α (also called ferrite)	b.c.c.	Random interstitial solid solution of C in b.c.c. Fe. Maximum solubility of 0.035 wt% C occurs at 723 °C. Pure α Fe is the stable polymorph below 914 °C (see Figure 2.1).
Fe ₃ C (also called iron carbide or cementite)	Complex	A hard and brittle chemical compound of Fe and C containing 25 atomic % (6.7 wt%) C.

in the Fe–Fe₃C system and Table 12.2 gives details of the composite eutectoid structure that occurs during slow cooling.

Figures 12.2–12.6 show how the room temperature microstructure of carbon steels depends on the carbon content. The limiting case of pure iron (Figure 12.2) is straightforward: when γ iron cools below

Table 12.2 Composite Structure Produced During the Slow Cooling of Fe–C Alloys

Name of Structure	Description and Comments
Pearlite	The composite eutectoid structure of alternating plates of α and Fe ₃ C produced when γ containing 0.80 wt% C is cooled below 723 °C. Pearlite nucleates at γ grain boundaries. It is sometimes, quite wrongly, called a phase. It is not a phase but is a <i>mixture</i> of the two separate phases α and Fe ₃ C in the proportions of 88.5% by weight of α to 11.5% by weight of Fe ₃ C. Because grains are single crystals it is <i>wrong</i> to say that pearlite forms in grains: we say instead that it forms in <i>nodules</i> .

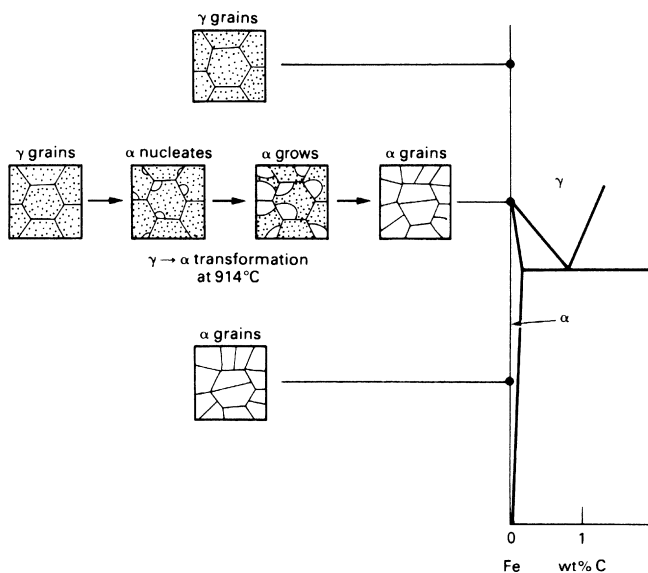


FIGURE 12.2

Microstructures during the slow cooling of pure iron from the hot working temperature.

914 °C α grains nucleate at γ grain boundaries and the microstructure transforms to α . If we cool a steel of eutectoid composition (0.80 wt% C) below 723 °C pearlite nodules nucleate at grain boundaries (Figure 12.3) and the microstructure transforms to pearlite. If the steel contains less than 0.80% C (a *hypoeutectoid* steel), then the γ starts to transform as soon as the alloy enters the $\alpha + \gamma$ field (Figure 12.4). “Primary” α nucleates at γ grain boundaries and grows as the steel is cooled from A_3 to A_1 . At A_1 the remaining γ (which is now of eutectoid composition) transforms to pearlite as usual. The room temperature microstructure is then made up of primary α + pearlite. If the steel contains more than 0.80% C (a *hypereutectoid* steel), then we get a room temperature microstructure of primary Fe_3C plus pearlite instead (Figure 12.5). These structural differences are summarized in Figure 12.6. Figures 12.7 and 12.8 show a real microstructure—from a polished and etched section of a low-carbon steel.

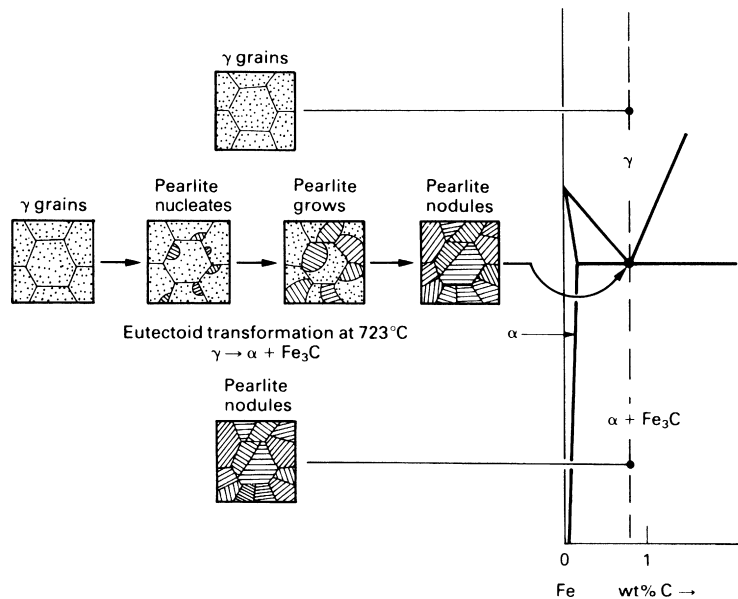


FIGURE 12.3

Microstructures during the slow cooling of a eutectoid steel from the hot working temperature. As a point of detail, when pearlite is cooled to room temperature, the concentration of carbon in the α decreases slightly, following the $\alpha/\alpha + \text{Fe}_3\text{C}$ boundary. The excess carbon reacts with iron at the $\alpha\text{--Fe}_3\text{C}$ interfaces to form more Fe_3C . This “plates out” on the surfaces of the existing Fe_3C plates which become very slightly thicker. The composition of Fe_3C is independent of temperature, of course.

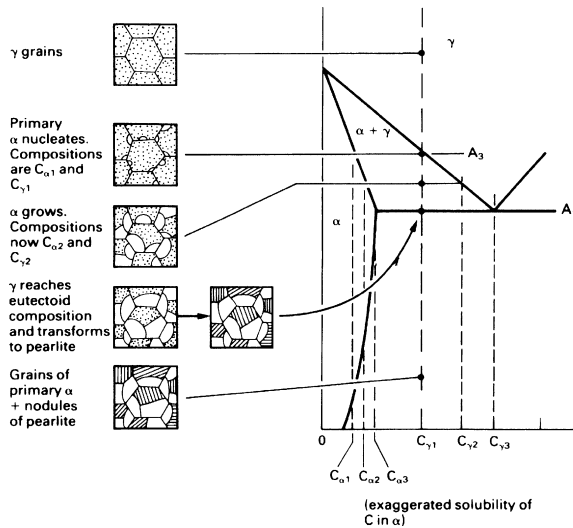


FIGURE 12.4

Microstructures during the slow cooling of a hypoeutectoid steel from the hot working temperature. A_3 is the standard labeling for the temperature at which α first appears, and A_1 is standard for the eutectoid temperature. *Hypoeutectoid* means that the carbon content is *below* that of a eutectoid steel (in the sense that hypodermic means "under the skin").

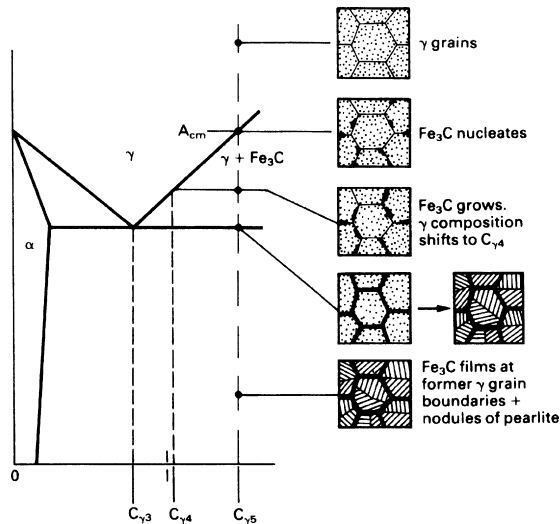
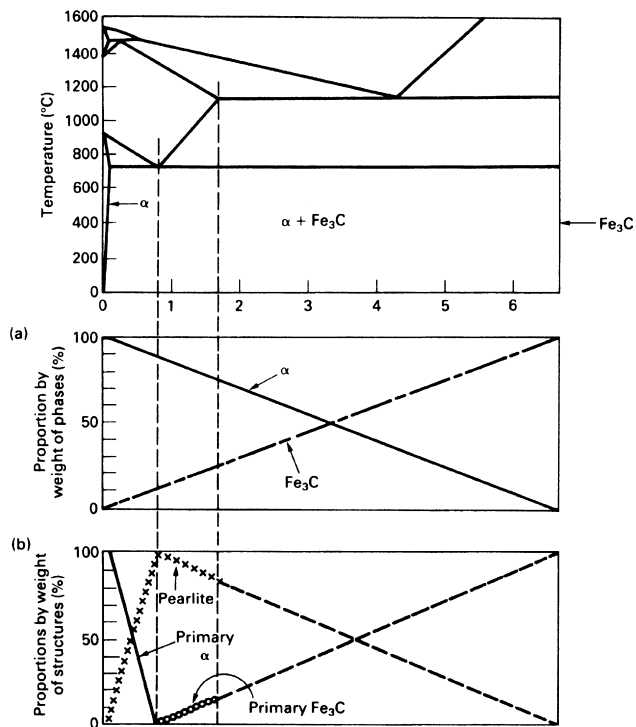


FIGURE 12.5

Microstructures during the slow cooling of a hypereutectoid steel. A_{cm} is the standard labeling for the temperature at which Fe_3C first appears. *Hypereutectoid* means that the carbon content is *above* that of a eutectoid steel (in the sense that a hyperactive child exhibits above-normal activity).

**FIGURE 12.6**

Room temperature microstructures in slowly cooled steels of different carbon contents. (a) The proportions by weight of the different phases. (b) The proportions by weight of the different *structures*.

**FIGURE 12.7**

Microstructure of a normalized low-carbon (hypoeutectoid) steel. The white areas are grains of primary α (ferrite) and the black areas are nodules of pearlite. Magnification $\times 95$. Refer to Figure 12.4 for the schematic of the transformations which produced this microstructure.

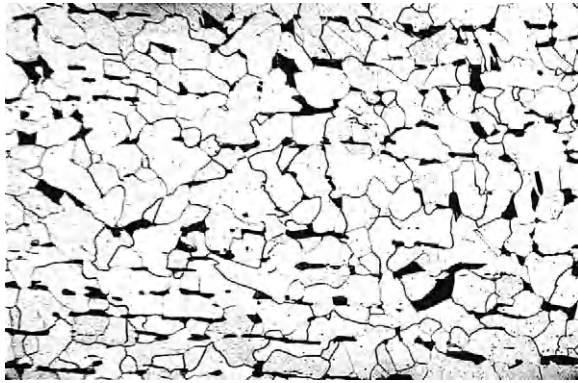


FIGURE 12.8

Structure of Figure 12.7 at a higher magnification ($\times 130$). This is still not enough to resolve the individual plates of α and Fe_3C in the pearlite, which is why the sectioned nodules still look uniform black.

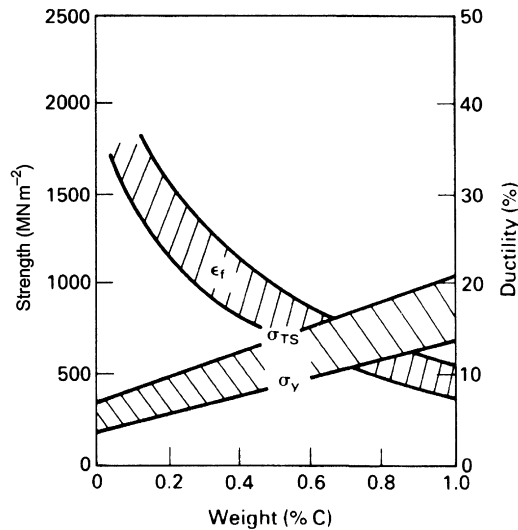
12.3 MECHANICAL PROPERTIES OF NORMALIZED STEELS

Figure 12.9 shows how the mechanical properties of normalized carbon steels change with carbon content. Both the yield strength and tensile strength increase linearly with carbon content. This is what we would expect: the Fe_3C acts as a strengthening phase, and the proportion of Fe_3C in the steel is linear in carbon concentration (Figure 12.6(a)). The ductility, on the other hand, falls rapidly as the carbon content goes up (Figure 12.9) because the α – Fe_3C interfaces in pearlite are good at nucleating cracks.

12.4 QUENCHED-AND-TEMPERED STEELS

We saw in Chapter 9 that if we cool eutectoid γ to 500°C at about 200°C s^{-1} , we will miss the nose of the C-curve. If we continue to cool below 280°C , the unstable γ will begin to transform to martensite. At 220°C half the γ will have transformed to martensite. And at -50°C , the steel will have become completely martensitic. Hypoeutectoid and hyper-eutectoid steels can be quenched to give martensite in exactly the same way (although, as Figure 12.10 shows, their C-curves are slightly different).

Figure 12.11 shows that the hardness of martensite increases rapidly with carbon content. This, again, is what we would expect. We saw in Chapter 9 that martensite is a supersaturated solid solution of C in Fe. Pure iron at room temperature would be b.c.c., but the supersaturated carbon distorts the lattice, making it tetragonal (Figure 12.11). The distortion increases linearly with the

**FIGURE 12.9**

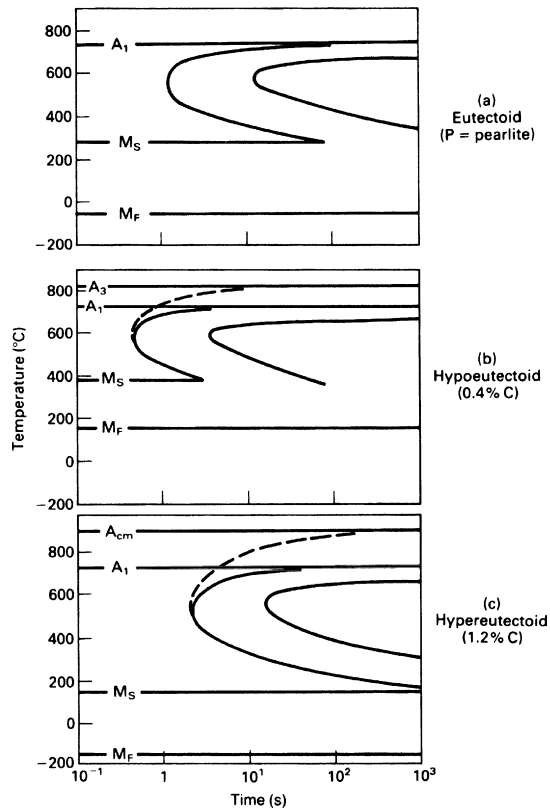
Mechanical properties of normalized carbon steels.

amount of dissolved carbon (Figure 12.11); and because the distortion is what gives martensite its hardness then this, too, must increase with carbon content.

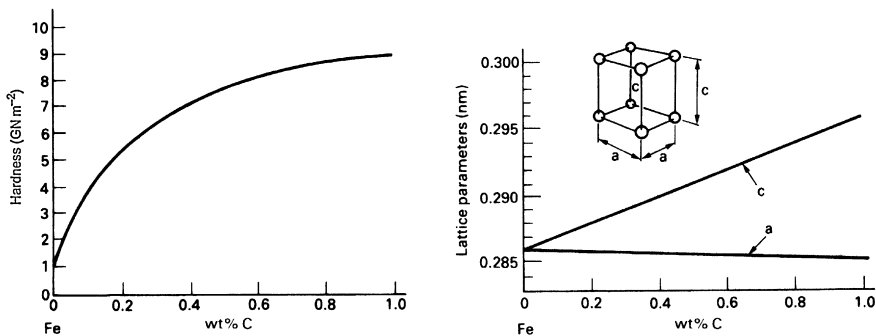
Although 0.8% carbon martensite is very hard, it is also very *brittle*. You can quench a 3 mm rod of tool steel into cold water and then snap it like a carrot. But if you *temper* martensite (reheat it to 300–600 °C), you can regain the lost toughness with only a moderate sacrifice in hardness. Tempering gives the carbon atoms enough thermal energy that they can diffuse out of supersaturated solution and react with iron to form small closely spaced precipitates of Fe_3C (Figure 12.12). The lattice relaxes back to the undistorted b.c.c. structure of equilibrium α , and the ductility goes up as a result. The Fe_3C particles precipitation harden the steel and keep the hardness up. If the steel is overtempered, however, the Fe_3C particles *coarsen* (they get larger and further apart) and the hardness falls. Figure 12.13 shows the big improvements in yield and tensile strength that can be obtained by quenching and tempering steels in this way.

12.5 NOTES ON THE TTT DIAGRAM

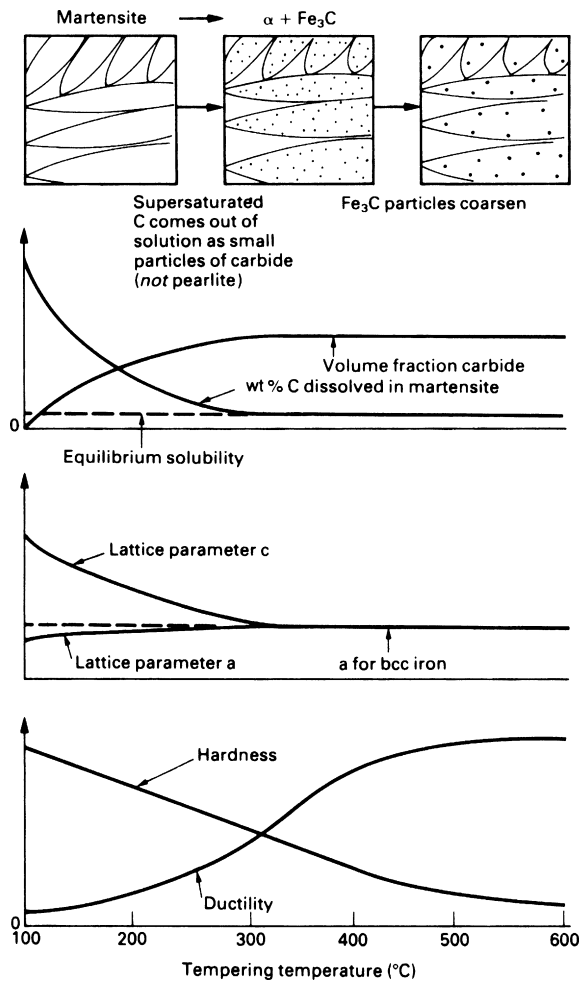
The C-curves of TTT diagrams are determined by quenching a specimen to a given temperature, holding it there for a given time, and quenching to room temperature (Figure 12.14). The specimen is then sectioned, polished, etched, and examined in the microscope. The percentage of Fe_3C present in the sectioned specimen allows one to find out how far the $\gamma \rightarrow \alpha + \text{Fe}_3\text{C}$

**FIGURE 12.10**

TTT diagrams for (a) eutectoid, (b) hypoeutectoid, and (c) hypereutectoid steels. (b) and (c) show (dashed lines) the C-curves for the formation of primary α and Fe₃C, respectively. Note that as the carbon content increases, both M_s and M_f decrease.

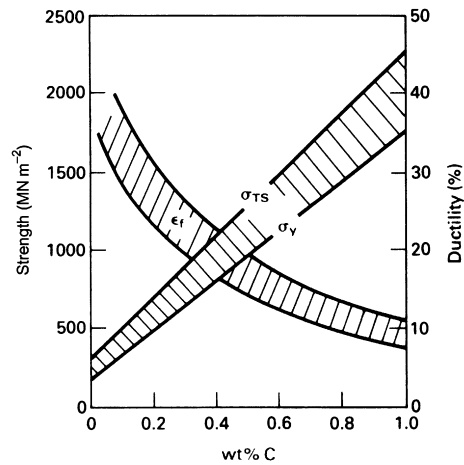
**FIGURE 12.11**

The hardness of martensite increases with carbon content because of the increasing distortion of the lattice.

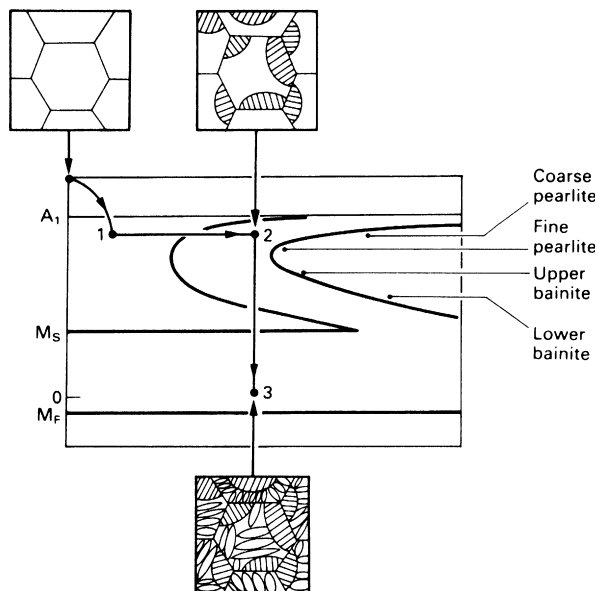
**FIGURE 12.12**

Changes during the tempering of martensite. There is a large driving force trying to make the martensite transform to the equilibrium phases of $\alpha + \text{Fe}_3\text{C}$. Increasing the temperature gives the atoms more thermal energy, allowing the transformation to take place.

transformation has gone (Figure 12.14). The complete set of C-curves can be built up by doing a large number of experiments at different temperatures and for different times. In order to get fast enough quenches, thin specimens are quenched into baths of molten salt kept at the various hold temperatures. A quicker alternative to quenching and sectioning is to follow the progress of the transformation with a high-resolution dilatometer: both α and Fe_3C are less dense than γ and the extent of the expansion observed after a given holding time tells us how far the transformation has gone.

**FIGURE 12.13**

Mechanical properties of quenched-and-tempered steels. Compare with Figure 12.9.

**FIGURE 12.14**

C-curves are determined using quench—hold—quench sequences.

When the steel transforms at a high temperature, with little undercooling, the pearlite in the steel is coarse—the plates in any nodule are relatively large and widely spaced. At slightly lower temperatures we get fine pearlite. Below the nose of the C-curve, the transformation is too fast for the Fe_3C to grow

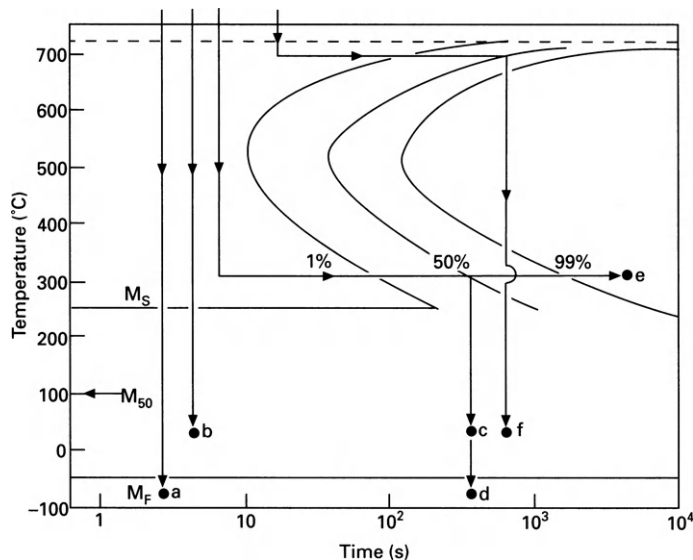
in nice, tidy plates. It grows instead as isolated stringers to give a structure called “upper bainite” (Figure 12.14). At still lower temperatures the Fe_3C grows as tiny rods and there is evidence that the α forms by a displacive transformation (“lower bainite”). The decreasing scale of the microstructure with increasing driving force (coarse pearlite \rightarrow fine pearlite \rightarrow upper bainite \rightarrow lower bainite in Figure 12.14) is an example of the general rule that, *the harder you drive a transformation, the finer the structure you get*.

Because C-curves are determined by quench—hold—quench sequences they can, strictly speaking, only be used to predict the microstructures that would be produced in a steel subjected to a quench—hold—quench heat treatment. But the curves do give a reasonable indication of the structures to expect in a steel that has been cooled *continuously*. For accurate predictions, however, we need to use *continuous cooling diagrams*.

A final note is that pearlite and bainite *only* form from undercooled γ . They *never* form from martensite. The TTT diagram *cannot* therefore be used to tell us anything about the rate of tempering in martensite.

EXAMPLES

12.1 The diagram which follows shows the TTT diagram for a coarse-grained, plain carbon steel of eutectoid composition. Samples of the steel are austenitized at 850°C and then subjected to the quenching treatments shown on the diagram. Describe the microstructure produced by each heat treatment.



12.2 You have been given samples of the following materials:

- (a) Pure iron.
- (b) 0.3 wt% carbon steel.
- (c) 0.8 wt% carbon steel.
- (d) 1.2 wt% carbon steel.

Sketch the structures that you would expect to see if you looked at polished and etched sections of the samples under a reflecting light microscope. Label the phases and any other features of interest. You may assume that each specimen has been cooled moderately slowly from a temperature of 1100 °C.

12.3 The densities of pure iron and iron carbide at room temperature are 7.87 and 8.15 Mg m⁻³, respectively. Calculate the percentages by volume of α and Fe₃C in pearlite.

Answers

α , 88.9%; Fe₃C, 11.1%.

12.4 Samples of plain carbon steel of eutectoid composition are to be heat treated to produce the following metallurgical structures:

- (a) pearlite
- (b) bainite
- (c) martensite
- (d) tempered martensite.

In each case, describe the structure (using simple sketches to illustrate your answer) and indicate a suitable heat treatment.

12.5 Indicate how the yield strength and tensile strength of normalized carbon steels depend on carbon content, and give a simple explanation for these dependencies.

12.6 Indicate how the tensile ductility of normalized carbon steels depends on carbon content, and give a simple explanation for this dependency.

12.7 Indicate how the hardness of martensite depends on the carbon content of the steel, and give a simple explanation for this dependency.

12.8 Explain what is meant by tempering. Why are martensitic steels usually tempered? Why is it important not to overtemper a quench-hardened steel?

12.9 Explain how you would determine the TTT diagram for a carbon steel of eutectoid composition. Why should TTT diagrams only be used as a guide to predicting the microstructure obtained in commercial heat treatments (where the steel is usually cooled continuously from the austenite region)?

12.10 State whether the following statements are true or false, and explain your answers.

- (a) The microstructure of a normalized hypoeutectoid steel consists of grains of ferrite and grains of pearlite.
- (b) The first new phase to nucleate when a hypereutectoid steel is cooled slowly from the austenite region is primary iron carbide.

- (c) When a 0.8% carbon martensite is overtempered, the structure changes to fine pearlite.

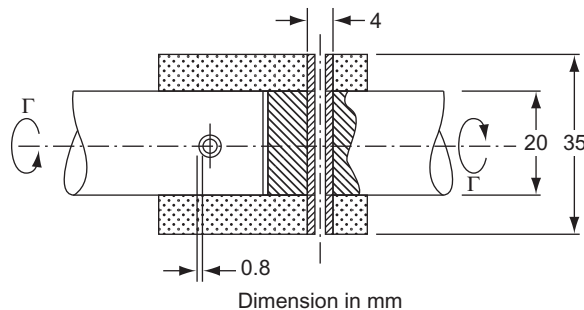
Answers

(a) False; (b) true; (c) false.

- 12.11** The diagram which follows shows a coupling between two rotating shafts designed to transmit power from a low-speed hydraulic motor to a gearbox. The coupling sleeve was a sliding fit on the shafts and the torque was carried by the two Bissell pins as shown in the diagram. During operation, one of the pins sheared, disconnecting the drive. You are called in as an engineering expert to determine the cause of the failure and decide that it was caused by a malfunction in the gearbox, which overloaded the coupling. However, an expert hired by the gearbox manufacturer (a metallurgist) alleges that the pin broke because it had not been tempered properly and was too brittle. In order to investigate this theory, you dismantle the assembly and measure the microhardness of the failed pin (on the flat end face). You find this to be approximately 500 GN m^{-2} . Does this indicate that the pin should be brittle as the metallurgist claims? Explain your answer. (The usual material for Bissell pins is spring steel containing about 0.8% carbon). What might you learn by measuring the hardness of the other pin (the one which did not fail)?

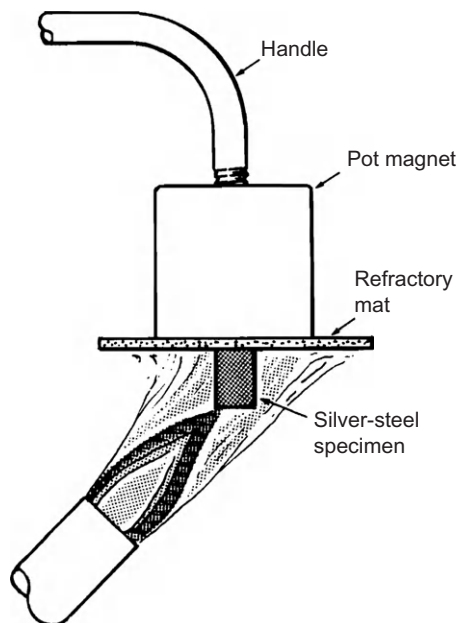
Answer

There is no evidence that the pin was brittle.



- 12.12** In what ways are the mechanical properties of quenched-and-tempered 1.0% carbon steel superior to those of normalized 1.0% carbon steel? How do the differences in microstructure between the two steels explain this superiority?
- 12.13** Briefly summarize (a) the similarities and (b) the differences between quenching and tempering in a 0.8% carbon steel, and age hardening in a Al–4% Cu alloy.

- 12.14** If a quenched carbon steel is overtempered, the Fe_3C particles coarsen (they get larger, further apart, and fewer in number). What is the driving force for this process?
- 12.15** Plain carbon tool steels typically contain 1% carbon and are quenched and tempered to get the appropriate trade-off between hardness (so they keep a sharp cutting edge) and toughness (so they do not break under the cutting forces). When sharpening these tools on a grinding wheel, why is it very important to keep them cooled with water?
- 12.16** The diagram which follows shows an experiment for demonstrating magnetism in steel. The steel specimen is a 10 mm length of 6 mm diameter silver-steel rod. Silver steel is a high-carbon tool steel containing typically 1.1% carbon. The specimen is suspended beneath a pot magnet, with a square of 1.5 mm thick ceramic fiber mat inserted between the two. The specimen is then heated to bright red heat, at which point it falls away from the magnet. Explain why this happens. Note: (a) b.c.c. iron is magnetic, but this magnetism vanishes at the Curie temperature (which is 768°C for b.c.c. iron); (b) f.c.c. iron is nonmagnetic.

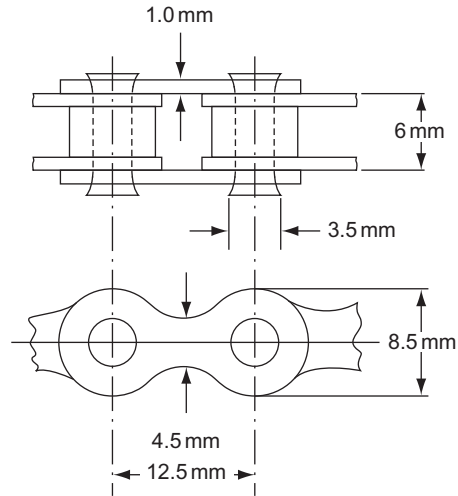


- 12.17** The diagram which follows shows the component parts of a bicycle chain. The average hardness measured on the face of a link is 530 GN m^{-2} ,

and on the end of a pin is 650 GN m^{-2} . Both links and pins are made from plain carbon steel. What is the minimum carbon content that the steels must have for (a) the links and (b) the pins? In practice, why must the carbon content of the steels be significantly greater than these minimum values?

Answers

(a) 0.2%; (b) 0.3%.



Steels 2—Alloy Steels

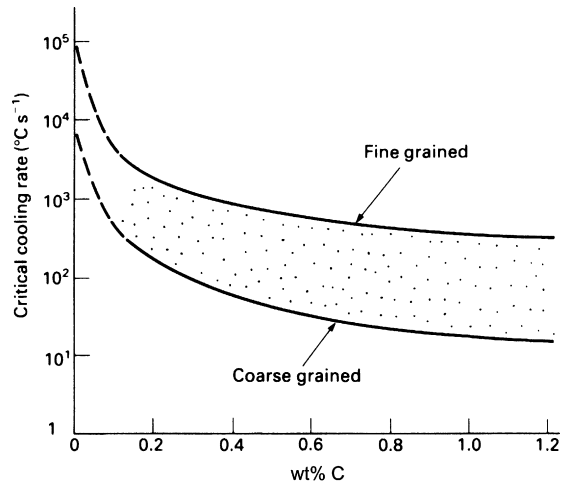
13.1 INTRODUCTION

A small, but extremely important, sector of the steel market is that of the alloy steels: the low-alloy steels, the high-alloy “stainless” steels, and the tool steels. Alloying elements are added to steels with four main aims in mind:

- (a) to improve the *hardenability* of the steel;
- (b) to give *solution strengthening* and *precipitation hardening*;
- (c) to give *corrosion resistance*;
- (d) to *stabilize austenite*, giving a steel that is austenitic (f.c.c.) at room temperature.

13.2 HARDENABILITY

We saw in the previous chapter that carbon steels could be strengthened by *quenching and tempering*. To get the best properties, we must quench the steel past the nose of the C-curve. The cooling rate that just misses the nose is called the *critical cooling rate* (CCR). If we cool at the critical rate, or faster, the steel will transform to 100% martensite. The CCR for a plain carbon steel depends on two factors—carbon content and grain size. We have already seen (in Chapter 9) that adding carbon decreases the rate of the diffusive transformation by orders of magnitude: the CCR decreases from $\approx 10^5\text{ }^\circ\text{C s}^{-1}$ for pure iron to $\approx 200\text{ }^\circ\text{C s}^{-1}$ for 0.8% carbon steel (Figure 13.1). We also saw in Chapter 9 that the rate of a diffusive transformation was related to the number of nuclei. Since grain boundaries are favorite nucleation sites, a fine-grained steel should produce more nuclei than a coarse-grained one. The fine-grained steel will

**FIGURE 13.1**

The effect of carbon content and grain size on the critical cooling rate.

therefore transform more rapidly than the coarse-grained steel and will have a higher CCR (Figure 13.1).

Quenching and tempering is usually limited to steels containing more than about 0.1% carbon. Figure 13.1 shows that these must be cooled at rates ranging from 100 to $2000\text{ }^{\circ}\text{C s}^{-1}$, if 100% martensite is to be produced. There is no difficulty in transforming the *surface* of a component to martensite—we simply quench the red-hot steel into a bath of cold water or oil. But if the component is at all large, the surface layers will tend to insulate the bulk of the component from the quenching fluid. The bulk will cool more slowly than the CCR and will not harden properly. Worse, a rapid quench can create shrinkage stresses which are quite capable of cracking brittle, untempered martensite.

These problems are overcome by alloying. The entire TTT curve is shifted to the right by adding a small percentage of the right alloying element to the steel—usually molybdenum (Mo), manganese (Mn), chromium (Cr), or nickel (Ni) (Figure 13.2). Numerous *low-alloy steels* have been developed with superior *hardenability*—the ability to form martensite in thick sections when quenched. This is one of the reasons for adding the 2–7% of alloying elements (together with 0.2–0.6% C) to steels used for things like crankshafts, high-tensile bolts, springs, connecting rods,

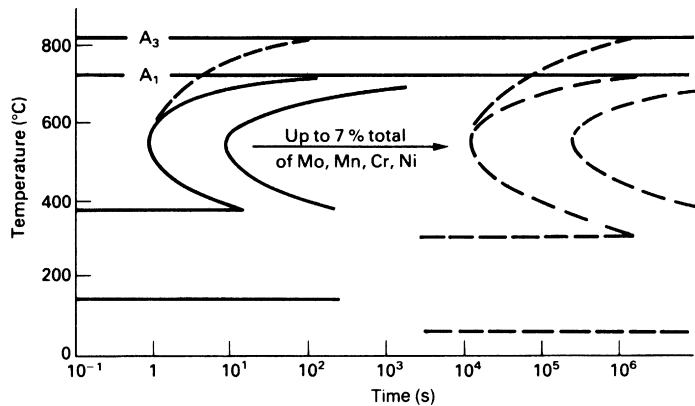


FIGURE 13.2

Alloying elements make steels more hardenable.

and spanners. Alloys with lower alloy contents give martensite when quenched into oil (a moderately rapid quench); the more heavily alloyed give martensite even when cooled in air. Having formed martensite, the component is tempered to give the desired combination of strength and toughness.

Hardenability is so important that a simple test is essential to measure it. The Jominy end-quench test, though inelegant from a scientific standpoint, fills this need. A bar 100 mm long and 25.4 mm in diameter is heated and held in the austenite field. When all the alloying elements have gone into solution, a jet of water is sprayed onto one end of the bar (Figure 13.3). The surface cools very rapidly, but sections of the bar behind the quenched surface cool progressively more slowly (Figure 13.3). When the whole bar is cold, the hardness is measured along its length. A steel of high hardenability will show a uniform, high hardness along the whole length of the bar (Figure 13.4). This is because the cooling rate, even at the far end of the bar, is greater than the CCR; and the whole bar transforms to martensite. A steel of medium hardenability gives quite different results (Figure 13.5). The CCR is much higher and is only exceeded in the first few centimeters of the bar. Once the cooling rate falls below the CCR, the steel starts to transform to bainite rather than martensite and the hardness drops off rapidly.

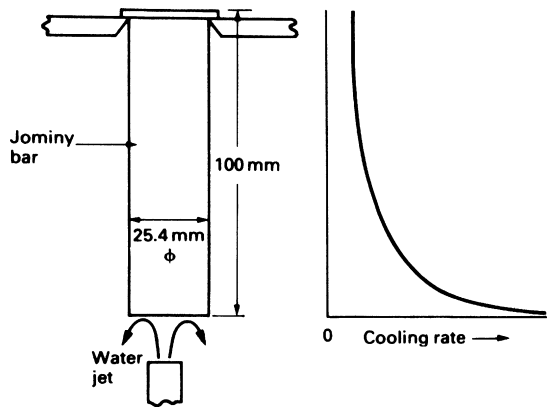


FIGURE 13.3
The Jominy end-quench test for hardenability.

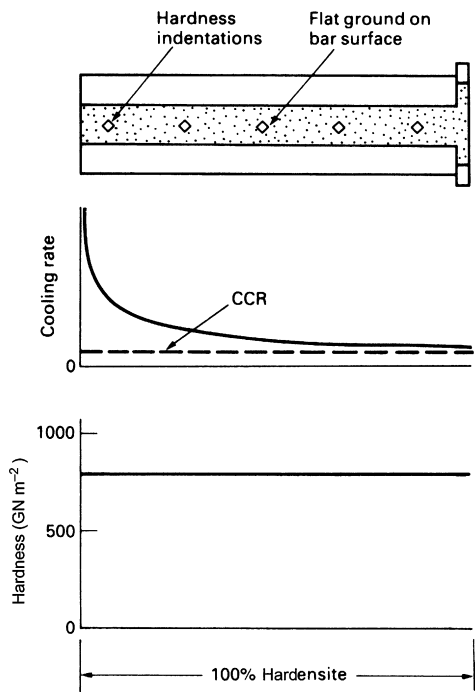


FIGURE 13.4
Jominy test on a steel of high hardenability.

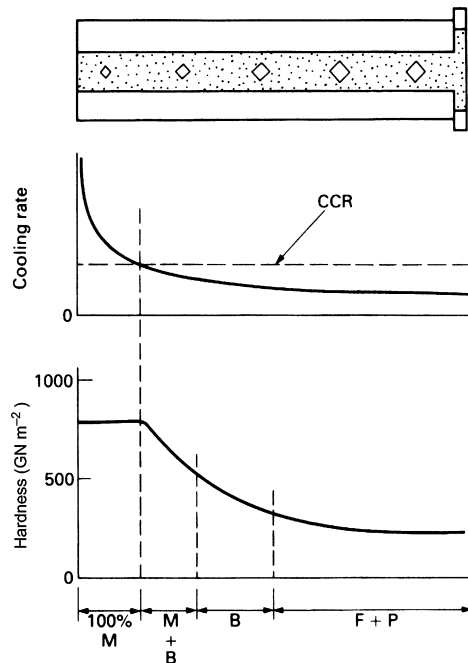


FIGURE 13.5

Jominy test on a steel of medium hardenability. M = martensite, B = bainite, F = primary ferrite, P = pearlite.

13.3 SOLUTION HARDENING

The alloying elements in the *low-alloy steels* dissolve in the ferrite to form a substitutional solid solution. This solution strengthens the steel and gives useful additional strength. The *tool steels* contain large amounts of dissolved tungsten (W) and cobalt (Co) as well to give the maximum feasible solution strengthening. Because the alloying elements have large solubilities in both ferrite and austenite, no special heat treatments are needed to produce good levels of solution hardening. In addition, the solution-hardening component of the strength is not upset by overheating the steel. For this reason, low-alloy steels can be welded and cutting tools can be run hot without affecting the solution-hardening contribution to their strength.

13.4 PRECIPITATION HARDENING

The *tool steels* are an excellent example of how metals can be strengthened by precipitation hardening. Traditionally, cutting tools have been made from 1% carbon steel with about 0.3% of silicon (Si) and manganese (Mn).

Used in the quenched and tempered state they are hard enough to cut mild steel and tough enough to stand up to the shocks of intermittent cutting. But they have one serious drawback. When cutting tools are in use they become hot: woodworking tools become warm to the touch, but metalworking tools can burn you. It is easy to “run the temper” of plain carbon metalworking tools, and the resulting drop in hardness will destroy the cutting edge. The problem can be overcome by using low cutting speeds and spraying the tool with cutting fluid. But this is an expensive solution—slow cutting speeds mean low production rates and expensive products. A better answer is to make the cutting tools out of *high-speed* steel. This is an alloy tool steel containing typically 1% C, 0.4% Si, 0.4% Mn, 4% Cr, 5% Mo, 6% W, 2% vanadium (V), and 5% Co. The steel is used in the quenched and tempered state (the Mo, Mn, and Cr give good hardenability) and owes its strength to two main factors: the fine dispersion of Fe_3C that forms during tempering, and the solution hardening that the dissolved alloying elements give.

Interesting things happen when this high-speed steel is heated to 500–600°C. The Fe_3C precipitates dissolve and the carbon that they release combines with some of the dissolved Mo, W, and V to give a fine dispersion of Mo_2C , W_2C , and VC precipitates. This happens because Mo, W, and V are strong *carbide formers*. If the steel is now cooled back down to room temperature, we will find that this *secondary hardening* has made it even stronger than it was in the quenched and tempered state. In other words, “running the temper” of a high-speed steel makes it harder, not softer; and tools made out of high-speed steel can be run at much higher cutting speeds (hence the name).

13.5 CORROSION RESISTANCE

Plain carbon steels rust in wet environments and oxidize if heated in air. But if chromium is added to steel, a hard, compact film of Cr_2O_3 will form on the surface and this will help to protect the underlying metal. The minimum amount of chromium needed to protect steel is about 13%, but up to 26% may be needed if the environment is particularly hostile. The iron–chromium system is the basis for a wide range of *stainless steels*.

13.6 STAINLESS STEELS

The simplest stainless alloy contains just iron and chromium (it is actually called *stainless iron*, because it contains virtually no carbon). [Figure 13.6](#) shows the Fe–Cr phase diagram. The interesting thing about this diagram is that alloys containing $\geq 13\%$ Cr have a b.c.c. structure all the way from 0 K to the melting point. They do not enter the f.c.c. phase field and cannot be

quenched to form martensite. Stainless irons containing $\geq 13\%$ Cr are therefore always *ferritic*.

Hardenable stainless steels usually contain up to 0.6% carbon. This is added in order to change the Fe–Cr phase diagram. As Figure 13.7 shows, carbon expands the γ field so that an alloy of Fe–15% Cr,

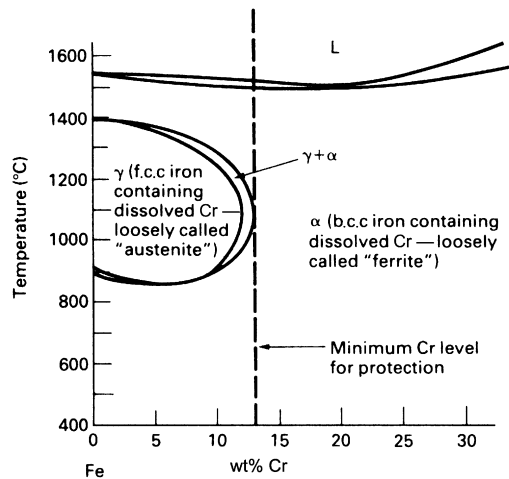


FIGURE 13.6
The Fe–Cr phase diagram.

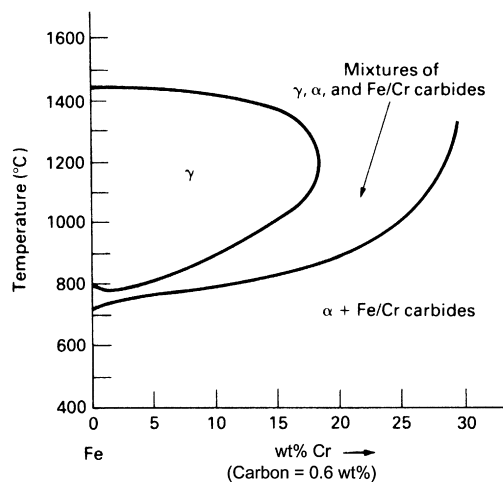


FIGURE 13.7
Simplified phase diagram for the Fe–Cr–0.6% C system.

0.6% C lies inside the γ field at 1000 °C. This steel can be quenched to give martensite; and the martensite can be tempered to give a fine dispersion of alloy carbides.

These quenched-and-tempered stainless steels are ideal for things like non-rusting ball-bearings, surgical scalpels, and kitchen knives.

Many stainless steels, however, are *austenitic* (f.c.c.) at room temperature. The most common austenitic stainless, “18/8”, has a composition Fe–0.1% C, 1% Mn, 18% Cr, 8% Ni. The chromium is added, as before, to give corrosion resistance. But *nickel* is added as well because it *stabilizes austenite*. The Fe–Ni phase diagram (Figure 13.8) shows why. Adding nickel lowers the temperature of the f.c.c.–b.c.c. transformation from 914 °C for pure iron to 720 °C for Fe–8% Ni. In addition, the Mn, Cr, and Ni slow the diffusive f.c.c.–b.c.c. transformation down by orders of magnitude. 18/8 stainless steel can therefore be cooled in air from 800 °C to room temperature without transforming to b.c.c. The austenite is, of course, unstable at room temperature. However, diffusion is far too slow for the metastable austenite to transform to ferrite by a diffusive mechanism. It is, of course, possible for the austenite to transform displacively to give martensite. But the large amounts of Cr and Ni lower the M_s temperature to ≈ 0 °C. This means that we would have to cool the steel well below 0 °C in order to lose much austenite.

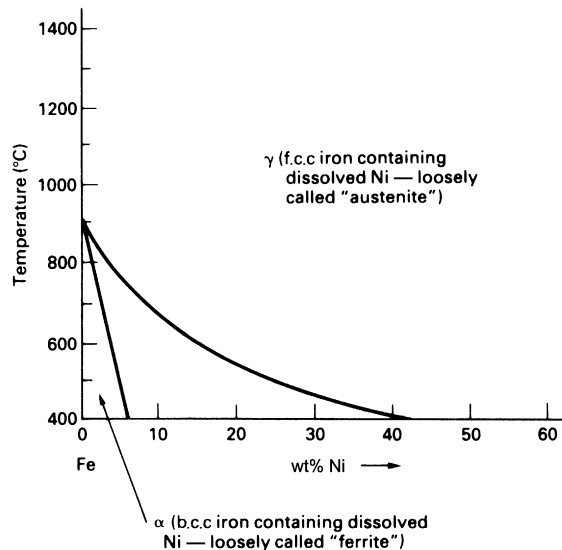


FIGURE 13.8

The Fe–Ni phase diagram.

Austenitic steels have a number of advantages over their ferritic cousins. They are tougher and more ductile. They can be formed more easily by stretching or deep drawing. Because diffusion is slower in f.c.c. iron than in b.c.c. iron, they have better creep properties. And they are nonmagnetic, which makes them ideal for instruments like electron microscopes and mass spectrometers.

But one drawback is that austenitic steels work harden very rapidly, which makes them rather difficult to machine.

13.7 PHASES IN STAINLESS STEELS

The structure of a stainless steel at room temperature depends to a large extent on its composition. Figure 13.9 shows the Schaeffler diagram, a map showing the fields of dominance of the phases as a function of composition. The labelings A, F, and M stand for austenite, ferrite, and martensite. Also shown is the region where sigma phase can form. This is an intermetallic with the approximate formula FeCr . Because sigma phase is brittle, stainless steels must have compositions which avoid it.

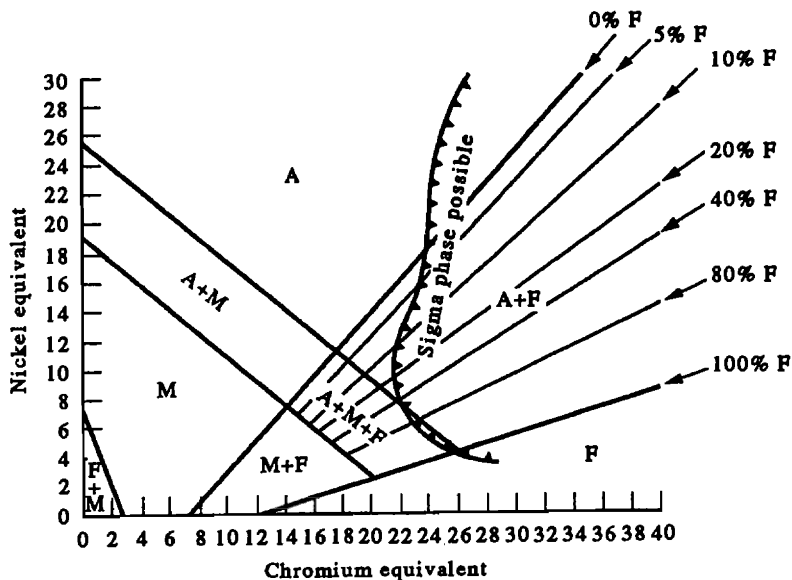


FIGURE 13.9
The Schaeffler diagram.

The vertical axis of the diagram is the nickel equivalent, which is given approximately by

$$\text{Nickel Equivalent} = \text{Ni} + 30 \text{ C} + 0.5 \text{ Mn} + 25 \text{ N.} \quad (13.1)$$

The horizontal axis is the chromium equivalent, given approximately by

$$\text{Chromium Equivalent} = \text{Cr} + \text{Mo} + 1.5 \text{ Si} + 0.5 \text{ Nb.} \quad (13.2)$$

The chemical symbols represent the concentration in weight % of the element concerned.

13.8 IMPROVING STAINLESS STEELS

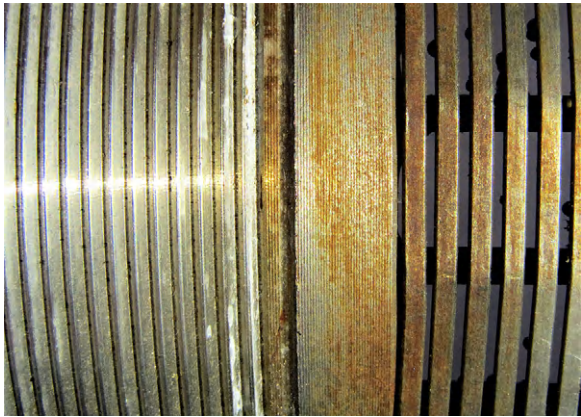
AISI 304 is the most common and basic stainless steel—it contains 18–20% Cr (and 8–10.5% Ni to make it f.c.c.). Its resistance to corrosion (especially pitting) can be improved a lot by adding molybdenum, which helps to stabilize the oxide film. The most common stainless steel containing Mo is AISI 316, which has 2–3% Mo, as well as 16–18% Cr (and 10–14% Ni). More recently, the super austenitics have been developed, such as 254 SMO and AL-6XN. These contain even more Mo (6%), Cr (20%), and Ni (20%), plus about 0.2% nitrogen. The N is absorbed as an interstitial solid solution—it is 16 times as effective as Cr in resisting pitting (and, incidentally, raises the yield strength by 25% because it pins dislocations). These alloys are also highly resistant to stress corrosion cracking. Finally, the new super duplex steels such as SAF 2507 have more Cr (25%), less Mo (4%) and Ni (7%) than the super austenitics. The low Ni content gives them a mixed (or duplex) f.c.c./b.c.c. structure, which has a yield strength twice that of 304 or 316. Because Ni is expensive, they are cheaper than the super austenitics yet are just as resistant to pitting and stress corrosion cracking. Such are the complications of developing alloys steels to resist corrosion!

WORKED EXAMPLE

The following three photographs show part of a water filter intended for use in borehole pumps on an irrigation project. The filter was a perforated tube with a diameter of 200 mm. The tube end was welded to a short threaded length of tube, which was used to connect the filter to a length of ordinary (nonperforated) tube. All the parts were made from 304 stainless steel. The perforated tube was made by assembling a tubular cage of steel rods (see photograph 1) and welding the end of each rod to the bore of the threaded coupling (see photograph 2).

A helix of wire was then wound around the outside of the cage to complete the wall (see photograph 3). The wire was fixed to the support rods by electrical resistance spot welding. The wire had a triangular-shaped cross section, and the width of the gap between adjacent wires was a minimum at the outside of the pipe wall, so the gaps would not become clogged with sand particles entrained in the water.





The filters were transported to site by sea. When they were unloaded, light rusting was observed on the machined surface of the coupling (see photograph 3) and on the bore of the coupling near to the heat-affected zone of the weld (see photograph 2). Concern was expressed that the steel might have been supplied to the wrong chemical composition. Indeed, it had failed the traditional workshop “test”: although an austenitic stainless steel like 304 should be nonmagnetic, some of the filters had shown a marked affinity for a magnet!

The following table gives data for the relative magnetic permeability of 304 stainless steel. When the steel is in the fully annealed condition, the permeability is very close to 1, and the metal is effectively nonmagnetic. However, the permeability increases with cold work: up to a hardness of about 320 the effect is small, but larger amounts of cold work result in a significant increase in permeability.

Magnetism of 304-Type Stainless Steel as a Function of Cold Work

Reduction in Thickness, $(t_0 - t)/t_0$	Diamond–Pyramid Hardness (HV)	Relative Permeability for $H = 4000 \text{ A m}^{-1}$	Relative Permeability for $H = 16,000 \text{ A m}^{-1}$
0	175	1.0037	1.0040
0.14	218	1.0048	1.0050
0.32	315	1.0371	1.062
0.65	390	1.540	2.12
0.85	437	2.20	4.75

Why can austenitic stainless steels go magnetic in this way? The thermodynamic stability of the austenite phase is controlled by the chemical composition of the steel. The range of composition over which austenite is stable at room temperature can be found from the Schaeffler diagram

(Figure 13.9). The vertical axis of the diagram plots the *nickel equivalent*, which is given by $\text{Ni} + 30 \text{ C} + 0.5 \text{ Mn} + 25 \text{ N}$. The horizontal axis plots the *chromium equivalent*, given by $\text{Cr} + \text{Mo} + 1.5 \text{ Si} + 0.5 \text{ Nb}$. Nickel, carbon, manganese, and nitrogen all stabilize austenite, but we need a nickel equivalent of at least 11 to get into the austenite field on the diagram.

The compositions of AISI 304 and the nearest BS equivalents are given in the next table; the corresponding nickel and chromium equivalents are 10–13, and 17–20. These values put us right at the bottom of the austenite field on the Schaeffler diagram. Depending on the precise composition the austenite in 304 stainless is unstable at room temperature; severe cold work can then trigger a displacive transformation where some of the austenite flips over into the magnetic martensite phase instead.

Compositions of 304-Type Stainless Steels in Weight %

Element	AISI 304	BS 304 S15	BS 304 S31
Carbon	0.08 max	0.06 max	0.07 max
Silicon	0.75/1.00 max	1.00 max	1.00 max
Manganese	2.00 max	2.00 max	2.00 max
Sulfur	0.030 max	0.030 max	0.030 max
Phosphorus	0.045 max	0.045 max	0.045 max
Chromium	18.00–20.00	17.5–19.0	17.0–19.0
Molybdenum	—	—	—
Nickel	8.00–10.50	8.0–11.0	8.0–11.0
Titanium	—	—	—
Niobium	—	—	—

Site engineers tend to be skeptical of complicated explanations, so it was decided to stage an experimental demonstration of this theory. A number of samples were removed from the filter and were tested with both a magnet and a hardness tester. The results, which are shown in the following table, were remarkably consistent with the data quoted above. An even better demonstration was to show that all traces of magnetism could be removed by heating the samples to red heat and cooling them down to room temperature again.

Magnetism of Filter Components

Component	Diamond–Pyramid Hardness (HV)	Magnetic Attraction
Coupling	180	Very weak
Rod/wire	350	Weak
Rod/wire	430	Strong

EXAMPLES

13.1 Explain the following.

- (a) The critical cooling rate (CCR) is approximately $700\text{ }^{\circ}\text{C s}^{-1}$ for a fine-grained 0.6% carbon steel but is only around $30\text{ }^{\circ}\text{C s}^{-1}$ for a coarse-grained 0.6% carbon steel.
- (b) A stainless steel containing 18% Cr has a b.c.c. structure at room temperature, whereas a stainless steel containing 18% Cr plus 12% Ni has an f.c.c. structure at room temperature.
- (c) High-speed steel cutting tools retain their hardness to well above the temperature at which the initial martensitic structure has become overtempered.

13.2 A steel shaft 40 mm in diameter is to be hardened by austenitizing followed by quenching into cold oil. The center of the bar must be 100% martensite. The following table gives the cooling rate at the center of an oil quenched bar as a function of bar diameter.

Bar Diameter (mm)	Cooling Rate ($^{\circ}\text{C s}^{-1}$)
500	0.17
100	2.5
20	50
5	667

It is proposed to make the shaft from a NiCrMo low-alloy steel. The critical cooling rates of NiCrMo steels are given quite well by the empirical equation

$$\log_{10}(\text{CCR in } ^{\circ}\text{C s}^{-1}) = 4.3 - 3.27 C - \frac{(\text{Mn} + \text{Cr} + \text{Mo} + \text{Ni})}{1.6}$$

where the symbol given for each element denotes its weight percentage. Which of the following steels would be suitable for this application?

Steel	Weight Percentages				
	C	Mn	Cr	Mo	Ni
A	0.30	0.80	0.50	0.20	0.55
B	0.40	0.60	1.20	0.30	1.50
C	0.36	0.70	1.50	0.25	1.50
D	0.40	0.60	1.20	0.15	1.50
E	0.41	0.85	0.50	0.25	0.55
F	0.40	0.65	0.75	0.25	0.85
G	0.40	0.60	0.65	0.55	2.55

(Hint: There is a log–log relationship between bar diameter and cooling rate.)

Answer

Steels B, C, D, G.

13.3 State whether the following statements are true or false, and explain your answers.

- (a) If a carbon steel of eutectoid composition is quenched from the austenite region into water at 10 °C, the final structure will be 100% martensite.
- (b) Stainless steels are always nonmagnetic.
- (c) When quenching steels to make hardened parts, it is much easier to avoid quench cracks if low-alloy steel is used instead of plain carbon steel.

Answers

(a) False; (b) false; (c) true.

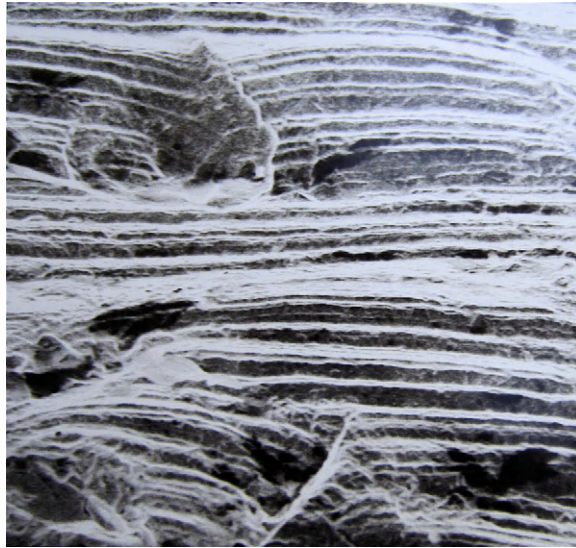
13.4 Using the compositions given in the Worked Example for AISI 304 stainless steel, calculate the *maximum permitted* value of the chromium equivalent (CrE), and the *minimum permitted* value of the nickel equivalent (NiE) (assume that the minimum C and Mn contents are 0.03 and 1). What approximate percentage of ferrite does the Schaeffler diagram give for this pair of values? What is the *maximum* permitted NiE? What percentage of ferrite does this give when combined with the maximum permitted CrE?

Answers

Max CrE = 21.5; min NiE = 9.4; 20% ferrite; max NiE = 13.9; 5% ferrite.

- 13.5** The super austenitic stainless steels typically contain 20 Cr, 6 Mo, 20 Ni, and 0.2 N. Estimate the CrE and NiE values (assuming that Si = 1, Nb = 0, C = 0.03, Mn = 1). Do these values place the structure inside the austenite field on the Schaeffler diagram, and if so how much “spare” NiE is there?
- 13.6** Extremely pure 316 stainless steel is much used for medical implants, such as bone screws, intramedullar nails, hip stems, and coronary stents. For highly stressed implants, a high-nitrogen variant, containing 0.4% nitrogen is used. This typically increases the tensile strength of the annealed steel from 500 to 750 MN m^{−2}. Explain why the nitrogen has this effect. High-tensile grades are also available, in the form of cold-drawn wires and rods. They typically have tensile strengths of 1100 MN m^{−2} (standard alloy) and 1350 MN m^{−2} (high-nitrogen alloy). Explain why these strengths are so much more than those of the annealed steels. What can you say about the contribution of the nitrogen to the strength of the cold-drawn compared to the annealed material? Why is it essential to use austenitic steels in the human body?
- 13.7** What are the most important service requirements to consider when selecting alloys for medical implants such as hip stems, knee joints, and spinal prostheses? Why is 316 much better than 304 stainless steel at meeting one

of these requirements? The photograph shows the fracture surface from a broken knee joint. Although it is not made from stainless steel (it is made from cobalt–chrome alloy containing 64 Co, 29 Cr, 6 Mo), it provides very clear indications of one very important service requirement. What is this requirement?



- 13.8** Threaded steel studs were used to hold together parts of a submersible pump in a borehole for extracting salty water. The studs had corroded badly after a relatively short time in service at 20 °C. The analysis of the steel was as follows (in wt%): 0.36 C, 0.72 Mn, 0.07 Ni, 1.00 Cr, 0.02 Mo. Explain why the studs corroded.
- 13.9** Compare the as-quenched hardness distributions along a Jominy test bar for steels of (a) medium hardenability and (b) high hardenability. Explain how the hardness distributions are related to the microstructures in the test bars.
- 13.10** What range of compositions is required so that stainless steel can be quenched to martensite? Give some practical applications of hardenable stainless steels. What secondary property of martensitic steels can be useful in some applications?

Case Studies in Steels

14.1 DETECTIVE WORK AFTER A BOILER EXPLOSION

The first case study shows how a knowledge of steel microstructures can help to trace the chain of events that led to a damaging engineering failure.

The failure took place in a large water-tube boiler used for generating steam in a chemical plant. The layout of the boiler is shown in [Figure 14.1](#). At the bottom of the boiler is a cylindrical pressure vessel—the mud drum—which contains water and sediments. At the top of the boiler is the steam drum, which contains water and steam. The two drums are connected by 200 tubes

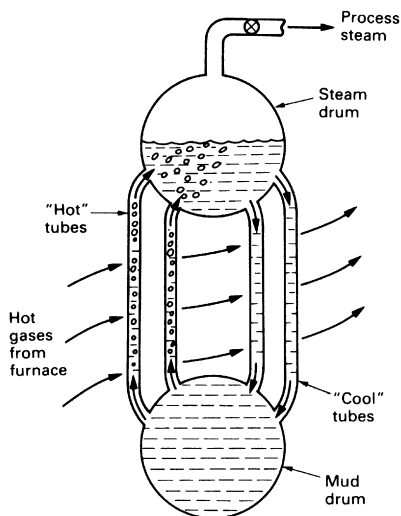


FIGURE 14.1

Schematic of water-tube boiler.

through which the water circulates. The tubes are heated from the outside by the flue gases from a coal-fired furnace. The water in the “hot” tubes moves upward from the mud drum to the steam drum, and the water in the “cool” tubes moves downward from the steam drum to the mud drum. A convection circuit is therefore set up where water circulates around the boiler and picks up heat in the process. The water tubes are 10 m long, have an outside diameter of 100 mm, and are 5 mm thick in the wall. They are made from a steel of composition Fe–0.18% C, 0.45% Mn, 0.20% Si. The boiler operates with a working pressure of 50 bar and a water temperature of 264 °C.

In the incident, some of the “hot” tubes became overheated and started to bulge. Eventually one of the tubes burst open and the contents of the boiler were discharged into the environment. No one was injured in the explosion, but it took several months to repair the boiler and the cost was high. In order to prevent another accident, a materials specialist was called in to examine the failed tube and comment on the reasons for the failure.

Figure 14.2 shows a schematic diagram of the burst tube. The first operation was to cut out a 20 mm length of the tube through the center of the failure. One of the cut surfaces of the specimen was then ground flat and tested for hardness. Figure 14.3 shows the data that were obtained. The hardness of most of the section was about 2.2 GN m^{-2} , but at the edges of the rupture the hardness went up to 4 GN m^{-2} . This indicates (see Figure 14.3) that the structure at the rupture edge is mainly martensite. However, away from the rupture, the structure is largely bainite. Hardness tests done on a

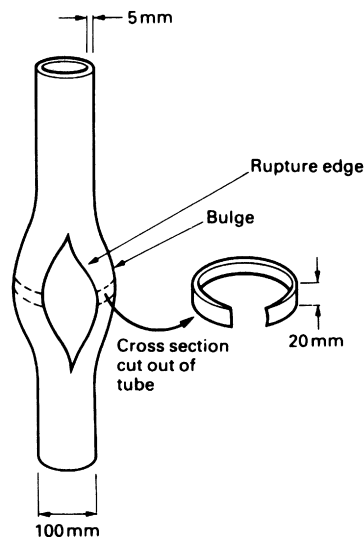


FIGURE 14.2

Schematic of burst tube.

spare boiler tube gave only 1.5 GN m^{-2} , showing that the failed tube would have had a ferrite + pearlite microstructure to begin with.

In order to produce martensite and bainite, the tube must have been overheated to at least the A_3 temperature of 870°C (Figure 14.4). When the rupture occurred, the rapid outrush of boiler water and steam cooled the steel rapidly down to 264°C . The cooling rate was greatest at the rupture edge, where the section was thinnest: high enough to quench the steel to martensite. In the main bulk of the tube the cooling rate was less, which is why bainite formed instead.

The hoop stress in the tube under the working pressure of 50 bar (5 MN m^{-2}) is $5 \text{ MN m}^{-2} \times 50 \text{ mm}/5 \text{ mm} = 50 \text{ MN m}^{-2}$. Creep data indicate that, at 900°C and 50 MN m^{-2} , the steel should fail after only 15 min or so. In all probability, then, the failure occurred by creep rupture during a short temperature excursion to at least 870°C .

How was it that water tubes reached such high temperatures? We can give two probable reasons. The first is that “hard” feed water will—unless properly treated—deposit scale inside the tubes (Figure 14.5). This scale will help to insulate the metal from the boiler water and the tube will tend to

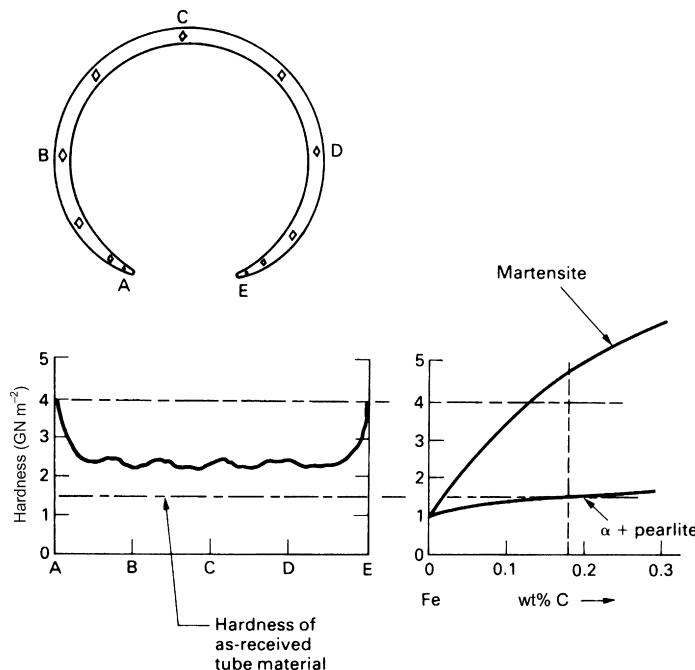
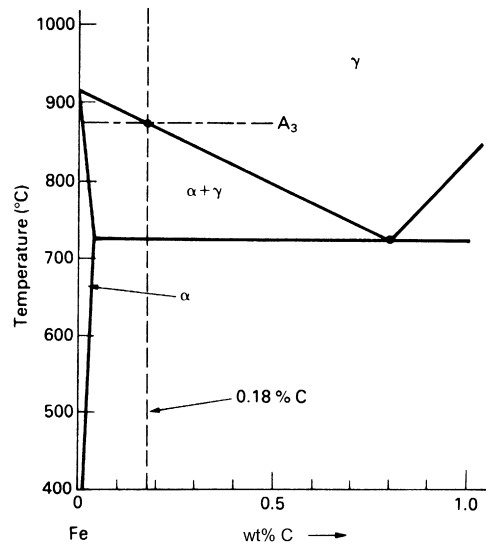
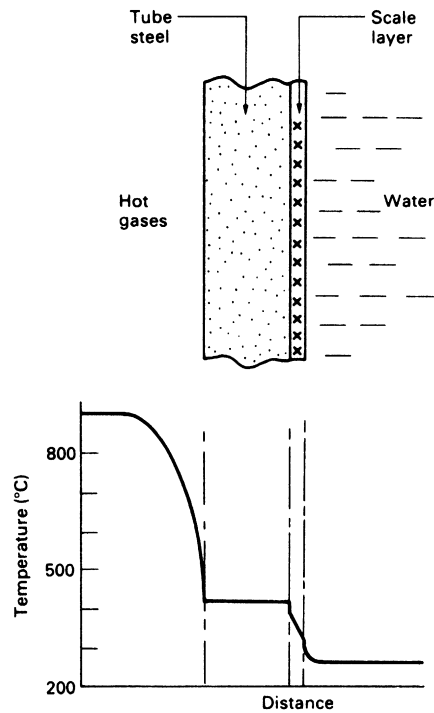


FIGURE 14.3

The hardness profile of the tube.

**FIGURE 14.4**

Part of the iron—carbon phase diagram.

**FIGURE 14.5**

Temperature distribution across the water-tube wall.

overheat. Secondly, water circulation in a natural convection boiler can be rather hit or miss; and the flow in some tubes can be very slow. Under these conditions, a stable layer of dry steam can form next to the inner wall of the tube and this, too, can be a very effective insulator.

14.2 WELDING STEELS SAFELY

Many steel structures—like bridges, storage tanks, and ships—are held together by welds. And when incidents arise from fast fractures or fatigue failures they can often be traced to the welds. The sinking of the Alexander Keilland oil platform in 1980 is an example [http://en.wikipedia.org/wiki/Alexander_L._Kielland_\(platform\)](http://en.wikipedia.org/wiki/Alexander_L._Kielland_(platform)).

Figure 14.6 is a schematic of a typical welding operation. An electric arc is struck between the electrode (which contains filler metal and flux) and the parent plates. The heat from the arc melts the filler metal which runs into the gap to form a molten pool. Although the pool loses heat to the surrounding cold metal this is replaced by energy from the arc. In fact some of the parent material is melted back as well. But as the arc moves on, the molten steel that it leaves behind solidifies rapidly, fusing the two plates together. Figure 14.6 shows how the temperature in the metal varies with distance from the weld pool. Because the electrode moves along the weld, the isotherms bunch up in front of the pool like the bow wave of a ship; behind the pool they are spaced more widely. The passage of this thermal “wave” along the weld leads to very rapid *heating* of the metal in front of the weld pool and slightly less rapid *cooling* of the metal behind (Figure 14.7). The section of the plate that is heated above $\approx 650^\circ\text{C}$ has its mechanical properties changed as a result. For this reason it is called the *heat-affected zone* (HAZ). Figure 14.8 shows an example of a HAZ.

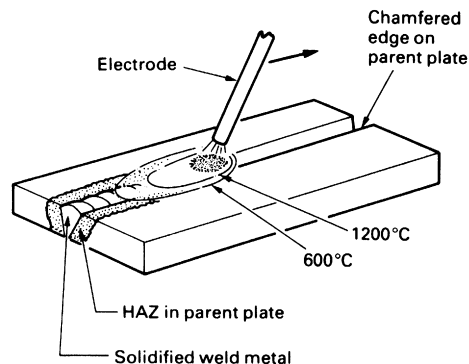
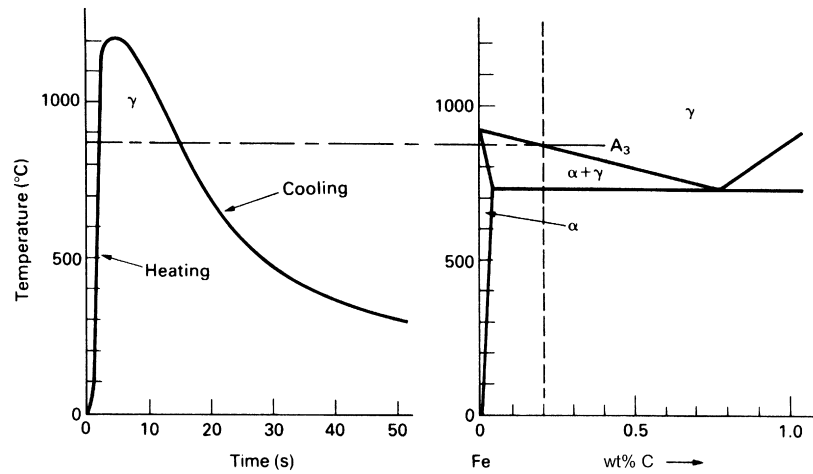
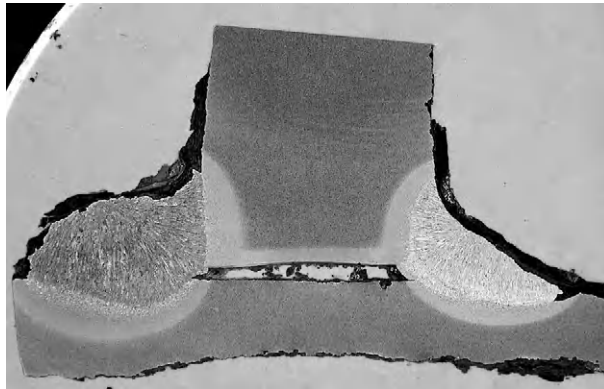


FIGURE 14.6

Schematic of a typical welding operation.

**FIGURE 14.7**

The left-hand graph shows how the temperature at one point in the parent plate changes as the welding arc passes by. The point chosen here is quite close to the edge of the plate, which is why it reaches a high peak temperature. A point further away from the edge would not reach such a high-peak temperature.

**FIGURE 14.8**

Polished and etched cross section through a pair of fillet welds between two low-carbon steel plates. Magnification $\times 2$. Because the weld pool solidified with a columnar structure, the interface between the weld metal and the parent plate can be seen clearly. The light-etching layer between the weld metal and the main body of the parent plate marks the extent of the HAZ. Interestingly, at the lower edge of the thick plate, there is also a shallow HAZ left by the flame-cutting process.

The most critical changes occur in the part of the HAZ that has been heated above the A_3 temperature (Figure 14.7). As the arc moves on, this part of the HAZ can cool as quickly as $100\text{ }^\circ\text{C s}^{-1}$. With a fine-grained carbon steel this should not be a problem: the CCR is more than $400\text{ }^\circ\text{C s}^{-1}$ (Figure 13.1) and little, if any, martensite should form. But some of the steel in the HAZ goes up to temperatures as high as $1400\text{ }^\circ\text{C}$. At such temperatures diffusion is extremely rapid, and in only a few seconds significant *grain growth* will take place (see Chapter 6). The CCR for this grain-growth zone will be reduced accordingly (Figure 13.1). In practice, it is found that martensite starts to appear in the HAZ when the carbon content is more than 0.5–0.6%.

The last thing that is wanted in a weld is a layer of hard, brittle martensite. It can obviously make the weld as a whole more brittle. And it can encourage *hydrogen cracking*. All welds contain quantities of atomic hydrogen (the molten steel in the weld pool rapidly reduces atmospheric moisture to give iron oxide and hydrogen). Because hydrogen is such a small atom, it can diffuse rapidly through steel (even at room temperature) and coalesce to give voids which, in a brittle material like martensite, will grow into cracks. These cracks can then extend (e.g., by fatigue) until they are long enough to cause fast fracture.

Example 1: Weldable structural steel to BS 4360 grade 43 A

BS 4360 is the structural steel workhorse. Grade 43 A has the following specifications: $C \leq 0.25\%$, $Mn \leq 1.60\%$, $Si \leq 0.50\%$; $\sigma_{TS} 430\text{--}510\text{ MN m}^{-2}$; $\sigma_y \geq 240\text{ MN m}^{-2}$.

The maximum carbon content of 0.25% is well below the 0.5–0.6% that may give HAZ problems. But, in common with all “real” carbon steels, 4360 contains manganese. This is added to react with harmful impurities like sulfur. Any unreacted manganese dissolves in ferrite where it contributes solid-solution strengthening and gives increased hardenability. But how do we know whether our 1.6% of manganese is likely to give HAZ problems? Most welding codes assess the effect of alloying elements from the empirical formula

$$CE = C + \frac{Mn}{6} + \frac{Cr + Mo + V}{5} + \frac{Ni + Cu}{15} \quad (14.1)$$

where CE is the *carbon equivalent* of the steel. The 1.6% Mn in our steel would thus be equivalent to $1.6\%/6 = 0.27\%$ carbon in its contribution to martensite formation in the HAZ. The total carbon equivalent is $0.25 + 0.27 = 0.52$. The cooling rate in most welding operations is unlikely

to be high enough to quench this steel to martensite. But poorly designed welds—like a small weld bead laid on a large plate—can cool very quickly. For this reason, failures often initiate not in the main welds of a structure but in small welds used to attach ancillary equipment like ladders and gangways. (It was a small weld of this sort which started the crack which led to the Alexander Keilland failure.)

Example 2: Pressure vessel steel to A 387 grade 22 class 2

A 387–22(2) is a creep-resistant steel which can be used at about 450 °C. It is a standard material for pipes and pressure vessels in chemical plants and oil refineries. The specification is: C ≤ 0.15%, Mn 0.25–0.66%, Si ≤ 0.50%, Cr 1.88–2.62%, Mo 0.85–1.15%; σ_{TS} 515–690 MN m^{−2}; σ_y ≥ 310 MN m^{−2}. The carbon equivalent for the maximum composition figures given is

$$CE = 0.15 + \frac{0.66}{6} + \frac{2.62 + 1.15}{5} = 1.01 \quad (14.2)$$

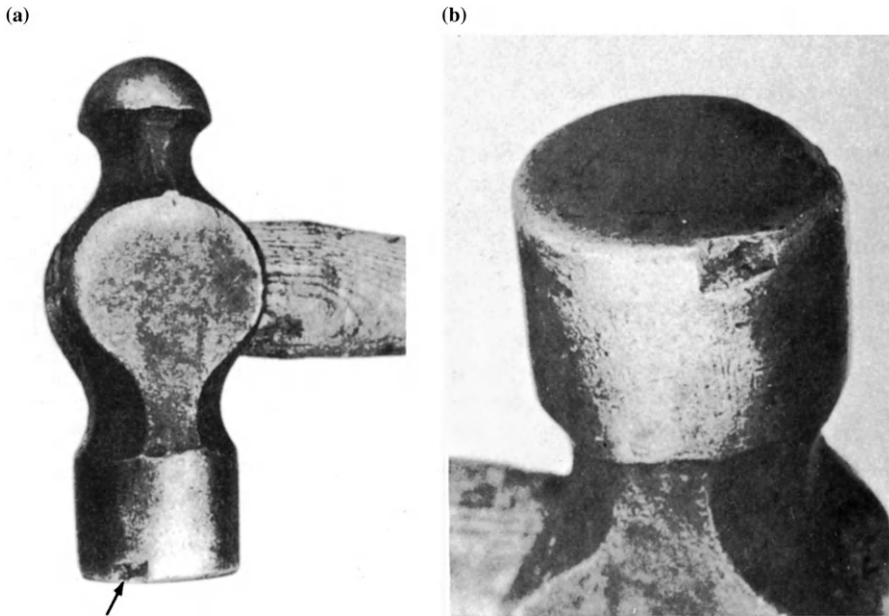
The Mn, Cr, and Mo in the steel have increased the hardenability considerably, and martensite is likely to form in the HAZ unless special precautions are taken. But the cooling rate can be decreased greatly if the parent plate is preheated to ≈ 350 °C before welding starts, and this is specified in the relevant welding code. Imagine yourself, though, as a welder working inside a large preheated pressure vessel: clad in an insulating suit and fed with cool air from outside you can only stand 10 min in the heat before making way for somebody else!

14.3 THE CASE OF THE BROKEN HAMMER

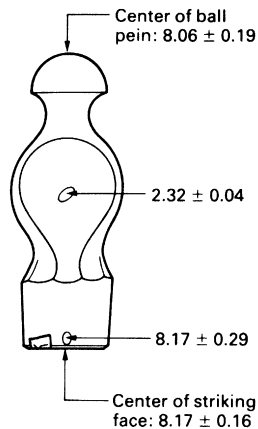
The father of one of the authors was breaking up some concrete slabs with an engineers' hammer when a large fragment of metal broke away and narrowly missed his eye. A 1½ lb hammer is not heavy enough for breaking up slabs, and he should have been wearing eye protection, but that is another matter. We examined the hammer to see whether the fracture might have been caused by faulty heat treatment.

Figure 14.9(a) shows the general shape of the hammer head and marks the origin of the offending fragment. Figure 14.9(b) is a close-up of the crater that the fragment left behind when it broke away.

The first thing that we did was to test the hardness of the hammer. The results are shown in Figure 14.10. The steel is very hard near the striking face and the ball pein, but the main body of the head is much softer.

**FIGURE 14.9**

(a) General view of hammer head. The origin of the fragment is marked with an arrow, (b) close-up of crater left by fragment.

**FIGURE 14.10**

Hardness results for hammer head (GN m^{-2}).

A typical standard for hammers (BS 876, 1995) states that hammers shall be made from a medium-carbon forging steel with the following limits on composition: 0.5–0.6% C, 0.5–0.9% Mn, and 0.1–0.4% Si. We would expect this steel to have a hardness of between 1.8 and 2.2 GN m^{-2} in the

as-received state. This is very close to the figure of 2.32 GN m^{-2} that we found for the bulk of the head, but much less than the hardness of face and pein. The bulk of the hammer was thus in the as-forged state, but both face and pein must have been hardened by quenching.

We can see from Figure 12.11 that untempered 0.55% carbon martensite should have a hardness of 8.0 GN m^{-2} . This is essentially identical to the hardnesses that we found on the striking face and the ball pein and suggests strongly that the face had not been tempered at all. In fact, the Standard says that faces and peins must be tempered to bring the hardness down into the range $5.1\text{--}6.6 \text{ GN m}^{-2}$. Presumably experience has shown that this degree of tempering makes the steel tough enough to stand up to normal wear and tear. Untempered martensite is far too brittle for hammer heads.

Having solved the immediate problem to our satisfaction, we still wondered how the manufacturer had managed to harden the striking faces without affecting the bulk of the hammer head. We contacted a maker of hammers who described the sequence of operations that is used. The heads are first shaped by hot forging and then allowed to cool slowly to room temperature. The striking face and ball pein are finished by grinding. The striking faces are austenitized as shown in Figure 14.11 and are then quenched into cold water. The only parts of the hammers to go above 723°C are the ends: so only these parts can be hardened by the quench. The quenched heads are then dried and the ends are tempered by completely immersing the heads in a bath of molten salt at 450°C . Finally, the heads are removed from the tempering bath and washed in cold water. The rather complicated austenitizing treatment is needed because the Standard insists that the hardened zone must not extend

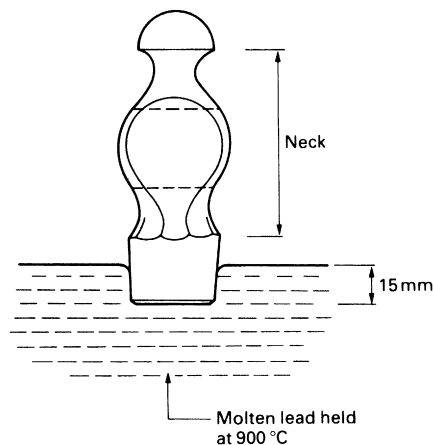


FIGURE 14.11
Austenitizing a striking face.

into the neck of the hammer (Figure 14.11). You can imagine how dangerous it would be if a hammer broke clean in two. The neck does not need to be hard, but it *does* need to be tough. Although there are standards for hammers, there is often no legislation which compels retailers to supply only standard hammers. It is, in fact, quite difficult to get standard hammers “over the counter.” But reputable makers spot check their hammers, because they will not knowingly sell improperly heat-treated hammers.

EXAMPLES

14.1 The heat exchanger in a reformer plant consisted of a bank of tubes made from a low-alloy ferritic steel containing 0.2 wt% carbon. The tubes contained hydrocarbon gas at high pressure and were heated from the outside by furnace gases. The tubes had an internal diameter of 128 mm and a wall thickness of 7 mm. Owing to a temperature overshoot, one of the tubes fractured and the resulting gas leak set the plant on fire.

When the heat exchanger was stripped down, it was found that the tube wall had bulged over a distance of about 600 mm. In the most expanded region of the bulge, the tube had split longitudinally over a distance of about 300 mm.

At the edge of the fracture, the wall had thinned down to about 3 mm.

Metallurgical sections were cut from the tube at two positions: (i) immediately next to the fracture surface half-way along the length of the split, (ii) 100 mm away from the end of the split in the part of the tube which, although slightly expanded, was otherwise intact.

The microstructure at position (ii) consisted of grains of ferrite and colonies of pearlite. It was noticed that the pearlite had started to “spheroidize” (see Example 6.2). The microstructure at position (i) consisted of grains of ferrite and grains of lower bainite in roughly equal proportions. Estimate the temperatures to which the tube been heated at positions (i) and (ii). Explain the reasoning behind your answers.

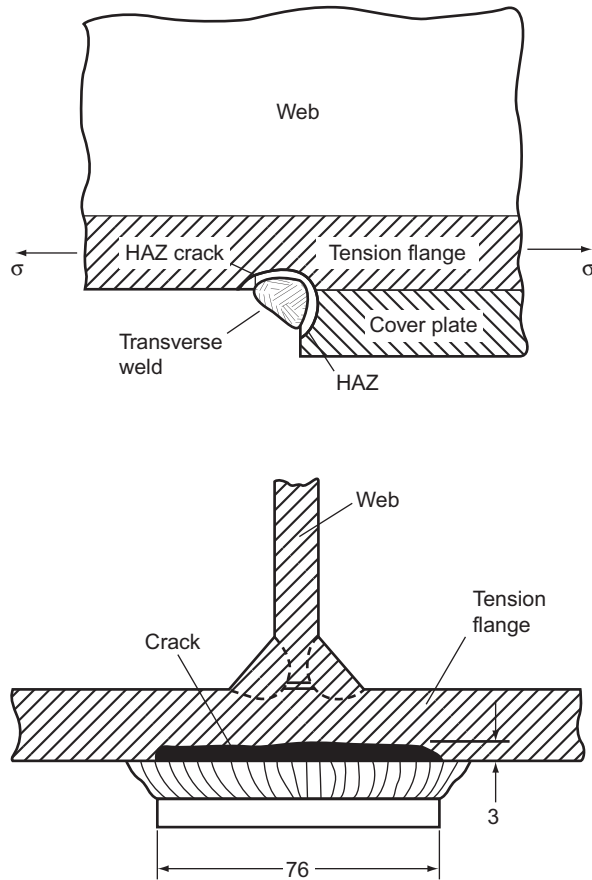
Answers

(i) 830 °C; (ii) 700 °C.

14.2 In 1962, a span of Kings Bridge (Melbourne, Australia) collapsed by brittle fracture. The fracture started from a crack in the heat-affected zone (HAZ) of a transverse fillet weld, which had been used to attach a reinforcing plate to the underside of a main structural I-beam (see the diagram). The concentrations of the alloying elements in the steel (in wt%) were: C 0.26; Mn 1.80; Cr 0.25.

The welding was done by hand, without any special precautions. The welding electrodes had become damp before use.

Account for the HAZ cracking. After the collapse, the other transverse welds in the bridge were milled-out and rewelded. What procedures would you specify to avoid a repeat of the HAZ cracking?



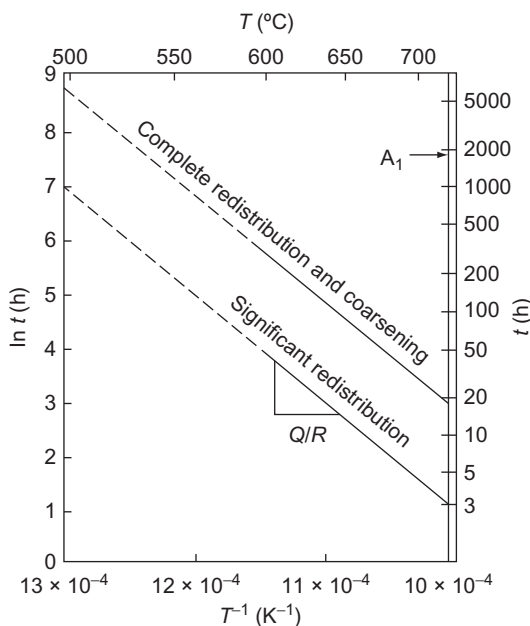
- 14.3** Steels for railroad rails typically contain 0.80 wt% carbon, 0.3 wt% silicon, and 1.0 wt% manganese. The steel is processed to give a fine-grained pearlitic structure with a hardness of approximately 2.8 GN m^{-2} . However, after a period in service, it is commonly found that a thin, hard layer (the “white layer”) forms in patches on the top (running) surface of the rail. The microhardness of this white layer is typically around 8 GN m^{-2} . Given that frictional heating between the wheels of rail vehicles and the running surface of the rail can raise the temperature at the interface to 800°C , explain why the white layer forms and account for its high hardness.
- 14.4** A rotating steel shaft from a high-speed textile machine was repaired with a circumferential surface weld. The shaft failed shortly after being put back into service by fatigue, which initiated in HAZ cracks. The composition of the steel

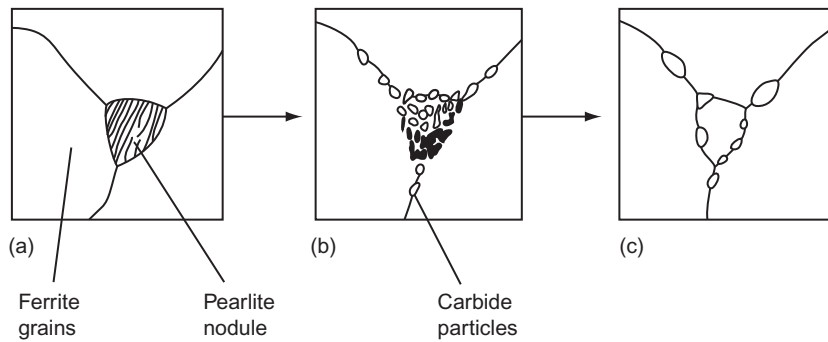
was (wt%): C 0.40; Mn 0.72; Cr 0.96; Mo 0.22; Ni 0.23. Explain why the HAZ cracked.

- 14.5** A superheater tube (to the same specification as the steel in the boiler-tube case study) had been in service for 7 years when it burst open. A metallurgical section taken from the tube wall close to the fracture showed pearlite which had spheroidized significantly. What does this tell us about the temperature history of the overheated length of tube? (Explain your answer.) The diagrams which follow show how the rate of spheroidization depends on temperature (t is the time of exposure at temperature T). Diagram (a) is the original structure of ferrite and fine pearlite, (b) shows significant redistribution of the carbide in the pearlite, and (c) shows complete redistribution of carbide, plus particle coarsening. Why is the plot of $(\ln t)$ versus (T^{-1}) linear? From the slope of the plot, find the value of Q , the activation energy for the process. Compare your value of Q to that for the diffusion of iron along ferrite grain boundaries (174 kJ mol^{-1}), and infer what the rate controlling process is. Explain why this rate-controlling process is reasonable.

Answers

Always $< 723^\circ\text{C}$; 166 kJ mol^{-1} .





14.6 With reference to [Figure 14.8](#), explain why flame cutting/should leave a HAZ beneath the cut surface of a low-carbon steel plate. The photograph which follows shows flame cutting being carried out in a shipyard.



- 14.7** The atomic diameters of hydrogen and carbon are 0.092 and 0.154 nm. The largest diameter of interstitial atom which can occupy an octahedral hole in b.c.c. iron without straining the lattice is 0.0383 nm. Calculate the increase in diameter Δd of the octahedral hole required to accommodate an atom of (a) hydrogen, (b) carbon. Carbon diffuses rapidly in b.c.c. iron at 700 °C. By making the crude assumption that the activation energy for diffusion of interstitial atoms is proportional to the atomic misfit, Δd , estimate the temperature (in °C) at which hydrogen will diffuse at a comparable speed. (Hint: think about way in which the diffusion coefficient depends on activation energy and temperature, and be careful to distinguish between degrees kelvin and degrees centigrade.)

Answers

(a) 0.0537 nm; (b) 0.1157 nm; 178 °C (which is far too accurate a figure, of course—call it 200 °C).

- 14.8** A pressure vessel is fabricated from steel plate 10 mm thick. Owing to a mistake in positioning one of the entry nozzles, the vessel wall is left with a circular hole 10 mm in diameter. It is decided to fill in the hole by machining up a circular disk from spare plate so it will just fit into the hole. The edges of both the hole and the disk are then chamfered back by 30°, and a full-penetration weld is run into the V-shaped groove. The heat from the welding warms up the plate in the vicinity of the weld. As the area cools back down toward room temperature it contracts, leaving a residual tensile stress which acts at right angles to the line of the weld bead. The contraction can be modeled by assuming that the heating effect is equivalent to the whole of the disk reaching a uniform temperature ΔT ($=200$ °C) above the (uniform) temperature of the surrounding plate.

The increase in the external radius of the disk Δa is given by the equation

$$\frac{\Delta a}{a} = \left(\frac{p}{E}\right)(1 - \nu),$$

where a is the disk radius, p is the (radial) tensile stress at the edge of the disk, E ($=212 \text{ GN m}^{-2}$) is Young's modulus, and ν is Poisson's ratio. The decrease in the radius of the hole ΔB is given by the equation

$$\frac{\Delta B}{B} = \left(\frac{p}{E}\right)(1 + \nu),$$

where B is the hole radius and p is the (radial) tensile stress at the edge of the hole.

Show that

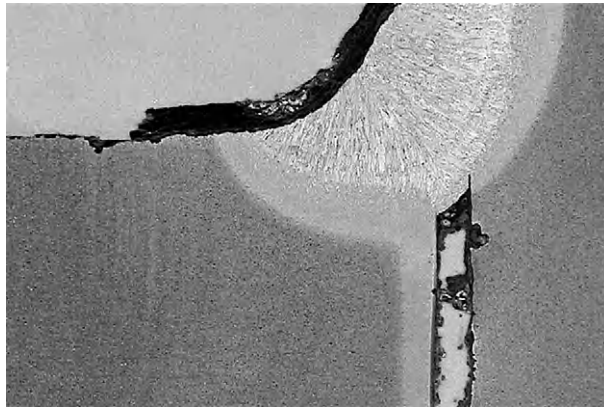
$$\frac{\Delta a}{a} + \frac{\Delta B}{B} = \alpha \Delta T,$$

where $a = B$, and $\alpha (=12 \times 10^{-6} \text{ }^\circ\text{C}^{-1})$ is the coefficient of thermal expansion of steel. Hence, show that $p = E\alpha\Delta T/2$ and estimate the value of the residual stress, p . Comment on this value in relation to the yield stress, σ_y ($=250 \text{ MN m}^{-2}$).

Answer

254 MN m^{-2} .

- 14.9** Explain the reasoning behind the carbon equivalent formula given in Equation (14.1). In typical welding processes, martensite should not form in the HAZ provided the carbon equivalent is about 0.45 or less. Explain why martensite may form at this CE value in the event that (a) significant grain growth occurs in the HAZ during welding, (b) a small weld bead is laid on top of a large thick plate.
- 14.10** The photograph shows a polished and etched cross section through a fillet weld between two low-carbon steel plates. The welding process has melted back some of the parent plate. Draw lines on a copy of the photograph to show the original surfaces of the plates. Draw lines to show the position of the interface between the weld metal and the parent plate (the “fusion boundary”). Also draw lines to show the low-temperature limit of the HAZ.



- 14.11** Cast iron is an alloy of carbon plus $>1.7 \text{ wt\%}$ carbon. Large diameter water pipes were made from a cast iron containing $3.5\% \text{ C}$ and were welded to cast iron flanges of the same composition. The welding rods were made from $\text{Fe} + 0.1 \text{ wt\% C}$. Soon after welding, the welds cracked through the middle of the weld beads. A weld bead was analyzed chemically, and the composition was found to be $\text{Fe} + 1.3 \text{ wt\% C}$. The hardness of the weld bead was $7\text{--}9 \text{ GN m}^{-2}$. Explain why the carbon content of the weld bead was so much higher than of the welding rods. What do the hardness values say about the microstructures in the weld bead? Why did the welds crack? (Hint: think about Example 14.10.)

- 14.12** The problem with the welds in Example 14.11 was solved by adding a second weld inside the flange using a weld metal composition of 50 wt% Fe + 50 wt% Ni. What crystal structure should this alloy have at all temperatures? What crystal structure should it have if it contains 1.3 wt% C? Why will this carbon content not cause cracking in the weld bead?
- 14.13** Low-alloy pressure-vessel steels with a carbon equivalent ≈ 1 are welded using the following special measures:
- (a) drying the welding rods in an oven immediately before using them,
 - (b) welding indoors in a fabrication shop,
 - (c) heating the steel to $\approx 350^\circ\text{C}$ before welding (“preheat”),
 - (d) heat treating the finished pressure vessel at $\approx 600^\circ\text{C}$ for 24 h (postweld heat treatment or PWHT).

Explain why each of these measures reduces the risk of cracking in the HAZs.

Processing Metals 1

15.1 INTRODUCTION

Figure 15.1 shows the main routes that are used for processing raw metals into finished articles. Conventional forming methods start by *melting* the basic metal and then *casting* the liquid into a mold. The casting may be a large prism-shaped ingot, or a continuously cast “strand,” in which case it is *worked* to standard sections (e.g., sheet, tube) or *forged* to shaped components. Shaped components are also made from standard sections by *machining* or *sheet metal-working*. Components are then assembled into finished articles by *joining* operations (e.g., welding) which are

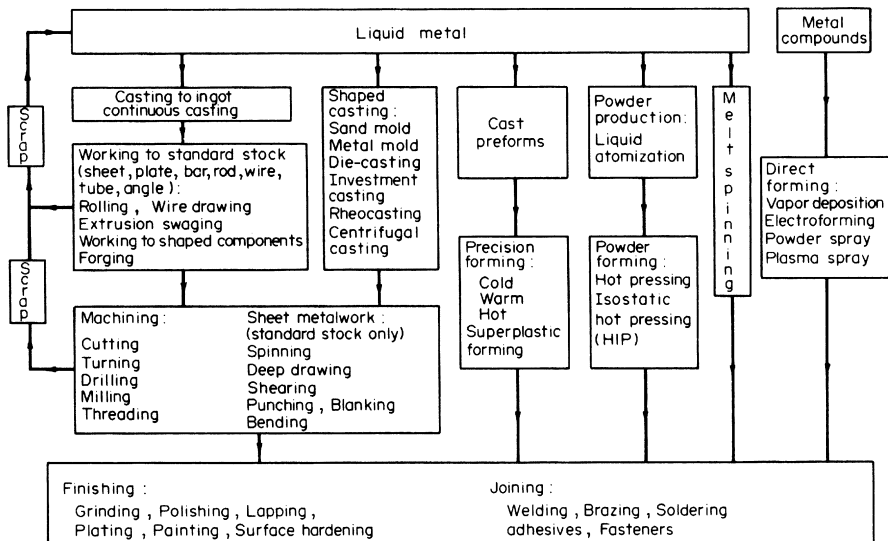


FIGURE 15.1

Processing routes for metals.

usually carried out in conjunction with *finishing* operations (e.g., grinding or painting). Alternatively, the casting can be made to the final shape of the component, although some light machining will usually have to be done on it.

Much use is now being made of alternative processing routes. In *powder metallurgy*, the liquid metal is atomized into small droplets which solidify to a fine powder. The powder is then *hot pressed* to shape (as we shall see in Chapter 20, hot-pressing is the method used for shaping high-technology ceramics). *Melt spinning* (Chapter 10) gives high cooling rates and is used to make amorphous alloys. Finally, there are a number of specialized processes in which components are formed directly from metallic compounds (e.g., *electro forming* or *chemical vapor deposition*).

It is not our intention here to give a comprehensive survey of the forming processes listed in Figure 15.1. This would itself take up a whole book and details can be found in the many books on manufacturing technology. Instead, we look at the underlying principles and relate them to the characteristics of the materials that we are dealing with.

15.2 CASTING

Ingots and Continuous Casting

We have already looked at casting structures in Chapter 10. Ingots tend to have the structure shown in Figure 15.2. When the molten metal is poured into the mold, *chill* crystals nucleate on the cold walls of the mold and grow inward. But the chill crystals are soon overtaken by the much larger columnar grains. Finally, nuclei are swept into the remaining liquid and these grow to produce *equiaxed* grains at the center of the ingot. As the

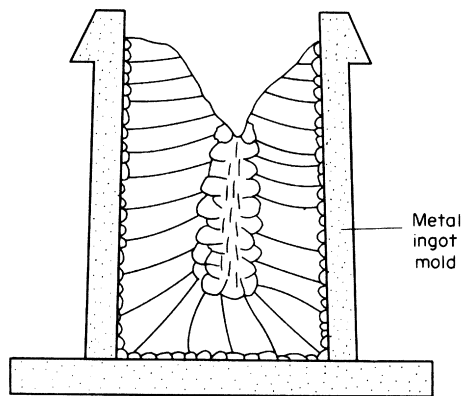


FIGURE 15.2

Typical ingot structure.

crystals grow, they reject dissolved impurities into the remaining liquid causing *segregation*. This can lead to bands of solid impurities (e.g., iron sulfide in steel) or to gas bubbles (e.g., from dissolved nitrogen). And because most metals contract when they solidify, there will be a substantial *contraction cavity* at the top of the ingot as well (Figure 15.2).

These *casting defects* are not disastrous in an ingot. The top, containing the cavity, can be cut off. And the gas pores will be squashed flat and welded solid when the white-hot ingot is sent through the rolling mill. But there are still a number of disadvantages in starting with ingots. Heavy segregation may persist through the rolling operations and can weaken the final product. And a great deal of work is required to roll the ingot down to the required section.

Many of these problems can be solved by using *continuous casting* (Figure 15.3). Contraction cavities do not form because the mold is continuously topped up with liquid metal. Segregation is reduced because the columnar grains grow over smaller distances. And, because the product has a small cross section, less work is needed to roll it to a finished section.

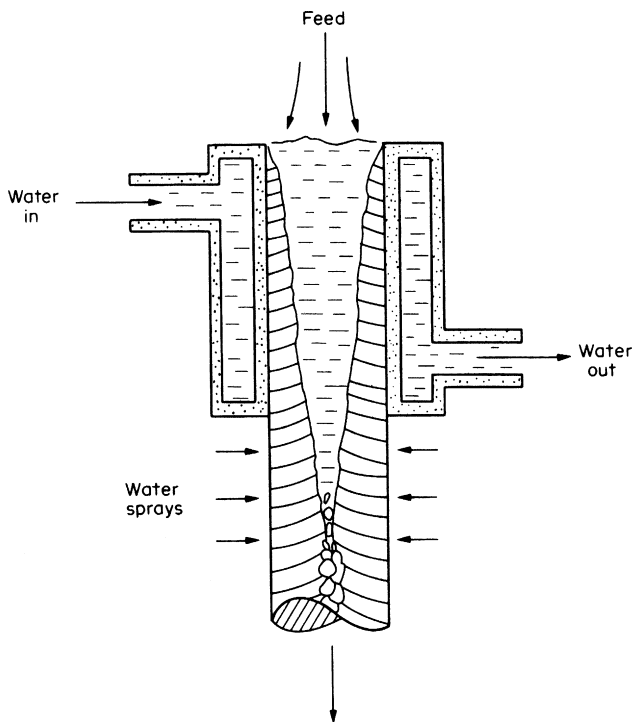


FIGURE 15.3
Continuous casting.

Shaped Castings

Shaped castings must be poured with much more care than ingots. Whereas the structure of an ingot will be greatly altered by subsequent working operations, the structure of a shaped casting will directly determine the strength of the finished article. Gas pores should be avoided, so the liquid metal must be *degassed* to remove dissolved gases (either by adding reactive chemicals or—for high-technology applications—casting in a vacuum). *Feeders* must be added to make up the contraction. And inoculants should be added to *refine* the grain size (Chapter 10). This is where powder metallurgy is useful. When atomized droplets solidify, contraction is immaterial. Segregation is limited to the size of the powder particles (2–150 μm); and the small powder size will give a small grain size in the hot-pressed product.

Sand Casting

Sand castings are poured into molds made of casting sand, a special sand mixture typically containing 90% silica, plus binders such as clay to hold the particles together (this is a major use of ceramics as *refractories* or heat-resistant materials). The first operation is to make a *pattern* (from wood, metal, or plastic) shaped like the required article (Figure 15.4). Sand is rammed around the pattern, and the mold is split open again to remove the pattern. Passages are then cut through the sand (by hand) for ingates and

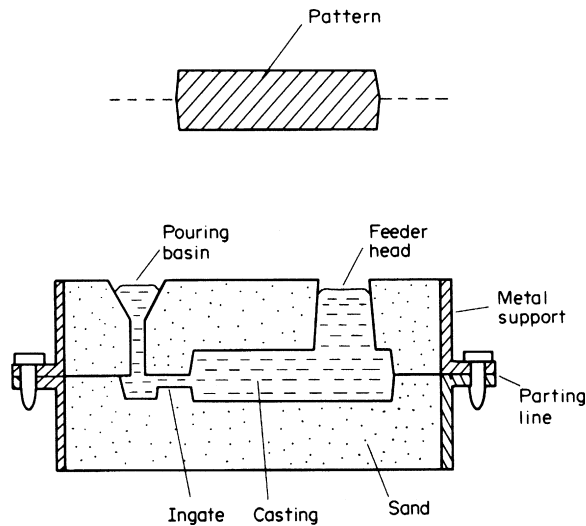


FIGURE 15.4

Sand casting. When the casting has solidified, it is removed by destroying the sand mold. The casting is then “fettled” by cutting off the ingate and the feeder head.

risers. The mold is reassembled and the molten metal poured into the mold cavity. When the casting has gone solid, it is removed by breaking up the (fragile) sand mold. The casting is then *fettled* (which involves sawing off the ingate and what is left of the metal in the feeder) before (as is often necessary) finishing critical areas (such as bolting surfaces and bores for bearings) by machining.

Even this apparently simple casting process involves a great deal of know-how and experience. The pattern must have slightly tapered sides, and a smooth shiny surface, so it can be withdrawn from the mold without pulling any sand away with it. It must also allow for thermal contraction when solid metal cools from its melting point to room temperature (patterns are generally made oversize by 1–2% to compensate). The shrinkage when molten metals solidify is large –3.8% for Zn alloys, 4.5% for Cu and Ni alloys, 5.7% for Mg alloys and a whopping 6.7% for Al alloys. The feeder must be able to top up the casting volume by at least this much. Obviously, the feeder must be the last part of the casting to solidify, or *contraction cavities* will form in unfed parts of the casting. Since the most massive part of the casting will solidify last, the feeder needs to be placed there. A useful guide to mold and feeder design is Chvorinov's rule

$$\text{Solidification time} = \text{Constant} \times (\text{volume/surface area})^2 = C(V/A)^2. \quad (15.1)$$

The mold needs to be designed so the feeder has a larger V/A than the maximum V/A for the mold cavity itself. The best shape for a feeder is a squat cylinder, which gives a large V/A . In a big or complex casting, several feeders will be needed to feed all parts of the casting adequately.

Figure 15.5 shows an example of an item—a truck footstep—made by sand casting. The separate bars of the footstep have a cross section about

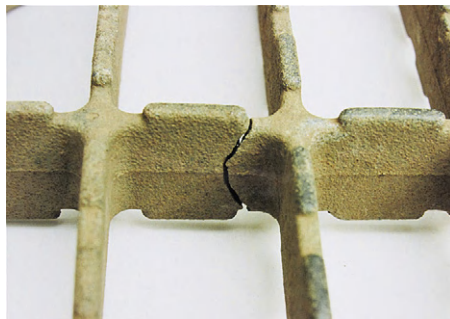


FIGURE 15.5

Close-up of part of a truck footstep, sand cast from Al–8% Si alloy.

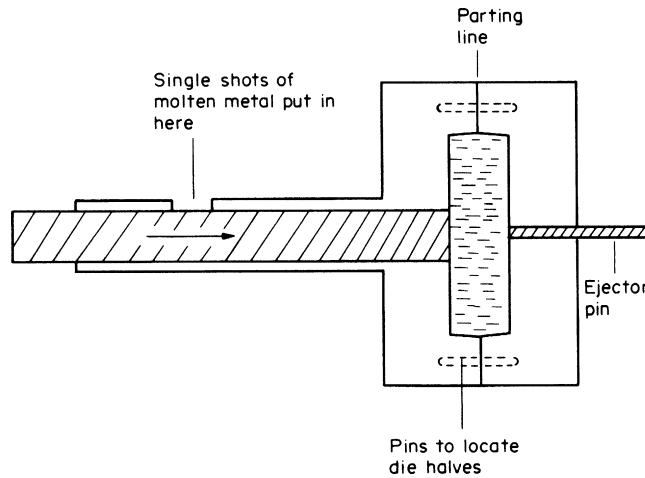


FIGURE 15.6
Pressure die-casting.

5 mm \times 20 mm. The horizontal ridge on the centerline of the bar caused by the parting line of the original sand mold is obvious, as is the rough surface finish produced by the sand particles. The bar is cracked right through by loads applied in service—the Al–8% Si alloy used has low toughness and ductility because brittle plates of silicon are present in the as-cast microstructure (see Figure 4.6 for the Al–Si phase diagram).

Permanent mold casting

This uses reusable metal molds, machined from solid. They must come apart in enough places that the casting can be removed. The molds are expensive (typically US\$ 15–50k), so high throughput is needed to offset this. The metal mold gives excellent surface finish and dimensional control. The main process which uses permanent molds is *pressure die-casting* (Figure 15.6). The molten metal is forced into the mold cavity at a pressure of 15–100 MN m^{−2} (the velocity of the fluid at the ingate is typically about 100 m s^{−1}). Solidification times are \approx 1 s for small parts. Under the pressure, the melt has good ability to fill sharp corners, so complex and detailed shapes can be cast. Production rates are very high, so the process is well suited to mass produced items. Figure 15.7 shows a good example of a cheap die-cast part made from a zinc-based alloy. Note the excellent definition of the index markings and numbers produced by the combination of high feeding pressure and a smooth steel mold surface.



FIGURE 15.7

Part of a workshop protractor, pressure die-cast from a zinc-based alloy.

Investment casting

This is used for especially intricate parts (where the pattern could not be removed from a sand mold or the part from a permanent mold) and for small parts where dimensional accuracy is vital. First, a wax pattern of the part is made (Figure 15.8). This is then coated with a ceramic slurry, which is dried to give it a little strength, and then fired (as we will see in Chapter 20, this is just how we make ceramic cups and plates). During the firing, the wax burns out of the ceramic mold, leaving a perfectly shaped mold cavity (this is why the process is also referred to as the “lost wax” process). If vents (called “sprues”) are added to the outside of the mold, the molten metal can be poured in under gravity, which generates enough pressure to push the air out of the mold cavity through the sprues. For critical applications (like turbine blades, which are made by investment casting), the metal is poured in a vacuum furnace; there is therefore no need to vent the mold (and the vacuum degasses the melt as well, so there should be no gas porosity).

Figure 15.9 shows a bronze sculpture produced by lost wax casting. It would be impossible to cast this any other way, and even so, the sculpture was made as a number of separate castings, which were brazed together with an oxyacetylene torch. Note that all the parts you see are in fact *hollow*. The sculpture would be immensely heavy (and ruinously expensive, given the high price of copper) if it were solid—and it would be impossible to braze the parts together because of their enormous thermal mass and high thermal conductivity. The original sculpting was done in clay, and the clay

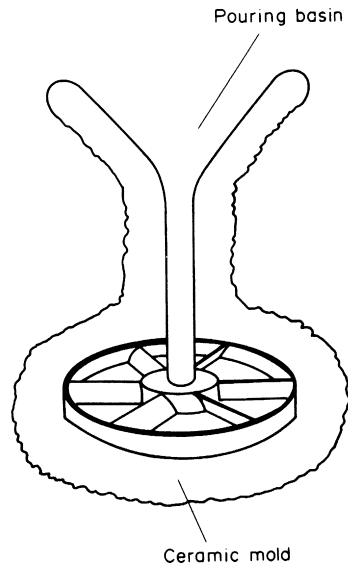


FIGURE 15.8
Investment casting.



FIGURE 15.9
Sculpture of the young Charles Darwin in Christ College, Cambridge UK 52 12 24.45 N 0 07 21.10 E.
Investment cast from bronze as separate pieces which were then welded together.

master was then coated with liquid silicone rubber compound. When the rubber had cured, it was peeled off the master, and the inside of the rubber negative was lined with a coating of wax several millimeter thick. Then, both the outside and the *inside* of the wax was coated with ceramic slurry, which was dried and fired. When the wax burnt out of the mold, it left a mold cavity only a few millimeter wide, which was fed with molten bronze by gravity and vented with lots of sprues. For further details, see http://www.christs.cam.ac.uk/darwin200/pages/index.php?page_id=i6 and the web site of the sculptor, Anthony Smith (born 1984) www.anthonysmithart.co.uk

Casting alloys

The main categories of casting alloys are the cast irons, cast steels, and casting alloys based on Al, Zn, Mg, and Cu. Table 15.1 gives data for typical alloys in each category. We will look at individual alloys in a moment, but the

Table 15.1. Typical Casting Alloys

Alloy	Approximate Composition (wt%)	Freezing Range (°C)	Tensile Strength (MN m ⁻²)	Ductility (%)	Typical Uses
Cast irons					
Gray	Fe + 3 C, 2 Si	1130–1250	>90, 150 mm >250, 15 mm	<1	Drain covers, machine tool parts
Ductile	Fe + 3 C, 2 Si, Mg	1130–1250	370	17	Water main pipes
Al					
356	Al + 7 Si, 0.4 Mg	577–624	240	2	Engine blocks and heads(heat treatable alloy)
380	Al + 8 Si, 4 Cu, 3 Zn	577–608	180	2	General engineering
S12C	Al + 12 Si	577	160	2	General engineering
S12C	+0.01 Na modifier	577 +	195	13	
S12C	Chill cast	577	195	4	
Zn					Pressure die-cast parts—cars, domestic appliances
MAZAK5	Zn + 4 Al, 1 Cu	382–388	300	10	
Mg (A8)	Mg + 8 Al, 1 Zn	500–600	140	2	Car/motorcycle wheels
Mg (A8)	Chill cast	500–600	185	4	(heat-treatable alloy)
Steels					
Carbon	Fe + 0.3 C	1450–1510	480	20	General engineering
Alloy (γ)	Fe + 1 C, 11 Mn	1250–1400	—	—	Crushers, tank tracks
Alloy (α)	Fe + 0.2 C, 3 Cr, Mo	1480–1520	600	13	High temperature (500 °C)
Cu					
Al Bronze	Cu + 10 Al, 5 Ni, Fe	1040	600	20	Marine parts (pumps, etc.)
Mn Brass	Cu + 40 Zn, 1 Mn, Al	900	460	25	Ship propellers (αβ brass)
Pb Brass	Cu + 30 Zn, 2 Pb, 1 Sn	920–950	200	20	Sand cast parts (α brass) (free machining, from Pb)

table shows two features of general interest. The first is the effect of processing parameters on the strength of the casting—a rapid solidification rate (produced by a small casting size or chill casting) can increase the strength considerably (see gray cast iron, Al Si2C, Mg A8). This is due to the finer microstructure produced by the faster phase transformation. (In Chapter 7, Section 7.6 and Chapter 12, Section 12.5, we explained the general rule that the harder you drive a transformation, the finer the microstructure you get.) The second is that most casting alloys have a small *freezing range*. We saw in Chapter 5, Section 5.2, that eutectic solders (which melt completely at the eutectic temperature) are free flowing, whereas solders with a large freezing range were pasty. In the casting world, alloys with a small freezing range are called “skin freezers,” and those with a large freezing range “mushy freezers.” In skin freezers, the zone of dendrites between the fully solidified metal and the liquid is thin, and it is easy for extra liquid to flow between the dendrites and feed the volume contraction. In mushy freezers, the opposite is the case, and pores can form between the dendrites.

Cast irons

Alloys of iron containing more than 1.7 wt% carbon are called *cast irons*. Carbon lowers the melting point of iron (see Figure 4.12): a medium-carbon steel must be heated to about 1500 °C to melt it, whereas a 4% cast iron is melted at only 1160 °C. This is why cast iron is called cast iron: it can be melted with primitive furnaces and can be cast into intricate shapes using very basic sand casting technology. Cast iron casting have been made for hundreds of years.

The world’s first cast iron bridge was put up in 1779 by the Quaker Ironmaster Abraham Darby III. Spanning the River Seven in Shropshire the bridge is still there; the local village is now called Ironbridge. You can see it on street view at 52 37 37.45 N 2 29 06.75 W.

Another early ironmaster, the eccentric “iron-mad” Wilkinson, lies buried in an iron coffin surmounted by an iron obelisk. He launched the world’s first ship and invented the machine for boring the cylinders of James Watt’s steam engines.

The Victorians used cast iron for everything they could: bridges, architectural beams and columns, steam-engine cylinders, lathe beds, even garden furniture.

But most cast irons are brittle and should not be used where they are subjected to shock loading or high tensile stresses.

There are two basic types of cast iron: *white* and *gray*. The phases in white iron are α and Fe_3C , and it is the large volume fraction of Fe_3C that makes the metal brittle. The name comes from the silvery appearances of the fracture surface, due to light being reflected from cleavage planes in the Fe_3C . In gray iron much of

the carbon separates out as elemental carbon (graphite) rather than Fe_3C . Gray irons contain $\approx 2 \text{ wt\% Si}$: this alters the thermodynamics of the system and makes iron–graphite more stable than iron– Fe_3C . If you cut a piece of gray iron with a hacksaw, the graphite in the sawdust will turn your fingers black, and the cut surface will look dark as well, giving gray iron its name. It is the graphite that gives gray irons their excellent wear properties—in fact gray is the only metal which does not “scuff” or “pick up” when it runs on itself. The properties of gray iron depend strongly on the shape of the graphite phase. If it is in the form of large *flakes*, the toughness is low because the flakes are planes of weakness. If it is in the form of *spheres* (spheroidal-graphite or “SG,” iron), the toughness is high and the iron is ductile. The graphite phase in gray iron is normally flaky, but SG irons were first produced in 1948: if small amounts of the elements cerium or magnesium are added to molten cast iron just before it is cast, the graphite precipitates as spherical particles rather than as flakes. When the graphite is in the form of spheres, it has a much smaller weakening effect than when it is present as flakes and SG iron has a much higher strength, ductility, and toughness than gray iron. For this reason, it is often called “ductile iron.”

The strength of flake graphite cast iron is determined largely by the shape and size of the flakes (the smaller the flakes, the smaller the cracks which they initiate under an applied stress). In turn, this is controlled by the rate at which the casting solidifies. The solidification rate is limited by the size of the casting—thin sections cool faster than thick ones—and have a higher tensile strength as a result. For example (see [Table 15.1](#)), a 150 mm diameter cast bar of medium-strength flake graphite cast iron has a tensile strength of $>90 \text{ MN m}^{-2}$, whereas a 15 mm diameter bar has a tensile strength of $>250 \text{ MN m}^{-2}$, a huge improvement.

Aluminum alloys

We saw from [Figure 15.5](#) that Al–Si alloys are brittle, because they contain plates of silicon (a brittle material). [Table 15.1](#) shows that these alloys have ductilities of only $\approx 2\%$. This can be cured in a spectacular way simply by adding 0.01 wt% sodium to the alloy just before it is poured into the mold. The silicon then forms as micron-sized particles (not extended plates), which are too small to nucleate cracks (*sodium modification*). The strength goes up significantly, but the ductility increases by a factor of 6! That such a small amount of sodium (like cerium or magnesium in SG iron) can have such a dramatic effect can only be due to coating the growing silicon with an atomic monolayer of the added element, altering the growth processes of the silicon (or the graphite in gray iron).

This takes us back to the Worked Example in Chapter 7, where we saw how the precise details of how atoms attach themselves to the surface of a

growing crystal can have a dramatic effect on the geometry of the crystal surface and the growth speed. If the growth of silicon requires the presence of surface steps, for example, the adsorption of only a small number of sodium atoms to steps could completely change the growth kinetics (by effectively “poisoning” the steps).

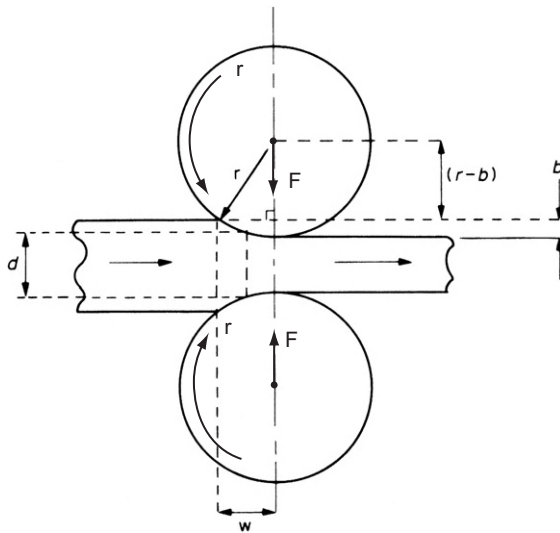
Chill casting increases the strength by the same amount as sodium, because the (faster growing) silicon particles are smaller. However, the particles are not as small as in the sodium modified alloy, so they are still able to nucleate cracks (although these are smaller) and the ductility is only doubled.

15.3 DEFORMATION PROCESSING

Because most metals and alloys are ductile, they can be worked to shape by processes which deform the material plastically, especially in compression (where necking cannot occur). Deformation may be carried out on materials which are cold (room temperature), warm ($\approx 0.3\text{--}0.5\ T_M$), or hot ($\approx 0.6\text{--}0.7\ T_M$). Increasing the temperature decreases the yield strength, making it easier to achieve large reductions in area without having to use excessive force (at the highest hot working temperatures, deformation is more like very rapid creep than conventional yielding). Cold deformation leads to work hardening—which strengthens the material (it also decreases its ductility)—and increases the forming loads considerably. The choice of temperature for the various stages involved in deformation processing a final product is largely determined by a balance between forming loads (and power consumption) and the properties specified for the final product. Other factors are the tendency for metals (especially carbon steel) to oxidize in air at high temperature (producing brittle “mill scale” on the exposed surfaces) and the fact that lubricants (necessary for some forming processes, like extrusion or wire drawing) break down at high temperatures.

Rolling

Steel ingots and concast strands are reduced to finished sections by hot rolling (Figure 15.10). Finished sections can be structural I-beams, channel sections and angles, round bars, plates, strip, rectangular or hexagonal sections, railroad rails, reinforcing bar, etc. Seamed tubes can be made by passing white-hot strip through rolls having concave grooves, which curve the strip up into a tubular form. The hot edges of the strip are then pressed together by more (downstream) grooved rolls, producing a longitudinal solid-state seam weld by diffusion bonding. Rolling carbon steels often produces a *banded* microstructure, where the nodules of pearlite are stretched out along the rolling direction (see Figure 12.7). (A striking example of a banded microstructure can be seen in samples of nineteenth century *wrought*

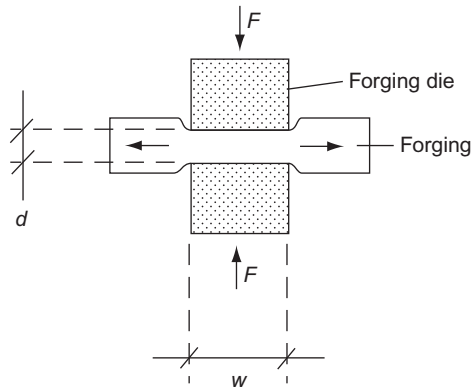
**FIGURE 15.10**

Cross section through a rolling mill.

iron, where the slag from the refining process has been elongated into stringers along the rolling direction.) Some rolled steel products are subjected to a final *cold* reduction in thickness in order to increase the yield strength by *work hardening* (so-called “bright” products, because they no longer have the layer of black iron oxide mill scale that forms on the surfaces during hot working). Rolling (cold, warm, and hot) is also used for most other major metals and alloys (such as aluminum, copper, etc.) but is less important than for steel, because finished product sections are generally produced by extrusion (see later).

Forging

Net or near net shape components can be made by forging (Figure 15.11). Figure 15.12 shows an example—the hot forging of a steel hammer head. The two halves of the forging die are recessed, so when they come together they form the hammer head. Note that when the die halves come together, they leave a gap which is filled by surplus material called “flash” (this type of forging is called “impression forging”). The flash is subsequently cropped off, then the claws are bent to the correct radius, and the hole for the handle is punched through. Before every shaping operation, the steel is heated to bright red heat (which is why the parts are covered in gray iron oxide scale). Forging is used for many engineering parts (e.g., engine crankshafts and connecting rods, turbine disks, gear blanks, bolt heads). A well-designed forging die can

**FIGURE 15.11**

Cross section through a forging operation. In this example, plastic flow takes place only in the plane of the drawing. The third dimension, L , is perpendicular to the drawing.

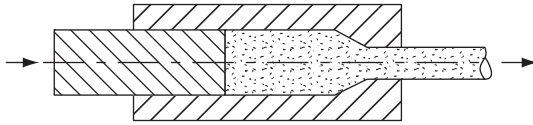
**FIGURE 15.12**

Stages in hot forging the head of a claw hammer from medium-carbon steel.

affect the microstructure in a favorable way, because the grains of deformed material “flow” around sharp changes in section and give the structure continuity there—this leads to better fatigue properties at stress concentrations.

Extrusion

Extrusion (Figure 15.13) is used extensively for producing finished sections in most metals, but especially aluminum, copper, and their alloys. A billet of

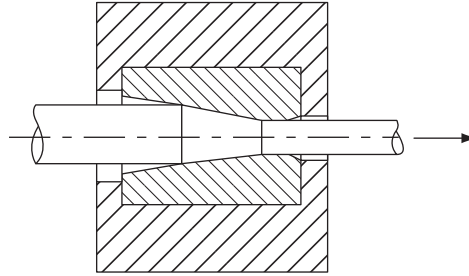
**FIGURE 15.13**

Schematic of a typical extrusion process.

the material is forced through a die made from a hard material (usually tool steel) and squeezed into the specified cross section. For this reason, sections can only be extruded in fixed lengths. It is important to have adequate boundary lubrication between the material and the die (e.g., soaps, fats, graphite, and molybdenum disulfide). Hollow sections (e.g., tube and box) can be made by inserting a core into the center of the die, supported by a rod passing along the axis of the billet. Common examples of extruded sections are copper water pipes (graphite residues have been known to initiate corrosion pitting from the bore in service!), complex aluminum alloy sections for double-glazed window frames, and a range of sizes of rod, round bar, hexagon bar, square and rectangular bar, tubes, hollow box and rectangular sections, etc.

Drawing

In a drawing process (Figure 15.14), the material is *pulled*, not pushed, through the die. This means that the length of the drawn product is limited only by the storage capacity on either side of the die. Wire is drawn to the correct size by *wire drawing*. This generally needs to be done in a number of separate passes, each using a smaller die bore than the previous one, because if the reduction in area in any pass is too great, the drawing force becomes sufficient to make the drawn wire deform plastically (or even break) under the drawing tension. Dies for wire drawing are usually made from inserts of WC-Co, or industrial diamond, surrounded by a tool steel ring to support them (and stop them bursting under the high hoop stress). Again, adequate lubrication is critical, both to minimize drawing force and to get a good surface finish (avoid scuffing by the die). The large amount of work hardening after a number of wire drawing passes gives an impressive tensile strength in the finished wire—probably the largest amount of work hardening in any deformation process ($\approx 2000 \text{ MN m}^{-2}$ in medium-carbon steel). Other sections may also be drawn, and the process is used to reduce the sizes of tubes made by other routes (*tube sinking*). When drawing tubes (or other hollow sections), the tube bore must be supported by a metal core, both to size the bore and to prevent the tube wall buckling in response to the compressive hoop strain.

**FIGURE 15.14**

Schematic of a typical drawing process.

Forces in forging and rolling

Referring to Figure 15.11 for the schematic of forging, even with boundary lubrication there is friction between the dies and the workpiece—and in hot forging there is essentially no lubrication at all. The worst case is that the workpiece “sticks” to the die faces, so when the die halves are closed, and material flows to right and left of the centerline, it has to deform in shear at the die–work interface, with shear stress = shear yield stress k . We looked at this problem in Example 11.2 of EM1Ed4. Because the interface shear requires an input of work (additional to just deforming the workpiece at the unconstrained yield stress, σ_y), the forming force F is *larger than its unconstrained value* of $wL\sigma_y$. It can be shown that the forming *pressure* at the centerline of the dies is given by

$$p_{\max} = \sigma_y \left(1 + \frac{w}{2d} \right). \quad (15.2)$$

At the edges of the dies, the (unconstrained) forming pressure is of course equal to σ_y . In between these limits, the forming pressure varies linearly (Figure 15.15), so the average forming pressure across the full width of the dies is given by

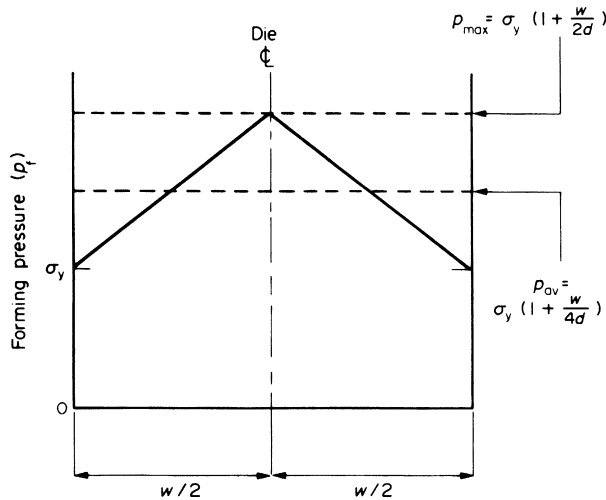
$$p_{\text{av}} = \sigma_y \left(1 + \frac{w}{4d} \right). \quad (15.3)$$

If the friction at the interface is less than k , say fk (where $0 < f < 1$), then the constrained forming pressures are less. The peak and average values are given approximately by

$$p_{\max} = \sigma_y \left(1 + \frac{fw}{2d} \right), \quad (15.4)$$

and

$$p_{\text{av}} = \sigma_y \left(1 + \frac{fw}{4d} \right). \quad (15.5)$$

**FIGURE 15.15**

How the forming pressure varies with position in the forging.

It is revealing to put typical numbers into Equation (15.2). If $w/d = 10$, then $p_{\max} = 6\sigma_y$. Pressures this large may deform the dies themselves; it is not surprising that hot forging is so popular, because of the large drop in σ_y at high temperature. In the forging of the hammer head (Figure 15.12), the flash has the largest ratio of w/d (but a relatively small area) and accounts for a significant part of the forging load as the dies close up. (In fact, this thin layer of flash is desirable—to squeeze the flash out through the gap requires a large pressure of metal inside the die cavity, which also pushes metal into every corner of the die cavity.)

This simple forging analysis can also be applied (approximately) to rolling. Referring to Figure 15.10, we can write

$$(r-b)^2 + w^2 = r^2. \quad (15.6)$$

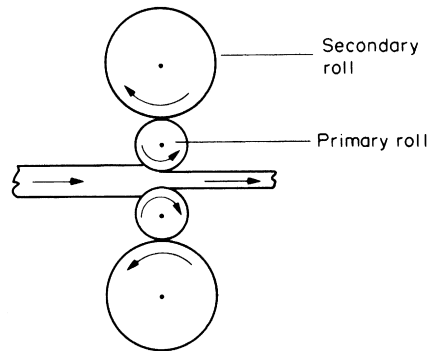
Provided $b \ll 2r$ this can be expanded to give

$$w = \sqrt{2rb}, \quad (15.7)$$

Thus

$$\frac{w}{d} = \frac{\sqrt{2rb}}{d} = \left(\frac{2r}{d}\right)^{1/2} \left(\frac{b}{d}\right)^{1/2} \quad (15.8)$$

Well-designed rolling mills therefore have rolls of small diameter. However, as Figure 15.16 shows, these may need to be supported by additional

**FIGURE 15.16**

In order to minimize the effects of friction, rolling operations should be carried out with minimum values of w/d . Small rolls give small w/d values, but they may need to be supported by additional secondary rolls.

secondary rolls which do not touch the workpiece. In fact, aluminum cooking foil is rolled by primary rolls the diameter of a pencil, backed up by a total of 18 secondary rolls.

15.4 RECRYSTALLIZATION

When metals are cold worked, they *work harden*. After a deformation of perhaps 80% a limit is reached, beyond which the metal cracks or fractures. Further rolling or drawing is possible if the metal is *annealed* (heated to about $0.6 T_M$). During annealing, old deformed grains are replaced by new, undeformed grains, and the working can be continued for a further 80% or so.

Figure 15.17 shows how the microstructure of a metal changes during plastic working and annealing. If the metal has been annealed to begin with (Figure 15.17(a)), it will have a comparatively low dislocation density (about 10^{12} m^{-2}) and will be relatively soft and ductile. Plastic working (Figure 15.17(b)) will greatly increase the dislocation density (to about 10^{15} m^{-2}). The metal will work harden and will lose ductility. Because each dislocation strains the lattice, the deformed metal will have a large strain energy (about 2 MJ m^{-3}). Annealing gives the atoms enough thermal energy that they can move under the driving force of this strain energy. The first process to occur is *recovery* (Figure 15.17(c)). Because the strain fields of the closely spaced dislocations interact, the total strain energy can be reduced by rearranging the dislocations into low-angle grain boundaries. These boundaries form the surfaces of irregular *cells*—small volumes which are relatively free of dislocations. During recovery, the dislocation density goes down only

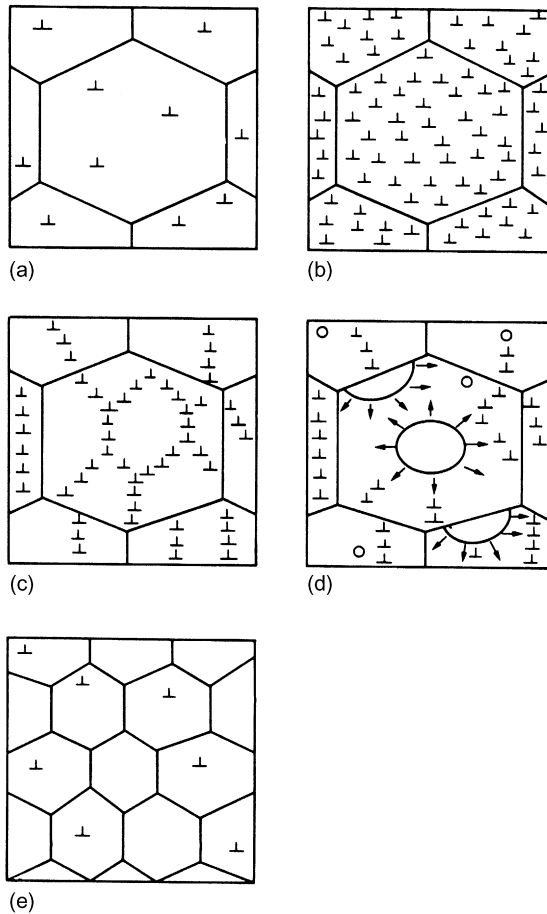
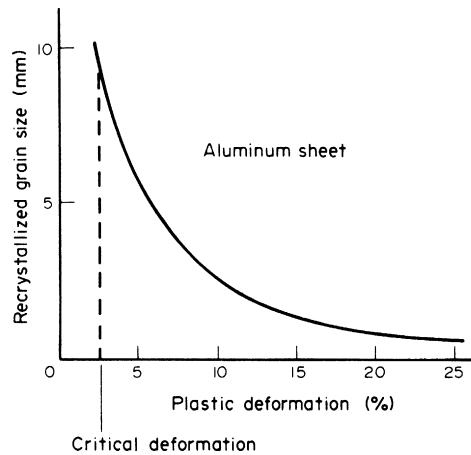


FIGURE 15.17

How the microstructure of a metal is changed by plastic working and annealing. (a) If the starting metal has already been annealed, it will have a comparatively low dislocation density. (b) Plastic working greatly increases the dislocation density. (c) Annealing leads initially to recovery—dislocations move to low-energy positions. (d) During further annealing new grains nucleate and grow. (e) The fully recrystallized metal consists entirely of new undeformed grains.

slightly: the hardness and ductility are almost unchanged. The major changes come from *recrystallization*. New grains nucleate and grow (Figure 15.17(d)) until the whole of the metal consists of undeformed grains (Figure 15.17(e)). The dislocation density returns to its original value, as do the values of the hardness and ductility.

Recrystallization is not limited just to getting rid of work hardening. It is also a powerful way of controlling the grain size of worked metals. Although

**FIGURE 15.18**

Typical data for recrystallized grain size as a function of prior plastic deformation. Note that, below a critical deformation, there is not enough strain energy to nucleate the new strain-free grains. This is just like the critical undercooling needed to nucleate a solid from its liquid (see Figure 8.4).

single crystals are desirable for a few specialized applications, the metallurgist almost always seeks a fine-grain size. To begin with, fine-grained metals are stronger and tougher than coarse-grained ones. And large grains can be undesirable for other reasons. For example, if the grain size of a metal sheet is comparable to the sheet thickness, the surface will rumple when the sheet is pressed to shape; and this makes it almost impossible to get a good surface finish on articles such as car-body panels or spun aluminum saucepans.

The ability to control grain size by recrystallization is due to the general rule that the harder you drive a transformation, the finer the structure you get. In the case of recrystallization, this means that the greater the prior plastic deformation (and hence the stored strain energy), the finer the recrystallized grain size (Figure 15.18). To produce a fine-grained sheet, for example, we simply reduce the thickness by about 50% in a cold rolling operation (to give the large stored strain energy) and then anneal the sheet in a furnace (to give the fine recrystallized structure).

WORKED EXAMPLE

The photograph shows a carved stone ornament on a gateway in a Cambridge college (UK). The squared motif (called a “portcullis”), together with its ornamental chains, is covered with *gold leaf*. Because gold does not corrode, it stays bright and shiny. The gold leaf is $0.10\ \mu\text{m}$ thick and is stuck to the stonework with a natural adhesive (called a “size”). The leaf is

supplied in squares measuring $3\frac{3}{8}$ " by $3\frac{3}{8}$ " (no metrication here!) separated by squares of tissue paper in the form of a booklet containing 25 leaves. It is applied to the sized stonework using a very soft brush made of squirrel hairs.



The thickness of $0.10\text{ }\mu\text{m}$ is not a misprint! We can work out how gold this thin might be rolled by using [Equations \(15.5\) and \(15.8\)](#). We choose plausible values of $w/d = 10$, $f = 0.5$, $b/d = 0.25$ for each rolling pass. For the final rolling pass, with gold foil $\approx 0.2\text{ }\mu\text{m}$ thick entering the rolls, we get a value for the roll diameter, $2r$ of $80\text{ }\mu\text{m}$ (3 thousandths of an inch). Rolling such thin foil is impossible—we could never make a rolling mill (together with its 18 secondary rolls) so small, and even if we could it would be impossible to machine the surface of the roll to the required tolerance. Yet the ancient Egyptians were making gold leaf 5000 years ago. How on earth did they do it?

To this day, gold leaf is made in the original way. First, the gold (usually 23 carat, 96% Au + Ag, Cu to get the color right) is reduced in a rolling mill to a thickness of 1 thou ($25.4\text{ }\mu\text{m}$). The rolled foil is then cut into 1-inch squares, and 150 of these squares are stacked one on top of the other, with a layer of “Goldbeater’s skin” (animal intestine membrane) interleaved between each piece of gold. This multilayer sandwich of gold and skin layers is then wrapped in protective sheets of parchment (thin material from animal skin, such as calfskin, sheepskin, or goatskin). Finally, the wrapped sandwich is placed on a granite block and pounded repeatedly with a 15 lb cast iron hammer (once a second for an hour). This expands the sandwich to an area of $4'' \times 4''$ —an expansion of 16 times in area, and therefore a reduction of 16 times in the thickness of each gold foil (which is now only $1.6\text{ }\mu\text{m}$ thick).

The sandwich is then dismantled, and each foil is cut into four separate 1 in². Then another sandwich is made up, this time containing 1500 gold foils. This is hammered for 3 h, until the gold has expanded to an area of 4" × 4", and the foil is now at the required thickness of 0.10 μm. The link gives details of a modern manufacturer of gold leaf.

http://www.eytzinger.com/gilding/gold-leaf-manufacturing/modern_art.php

The beauty of the method is that the sandwich of gold foils and skins behaves as a layered composite, with both foils and skins expanding sideways together, so the hammering process is equivalent to forging with a relatively small value of w/d . We can only marvel at how this was originally discovered.

EXAMPLES

- 15.1** Estimate the percentage volume contraction due to solidification in pure copper. Use the following data: $T_M = 1083\text{ }^\circ\text{C}$; density of solid copper at $20\text{ }^\circ\text{C} = 8.96\text{ Mg m}^{-3}$; average coefficient of thermal expansion in the range $20\text{--}1083\text{ }^\circ\text{C} = 20.6\text{ MK}^{-1}$; density of liquid copper at $T_M = 8.00\text{ Mg m}^{-3}$.

Answer

5%.

- 15.2** A silver replica of a holly leaf is to be made by investment casting. (A natural leaf is coated with ceramic slurry which is then dried and fired. During firing the leaf burns away, leaving a mold cavity.) The thickness of the leaf is 0.4 mm. Calculate the liquid head needed to force the molten silver into the mold cavity. It can be assumed that molten silver does not wet the mold walls.

(Hint: The pressure needed to force a nonwetting liquid into a parallel-sided cavity of thickness t is given by

$$p = \frac{T}{(t/2)}$$

where T is the surface tension of the liquid.) The density and surface tension of molten silver are 9.4 Mg m^{-3} and 0.90 N m^{-1} .

Answer

49 mm.

- 15.3** Aluminum sheet is to be rolled according to the following parameters: starting thickness 1 mm, reduced thickness 0.8 mm, yield strength 100 MN m^{-2} . What roll radius should be chosen to keep the forming pressure below 200 MN m^{-2} ?

Answer

16.2 mm or less.

- 15.4** Aluminum sheet is to be rolled according to the following parameters: sheet width 300 mm, starting thickness 1 mm, reduced thickness 0.8 mm, yield strength 100 MN m^{-2} , maximum forming pressure 200 MN m^{-2} , roll radius 16.2 mm, roll length 300 mm. Calculate the force F that the rolling pressure will exert on each roll.

(Hint: Use the average forming pressure, p_{av} , shown in Figure 15.15.)

The design states that the roll must not deflect by more than 0.01 mm at its center. To achieve this bending stiffness, each roll is to be backed up by one secondary roll as shown in Figure 15.16. Calculate the secondary roll radius needed to meet the specification. The central deflection of the secondary roll is given by

$$\delta = \frac{5FL^3}{384EI}$$

where L is the roll length and E is the Young's modulus of the roll material. I , the second moment of area of the roll section, is given by

$$I = \pi r_s^4 / 4$$

where r_s is the secondary roll radius. The secondary roll is made from steel, with $E = 210 \text{ GN m}^{-2}$. You may neglect the bending stiffness of the primary roll.

Answers

$F = 81 \text{ kN}$; $r_s = 64.5 \text{ mm}$.

- 15.5** Describe the processes of recovery and recrystallization that occur during the high-temperature annealing of a work-hardened metal. How does the grain size of the fully recrystallized metal depend on the initial amount of work hardening? Mention some practical situations in which recrystallization is important.
- 15.6** A bar of cold-drawn copper had a yield strength of 250 MN m^{-2} . The bar was later annealed at 600°C for 5 min. The yield strength after annealing was 50 MN m^{-2} . Explain this change. (Both yield strengths were measured at 20°C .)
- 15.7** Explain why continuous casting has almost entirely replaced ingot casting as the primary processing step in the production of rolled steel sections.
- 15.8** What casting process would you use to make each of the following parts.
- (a) A large propeller for a ship.
 - (b) Small turbine blades, with accurate dimensions and good surface finish.
 - (c) The wheels of a small toy railway locomotive.
 - (d) The bed of a metal turning lathe.

In each case, explain your choice of casting process and suggest a suitable alloy.

- 15.9** Explain the following.
- (a) A sand-cast bar of flake graphite (gray) cast iron 15 mm in diameter had a tensile strength of 247 MN m^{-2} , but an otherwise identical bar 150 mm in diameter had a tensile strength of 93 MN m^{-2} .
 - (b) A sand-cast bar of eutectic Al–Si alloy had a tensile strength and ductility of 160 MN m^{-2} and 2%, but an identical bar cast after the addition of 0.01% Na to the melt had a tensile strength and ductility of 195 MN m^{-2} and 13%.
 - (c) A sand-cast bar of flake graphite (gray) cast iron 25 mm in diameter had a tensile strength of 200 MN m^{-2} and a ductility of 1%, but a sand-cast bar of spheroidal-graphite cast iron 25 mm in diameter had a tensile strength of 350 MN m^{-2} and a ductility of 17%.
- 15.10** Distinguish between skin freezers and mushy freezers. What types of alloy are skin freezers, and what types are mushy freezers?
- 15.11** Explain how Chvorinov's rule can be used to help design the size and positioning of feeders in sand casting molds.

Processing Metals 2

16.1 MACHINING

The ability of most metals and alloys to deform plastically also allows them to be shaped by machining and grinding. Traditionally, machining takes many geometrical forms, such as lathe turning, milling, drilling, sawing, etc., although more recently computer controlled five-axis machining centers are being used to carry out many operations in one sequence, without moving the workpiece from one machine to another.

As shown in [Figure 16.1](#), the cutting tool (or the abrasive particles in grinding) removes material from the workpiece by *plastic shear*. Thermodynamically, all that is required is the energy of the two new surfaces created when the chip peels off the surface. In reality, the work done in shear (a shear strain of order 2, dependent on the cutting geometry) greatly exceeds this minimum necessary energy. In addition, friction between the chip and the tool is very high, because of the high pressures involved. This has several consequences—the tool gets very hot (near the tool tip, the temperature can reach 700 °C when fast machining steel), the tool wears (so it needs resharpening), and still further work input is required. These effects can be reduced by generous lubrication and cooling with oil–water emulsions. Some alloys can be made *free machining*: adding 2% lead to brass (see Table 15.1) makes the chip break up as it comes off the workpiece (Pb does not dissolve in Cu or Zn and segregates as small inclusions between dendrites); this alloy machines so easily that no coolant is required. (This is an interesting example of the how the microstructure of a material is altered not to improve the mechanical properties of the final product but to make it easier to make the product!) Machining imposes high demands on the properties of the *tool material*, and most high-speed machining and grinding now uses tools (or tool tips) made from ceramic–metal composites (e.g., WC-Co) or pure ceramics (e.g., SiC, Al₂O₃, diamond).

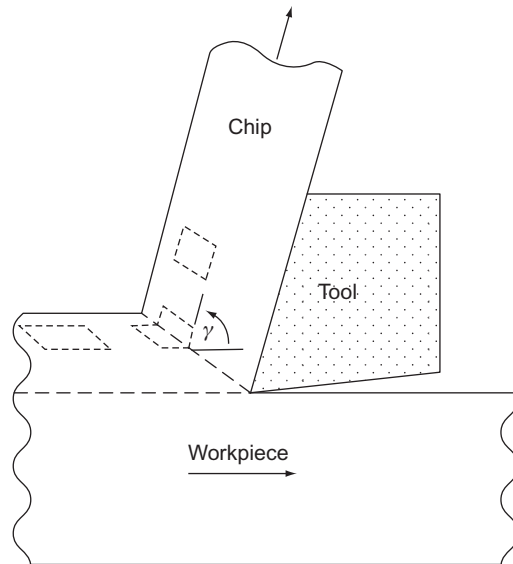


FIGURE 16.1
Machining.

16.2 JOINING

Many of the processes used to join one metal to another are based on casting. We have already looked at *fusion welding* (Figure 14.6). The most widely used welding process is arc welding: an electric arc is struck between an electrode of filler metal and the workpieces, providing the heat needed to melt the filler and fuse it to the parent plates. The electrode is coated with a *flux* which melts and forms a protective cover on the molten metal. In *submerged arc* welding, used for welding thick sections automatically, the arc is formed beneath a pool of molten flux. In *gas welding* the heat source is an oxyacetylene flame. In *spot welding* the metal sheets to be joined are pressed together between thick copper electrodes and fused together locally by a heavy current. Small, precise welds can be made using either an electron beam or a laser beam as the heat source.

Brazing and soldering are also fine-scale casting processes. But they use filler metals which melt more easily than the parent metal (see Table 5.1). The filler does not join to the parent metal by fusion (melting together). Instead, the filler spreads over, or wets, the solid parent metal and, when it solidifies, becomes firmly stuck to it. True metal-to-metal contact is essential for good wetting. Before brazing, the parent surfaces are either mechanically abraded or acid pickled to remove as much of the surface oxide film as possible.

Then a flux is added which chemically reduces any oxide that forms during the heating cycle. Specialized brazing operations are done in a vacuum furnace which virtually eliminates oxide formation.

There are of course many ways of joining metal parts together by purely *mechanical methods* (some pre-date the invention of fusion welding by centuries). These include: fasteners, like rivets and bolts (riveted ship hulls, steam boilers, and bridge girders were standard until the 1940s, even 1950s); crimping (e.g., crimped ferrules on rubber brake hose terminations); rolled-over joints (e.g., bases of cans and aerosols); fold-over tabs (e.g., in tinplate toys—a future engineer’s first experience of low-cycle fatigue was often finding that such toys could not be dismantled and reassembled more than once!); threaded connections (e.g., water fittings and metal screw-top cans). Today, although fusion welding has replaced fasteners in things like large-scale construction and pressure vessels (and made it feasible to produce large diameter steel piping by longitudinal seam welding), parts in aircraft are still held together by rivets and bolts, automotive engines by bolts and threaded studs, and laptop cases by screws (often deigned with a head which makes it impossible for you to unscrew them!). Many methods of mechanical joining are closely related to materials properties and microstructures. (A prime example is the use of quenched and tempered steels in forged-head and thread-rolled “high tensile” bolts, which use “every trick in the trade” to get the best tensile capacity and fatigue properties.)

In spite of the enduring popularity of mechanical fasteners, polymer-based *adhesives* have made huge advances over the last 70 years. We will look at their extensive use in joining airframe parts together in the Worked Example of Chapter 24. We are familiar with two-part epoxy (thermoset) resins such as Araldite, which are mixed, applied, and cured at room temperature (although they can be cured much faster at $\approx 100^\circ\text{C}$). Airframe applications generally use one-part phenolic resins, cured under pressure at $\approx 170^\circ\text{C}$, but the principle is the same. Thermoset adhesives are widely used in mechanical engineering, replacing traditional assembly methods. For example, wheels can be slid onto axles coated with a liquid *anaerobic adhesive* such as Loctite. This contains an acrylic monomer, plus OH^- ions reacted with oxygen from the air. Once the liquid is in the joint, the lack of oxygen frees up the OH^- ions, which instead attach to carbon atoms in the monomers and make them polymerize (the metal surfaces act as the catalyst for this reaction). Connections made in this way are as strong as traditional connections made with splines, keyways, or press fits but are cheaper (and better in fatigue); they can be taken apart (with difficulty) by heating to high temperature to burn-out the thermoset. Other well-known adhesives are cyanoacrylate (Superglue), another acrylic-based thermoset. The adhesive stays liquid in the tube because water vapor is excluded, but when assembled to

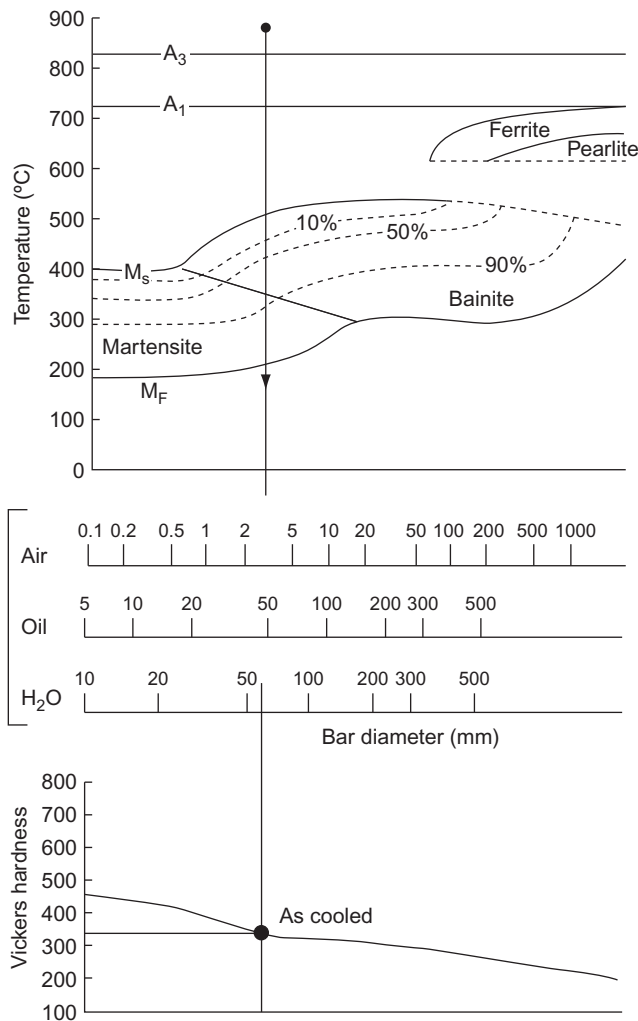
the joint, water vapor in the air initiates polymerization. (Have you ever wondered why Superglue always seems to stick your fingers together much faster than the pieces you are holding? The likely answer is sweat on your skin causes faster polymerization! Superglue is increasingly used for fixing wounds during surgery, because it sets fast and is quicker, neater, and more hygienic than stitching.) A tip for getting Superglue to cure faster is to breathe on the wetted joint just before you assemble the pieces (DRHJ received this advice—and much more—from the workshop staff in Cambridge University’s Engineering Department, who seem to know everything).

16.3 HEAT TREATING

With heat-treatable alloys—such as age-hardening aluminum alloys and low-alloy steels—the properties of the end product depend on *heat treating* the alloys in closely specified ways. We have already seen the principles of how this is done in Chapters 11 (for Al alloys) and 12 (for steels). Particularly with steels, heat treatments intended to raise the yield strength are done on parts which have been machined to their specified dimensions. It would be difficult or impossible to machine them once hardened, although they may be finished to final tolerances and surface finishes by fine grinding (e.g., honing bores or surface grinding flat surfaces). Because of this, heat treating of steels is very much a secondary processing step (done at the end of the processing chain). In contrast, heat treatable Al alloys can be solution treated, quenched, and stored in refrigerators; then later on formed, machined, or assembled in the soft condition, before being aged in an oven to get full age hardening. In this case, only the final stage of the heat treatment is a secondary processing step. For example, solution treated and quenched rivets can be used to joint sheets in a riveted structure (it is easy to close the rivets in the soft state), and the rivets afterward allowed to age naturally at room temperature (in the assembled structure) to develop their full strength.

In Chapter 12 (Section 12.5), we saw that TTT diagrams are useful for gathering and explaining basic data, but *continuous cooling transformation* diagrams (CCT for short) are needed to define the process conditions in real heat treatments. Here, we give a typical example of a CCT diagram (Figure 16.2), and explain how to use it. (At the end of this chapter, we give critical cooling rate (CCR) data for a range of steel compositions, useful for the preliminary assessment of a heat treatment schedule). The CCT diagram in Figure 16.2 is for a low-alloy steel with a composition of 0.17 C, 0.25 Si, 0.5 Mn, 1.6 Cr, 0.3 Mo, 1.55 Ni.

Look first at the solid vertical line (with downward pointing arrow) going down through all three parts of the diagram. This shows that the steel was

**FIGURE 16.2**

CCT diagram for a low-alloy steel containing 0.17 wt% carbon.

solution treated at 880 °C in the austenite field (i.e., above the A_3 temperature), then quenched to room temperature (see top diagram). But what was the rate of quench? The *cooling history* $T(t)$ in this example is what the steel would “see” if located at the center of a long circular bar of diameter 50 mm which was quenched from 880 °C into still oil at room temperature (see middle diagram). As shown in the middle diagram, the same $T(t)$ could alternatively

be produced by quenching a 64 mm bar into *still cold water* or allowing a 3 mm bar to cool naturally in *still air at room temperature*. (Water is a more severe quench medium than oil, because it has a higher thermal mass, so to keep the same $T(t)$ we need more steel “insulating” the center of the bar; air is a vastly less effective quench medium than oil, so to keep the same $T(t)$ we need to remove nearly all of the steel “insulation” from around the center of the bar; all of which makes intuitive sense.)

The bottom diagram shows that this $T(t)$ would produce a microstructure having a hardness of 340 Vickers. (The Vickers hardness test—which is widely used for industrial QA purposes—uses a diamond pyramid indenter (see EM1Ed4, Figure 8.12) and stress units of kg f mm^{-2} ; a Vickers hardness of 500 therefore corresponds to a hardness of 4.9 GN m^{-2} , because $g = 9.81 \text{ m s}^{-2}$.) But what is this microstructure? To find out, we go back to the top diagram. The answer is $\approx 85\%$ bainite plus $(100 - 85) = 15\%$ martensite.

The top diagram also shows how the microstructure develops *during* cooling. At 510°C , we start to enter the bainite field, so unstable (undercooled) austenite starts to transform to bainite. As the temperature falls further, more bainite forms from austenite (see the 10% and 50% transformation lines). Then, at 350°C , we enter the martensite field (after $\approx 85\%$ of the austenite has transformed), so the remaining 15% austenite starts to transform progressively to martensite as the temperature decreases further. Finally, at 210°C (the M_F temperature), the transformation is 100% complete (no austenite is left). We give further examples of how to use CCT diagrams in the examples, so you can get more practice. But plotted in this form, they are very user friendly (much more than TTT diagrams).

Real parts, of course, do not all come in the shape of a long cylindrical bar. Then, the *diameter of the equivalent bar*, D_e needs to be estimated from

$$D_e = f \times Z, \quad (16.1)$$

where Z is a characteristic dimension of the real part (e.g., the short side of a rectangular section bar) and f is a dimensionless shape factor. The compendium at the end of this chapter shows how to make these conversions.

Finally, remember that CCT diagrams should only be used as a rough guide to the final microstructure and hardness: there is often a lot of variability between different steels of the same nominal composition (from differences in prior thermal and mechanical history, grain size, solution treating time, etc.). When planning a production run, it is always wise to trial the heat treatment schedule on actual parts, and check out the results using hardness tests, etc.

16.4 SPECIAL TOPICS

Surface engineering

Often, the *surface* of a component needs to have special properties, distinct from those of the bulk material. Examples are high hardness, low wear/friction, low thermal conductivity, or good corrosion resistance. Then the desired properties are achieved by treating the surface. Examples are given in [Table 16.1](#). This is a huge subject in its own right, and we can only give a flavor of it here (it takes up a whole volume of the multivolume set of ASM Metals Handbooks). If you are interested in knowing more, here are a few web sites to begin with, and you can find many others.

Table 16.1 Typical Surface Engineering Processes

Process	Method	Typical Applications
Case carburizing	C diffused into steel surface when austenite ($\approx 900^\circ\text{C}$). Part then quenched into oil.	Hard, wear-resistant surfaces in bearings, pins, etc.
Nitriding	N (from NH_3) diffused into steel surface at 600°C . Reacts with Al in steel to form hard Al nitride.	Crankshaft journals.
Induction hardening	Surface heated to austenite by high frequency induction coil, then quenched by oil/water.	Wear-resistant sliding surfaces in cast iron machine tools, saw. and knife blades, etc.
Flame hardening	Surface heated to austenite by gas torch, then quenched by oil/water.	Wear- and fatigue-resistant surfaces of gear teeth, etc.
Laser hardening	Surface heated to austenite by scanned laser beam, then self-quenched by thermal mass of part.	Wear- and fatigue-resistant surfaces of engine camshaft lobes, etc.
Electroplating	Make surface or part the cathode in plating bath; plate onto conducting former to make parts.	Cr for wear resistance of rotating and sliding surfaces; forming thin/small parts by electroforming.
Weld deposition: arc, gas, plasma transferred arc (PTA)	Welded-on layers of hard metals, e.g., Stellite (Co—Cr alloy).	Wear-resistant engineering parts (new and reclaimed), valve faces.
Thermal spraying: flame, plasma, high-velocity oxygen fuel (HVOF), etc	Hot-sprayed layers of WC-Co, ceramics and alloys.	Wear- and corrosion-resistant applications. Thermal barrier coatings (TBCs)—gas turbine parts, etc.
Chemical vapor deposition (CVD)	Reaction of gas-phase chemical compounds on surface of heated part, usually under low pressure.	TiC and TiN hard layers on forming/cutting tools, manufacture of complex thin-walled parts.
Physical vapor deposition (PVD)	Evaporation of coating materials from heated source and deposition on part (with gas-phase elements for compound formation).	TiC and TiN hard layers on forming/cutting tools. Less heat distortion of parts (lower deposition temperature than CVD).

http://en.wikipedia.org/wiki/Thermal_spraying

<http://www.youtube.com/watch?v=ke7uRekOYws>

<http://www.youtube.com/watch?v=SvVuhMUZWmc>

<http://www.youtube.com/watch?v=IIIExrjIRg>

<http://www.richterprecision.com/pvd-coatings.html>

Friction welding

Figure 16.3 shows how friction welding is done. Frictional heat is produced at the joint interface by relative rotation (under pressure) of the pieces to be joined. This does not melt the material, but heats it to a high enough temperature that it bonds.

http://en.wikipedia.org/wiki/Friction_welding

(Because the process does not involve the melting of the material, it is really a specialized forging process—it has similarities to the traditional blacksmith's method of “welding” bars of wrought iron together by heating the (tapered) ends to white heat, overlapping them, and beating them with a hammer.)

Friction welding has many advantages over fusion welding. Because the joining time is very short (several seconds) and the interface temperature does not go as high, the HAZ is thinner, and its thermal cycle is less severe—there is no time for grain growth, and annealing (removal of work hardening) occurs over a narrower band of parent material. There is

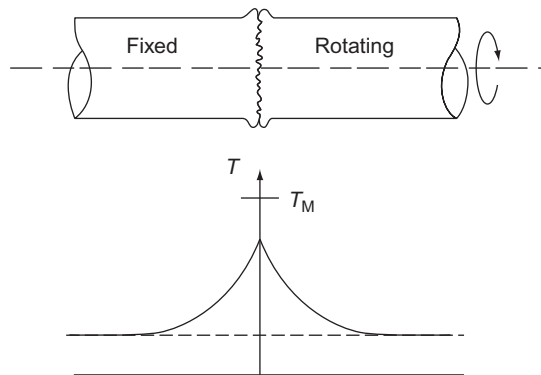


FIGURE 16.3

Schematic of friction welding.

no bead of weld metal to cause chemical or microstructural variations (or introduce weld defects) across the joint. There is no postweld distortion, and because friction welding is done by machine, it is easy to get accurate relative alignment of the parts. Thick sections, like thick-walled tube (e.g., drill strings for oil and gas drilling) and large diameter bar (e.g., for drive shafts) can easily be joined with a uniform 100% area joint. This would be difficult or impossible to achieve to an acceptable standard with fusion welding. Reactive metals (like Al, Ti, Mg, which have to be fusion welded in an inert gas atmosphere) can easily be joined in air. Finally, different metals can be joined together, in impossible combinations for fusion welding (e.g., Al alloys to steels or nickel alloys).

The principle of friction welding has recently been adapted for joining *plates* together by a process called *friction stir welding* (Figure 16.4).

http://en.wikipedia.org/wiki/Friction_stir_welding

<http://www.youtube.com/watch?v=niVsJPFgl1Y>

This is mainly used for joining Al alloys to avoid postweld distortion and minimize loss of strength of the parent material (annealing of work-hardened alloys or overaging of age-hardened alloys). Mg and Cu can also be joined this way. In a workshop environment, a simple vertical milling machine, with automatic feed and special tool, is all that is needed to make friction stir welds. The process is now widely used for welding aluminum in

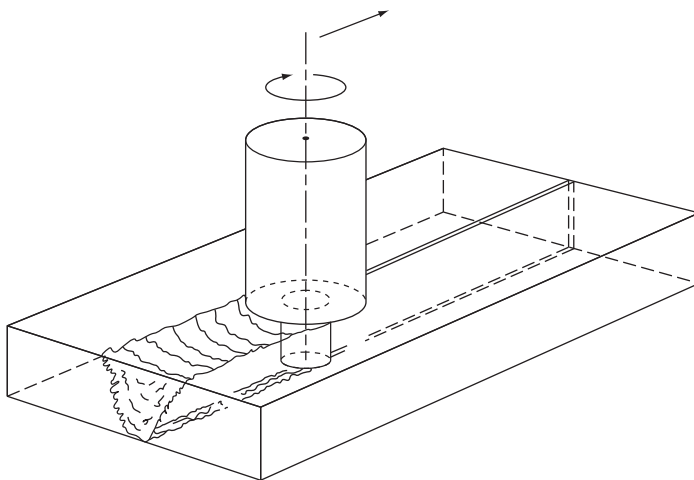


FIGURE 16.4
Schematic of friction-stir welding.

ship hulls and superstructures, train carriage bodies, spacecraft fuel tanks, aircraft and automotive parts, etc.

Superplastic forming

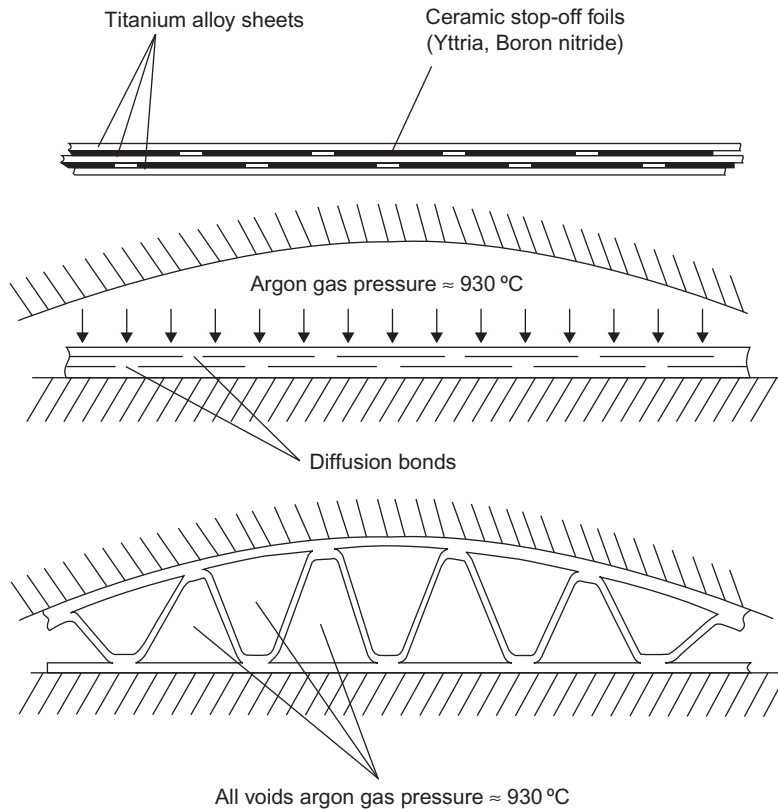
We saw in EM1Ed4, Chapter 22 that materials creep very fast by diffusion creep if they have a fine-grain size. As shown by Equation (22.2) in EM1Ed4, the strain rate scales as stress to the power 1 (not some higher power, as in power-law creep). This means that if we stretch a fine-grained alloy at high temperature, it will not easily form necks (see Example 16.5 for the reason). This principle is used in *superplastic forming* (SPF). The main material used for SPF is the titanium alloy Ti + 6 Al 4V, although there are a few others which can be formed this way. Ti6Al4V has a two phase $\alpha + \beta$ structure, and this is critical in stopping the grains coarsening at the high temperature of the forming process. Typical creep properties of this alloy at 930 °C and strain rate = 10^{-4} s^{-1} are: flow stress = 2 MN m^{-2} (12 μm grain size), and 11 MN m^{-2} (20 μm grain size). Strains to failure are $\approx 1000\%$, so huge tensile extensions are possible when forming parts (far greater than in plastic deformation).

One of the most dramatic applications of SPF is in the big fan blades at the front end of aircraft turbofan engines. These are made from three layers of Ti6Al4V sheet, which are first diffusion bonded together in the right places (using high temperature and inert gas pressure), then inflated into a mold cavity (again using inert gas pressure at high temperature) to make a hollow, internally stiffened airfoil shape all in one go. The sequence of operations is shown schematically in Figure 16.5. This can only be regarded as an astonishing triumph of materials engineering.

<http://www.youtube.com/watch?v=sQPpdmoZhj8&feature=relmfu>

Shape memory alloys

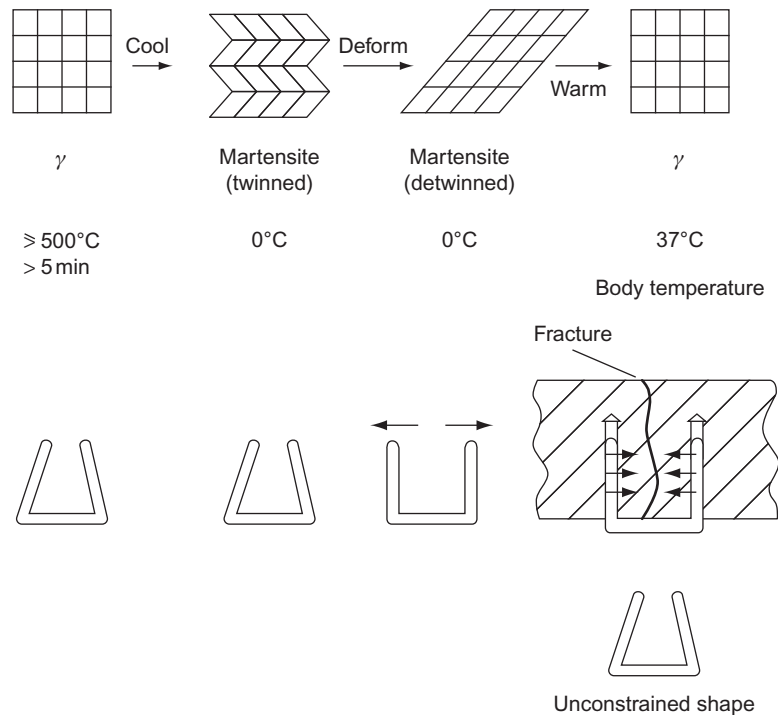
Most applications of shape memory alloys (SMAs) use a Ni–Ti alloy in an atom ratio of $\approx 50/50$. Above a high enough temperature (0–115 °C, depending on the exact Ni/Ti ratio), the alloy has a single phase b.c.c. structure, with $a = 0.301 \text{ nm}$, and $T_M = 1300 \text{ °C}$. (This phase is labeled γ on the phase diagram and is referred to as “austenite” in the literature, which is highly confusing because it is *not* an f.c.c. structure!) When the γ is cooled to a low enough temperature, it transforms to a martensite phase, by a process (called “twinning”) which involves the sliding (by dislocation glide) of crystal planes over one another. In this condition, the part can easily be deformed. This takes place by a mechanism known as “detwinning,” where some of the twins which formed when the γ transformed to martensite are “undone” (again, by dislocation glide). However, the remarkable thing

**FIGURE 16.5**

Schematic of superplastic forming of an aero engine fan blade.

about the alloy is that if it is heated up again to a temperature at which the γ is stable, the twins all “unzip,” and return the part to its original (high temperature) shape. In other words, the part “remembers” its original shape.

This is the basis of party jokes and tricks. You can take a length of NiTi wire, coil it up into a helix, then give it to someone to put into a mug of warm water—whereupon it will (with great force) straighten out, and leap out of the mug to the great surprise of the victim. But there are many more serious niche applications for this extraordinary alloy. One example, clamping bones together after orthopedic surgery is shown in [Figure 16.6](#). The beauty of this method is that the clamp always exerts a large force on the bone joint, which allows the bones to fuse together well. (You need to insert the clamps into the holes pretty smartly or they will warm up and transform back to γ before they go in.) Conventional clamps can work loose allowing the bone joint to separate. The clamp has to be manufactured to the correct shape in the first

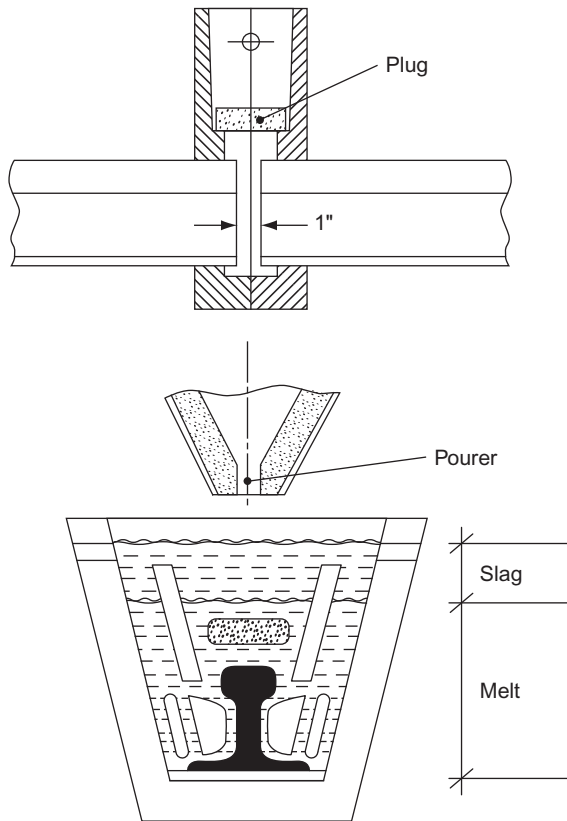
**FIGURE 16.6**

Schematic of NiTi SMA clamp inserted into bone parts during orthopedic surgery.

place by cold forming, then held in a shaped jig (so it cannot move) and heated to $\geq 500^\circ\text{C}$ for $\geq 5\text{ min}$ to set the shape.

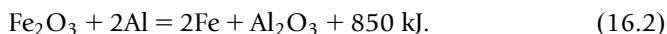
WORKED EXAMPLE

New railroad rails are usually transported to the site in the form of long lengths ($\approx 400\text{ m}$), previously assembled by welding shorter lengths of rail end to end. These joints are done by flash butt welding at the workshops <http://www.youtube.com/watch?v=8H0tXj0qIG8>. This involves heating the two rail ends with a large low voltage DC current (which initially arcs across a narrow gap between the ends), then pressing the ends together (with the current still flowing) to make a hot forged joint across the full cross section of the rail. Once at the site, the ends of the long rail lengths are joined by *aluminothermic welding* (also called *thermit welding*). The geometry of this process is shown in the following diagram and described in the link http://www.thermit-welding.com/thermit_welding_process.php.



Schematic of thermite welding mold, pouring, and feeding geometry. The plug is inserted after preheating the rail ends. The Al_2O_3 slag floats to the top and overflows into slag trays. See <http://www.youtube.com/watch?v=19jqMckL8bA>.

The ends of the rails to be joined are spaced apart by about an inch and enclosed by a factory-made split ceramic mold. The rail ends are then preheated with gas torches. The welding process uses a steel canister (lined with refractory ceramic) containing a mixture of iron oxide and aluminum powders. This is positioned on top of the ceramic mold, and the powder is ignited. It reacts according to the equation



The reaction heats the contents of the canister to $\approx 2500^\circ\text{C}$, which melts the reduced iron. (The powders also contain pellets of alloying elements, so the molten metal is actually a steel, matching the composition of the rail steel). The molten steel then runs into the bottom of the mold cavity and rises up inside the gap between the rail ends. Some of the rail end is melted back, then the liquid steel solidifies to give a cast structure. Once the weld

has gone solid, the mold is broken off, and the excess metal trimmed away. Finally, when the joint has cooled to room temperature, the profile of the running surface is accurately ground using a special rail mounted grinding wheel. The following clips show this actually being done (with varying degrees of safety precautions!).

<http://www.youtube.com/watch?v=nR6K90cR8Lg>

http://www.youtube.com/watch?v=unr_cbe335c&feature=related

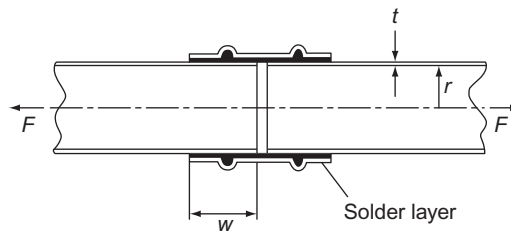
<http://www.youtube.com/watch?feature=endscreen&NR=1&v=foiY79zhF4>

Obviously, the thermit process is also good for replacing short lengths of worn or cracked rail on site (these are cut out with an oxy-gas torch, a replacement length inserted into the gap, and the ends joined with thermit welds).

We are so used to thinking of welding in terms of electric arc welding that it is hard to realize that the thermit process was first used to make rail joints way back in 1899, before electric arc welding became popular. Although arc welding is a versatile joining method, we have seen that it has a number of potential disadvantages: metallurgical damage to parent material, distortion, hard to fully weld large cross sections, need for skilled workers, etc. Innovation often means exploring every possible joining method in order to achieve the optimum for the particular application, from friction welding lengths of oil pipe to electron beam welding thin diaphragms for aircraft pressure sensors <http://www.camvaceng.com/aneroid-capsules.asp>.

EXAMPLES

16.1 Copper capillary fittings are to be used to solder copper water pipes together as shown below:



The joint is designed so that the solder layer will yield in shear at the same axial load F that causes the main tube to fail by tensile yield. Estimate the required value of w , given the following data: $t = 1 \text{ mm}$; σ_y (copper) = 120 MN m^{-2} ; σ_y (solder) = 10 MN m^{-2} .

Answer

24 mm.

- 16.2** A piece of plain carbon steel containing 0.2 wt% carbon was case-carburized to give a case depth of 0.3 mm. The carburizing was done at a temperature of 1000 °C. The Fe–C phase diagram shows that, at this temperature, the iron can dissolve carbon to a maximum concentration of 1.4 wt%. Diffusion of carbon into the steel will almost immediately raise the level of carbon in the steel to a constant value of 1.4 wt% just beneath the surface of the steel. However, the concentration of carbon well below the surface will increase more slowly toward the maximum value of 1.4 wt% because of the time needed for the carbon to diffuse into the interior of the steel.

The diffusion of carbon into the steel is described by the time-dependent diffusion equation.

$$C(x, t) = (C_s - C_0) \left\{ 1 - \operatorname{erf} \left(\frac{x}{2\sqrt{Dt}} \right) \right\} + C_0.$$

The symbols have the meanings: C , concentration of carbon at a distance x below the surface after time t ; C_s , 1.4 wt% C; C_0 , 0.2 wt% C; D , diffusion coefficient for carbon in steel. The “error function,” $\operatorname{erf}(y)$, is given by

$$\operatorname{erf}(y) = \frac{2}{\sqrt{\pi}} \int_0^y e^{-z^2} dz.$$

The following table gives values for this integral.

y	0	0.1	0.2	0.3	0.4	0.5	0.6	0.7	
$\operatorname{erf}(y)$	0	0.11	0.22	0.33	0.43	0.52	0.60	0.68	
y	0.8	0.9	1.0	1.1	1.2	1.3	1.4	1.5	∞
$\operatorname{erf}(y)$	0.74	0.80	0.84	0.88	0.91	0.93	0.95	0.97	1.00

The diffusion coefficient may be taken as

$$D = 9 \times 10^{-6} \text{ m}^2 \text{ s}^{-1} \exp \left\{ \frac{-125 \text{ kJ mol}^{-1}}{RT} \right\}$$

where R is the gas constant and T is the absolute temperature.

Calculate the time required for carburization, if the depth of the case is taken be the value of x for which $C = 0.5$ wt% carbon.

Answer

8.8 min.

- 16.3** Using the equations and tabulated error function data from Example 16.2, show that the expression $x = \sqrt{Dt}$ gives the distance over which the concentration of the diffusion profile halves.

- 16.4** Outline the ways in which the surfaces of engineering materials may be treated to improve their wear resistance.
- 16.5** A bar of hot material (area A , length l) is subjected to a constant tensile load F along its axis. The material creeps under the load according to the equation

$$\dot{\epsilon} = B\sigma^n,$$

where σ ($=F/A$) is the stress and B and n are constants. The bar contains a length of slightly reduced cross-sectional area. Show how the value of n affects the tendency of the bar to develop necks as it creeps. (Hints: The volume of the bar, $Al = \text{constant}$; differentiate this to show that $dA/A = -dl/l = -d\epsilon$; hence, show that $\dot{A}/A = -B(F/A)^n = \text{constant}/A^n$.)

- 16.6** Refer to the CCT diagram in Figure 16.2. Long cylindrical bars of this steel having diameters of 10, 50, and 200 mm are austenitized at 900 °C, then quenched into cold oil. For each bar, estimate the proportion of the various phases present in the as-quenched condition, and estimate the as-quenched Vickers hardness.

Answers

10 mm: 100% M, 460; 50 mm: 85% B, 15% M, 340; 200 mm: 100% B, 310.

- 16.7** Referring to Figure 16.2, explain the difference in the diameter scales for bars quenched in air, oil, and water.
- 16.8** Explain briefly what is meant by *hardenability*. Referring to the table in the data section at the end of the chapter, arrange the following steels in order of increasing hardenability: 0.40 C nickel steel; 0.40 C carbon steel; 0.40 C nickel–chromium steel; 0.40 C chromium–molybdenum steel; 0.39 C chromium steel.
- 16.9** The lower half of a forming die (for cold pressing an automotive subframe from thin sheet) has overall external dimensions of 1 m \times 1 m \times 0.2 m. Calculate the equivalent diameter, D_e for the die. Why is your value on the conservative side? Choose steels from the table in the data section which would give the die a fully martensitic structure after an oil quench. You are now told that the as-quenched hardness of the die must be 9 GN m⁻². How much carbon should you have in the steel to achieve this? What would this amount of carbon do to the hardenability of the steels you identified earlier?
- 16.10** What are the advantages of friction welding compared to arc welding for joining lengths of thick-walled drill pipes?
- 16.11** What are the advantages of friction stir welding compared to arc welding for joining plates of work-hardened aluminum alloys?
- 16.12** Make a list of the devices you could envisage which utilize the special properties of SMAs.
- 16.13** What are the advantages of thermit welding compared to arc welding for joining railroad rails?
- 16.14** Give examples of how and why anaerobic adhesives have replaced traditional methods of joining in mechanical engineering.

- 16.15** Explain why the processes which take place during machining cause heating and wear of the cutting tool. How does this affect the choice of tool materials?

Heat treating steels

The addition of the alloying elements C, Mn, Cr, Mo, and Ni decreases the CCR for the formation of martensite and increases the size of section that can be quenched to give a fully martensitic structure. The following table gives approximate values for the maximum diameter of round bar which can be quenched in oil to give 100% martensite. The table lists typical ranges of compositions for carbon, carbon–manganese, and low-alloy steels as used in engineering applications. The concentrations of the alloying elements are given as weight %.

Steel Type	C	Si	Mn	Cr	Mo	Ni	Diameter (mm)
C	0.13	—	0.60	—	—	—	—
	0.25	0.20	0.70	—	—	—	5
	0.40	0.20	0.70	—	—	—	10
	0.86	0.20	0.60	—	—	—	15
C–Mn	0.19	0.20	1.20	—	—	—	4
	0.28	0.20	1.20	—	—	—	8
	0.28	0.20	1.50	—	—	—	11
	0.36	0.20	1.20	—	—	—	13
Ni	0.38	0.25	1.80	—	—	—	30
	0.10	0.26	0.53	—	—	3.65	7
	0.16	0.25	0.60	0.20	—	1.50	15
	0.10	0.20	0.40	—	—	4.8	20
Ni–Cr	0.09	0.25	0.45	0.10	—	9.00	60
	0.40	0.26	0.62	0.23	0.10	3.45	60
	0.16	0.20	0.80	0.85	—	1.15	8
	0.16	0.31	0.50	1.95	—	2.02	25
Cr	0.40	0.23	0.75	0.65	—	1.30	25
	0.15	0.15	0.40	1.15	—	4.10	40
	0.30	0.20	0.50	1.25	—	4.10	300
	0.20	0.30	0.75	0.95	—	—	8
Cr–Mo	0.38	0.25	0.70	0.50	—	—	20
	0.39	0.20	0.70	1.05	—	—	30
	0.59	0.25	0.60	0.65	—	0.20	40
	0.24	0.37	0.27	13.3	—	0.32	500
	0.14	0.25	0.55	0.60	0.55	—	5
	0.12	0.30	0.45	0.85	0.60	0.16	8
	0.27	0.13	0.60	0.74	0.55	0.19	20
	0.40	0.20	0.85	1.05	0.30	—	50
	0.32	0.25	0.55	3.05	0.40	0.30	110

The data have been obtained from CCT diagrams. The diagrams show significant variability even between steels of very similar composition. This is because the CCR is affected by the prior thermal and mechanical history of the steel. The data should be used only as a rough guide to tell us whether a quenched component of a particular size is likely to be fully martensitic.

Shape factors

See Equation (16.1). The f values given here are first order fits to more complex relationships obtained from finite element heat transfer modeling. They are therefore *approximate* only.

Infinitely long bar of rectangular cross section: thickness t , width b ($0 \leq t/b \leq 1$)

$$D_e = f \times t, f \approx 1.7 - 0.6(t/b).$$

Circular bar length l , diameter d with axial hole diameter ϕ .

$$D_e = f \times d.$$

(a) $\phi/d = 0$:

$$f \approx 1 \quad (0.75 \leq l/d \leq \infty),$$

$$f \approx 1.33l/d \quad (0 \leq l/d \leq 0.75).$$

(b) $\phi/d = 0.2$:

$$f \approx 0.6 \quad (0.45 \leq l/d \leq \infty),$$

$$f \approx 1.33l/d \quad (0 \leq l/d \leq 0.45).$$

(c) $\phi/d = 0.5$:

$$f \approx 0.4 \quad (0.3 \leq l/d \leq \infty),$$

$$f \approx 1.33l/d \quad (0 \leq l/d \leq 0.3).$$

Ceramics

17.1 INTRODUCTION

Ceramics are *inorganic, nonmetallic* solids. They have a structure which is crystalline, amorphous, or a mixture of both. Most are compounds of oxygen, carbon, or nitrogen with metals such as aluminum or silicon—these are some of the most abundant elements in the Earth's crust. The word “ceramic” comes from the Greek *keramikos*, meaning “of pottery,” and is traditionally associated with the production of things like pottery or tiles by the human hand from starting materials which are “fired” at high temperature. (The description “terra-cotta” for roof tiles is the Italian for “baked earth.”) However, in the context of engineering materials, the definition extends to include naturally occurring materials such as rock and stone—which may be igneous (formed at high temperature) or sedimentary (formed at low temperature, often by deposition or crystallization from water)—plus particles produced by the mechanical breakdown of rock and stone (such as sand and gravel). Although there is a wide range of chemical compounds that are classed as ceramics, and many different forms and ways in which they occur naturally—or can be processed by the human hand—they have common characteristics which define how they are used: most are (a) *hard* (diamond, a form of pure carbon, is the hardest material known), (b) *inherently brittle*, (c) *chemically stable*, (d) *refractory* (they melt or soften at high temperatures), and (e) *electrical insulators* (carbon, in the form of graphite, is a notable—and essential—exception). Finally, *glass* is *optically transparent*—no other material can remotely approach its performance for windows or precision optical systems.

It is difficult to appreciate from our twenty-first century viewpoint that further back in time than 4000 years (more in China), humans did not have access to metals (with the possible exception of gold, which—because it is chemically stable—occurs naturally as the metal rather than an ore). Apart from articles manufactured from ceramic starting materials such as pottery

and glassware, they were totally dependent on natural materials such as rock and stone, wood, plant and insect fibers, and the products of animals, birds, and marine life forms. It is therefore interesting that with the present abundance of metals (and synthetic polymers and composites), ceramics have not been superseded, and in fact are used in greater quantities than ever before—although stone has mainly been replaced by processed ceramics such as cement and concrete, bricks and blocks, tiles, and composites of ceramic particles in polymer matrices.

Two of the most iconic structures made from ceramics—built nearly 2000 years apart—are the Roman aqueduct at Segovia, Spain (Figures 17.1–17.3) and the Sydney Opera House, Australia (Figures 17.4 and 17.5).

The aqueduct was constructed in about 50 AD from granite blocks (no mortar is used to hold it together—the blocks simply fit snugly together). Granite—an



FIGURE 17.1

The Roman aqueduct at Segovia, Spain. The locals take it for granted (40 56 51.90 N 4 07 03.25 W).

igneous rock—is the hardest and most weather-resistant stone available for construction. The close-up in [Figure 17.3](#) shows how well it has resisted its 2000 years of exposure to wind, rain, and frost. One can imagine the incredible effort required to cut the granite blocks out of the rock face in the quarry, and trim



FIGURE 17.2

The Roman aqueduct at Segovia, Spain. The granite is as hard as the winters (40 56 51.90 N 4 07 03.25 W).



FIGURE 17.3

The Roman aqueduct at Segovia, Spain. Arches in the sky (40 56 51.90 N 4 07 03.25 W).

them to shape—all by hand, with hammers and chisels. It is such an important historical structure that it is a UNESCO World Heritage Site.

<http://www.romanaqueducts.info/aquasite/segovia/index.html>

http://en.wikipedia.org/wiki/Aqueduct_of_Segovia

<http://whc.unesco.org/en/list/311>



FIGURE 17.4

The Sydney Opera House, Australia. A triumph of concrete and glass (33 51 24.50 S 151 12 54.30 E).

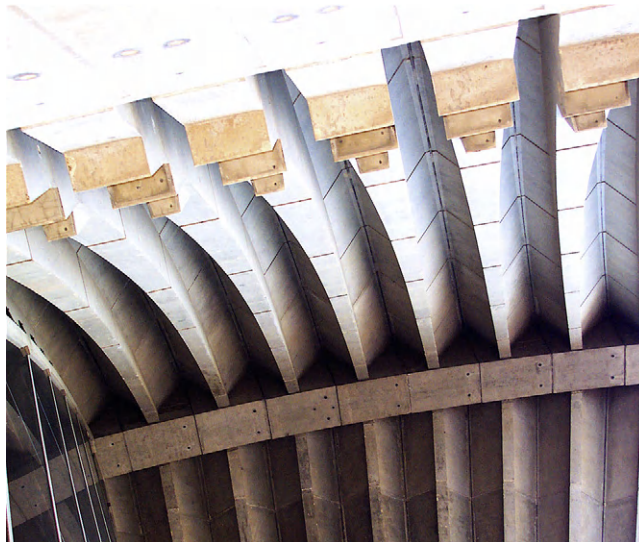


FIGURE 17.5

The Sydney Opera House, Australia. Limbs of concrete (33 51 24.50 S 151 12 54.30 E).

The Sydney Opera House was conceived and largely designed by Danish architect Jørn Utzon and opened in 1973. The curved shell elements of the building are constructed from reinforced concrete, and the walls are made from plate glass (supported against wind loading by steel trusses). In 2003, Utzon received the Pritzker Prize, architecture's highest award, for the design. The citation stated: "There is no doubt that the Sydney Opera House is his masterpiece. It is one of the great iconic buildings of the 20th century, an image of great beauty that has become known throughout the world—a symbol for not only a city, but a whole country and continent." (As Engineers, you will be intrigued by a special feature of the design which is not apparent to the casual observer. Each of the curved surfaces which makes up the roof is a part of a single spherical cap—if all the curved surfaces were to be assembled together, they would form a single spherical surface with no gaps. This allows arches of varying length to be cast in a mold of standard curvature and cross section, and a series of arch segments to be placed adjacent to one another, to form each curved surface.) The Opera House is such an important piece of modern architecture that it is a UNESCO World Heritage Site.

http://en.wikipedia.org/wiki/Sydney_Opera_House

<http://www.sydneyoperahouse.com/>

Even stone is making a comeback when there is money to pay for it (extracting it from the quarry and cutting it to size is still an expensive business, even with the latest power tools, explosives, and diamond-tipped saws). [Figure 17.6](#) shows a nice example of stone used in a modernist home together with glass and concrete. The stone wall is made from slabs of *slate*, a sedimentary stone formation which has subsequently been subjected to



FIGURE 17.6

A modernist home in Sydney. Glass, stone, and concrete together (33 50 01.70 S 151 15 06.35 E).

high temperature and pressure by geological processes (an example of a *metamorphic* rock). Because it can be split into very thin flat “slates,” it was much used in the past as a lighter and longer-lasting alternative to roofing tiles (it still is if cost is not important).

However, within the last 50 years, there has been a rapid increase in the use of *manufactured* ceramics for small-scale specialized applications. Of course, niche applications of ceramics go back a lot further than this. A good example is the use of glazed ceramics as electrical insulators. But the importance of the modern *high-performance engineering ceramics* cannot be overemphasized. It would be hard these days to imagine drilling oil wells without teeth coated with industrial diamond, or machining metal and sawing wood without tungsten carbide/cobalt cutting tool tips, or reentry of a space shuttle without reinforced carbon–carbon (RCC) wing leading edges.

http://en.wikipedia.org/wiki/Space_Shuttle_thermal_protection_system

This is the area where scientific research and development of the highest order has been required to produce materials capable of surviving extreme service conditions.

The next five chapters focus on ceramics. Five classes of materials are of interest to us here:

- (a) *Glasses*, all of them based on silica (SiO_2), with additions to reduce the melting point, or give other special properties.
- (b) The traditional *vitreous ceramics*, or clay products, used in large quantities for plates and cups, sanitary ware, tiles, bricks, and so forth.
- (c) The new *high-performance ceramics*, finding ever-increasing application for resistance to wear and temperature.
- (d) *Cement and concrete*: a complex ceramic with many phases, and one of three essential bulk materials of civil engineering.
- (e) *Rocks and minerals*, including ice.

As with metals, the number of different ceramics is vast. But there is no need to remember them all: the generic ceramics listed below (which you *should* remember) embody the important features; others can be understood in terms of these. They are, potentially or actually, cheap. The processing costs may be high, but the raw ingredients are generally abundant.

17.2 GENERIC CERAMICS

Glasses

Glasses are used in enormous quantities: as much as 80% of the surface area of a modern office block can be glass; and glass is used in a vast range of products, from car windscreens to jam jars. All important glasses are based

on silica (SiO_2). Two are of primary interest: common window glass and the temperature-resisting borosilicate glasses. Table 17.1 gives details.

Vitreous ceramics

Potters have been respected members of society since ancient times; the pottery of an era or civilization often gives the clearest picture of its state of development and its customs. Modern pottery, porcelain, tiles, and structural and refractory bricks are made by processes which, though automated, differ little from those of 2000 years ago. All are made from clays, which are formed in the wet, plastic state and then dried and fired. After firing, they consist of crystalline phases (mostly silicates) held together by a glassy phase based on silica (SiO_2). The glassy phase forms and melts when the clay is fired and spreads around the surface of the inert, but strong, crystalline phases, bonding them together. The basic information is summarized in Table 17.2.

High-performance engineering ceramics

Diamond (the synthetic variety) is the ultimate engineering ceramic; it has for many years been used for cutting tools, dies, rock drills, and as an abrasive. But it is extremely expensive. The strength of a ceramic is largely determined by two characteristics: its *toughness* (K_c), and the size distribution of *microcracks* it contains. A new class of fully dense, high-strength ceramics is now emerging which combine a higher K_c with a much narrower

Table 17.1 Generic Glasses

Glass	Typical Composition (wt%)	Typical Uses
Soda-lime glass	70 SiO_2 , 10 CaO , 15 Na_2O	Windows, bottles, etc.; easily formed and shaped.
Borosilicate glass	80 SiO_2 , 15 B_2O_3 , 5 Na_2O	Pyrex; cooking and chemical glassware; high-temperature strength, low coefficient of expansion, good thermal shock resistance.

Table 17.2 Generic Vitreous Ceramics

Ceramic	Typical Composition	Typical Uses
Porcelain	Made from clays: hydrous aluminosilicate such as $\text{Al}_2(\text{Si}_2\text{O}_5)(\text{OH})_4$ mixed with other inert minerals.	Electrical insulators.
China		Artware and tableware tiles.
Pottery		Construction; refractory uses.
Brick		

distribution of smaller microcracks, giving properties which make them competitive with metals, cermets, even with diamond, for cutting tools, dies, and engine parts. And (at least potentially) they are cheap. The most important are listed in Table 17.3.

Cement and concrete

Cement and concrete are used in construction on an enormous scale, equaled only by structural steel, brick, and wood. *Cement* is a mixture of a combination of lime (CaO), silica (SiO₂), and alumina (Al₂O₃), which sets when mixed with water. Concrete is sand and stones (aggregate) held together by cement. Table 17.4 summarizes the most important facts.

Natural ceramics

Stone is the oldest of all construction materials and the most durable. Stone used in a load-bearing capacity behaves like any other ceramic; and the criteria used in design with stone are the same. One natural ceramic, however, is unique. Ice forms on the Earth’s surface in enormous volumes: the Antarctic ice cap, for instance, is up to 3 km thick and almost 3000 km across; something like 10¹³ m³ of pure ceramic. The mechanical properties are of primary importance in some major engineering problems, notably ice breaking, and the construction of offshore oil and gas rigs in polar regions. Table 17.5 lists the important natural ceramics.

Table 17.3 Generic High-Performance Ceramics		
Ceramic	Typical Composition	Typical Uses
Dense alumina	Al ₂ O ₃	Cutting tools, dies; wear-resistant surfaces, bearings; medical implants; engine and turbine parts; armor.
Silicon carbide, nitride	SiC, Si ₃ N ₄	
Sialons	Si ₂ AlON ₃	
Cubic zirconia	ZrO ₂ + 5 wt% MgO	

Table 17.4 Generic Cements and Concretes		
Cement	Typical Composition	Typical Uses
Portland cement	CaO + SiO ₂ + Al ₂ O ₃	Cast facings, walkways, etc. and as component of concrete. General construction.

17.3 CERAMIC COMPOSITES

The great stiffness and hardness of ceramics can sometimes be combined with the toughness of polymers or metals by making composites. Glass- and carbon-fiber reinforced plastics are examples: the glass or carbon fibers stiffen the rather floppy polymer; but if a fiber fails, the crack runs out of the fiber and blunts in the ductile polymer without propagating across the whole section. Cermets are another example: particles of hard tungsten carbide bonded by metallic cobalt, much as gravel is bonded with tar to give a hard-wearing road surface (another ceramic composite). Bone is a natural ceramic composite: particles of hydroxyapatite (the ceramic) bonded together by collagen (a polymer). Synthetic ceramic–ceramic composites are increasingly used in high-temperature applications. Examples are summarized in Table 17.6.

17.4 DATA FOR CERAMICS

Ceramics are hard, brittle solids. When designing with metals, failure by plastic collapse and by fatigue are the primary considerations. For ceramics, plastic collapse and fatigue are seldom problems; it is brittle failure, caused by direct loading or by thermal stresses, that is the overriding consideration.

Table 17.5 Generic Natural Ceramics

Ceramic	Composition	Typical Uses
Limestone (marble)	Largely CaCO_3	Building foundations, construction.
Sandstone	Largely SiO_2	
Granite	Aluminium silicates	
Ice	H_2O	Polar engineering.

Table 17.6 Ceramic Composites

Ceramic Composite	Components	Typical Uses
Fiber glass	Glass – polymer	High-performance structures.
CFRP	Carbon – polymer	
Cermet	Tungsten carbide–cobalt	Cutting tools, dies.
Bone	Hydroxyapatite–collagen	Main structural material of animals.
New ceramic composites	Alumina–silicon carbide	High temperature and high toughness applications.

Because of this, the data listed in Table 17.7 for ceramic materials differ in emphasis from those listed for metals. In particular, the table shows the *modulus of rupture* (the maximum surface stress when a beam breaks in bending) and the *thermal shock resistance* (the ability of the solid to withstand sudden changes in temperature). These, rather than the yield strength, tend to be the critical properties in any design exercise.

As before, the data presented here are approximate, intended for the first phase of design. When the choice has narrowed sufficiently, it is important to consult more exhaustive data compilations; and then to obtain detailed specifications from the supplier of the material you intend to use. Finally, if the component is a critical one, you should conduct your own tests. The properties of ceramics are more variable than those of metals: the same material, from two different suppliers, could differ in toughness and strength by a factor of two.

There are, of course, many more ceramics available than those listed here. As before, the structure-insensitive properties (density, modulus, and melting point) depend little on quality—they do not vary by more than 10%. But the structure-sensitive properties (fracture toughness, modulus of rupture, and some thermal properties including expansion) are much more variable. For these, it is essential to consult manufacturers' data sheets or conduct your own tests.

EXAMPLES

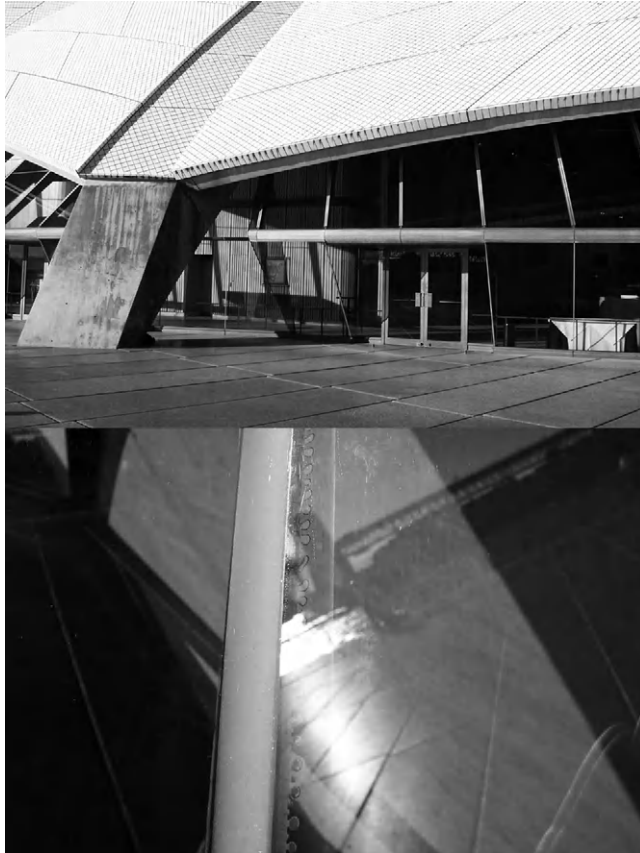
- 17.1 What are the five main generic classes of ceramics? For each generic class:
 - (a) give one example of a specific component made from that class,
 - (b) indicate why that class was selected for the component.
- 17.2 How do the unique characteristics of ceramics influence the way in which these materials are used?
- 17.3 The glass walls of the Sydney Opera House are constructed from glass panels butted together with a 10 mm expansion gap between adjacent panels. The gap is injected with a flexible polymer which is cured in situ and also sticks to the edge of the glass (see photographs). Taking a notional panel width of 3 m, and a maximum temperature variation of 40 °C, calculate the minimum strain capacity required from the polymer. See Table 17.7 for the thermal expansion coefficient of soda glass. Apart from tensile fracture of the polymer, what additional mechanical failure mechanism is possible in the jointing system?

Table 17.7 Properties of Ceramics

	Density (Mg m ₋₃)	Youngs Modulus (GN m ₋₂)	Compressive Strength (MN m ₋₂)	Modulus of Rupture (MN m ₋₂)	Weibull Exponent <i>m</i>	Time exponent <i>n</i>	Fracture Toughness (MN m _{-3/2})	Melting (softening) Temperature (K)	Specific Heat (J kg ₋₁ K ₋₁)	Thermal Conductivity (W m ₋₁ K ₋₁)	Thermal Expansion Coefficient (MK ⁻¹)	Thermal Shock Resistance (K)
Glasses												
Soda glass	2.48	74	1000	50	Assume 10 in design	10	0.7	(1000)	990	1	8.5	84
Borosilicate glass	2.23	65	1200	55		10	0.8	(1100)	800	1	4.0	280
Pottery, etc.,												
Porcelain	2.3–2.5	70	350	45		—	1.0	(1400)	800	1	3	220
High- performance engineering ceramics												
Diamond	3.52	1050	5000	—		—	—	—	510	70	1.2	1000
Dense alumina	3.9	380	3000	300–400	10	10	3–5	2323 (1470)	795	25.6	8.5	150
Silicon carbide	3.2	410	2000	200–500	10	40	—	3110	1422	84	4.3	300
Silicon nitride	3.2	310	1200	300–850	—	40	4	2173	627	17	3.2	500
Zirconia	5.6	200	2000	200–500	10–21	10	4–12	2843	670	1.5	8	500
Sialons	3.2	300	2000	500–830	15	10	5	—	710	20–25	3.2	510
Cement, etc.												
Cement	2.4–2.5	20–30	50	7	12	40	0.2	—	—	1.8	10–14	<50
Concrete	2.4	30–50	50	7	12	40	0.2	—	—	2	10–14	
Rocks and ice												
Limestone	2.7	63	30–80	20	—	—	0.9	—	—	—	8	≈ 100
Granite	2.6	60–80	65–150	23	—	—	—	—	—	—	8	
Ice	0.92	9.1	6	1.7	—	—	0.12	273 (250)	—	—	—	

Answer

10%

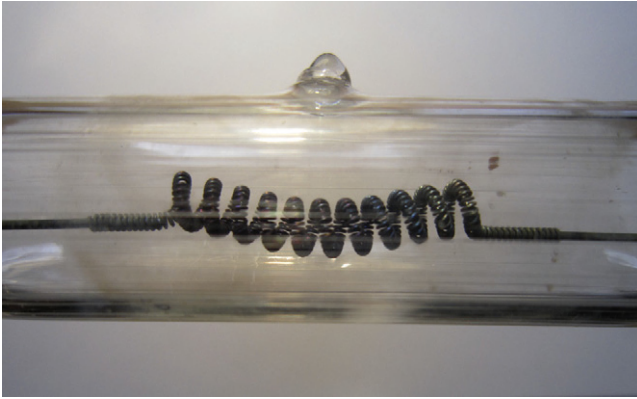


Glass walls of Sydney Opera House (33 51 24.50 S 151 12 54.30 E).

- 17.4** The photograph shows part of a tungsten filament light bulb. The envelope is made from glass.

http://en.wikipedia.org/wiki/Incandescent_light_bulb

What service environment must the glass withstand? Why is glass (or quartz—pure SiO_2) the only material which is suitable for lamp envelopes?



- 17.5** Write a brief description of the use of ceramics as refractory materials for making molds for casting molten metals. What properties make them the material of choice for many casting processes?
- 17.6** Ceramic inserts of tungsten carbide/cobalt are much used in wire drawing. <http://www.fwwd.com/>
Why is WC/Co used for this purpose? What measures are taken to prevent ceramic dies fracturing under the radial forces generated by the wire drawing process? What other ceramic materials can be used for wire drawing?
- 17.7** The photograph shows the valve sectors from a quarter-turn water faucet (tap). They are made from alumina (Al_2O_3). Why is alumina a good material choice for this application?



- 17.8** Figure 1.4 shows the water-level gauge in a model steam engine. The gauge tube itself is made from glass. Would you use soda glass or borosilicate (Pyrex) glass? Explain your choice. (The clip <http://www.youtube.com/watch?v=f3lfFKq1fhA> shows a thrilling cab ride on the steam loco Blanche on the Ffestiniog narrow-gauge railway in North Wales, UK. At various points, you can see the two water gauges mounted on the back of the firebox. The gauge glass tubes themselves are protected by rectangular glass panels, or “gauge glass protectors” (52 55 09.80 N 4 06 24.90 W.)

Why are gauge glass protectors always necessary for the safe use of boiler water gauges?

- 17.9** Synthetic sapphire is next in hardness to diamond. It is used for spindle bearings in mechanical watches. Why is sapphire used for miniature bearings of this type?
http://en.wikipedia.org/wiki/Jewel_bearing
- 17.10** Why are champagne bottles much thicker than wine bottles?
- 17.11** Take a look around your home. Write a representative list of the things you see which are made from ceramics. Assign each item to one of the five generic classes of ceramic. List specialized applications of ceramics (where only one or a very limited range of ceramics will perform adequately in the service environment). Make sure you think of electrical or electronic applications.
- 17.12** The lenses of reading glasses were traditionally made from glass. However, they are now being made from polymers as well.
http://en.wikipedia.org/wiki/Corrective_lens
Polymer lenses are lighter than glass lenses (polymers have a much lower density than glass), so they are more comfortable to wear. However, their useful life is much less. Explain why.

Ceramic Structures

18.1 INTRODUCTION

A ceramic, like a metal, has structure at the atomic scale: its crystal structure (if crystalline) or its amorphous structure (if glassy). It has structure at a larger scale too: the shape and arrangement of its grains or phases; the size and volume fraction of pores it contains (most ceramics are porous). Ceramic structures differ from those of metals. Their intricate details (and they can be intricate) are the province of the ceramic specialist; but you need a working knowledge of their basic features to understand the processing and engineering uses of ceramics and appreciate the recently developed high-strength ceramics.

18.2 IONIC AND COVALENT CERAMICS

A critical distinction must be made between predominantly *ionic* ceramics and those which are predominantly *covalent* in their bonding. Ionic ceramics are, typically, compounds of a metal with a nonmetal: sodium chloride, NaCl; magnesium oxide, MgO; alumina, Al_2O_3 ; zirconia, ZrO_2 . The metal and nonmetal have unlike electric charges: in sodium chloride, for instance, the sodium atoms have one positive charge and the chlorine atoms have one negative charge each. The electrostatic attraction between the unlike charges gives most of the bonding. So the ions pack *densely* (to get as many plus and minus charges close to each other as possible) but with the *constraint* that ions of the same type (and so with the same charge) must not touch. This leads to certain basic ceramic structures, typified by rocksalt, NaCl, or by alumina, Al_2O_3 , which we will describe later.

Covalent ceramics are different. They are compounds of two nonmetals (like silica, SiO_2), or, occasionally, are just pure elements (like diamond, C, or silicon, Si). An atom in this class bonds by sharing electrons with its neighbors to give a fixed number of directional bonds. Covalent atoms are a bit like

the units of a child's construction kit which snap together: the position and number of neighbors are rigidly fixed by the number and position of the connectors on each block. The resulting structures are quite different from those given by ionic bonding; and as we will see later, the mechanical properties are different too. The energy is minimized, not by dense packing, but by forming *chains, sheets, or three-dimensional networks*. Often these are non-crystalline; all commercial glasses, for instance, are three-dimensional amorphous networks based on silica, SiO_2 .

We will first examine the simple structures given by ionic and covalent bonding, and then return to describe the microstructures of ceramics.

18.3 SIMPLE IONIC CERAMICS

The classic ionic ceramic is sodium chloride ("rocksalt"), NaCl , shown in Figure 18.1(a). Each sodium atom loses an electron to a chlorine atom; it is the electrostatic attraction between the Na^+ ions and the Cl^- ions that holds the crystal together. To achieve the maximum electrostatic interaction, each Na^+ has 6 Cl^- neighbors and no Na^+ neighbors (and vice versa);

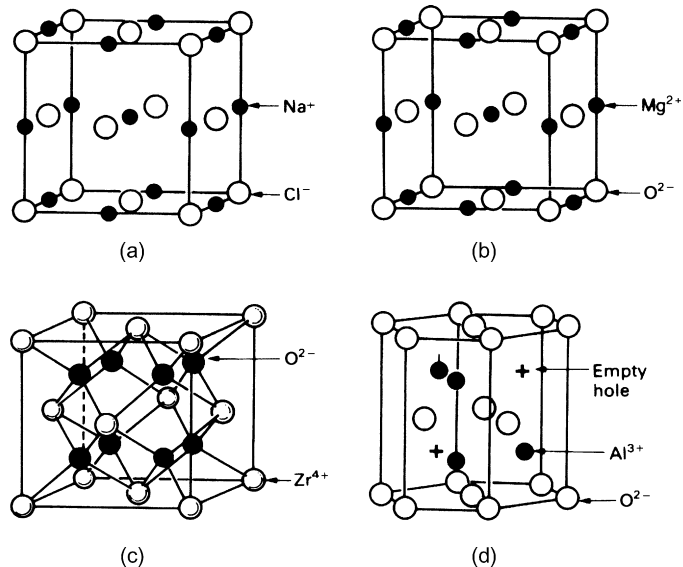


FIGURE 18.1

Ionic ceramics. (a) The rocksalt, or NaCl , structure. (b) Magnesia, MgO , has the rocksalt structure. It can be thought of as an f.c.c. packing with Mg ions in the octahedral holes. (c) Cubic zirconia, ZrO_2 : an f.c.c. packing of Zr with O in the tetrahedral holes. (d) Alumina, Al_2O_3 : a c.p.h. packing of oxygen with Al in two-thirds of the octahedral holes.

there is no way of arranging single-charged ions that does better than this. So most of the simple ionic ceramics with the formula AB have the rocksalt structure.

Magnesia, MgO , is an example (Figure 18.1(b)). It is an engineering ceramic, used as a refractory in furnaces, and its structure is exactly the same as that of rocksalt: the atoms pack to maximize the density, with the constraint that like ions are not nearest neighbors.

But there is another way of looking at the structure of MgO , and one which greatly simplifies the understanding of many of the more complex ceramic structures. Look at Figure 18.1(b) again: the oxygen ions (open circles) form an f.c.c. packing. Figure 18.2 shows that the f.c.c. structure contains two sorts of interstitial holes: the larger octahedral holes, of which there is one for each oxygen atom; and the smaller tetrahedral holes, of which there are two for each oxygen atom. Then the structure of MgO can be described as an *f.c.c. packing of oxygen with an Mg ion squeezed into each octahedral hole*. Each Mg^{2+} has six O^{2-} as immediate neighbors, and vice versa: the coordination number is 6. The Mg ions wedge the oxygens apart, so that they do not touch. Then the attraction between the Mg^{2+} and the O^{2-} ions greatly outweighs the repulsion between the O^{2-} ions, and the solid is very strong and stable (its melting point is over 2000°C).

This “packing” argument may seem an unnecessary complication. But its advantage comes now. Consider cubic zirconia, ZrO_2 , an engineering ceramic of growing importance. The structure (Figure 18.1(c)) looks hard to describe, but it isn’t. It is simply an *f.c.c. packing of zirconium with the O^{2-} ions in the tetrahedral holes*. Since there are two tetrahedral holes for each atom of the f.c.c. structure, the formula works out at ZrO_2 .

Alumina, Al_2O_3 (Figure 18.1(d)), is a structural ceramic used for cutting tools and grinding wheels, and a component in brick and pottery. It has a structure which can be understood in a similar way. The oxygen ions are close-packed, but this time in the c.p.h. arrangement, like zinc or titanium.

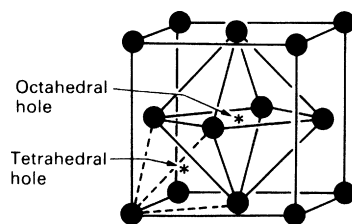


FIGURE 18.2

Both the f.c.c. and the c.p.h. structures are close-packed. Both contain one octahedral hole per atom and two tetrahedral holes per atom. The holes in the f.c.c. structures are shown here.

The hexagonal structure (like the f.c.c. one) has one octahedral hole and two tetrahedral holes per atom. In Al_2O_3 , the Al^{3+} ions are put into the octahedral interstices, so that each is surrounded by six O^{2-} ions. But if the charges are to balance (as they must), there are only enough Al ions to fill two-thirds of the sites. So one-third of the sites, in an ordered pattern, remain empty. This introduces a small distortion of the original hexagon, but from our point of view this is unimportant.

There are many other ionic oxides with structures which are more complicated than these. We will not go into them here. But it is worth knowing that most can be thought of as a dense (f.c.c. or c.p.h.) packing of oxygen, with various metal ions arranged, in an orderly fashion, in the octahedral or the tetrahedral holes.

18.4 SIMPLE COVALENT CERAMICS

The ultimate covalent ceramic is diamond, widely used where wear resistance or very great strength are needed. Its structure, shown in Figure 18.3 (a), shows the four coordinated arrangement of the atoms within the cubic unit cell: each atom is at the center of a tetrahedron with its four bonds

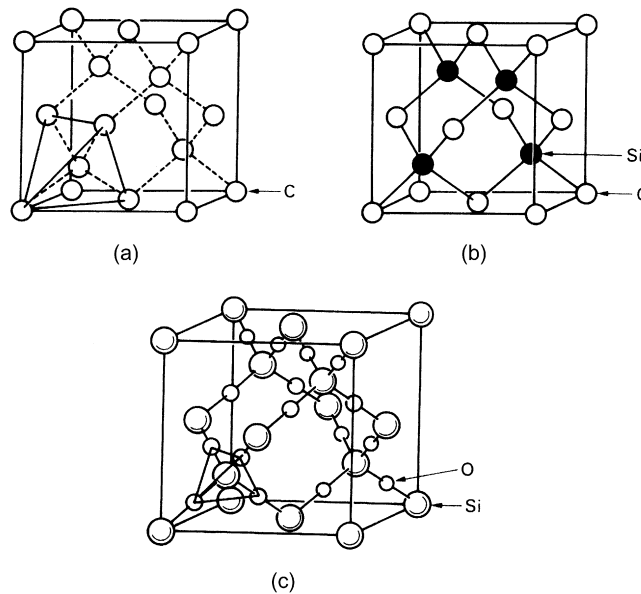


FIGURE 18.3

Covalent ceramics. (a) The diamond cubic structure: each atom bonds to four neighbors. (b) Silicon carbide: the diamond cubic structure with half the atoms replaced by silicon. (c) Cubic silica: the diamond cubic structure with an SiO_4 tetrahedron on each atom site.

directed to the four corners of the tetrahedron. It is not a close-packed structure (atoms in close-packed structures have 12, not four, neighbors) so its density is low.

The very hard structural ceramics silicon carbide, SiC , and silicon nitride, Si_3N_4 (used for load-bearing components such as high-temperature bearings and engine parts) have a structure closely related to that of diamond. If, in the diamond cubic structure, every second atom is replaced by silicon, we get the *sphalerite* structure of SiC , shown in Figure 18.3(b). Next to diamond, this is one of the hardest of known substances, as the structural resemblance would suggest.

18.5 SILICA AND SILICATES

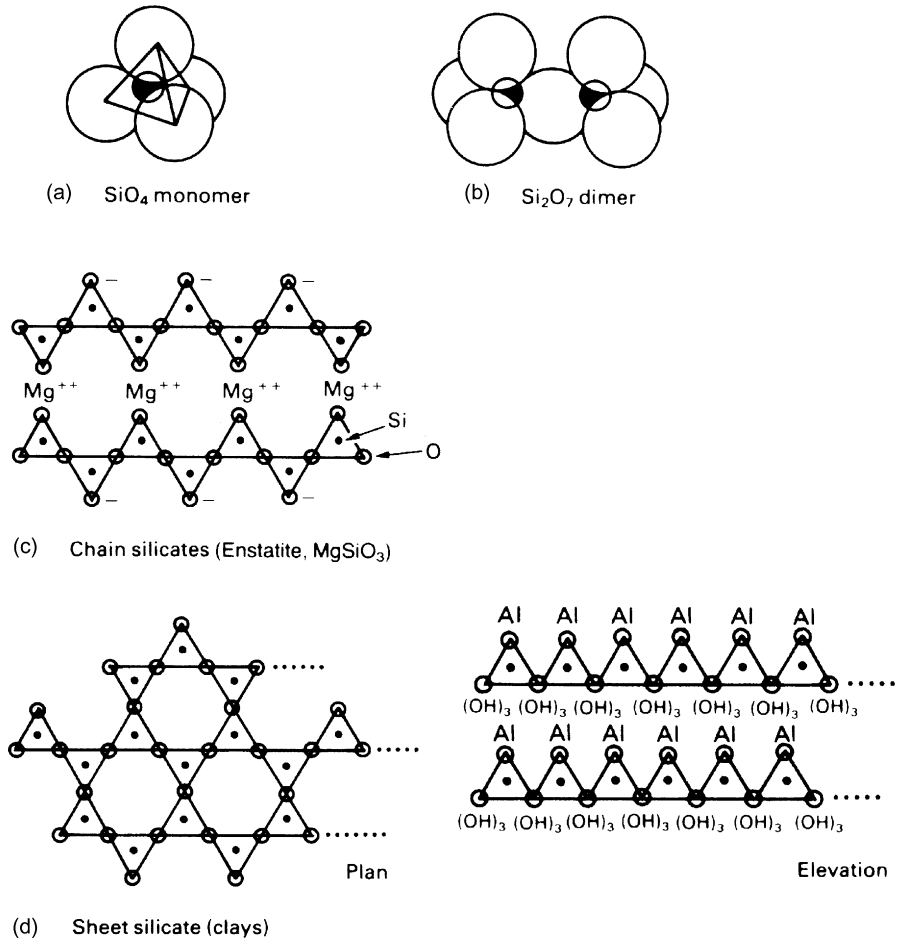
The Earth's crust is largely made of silicates. Of all the raw materials used by humans, silica and its compounds are the most widespread, plentiful, and cheap.

Silicon atoms bond strongly with four oxygen atoms to give a tetrahedral unit (Figure 18.4(a)). This stable *tetrahedron* is the basic unit in all silicates, including that of pure silica (Figure 18.3(c)); note that it is just the diamond cubic structure with every C atom replaced by a SiO_4 unit. But there are a number of other, quite different, ways in which the tetrahedra can be linked together.

The way to think of them all is as SiO_4 tetrahedra (or, in polymer terms, *monomers*) linked to each other either directly or via a metal ion (M) link. When silica is combined with metal oxides like MgO , CaO , or Al_2O_3 such that the ratio MO/SiO_2 is 2/1 or greater, then the resulting silicate is made up of separated SiO_4 monomers (Figure 18.4(a)) linked by the MO molecules. (Olivine, the dominant material in the Earth's upper mantle, is a silicate of this type.)

When the ratio MO/SiO_2 is a little less than 2/1, silica *dimers* form (Figure 18.4(b)). One oxygen is shared between two tetrahedra; it is called a *bridging oxygen*. This is the first step in the polymerization of the monomer to give chains, sheets, and networks.

With decreasing amounts of metal oxide, the degree of polymerization increases. *Chains* of linked tetrahedra form, like long chain polymers with a $-\text{C}-\text{C}-$ backbone, except that here the backbone is a $-\text{Si}-\text{O}-\text{Si}-\text{O}-\text{Si}-$ chain (Figure 18.4(c)). Two oxygens of each tetrahedron are shared (there are two bridging oxygens). The others form ionic bonds between chains, joined by the MO. These are weaker than the $-\text{Si}-\text{O}-\text{Si}-$ bonds which

**FIGURE 18.4**

Silicate structures. (a) The SiO_4 monomer. (b) The Si_2O_7 dimer with a bridging oxygen. (c) A chain silicate. (d) A sheet silicate. Each triangle is the projection of a SiO_4 monomer.

form the backbone, so these silicates are fibrous; asbestos, for instance, has this structure.

If three oxygens of each tetrahedron are shared, *sheet structures* form (Figure 18.4(d)). This is the basis of clays and micas. The additional M attaches itself preferentially to one side of the sheet—the side with the spare oxygens on it. Then the sheet is polarized: it has a net positive charge on one surface and a negative charge on the other. This interacts strongly with water, attracting a layer of water between the sheets. This is what makes clays plastic: the sheets of silicate slide over each other readily, lubricated by the

water layer. As you might expect, sheet silicates are very strong in the plane of the sheet, but cleave or split easily between the sheets: mica and talc do this.

Pure silica contains no metal ions and every oxygen becomes a bridge between two silicon atoms giving a *three-dimensional network*. The high-temperature form, shown in Figure 18.3(c), is cubic; the tetrahedra are stacked in the same way as the carbon atoms in the diamond cubic structure. At room temperature, the stable crystalline form of silica is more complicated but, as before, it is a three-dimensional network in which all the oxygens bridge silicons.

18.6 SILICATE GLASSES

Commercial glasses are based on silica. They are made of the same SiO_4 tetrahedra on which the crystalline silicates are based, but they are arranged in a noncrystalline, or *amorphous*, way. The difference is shown schematically in Figure 18.5. In the glass, the tetrahedra link at the corners to give a random (rather than a periodic) network. Pure silica forms a glass with a high softening temperature (about 1200°C). Its great strength and stability, and its low thermal expansion, suit it for certain special applications, but it is hard to work because its viscosity is high.

This problem is overcome in commercial glasses by introducing *network modifiers* to reduce the viscosity. They are metal oxides, usually Na_2O and

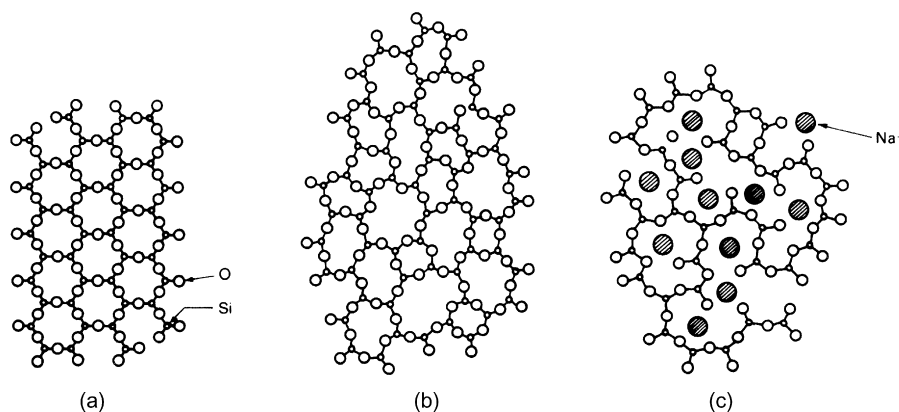


FIGURE 18.5

Glass formation. A three-coordinated crystalline network is shown at (a). But the bonding requirements are still satisfied if a random (or glassy) network forms, as at (b). The network is broken up by adding network modifiers, like Na_2O , which interrupt the network as at (c).

CaO, which add positive ions to the structure and break up the network (Figure 18.5(c)). Adding one molecule of Na_2O , for instance, introduces two Na^+ ions, each of which attaches to an oxygen of a tetrahedron, making it nonbridging. This reduction in cross-linking softens the glass, reducing its *glass temperature* T_G (the temperature at which the viscosity reaches such a high value that the glass is a solid). Look at Table 17.1 in Chapter 17 for generic glasses: common window glass is only 70% SiO_2 ; it is heavily modified and easily worked at 700 °C. Pyrex is 80% SiO_2 ; it contains less modifier and has a much better thermal shock resistance (because its thermal expansion is lower), but it is harder to work, requiring temperatures above 800 °C.

18.7 CERAMIC ALLOYS

Ceramics form alloys with each other, just as metals do. But the reasons for alloying are quite different: in metals it is usually to increase the yield strength, tensile strength, or corrosion resistance; in ceramics, it is generally to allow sintering to full density or to improve the fracture toughness. But for the moment this is irrelevant; the point here is that we deal with ceramic alloys just as we did with metallic alloys. Molten oxides, for the most part, have large solubilities for other oxides (that is why they make good *fluxes*, dissolving undesirable impurities into a harmless slag). On cooling, they solidify as one or more phases: solid solutions or new compounds. Just as for metals, the *constitution of a ceramic alloy* is described by the appropriate phase diagram.

Take the silica–alumina system as an example. It is convenient to treat the components as the two pure oxides SiO_2 and Al_2O_3 (instead of the three elements Si, Al, and O). Then the phase diagram is particularly simple, as shown in Figure 18.6. There is a compound, *mullite*, with the composition $(\text{SiO}_2)_2 (\text{Al}_2\text{O}_3)_3$, which is slightly more stable than the simple solid solution, so the alloys break up into mixtures of mullite and alumina, or mullite and silica. The phase diagram has two eutectics but is otherwise straightforward.

The phase diagram for MgO and Al_2O_3 is similar with a central compound, *spinel*, having the composition MgOAl_2O_3 . That for MgO and SiO_2 , also is simple with a compound, *forsterite*, having the composition $(\text{MgO})_2 \cdot \text{SiO}_2$. Given the composition, the equilibrium constitution of the alloy is read off the diagram in exactly the way described in Chapters 4 and 5.

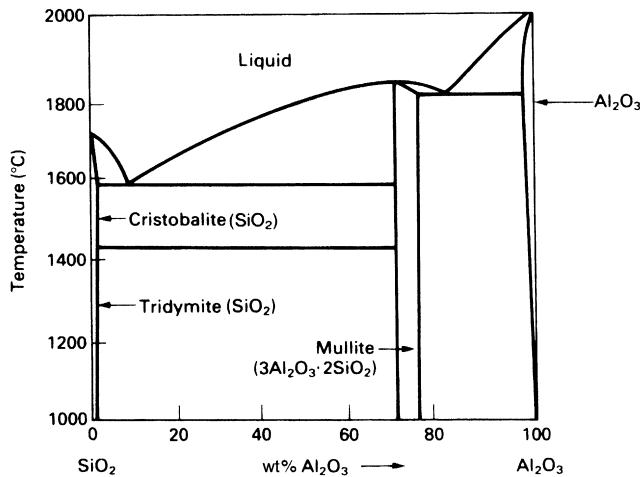


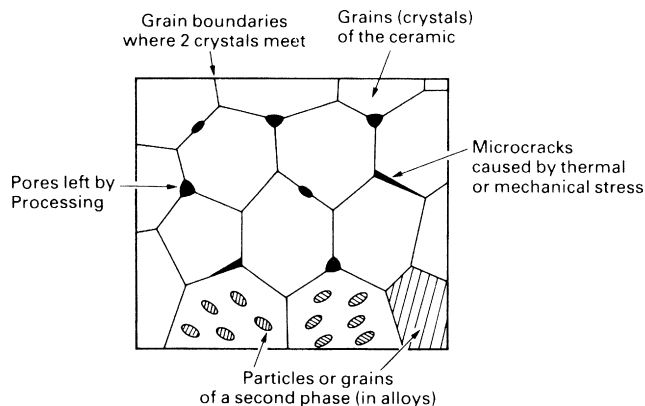
FIGURE 18.6

A typical ceramic phase diagram: for alloys of SiO₂ with Al₂O₃. The intermediate compound 3Al₂O₃ · SiO₂ is called mullite.

18.8 MICROSTRUCTURES OF CERAMICS

Crystalline ceramics form polycrystalline microstructures, very like those of metals (Figure 18.7). Each grain is a more or less perfect crystal, meeting its neighbors at grain boundaries. The structure of ceramic grain boundaries is obviously more complicated than those in metals: ions with the same sign of charge must still avoid each other and, as far as possible, valency requirements must be met in the boundary, just as they are within the grains. But none of this is visible at the microstructural level, which for a pure, dense ceramic, looks just like that of a metal.

Many ceramics are not fully dense. Porosities as high as 20% are a common feature of the microstructure (Figure 18.7). The pores weaken the material, though if they are well rounded, the stress concentration they induce is small. More damaging are cracks; they are much harder to see, but they are nonetheless present in most ceramics, left by processing, or nucleated by differences in thermal expansion or modulus between grains or phases. These, as we shall see in the next chapter, ultimately determine the strength of the material. Recent developments in ceramic processing aim to reduce the size and number of these cracks and pores, giving ceramic bodies with tensile strengths as high as those of high-strength steel.

**FIGURE 18.7**

Microstructural features of a crystalline ceramic: grains, grain boundaries, pores, microcracks, and second phases.

18.9 VITREOUS CERAMICS

Pottery and tiles survive from antiquity, evidence of their corrosion resistance and durability. Vitreous ceramics today are the basis of an enormous industry, turning out bricks, tiles, and white-ware. All are made from clays: sheet silicates such as the hydrated aluminosilicate *kaolin*, $\text{Al}_2(\text{Si}_2\text{O}_5)(\text{OH})_4$. When wet, the clay draws water between the silicate sheets (because of its polar layers) making it plastic and easily worked. It is then dried to the green state, losing its plasticity and acquiring enough strength to be handled for firing. The firing—at a temperature between 800 and 1200 °C—drives off the remaining water and causes the silica to combine with impurities like CaO to form a liquid glass which wets the remaining solids. On cooling, the glass solidifies (but is still a glass) giving strength to the final composite of crystalline silicates bonded by vitreous bonds. The amount of glass which forms during firing has to be carefully controlled: too little, and the bonding is poor; too much, and the product slumps or melts completely.

As fired, vitreous ceramics are usually porous. To seal the surface, a glaze is applied, and the product refired at a lower temperature than before. The glaze is simply a powdered glass with a low melting point. It melts completely, flows over the surface, and wets the underlying ceramic, being sucked into the pores by surface tension. When cold again, the surface is not only impervious to water, it is also smooth and free of the holes and cracks which would lead to easy fracture.

18.10 STONE AND ROCK

Sedimentary rocks (like sandstone) have a microstructure rather like that of a vitreous ceramic. Sandstone is made of particles of silica, bonded together either by more silica or by calcium carbonate (CaCO_3). Like pottery, it is porous. The difference lies in the way the bonding phase formed: it is precipitated from solution in ground water, rather than formed by melting.

Igneous rocks (like granite) are much more like the $\text{SiO}_2\text{--Al}_2\text{O}_3$ alloys described in the phase diagram of Figure 18.6. These rocks have, at some point in their history, been hot enough to melt. Their structure can be read from the appropriate phase diagram: they generally contain several phases and, since they have melted, they are fully dense (though they still contain cracks nucleated during cooling).

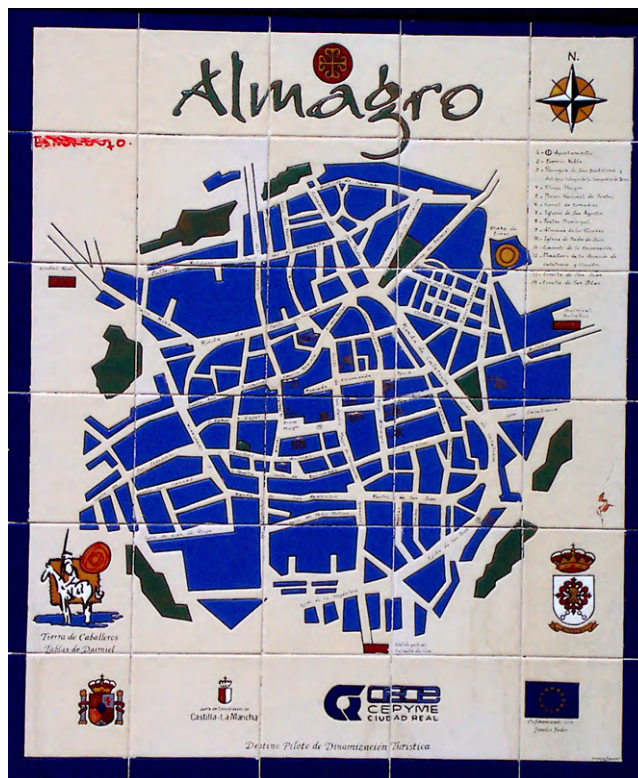
18.11 CERAMIC COMPOSITES

Most successful composites combine the stiffness and hardness of a ceramic (like glass, carbon, or tungsten carbide) with the ductility and toughness of a polymer (like epoxy) or a metal (like cobalt). We will look at them in more detail in later chapters.

WORKED EXAMPLE

The following photograph was taken in Almagro, Spain—a small but very historic town in the province of Castilla la Mancha (famous as the setting for Cervantes's legendary character *Don Quijote*) (38° 53' 18.55" N 3° 42' 42.14" W).

It shows a map of the town assembled from ceramic tiles and fixed to a panel on the wall of an old building in the town center. It is a good example of hand-painted tiles. The plain white ceramic tiles were first fired, and after removal from the kiln and cooling were hand-painted. They were then coated with glazing compound and refired at a lower temperature. The glaze seals the surface (protecting the paint and keeping dirt and water out) and also makes the outer surface of the tile stronger in tension.



EXAMPLES

- 18.1** Describe in a few words (using examples or sketches if you want to) what is meant by the following:
 - (a)** An ionic ceramic.
 - (b)** A covalent ceramic.
- 18.2** Describe in a few words (using examples or sketches if you want to) what is meant by the following:
 - (a)** A chain silicate.
 - (b)** A sheet silicate.
- 18.3** Describe in a few words (using examples or sketches if you want to) what is meant by the following:
 - (a)** A glass.
 - (b)** A network modifier.
 - (c)** The glass temperature.
- 18.4** Describe in a few words (using examples or sketches if you want to) what is meant by the following:

- (a) A vitreous ceramic.
 - (b) A glaze.
- 18.5** Describe in a few words (using examples or sketches if you want to) what is meant by the following:
- (a) A sedimentary rock.
 - (b) An igneous rock.
- 18.6** The following photograph shows the sandstone cliffs next to the Fitzroy Falls, near Kangaroo Valley, New South Wales, Australia—34 38 55.00 S 150 28 40.20 E. How can you tell by looking at these formations that the rock is a sedimentary rock?



Mechanical Properties of Ceramics

19.1 INTRODUCTION

A Ming vase should perform its primary function—of pleasing the eye of the beholder—without being subjected to much stress. Unfortunately, accidents do sometimes happen, as on 25 January 2006 when a visitor to the University of Cambridge's Fitzwilliam Museum collided with three priceless oriental vases which ended up on the floor in tiny pieces!

<http://www.fitzmuseum.cam.ac.uk/gallery/chinesevases/521158.90N00711.70E>

However, most glassware, vitreous ceramic and porcelain fulfills its function without experiencing excessive static load, although it must be handled carefully (it should not be allowed to bang into other hard objects), and it must not be subjected to excessive thermal shock (fine glassware should be washed by hand in very tepid water).

Many other ceramics, of course, *are* expected to carry significant loads—concrete, bricks, structural glass are some examples. Their strength has a major impact on the design of the structures in which they are used. And high-performance ceramics are used under even more demanding conditions of stress (and temperature).

In this chapter, we look at the mechanical properties of ceramics which we need to know about in order to design adequately with these materials.

19.2 ELASTIC MODULI

Ceramics, like metals (but unlike polymers), have a well-defined Young's modulus: the value does not depend significantly on loading time (or, if the loading is cyclic, on frequency). Ceramic moduli are generally larger than those of metals, reflecting the greater stiffness of the ionic bond in

Table 19.1 Specific Moduli: Ceramics Compared to Metals

Material	Modulus E (GN m ⁻²)	Density ρ (Mg m ⁻³)	Specific Modulus E/ρ
Steels	210	7.8	27
Al alloys	70	2.7	26
Alumina, Al ₂ O ₃	390	3.9	100
Silica, SiO ₂	69	2.6	27
Cement	45	2.4	19

simple oxides and of the covalent bond in silicates. And since ceramics are largely composed of light atoms (oxygen, carbon, silicon, aluminum) and their structures are often not close-packed, their densities are low. Because of this, their specific moduli (E/ρ) are attractively high. Table 19.1 shows that alumina, for instance, has a specific modulus of 100 (compared to 27 for steel). This is one reason ceramic or glass fibers are used in composites: their presence raises the specific stiffness of the composite enormously. Even cement has a reasonable specific stiffness—high enough to make boats out of it.

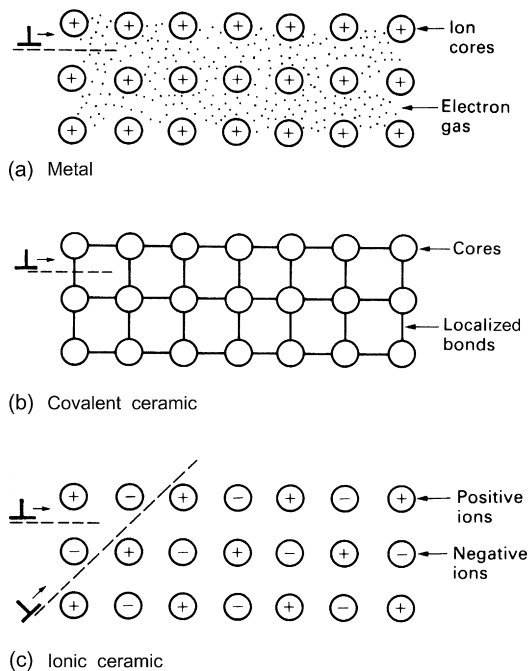
19.3 STRENGTH, HARDNESS, AND LATTICE RESISTANCE

Ceramics are the hardest of solids. Corundum (Al₂O₃), silicon carbide (SiC) and, of course, diamond (C) are used as abrasives: they will cut, or grind, or polish almost anything—even glass, and glass is itself a very hard solid. Table 19.2 gives some feel for this: it lists the hardness H , normalized by Young's modulus E , for a number of pure metals and alloys, and for four pure ceramics. Pure metals (Table 19.2, first column) have a very low hardness and yield strength (remember $H \approx 3\sigma_y$). The main purpose of alloying is to raise these. The second column shows that this technique is very successful: the hardness has been increased from around $10^{-3}E$ to about $10^{-2}E$. But now look at the third column: even pure, unalloyed ceramics have hardnesses which far exceed even the best metallic alloys. Why is this?

When a material yields in a tensile test, or when a hardness indenter is pressed into it, dislocations move through its structure. Each test, in its own way, measures the difficulty of moving dislocations in the material. Metals are *intrinsically soft*. When atoms are brought together to form a metal, each loses one (or more) electrons to the gas of free electrons which moves freely around the ion cores (Figure 19.1(a)). The binding energy comes from the general electrostatic interaction between the positive ions and the negative

Table 19.2 Normalized Hardness of Pure Metals, Alloys, and Ceramics

Pure Metal	H/E	Metal alloy	H/E	Ceramic	H/E
Copper	1.2×10^{-3}	Brass	9×10^{-3}	Diamond	1.5×10^{-1}
Aluminum	1.5×10^{-3}	Dural (Al 4% Cu)	1.5×10^{-2}	Alumina	4×10^{-2}
Nickel	9×10^{-4}	Stainless steel	6×10^{-3}	Zirconia	6×10^{-2}
Iron	9×10^{-4}	Low alloy steel	1.5×10^{-2}	Silicon carbide	6×10^{-2}
Mean, metals	1×10^{-3}	Mean, alloys	1×10^{-2}	Mean, ceramics	8×10^{-2}


FIGURE 19.1

(a) Dislocation motion is intrinsically easy in pure metals—though alloying to give solid solutions or precipitates can make it more difficult. (b) Dislocation motion in covalent solids is intrinsically difficult because the interatomic bonds must be broken and reformed. (c) Dislocation motion in ionic crystals is easy on some planes, but hard on others. The hard systems usually dominate.

electron gas, and the bonds are not localized. If a dislocation passes through the structure, it displaces the atoms above its slip plane over those which lie below, but this has only a small effect on the electron–ion bonding. Because of this, there is only a slight *drag* on the moving dislocation.

Most ceramics are *intrinsically hard*; ionic or covalent bonds present an enormous *lattice resistance* to the motion of a dislocation. Take the covalent bond first. The covalent bond is localized; the electrons which form the bond are concentrated in the region between the bonded atoms; they behave like little elastic struts joining the atoms (Figure 19.1(b)). When a dislocation moves through the structure, it must break and reform these bonds as it moves: there is a big drag on the moving dislocations as a result.

Most ionic ceramics are hard, though for a slightly different reason. The ionic bond, like the metallic one, is electrostatic: the attractive force between a sodium ion (Na^+) and a chlorine ion (Cl^-) is simply proportional to q^2/r where q is the charge on an electron and r is the separation of the ions. If the crystal is sheared on the 45° plane shown in Figure 19.1(c) then like ions remain separated: Na^+ ions do not ride over Na^+ ions, for instance. This sort of shear is relatively easy—the lattice resistance opposing it is small. But look at the other shear—the horizontal one. This *does* carry Na^+ ions over Na^+ ions and the electrostatic repulsion between like ions opposes this strongly. The lattice resistance is high. In a polycrystal, you will remember, many slip systems are necessary, and some of them are the hard ones. So the hardness of a polycrystalline ionic ceramic is usually high (though not as high as a covalent ceramic), even though a single crystal of the same material might—if loaded in the right way—have a low yield strength.

So ceramics, at room temperature, generally have a very large lattice resistance. The stress required to make dislocations move is a large fraction of Young's modulus: typically around $E/30$, compared with $E/10^3$ or less for the soft metals like copper or lead. This gives ceramics yield strengths which are of order 5 GN m^{-2} —so high that the only way to measure them is to indent the ceramic with a diamond and measure the hardness.

This enormous hardness is exploited in grinding wheels which are made from small particles of a high-performance engineering ceramic (Table 17.3) bonded with an adhesive or a cement. In design with ceramics, it is never necessary to consider plastic collapse of the component: fracture always intervenes first.

19.4 FRACTURE STRENGTH OF CERAMICS

The penalty that must be paid for choosing a material with a large lattice resistance is brittleness: the fracture toughness is low. Even at the tip of a crack, where the stress is intensified, the lattice resistance makes slip very difficult. It is the crack-tip plasticity which gives metals their high toughness: energy is absorbed in the plastic zone, making the propagation of the crack

much more difficult. Although some plasticity can occur at the tip of a crack in a ceramic too, it is very limited; the energy absorbed is small and the fracture toughness is low.

The result is that the fracture toughness K_c of ceramics is very low compared to that of metals. Cement and ice have the lowest K_c at $\approx 40.2 \text{ MN m}^{-3/2}$. Traditional manufactured ceramics (brick, pottery, china, porcelain) and natural stone or rock are better, at $\approx 0.5\text{--}2 \text{ MN m}^{-3/2}$. But even engineering ceramics such as silicon nitride, alumina, and silicon carbide only reach $\approx 4 \text{ MN m}^{-3/2}$. This low fracture toughness makes ceramics very vulnerable to the presence of crack-like defects. They are *defect-sensitive* materials, liable to fail by fast fracture from defects well before they can yield.

Unfortunately, many manufactured ceramics contain cracks and flaws left by the production process (e.g., the voids left between the particles from which the ceramic was fabricated). The defects are worse in cement, because of the rather crude nature of the mixing and setting process. Ice usually contains small bubbles of trapped air (and, in the case of sea ice, concentrated brine). And all but the hardest brittle materials accumulate additional defects when they are handled or exposed to an abrasive environment.

The design strength of a brittle material in tension is therefore determined by its low fracture toughness in combination with the lengths of the crack-like defects it contains. If the longest microcrack in a given sample has length $2a_m$ then the tensile strength is simply given by

$$\sigma_{TS} \approx \frac{K_c}{\sqrt{\pi a_m}} \quad (19.1)$$

from the fast fracture equation. Some engineering ceramics have tensile strengths about half that of steel—around 200 MN m^{-2} . Taking a typical fracture toughness of $2 \text{ MN m}^{-3/2}$, the largest microcrack has a size of $60 \mu\text{m}$, which is of the same order as the original particle size. Pottery, brick, and stone generally have tensile strengths that are much lower than this—around 20 MN m^{-2} . These indicate defects of the order of 2 mm for a typical fracture toughness of $1 \text{ MN m}^{-3/2}$. The tensile strength of cement and concrete is even lower— 2 MN m^{-2} in large sections—implying the presence of at least one crack 6 mm or more in length for a toughness of $0.2 \text{ MN m}^{-3/2}$.

We saw in EM1Ed4, Chapter 15, that ceramics, like most other brittle materials, show a *statistical variation* in strength. This is a consequence of a sample or component containing multiple crack-like defects, with a distribution of crack lengths and orientations. Although a tensile test on one sample will give a single value of strength (for that sample only), there is no single tensile strength for the material in general, only a *distribution* of strength. When designing ceramic components for high-performance applications, it is

necessary to specify an acceptable *survival probability* P_s rather than an acceptable stress σ . This is calculated using the Weibull equation (EM1Ed4, Equation 15.5)

$$P_s(V) = \exp \left\{ -\frac{1}{\sigma_0^m V_0} \int_V \sigma^m dV \right\}, \quad (19.2)$$

which can be simplified to

$$P_s(V) = \exp \left\{ -\frac{V}{V_0} \left(\frac{\sigma}{\sigma_0} \right)^m \right\} \quad (19.3)$$

when the stress is uniform throughout the sample or component. Values of σ_0 (σ for $P_s = 1/e = 37\%$) and m (the Weibull modulus) are found by doing tensile tests on a large number of samples of volume V_0 . Values of m are given in Table 17.7 for the generic ceramics.

19.5 MODULUS OF RUPTURE

We saw in EM1Ed4, Section 15.4, that it is difficult to perform tensile tests on brittle materials—the specimens tend to break prematurely where they are gripped by the testing machine. The preferred method for testing ceramics in tension is the three-point bend test, which measure the *modulus of rupture*. The test geometry is shown in Figure 19.2, and the modulus of rupture is calculated using the equation

$$\sigma_r = \frac{3F\ell}{2bd^2}. \quad (19.4)$$

As explained in EM1Ed4, Section 15.4, the modulus of rupture is larger than the tensile strength. This is a consequence of the (nonuniform) stress state in three-point bending acting selectively on the distribution of crack-like

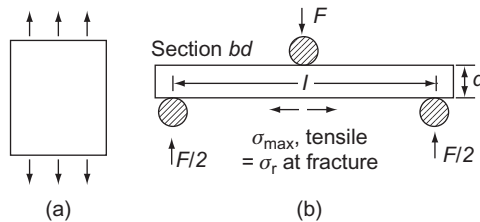


FIGURE 19.2

Tests for measuring the strengths of ceramics in tension. (a) The tensile test measures the tensile strength σ_{TS} . (b) The three-point bend test measures the modulus of rupture σ_r .

defects. The tensile strength may be found from the modulus of rupture using the equation

$$\sigma_{TS} = \frac{\sigma_r}{\{2(m+1)^2\}^{1/m}}. \quad (19.5)$$

For example, if $m = 10$, $\sigma_{TS} = \sigma_r/1.73$. If $m = 5$, $\sigma_{TS} = \sigma_r/2.35$. Values of σ_r are given in Table 17.7 for the generic ceramics.

How do we find σ_0 and m from a set of n individual three-point bend tests? First, the test results are ranked in order of increasing modulus of rupture. Then P_s for each test can be found from its rank j ($1 \leq j \leq n$) using the standard statistical result

$$P_s = 1 - \frac{j - 0.375}{n + 0.25}. \quad (19.6)$$

For example, if there are 6 bend tests in the data set, the value of P_s for the strongest sample ($j = 6$) would be

$$P_s = 1 - \frac{6 - 0.375}{6 + 0.25} = 0.100. \quad (19.7)$$

Paired values of P_s (V_0) and σ_r are then plotted according to the equation

$$\ln \left\{ \ln \left(\frac{1}{P_s(V_0)} \right) \right\} = m \ln \sigma_r - m \ln \sigma_0. \quad (19.8)$$

The value of m is found from the slope of the plot, and σ_0 is read off the plot at the position where the “ln–ln term” is zero (corresponding to $P_s = 1/e = 0.37$).

19.6 COMPRESSION TEST

Many ceramics carry load in compression, deliberately avoiding the perils (and uncertainties) of tensile loading. The compression test measures the compressive strength, σ_c (Figure 19.3).

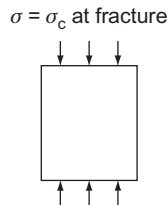


FIGURE 19.3

Test for measuring the compressive strength σ_c of ceramics.

Values of σ_C are given in Table 17.7 for the generic ceramics. This test is much used on standard-sized samples of cement and concrete for quality control during construction. For metals (or any plastic solid), the strength measured in compression is the same as in tension. But for brittle solids this is not so; for these, the compressive strength is roughly 15 times larger, with

$$\sigma_C \approx 15\sigma_{TS}. \quad (19.9)$$

The reason for this is explained by Figure 19.4(b). Cracks in compression propagate *stably*, and twist out of their original orientation to propagate *parallel to the compression axis*. Fracture is not caused by the rapid unstable propagation of one crack, but the slow extension of many cracks to form a crushed zone. It is not the size of the largest crack (a_m) that counts but that of the average \bar{a} . The compressive strength is still given by a formula like Equation (19.1), with

$$\sigma_C \approx C \frac{K_C}{\sqrt{\pi \bar{a}}} \quad (19.10)$$

but the constant C is about 15, instead of 1.

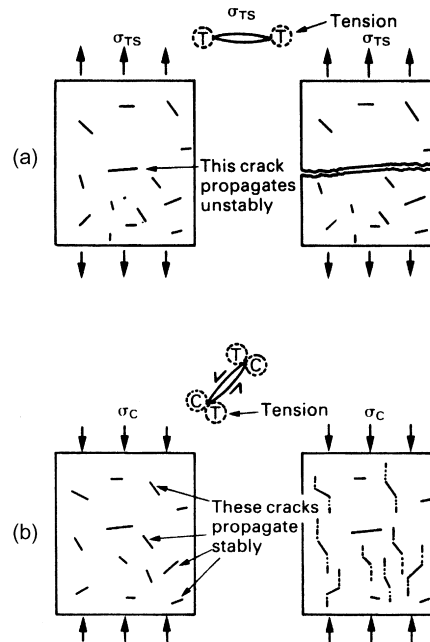


FIGURE 19.4

(a) In tension the largest flaw propagates unstably. (b) In compression, many flaws propagate stably to give general crushing.

19.7 THERMAL SHOCK RESISTANCE

When you pour boiling water into a cold bottle and discover that the bottom drops out with a smart pop, you have reinvented the standard test for thermal shock resistance. Fracture caused by sudden changes in temperature is a problem with ceramics. But while some (like ordinary glass) will only take a temperature “shock” of 80 °C before they break, others (like silicon nitride) will stand a sudden change of 500 °C, and this is enough to fit them for use in environments as violent as an internal combustion engine.

One way of measuring *thermal shock resistance* is to drop a piece of the ceramic, heated to progressively higher temperatures, into cold water. The maximum temperature drop ΔT (in K) which it can survive is a measure of its thermal shock resistance. If its coefficient of expansion is α , then the quenched surface layer suffers a shrinkage strain of $\alpha \Delta T$. But it is part of a much larger body which is still hot, and this constrains it to its original dimensions: it then carries an elastic tensile stress $E\alpha\Delta T$. If this tensile stress exceeds that for tensile fracture, σ_{TS} , the surface of the component will crack and ultimately spall off. So the maximum temperature drop ΔT is given by

$$E\alpha\Delta T = \sigma_{TS}. \quad (19.11)$$

Values of ΔT are given in Table 17.7. For ordinary glass, α is large and ΔT is small—about 80 °C, as we have said. But for most of the high-performance engineering ceramics, α is small and σ_{TS} is large, so they can be quenched suddenly through several hundred degrees without fracturing.

19.8 TIME DEPENDENCE OF STRENGTH

Many people, at some point in their lives, have been startled by the sudden disintegration, apparently without cause, of a drinking glass (a “toughened” glass, almost always), or the spontaneous failure of an automobile windshield. These poltergeist-like happenings are caused by *slow crack growth*.

To be more specific, if a glass rod at room temperature breaks under a stress σ in a short time t , then an identical rod stressed at 0.75σ will break in a time of order $10t$. Most oxides behave like this, which is something that must be taken into account in engineering design. Carbides and nitrides (e.g., SiC or Si₃N₄) do not suffer from this *time-dependent failure* at room temperature, although at high temperature they may do so. Its origin is the slow growth of surface microcracks caused by a chemical

interaction between the ceramic and the water in its environment. Water or water vapor reaching the crack tip reacts chemically with molecules there to form a hydroxide, breaking the Si–O–Si or M–O–M bonds (Figure 19.5). When the crack has grown to the critical length for failure at that stress level the part fails suddenly, often after a long period. Because it resembles fatigue failure, but under static load, it is sometimes called “static fatigue.” Toughened glass is particularly prone to this sort of failure because it contains internal stresses which can drive the slow crack growth, and which drive spontaneous fast fracture when the crack grows long enough.

Fracture mechanics can be applied to this problem, much as it is to fatigue. We use only the final result, as follows. If the standard test which was used to measure σ_{TS} takes a time t (test), then the stress σ which the sample will support safely for a time t is given by

$$\left(\frac{\sigma}{\sigma_{TS}}\right)^n = \frac{t(\text{test})}{t} \quad (19.12)$$

where n is the slow crack growth exponent. Its value for oxides is between 10 and 20 at room temperature. When $n = 10$, a factor of 10 in time reduces the strength by 20%. For carbides and nitrides, n can be as large as 100; then a factor of 10 in time reduces the strength by only 2%. Data for n are included in Table 17.7.

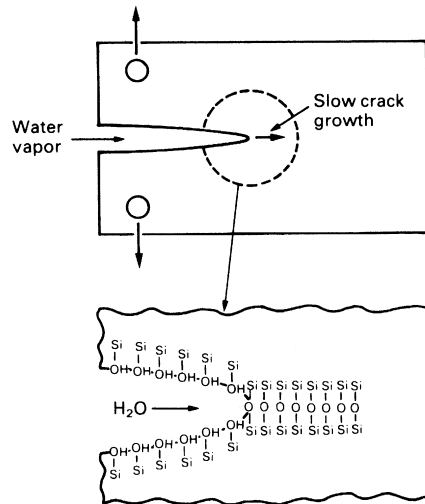


FIGURE 19.5

Slow crack growth caused by surface hydration of oxide ceramics.

19.9 CREEP OF CERAMICS

Like metals, ceramics creep when they are hot. The creep curve (Figure 19.6) is just like that for a metal (see EMIEd4, Chapter 20). During primary creep, the strain rate decreases with time, tending toward the steady-state creep rate

$$\dot{\epsilon}_{ss} = A\sigma^n \exp(-Q/RT). \quad (19.13)$$

Here σ is stress, A and n are creep constants and Q is the activation energy for creep. Most engineering design against creep is based on this equation. Finally, the creep rate accelerates again into *tertiary creep* and *fracture*.

But what is “hot”? Creep becomes a problem when the temperature is greater than about $(1/3) T_M$. The melting point T_M of engineering ceramics is high—over 2000 °C—so creep is design-limiting only in very high temperature applications (refractories, for instance). There is, however, one important ceramic—ice—which has a low melting point and creeps extensively, following Equation (19.13). The sliding of glaciers, and even the spreading of the Antarctic ice-cap, are controlled by the creep of ice; geophysicists who model the behavior of glaciers use Equation (19.13).

Because glasses have a liquid structure, their creep behavior is less complicated. In the creep regime, they behave as (very stiff) liquids—creep is governed by viscous flow, and the strain rate is proportional to the driving stress ($n = 1$ in Equation (19.13)). The viscosity of glasses falls slowly and continuously as they are heated. Viscosity is defined in the way shown in Figure 19.7. If shear stress σ_s is applied to the hot glass, it shears at a shear strain rate $\dot{\gamma}$. Then the viscosity, η , is defined by

$$\eta = \frac{\sigma_s}{10\dot{\gamma}}. \quad (19.14)$$

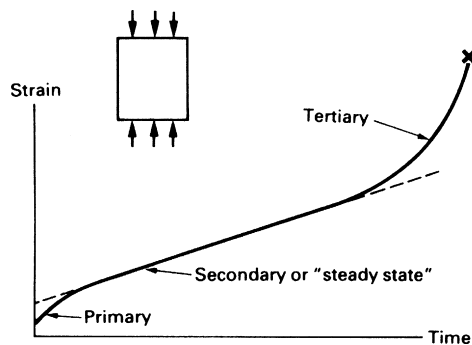
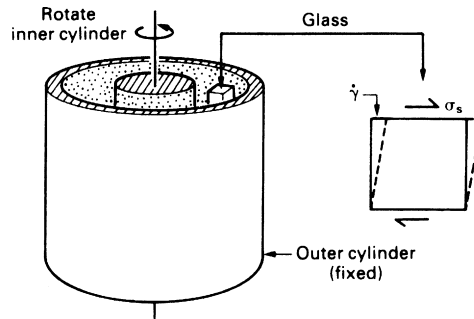
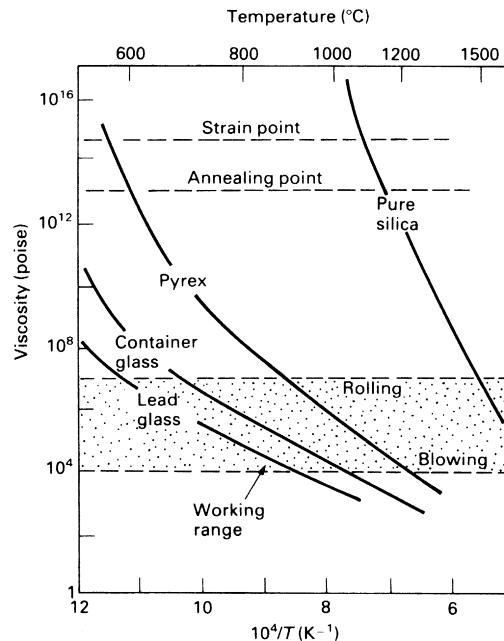


FIGURE 19.6

Creep curve for a ceramic.

**FIGURE 19.7**

A rotation viscometer. Rotating the inner cylinder shears the viscous glass. The torque (and thus the shear stress σ_s) is measured for a given rotation rate (and thus shear strain rate $\dot{\gamma}$).

**FIGURE 19.8**

The variation of glass viscosity with temperature. It follows an Arrhenius law ($\eta \propto \exp(Q/RT)$) at high temperature.

It has units of poise (P) or $10^{-1} \text{ NM}^{-2} \text{ s}$. Glasses are worked in the temperature range in which their viscosity is between 10^4 and 10^7 poise (Figure 19.8).

Viscous flow is a thermally activated process. For flow to take place, the network must break and reform locally. Below the glass temperature, T_G there is

insufficient thermal energy to allow this breaking and reforming to occur, and the glass ceases to flow; it is convenient to define this as the temperature at which the viscosity reaches 10^{17} P. (At T_G , it would take a large window 10,000 years to deform perceptibly under its own weight. The story that old windows do so at room temperature is a myth.) Above T_G , the thermal energy of the molecules is sufficient to break and remake bonds at a rate which is fast enough to permit flow. As with all simple thermally activated processes, the rate of flow is given by

$$\text{rate of flow} \propto \exp(-Q/RT) \quad (19.15)$$

where Q is the activation energy for viscous flow. The viscosity, η , is proportional to $(\text{rate of flow})^{-1}$, so

$$\eta \propto \exp(Q/RT). \quad (19.16)$$

The figure shows how the viscosity of three sorts of glass and of silica itself, vary with temperature. On it, $\log \eta$ is plotted against $1/T$, to give lines with slope Q/R . The viscosity corresponding to the glass temperature is at the top of the figure. The working range is shown as a shaded band: it is wide because working procedures vary.

EXAMPLES

19.1 Explain why the yield strengths of ceramics can approach the ideal strength $\bar{\sigma}$, whereas the yield strengths of metals are usually much less than $\bar{\sigma}$. How would you attempt to measure the yield strength of a ceramic, given that the fracture strengths of ceramics in tension are usually much less than the yield strengths?

19.2 Why are ceramics usually much stronger in compression than in tension?

Al_2O_3 has a fracture toughness K_{IC} of about $3 \text{ MN m}^{-3/2}$. A batch of Al_2O_3 samples is found to contain surface flaws about $30 \mu\text{m}$ deep. Estimate (a) the tensile strength and (b) the compressive strength of the samples. Assume that $Y = 1.12$ when the flaws are in tension.

Answers

(a) 276 MN m^{-2} , (b) 4635 MN m^{-2} .

19.3 Estimate the thermal shock resistance ΔT for the ceramics listed in Table 17.7. Use the data for Young's modulus E , modulus of rupture σ_r and thermal expansion coefficient α given in Table 17.7. How well do your calculated estimates of ΔT agree with the values given for ΔT in Table 17.7? (Hints: (a) assume that $\sigma_{\text{TS}} \approx \sigma_r$ for the purposes of your estimates; (b) where there is a spread of values for E , σ_r or α , use the average values for your calculation.)

- 19.4** The photograph shows part of the cloisters of a monastery near the city of Huelva, Andalusia, Spain. Explain in a qualitative way why none of the elements in the structure experiences tensile loading. Why is this important in masonry structures? (This place is of historical importance, because it was from here in August 1492 that Christopher Columbus set sail for his voyage of discovery to North America.)



Cloisters at El Monasterio de Santa María de la Rábida (37 12 27.90N 6 55 32.50 W).

- 19.5** You have been asked to design a hydraulic rock splitter for excavating rock in situations where blasting is not permitted (e.g., where the rock face is unstable or where there are buildings nearby). The procedure is to drill a hole deep into the rock, and insert into it a hydraulically operated device capable of exerting an outward radial pressure on the wall of the hole. Estimate the maximum pressure required if the rock has a fracture strength of 20 MN m^{-2} . (The tensile hoop stress in a thick-walled tube carrying an internal pressure p is given by

$$\sigma = \frac{pb^2(a^2 + r^2)}{r^2(a^2 - b^2)},$$

where a and b are the external and internal radii of the tube and r is the radius at the position where σ is calculated. You may assume that $a \gg b$ in the present situation.)

Answer

20 MN m^{-2} .

- 19.6** If the diameter of the hole in Example 19.5 is 50 mm, and Young's modulus E for the rock is 60 GN m^{-2} , estimate the radial expansion of the hole just before

fracture takes place. (The increase in the bore radius of a thick-walled tube is given by

$$\Delta b = b \left(\frac{P}{E} \right) \left\{ \left(\frac{a^2 + b^2}{a^2 - b^2} \right) + \nu \right\},$$

where ν (≈ 0.3) is Poisson's ratio.)

Answer

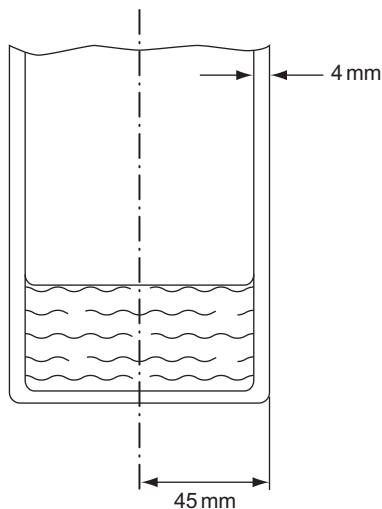
0.01 mm.

- 19.7** Modulus of rupture tests on samples of soda glass gave a median strength ($P_s = 0.5$) of 50 MN m^{-2} . In each test, the beam was fully loaded for approximately 1 min. If the design life of the glass component is to be 100 years, and the time exponent n is 10, estimate the strength reduction factor to be applied to take into account slow crack growth. What would the reduction factor be if the time at full load had been 5 min? What would the reduction factor be for 5 min at full load and $n = 20$?

Answers

0.17; 0.20; 0.45.

- 19.8** The diagram shows the lower end of a laboratory storage bottle made from soda glass. The bottle was used to dilute sulfuric acid in the approved way by putting some water into the bottle first, and then slowly adding the acid. The dissolution reaction generated a significant amount of heat but there was no spitting or other side effect until, after a minute or two, a crack formed in the glass at the level of the meniscus. This quickly propagated into a through-thickness fully circumferential crack, and the top of the bottle separated cleanly from the base. Account in a qualitative way for the failure. How would you avoid this dangerous type of failure in future?



- 19.9** Explain why, when designing with ceramics, it is never necessary to consider plastic collapse as a potential failure mode.
- 19.10** Explain briefly why the fracture toughnesses of ceramics are much less than those of nearly all metals.
- 19.11** Why is the three-point bend test preferred over the simple tensile test for measuring the strength of ceramics in tension? How is the tensile strength (as found from a simple tensile test) related to the modulus of rupture?
- 19.12** A tube of soda glass has an internal diameter of 20 mm and a wall thickness of 2 mm. Use the appropriate equation from the section on Thermal Stresses at the end of this chapter to estimate the maximum value of temperature difference between the outer and inner surfaces of the tube that the glass can stand without fracturing. Use data from Table 17.7, and assume a value for Poisson's ratio of 0.3. Assume that the tensile strength of the glass in this application is approximated by the modulus of rupture. If the tube did fracture, where would you expect the fracture to start?

Answers

111 °C.

- 19.13** The tube in Example 19.12 is to be used as a heat exchanger, with the outer surface immersed in agitated boiling water, and ice-cold fluid flowing through the bore. Using the maximum temperature difference calculated in Example 19.12, estimate the maximum heat flow rate (expressed per 100 mm length of tube) which the tube can stand. Explain how differences between the properties of soda glass and Pyrex borosilicate glass (see Table 17.7) would help to increase the maximum temperature difference if Pyrex were used instead. Why is Pyrex glass always used for chemistry experiments?

Answer

209 W per 100 mm length.

Thermal Stresses

Thermal strain = $\alpha\Delta T$.

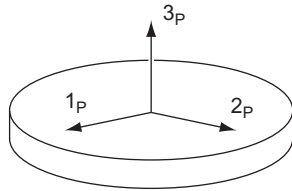
Thus,

$$\varepsilon_1 = \frac{\sigma_1}{E} - \nu \frac{\sigma_2}{E} - \nu \frac{\sigma_3}{E} + \alpha\Delta T.$$

$$\varepsilon_2 = \frac{\sigma_2}{E} - \nu \frac{\sigma_1}{E} - \nu \frac{\sigma_3}{E} + \alpha\Delta T.$$

$$\varepsilon_3 = \frac{\sigma_3}{E} - \nu \frac{\sigma_1}{E} - \nu \frac{\sigma_2}{E} + \alpha\Delta T.$$

Example



Derive an equation for calculating the surface stresses that are produced when a hot disk of a poor thermal conductor is dropped into cold water. Assume that the stresses are not relieved by cracking.

Since the surface layers are constrained by the bulk material, $\varepsilon_1 = 0$, $\varepsilon_2 = 0$. In addition, $\sigma_3 = 0$ (free surface). Thus

$$0 = \frac{\sigma_1}{E} - \nu \frac{\sigma_2}{E} + \alpha \Delta T,$$

$$0 = \frac{\sigma_2}{E} - \nu \frac{\sigma_1}{E} + \alpha \Delta T,$$

which gives $\sigma_1 = \sigma_2 = \sigma$ (equi-biaxial stress state). Then

$$0 = \frac{\sigma}{E} - \nu \frac{\sigma}{E} + \alpha \Delta T$$

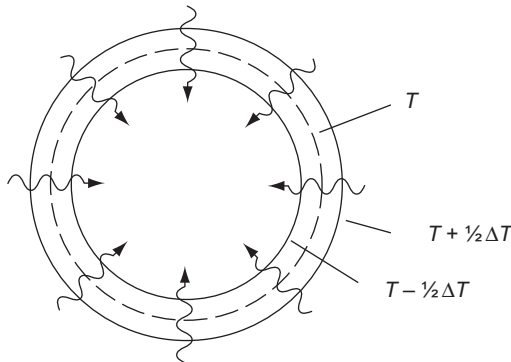
which gives

$$\sigma = \frac{\alpha \Delta T E}{(1 - \nu)}.$$

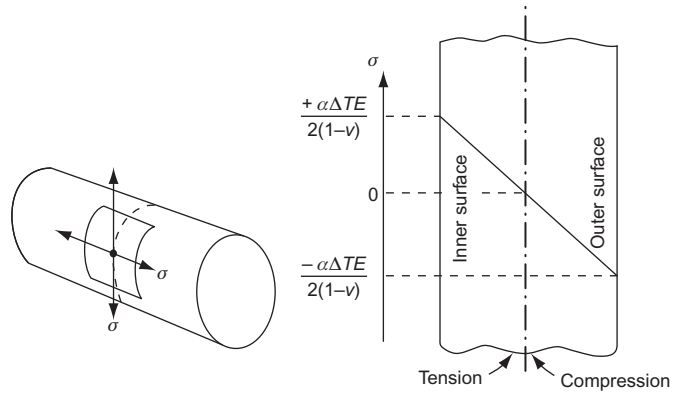
Since ΔT in a cooling situation is negative, the stress is tensile one.

Example

Calculate the thermal stresses in a long tube subjected to a uniform radial flow of heat through the tube wall. The temperature of the outside of the tube is greater than the temperature of the inside by amount ΔT .



The stress state is equi-biaxial, as in the previous example. The situation is as follows:



$$\sigma_{\max} = \pm \frac{\alpha\Delta TE}{2(1-\nu)}.$$

Processing Ceramics

20.1 INTRODUCTION

When you squeeze snow to make a snowball, you are hot-pressing a ceramic. Hot-pressing of powders is one of several standard *sintering methods* used to form ceramics which require methods appropriate to their special properties.

Glass, it is true, becomes liquid at a modest temperature (1000 °C) and can be cast like a metal. At a lower temperature (around 700 °C) it is very viscous and can again be formed by the methods used for metals: rolling, pressing, and forging. But the engineering ceramics have high melting points—typically 2000 °C—precluding the possibility of melting and casting. And they lack the plasticity which allows the wide range of secondary forming processes used for metals: forging, rolling, machining, and so forth. So most ceramics are made from *powders* which are pressed and fired, in various ways, to give the final product shape.

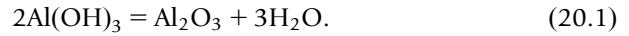
Vitreous ceramics are different. Clay, when wet, is *hydroplastic*: the water is drawn between the clay particles, lubricating their sliding, and allowing the clay to be formed by hand or with simple machinery. When the shaped clay is dried and fired, one component in it melts and spreads round the other components, bonding them together.

Low-grade ceramics—stone and certain refractories—are simply mined and shaped. We are concerned here not with these but with the production and shaping of high-performance engineering ceramics, clay products, and glasses. Cement and concrete are discussed separately in Chapter 21. We start with engineering ceramics.

20.2 PRODUCTION OF ENGINEERING CERAMICS

Alumina powder is made from bauxite, a hydrated aluminum oxide with the formula $\text{Al}(\text{OH})_3$, of which there are large deposits in Australia, the

Caribbean, and Africa. After crushing and purification, the bauxite is heated at 1150 °C to decompose it to alumina, which is then milled and sieved:



Zirconia, ZrO_2 , is made from the natural hydrated mineral or from zircon, a silicate. Silicon carbide and silicon nitride are made by reacting silicon with carbon or nitrogen. Although the basic chemistry is very simple, the processes are complicated by the need for careful quality control, and the goal of producing fine ($<1\text{ }\mu\text{m}$) powders which, almost always, lead to a better final product. These powders are then consolidated by one of a number of methods.

20.3 FORMING ENGINEERING CERAMICS

The surface area of fine powders is enormous. A cupful of alumina powder with a particle size of $1\text{ }\mu\text{m}$ has a surface area of about 10^3 m^2 . If the surface energy of alumina is 1 J m^{-2} , the surface energy of the cupful of powder is 1 kJ.

This energy drives *sintering* (Figure 20.1). When the powder is packed together and heated to a temperature at which diffusion becomes very rapid (generally, to around $(2/3) T_M$), the particles *sinter*, that is, they bond together to form small necks which then grow, reducing the surface area, and causing the powder to densify. Full density is not reached by this sort of sintering, but the residual porosity is in the form of small, rounded holes which have only a small effect on mechanical strength.

Figure 20.2 shows, at a microscopic level, what is going on. Atoms *diffuse* from the grain boundary which must form at each neck (since the particles which meet there have different orientations), and deposit in the pore, tending to fill it up. The atoms move by *grain-boundary diffusion* (helped a little by lattice diffusion, which tends to be slower). The reduction in surface area drives the process, and the rate of diffusion controls its rate. This

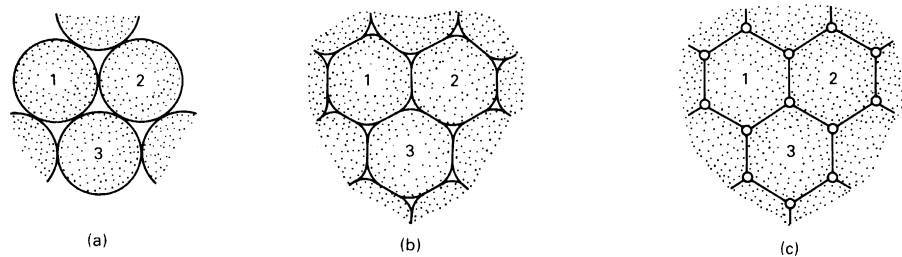


FIGURE 20.1

Powder particles pressed together at (a) sinter, as shown at (b), reducing the surface area (and thus energy) of the pores; the final structure usually contains small, nearly spherical pores (c).

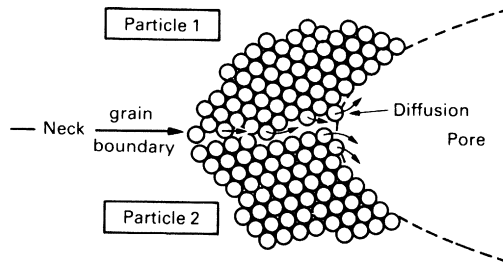


FIGURE 20.2

The microscopic mechanism of sintering. Atoms leave the grain boundary in the neck between two particles and diffuse into the pore, filling it up.

immediately tells us the two most important things we need to know about solid state sintering:

- (a) Fine particles sinter much faster than coarse ones because the surface area (and thus the driving force) is higher and the diffusion distances are smaller.
- (b) The rate of sintering varies with temperature in exactly the same way as the diffusion coefficient. Thus, the rate of densification is given by

$$\frac{d\rho}{dt} = \frac{C}{a^n} \exp(-Q/RT). \quad (20.2)$$

Here ρ is the density, a is the particle size, C and n are constants, Q is the activation energy for sintering, R is the gas constant, and T is the absolute temperature. n is typically about 3, and Q is usually equal to the activation energy for grain-boundary diffusion.

The sintering of powder is a production method used not only for ceramics but also for metals and polymers too. In practice, the powder is first pressed to an initial shape in a die, mixing it with a binder, or relying on a little plasticity, to give a “green compact” with just enough strength to be moved into a sintering furnace. Considerable shrinkage occurs, of course, when the compact is fired. But by mixing powders of different sizes to get a high density to start with, and by allowing for the shrinkage in designing the die, a product can be produced which requires the minimum amount of finishing by machining or grinding. The final microstructure shows grains with a distribution of small, nearly spherical pores at the edges of the grains. The pore size and spacing are directly proportional to the original particle size, so the finer the particles, the smaller are these defects, and the better the mechanical strength. During sintering, the grains in the ceramic grow, so the final grain size is often much larger than the original particle size.

Higher densities and smaller grains are obtained by *hot-pressing*: the simultaneous application of pressure and temperature to a powder. The powder is squeezed in a die (Figure 20.3) or in a pressure vessel which is pumped up to a high gas pressure (hot isostatic pressing, Figure 20.4). At the same time the powder is heated to the sintering temperature. The pressure adds to the surface energy to drive sintering more quickly than before. The rate is still controlled by diffusion, and so it still varies with temperature according to Equation (20.2). But the larger driving force shortens the sintering time from hours to minutes and increases the final density. Indeed, full density can only be reached by pressure sintering, and the short time gives no opportunity for grain growth, so the mechanical properties of the product are good. Die pressing allows such precision that no subsequent finishing processes are necessary; but the dies, and thus the process, are expensive.

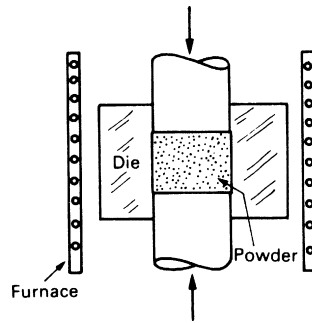


FIGURE 20.3

Die pressing: the powder is heated and compressed in a shaped die.

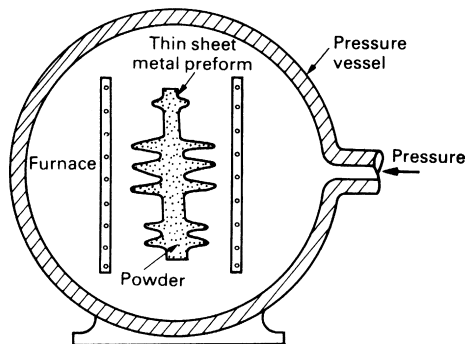


FIGURE 20.4

Hot isostatic pressing ("HIPing"): the powder, in a thin steel preform, is heated and compressed by high-pressure argon.

Full density can be reached by another route—though with some loss of mechanical strength. Small amounts of additive, such as MgO in the sintering of Al_2O_3 or Si_3N_4 , greatly increase the rate of sintering. The additive reacts with the powder (and any impurities it may contain) to form a low melting point glass which flows between the powder particles at the sintering temperature. Diffusional transport through the melt is high—it is like squeezing wet sugar—and the rate of sintering of the solid is increased. As little as 1% of glass is all that is needed, but it remains at the boundaries of the grains in the final product and (because it melts again) drastically reduces their high-temperature strength. This process of *liquid phase sintering* (Figure 20.5) is widely used to produce dense ceramics.

There are two further processes. Silicon-based ceramics can be fabricated by sintering or by hot-pressing. But a new route, *reaction bonding* (Figure 20.6), is cheaper and gives good precision. If pure silicon powder is heated in nitrogen gas, or a mixture of silicon and carbon powders is sintered together, then the reactions



and

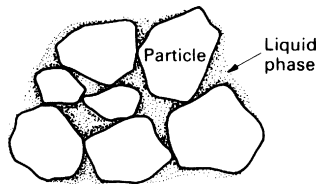


FIGURE 20.5

Liquid phase sintering: a small amount of additive forms a liquid which accelerates sintering and gives fully dense products but with some loss of high-temperature strength.

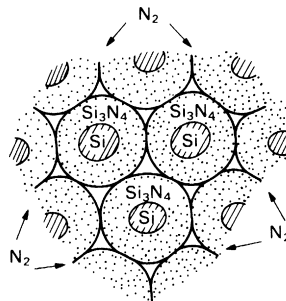


FIGURE 20.6

Silicon ceramics (SiC , Si_3N_4) can be shaped by reaction bonding.

occur during the sintering, and bonding occurs simultaneously. In practice, silicon, or the silicon–carbon mixture, is mixed with a polymer to make it plastic, and then formed by rolling, extrusion, or pressing, using methods which are normally used for polymer forming: thin shells and complicated shapes can be made in this way. The polymer additive is then burnt out and the temperature raised so that the silicon and carbon react. The final porosity is high (because nitrogen or carbon must be able to penetrate through the section), but the dimensional change is so small (0.1%) that no further finishing operations need be necessary.

Finally, some ceramics can be formed by *chemical vapor deposition* (CVD) processes. Silicon nitride is an example: Si_3N_4 can be formed by reacting suitable gases in such a way that it deposits on (or in) a former to give a shell or a solid body. When solids grow from the vapor they usually have a structure like that of a casting: columnar grains grow from the original surface and may extend right through the section. For this reason, CVD products often have poor mechanical properties.

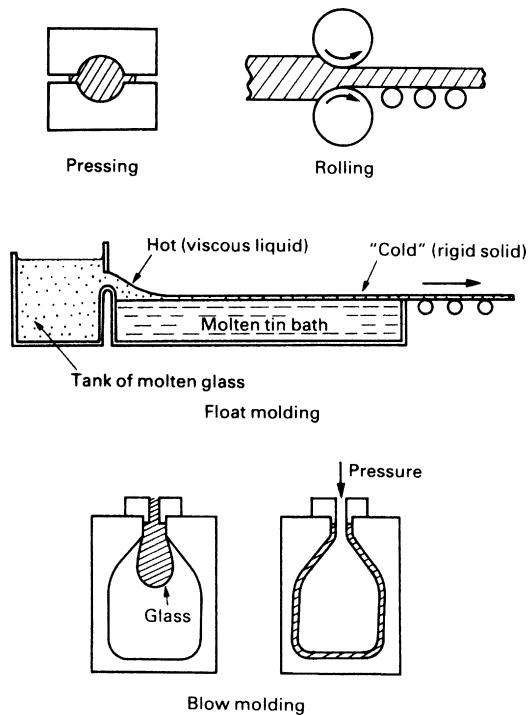
20.4 PRODUCTION AND FORMING OF GLASS

Commercial glasses are based on silica, SiO_2 , with additives: 30% of additives in a soda glass, about 20% in high-temperature glass like Pyrex. The additives lower the viscosity by breaking up the network. Raw glasses are produced, like metals, by melting the components together and then casting them. Glasses are formed by deformation involving viscous flow.

The working range is shown in Figure 19.8 as a shaded band: it is wide because working procedures vary. Typical processes, shown in Figure 20.7, are:

- (a) Hot-pressing, in which a slug of hot glass is pressed between dies (like the forging of metals); it is used to make heavy glass insulators, and requires a high viscosity.
- (b) Rolling, to produce a glass sheet; again, requires a high viscosity.
- (c) Float molding, to produce optically smooth window glass; needs a *low* viscosity.
- (d) Blow molding, to produce bottles or the thin envelopes for light bulbs, at rates of several thousand per hour; requires a low viscosity.

Two other temperatures are important in the working of glass (see Figure 19.8). At the *annealing point* ($\eta = 10^{13}$ p) there is still enough fluidity to relax internal stresses in about 15 min. Most glass products are held briefly at this temperature to remove tensile stresses that might otherwise induce fracture. At the *strain point* ($\eta = 10^{14}$ p) atom motion in the glass is

**FIGURE 20.7**

Forming methods for glass: pressing, rolling, float molding, and blow molding.

so sluggish that rapid cooling from this temperature does not introduce new stresses. So, in processing, the product is cooled slowly from the annealing point to the strain point and faster from there to room temperature.

Residual tensile stresses, as we have seen, are a problem. But compressive residual stresses, in the right place, can be used to advantage. *Toughened glass* is made by heating the product above its annealing point and then cooling rapidly. The surface contracts and hardens while the interior is still hot and more fluid; it deforms, allowing the tensile stress in the surface to relax. Then the interior cools and contracts. But the surface is below its strain point; it cannot flow, so it is put into compression by the contracting interior. With the surface in compression, the glass is stronger, because the microcracks which initiate failure in a glass are always in the surface (caused by abrasion or corrosion). The interior, of course, is in tension; and if a crack should penetrate through the protective compressive layer it is immediately unstable and the toughened glass shatters spontaneously.

20.5 PROCESSING POTTERY, PORCELAIN, AND BRICK

Pottery is one of the oldest materials. Clay artifacts as old as the pyramids (5000 BC) are sophisticated in their manufacture and glazing; and shards of pottery of much earlier date are known. Then, as now, the clay was *mined* from sites where weathering had deposited them, *hydroplastically formed*, *fired*, and then *glazed*.

Clays have plate-like molecules with charges on their surfaces (Chapter 18). The charges draw water into the clay as a thin lubricating layer between the plates. With the right moisture content, clays are *plastic*: they can be molded, extruded, turned, or carved. But when they are dried, they have sufficient strength to be handled and stacked in kilns for firing.

In *slip casting*, a thin slurry, or suspension, of clay in water is poured into a porous mold. Water is absorbed into the mold wall, causing a layer of clay to form and adhere to it. The excess slurry is tipped out of the mold and the slip-cast shell, now dry enough to have strength, is taken out and fired. The process allows intricate shapes (like plates, cups, vases) to be made quickly and accurately.

When a clay is *fired*, the water it contains is driven off and a silicate glass forms by reaction between the components of the clay. The glass melts and is drawn by surface tension into the interstices between the particles of clay, like water into a sponge. Clays for brick and pottery are usually a blend of three constituents which occur together naturally: pure clay, such as the $\text{Al}_2\text{O}_3 \cdot 2\text{SiO}_2 \cdot 2\text{H}_2\text{O}$ (kaolinite) described in Chapter 18; a flux (such as feldspar) which contains the Na or K used to make the glass; and a filler such as quartz sand, which reduces shrinkage but otherwise plays no role in the firing. Low-fire clays contain much flux and can be fired at 1000 °C. High-fire clays have less and require temperatures near 1200 °C. The final microstructure shows particles of filler surrounded by particles of mullite (the reaction product of SiO_2 and Al_2O_3 in the clay) all bonded together by the glass.

Vitreous ceramics are made waterproof and strengthened by glazing. A slurry of powdered glass is applied to the surface by spraying or dipping, and the part is refired at a lower temperature (typically 800 °C). The glass melts, flows over the surface, and is drawn by capillary action into pores and microcracks, sealing them.

20.6 IMPROVING CERAMICS

When we speak of the “strength” of a metal, we mean its yield strength or tensile strength; to strengthen metals, they are alloyed in such a way as to obstruct dislocation motion, and thus raise the yield strength. By contrast,

the “strength” of a ceramic is its fracture strength; to strengthen ceramics, we must seek ways of making fracture more difficult. There are two, and they are complementary. The tensile fracture strength (Equation (19.1)) is given by

$$\sigma_{TS} \approx \frac{K_c}{\sqrt{\pi a_m}}. \quad (20.5)$$

The compressive strength is about 15 times this. First, we can seek to reduce the inherent flaw size; and second (though this is more difficult), we can seek to increase the fracture toughness.

Most ceramics (as we have seen) contain flaws: holes and cracks left by processing, cracks caused by thermal stress, corrosion, or abrasion. Even if there are no cracks to start with, differences in elastic moduli between phases will nucleate cracks on loading. And most of these flaws have a size which is roughly that of the powder particles from which the ceramic was made. If the flaw size can be reduced, or if samples containing abnormally large flaws can be detected and rejected, the mean strength of the ceramic component is increased.

This is largely a problem of *quality control*. It means producing powders of a controlled, small size; pressing and sintering them under tightly controlled conditions to avoid defects caused by poor compaction or by grain growth; and careful monitoring of the product to detect any drop in standard. By these methods, the modulus of rupture for dense Al_2O_3 and silicon carbide can be raised to 1000 MN m^{-2} , making them as strong in tension as a high-strength steel; in compression, they are 15 times stronger again.

The other alternative is to attempt to increase K_c . Pure ceramics have a fracture toughness between 0.2 and $2 \text{ MN m}^{-3/2}$. A dispersion of *particles of a second phase* can increase this a little: the advancing crack is pinned by the particles and bows between them, much as a dislocation is pinned by strong second phase particles.

A more complicated, and more effective, mechanism operates in *partially stabilized zirconia* (PSZ), which has general application to other ceramics. Consider the analogy of a chocolate bar. Chocolate when cold is a brittle solid and because of this it is notch sensitive: notches are molded into chocolate to help you break it in a fair, controlled way. Some chocolate bars have raisins and nuts in them, and they are less brittle: a crack, when it runs into a raisin, is arrested; and more energy is needed to break the bar in half. PSZ works in rather the same way. When ZrO_2 is alloyed with MgO , a structure can be created which has small particles of tetragonal zirconia (the raisins). When a crack approaches a particle, the particle transforms by a displacive transformation to a new (monoclinic) crystal structure, and this process absorbs energy. The details are complicated, but the result is

simple: the toughness is increased from 2 to $8 \text{ MN m}^{-3/2}$. This may not seem much compared with $100 \text{ MN m}^{-3/2}$ for a tough steel, but it is big for a ceramic, dramatically increasing its strength and resistance to thermal shock, and opening up new applications for it.

Ceramics can be *fiber strengthened* to improve their toughness. The plaster in old houses contains horse hair; and from the earliest times straw has been put into mud brick, in both cases to increase the toughness. In Arctic regions, ice is used for aircraft runways; the problem is that heavy aircraft knock large chips out of the brittle surface. One solution is to spread sawdust or straw onto the surface, flood it with water, and refreeze it; the fibers toughen the ice and reduce cracking. More recently, methods have been developed to toughen cement with glass fibers to produce high-strength panels and pipes. The details of the toughening mechanisms are the same as those for fiber-reinforced polymers. The effect can be spectacular: toughnesses of over $10 \text{ MN m}^{-3/2}$ are possible.

An older and successful way of overcoming the brittleness of ceramics is to make a sort of composite called a *cermet*. The best example is the cemented carbide used for cutting tools. Brittle particles of tungsten carbide (WC) are bonded together with a film of cobalt (Co) by sintering the mixed powders. If a crack starts in a WC particle, it immediately runs into the ductile cobalt film, which deforms plastically and absorbs energy (Figure 20.8). The composite has a fracture toughness of around $15 \text{ MN m}^{-3/2}$, even though that of the WC is only $1 \text{ MN m}^{-3/2}$.

The combination of better processing to give smaller flaws with alloying to improve toughness is a major advance in ceramic technology. The potential, not yet fully realized, appears to be enormous. Table 20.1 lists some of the areas in which ceramics have, or may soon, replace other materials.

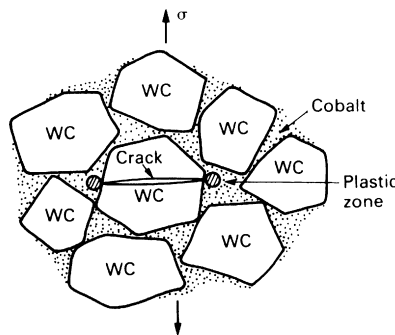


FIGURE 20.8

A cermet is a particulate composite of a ceramic (WC) in a metal (Co). A crack in the ceramic is arrested by plasticity in the cobalt.

Table 20.1 Applications of High-Performance Ceramics

Application	Property	Material
Cutting tools	Hardness, toughness	Alumina, sialons
Bearings, liners, seals	Wear resistance	Alumina, zirconia
Agricultural machinery	Wear resistance	Alumina, zirconia
Engine and turbine parts, burner nozzles	Heat and wear resistance	SiC, Si ₃ N ₄ , alumina, sialons, ceramic–ceramic composites
Shielding, armor	Hardness, toughness	Alumina, boron carbide
High-performance windows	Translucence and strength	Alumina, magnesia
Artificial bone, teeth, joints	Wear resistance, strength	Zirconia, alumina
Integrated circuit substrates	Insulation, heat resistance	Alumina, magnesia

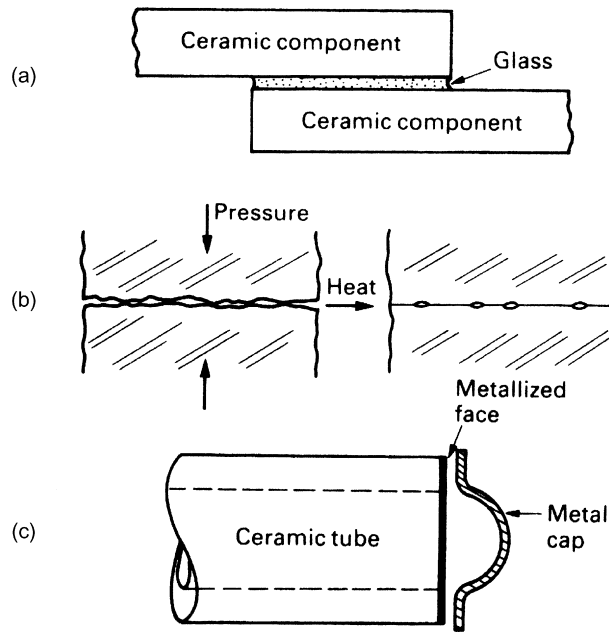
20.7 JOINING CERAMICS

Ceramics cannot be put into direct contact with bolts or rivets: the contact stresses would cause brittle fracture. Instead, ceramic components are fixed to other ceramic or metal parts by techniques which avoid or minimize stress concentrations.

Two such techniques are *diffusion bonding* and *glaze bonding* (Figure 20.9). In diffusion bonding, the parts are heated while being pressed together; then, by processes like those which give sintering, the parts bond together. Even dissimilar materials can be bonded in this way. In glaze bonding, the parts are coated with a low-melting (600 °C) glass; the parts are placed in contact and heated above the melting point of the glass.

Ceramics are joined to metals by *metal coating and brazing* and by the use of *adhesives*. In metal coating, the mating face of the ceramic part is coated in a thin film of a refractory metal such as molybdenum (usually applied as a powder and then heated). The metal film is then electroplated with copper, and the metal part brazed to the copper plating. Adhesives, usually epoxy resins, are used to join parts at low temperatures. Finally, ceramic parts can be clamped together, provided the clamps avoid stress concentrations, and are provided with soft (e.g., rubber) packing to avoid contact stresses.

The forming and joining of ceramics is summarized in the flowchart of Table 20.2.

**FIGURE 20.9**

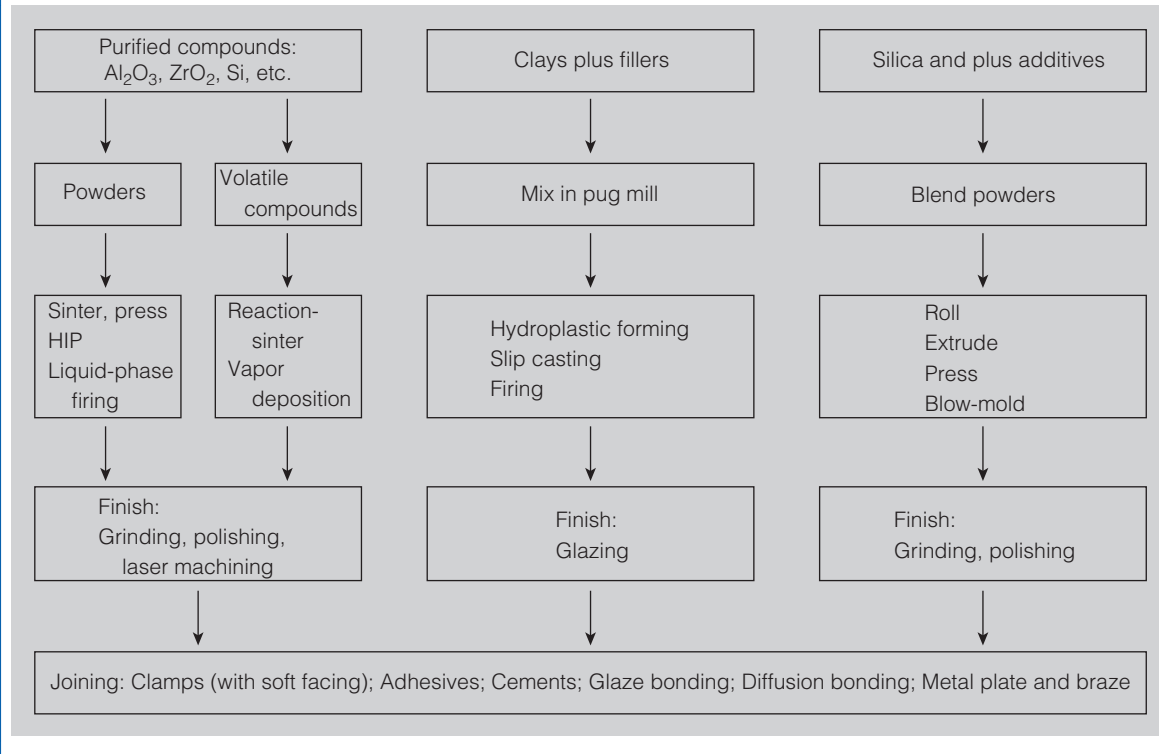
Joining methods for ceramics: (a) glaze bonding, (b) diffusion bonding, and (c) metallization plus brazing. In addition, ceramics can be clamped and can be joined with adhesives.

WORKED EXAMPLE

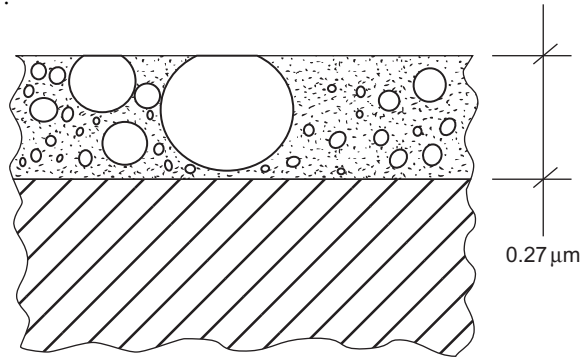
Glazed layers are not used just to seal, protect, and strengthen vitreous ceramics like tiles. Before plastics became so widely used, glazes (referred to as “vitreous enamel”) were much used to coat thin sheet steel in applications like domestic washing-up bowls, water jugs, and other containers (like bread bins), to protect the steel from corrosion and add an attractive finish. They are still used to coat baths made from pressed steel (as in bathrooms)—although expensive, these are vastly superior to plastic baths, which flex annoyingly (and therefore feel as cheap as they indeed are) and also degrade with time (it is not unknown for someone standing in an old plastic bath to put their foot through the bottom of it, with unfortunate consequences both to the person and to the decoration of the room below). Large storage tanks are also made from vitreous enameled sheet steel to protect them from corrosion.

Of course, if there are defects in the vitreous enamel coating, corrosion can set in. This was the case with a large water tank in a sewage farm after only 5 months in service from new. Granted that the water was aggressive to steel,

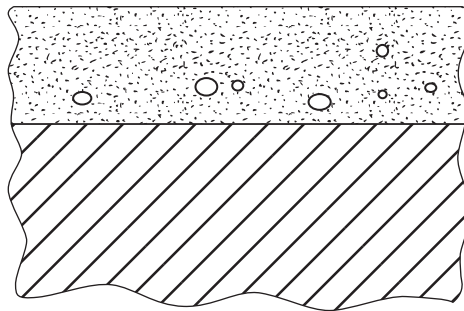
Table 20.2 Forming and Joining of Ceramics



but one does not expect water tanks to start pinholing and leaking after such a short time. When small samples from the tank wall were sectioned and polished, large through-thickness pores were found in the enamel coating, as shown below.



But why did the glazed layer have such large pores? The enameling process involved a number of steps as follows: degrease steel sheet; acid etch sheet surface; electroplate with nickel (very thin layer); spray with “frit” (glass powder with organic binder); “biscuit” dry at $\approx 250^\circ\text{C}$; fire at $\approx 900^\circ\text{C}$ for 3–4 min; air cool to room temperature. To find out why the pores were there, tests were done by removing small samples from the tank and reheating them to high temperature. After 3 min at 850°C and cooling to room temperature, no change to the porosity was observed when the samples were sectioned and polished. When samples were heated to 900°C , the number of pores and their sizes decreased hugely.



This glaze layer would have been fine as a barrier layer. When samples were heated to 950°C , the pores vanished altogether, but because the viscosity of the glass was too low at this temperature, it flowed too easily over the steel surface, and this made the coating thickness much too uneven and thin in places. So, 900°C is the correct temperature, and the steel sheet had been fired at a temperature 50°C too low. This just goes to show how critical processing temperature can be.

EXAMPLES

20.1 You have been given samples of the following ceramics.

- (a) A hot-pressed thermocouple sheath of pure alumina.
- (b) A piece of window glass.
- (c) An unglazed fired clay pot.
- (d) A tungsten carbide/cobalt cutting tool.

Sketch the structures that you would expect to see if you looked at polished sections of the samples under a reflecting light microscope. Label the phases and any other features of interest.

20.2 Describe briefly how the tensile strength of ceramic materials is determined by their microstructures. How may the tensile strength of ceramics be improved?

20.3 Describe the stages which might typically be followed in producing a small steel gear wheel by powder processing. Discuss the relative advantages and disadvantages of producing the gear wheel by powder processing or machining.

20.4 Why are special precautions necessary when joining ceramic components to metal components? What methods are available for the satisfactory joining of ceramics to metals?

20.5 The window glass in old buildings often has an uneven surface, with features which look like flow marks. The common explanation is that the glass has suffered creep deformation over the years under its own weight. Explain why this scenario is complete rubbish (why do you think the glass does appear to have “flow marks”?).

20.6 In addition to its dominant use for windows, glass is increasingly being used in innovative architectural applications such as bathroom panels, balcony walls, staircase treads, and roofs. How would you design a bolted joint type for attaching a glass panel to the steel framing of a balcony wall? Indicate how and why your joint type differs from that used to attach a metal panel to the framing.

20.7 The table shows the compositions and coefficients of thermal expansion (20–500 °C) for Fe–Ni alloys. Which of these alloys would you use when making glass–metal seals with borosilicate glass?

Alloy	Ni	Co	Cr	Fe	α (MK ⁻¹)
36	36			64	10.1
40	40			60	8.0
42	42			58	8.0
48	48			52	9.1
50	50			50	9.7
K	29	17		54	6.1
475	47		5	48	10.7

Answer

K alloy.

- 20.8** In a microwave device application, wafers of alumina are soldered to small flat plates made from K alloy. The K alloy is plated with $5\text{ }\mu\text{m}$ layers of nickel and then gold. The alumina is sputtered with a $5\text{ }\mu\text{m}$ adhesion layer of titanium–tungsten, then plated with $5\text{ }\mu\text{m}$ layers of nickel and then gold (neither nickel nor gold will stick to alumina). The joint is soldered using gold–germanium eutectic solder (88 Au, 12 Ge) which melts at $356\text{ }^{\circ}\text{C}$. The solder is supplied as strip 25 mm wide by $25\text{ }\mu\text{m}$ thick. Solder preforms are cut from this strip to match the dimensions of the area to be joined, the components are assembled, pressed together with an inconel spring, and heated in an infrared furnace to melt the solder. Why is it not necessary to flux the joint before the soldering operation? What might be the disadvantages of having to use flux in a thin solder joint having a large area? Why is K alloy physically compatible with alumina?
- 20.9** “Maltesers” are approximately spherical “chocolates” consisting of crisp, light honeycomb centers covered with a layer of milk chocolate. The photographs show (a) some loose Maltesers straight out of the bag and (b) a batch of Maltesers which had been warmed up in a low oven. Comment on the essential difference between the two photographs, explain that difference, and relate it to the processing of ceramics.



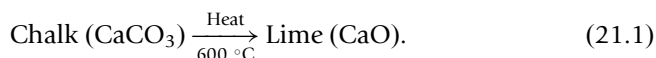
Cement and Concrete

21.1 INTRODUCTION

Concrete is a *particulate composite* of stone and sand, held together by an adhesive. The adhesive is usually a *cement paste* (used also as an adhesive to join bricks or stones), but asphalt or even polymers can be used to give special concretes. In this chapter, we examine three cement pastes: the early pozzolana; the widespread Portland cement; and the newer, and somewhat discredited, high-alumina cement. And we consider the properties of the principal cement-based composite, concrete. The chemistry will be unfamiliar, but it is not difficult. The properties are exactly those expected of a ceramic containing a high density of flaws.

21.2 CHEMISTRY OF CEMENT

Cement was known to the ancient Egyptians and Greeks. Their lime cement was mixed with volcanic ash by the Romans to give a lime mortar; its success can be judged by the number of Roman buildings still standing 2000 years later. In countries which lack a developed manufacturing and distribution system, these *pozzolana cements* are still used (they are named after Pozzuoli, near Naples, where the ash came from, and which was subject to considerable volcanic activity—see Vesuvius 40 49 31.70 N 14 25 25.54 E). To make them, chalk is heated at a relatively low temperature in simple wood-fired kilns to give lime



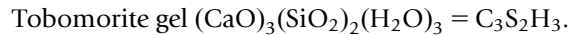
The lime is mixed with water and volcanic ash and used to bond stone, brick, or even wood. The water reacts with lime, turning it into Ca(OH)_2 ; but in doing so, a surface reaction occurs with the ash (which contains SiO_2) probably giving a small amount of $(\text{CaO})_3(\text{SiO}_2)_2(\text{H}_2\text{O})_3$ and forming

a strong bond. Only certain volcanic ashes have an active surface which will bond in this way; but they are widespread enough to be readily accessible.

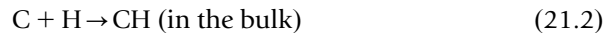
The chemistry, obviously, is one of the curses of the study of cement. It is greatly simplified by the use of a *reduced nomenclature*. The four ingredients that matter in any cement are, in this nomenclature

Lime	CaO	= C
Alumina	Al ₂ O ₃	= A
Silica	SiO ₂	= S
Water	H ₂ O	= H.

The key product, which bonds everything together, is



In this terminology, pozzolana cement is C mixed with a volcanic ash which has active S on its surface. The reactions which occur when it sets (Figure 21.1) are



and



The tobomorite gel bonds the hydrated lime (CH) to the pozzolana particles. These two equations are all you need to know about the chemistry of pozzolana cement. Those for other cements are only slightly more complicated.

The world's construction industry continued to rely on lime cements until relatively recently (mid to late nineteenth century) and they are still used for specific applications such as repairing historic buildings (Figures 21.2 and 21.3). However, in 1824, an English entrepreneur, Jo Aspdin, took out a

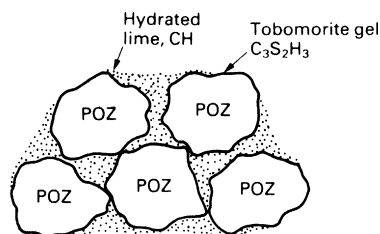


FIGURE 21.1

A pozzolana cement. The lime (C) reacts with silica (S) in the ash to give a bonding layer of tobomorite gel $\text{C}_3\text{S}_2\text{H}_3$.

patent for “a cement of superior quality, resembling Portland stone” (a white limestone from the island of Portland, UK). This *Portland cement* is prepared by firing a controlled mixture of chalk (CaCO_3) and clay (which is just S_2AH_2) in a kiln at 1500°C (a high temperature, requiring special kiln



FIGURE 21.2

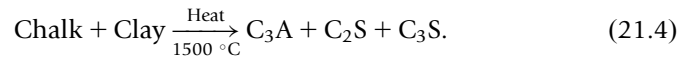
Lime mortar used to bind bricks together. Christ's College, Cambridge, UK (52 12 19.80 N 0 07 18.75 E). Rear elevation of First Court, which dates from 1505. One of the few areas of the original Tudor facade in original condition (the elevations facing into the court were faced in stone at a later date to protect them from weathering). Note frost damage to one of the original Tudor bricks (top right of photograph), and two weathered bricks replaced with thin replica Tudor bricks and fresh lime mortar. The old bricks and mortar are smoke blackened from the time when coal was burnt in fireplaces in the city.



FIGURE 21.3

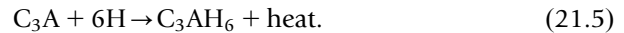
Lime cement render, with imitation stone parting lines added with a pointed tool before the render set. Christ's College, Cambridge, UK (52 12 19.80 N 0 07 22.60 E). Front elevation in Second Court. The existing render had become cracked and weathered and was replaced with authentic render in 2011/12.

materials and fuels, so it is a technology adapted to a developed country). Firing gives three products



When Portland cement is mixed with water, it hydrates, forming *hardened cement paste* (“h.c.p.”). All cements harden by reaction, not by drying; indeed, it is important to keep them wet until full hardness is reached. Simplified a bit, two groups of reactions take place during the hydration of Portland cement.

The first is fast, occurring in the first 4 h and causing the cement to *set*. It is the hydration of the C_3A



The second is slower and causes the cement to *harden*. It starts after a delay of 10 h or so, and takes 100 days or more before it is complete. It is the hydration of C_2S and C_3S to tobomorite gel, the main bonding material which occupies 70% of the structure



↑
Tobomorite gel.

Portland cement is stronger than pozzolana because gel forms in the bulk of the cement, not merely at its surface with the filler particles. The development of strength is shown in Figure 21.4(a). The reactions give off a good deal of heat (Figure 21.4(b)). It is used, in cold countries, to raise the temperature of the cement, preventing the water it contains from freezing. But in very large structures such as dams, heating is a problem: then cooling pipes are embedded in the concrete to take the heat out, and left in place afterward as extra reinforcement.

The classic example of this is in the construction of the Hoover dam, on the Colorado River (Black Canyon) between Arizona and Nevada, USA (built 1931–1936)—36 00 57.70 N 114 44 16.00 W.

http://en.wikipedia.org/wiki/Hoover_Dam

<http://www.youtube.com/watch?v=gcBGYNpohs4>

The engineers calculated that if the dam had been built in a single continuous pour, the concrete would have taken 125 years to cool and the resulting stresses would have caused the dam to crack and crumble. Instead, the ground was marked out into rectangles and separate concrete blocks were

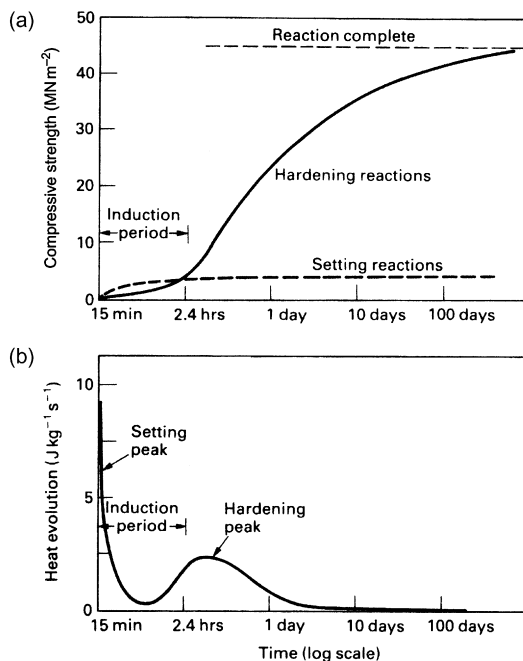


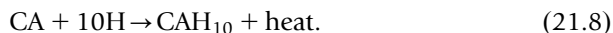
FIGURE 21.4

(a) The hardening of Portland cement. The setting reaction (Equation (21.5)) is followed by the hardening reactions (Equations (21.6) and (21.7)). Each is associated with the evolution of heat, as shown in (b).

poured side by side and on top of one another, to make up the full width and height of the dam. Some blocks were as large as 50 ft^2 by 5 ft high. Each block contained a series of 1 in. steel pipes through which water was run (cool river water to start with, then ice-cold water from a refrigeration plant as the setting and hardening progressed).

Figure 21.5 shows a less spectacular (but no less important) example of the use of modern Portland cement—binding bricks together in standard brick-laying practice. Many homes have double skin walls with an outer skin laid from bricks (the inner skin may be cement blocks or wooden framed). Brick skins are also much used on the external elevations of larger steel or concrete framed buildings.

High-alumina cement is fundamentally different from Portland cement. As its name suggests, it consists mainly of CA, with very little C_2S or C_3S . Its attraction is its high hardening rate: it achieves in a day what Portland cement achieves in a month. The hardening reaction is



But its long-term strength can be a problem. Depending on temperature and environment, the cement may deteriorate suddenly and without warning by “conversion” of the metastable CAH_{10} to the more stable C_3AH_6 (which formed in Portland cement). There is a substantial decrease in volume, creating porosity and causing drastic loss of strength. In cold, dry environments, the changes are slow, and the effects may not be evident for years. But warm, wet conditions are disastrous, and strength may be lost in a few weeks.

21.3 STRUCTURE OF PORTLAND CEMENT

The structure of cement, and the way in which it forms, are really remarkable. The angular cement powder is mixed with water (Figure 21.6). Within 15 min the setting reaction (Equation (21.5)) coats the grains with a gelatinous envelope of hydrate (C_3AH_6). The grains are bridged at their point of contact by these coatings, giving a network of weak bonds which cause a loss of plasticity. The bonds are easily broken by stirring, but they quickly form again.

Hardening (Equations (21.6) and (21.7)) starts after about 3 h. The gel coating develops protuberances which grow into thin, densely packed rods radiating like the spines of a sea urchin from the individual cement grains. These spines are the $\text{C}_3\text{S}_2\text{H}_3$ of the second set of reactions. As hydration continues, the spines grow, gradually penetrating the region between the cement grains. The interlocked network of needles eventually consolidates into a rigid mass and has the further property that it grows into, and binds to, the porous surface of brick, stone, or precast concrete.



FIGURE 21.5

A mixture of Portland cement and sand (1 part by volume cement + 4 parts by volume sand) used to bind bricks together in modern construction. Individual sand particles can be seen in the mix. A plasticizer is usually added to the wet mix before use in order to make it easier to lay it with the bricklaying trowel.

The mechanism by which the spines grow is fascinating (Figure 21.7). The initial envelope of hydrate on the cement grains, which gave setting, also acts as a semipermeable membrane for water. Water is drawn through the coating because of the high concentration of calcium inside, and a pressure

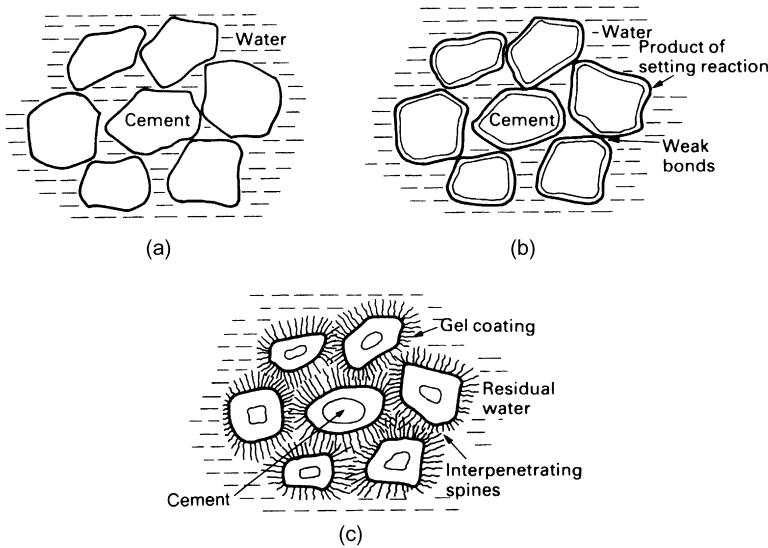


FIGURE 21.6

The setting and hardening of Portland cement. At the start (a) cement grains are mixed with water, H. After 15 min (b) the setting reaction gives a weak bond. Real strength comes with the hardening reaction (c), which takes some days.

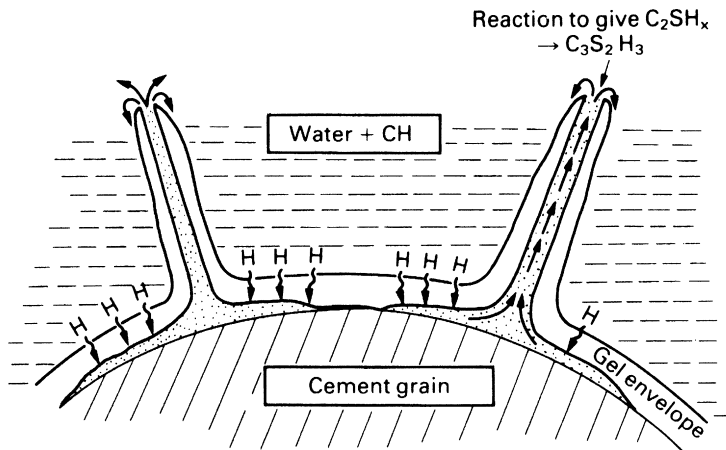


FIGURE 21.7

The mechanism by which the spiny structure of $\text{C}_3\text{S}_2\text{H}_3$ grows.

builds up within the envelope (the induction period, shown in Figure 21.4). This pressure bursts through the envelope, squirting little jets of a very concentrated solution of C_3S and C_2S into the surrounding water. The outer surface of the jet hydrates further to give a tube of $C_3S_2H_3$. The liquid within the tube, protected from the surrounding water, is pumped to the end by the osmotic pressure where it reacts, extending the tube. This osmotic pump continues to operate, steadily supplying reactants to the tube ends, which continue to grow until all the water or all the unreacted cement are used up.

Hardening is just another (rather complicated) example of nucleation and growth. Nucleation requires the formation, and then breakdown, of the hydrate coating; the “induction period” shown in Figure 21.4 is the nucleation time. Growth involves the passage of water by osmosis through the hydrate film and its reaction with the cement grain inside. The *driving force* for the transformation is the energy released when C_2S and C_3S react to give tobermorite gel $C_3S_2H_3$. The rate of the reaction is controlled by the rate at which water molecules diffuse through the film, and thus depends on temperature as

$$\text{rate} \propto \exp(-Q/RT). \quad (21.9)$$

Obviously, the rate will depend on the total surface area of cement grains available for reaction, and thus on the fineness of the powder. So hardening is accelerated by raising the temperature and by grinding the powder more finely.

21.4 CONCRETE

Concrete is a mixture of stone and sand (the *aggregate*) glued together by cement (Figure 21.8). The aggregate is dense and strong, so the weak phase is the hardened cement paste, and this largely determines the strength. Compared with other materials, cement is cheap; but aggregate is cheaper, so it is normal to pack as much aggregate into the concrete as possible whilst still retaining workability.

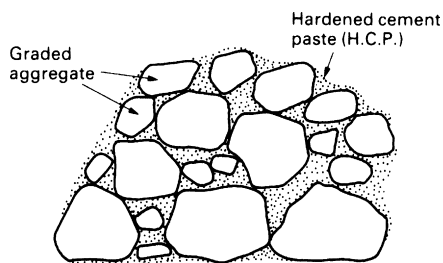


FIGURE 21.8

Concrete is a particulate composite of aggregate (60% by volume) in a matrix of hardened cement paste.

The best way to do this is to grade the aggregate so that it packs well. If particles of equal size are shaken down, they pack to a relative density of about 60%. The density is increased if smaller particles are mixed in: they fill the spaces between the bigger ones. A good combination is a 60–40 mixture of sand and gravel. The denser packing helps to fill the voids in the concrete, which are bad for obvious reasons: they weaken it, and they allow water to penetrate (which, if it freezes, will cause cracking).

When concrete hardens, the cement paste shrinks. The gravel, of course, is rigid, so that small shrinkage cracks are created. It is found that *air entrainment* (mixing small bubbles of air into the concrete before pouring) helps prevent the cracks spreading. Figure 21.9 shows a typical example of modern concrete construction.



FIGURE 21.9

Modular construction using precast sections of concrete (reinforced with steel bars and meshes). Christ's College, Cambridge, UK (52 12 25.20 N 0 07 21.80 E). Main elevation of New Court, designed by Sir Denys Lasdun (built 1969/70). A major refurbishment program was completed in 2008. This included (a) repairing areas of concrete which had cracked and started to come away from the leading edges of the roof slabs, (b) adding zinc sacrificial anodes to protect the steel reinforcement (by cathodic protection), (c) treating all exposed surfaces with a colorless polymer-based sealant to keep water out.

21.5 STRENGTH OF CEMENT AND CONCRETE

The strength of Portland cement largely depends on its *age* and its *density*. The development of strength with time was shown in Figure 21.4(a): it still increases slowly after a year. Too much water in the original mixture gives a weak low-density cement (because of the space occupied by the excess water). Too little water is bad too because the workability is low and large voids of air get trapped during mixing. A water/cement ratio of 0.5 is a good compromise, though a ratio of 0.38 actually gives enough water to allow the reactions to go to completion.

The Young's modulus of cement paste varies with density as

$$\frac{E}{E_s} = \left(\frac{\rho}{\rho_s} \right)^3. \quad (21.10)$$

where E_s and ρ_s are the modulus and the density of solid tobermorite gel (32 GN m^{-2} and 2.5 Mg m^{-3}). Concrete, of course, contains a great deal of gravel with a modulus three or so times greater than that of the paste. Its modulus can be calculated by the methods used for composite materials, giving

$$E_{\text{concrete}} = \left\{ \frac{V_a}{E_a} + \frac{V_p}{E_p} \right\}^{-1}. \quad (21.11)$$

Here, V_a and V_p are the volume fractions of aggregate and cement paste and E_a and E_p are their moduli. As Figure 21.10 shows, experimental data for typical concretes fit this equation well.

When cement is made, it inevitably contains flaws and cracks. The gel (like all ceramics) has a low fracture toughness: K_c is about $0.3 \text{ MN m}^{-3/2}$. In

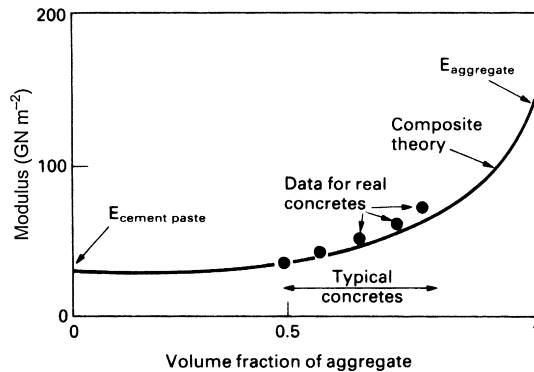


FIGURE 21.10

The modulus of concrete is very close to that given by simple composite theory (Equation (21.11)).

tension, it is the longest crack which propagates causing failure. The tensile strength of cement and concrete is around 4 MN m^{-2} , implying a flaw size of 1 mm or so. The fracture toughness of concrete is a little higher than that of cement, typically $0.5 \text{ MN m}^{-3/2}$. This is because the crack must move round the aggregate, so the total surface area of the crack is greater. But this does not mean that the tensile strength is greater. It is difficult to make the cement penetrate evenly throughout the aggregate, and if it does not, larger cracks or flaws are left. And shrinkage, mentioned earlier, creates cracks on the same scale as the largest aggregate particles. The result is that the tensile strength is usually a little lower than that of carefully prepared cement. These strengths are so low that engineers, when designing with concrete and cement, arrange that it is always loaded in compression (or reinforce it with materials which can take tensile loads).

In compression, a single large flaw is not fatal (as it is tension). As explained in Chapter 19, cracks at an angle to the compression axis propagate in a *stable* way (requiring a progressive increase in load to make them propagate further). And they bend so that they run parallel to the compression axis (Figure 21.11). The stress–strain curve therefore rises (Figure 21.12), and finally reaches a maximum when the density of cracks is so large that they link to give a general crumbling of the material. In slightly more detail:

- (a) Before loading, the cement or concrete contains cracks due to porosity, incomplete consolidation, and shrinkage stresses.
- (b) At low stresses, the material is linear elastic, with modulus given in Table 17.7. But even at low stresses, new small cracks nucleate at the surfaces between aggregate and cement.
- (c) Above 50% of the ultimate crushing stress, cracks propagate stably, giving a stress–strain curve that continues to rise.

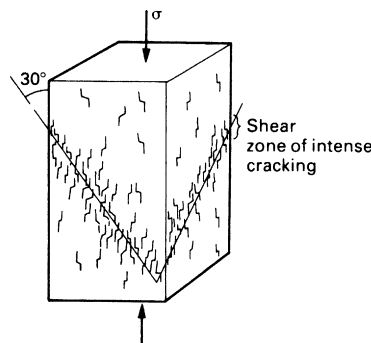
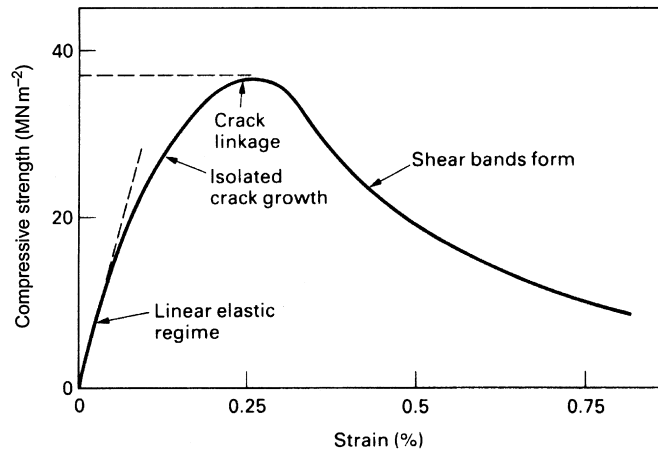


FIGURE 21.11

The compressive crushing of a cement or concrete block.

**FIGURE 21.12**

The stress—strain curve for cement or concrete in compression. Cracking starts at about half the ultimate strength.

- (d) Above 90% of the maximum stress, some of the cracks become unstable and continue to grow at constant load, linking with their neighbors. A failure surface develops at an angle of 30° to the compression axis. The load passes through a maximum and then drops—sometimes suddenly, but more usually rather slowly.

A material as complicated as cement shows considerable variation in strength. The mean crushing strength of 100 mm cubes of concrete is (typically) 50 MN m^{-2} ; but a few of the cubes fail at 40 MN m^{-2} and a few survive to 60 MN m^{-2} . There is a size effect too: 150 mm cubes have a strength which is lower, by about 10%, than that of 100 mm cubes. This is exactly what we would expect from Weibull's treatment of the strength of brittle solids (Chapter 19). There are, for concrete, additional complexities. But to a first approximation, design can be based on a median strength of 30 MN m^{-2} and a Weibull exponent of 12, provided the mixing and pouring are good. When these are poor, the exponent falls to about 8.

21.6 HIGH-STRENGTH CEMENT

The low tensile strength of cement paste is, as we have seen, a result of low fracture toughness ($0.3 \text{ MN m}^{-3/2}$) and a distribution of large inherent flaws. The scale of the flaws can be greatly reduced by four steps:

- (a) Milling the cement to finer powder.
- (b) Using the "ideal" water/cement ratio (0.38).

- (c) Adding polymeric lubricants (which allow the particles to pack more densely).
- (d) Applying pressure during hardening (which squeezes out residual porosity).

The result of doing all four things together is a remarkable material with a porosity of less than 2% and a tensile strength of up to 90 MN m^{-2} . It is light (density 2.5 Mg m^{-3}) and, potentially, a cheap competitor in many low-stress applications now filled by polymers.

21.7 REINFORCING CEMENT AND CONCRETE

Since the early 1900s, cement has been reinforced with naturally occurring asbestos fibers to make *asbestos cement* (AC). This is much used for things like water pipes, corrugated roofing sheet, and building board. Manufacture and new-build use of AC has been banned in many countries (owing to the risk of workers contracting lung cancer by breathing in asbestos dust), but AC continues to be made and used elsewhere.

<http://www.hse.gov.uk/contact/faqs/asbestos-health-risks.htm>

<http://en.wikipedia.org/wiki/Asbestos>

Fine asbestos fibers can have considerable tensile strength ($\approx 1 \text{ GN m}^{-2}$). The processed fiber bundles are not continuous, but can be up to several centimeters in length. They are mixed with wet cement paste and formed into a thin layer ($\approx 0.25 \text{ mm}$ thick). The fibers become oriented parallel to the layer surfaces but are oriented randomly within the layers. When manufacturing water pipes, for example, the layer is wound on to a cylindrical mandrel and compressed (whilst still wet) so as to build up to the required thickness of the finished AC pipe. The wet pipe is then dried and cured (which takes up to 4 weeks). The end result is a chopped fiber composite of cement paste with $\approx 15\%$ volume fraction asbestos fibers. [Figure 21.13](#) shows an external view in close-up of a length of AC water pipe which failed in service. Asbestos fibers can be seen protruding from the fracture surface. Other fiber reinforcement materials have also been developed to replace asbestos, including coated glass fibers (to protect the glass from the alkaline cement), polypropylene and polyvinyl alcohol fibers, and more recently cellulose fibers. These are processed in essentially the same way as asbestos fibers.

For large structures, concrete is almost always reinforced with steel meshes and bars (“rebar”) (more recently, rebars of high specific stiffness, made from aligned kevlar fibers in an epoxy matrix, are being used for demanding applications). Concrete beams which have to support large bending

**FIGURE 21.13**

External view in close-up of a length of AC water pipe which failed in service. The internal diameter and wall thickness were 150 and 15 mm. The internal pressure has pushed a section out of the pipe wall. Note the bundle of asbestos fibers protruding from the fracture surface. These had pulled out of the mating fracture surface.

moments (e.g., bridge girders) go one step further and have longitudinal prestressing tendons located in the concrete near the position of maximum tensile stress in service (Figure 21.14).

http://en.wikipedia.org/wiki/Prestressed_concrete

There are two ways of generated the prestress. In the first (“pretensioning”), the tendons are passed along the length of the shuttering (mold) and out at the ends, where they are hooked up to hydraulic jacks and put into tension (they almost yield). The concrete is then poured and allowed to set and harden. Once the concrete has developed enough shear strength to grip the tendons firmly, the jacks are removed from the tendons, which contract elastically and put the concrete in the lower half of the beam into compression. In the second (“posttensioning”), the concrete beam is cast containing plastic tubes which run along the length of the beam where the tendons are to be located. Once the concrete has developed enough compressive strength, tendons are passed along the tubes and attached to hydraulic jacks at the ends of the beam (these bear on substantial steel plates to spread the load). The tendons are then stretched and made fast with split tapered collets. The idea in both cases is that when the beams are loaded in service, the *concrete* in the lower half of the beam stays in (reduced) compression, so will not crack (and let in air or water). The tensile load is taken by the steel tendons and not by the (weak in tension) concrete. Of course, concrete reinforced by rebar or prestressed tendons is far closer to being an engineering structure than a material (even a composite material). But it

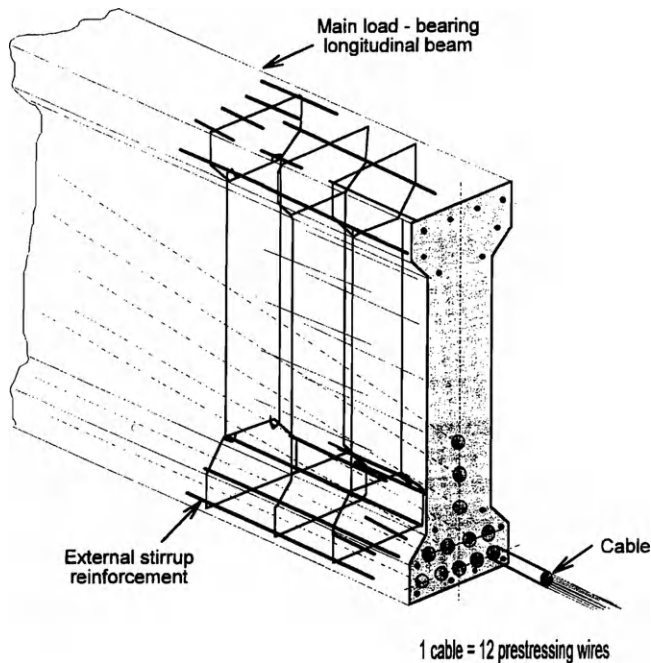


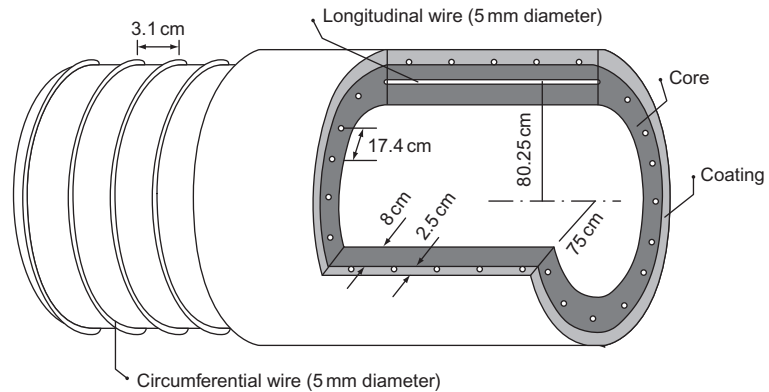
FIGURE 21.14

Typical arrangement of prestressing tendons (posttensioned) in a concrete bridge girder. The diagram also shows the geometry of the fixed steel rebar.

is essential to know about the processing and properties of concrete in order to be able to overcome its shortcomings when used in serious structural applications.

WORKED EXAMPLE

The diagram shows a schematic of an internally pressurized water pipe. The concrete core is reinforced with two types of steel prestressed wires (all 5 mm diameter)—longitudinal (to take axial forces) and circumferential (to take the hoop stress from the internal pressure). The longitudinal wires were tensioned in the mold and the concrete core was then poured. After the core had developed sufficient strength, the circumferential wire was pretensioned and wrapped around the core as a helical winding. The yield strength and tensile strength of the (cold drawn) wire were 1700 and 1800 MN m^{-2} , and the strain before necking was $\approx 2\%$. The winding was covered with a layer of cement mortar to protect it from damage and corrosion (the pipe was buried in soil in service).



The pipe burst open only after 6 years. When the trench was excavated, a piece of pipe wall measuring 1 m by 0.5 m was found to be shattered and the prestressing wires crossing this area had snapped. Tests on wire samples showed that the tensile strength had decreased to $\approx 1400 \text{ MN m}^{-2}$ and fracture was macroscopically brittle (the stress–strain curve was linear up to failure). Cracks ($\approx 1.4 \text{ mm}$ deep) were found on the fracture surfaces; they had started at the wire surface and propagated inward with time (the crack surfaces were corroded) until they reached the critical crack size for fast fracture. The cracking was caused by stress corrosion cracking of the wires, in turn caused by a combination of a susceptible material (very hard, cold drawn steel) and aggressive environment (soil and groundwater). The outer skin of mortar had obviously not been thick enough to protect the steel wires from the environment. Prestressing of concrete structures is not a simple low-tech fix!

EXAMPLES

- 21.1** In what way would you expect the setting and hardening reactions in cement paste to change with temperature? Indicate the practical significance of your result.
- 21.2** A concrete consists of 60% by volume of limestone aggregate plus 40% by volume of cement paste. Estimate Young's modulus of the concrete, given that E for limestone is 63 GN m^{-2} and E for cement paste is 25 GN m^{-2} .

Answer

39 GN m^{-2} .

- 21.3** Why is the tensile strength of conventional cement only about 4 MN m^{-2} ? How can the tensile strength of cement be increased by improvements in processing? What is the maximum value of tensile strength which can be achieved by processing improvements?

Answer

90 MN m^{-2} approximately.

- 21.4** Make a list, based on your own observations, of selected examples of components and structures made from cement and concrete. Discuss how the way in which the materials are used in each example is influenced by the low (and highly variable) tensile strength of cement and concrete.
- 21.5** The concrete roof of the Sydney Opera House is not left bare but is covered with a layer of glazed ceramic tiles (see photograph below). What are the advantages of this form of construction? How would you fix the tiles in place?



The roof of the Sydney Opera House.

- 21.6** Why is it necessary to cool large volumes of poured concrete while it is setting and hardening? How would you do this in practice? What could happen if you did not cool the concrete?
- 21.7** Referring to the Worked Example, estimate the fracture toughness of the prestressing wire. Assume $Y = 1$. Why was the stress–strain curve of the cracked wire samples linear, when the curve for the uncracked wire showed significant yielding before final failure?

Answer

$93 \text{ MN m}^{-3/2}$.

- 21.8** Referring to [Figure 21.14](#), real bridge girders of this type in a motorway viaduct developed vertical cracks up to 2 m long following the line of the external stirrup rebars. Brown rust deposits were seen leaking out of the cracks. Analysis of the concrete and corrosion deposits showed a high concentration of chloride ions (from road salting). Look at EM1Ed4, Section 27.3 (p. 408) and answer the following questions. Why did the rebars corrode? Why did the concrete crack? What could be done to stop further corrosion?

- 21.9** What are the benefits of making products from cement–fiber composites?
Give specific examples of products made from this type of material.
- 21.10** Why is structural concrete usually reinforced with steel bars and meshes?
Give specific examples of the use of reinforced concrete.
- 21.11** Why are concrete bridge beams reinforced with prestressing tendons?

Case Studies in Ceramics

22.1 HARD AS FLINT

The expression “hard as flint” was well known for equating something (or someone!) to a very hard natural ceramic. Flint has been used extensively for all sorts of cutting, splitting, and scraping tools, as well as things like arrowheads and spear points, by humans, and their predecessors the hominids, since the furthest distances of time. At the archeological site of Atapuerca, Burgos, Spain—42° 22' 09.70" N 3° 31' 26.15" W—flint tools dating back 1.2 *million* years have been excavated from the caves; many others date from 200,000 to 400,000 years ago. Cutting marks have been found on the bones of bears dating back to more than 800,000 years. Atapuerca has the oldest evidence of human/hominid occupation in Europe and is a UNESCO World Heritage Site <http://whc.unesco.org/en/list/989/>. Without flint as a tool material, human progress would have been slowed significantly—it is an early example of materials as a *key enabling technology*.

What is flint? It is usually found as three-dimensional shapes or *nodules* up to ≈ 10 cm diameter by ≈ 30 cm long (often branched or with large surface protrusions), which have formed within sedimentary rocks such as chalk and limestone. The flint nodules consist of quartz, which crystallized inside preexisting inclusions of organic material (which defined the shape of the flint nodules). The quartz is thought to have originated from skeletons of marine organisms, and in fact flint sometimes contains fossilized remains. Flint nodules were often dug out of chalk deposits—an old (5000 years) flint mine can be visited at Grimes Graves, Lynford, Thetford, Norfolk, UK—52° 28' 34.00" N 0° 40' 30.60" E.

<http://www.english-heritage.org.uk/daysout/properties/grimes-graves-prehistoric-flint-mine/>

There are the remains of about 400 separate shafts in the area (which looks like a mini lunar landscape when viewed on Google Earth). Flint was much

used as a building material (and still is for repairs and new build in heritage areas). Because of its hardness and lack of permeability to water, it is extremely resistant to weathering and frost damage. An excellent example can be seen in the flint “checkerboard” facade of Trinity Guildhall (built 1420 AD), in St. Margaret’s Place, King’s Lynn, Norfolk, UK—52 45 07.42 N 0 23 40.09 E.

But why is flint so special as a *tool* material? It is classified as a *microcrystalline* quartz mineral, because the size of the individual crystals is only 0.5–20 μm .

<http://www.agateworld.co.uk/>

<http://www.quartzpage.de/flint.html>

<http://en.wikipedia.org/wiki/Flint>

In most rocks, the crystals are much larger; when viewed with a hand lens, they can easily be seen, whereas a fractured surface of flint looks smooth and “glassy.” Because of this, flint is still loosely (and incorrectly) referred to as having an “amorphous” structure—which could only be the case if the quartz had been melted (heated to 1800 °C) and then cooled like a conventional glass. The very small crystal size leads to several key attributes of flint. First, it is tougher than many other rocks or stones. Second, it has no preferred fracture plane—it can be broken (“knapped”) to give smooth, curved surfaces (conchoidal fractures—like glass fractures, but less curved and more predictable). Third, because of the small crystal size, when two conchoidal fractures meet, the edge is extremely sharp (edge radius \approx crystal size).

This means that flint tools can be formed to give very sharp and durable cutting edges (although this is a highly skilled operation).

<http://www.belchalwell.org.uk/artifacts-flint.asp>

<http://www.stoneagetools.co.uk/identifying-flint-tools.htm>

Figure 22.1 shows some pieces of flint, together with DRHJ’s crude attempt to knap a cutting edge. Knapping a complete knife or arrowhead is best left to the experts! One can only marvel at how these special features of flint were discovered, entirely empirically, by ancient humanoids and extrapolated to the skilled manufacture of sophisticated tools.

22.2 SLATE—NATURAL ROOFING MATERIAL

For our second case study, we look at another naturally occurring ceramic—*slate*, which (like flint) has very special properties (but quite unlike those of flint) that make it ideal for a very different, specialized application—roofing



FIGURE 22.1

Pieces of flint.



FIGURE 22.2

Modern house roofed with Spanish slates, Cambridge, UK.

material for buildings. [Figures 22.2 and 22.3](#) show typical examples of slates used on the roof of a house. Slate has been used for “slates” like this for centuries—and for many other things too. The individual slates are thin (≈ 4 mm) sheets of slate, which have been trimmed to the correct width and length by cropping (using a guillotine). As shown in [Figure 22.3](#), the cropping works by initiating multiple brittle fractures in the slate sheets, and

this leads to randomly chipped edges. In this context, the tendency of ceramics to suffer brittle fracture is actually a *useful* property and allows the sheets to be cut to size quickly and easily using primitive machinery.

However, the surfaces of the slate sheets are very flat, smooth, and parallel (see Figure 22.3). How can such perfect sheets be made from slate using primitive technology? The video clip shows how

<http://www.youtube.com/watch?v=w2Wdbn-W0R0>

Quarried slate can be *split* easily, using only a hammer and bolster (and considerable manual skill). But what is so special about slate that it can be split in this way? Slate originates from shale-type sedimentary rocks composed of clay or volcanic ash. But the slate does *not* usually split along the bedding planes of the sedimentary rock as one might think. Instead, the rock was later subjected to high pressure and temperature, which transformed the crystal structure by a process of *metamorphism*. The result is a very fine-grained rock with a layered (*foliated*) arrangement of crystals (often silicates) having a *preferred orientation* (perpendicular to the direction of maximum compressive stress during metamorphism). The special, complex microstructure of slate allows it to be split easily along distinct *cleavage planes*. (The ease with which thin sheets of slate can be produced means that a slate roof is much *lighter* than a tiled roof; and because slate absorbs very little water, it is also highly resistant to frost damage.)

The following links give an idea of the scale of quarrying (and the devastation of landscape) undertaken in the nineteenth century to extract slate

Oakley Quarry, Blaenau Ffestiniog, North Wales, UK—53 00 21.00 N 3 57 02.40 W and the narrow-gauge railways used to convey slates from the quarries to the ports ready for export



FIGURE 22.3

Close up of slates on house roof. Note chipped edges of slates, where they have been trimmed to size by guillotining.

<http://www.youtube.com/watch?v=a4bl9AoNLTw&feature=endscreen&NR=1>
http://www.festipedia.org.uk/wiki/Gravity_Slate_Trains

The video clip shows how the workman methodically splits the slab of slate in half down the its centerline, then does the same to one of the halves, and so on, halving each piece until the correct thickness of slate is reached. It was obviously discovered empirically a long time ago that this was the best way to do the splitting. It is fascinating that we now know why—but only because of fracture mechanics! The situation is shown in Figure 22.4, and the analysis is given below.

For fast fracture at fixed displacements, the energy equation is (EM1Ed4, p. 190, Equation (13.2)):

$$-\frac{dU_{el}}{da} = G_{ct}. \quad (22.1)$$

For the single cantilever situation (left of Figure 22.4), the stored strain energy is

$$U_{el} = \int_0^{\delta_1} F d\delta. \quad (22.2)$$

The end deflection of the cantilever is given by (EM1Ed4, p. 48)

$$\delta = \frac{Fa^3}{3EI}. \quad (22.3)$$

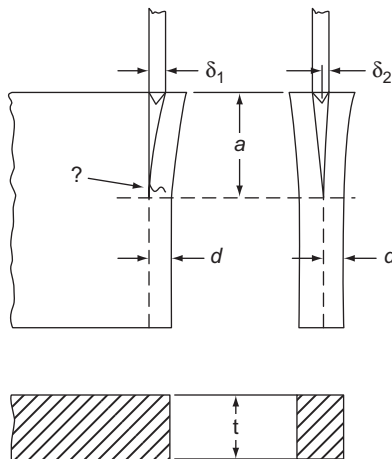


FIGURE 22.4

Splitting slate. If the slate is split nonsymmetrically (as at left), there is a greater chance it will snap during the splitting operation (note that $\delta_1 \approx \sqrt{2\delta_2}$).

Thus

$$U_{el} = \frac{3EI}{a^3} \int_0^{\delta_1} \delta \, d\delta = \frac{3}{2} \left(\frac{EI\delta_1^2}{a^3} \right), \quad (22.4)$$

$$-\frac{dU_{el}}{da} = \frac{9}{2} \left(\frac{EI\delta_1^2}{a^4} \right) = G_c t, \quad (22.5)$$

$$\delta_1 = \frac{\sqrt{2}}{3} \left(\frac{\sqrt{EG_c}}{E} \right) \left(\frac{t}{l} \right)^{1/2} a^2. \quad (22.6)$$

For the double cantilever situation (right of Figure 22.4), the stored strain energy is

$$U_{el} = 2 \int_0^{\delta_2} F \, d\delta. \quad (22.7)$$

Thus,

$$\delta_2 = \frac{1}{3} \left(\frac{\sqrt{EG_c}}{E} \right) \left(\frac{t}{l} \right)^{1/2} a^2, \quad (22.8)$$

$$\delta_1 = \sqrt{2}\delta_2. \quad (22.9)$$

The maximum bending stress in the cantilever occurs next to the tip of the cleavage crack (split). If it is large enough, a tensile brittle fracture will initiate at (or near to) the tip of the split, and then run through the thickness of the cantilever at right angles to the plane of the split. The maximum tensile stress is proportional to δ , so the stress in the nonsymmetrical splitting operation is 1.414 times larger than in the symmetrical one. By always splitting the slate symmetrically, the risk of fractures (and therefore wasted material and time) is minimized.

22.3 GLASS ROOF BEAMS

Glass is an inherently brittle material. Although its theoretical strength is extremely high, even small flaws will propagate at low stress because of the low fracture toughness (typical of a ceramic material). It is not the most obvious choice for load-bearing structures. However, even a pane of window glass is a load-bearing structure. It may be supported by a window frame, but it is still subjected to wind loading—and impacts from children, birds, footballs, and burglars. Small panes of ordinary (untoughened) glass can fulfil this function quite well (although as a small child there is always that heart-stopping moment when one's baseball goes over into next-door's back yard, to be followed by the tinkling of glass and a loud shout!). Even so, full-length windows must nowadays be made from "safety glass," because shards of broken glass can lead to very serious injury.

In many modern buildings, the external skin is made from large panels of glass. The wind loadings (and the consequences of failure) are then very serious, because of the large area of glass, and its height above ground level. Modern architects dislike having the supporting structures on view (as they are in a glass-walled building of an earlier era—the Sydney Opera House, see Figures 17.4 and 17.5). The ideal is to have a completely transparent glass wall, or glass roof, with “no visible means of support.” The following case study shows a mouth-watering example of an all-glass roof on an extension to an old house.

http://www.trombe.co.uk/case_studies_-_case_05.php

The very considerable weight of the double-glazed roof panels (and the snow and ice loading on the roof in winter) is supported entirely by glass beams of rectangular cross-section spanning between the walls and the ridge girder. This is a classic example of how glass is now being used as steel, reinforced concrete, and wood were in conventional construction. But how can glass be manufactured for applications where it is loaded in considerable tension, but cannot be allowed to fail?

For a start, *toughened glass* (also called *tempered glass*) must be used (see Chapter 20, Section 20.4). As shown in Figure 22.5, the tempering process

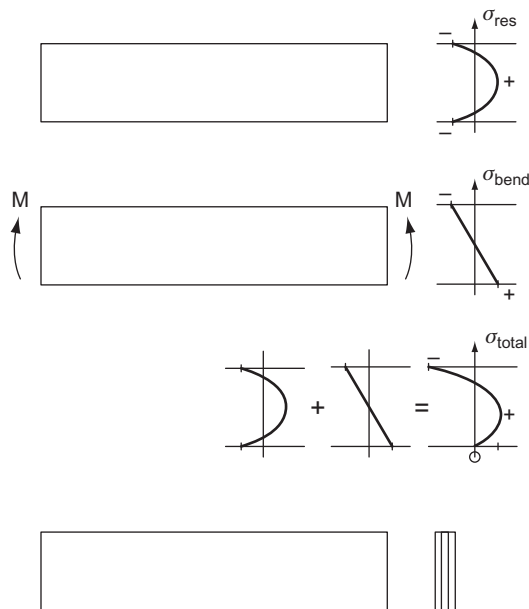


FIGURE 22.5

Use of toughened (tempered) glass in a structural beam.

puts the surface regions of the glass beam into *residual compression*, with a balancing *residual tension* in the core of the beam. Because glass is formed as a liquid and cools without any changes in its microstructure, bulk glass is essentially defect-free. So, although the core is in considerable tension, it does not break because it does not have any flaws (its strength could conceivably approach the theoretical strength). The problem lies with the surfaces of the glass beam: there is a finite risk that they will contain scratches, for example, made by particles of cement or stone dust (also hard ceramics) brought into contact with the beam when it is handled on site. And even if these scratches are not deep enough to reach the critical crack depth for fast fracture, they can still grow under static load by *slow crack growth* (see Chapter 19, Section 19.8). However, as long as the surface is in residual compression, surface flaws cannot propagate, either by fast fracture or slow crack growth.

When the glass beam is loaded, of course, there is a transfer of compressive stress from the bottom of the beam to the top (see Figure 22.5). At a sufficiently large bending moment, the net compressive stress at the bottom of the beam becomes zero. If the beam is designed so that it does not go into tension in service, then there should be a very low risk of failure.

As an additional precaution against catastrophic failure, the beam may be *laminated* from a number of separate toughened glass plates stuck together with *interlayers* made from thermoplastic polymers (see Figure 22.5). The interlayers are produced as thin sheet ≈ 1 mm thick. They are placed between the glass plates, and the assembly is then subjected to high temperature and pressure in an autoclave (to melt the polymer, stick it to the glass surfaces, and weld-up any voids). The following link gives details of a commercial interlayer product for high-stress structural use (SentryGlas) which has a large modulus (0.3 GN m^{-2}), tensile strength (35 MN m^{-2}), and strain to failure (400%).

http://www2.dupont.com/SafetyGlass/en_US/products/sentryglas.html

If one of the glass plates were to fail, the interlayer would stop the cracks propagating into the next plate. If a large factor of safety is required, the beam can be designed so that it can carry the required load even if one or more of the individual glass plates were to fail.

Figures 22.6 and 22.7 show an example of a design for a large glass roof, at Christ's College, Cambridge, UK—52 12 18.70 N 0 07 21.00 E. The project involves building a new library on the site of an earlier building dating from the 1970s.

http://www.christs.cam.ac.uk/college-life/library/library_court_project/



FIGURE 22.6
Library Court, Christ's College, Cambridge, UK.

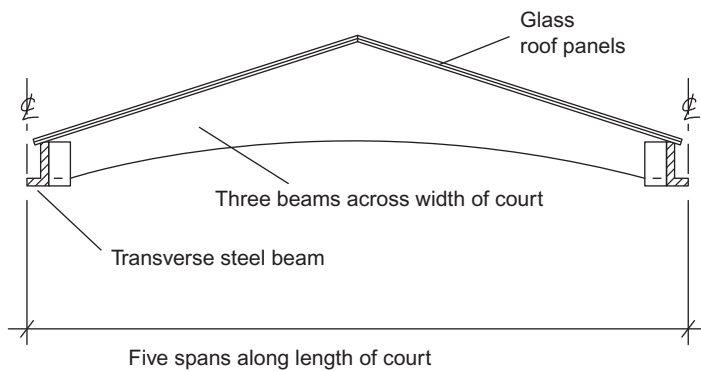


FIGURE 22.7
Schematic of glass roof for Library Court.

As part of this project, the open space between the old college buildings (dating from 1505) and the new library ("Library Court") is to be covered with a glass roof, level with the roof of the 1505 building. The area of the court is too large to allow the roof to be supported entirely with glass beams,

but although the beams across the width of the court are steel, those along its length are glass. Each beam is fabricated from three separate glass plates stuck together with a polymer interlayer (for the reasons given above) and is designed to take the load of the roof even if two of the three plates were to fail.

WORKED EXAMPLE

A danger of working in a particular discipline—like structural engineering, for example—is that you can develop a degree of tunnel vision and be unaware of things that people in other areas of technology and commerce take for granted. We can easily become so focussed on the need to stop ceramics suffering brittle, catastrophic failure in structural applications that we lose sight of the fact that we could not actually use natural ceramics unless they *were* brittle and fractured easily. Of course, one could argue that the era of making tools by knapping (fracturing) flint is now long gone (although it is not certain how far we would have developed without the flint tools of our forebears); and vitreous tiles could replace the slates previously split and trimmed from natural slate. However, we would still like to cut tiles or glass sheets to shape by scoring the surface with a diamond point and bending them; or demolish a brick building with a ball crane; or break up reinforced concrete with jackhammers. Not being able to do such things would be but a small inconvenience when you realize that without the very low fracture toughness of ceramics, we could not quarry stone (no amount of explosives would shatter a ductile rock face) or make cement; we could not excavate cuttings or tunnels, or drill for oil, or mine for minerals; and ice (another natural ceramic) could not be broken by icebreakers, or chipped away by the crampons, ice axes, and ice screws of winter climbers. If ceramics were as tough as metals, we could make wonderful aero engines. But most other things in life would be impossible. Reflect that, on balance, it is a very good thing that ceramics *are* so brittle!

EXAMPLES

- 22.1** Explain why glass must always be cut to its final dimensions (and any holes drilled) *before* tempering and never afterward.
- 22.2** Rewrite the Weibull equations, Equations (19.2) and (19.3), for the situation where flaws are only present in the *surface* of the material (as in glass).
- 22.3** Modulus of rupture tests are carried out on glass microscope slides (loaded and supported on their faces, not their edges). The width of the slides, w , is much greater than their thickness, t . The distance between

the support rollers is ℓ . Show that the stress integral in Equation (19.2) is given by

$$\frac{w\ell\sigma_r^m}{(m+1)},$$

where m is the Weibull modulus for the glass. Hence, show that the tensile strength of the glass is related to the modulus of rupture by the equation

$$\sigma_{TS} = \frac{\sigma_r}{\{2(m+1)\}^{1/m}}.$$

Calculate the ratio σ_r/σ_{TS} for $m = 10$.

Answer

1.36.

- 22.4** The glass slides are now tested by applying a bending moment to each end (putting them into a state of *pure bending*). Show that the tensile strength is related to the maximum bending stress σ_b by the equation

$$\sigma_{TS} = \frac{\sigma_b}{2^{1/m}}.$$

Calculate the ratio σ_b/σ_{TS} for $m = 10$. Explain why σ_b is only 7% greater than σ_{TS} , whereas in Example 22.3, σ_r is 36% greater than σ_{TS} .

Answer

1.07.

- 22.5** Give examples of how brittle fracture in ceramics is *useful*.
- 22.6** What type of glass was used for the following items which were subjected to a big impact: (a) a shower screen which broke up into a huge number of small dice-shaped pieces, (b) a car windscreen which developed a long crack going right across the driver's field of view, (c) a window pane which broke up into large shards?
- 22.7** Ballast for railroad tracks is usually obtained from quarried stone (such as granite), broken down in crushing mills to produce the correct size of stones. <http://www.cloburn.co.uk/commercial-products/railway-track-ballast>
Because the stones are angular in shape, with sharp edges, they interlock in the compacted ballast and provide a stable (nonshifting) base for the track ties. (Pebbles and gravel, worn smooth by the passage of water over geological time are useless as track ballast—just see how they move when you walk on them.) Why does the crushing mill produce angular stones?

Polymers

23.1 INTRODUCTION

Almost all biological systems are built of polymers which not only perform mechanical functions (like wood, bone, cartilage, and leather) but also contain and regulate chemical reactions (like leaf, veins, and cells). People use these natural polymers, of course, and have done so for many thousands of years. But it was only in the last 100 years or so that they learned how to make polymers of their own. Early efforts (bakelite, celluloid, formaldehyde plastics) were floppy and not very strong; it is a characteristic of most simple synthetic polymers that their stiffness (for a given section) is much less than that of metal or, indeed, wood, or bone. That is because wood and bone are composites: they are really made up of stiff fibers or particles, embedded in a matrix of simple polymer.

People have learned how to make composites too: the industries which make glass-, carbon-, or Kevlar-fiber-reinforced polymers (GFRP, CFRP, or KFRP) enjoy a faster growth rate than most other branches of materials production. These materials are stiff, strong, and light. Though expensive, they are finding increasing use in aerospace, transport, and sporting goods. And there are many opportunities for their wider application in other fields like hiking equipment, medical goods, and even apparently insignificant things like spectacle frames: worldwide at least 10^9 people wear spectacles.

The newer polymers are as exciting as the newer composites. By crystallizing, or by cross-linking, or by orienting the chains, new polymers are made which are as stiff as aluminum; they quickly find their way into production. New processing methods can impart resistance to heat as well as to mechanical deformation, opening up ranges of application for polymers which have penetrated heavily into a market which used to be dominated by metals. No designer can afford to neglect the opportunities offered by polymers and composites.

But it is a mistake to imagine that metal components can simply be replaced by components of these newer materials without rethinking the design. Polymers are less stiff, less strong, and less tough than most metals, so the new component requires careful redesign. Composites, it is true, are stiff and strong. But they are often very anisotropic, and because they are bound by polymers, their properties can change significantly with small changes in temperature. Proper design with polymers requires a good understanding of their properties and where they come from. That is the function of these next five chapters.

In this chapter, we introduce the main engineering polymers. They form the basis of a number of major industries, among them paints, rubbers, plastics, synthetic fibers, and paper. As with metals and ceramics, there is a bewilderingly large number of polymers and the number increases every year. So we shall select a number of “generic” polymers which typify their class; others can be understood in terms of these. The classes of interest to us here are:

- (a) *Thermoplastics* such as polyethylene, which soften on heating.
- (b) *Thermosets* or *resins* such as epoxy which harden when two components (a resin and a hardener) are heated together.
- (c) *Elastomers* or *rubbers*.
- (d) *Natural polymers* such as cellulose, lignin, and protein, which provide the mechanical basis of most plant and animal life.

Although their properties differ widely, all polymers are made up of long molecules with a covalently bonded backbone of carbon atoms. These long molecules are bonded together by weak Van der Waals and hydrogen (“secondary”) bonds, or by these plus covalent cross-links. The melting point of the weak bonds is low, not far from room temperature. So we use these materials at a high fraction of the melting point of the weak bonds (though not of the much stronger covalent backbone). Not surprisingly, they show some of the features of a material near its melting point: they *creep*, and the elastic deflection which appears on loading increases with time. This is just one important way in which polymers differ from metals and ceramics, and it necessitates a different design approach.

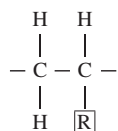
Most polymers are made from oil; the technology needed to make them from coal is poorly developed. But one should not assume that dependence on oil makes the polymer industry specially vulnerable to oil price or availability. The value added when polymers are made from crude oil is large. So doubling the price of oil does not double the price of the polymer. And the energy content of metals is large too: that of aluminum is nearly twice as great as that of most polymers. So polymers are no more sensitive to energy prices than are most other commodities, and they are likely to be with us for a very long time to come.

23.2 GENERIC POLYMERS

Thermoplastics

Polyethylene is the commonest of the thermoplastics. They are often described as *linear* polymers, that is the chains are not cross-linked (though they may branch occasionally). That is why they soften if the polymer is heated: the secondary bonds which bind the molecules to each other melt so that it flows like a viscous liquid, allowing it to be formed. The molecules in linear polymers have a range of molecular weights, and they pack together in a variety of configurations. Some, like polystyrene, are amorphous; others, like polyethylene, are partly crystalline. This range of molecular weights and packing geometries means that thermoplastics do not have a sharp melting point. Instead, their viscosity falls over a range of temperature, like that of an inorganic glass.

Thermoplastics are made by adding together (“polymerizing”) subunits (“monomers”) to form long chains. Many of them are made of the unit



repeated many times. The radical $\boxed{\text{R}}$ may simply be hydrogen (as in polyethylene), or $-\text{CH}_3$ (polypropylene) or $-\text{Cl}$ (polyvinylchloride). A few, like nylon, are more complicated. The generic thermoplastics are listed in Table 23.1. The fiber and film-forming polymers polyacrylonitrile (ACN) and polyethylene terephthalate (PET, Terylene, Dacron, Mylar) are also thermoplastics.

Thermosets or resins

Epoxy, familiar as an adhesive and as the matrix of fiberglass, is a thermoset (Table 23.2). Thermosets are made by mixing two components (a *resin* and a *hardener*) which react and harden, either at room temperature or on heating. The resulting polymer is usually heavily cross-linked, so thermosets are sometimes described as *network* polymers. The cross-links form during the polymerization of the liquid resin and hardener, so the structure is almost always amorphous. On reheating, the additional secondary bonds melt, and the modulus of the polymer drops; but the cross-links prevent true melting or viscous flow so the polymer cannot be hot-worked (it turns into a rubber). Further heating just causes it to decompose.

The generic thermosets are the epoxies and the polyesters (both widely used as matrix materials for fiber-reinforced polymers) and the formaldehyde-based

Table 23.1 Generic Thermoplastics

Thermoplastic	Composition	Uses
Polyethylene, PE	$\left(\begin{array}{c} \text{H} \\ \\ -\text{C}- \\ \\ \text{H} \end{array} \right)_n$ Partly crystalline.	Tubing, film, bottles, cups, electrical insulation, packaging.
Polypropylene, PP	$\left(\begin{array}{cc} \text{H} & \text{H} \\ & \\ -\text{C} & -\text{C}- \\ & \\ \text{H} & \text{CH}_3 \end{array} \right)_n$ Partly crystalline.	Same uses as PE, but lighter, stiffer, more resistant to sunlight.
Polytetrafluoroethylene, PTFE	$\left(\begin{array}{c} \text{F} \\ \\ -\text{C}- \\ \\ \text{F} \end{array} \right)_n$ Partly crystalline.	Teflon. Good, high-temperature polymer with very low friction and adhesion characteristics. Nonstick saucepans, bearings, seals.
Polystyrene, PS	$\left(\begin{array}{cc} \text{H} & \text{H} \\ & \\ -\text{C} & -\text{C}- \\ & \\ \text{H} & \text{C}_6\text{H}_5 \end{array} \right)_n$ Amorphous.	Cheap molded objects. Toughened with butadiene to make high-impact polystyrene (HIPS). Foamed with CO ₂ to make common packaging.
Polyvinylchloride, PVC	$\left(\begin{array}{cc} \text{H} & \text{H} \\ & \\ -\text{C} & -\text{C}- \\ & \\ \text{H} & \text{Cl} \end{array} \right)_n$ Amorphous.	Architectural uses (window frames, etc.). Plasticized to make artificial leather, hoses, clothing.
Polymethylmethacrylate, PMMA	$\left(\begin{array}{cc} \text{H} & \text{CH}_3 \\ & \\ -\text{C} & -\text{C}- \\ & \\ \text{H} & \text{COOCH}_3 \end{array} \right)_n$ Amorphous.	Perspex, lucite. Transparent sheet and moldings. Aircraft windows, laminated windscreens.
Nylon 66	$(-\text{C}_6\text{H}_{11}\text{NO}-)_n$ Partly crystalline when drawn.	Textiles, rope, moldings.

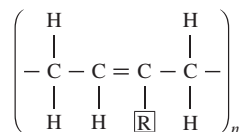
Table 23.2 Generic Thermosets or Resins

Thermoset	Composition	Uses
Epoxy	$\left(\begin{array}{c} \text{CH}_3 \qquad \qquad \text{OH} \\ \qquad \qquad \qquad \\ -\text{O}-\text{C}_6\text{H}_4-\text{C}-\text{C}_6\text{H}_4-\text{O}-\text{CH}_2-\text{CH}-\text{CH}_2- \\ \\ \text{CH}_3 \end{array} \right)_n$ <p>Amorphous.</p>	Fiberglass, adhesives. Expensive.
Polyester	$\left(\begin{array}{c} \text{O} \qquad \qquad \text{O} \qquad \qquad \text{CH}_2\text{OH} \\ \qquad \qquad \qquad \qquad \\ -\text{C}-(\text{CH}_2)_m-\text{C}-\text{O}-\text{C}- \\ \\ \text{CH}_2\text{OH} \end{array} \right)_n$ <p>Amorphous.</p>	Fiberglass, laminates. Cheaper than epoxy.
Phenolformaldehyde	$\left(\begin{array}{c} \text{OH} \\ \\ -\text{C}_6\text{H}_2-\text{CH}_2- \\ \\ \text{CH}_2 \end{array} \right)_n$ <p>Amorphous.</p>	Bakelite, Tufnol, Formica. Rather brittle.

plastics (widely used for molding and hard surfacing). Other formaldehyde plastics, which now replace bakelite, are ureaformaldehyde (used for electrical fittings) and melamine–formaldehyde (used for tableware).

Elastomers

Elastomers or rubbers are almost-linear polymers with occasional cross-links in which, at room temperature, the secondary bonds have already melted. The cross-links provide the “memory” of the material so that it returns to its original shape on unloading. The common rubbers are all based on the single structure



with the position $\boxed{\text{R}}$ occupied by H, CH₃, or Cl. They are listed in [Table 23.3](#).

Table 23.3 Generic Elastomers (Rubbers)

Elastomer	Composition	Uses
Polyisoprene	$\left(\begin{array}{c} \text{H} \qquad \qquad \text{H} \\ \qquad \qquad \\ -\text{C} - \text{C} = \text{C} - \text{C}- \\ \qquad \qquad \qquad \\ \text{H} \quad \text{H} \quad \text{CH}_3 \quad \text{H} \end{array} \right)_n$ <p>Amorphous except at high strains.</p>	Natural rubber.
Polybutadiene	$\left(\begin{array}{c} \text{H} \qquad \qquad \text{H} \\ \qquad \qquad \\ -\text{C} - \text{C} = \text{C} - \text{C}- \\ \qquad \qquad \qquad \\ \text{H} \quad \text{H} \quad \text{H} \quad \text{H} \end{array} \right)_n$ <p>Amorphous except at high strains.</p>	Synthetic rubber, car tires.
Polychloroprene	$\left(\begin{array}{c} \text{H} \qquad \qquad \text{H} \\ \qquad \qquad \\ -\text{C} - \text{C} = \text{C} - \text{C}- \\ \qquad \qquad \qquad \\ \text{H} \quad \text{H} \quad \text{Cl} \quad \text{H} \end{array} \right)_n$ <p>Amorphous except at high strains.</p>	Neoprene. An oil-resistant rubber used for seals.

Natural polymers

The rubber polyisoprene is a natural polymer. So, too, are cellulose and lignin, the main components of wood and straw, and so are proteins like wool or silk. We use cellulose in vast quantities as paper and (by treating it with nitric acid), we make celluloid and cellophane out of it. But the vast surplus of lignin left from wood processing, or available in straw, cannot be processed to give a useful polymer. If it could, it would form the base for a vast new industry. The natural polymers are not as complicated as you might expect. They are listed in [Table 23.4](#).

23.3 MATERIAL DATA

Data for the properties of the generic polymers are shown in [Table 23.5](#). But you have to be particularly careful in selecting and using data for the properties of polymers. Specifications for metals and alloys are defined fairly tightly; two pieces of Type 316 L stainless steel from two different manufacturers will differ very little. Not so with polymers: polyethylene made by one manufacturer may be very different from polyethylene made by another. It is

Table 23.4 Generic Natural Polymers

Natural Polymer	Composition	Uses
Cellulose	$(-C_6H_9O_6-)_n$ Crystalline.	Framework of all plant life, as the main structural component in cell walls.
Lignin	Amorphous.	The other main component in cell walls of all plant life.
Protein	$\left(\begin{array}{c} \boxed{R} \\ \\ -NH-C-C- \\ \quad \\ H \quad O \end{array} \right)_n$ <p>\boxed{R} is a radical. Partly crystalline.</p>	Gelatin, wool, silk.

partly because all polymers contain a spectrum of molecular lengths; slight changes in processing change this spectrum. But it is also because details of the polymerization change the extent of molecular branching and the degree of crystallinity in the final product; and the properties can be further changed by mechanical processing (which can, in varying degrees, align the molecules) and by proprietary additives. For all these reasons, data from compilations (like Table 23.5), or data books, are at best *approximate*. For accurate data, you *must* use the manufacturers' data sheets or conduct your own tests.

There are other ways in which polymer data differ from those for metals or ceramics. Polymers are held together by two sorts of bonds: strong covalent bonds which form the long chain backbone and weak secondary bonds which stick the long chains together. At the glass temperature T_G , which is always near room temperature, the secondary bonds melt, leaving only the covalent bonds. The moduli of polymers reflect this. Below T_G most polymers have a modulus of around 3 GN m^{-2} . (If the polymer is *drawn* to fibers or sheet, the molecules are aligned by the drawing process, and the modulus in the draw-direction can be larger.) But even if T_{room} is below T_G , T_{room} will still be a large fraction of T_G . Under load, the secondary bonds creep, and the modulus falls. Table 23.5 lists moduli for a loading time of 100 s at room temperature (20°C); for loading times of 1000 h, the modulus can fall to one-third of that for the short (100 s) test. And above T_G , the secondary bonds melt completely: linear polymers become very viscous liquids and cross-linked polymers become rubbers. Then the modulus can fall dramatically, from 3 GN m^{-2} to 3 MN m^{-2} or less.

Table 23.5 Properties of Polymers

Polymer	Density (Mg m ⁻³)	Youngs Modulus (20 °C 100 s) (GN m ⁻²)	Tensile Strength (MN m ⁻²)	Fracture Toughness (20 °C) (MN m ^{-3/2})	Glass Temperature <i>T_G</i> (K)	Softening Temperature <i>T_s</i> (K)	Specific Heat (J Kg ⁻¹ K ⁻¹)	Thermal Conductivity (Wm ⁻¹ K ⁻¹)	Thermal Coefficient (MK ⁻¹)
<i>Thermoplastics</i>									
Polyethylene, PE (low density)	0.91–0.94	0.15–0.24	7–17	1–2	270	355	2250	0.35	160–190
Polyethylene, PE (high density)	0.95–0.98	0.55–1.0	20–37	2–5	300	390	2100	0.52	150–300
Polypropylene, PP	0.91	1.2–1.7	50–70	3.5	253	310	1900	0.2	100–300
Polytetrafluoroethylene, PTFE	2.2	0.35	17–28	–	–	395	1050	0.25	70–100
Polystyrene, PS	1.1	3.0–3.3	35–68	2	370	370	1350–1500	0.1–0.15	70–100
Polyvinyl chloride, PVC (unplasticized)	1.4	2.4–3.0	40–60	2.4	350	370	–	0.15	50–70
Polymethylmethacrylate, PMMA	1.2	3.3	80–90	1	378	400	1500	0.2	54–72
Nylons	1.15	2–3.5	60–110	3–5	340	350–420	1900	0.2–0.25	80–95
<i>Resins or thermosets</i>									
Epoxies	1.2–1.4	2.1–5.5	40–85	0.6–1.0	380	400–440	1700–2000	0.2–0.5	55–90
Polyesters	1.1–1.4	1.3–4.5	45–85	0.5	340	420–440	1200–2400	0.2–0.24	50–100
Phenolformaldehyde	1.27	8	35–55	–	–	370–550	1500–1700	0.12–0.24	26–60
<i>Elastomers (rubbers)</i>									
Polyisoprene	0.91	0.002–0.1	≈ 10	–	220	≈ 350	≈ 2500	≈ 0.15	≈ 600
Polybutadiene	1.5	0.004–0.1	–	–	171	≈ 350	≈ 2500	≈ 0.15	≈ 600
Polychloroprene	0.94	≈ 0.01	–	–	200	≈ 350	≈ 2500	≈ 0.15	≈ 600
<i>Natural polymers</i>									
Cellulose fibers	1.5	25–40	≈ 1000	–	–	–	–	–	–
Lignin	1.4	2.0	–	–	–	–	–	–	–
Protein	1.2–1.4	–	–	–	–	–	–	–	–

You can see that design with polymers involves considerations which may differ from those for design with metals or ceramics. And there are other differences. One of the most important is that the yield or tensile strength of a polymer is a large fraction of its modulus; typically, $\sigma_y = E/20$. This means that design based on general yield (plastic design) gives large elastic deflections, much larger than in metals and ceramics. The excessive “give” of a poorly designed polymer component is a common experience, although it is often an advantage to have deflections without damage—as in polyethylene bottles, tough plastic luggage, or car bumpers.

The nearness of T_G to room temperature has other consequences. Near T_G most polymers are fairly tough, but K_c can drop steeply as the temperature is reduced. (The early use of polymers for shelving in refrigerators resulted in frequent fractures at $+4^\circ\text{C}$. These were not anticipated because the polymer was ductile and tough at room temperature.)

The specific heats of polymers are large—typically 5 times more than those of metals when measured per kilogram. When measured per meter cube, however, they are about the same because of the large differences in density. The coefficients of thermal expansion of polymers are enormous, 10–100 times larger than those of metals. This can lead to problems of thermal stress when polymers and metals are joined. And the thermal conductivities are small, 100–1000 times smaller than those of metals. This makes polymers attractive for thermal insulation, particularly when foamed.

In summary, then, design with polymers requires special attention to time-dependent effects, large elastic deformation, and the effects of temperature, even close to room temperature. Room temperature data for the generic polymers are presented in [Table 23.5](#). As emphasized already, they are approximate, suitable only for the first step of the design project. For the next step, you should consult books, and when the choice has narrowed to one or a few candidates, data for them should be sought from manufacturers’ data sheets, or from your own tests. Many polymers contain additives—plasticizers, fillers, colorants—which change the mechanical properties. Manufacturers will identify the polymers they sell but will rarely disclose their additives. So it is essential, in making a final choice of material, that both the polymer and its source are identified and data *for that polymer, from that source*, are used in the design calculations.

WORKED EXAMPLE

The photograph below shows an aluminum alloy car wheel, complete with rubber tire. It is from an old Volvo and is as far away from a trendy high-performance car with huge alloy wheels and low-profile tires as you can get. Actually, alloy wheels of any sort are silly, because they are made from rather

brittle casting alloy (and they are expensive). Pressed steel wheels are more robust and a lot cheaper. Low-profile tires are silly too—they handle less well, and they put the wheel rims too close to the ground (which makes them liable to be smashed-up when driving over obstacles like speed humps or potholes). However, as engineers, it is all too easy to get diverted from where we are going by irritation at silly engineering driven by mere “fashion.” We must concentrate on the fact that rubber is the *only* material from which car tires can be made.

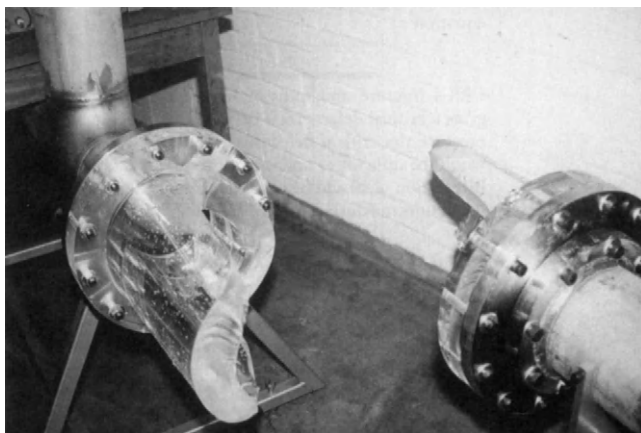


Why is this? It is because rubber has a huge elastic range, it springs back almost instantaneously after being deformed, it has adequate static strength and good fatigue resistance, it has a very large coefficient of friction against road surface materials, it has adequate resistance to wear against road surface materials, and it retains all these properties over a very large range of temperature. We would be set back 120 years without rubber tires. Road vehicles would have wheels shod with steel (like the steam engine in Figure 1.1), and road transport would be limited to low speeds over small distances. Higher speeds would quickly destroy wheels, suspension, goods, people, roads. And, as anyone who has driven a steam roller will verify, you cannot stop in a hurry (or traverse a steep hill) without risking a disastrous runaway skid. All long-distance transport would be by rail (the use of steel tired wheels is made possible by a road of steel—literally the “railroad”—which is flat, true, hard, and dead level). Transport within all urban areas would be by trams. Of course, many would argue that we were very stupid in the 1950s and 1960s to have torn up so much of the investment made in railway networks and tram systems in the nineteenth and early twentieth centuries—a policy which can be blamed squarely on the explosive growth of motor car

ownership over that period—and it would be nice to go back to an age before the motor car destroyed so much. But reflect on the fact that you cannot land an aeroplane without rubber tires (well, apart from a sea-plane, and they were slow and lumbering). Now, not being able to do that really would mean a massive step backward for the planet as we know it.

EXAMPLES

- 23.1** What are the four main generic classes of polymers? For each generic class:
- (a) give one example of a specific component made from that class,
 - (b) indicate why that class was selected for the component.
- 23.2** How do the unique characteristics of polymers influence the way in which these materials are used?
- 23.3** The photograph shows a flanged connector in an internally pressurized piping system. The material is a polymethylmethacrylate (PMMA). The connector failed during a hydrostatic pressure test, at a pressure of only 70% of the working pressure. At this point, the maximum hoop stress had reached 10 MN m^{-2} . Table 23.5 gives a tensile strength of 80 MN m^{-2} minimum for PMMA. Why do you think the connector failed at only 1/8 of this value? Justify your explanation with a short calculation. Why is PMMA a poor choice of material for the connector? What materials property in Table 23.5 is the critical design parameter in this application? The wall thickness of the tubular portion of the connector is 50 mm.



Flanged connector in an internally pressurized piping system.

- 23.4** Take a look around your home. Write a representative list of the things you see which are made from polymers. Assign each item to one of the four generic classes of polymers. List specialized applications of polymers (where only one or a very limited range of polymers will perform adequately in the service environment).

- 23.5** The lenses of reading glasses were traditionally made from glass. However, they are now being made from polymers as well.

http://en.wikipedia.org/wiki/Corrective_lens

What are the advantages and disadvantages of polymer lenses over glass lenses?

- 23.6** A specimen of polymer is tested in tension to measure its Young's modulus. It is found that the modulus (nominal stress divided by nominal strain) decreases as the duration of the test increases. Explain this observation.
- 23.7** What properties of rubber makes it the best material for road vehicle tires?
- 23.8** Explain why hot-working operations can be done on thermoplastics but not thermosets.
- 23.9** Explain briefly why the properties of a component made from a polymer like polyethylene can be strongly influenced by details of how the various processes are carried out.
- 23.10** Summarize briefly the ways in which design with polymers differs from design with (a) metals and (b) ceramics.

Polymer Structures

24.1 INTRODUCTION

If the architecture of metal crystals is thought of as classical, then that of polymers is baroque. The metal crystal is infused with order, as regular and symmetrical as the Parthenon; polymer structures are as exotic and convoluted as an Austrian altarpiece. Some polymers, it is true, form crystals, but the molecular packing in these crystals is more like that of the woven threads in a horse blanket than like the neat stacking of spheres in a metal crystal. Most are amorphous, and then the long molecules twine around each other like a bag full of tangled rope. And even the polymers which can crystallize are, in the bulk form in which engineers use them, only partly crystalline: segments of the molecules are woven into little crystallites, but other segments form a hopeless amorphous tangle in between.

The simpler polymers (like polyethylene, PMMA, and polystyrene) are linear: the chains, if straightened out, would look like a piece of string. These are the thermoplastics: if heated, the strings slither past each other and the polymer softens and melts. And, at least in principle, these polymers can be drawn in such a way that the flow orients the strings, converting the amorphous tangle into sheet or fiber in which the molecules are more or less aligned. Then the properties are much changed: if you pull on the fiber (for example) you now stretch the molecular strings instead of merely unraveling them, and the stiffness and strength you measure are much larger than before.

The less simple polymers (like the epoxies, polyesters, and formaldehyde-based resins) are networks: each chain is cross-linked in many places to other chains, so that, if stretched out, the array would look like a piece of Belgian lace, somehow woven in three dimensions. These are the thermosets: if heated, the structure softens but it does not melt; the cross-links prevent viscous flow. Thermosets are usually a bit stiffer than amorphous thermoplastics

because of the cross-links, but they cannot easily be crystallized or oriented, so there is less scope for changing their properties by processing.

In this chapter, we review the essential features of polymer structures. They are more complicated than those of metal crystals, and there is no formal framework (like that of crystallography) in which to describe them exactly. But a looser, less precise description is possible and is of enormous value in understanding the properties that polymers exhibit.

24.2 MOLECULAR LENGTH

Ethylene, C_2H_4 , is a molecule. We can represent it as shown in Figure 24.1 (a), where the square box is a carbon atom and the small circles are hydrogen. Polymerization breaks the double bond, activating the ethylene monomer (Figure 24.1(b)), and allowing it to link to others, forming a long chain or *macromolecule* (Figure 24.1(c)). The ends of the chain are a problem: they either link to other macromolecules or end with a *terminator* (such as an $-OH$ group), shown as a round blob.

If only two or three molecules link, we have created a polymer. But to create a solid with useful mechanical properties, the chains must be longer—at least 500 monomers long. They are called *high polymers* (to distinguish them

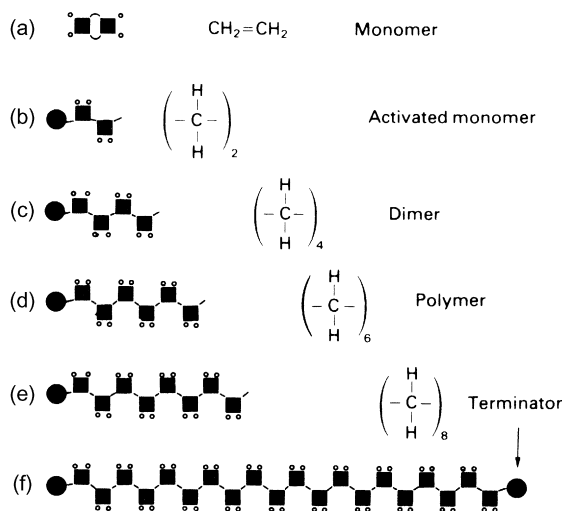


FIGURE 24.1

(a) The ethylene molecule or monomer; (b) the monomer in the activated state, ready to polymerize with others; (c)–(f) the ethylene polymer (“polyethylene”); the chain length is limited by the addition of terminators like $-OH$. The DP is the number of monomer units in the chain.

from the short ones) and, obviously, their length, or total molecular weight, is an important feature of their structure. It is usual to speak of the *degree of polymerization* or DP: the number of monomer units in a molecule. Commercial polymers have a DP in the range 10^3 – 10^5 .

The molecular weight of a polymer is simply the DP times the molecular weight of the monomer. Ethylene, C_2H_4 , for example, has a molecular weight of 28. If the DP for a batch of polyethylene is 10^4 , then the molecules have an *average* molecular weight of 280,000. The word “average” is significant. In all commercial polymers there is a range of DP, and thus of molecular lengths (Figure 24.2(a)). Then the average is simply

$$\overline{DP} = \int_0^{\infty} DP P(DP) d(DP) \quad (24.1)$$

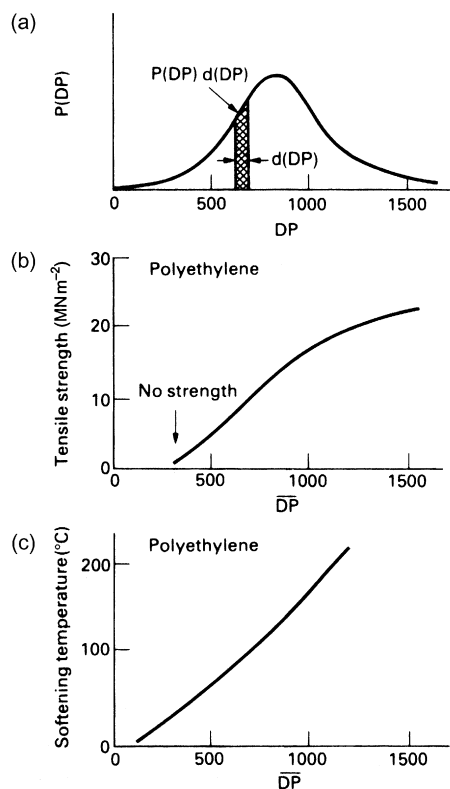


FIGURE 24.2

(a) Linear polymers are made of chains with a spectrum of lengths or DPs. The probability of a given DP is $P(DP)$; (b) and (c) the strength, the softening temperature, and many other properties depend on the average DP.

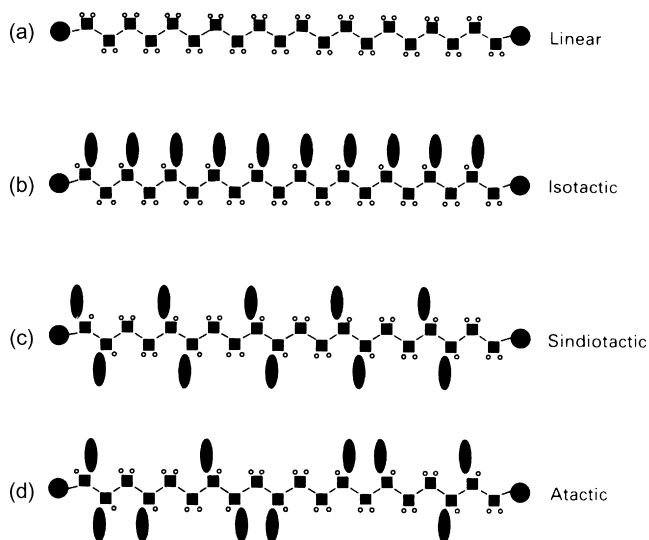
where $P(\text{DP})d(\text{DP})$ is the fraction of molecules with DP values between DP and $\text{DP} + d(\text{DP})$. The molecular weight is just $m\overline{\text{DP}}$, where m is the molecular weight of the monomer.

Most polymer properties depend on the average DP. Figure 24.2(b,c), for polyethylene, shows two: the tensile strength and the softening temperature. $\overline{\text{DP}}$ s of less than 300 give no strength because the short molecules slide apart too easily. The strength rises with $\overline{\text{DP}}$, but so does the viscosity; it is hard to mold polyethylene if the $\overline{\text{DP}}$ is much above 10^3 . The important point is that a material like polyethylene does not have a unique set of properties. There are many polyethylenes; the properties of a given batch depend on (among other things) the molecular length or $\overline{\text{DP}}$.

24.3 MOLECULAR ARCHITECTURE

Thermoplastics are the largest class of engineering polymer. They have linear molecules: they are not cross-linked, and for that reason they soften when heated, allowing them to be formed (ways of doing this are described in Chapter 26). Monomers which form linear chains have two active bonds (they are *bifunctional*). A molecule with only one active bond can act as a chain terminator, but it cannot form a link in a chain. Monomers with three or more active sites (*polyfunctional* monomers) form networks: they are the basis of thermosetting polymers or resins.

The simplest linear-chain polymer is polyethylene (Figure 24.3(a)). By replacing one H atom of the monomer by a *side-group* or *radical* R (ovals in Figure 24.3(b–d)), we obtain the *vinyl* group of polymers: R = Cl gives polyvinyl chloride; R = CH₃ gives polypropylene; R = C₆H₅ gives polystyrene. The radical gives asymmetry to the monomer unit, and there is then more than one way in which the unit can be attached to form a chain. Three arrangements are shown in Figure 24.3. If all the side-groups are on the same side, the molecule is called *isotactic*. If they alternate in some regular way round the chain, it is called *sindiotactic*. If they alternate randomly, it is called *atactic*. These distinctions may seem like splitting hairs (protein, another linear polymer), but they are important: the tacticity influences properties. The regular molecules (Figure 24.3(a–c)) can stack side by side to form crystals: the regularly spaced side-groups nestle into the regular cavities of the next molecule. The irregular, atactic, molecules cannot: their side-groups clash and the molecules are forced into lower density, noncrystalline arrangements. Even the type of symmetry of the regular molecules matters: the isotactic (one sided) molecules carry a net electric dipole and can be electroactive (showing piezoelectric effects, for instance) and others cannot.

**FIGURE 24.3**

(a) Linear polyethylene; (b) an isotactic linear polymer: the side-groups are all on the same side; (c) a syndiotactic linear polymer: the side-groups alternate regularly; (d) an atactic linear polymer: the side-groups alternate irregularly.

Some polymerization processes (such as the Ziegler process for making polyethylene) are delicate and precise in their operation: they produce only linear chains and with a narrow spread of lengths. Others (like the older, high-pressure process) are crude and violent: side-groups may be torn from a part-formed molecule and other growing molecules may attach themselves there, giving *branching*. Branching hinders crystallization, just as atacticity does. Low-density polyethylene is branched, and for that reason has a low fraction of crystal ($\approx 50\%$), a low density and low softening temperature (75°C). High-density PE is not branched: it is largely crystalline ($\approx 80\%$), it is 5% denser, and it softens at a temperature which is 30°C higher.

The next simplest group of linear polymers is the *vinylidene* group. Now *two* of the hydrogens of ethylene are replaced by radicals. Polymethylmethacrylate (PMMA, Perspex, Plexiglas, or Lucite) is one of these: the two radicals are $-\text{CH}_3$ and $-\text{COOCH}_3$. Now the difficulties of getting regular arrangements increases, and most of these polymers are amorphous.

Linear-chain thermoplastics are the most widely used of polymers, partly because of the ease with which they can be formed. Their plasticity allows them to be drawn into sheet, and in so doing, the molecules become aligned in the plane of the sheet, increasing the modulus and strength in this plane. Alignment is even more dramatic when linear polymers are drawn to

fibers: the high strength of nylon, Dacron, and Kevlar fibers reflects the near-perfect lining up of the macromolecules along the fiber axis.

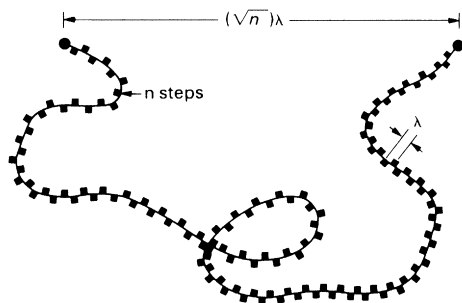
Most *thermosets* start from large polyfunctional monomers. They react with each other or with small, linking molecules (like formaldehyde) in a condensation reaction—one which plucks a —OH from one molecule and a —H from the other to give H_2O (a by-product), welding the two molecules together at the severed bonds. Since one of the two molecules is polyfunctional, random three-dimensional networks are possible. Because of the cross-linking, thermosets do not melt when heated (though they ultimately decompose), they do not easily dissolve in solvents (as linear polymers do), and they cannot be formed after polymerization (as linear polymers can). But for the same reason they are chemically more stable, are useful to a higher temperature, and are generally stiffer than thermoplastics. The irreversible setting reaction makes thermosets particularly good as adhesives, coatings, and the matrix for composites.

Elastomers are a special sort of cross-linked polymer. First, they are really linear polymers with just a few cross-links—one every hundred or more monomer units—so that a molecule with a DP of 500 might have fewer than five cross-link points along its length. And second, the polymer has a glass temperature which is well below the room temperature, so that (at room temperature) the secondary bonds have melted. Why these two features give an elastomer is explained later (Chapter 25).

24.4 MOLECULAR PACKING AND GLASS TRANSITION

Although we have drawn them as straight, a free polymer molecule is never so. Each C—C joint in its backbone has rotational freedom, so that the direction of the molecule changes at each step along the chain, allowing it to spiral, twist, and tangle in the most extravagant way. When a linear polymer melts, its structure is that of a dense spaghetti-like tangle of these meandering molecules. Each is free to slither past the others in the melt, so the chain-links bend in a random way (Figure 24.4). The average distance between the start of the chain and its end is then calculated in the same way that you calculate the distance a drunk staggers from a bar: if steps (of length λ) are equally likely in all directions (a “random walk”), the distance from the bar after n steps is $(\sqrt{n})\lambda$. So, if the polymer has n units of length λ , the distance from its head to its tail is, on average, $(\sqrt{n})\lambda$, not $n\lambda$ as you might at first think.

When the melt is cooled, the spaghetti tangle may simply freeze without rearranging; the resulting solid polymer then has an *amorphous* structure. But

**FIGURE 24.4**

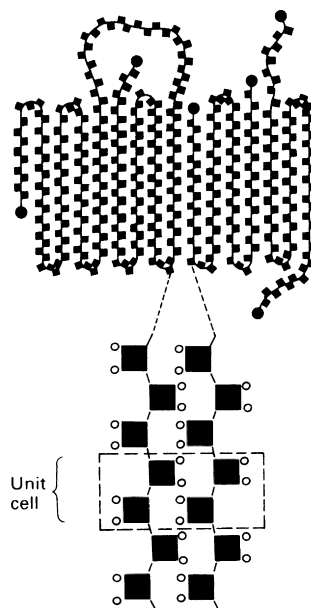
The random walk of a chain in a polymer melt, or in a solid, glassy polymer means that, on average, one end of the molecule is $(\sqrt{n}) \lambda$ away from the other end. Very large strains (≈ 4) are needed to straighten the molecule out.

during cooling, molecules can move, and (depending on their architecture) they may partly line up to form *crystallites*. We now consider each of the structures, starting with the crystallites.

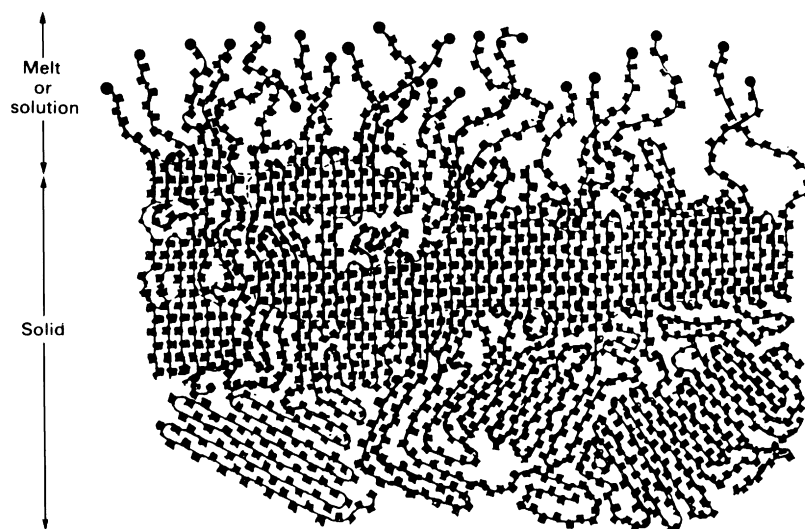
Polymer crystals

Linear-chain molecules can crystallize. High-density polyethylene is an example. The molecules have no side-groups or branches. On cooling, secondary bonds tend to pull the molecules together into parallel bundles, not perfectly crystalline, but not amorphous (devoid of all order) either. Under some circumstances, well-defined *chain-folded* crystals form (Figure 24.5): the long molecules fold like computer paper into a stack with a width much less than the length of the molecule. Actually, the crystals are rarely as neatly folded as computer paper. The folds are not perfectly even, and the tails of the molecules may not tuck in properly; it is more like a badly woven carpet. Nonetheless, the crystallinity is good enough for the polymer to diffract X-rays like a metal crystal, and a unit cell can be defined (Figure 24.5). Note that the cell is much smaller than the molecule itself.

But even the most crystalline of polymers (e.g., high-density PE) is only 80% crystal. The structure probably looks something like Figure 24.6: bundles, and chain-folded segments, make it largely crystalline, but the crystalline parts are separated by regions of disorder—amorphous, or glassy regions. Often the crystalline platelets organize themselves into *spherulites*: bundles of crystallites that, at first sight, seem to grow radially outward from a central point, giving crystals with spherical symmetry. The structure is really more complicated than that. The growing ends of a small bundle of crystallites (Figure 24.7(a)) trap amorphous materials between them, wedging them apart. More crystallites nucleate on the bundle, and they, too, splay out as

**FIGURE 24.5**

A chain-folded polymer crystal. The structure is like that of a badly woven carpet. The unit cell, shown below, is relatively simple and is much smaller than the polymer chain.

**FIGURE 24.6**

A schematic drawing of a largely crystalline polymer like high-density polyethylene. At the top the polymer has melted and the chain-folded segments have unwound.

they grow. The splaying continues until the crystallites bend back on themselves and touch; then it can go no further (Figure 24.7(b)). The spherulite then grows as a sphere until it impinges on others, to form a grain-like structure. Polythene is, in fact, like this, and polystyrene, nylon, and many other linear polymers do the same thing.

When a liquid crystallizes to a solid, there is a sharp, sudden decrease of volume at the melting point (Figure 24.8(a)). The random arrangement of the atoms or molecules in the liquid changes discontinuously to the ordered, neatly packed, arrangement of the crystal. Other properties change discontinuously at the melting point also: the viscosity, for example, changes sharply by an enormous factor (10^{10} or more for a metal). Broadly speaking, polymers behave in the same way: a crystalline polymer has a fairly well-defined melting point at which the volume changes rapidly, though the sharpness found when metals crystallize is blurred by the range of molecular weights (and thus melting points) as shown in Figure 24.8(b). For the same reason, other polymer properties (like the viscosity) change rapidly at the melting point, but the true discontinuity of properties found in simple crystals is lost.

When, instead, the polymer solidifies to a glass (an amorphous solid), the blurring is much greater, as we shall now see.

Amorphous polymers

Cumbersome side-groups, atacticity, branching, and cross-linking all hinder crystallization. In the melt, thermal energy causes the molecules to rearrange

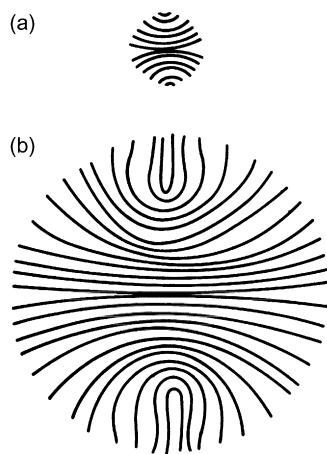
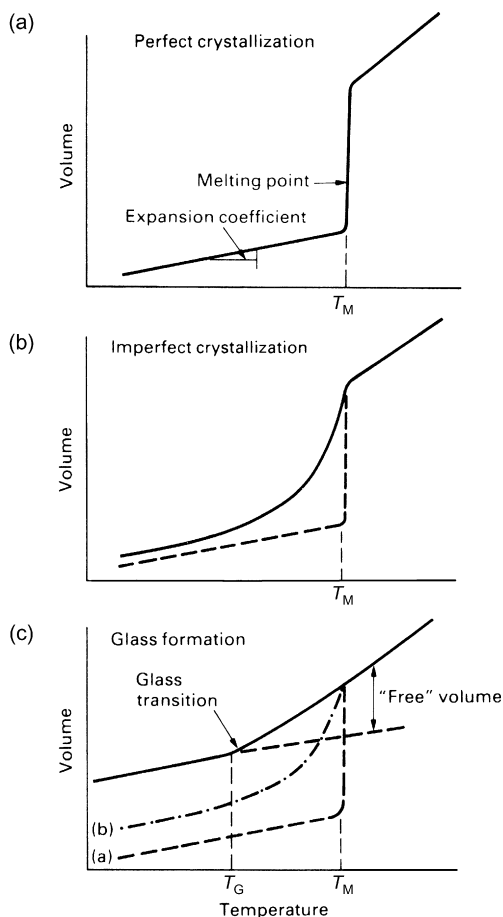


FIGURE 24.7

The formation and structure of a spherulite.

**FIGURE 24.8**

(a) The volume change when a simple melt (like a liquid metal) crystallizes defines the melting point, T_M ; (b) the spread of molecular weights blurs the melting point when polymers crystallize; (c) when a polymer solidifies to a glass the melting point disappears completely, but a new temperature at which the free volume disappears (the glass temperature, T_G) can be defined and measured.

continuously. This wriggling of the molecules increases the volume of the polymer. The extra volume (over and above that needed by tightly packed, motionless molecules) is called the *free volume*. It is the free volume, aided by the thermal energy, that allows the molecules to move relative to each other, giving viscous flow.

As the temperature is decreased, free volume is lost. If the molecular shape or cross-linking prevent crystallization, then the liquid structure is retained, and

free volume is not all lost immediately (Figure 24.8(c)). As with the melt, flow can still occur, though naturally it is more difficult, so the viscosity increases. As the polymer is cooled further, more free volume is lost. There comes a point at which the volume, though sufficient to contain the molecules, is too small to allow them to move and rearrange. All the free volume is gone, and the curve of specific volume flattens out (Figure 24.8(c)). This is the *glass transition temperature*, T_G . Below this temperature, the polymer is a *glass*.

The glass transition temperature is as important for polymers as the melting point is for metals (data for T_G are given in Table 23.5). Below T_G , secondary bonds bind the molecules into an amorphous solid; above, they start to melt, allowing molecular motion. The glass temperature of PMMA is 100 °C, so at room temperature it is a brittle solid. Above T_G , a polymer becomes first *leathery*, then *rubbery*, capable of large elastic extensions without brittle fracture. The glass temperature for natural rubber is around −70 °C, and it remains flexible even in the coldest winter; but if it is cooled to −196 °C in liquid nitrogen, it becomes hard and brittle, like PMMA at room temperature.

That is all we need to know about structure for the moment, though more information can be found in the books listed under References. We now examine the origins of the strength of polymers in more detail, seeking the criteria which must be satisfied for good mechanical design.

WORKED EXAMPLE

The photograph shows an everyday example of a thermoset—the well-known “Araldite” glue, much used in home and shed for gluing things together. This is a *two-part epoxy resin*—the *resin* (called “adhesive” on the tube) and the *hardener* are mixed together in equal quantities by volume, then applied to the areas to be joined. The mixture needs to be used within about an hour, otherwise the polymerization reaction starts to increase the viscosity significantly. Ninety percent of full strength is reached after about 48 h of curing at room temperature (20 °C). If the mixture is heated to say 100 °C, the viscosity decreases dramatically—the glue flows over and into the joint surfaces much better. The curing rate goes up dramatically too—because the reaction is a thermally activated process, which obeys Arrhenius’s law. At 100 °C, 90% of full strength is reached after only 2 h.



Epoxy resins were developed in the 1930s and, along with other thermoset adhesives, soon found their way into an increasingly large number of applications.

<http://en.wikipedia.org/wiki/Epoxy>

One of the most major (and critical) uses was (and is) in aircraft structures—bonding together aluminum airframe parts (and wood in the early days). A pioneering example of this was in the ill-fated Comet aircraft of 1952. In the fuselage, all the longitudinal stringers were glued to the skin, as were the seams of the rear pressure dome. In the wings, internal stringers, stiffeners, and doublers were glued, as were internals within the ailerons and flaps. There are many manufacturing advantages to gluing structural elements together instead of riveting or bolting, one of the most important being that gluing does away with rivet holes, which are a major source of stress concentrations—and hence of fatigue cracking. We saw in EM1Ed4, Section 19.1 that the Comet air disasters were caused by fatigue cracking which started at rivet holes near the edges of openings in the fuselage (for ADF windows and escape hatches). The irony was that doublers which were riveted around the edges of these openings were originally meant to be glued to the fuselage skin. However, at a late stage this method was abandoned, and riveted connections were used instead, in the interests of easier assembly. Had this change not been made, it is probable that the Comet disasters would not have occurred.

Many aircraft in service today have major components joined together by thermoset adhesives. These include bonding stringers to skins in both fuselage and wing structures, and bonding aluminum honeycomb cores to skins of control surfaces such as elevators, ailerons, and spoilers. Well-known types of aircraft that have seen long service using structural adhesives include the Boeing 737 (1967) and Airbus A310 (1982).

Adhesives for bonding aircraft structures generally use *one-part resins* rather than two-part resins (as in Araldite). The components are supplied ready mixed and have a long shelf life, especially if kept refrigerated (≈ 12 months at 0°C , ≈ 3 months at 20°C). Once the joints have been assembled, the adhesive is cured by heating the parts in heated presses or autoclaves (typically 170°C for 1 h). The adhesive used for the Comet was in fact a *phenolic resin* (not an epoxy resin), with the proprietary name of Redux 775.

<http://www.hexcel.com/products>

This is still the most widely used airframe adhesive, not because it is the strongest (that is epoxy), but because it has the best long-term durability in service, especially when exposed to things like warm water and warm humid air.

Until the 1960s, the glue was brushed on to the surfaces to be joined, which were then clamped together and warmed up to the curing temperature. Then came a major development which transformed the assembly process. The adhesive mix was processed into a thin film, backed with paper on one side and polythene sheet on the other (a bit like double-sided cellotape, but with paper backing on *both* sides). Strips or patches of sheet were then cut to the outline of the areas to be joined. The paper was peeled off, and the newly exposed surface of the film was pressed down on to the lower of the two joint surfaces. The polythene was then peeled off the other side of the film, and the upper joint surface was pressed down on to the film. The joint was then clamped and cured as normal.

As always in any manufacturing process, the devil is in the detail—this is why on-the-job know-how is so important. There are all sorts of little things that are important to the success of the joining process and the end result. For example, the phenolic resins involve a *condensation reaction*, which generates water as a by-product (see Chapter 26). The steam produced at the curing temperature would push the joint surfaces apart unless they were clamped firmly together (a pressure of at least 700 kN m^{-2} is needed). The aluminum joint surfaces must be cleaned and treated so the adhesive will bond properly when cured. The strength and toughness of the glue may be increased by adding small powdered particles of aluminum, thermoplastic (polyvinyl formal, polyvinyl butyral, nitrile rubber), or minerals (asbestos was one such, until banned). The glue may contain very fine spheres of glass ($\approx 0.13\text{ mm}$ diameter) to keep the joint surfaces apart, and thus get a glue layer of uniform controlled thickness. Spun rock wool may be incorporated into the glue film in order to stop the glue flowing out of the joint during curing. Glass, nylon, or polyester fiber “scrim” (a very coarsely woven fabric) is sometimes incorporated into the film to give it some handling strength, to control the flow of adhesive during curing, and to keep the joint surfaces apart. A far cry from Araldite glue as used in the home or the shed!

EXAMPLES

- 24.1** Describe in a few words (using examples or sketches if you want to) what is meant by the following:
- (a) A linear polymer.
 - (b) An isotactic polymer.
 - (c) A syndiotactic polymer.
 - (d) An atactic polymer.
- 24.2** Describe in a few words (using examples or sketches if you want to) what is meant by the following:
- (a) Degree of polymerization.
 - (b) Tangling.
 - (c) Branching.
 - (d) Cross-linking.
- 24.3** Describe in a few words (using examples or sketches if you want to) what is meant by the following:
- (a) An amorphous polymer.
 - (b) A crystalline polymer.
 - (c) A network polymer.
- 24.4** Describe in a few words (using examples or sketches if you want to) what is meant by the following:
- (a) A thermoplastic.
 - (b) A thermoset.
 - (c) An elastomer or rubber.
- 24.5** Describe in a few words (using examples or sketches if you want to) what is meant by the glass transition temperature.
- 24.6** The density of a polyethylene (PE) crystal is 1.014 Mg m^{-3} at 20°C . The density of amorphous PE at 20°C is 0.84 Mg m^{-3} . Estimate the percentage crystallinity in:
- (a) A low-density PE having a density of 0.92 Mg m^{-3} at 20°C .
 - (b) A high-density PE having a density of 0.97 Mg m^{-3} at 20°C .

Answers

(a) 46%; (b) 75%.

- 24.7** Explain why fibers drawn from linear thermoplastics have very high moduli and tensile strengths.
- 24.8** For rubber, $T_G \approx -50^\circ\text{C}$ to -100°C . Why is this so important in engineering applications of rubber?
- 24.9** What factors determine the extent to which polymers are crystalline or amorphous? Explain how these factors determine the degree of crystallinity.

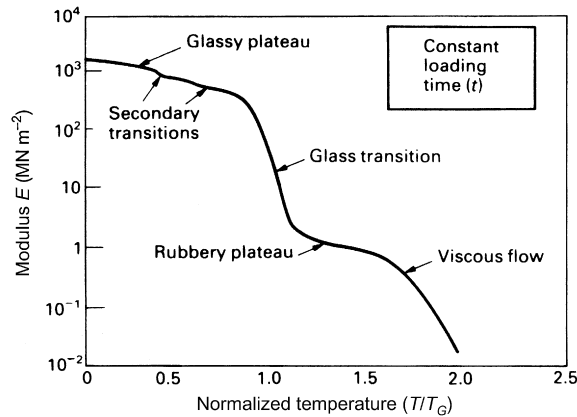
Mechanical Properties of Polymers

25.1 INTRODUCTION

Polymers have a spectrum of mechanical behavior, from *brittle–elastic* at low temperature, through *plastic* to *viscoelastic* or *leathery*, to *rubbery* and finally to *viscous* at high temperature. Metals and ceramics have a range of mechanical behavior, but, because their melting points are high, the variation near room temperature is unimportant. With polymers it is different: between $-20\text{ }^{\circ}\text{C}$ and $+200\text{ }^{\circ}\text{C}$ a polymer can pass through all of the mechanical states listed above, and in doing so its modulus and strength can change by a factor of 10^3 or more. So while we could treat metals and ceramics as having a constant stiffness and strength for design near ambient temperatures, we cannot do so for polymers.

The mechanical state of a polymer depends on its molecular weight and on the temperature; or more precisely, on how close the temperature is to its glass temperature T_G . Each mechanical state covers a certain range of *normalized temperature* T/T_G (Figure 25.1). Some polymers, like PMMA, and many epoxies, are brittle at room temperature because their glass temperatures are high and room temperature is only $0.75\ T_G$. Others, like polyethylene, are leathery; for these, room temperature is about $1.0\ T_G$. Still others, like polyisoprene, are elastomers; for these, room temperature is well above T_G (roughly $1.5\ T_G$). So it makes sense to plot polymer properties not against temperature T , but against T/T_G , since that is what really determines the mechanical state. The modulus and strength diagrams described in this chapter are plotted in this way.

It is important to distinguish between the *stiffness* and the *strength* of a polymer. The stiffness describes the resistance to elastic deformation, the strength describes the resistance to collapse by plastic yielding or by fracture. Depending on the application, one or the other may be design-limiting. And both, in polymers, have complicated origins, which we will now explain.

**FIGURE 25.1**

Schematic showing the way in which Young's modulus E for a linear polymer changes with temperature for a fixed loading time.

25.2 STIFFNESS—TIME AND TEMPERATURE DEPENDENT MODULUS

Much engineering design—particularly with polymers—is based on *stiffness*: the designer aims to keep the elastic deflections below some critical limit. Then the material property which is most important is Young's modulus, E . Metals and ceramics have Young's moduli which, near room temperature, can be thought of as constant. Those of polymers cannot. When a polymer is loaded, it deflects by an amount which increases with the loading time t and with the temperature T . The deflection is elastic—on unloading, the strain disappears again (though that, too, may take time). So it is usual to speak of the *time and temperature dependent modulus*, $E(t, T)$ (from now on called E). It is defined, just like any other Young's modulus, as the stress σ divided by the elastic strain ε

$$E = \frac{\sigma}{\varepsilon(t, T)}. \quad (25.1)$$

The difference is that the strain now depends on time and temperature.

The modulus E of a polymer can change enormously—by as much as a factor of 1000—when the temperature is changed. We will focus first on the behavior of linear-amorphous polymers, examining the reasons for the enormous range of modulus, and digressing occasionally to explain how cross-linking, or crystallization, change things.

Linear-amorphous polymers (like PMMA or PS) show five regimes of deformation in each of which the modulus has certain characteristics, illustrated by Figure 25.1. They are:

- (a) The glassy regime, with a large modulus, around 3 GN m^{-2} .
- (b) The glass-transition regime, in which the modulus drops steeply from 3 GN m^{-2} to around 3 MN m^{-2} .
- (c) The rubbery regime, with a low modulus, around 3 MN m^{-2} .
- (d) The viscous regime, when the polymer starts to flow.
- (e) The regime of decomposition, in which chemical breakdown starts.

We now examine each regime in more detail.

Glassy regime and secondary relaxations

The glass temperature, T_G , is the temperature at which the secondary bonds start to melt. Well below T_G the polymer molecules pack tightly together, either in an amorphous tangle, or in poorly organized crystallites with amorphous material in between. Load stretches the bonds, giving elastic deformation which is recovered on unloading. But there are two sorts of bonds: the taut, muscular, covalent bonds that form the backbone of the chains; and the flabby, soft, secondary bonds between them. Figure 25.2 illustrates this: the covalent chain is shown as a solid line and the side groups or radicals as full circles; they bond to each other by secondary bonds shown as dotted lines (this scheme is helpful later in understanding elastic deformation).

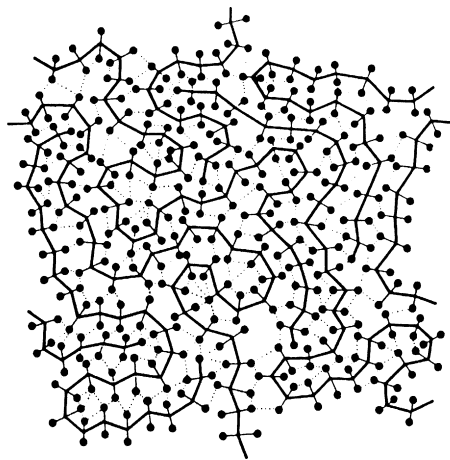


FIGURE 25.2

Schematic of a linear-amorphous polymer, showing the strong covalent bonds (full lines) and the weak secondary bonds (dotted lines). When the polymer is loaded below T_G , it is the secondary bonds which stretch.

The modulus of the polymer is an average of the stiffnesses of its bonds. But it obviously is not an arithmetic mean: even if the stiff bonds were completely rigid, the polymer would deform because the weak bonds would stretch. Instead, we calculate the modulus by summing the deformation in each type of bond using the methods of composite theory. A stress σ produces a strain which is the weighted sum of the strains in each sort of bond

$$\varepsilon = f \frac{\sigma}{E_1} + (1-f) \frac{\sigma}{E_2} = \sigma \left\{ \frac{f}{E_1} + \frac{(1-f)}{E_2} \right\}. \quad (25.2)$$

Here f is the fraction of stiff, covalent bonds (modulus E_1) and $1-f$ is the fraction of weak, secondary bonds (modulus E_2). The polymer modulus is

$$E = \frac{\sigma}{\varepsilon} = \left\{ \frac{f}{E_1} + \frac{(1-f)}{E_2} \right\}^{-1}. \quad (25.3)$$

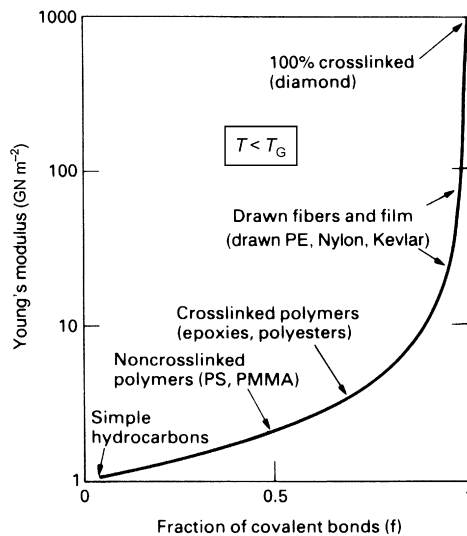
If the polymer is completely cross-linked ($f=1$), then the modulus (E_1) is known: it is that of diamond, 10^3 GN m^{-2} . If it has no covalent bonds at all, then the modulus (E_2) is that of a simple hydrocarbon like paraffin wax, and that, too, is known: it is 1 GN m^{-2} .

Substituting this information into Equation (25.3) gives the glassy modulus as a function of the fraction of covalent bonding

$$E = \left\{ \frac{f}{10^3} + \frac{(1-f)}{1} \right\}^{-1} \text{ GN m}^{-2} \quad (25.4)$$

This function is plotted in Figure 25.3. The glassy modulus of random, linear polymers ($f=0.5$) is always around 3 GN m^{-2} . Heavily cross-linked polymers have a higher modulus because f is larger—as high as 0.75—giving $E = 8 \text{ GN m}^{-2}$. Drawn polymers are different: they are anisotropic, having the chains lined up along the draw direction. Then the fraction of covalent bonds in the loading direction is increased dramatically. In extreme drawing of fibers like nylon or Kevlar this fraction reaches 98%, and the modulus rises to 100 GN m^{-2} , about the same as that of aluminum. This *orientation strengthening* is a potent way of increasing the modulus of polymers. The stiffness normal to the drawing direction, of course, decreases because f falls toward zero in that direction.

You might expect that the glassy modulus (which, like that of metals and ceramics, is just due to bond-stretching) should not depend much on temperature. At very low temperatures this is correct. But the tangled packing of polymer molecules leaves some “loose sites” in the structure: side groups or chain segments, with a little help from thermal energy,

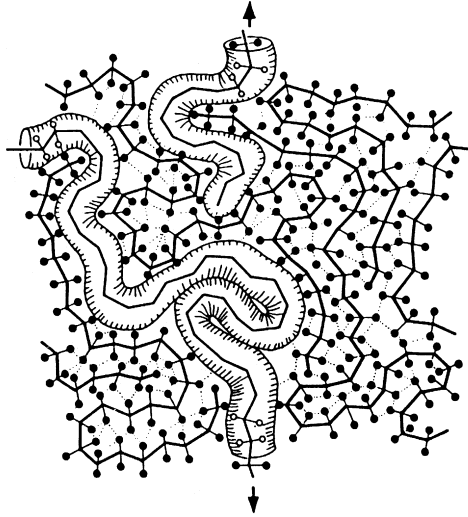
**FIGURE 25.3**

How the modulus of polymers changes with the fraction of covalent bonds in the loading direction. Cross-linking increases this fraction a little; drawing increases it much more.

readjust their positions to give a little extra strain. These secondary relaxations (Figure 25.1) can lower the modulus by a factor of 2 or more, so they cannot be ignored. But their effect is small compared with that of the viscoelastic, or glass transition, which we come to next.

Glass or viscoelastic transition

As the temperature is raised, the secondary bonds start to melt. Then segments of the chains can slip relative to each other like bits of greasy string, and the modulus falls steeply (Figure 25.1). It is helpful to think of each polymer chain as contained within a tube made up by the surrounding nest of molecules (Figure 25.4). When the polymer is loaded, bits of the molecules slide slightly in the tubes in a snake-like way (called “reptation”) giving extra strain and dissipating energy. As the temperature rises past T_G , the polymer expands and the extra free volume (Chapter 24) lowers the packing density, allowing more regions to slide, and giving a lower apparent modulus. But there are still nonsliding (i.e., elastic) parts. On unloading, these elastic regions pull the polymer back to its original shape, though they must do so against the reverse viscous sliding of the molecules, and that takes time. The result is that the polymer has *leathery* properties, as do low-density polyethylene and plasticized PVC at room temperature.

**FIGURE 25.4**

Each molecule in a linear polymer can be thought of as contained in a tube made up by its surroundings. When the polymer is loaded at or above T_g , each molecule can move (reptate) in its tube, giving strain.

Within this regime it is found that the modulus E at one temperature can be related to that at another by a change in the time scale only: there is an *equivalence between time and temperature*. This means that the curve describing the modulus at one temperature can be superimposed on that for another by a constant horizontal displacement $\log(a_T)$ along the $\log(t)$ axis, as shown in Figure 25.5.

A well-known example of this time–temperature equivalence is the steady-state creep of a crystalline metal or ceramic, where it follows immediately from the kinetics of thermal activation. At a constant stress σ the creep rate varies with temperature as

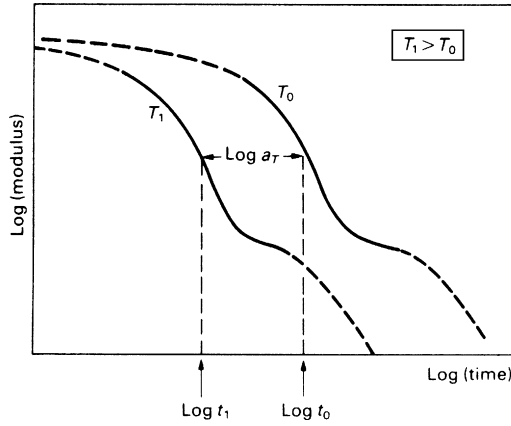
$$\dot{\epsilon}_{ss} = \frac{\epsilon}{t} = A \exp(-Q/RT) \quad (25.5)$$

giving

$$\epsilon(t, T) = tA \exp(-Q/RT). \quad (25.6)$$

From Equation (25.1), the apparent modulus E is given by

$$E = \frac{\sigma}{\epsilon(t, T)} = \frac{\sigma}{tA} \exp(Q/RT) = \frac{B}{t} \exp(Q/RT). \quad (25.7)$$

**FIGURE 25.5**

Schematic of the time—temperature equivalence for the modulus. Every point on the curve for temperature T_1 lies at the same distance, $\log(a_T)$, to the left of that for temperature T_0 .

If we want to match the modulus at temperature T_1 to that at temperature T_0 (see Figure 25.5), then we need

$$\frac{\exp(Q/RT_1)}{t_1} = \frac{\exp(Q/RT_0)}{t_0} \quad (25.8)$$

or

$$\frac{t_1}{t_0} = \frac{\exp(Q/RT_1)}{\exp(Q/RT_0)} = \exp \frac{Q}{R} \left\{ \frac{1}{T_1} - \frac{1}{T_0} \right\}. \quad (25.9)$$

Thus

$$\ln \left(\frac{t_0}{t_1} \right) = -\frac{Q}{R} \left\{ \frac{1}{T_1} - \frac{1}{T_0} \right\}, \quad (25.10)$$

and

$$\begin{aligned} \log(a_T) &= \log(t_0/t_1) = \log t_0 - \log t_1 \\ &= \frac{-Q}{2.3R} \left\{ \frac{1}{T_1} - \frac{1}{T_0} \right\}. \end{aligned} \quad (25.11)$$

This result says that a simple shift along the time axis by $\log(a_T)$ will bring the response at T_1 into coincidence with that at T_0 (see Figure 25.5).

Polymers are a little more complicated. The drop in modulus (like the increase in creep rate) is caused by the increased ease with which molecules

can slip past each other. In metals, which have a crystal structure, this reflects the increasing number of vacancies and the increased rate at which atoms jump into them. In polymers, which are amorphous, it reflects the increase in free volume which gives an increase in the rate of reptation. Then the shift factor is given, not by Equation (25.11) but by

$$\log(a_T) = \frac{C_1(T_1 - T_0)}{C_2 + T_1 - T_0} \quad (25.12)$$

where C_1 and C_2 are constants. This is called the “WLF equation” after its discoverers, Williams, Landel, and Ferry, and (like the Arrhenius law for crystals) is widely used to predict the effect of temperature on polymer behavior. If T_0 is taken to be the glass temperature, then C_1 and C_2 are roughly constant for all amorphous polymers (and inorganic glasses too); their values are $C_1 = 17.5$ and $C_2 = 52$ K.

Rubbery behavior and elastomers

As the temperature is raised above T_G , one might expect that flow in the polymer should become easier and easier, until it becomes a rather sticky liquid. Linear polymers with fairly short chains ($\overline{DP} < 10^3$) do just this. But polymers with longer chains ($\overline{DP} > 10^4$) pass through a *rubbery state*.

The origin of rubber elasticity is more difficult to picture than that of a crystal or glass. The long molecules, intertwined like a jar of exceptionally long worms, form *entanglements*—points where molecules, because of their length and flexibility, become knotted together (Figure 25.6). On loading,

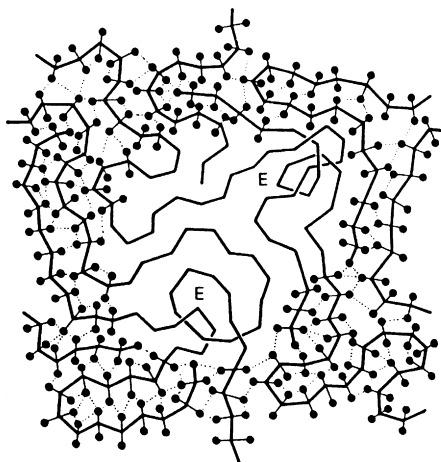


FIGURE 25.6

Schematic of a linear-amorphous polymer, showing entanglement points (marked “E”) which act like chemical cross-links.

the molecules reptate (slide) except at entanglement points. The entanglements give the material a shape-memory: load it, and the segments between entanglements straighten out; remove the load and the wriggling of the molecules (being above T_G) draws them back to their original configuration, and thus shape. Stress tends to *order* the molecules of the material; removal of stress allows it to *disorder* again. The rubbery modulus is small, about one-thousandth of the glassy modulus, T_G , but it is there nonetheless and gives the plateau in the modulus shown in Figure 25.1.

Much more pronounced rubbery behavior is obtained if the chance entanglements are replaced by deliberate cross-links. The number of cross-links must be small—about 1 in every few hundred monomer units. But, being strong, the covalent cross-links do not melt, and this makes the polymer above T_G into a true *elastomer*, capable of elastic extensions of 300% or more (the same as the draw ratio of the polymer in the plastic state—see the next section) which are recovered completely on unloading. Over-frequent cross-links destroy the rubbery behavior. If every unit on the polymer chain has one (or more) cross-links to other chains, then the covalent bonds form a three-dimensional network, and melting of the secondary bonds does not leave long molecular spans which can straighten out under stress. So good elastomers, like polyisoprene (natural rubber) are linear polymers with just a few cross-links, well above their glass temperatures (room temperature is $1.4 T_G$ for polyisoprene). If they are cooled below T_G , the modulus rises steeply and the rubber becomes hard and brittle, with properties like those of PMMA at room temperature.

Viscous flow

At yet higher temperatures ($>1.4 T_G$), the secondary bonds melt completely and even the entanglement points slip. This is the regime in which thermoplastics are molded: linear polymers become viscous liquids. The viscosity is always defined (and usually measured) in shear: if a shear stress σ_s produces a rate of shear $\dot{\gamma}$ then the viscosity is

$$\eta = \frac{\sigma_s}{10\dot{\gamma}}. \quad (25.13)$$

Its units are poise (P) or $10^{-1} \text{ Nm}^{-2} \text{ s}$.

Polymers, like inorganic glasses, are formed at a viscosity in the range 10^4 – 10^6 poise, when they can be blown or molded. (When a metal melts, its viscosity drops discontinuously to a value near 10^{-3} poise—about the same as that of water; that is why metals are formed by casting, not by the more convenient methods of blowing or molding.) The viscosity depends on temperature, of course; and at very high temperatures the

dependence is well described by an Arrhenius' law, like inorganic glasses. But in the temperature range $1.3\text{--}1.5\ T_G$, where most thermoplastics are formed, the flow has the same time–temperature equivalence as that of the viscoelastic regime (Equation (25.12)) and is called “rubbery flow” to distinguish it from the higher temperature Arrhenius' flow. Then, if the viscosity at one temperature T_0 is η_0 , the viscosity at a higher temperature T_1 is

$$\eta_1 = \eta_0 \exp \left\{ -\frac{C_1(T_1 - T_0)}{C_2 + T_1 - T_0} \right\}. \quad (25.14)$$

When you have to estimate how a change of temperature changes the viscosity of a polymer (in calculating forces for injection molding, for instance), this is the equation to use.

Cross-linked polymers do not melt. But if they are made hot enough they, like linear polymers, decompose.

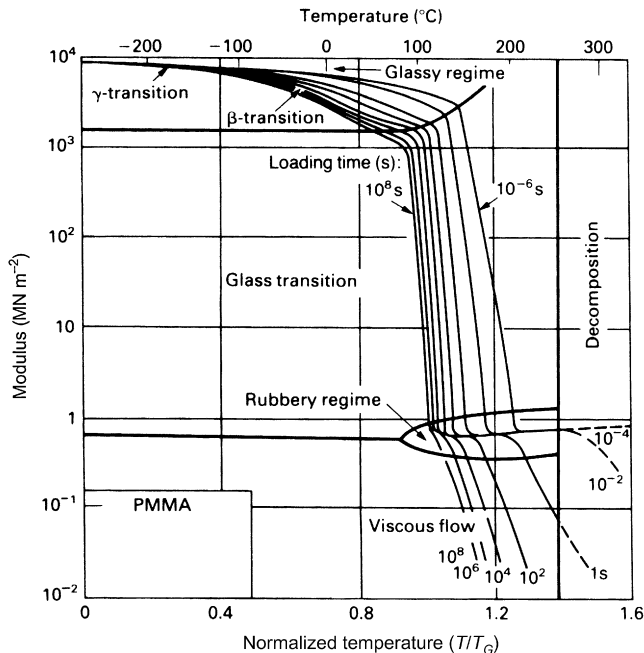
Decomposition

If a polymer gets too hot, the thermal energy exceeds the cohesive energy of some part of the molecular chain, causing depolymerization or degradation. Some (like PMMA) decompose into monomer units; others (PE, for instance) randomly degrade into many products. It is commercially important that no decomposition takes place during high-temperature molding, so a maximum safe working temperature is specified for each polymer; typically, it is about $1.5\ T_G$.

Modulus diagrams for polymers

The above information is conveniently summarized in the *modulus diagram* for a polymer. Figure 25.7 shows an example: it is a modulus diagram for PMMA and is typical of linear-amorphous polymers (PS, for example, has a very similar diagram). The modulus E is plotted, on a log scale, on the vertical axis: it runs from 0.01 to 10,000 MN m⁻². The temperature, normalized by the glass temperature T_G , is plotted linearly on the horizontal axis: it runs from 0 (absolute zero) to $1.6\ T_G$ (below which the polymer decomposes).

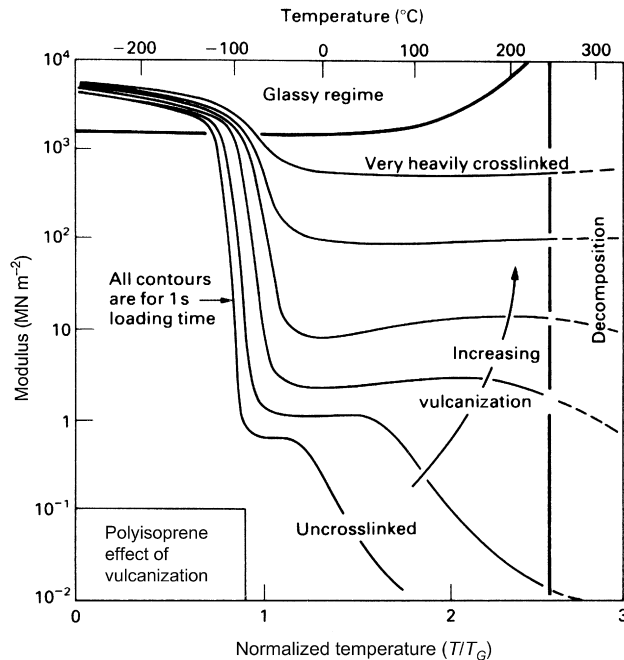
The diagram is divided into five *fields*, corresponding to the five regimes described earlier. In the glassy field, the modulus is large—typically 3 GN m⁻²—but it drops slightly as the secondary transitions cause local relaxations. In the glassy or viscoelastic–transition regime, the modulus drops steeply, flattening out again in the rubbery regime. Finally, true melting or decomposition causes a further drop in modulus.

**FIGURE 25.7**

Modulus diagram for PMMA. It shows the glassy regime, the glass–rubber transition, the rubbery regime, and the regime of viscous flow. The diagram is typical of linear-amorphous polymers.

Time, as well as temperature, affects the modulus. This is shown by the *contours of loading time*, ranging from very short (10^{-6} s) to very long (10^8 s). The diagram shows how, even in the glassy regime, the modulus at long loading times can be a factor of 2 less than that for short times; and in the glass-transition region the factor increases to 100 or more. The diagrams give a compact summary of the small-strain behavior of polymers and are helpful in seeing how a given polymer will behave in a given application.

Cross-linking raises and extends the rubbery plateau, increasing the rubber-modulus, and suppressing melting. [Figure 25.8](#) shows how, for a single loading time, the contours of the modulus diagram are pushed up as the cross-link density is increased. Crystallization increases the modulus too (the crystal is stiffer than the amorphous polymer because the molecules are more densely packed), but it does not suppress melting, so crystalline linear polymers (like high-density PE) can be formed by heating and molding them, just like linear-amorphous polymers; cross-linked polymers cannot.

**FIGURE 25.8**

Influence of cross-linking on a contour of the modulus diagram for polyisoprene.

25.3 STRENGTH—COLD DRAWING AND CRAZING

Engineering design with polymers starts with stiffness. But strength is also important, sometimes overridingly so. A plastic chair need not be very stiff—it may be more comfortable if it is a bit flexible—but it must not collapse from plastic yield, or fail in a brittle manner, when sat upon. There are numerous examples of the use of polymers (luggage, casings of appliances, interior components for automobiles) where strength, not stiffness, is the major consideration.

The “strength” of a solid is the stress at which something starts to happen which gives a permanent shape change: plastic flow or the propagation of a brittle crack, for example. At least five strength-limiting processes are known in polymers. Roughly in order of increasing temperature, they are:

- (a) Brittle fracture, like that in ordinary glass.
- (b) Cold drawing, the drawing-out of the molecules in the solid state, giving a large shape change.

- (c) Shear banding, giving slip bands rather like those in a metal crystal.
- (d) Crazing, a kind of microcracking, associated with local cold drawing.
- (e) Viscous flow, when the secondary bonds in the polymer have melted.

We now examine each of these in a little more detail.

Brittle fracture

Below about $0.75 T_G$, polymers are brittle (Figure 25.9). Unless special care is taken to avoid it, a polymer sample has small surface cracks (depth c) left by machining or abrasion, or caused by environmental attack. Then a tensile stress σ will cause brittle failure if

$$\sigma \approx \frac{K_c}{\sqrt{\pi c}} \quad (25.15)$$

where K_c is the fracture toughness of the polymer. The fracture toughness of most polymers (Table 23.5) is, very roughly, $1 \text{ MN m}^{-3/2}$, and the incipient crack size is, typically, a few micrometers. Then the fracture strength in the brittle regime is about 100 MN m^{-2} . But if deeper cracks or stress concentrations are cut into the polymer, the stress needed to make them propagate is, of course, lower. When designing with polymers, you must remember that below $0.75 T_G$ they are low-toughness materials and that anything that concentrates stress (like cracks, notches, or sharp changes of section) is dangerous.

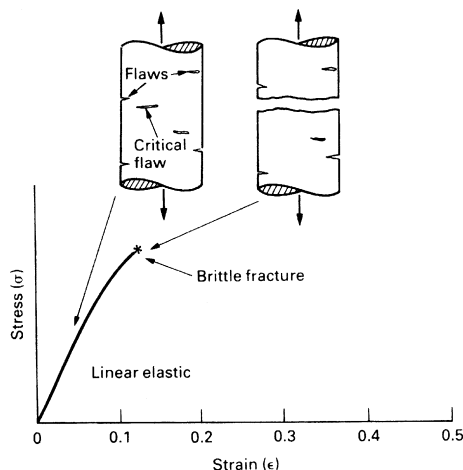


FIGURE 25.9

Brittle fracture: the largest crack propagates when the fast-fracture criterion is satisfied.

Cold drawing

At temperatures 50 °C or so below T_G , thermoplastics become plastic (hence the name). The stress–strain curve typical of polyethylene or nylon, for example, is shown in Figure 25.10. It shows three regions.

At low strains, the polymer is *linear elastic*, which is the modulus we have just discussed. At a strain of about 0.1, the polymer *yields* and then *draws*. The chains unfold (if chain-folded) or draw out of the amorphous tangle (if glassy), and straighten and align. The process starts at a point of weakness or of stress concentration, and a segment of the gauge length draws down, like a neck in a metal specimen, until the *draw ratio* (l/l_0) is sufficient to cause alignment of the molecules (like pulling cotton wool). The draw ratio for alignment is between 2 and 4 (nominal strains of 100–300%). The neck propagates along the sample until it is all drawn (Figure 25.10).

The drawn material is stronger in the draw direction than before; that is why the neck spreads instead of simply causing failure. When drawing is complete, the stress–strain curve rises steeply to final fracture. This draw-strengthening is widely used to produce high-strength fibers and film. An example is nylon made by melt spinning: the molten polymer is squeezed through a fine nozzle and then pulled (draw ratio ≈ 4), aligning the molecules along the fiber axis; if it is then cooled to room temperature, the

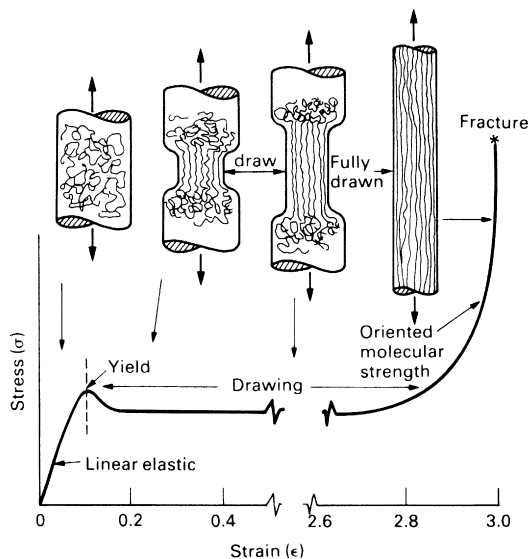


FIGURE 25.10

Cold drawing of a linear polymer: the molecules are drawn out and aligned giving, after a draw ratio of about 4, a material which is much stronger in the draw direction than it was before.

reorientated molecules are frozen into position. The drawn fiber has a modulus and strength some 8 times larger than that of the bulk, unoriented, polymer.

Crazing

Many polymers, among them PE, PP, and nylon, draw at room temperature. Others with a higher T_G , such as PS, do not—although they draw well at higher temperatures. If PS is loaded in tension at room temperature, it *crazes*. Small crack-shaped regions within the polymer draw down, but being constrained by the surrounding undeformed solid, the drawn material ends up as ligaments which link the craze surfaces (Figure 25.11). The crazes are easily visible as white streaks or as general whitening when cheap injection-molded articles are bent (plastic pen tops, appliance casings, plastic caps). The crazes are a precursor to fracture. Before drawing becomes general, a crack forms at the center of a craze and propagates—often with a crazed zone at its tip—to give final fracture (Figure 25.11).

Shear banding

When crazing limits the ductility in tension, large plastic strains may still be possible in compression *shear banding* (Figure 25.12). Within each band a finite shear has taken place. As the number of bands increases, the total overall strain accumulates.

Viscous flow

Well above T_G polymers flow in the viscous manner we have described already. When this happens the strength falls steeply.

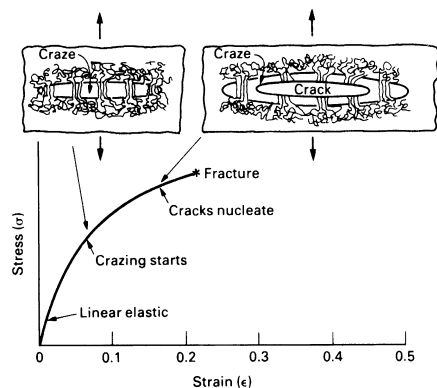
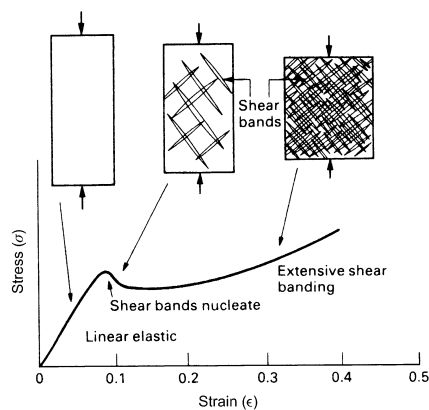


FIGURE 25.11

Crazing in a linear polymer: molecules are drawn out as in Figure 25.10, but on a much smaller scale, giving strong strands which bridge the microcracks.

**FIGURE 25.12**

Shear banding, an alternative form of polymer plasticity which appears in compression.

Strength diagrams for polymers

Most of this information can be summarized as a *strength diagram* for a polymer. Figure 25.13 is an example, again for PMMA. Strength is less well understood than stiffness, but the diagram is broadly typical of other linear polymers. The diagram is helpful in giving a broad, approximate picture of polymer strength. The vertical axis is the strength of the polymer: the stress at which inelastic behavior becomes pronounced. The right-hand scale gives the strength in MN m^{-2} ; the left-hand scale gives the strength normalized by Young's modulus at 0 K. The horizontal scale is the temperature, unnormalized across the top and normalized by T_G along the bottom. (The normalizations make the diagrams more general: similar polymers should have similar normalized diagrams.)

The diagram is divided, like the modulus diagram, into *fields* corresponding to the five strength-limiting processes described earlier. At low temperatures, there is a brittle field; here the strength is calculated by linear-elastic fracture mechanics. Below this lies the crazing field: the stresses are too low to make a single crack propagate unstably, but they can still cause the slow growth of microcracks, limited and stabilized by the strands of drawn material which span them. At higher temperatures, true plasticity begins: cold drawing and, in compression, shear banding. And at high temperature lies the field of viscous flow.

The strength of a polymer depends on the strain rate as well as the temperature. The diagram shows *contours of constant strain rate*, ranging from very slow (10^{-6} s^{-1}) to very fast (1 s^{-1}). The diagram shows how the strength varies with temperature and strain rate and helps identify the dominant

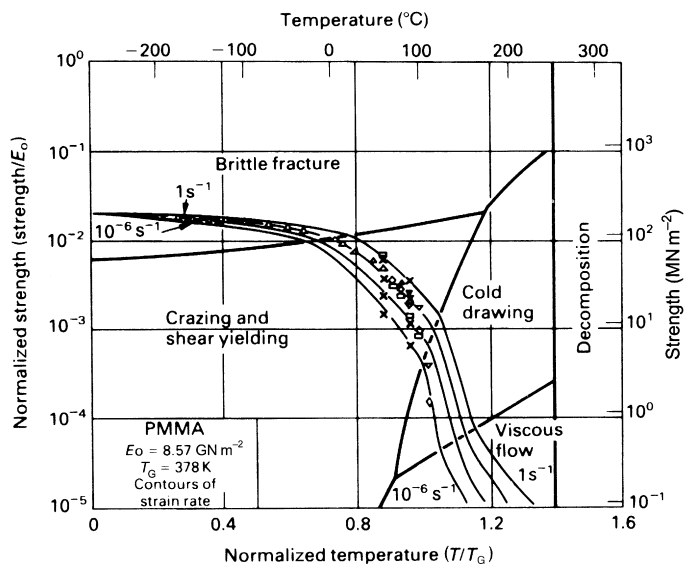


FIGURE 25.13

Strength diagram for PMMA. The diagram is broadly typical of linear polymers.

strength-limiting mechanism. This is important because the ductility depends on mechanism: in the cold drawing regime it is large, but in the brittle fracture regime it is zero.

Strength is a much more complicated property than stiffness. Strength diagrams summarize the behavior of laboratory samples tested in simple tension. But they (or equivalent compilations of data) must be used with circumspection. In an engineering application, the stress-state may be multiaxial, not simple tension; and the environment (even simple sunlight) may attack and embrittle the polymer, reducing its strength. These, and other, aspects of design with polymers are discussed in the books listed in the References.

EXAMPLES

25.1 Estimate the loading time needed to give a modulus of 0.2 GN m^{-2} in low-density polyethylene at the glass-transition temperature.

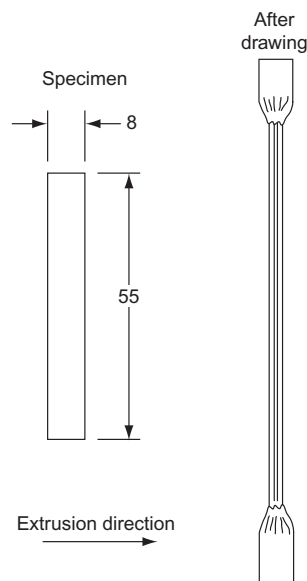
Answer

270 days.

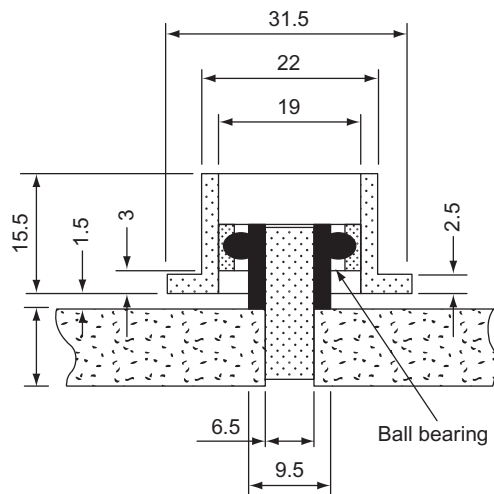
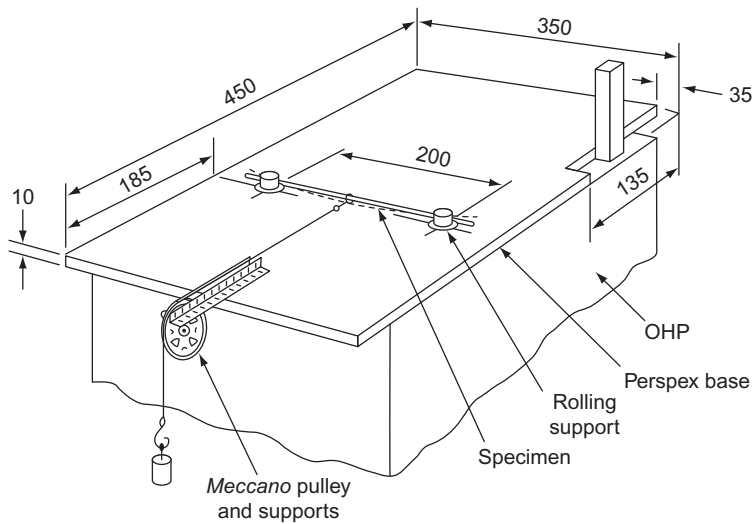
25.2 Explain how the modulus of a polymer depends on the following factors:

- Temperature.
- Loading time.
- Fraction of covalent cross-links.

- (d) Molecular orientation.
 - (e) Crystallinity.
 - (f) Degree of polymerization.
- 25.3** Explain how the tensile strength of a polymer depends on the following factors:
- (a) Temperature.
 - (b) Strain rate.
 - (c) Molecular orientation.
 - (d) Degree of polymerization.
- 25.4** Explain how the toughness of a polymer is affected by:
- (a) Temperature.
 - (b) Strain rate.
 - (c) Molecular orientation.
- 25.5** The Young's modulus of natural rubber decreases from 3 GN m^{-2} at -200°C to 3 MN m^{-2} at room temperature, whereas the Young's modulus of epoxy resin is approximately 10 GN m^{-2} at both temperatures. Explain this difference in behavior.
- 25.6** Detach a polythene bag from a roll of freezer bags, and using a pair of scissors, cut a strip from it as shown in the diagram below (dimensions in millimeter). Make sure that the axis of the specimen is parallel to the width of each bag, and at right angles to the extrusion direction of the polythene (which is the unrolling direction of the freezer bags). Grip each end of the strip between thumb and forefinger, and pull out the strip as shown. Note what happens as you pull the strip out, and explain why the strip behaves in the way it does.

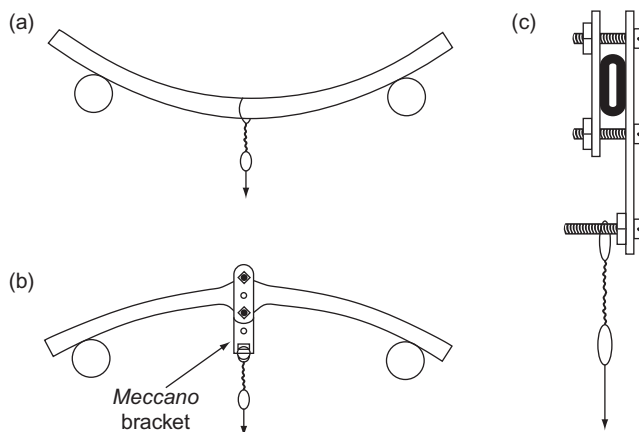


25.7 The two diagrams which follow show a jig for use on the table of an overhead projector (OHP) for projecting the image of a beam being loaded in three-point bending. All dimensions are given in millimeters. The span of the beam is 200 mm.



- Assemble parts with light interference fits or anaerobic adhesive
- Materials: central shaft and spacer, mild steel; outer wheel, aluminum

A 400 mm length of polythene tube (OD ≈ 9 mm, wall thickness ≈ 1.5 mm) is placed in a vacuum flask of liquid nitrogen until it no longer boils off nitrogen, then removed and loaded in the rig as shown in (a) of the following diagram. (Note that the tube is shown curved because polythene tube is usually stored on a reel and comes off the reel with curved set.)



If a weight of 150 g is applied to the tube, it will produce a negligible deflection at the center of the test span. Explain this observation. (If anyone carries out this test for themselves, it is entirely at their own risk, and suitable precautions should be taken to avoid cold burns. Safety glasses must be worn, and cold parts must absolutely not be allowed to come into contact with your skin. The tube will need to be placed vertically down into the vacuum flask, and for the first minute liquid nitrogen will squirt out of the upper end of the tube, so the tube end must be directed away from you—and nobody else must be within range of the stream of liquid nitrogen.)

- 25.8** The length of polythene tube is then removed from the rig, and allowed to warm up to room temperature. It is reloaded in the rig as shown in (b) of the diagram (still using the 150 g weight). The tube deflects instantaneously by ≈ 20 mm. Explain the difference in behaviors observed at (a) liquid nitrogen temperature and (b) room temperature. (Note that if the tube were to be loaded as in (a) of the diagram, it would just bow inward, and slide through the gap between the support rollers. This is overcome by loading the tube as shown in (b) of the diagram and clamping a special loading bracket to the tube to stop it flipping over from a (b) type to an (a) type configuration.)
- 25.9** The polythene tube is left in the rig (still carrying the 150 g test load) and continues to deflect. Explain this observation. The load is then removed, and the deflection of the tube decreases, until all the earlier deformation is

recovered. Explain this observation. Also explain why the polythene tube was set into a curve when it was taken off the reel, whereas it would have been straight when it came out of the extrusion die during manufacture.

- 25.10** The polythene tube is heated by warming it in a very gentle gas flame, rotating the tube (and moving it axially from side to side) so that it is heated uniformly. The tube is then removed from the flame, and the investigator pulls the tube ends apart sharply. It is found that the tube behaves almost as if it were made from rubber. Explain this observation. (If anyone carries out this test for themselves, it is entirely at their own risk, and suitable precautions should be taken to avoid burns and risk of fire. Safety glasses and fireproof gloves must be worn. Make sure the tube is not overheated, and does not start to catch fire. Have a bowl of water handy in case a small fire needs to be put out.)
- 25.11** The central 50 mm length of the polythene tube is heated to a higher temperature by warming it in the gentle gas flame, rotating the tube so that it is heated uniformly. The tube will start to flow readily, and the heated length can easily be pulled to failure by the investigator. Explain this observation. (If anyone carries out this test for themselves, it is entirely at their own risk, and suitable precautions should be taken to avoid burns and risk of fire. Safety glasses and fireproof gloves must be worn. Make sure the tube does not start to catch fire. Have a bowl of water handy in case a small fire needs to be put out.)
- 25.12** A 400 mm length of *rubber* tube (OD \approx 9 mm, wall thickness \approx 1.5 mm) is placed in a vacuum flask of liquid nitrogen until it no longer boils off nitrogen. It is then removed, placed on a piece of wood on the bench, and hit with a hammer. If hit hard enough, it will shatter into several pieces. Explain this observation. Why will rubber not shatter if this test is done at room temperature? (This experiment is quite dangerous, as pieces of hard, sharp rubber will fly off in all directions. If anyone carries out this test for themselves, it is entirely at their own risk, and suitable precautions should be taken to avoid injury from fragmenting rubber and cold burns. Safety glasses must be worn, and cold parts must absolutely not be allowed to come into contact with your skin. The tube will need to be placed vertically down into the vacuum flask and for the first minute liquid nitrogen will squirt out of the upper end of the tube, so the tube end must be directed away from you—and nobody else must be within range of the stream of liquid nitrogen. If there is an audience, a transparent safety screen must be placed between the demonstrator and the audience.)
- 25.13** Explain why drawn threads of nylon have both a Young's modulus and a tensile strength which are approximately 8 times those of bulk molded nylon.
- 25.14** Explain what is meant by shear banding. Under what conditions is shear banding likely to occur?

- 25.15** What molecular arrangement gives the best rubbers?
- 25.16** The long-chain molecules in rubber behave a bit like violin strings, in that segments of the chains between adjacent cross-links are equivalent to “string lengths”, and thermal energy nkT makes the segments “vibrate.” According to this model, as the temperature is increased, the “amplitude” of “vibration” should increase, which has the effect of shortening the segments, and therefore generating a negative strain. (This is counter-intuitive, because increasing the temperature of a material would normally be expected to produce a *positive* strain, equal to a (positive) coefficient of thermal expansion times the temperature rise.) Devise a simple (and safe) experiment, using items easily available in the average home, and use it to demonstrate this effect.

Processing Polymers

26.1 INTRODUCTION

People have used natural polymers for far longer than metals. From the earliest times, wood, leather, wool, and cotton have been used for shelter and clothing. Many natural polymers are cheap and plentiful (though not all—think of silk) and remarkably strong. But they evolved for specific natural purposes—to support a tree, to protect an animal—and are not always in the form best suited to meet the needs of engineering.

So people have tried to improve on nature. First, they tried to extract natural polymers, and reshape them to their purpose. Cellulose (Table 23.4), extracted from wood shavings and treated with acids, allows the replacement of the $-\text{OH}$ side group by $-\text{COOCH}_3$ to give *cellulose acetate*, familiar as rayon (used to reinforce car tires) and as transparent acetate film. Replacement by $-\text{NO}_3$ instead gives *cellulose nitrate*, the celluloid of the film industry and a component of many lacquers. Natural latex from the rubber tree is vulcanized to give rubbers and filled (with carbon black, for instance) to make it resistant to sunlight. But the range of polymers obtained in this way is limited.

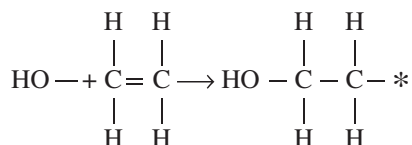
The real breakthrough came when chemists developed processes for making large molecules from their smallest units. Instead of the ten or so natural polymers and modifications of them, the engineer was suddenly presented with hundreds of new materials with remarkable and diverse properties. The number is still increasing.

And we are still learning how best to fabricate and use them. As emphasized in the last chapter, the mechanical properties of polymers differ in certain fundamental ways from those of metals and ceramics, and the methods used to design with them differ accordingly. Their special properties also need special methods of fabrication. This chapter outlines how polymers are fabricated and joined. To understand this, we must first look, in more detail, at their synthesis.

26.2 POLYMER SYNTHESIS

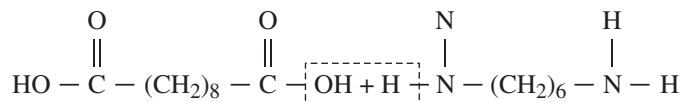
Plastics are made by a chemical reaction in which monomers add (with nothing left over) or condense (with H_2O left over) to give a high polymer.

Polyethylene, a linear polymer, is made by an *addition reaction*. It is started with an initiator, such as H_2O_2 , which gives free and very reactive $-\text{OH}$ radicals. One of these breaks the double bond of an ethylene molecule, C_2H_4 , when it is heated under pressure, to give



The left-hand end of the activated monomer is sealed off by the OH terminator, but the right-hand end (with the star) is aggressively reactive and now attacks another ethylene molecule, as we illustrated earlier in Figure 24.1. The process continues, forming a longer and longer molecule by a sort of chain reaction. The $-\text{OH}$ used to start a chain will, of course, terminate one just as effectively, so excess initiator leads to short chains. As the monomer is exhausted, the reaction slows down and finally stops. The DP depends not only on the amount of initiator, but on the pressure and temperature as well.

Nylon, also a linear polymer, is made by a *condensation reaction*. Two different kinds of molecule react to give a larger molecule and a by-product (usually H_2O); the ends of large molecules are active and react further, building a polymer chain. Note how molecules of one type condense with those of the other in this reaction of two symmetrical molecules.



The resulting chains are regular and symmetrical, and tend to crystallize easily. Condensation reactions do not rely on an initiator, so the long molecules form by the linking of shorter (but still long) segments, which in turn grow from smaller units. In this they differ from addition reactions, in which single monomer units add one by one to the end of the growing chain.

Most network polymers (the epoxies and the polyesters, for instance) are made by condensation reactions. The only difference is that one of the two reacting molecules is multifunctional (polyester is three-functional), so the

reaction gives a three-dimensional lacework, not linear threads, and the resulting polymer is a thermoset.

26.3 POLYMER ALLOYS

Copolymers

If, when making an addition polymer, two monomers are mixed, the chain which forms contains both units (*copolymerization*). Usually the units add randomly, and by making the molecule less regular, they favor an amorphous structure with a lower packing density, and a lower T_G . PVC, when pure, is brittle; but copolymerizing it with vinyl acetate (which has a $-\text{COOCH}_3$ radical in place of the $-\text{Cl}$) gives the flexible copolymer shown in Figure 26.1(a). Less often, the two monomers group together in blocks along the chain; the result is called a *block copolymer* (Figure 26.1(b)).

Solid solutions: plasticizers

Plasticizers are organic liquids with relatively low molecular weights (100–1000) which dissolve in large quantities (up to 35%) in solid polymers. The chains are forced apart by the oily liquid, which lubricates them, making it easier for them to slide over each other. So the plasticizer does what its name suggests: it makes the polymer more flexible (and makes its surface feel slightly oily). It achieves this by lowering T_G , but this also reduces the tensile strength—so moderation must be exercised in its use. And the plasticizer must have a low vapor pressure or it will evaporate and leave the polymer brittle.

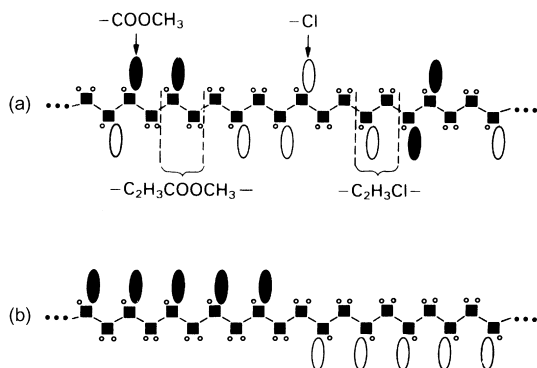


FIGURE 26.1

(a) A copolymer of vinyl chloride and vinyl acetate; the “alloy” packs less regularly, has a lower T_G , and is less brittle than simple polyvinylchloride (PVC). (b) A block copolymer: the two different molecules in the alloy are clustered into blocks along the chain.

Two-phase alloys: toughened polymers

When styrene and butadiene are polymerized, the result is a mixture of distinct molecules of polystyrene and of a rubbery copolymer of styrene and butadiene. On cooling, the rubbery copolymer precipitates out, much as CuAl_2 precipitated out of aluminum alloys, or Fe_3C out of steels. The resulting microstructure is shown in Figure 26.2: the matrix of glassy polystyrene contains rubbery particles of the styrene–butadiene copolymer. The rubber particles stop cracks in the material, increasing its fracture toughness—for this reason the alloy is called *high-impact polystyrene*. Other polymers can be toughened in the same way.

Stabilization and vulcanization

Polymers are damaged by radiation, particularly by the ultraviolet in sunlight. An ultraviolet photon has enough energy to break the C–C bond in the polymer backbone, splitting it into shorter chains. Paints, especially, are exposed to this sort of radiation damage. The solution is to add a pigment or filler (like carbon) which absorbs radiation, preventing it from hitting the delicate polymer chains. Car tires contain as much as 30 wt% of carbon to *stabilize* the polymer against attack by sunlight.

Oxygen, too, can damage polymers by creating –O– cross-links between polymer chains; it is a sort of unwanted vulcanization. The cross-links raise T_G and make the polymer brittle; it is a particular problem with rubbers, which lose their elasticity. Ozone (O_3) is especially damaging because it supplies oxygen in an unusually active form. Sunlight (particularly ultraviolet again) promotes oxidation, partly because it creates O_3 . Polymers containing a C=C double bond are particularly vulnerable, because oxygen links to it to give –C–O–C cross-links; that is why rubbers are attacked by oxygen more than other polymers (see their structure in Table 23.3). The way to

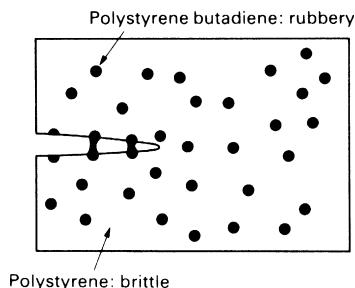


FIGURE 26.2

A two-phase polymer alloy made by copolymerizing styrene and butadiene in polystyrene. The precipitates are a polystyrene–butadiene copolymer.

avoid oxygen attack is to avoid polymers containing double-bonds and to protect the polymer from direct sunlight by stabilizing it.

26.4 FORMING POLYMERS

Thermoplastics soften when heated, allowing them to be formed by processes such as *injection molding*, *vacuum forming*, *blow molding*, and *compression molding*. Thermosets, on the other hand, are heated, formed, and cured simultaneously, usually by *compression molding*. Rubbers are formed like thermosets, by pressing and heating a mix of elastomer and vulcanizing agent in a mold.

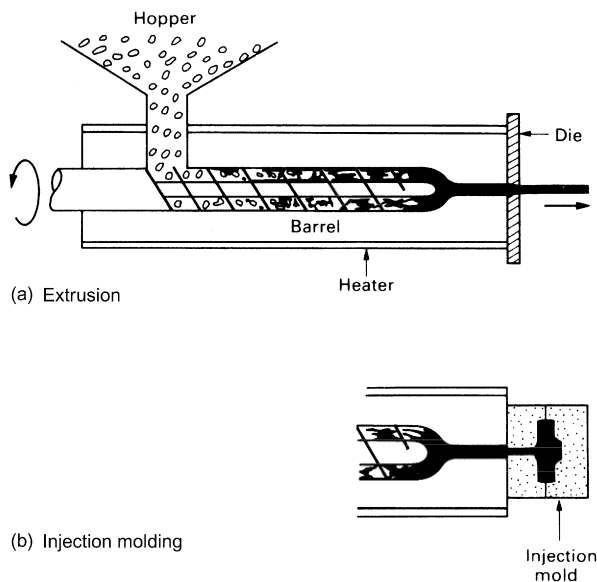
Polymers can be used as surface coatings. Linear polymers can be applied as a solution; the solvent evaporates leaving a film of the polymer. Thermosets can be applied as a fluid mixture of resin and hardener which is mixed just before it is used and cures soon after it is applied.

Polymer fibers are produced by forcing molten polymer or polymer in solution through fine nozzles (spinnerettes). The fibers so formed can be twisted into yarn and woven into fabric. Finally, polymers may be expanded into foams by mixing in chemicals that release CO₂ bubbles into the molten polymer or the curing resin, or by expanding a dissolved gas into bubbles by reducing the pressure.

The full technical details of these processes are beyond the scope of this book, but it is worth having a slightly closer look at them to get a feel for the engineering context in which each is used.

Extrusion

A polymer extruder is like a giant cake-icer. Extrusion is a cheap continuous process for producing shapes of constant section (called “semis,” meaning “semifinished” products or stock). Granules of polymer are fed into a screw like that of an old-fashioned meat mincer, turning in a heated barrel (Figure 26.3(a)). The screw compacts, heats, and mixes the polymer, which melts as it approaches the hot end of the barrel, where it is forced through a die and then cooled (so that its new shape is maintained) to give tubes, sheet, ribbon, and rod. The shear-flow in the die orients the molecules in the extrusion direction and increases the strength. As the extrusion cools, it recovers a bit, and this causes a significant transverse expansion. Complex die shapes lead to complex recovery patterns, so that the final section is not the same as that of the die opening. But die-makers can correct for this, and the process is so fast and cheap that it is very widely used (60% of all thermoplastics undergo some form of extrusion). It has been adopted by the manufacturers of ceramic components who mix the powdered ceramic with

**FIGURE 26.3**

(a) Extrusion: polymer granules are heated, mixed, and compressed by the screw which forces the now molten polymer out through a die. (b) Injection molding is extrusion into a mold. If the molding is cooled with the pressure on, good precision and detail are obtained.

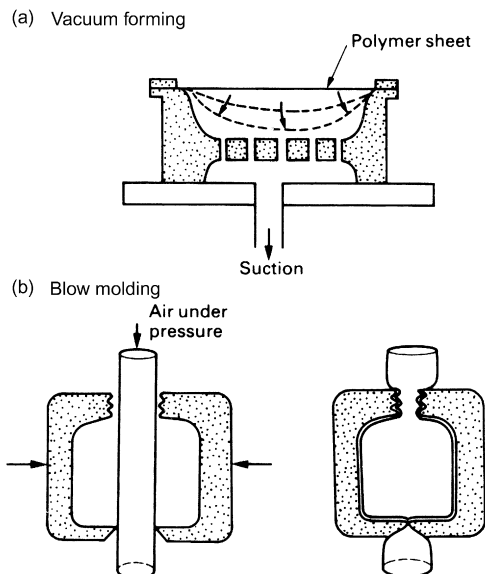
a polymer binder, extrude the mixture, and then burn off the polymer while firing the ceramic.

Injection molding

In *injection molding*, polymer granules are compressed by a ram or screw, heated until molten and squirted into a cold, split mold under pressure (Figure 26.3(b)). The molded polymer is cooled below T_G , the mold opens and the product is ejected. Excess polymer is injected to compensate for contraction in the mold. The molecules are oriented parallel to the flow direction during injection, giving useful strengthening, but properties that are anisotropic. The process gives high-precision moldings, because the polymer cools with the pressure still on but is slow (the cycle time is between 1 and 5 min), and the molds are expensive. Typically, molding temperatures for thermoplastics are between 150 and 350 °C (1.3 and 1.6 T_G) and the pressures needed to give good detail are high—typically 30–120 MN m⁻².

Vacuum and blow forming of sheet

In *vacuum* and *blow forming*, sheets produced by extrusion are shaped by vacuum or pressure forming. Heat-softened sheet is pressed into a mold by atmospheric pressure when a vacuum is created between the mold and the

**FIGURE 26.4**

(a) Vacuum forming is good for making simple shapes out of sheet. (b) Blow molding is used to make plastic containers.

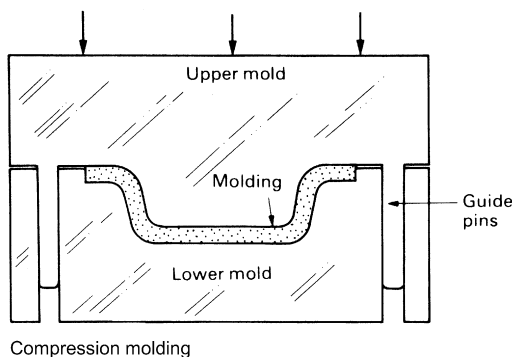
sheet, Figure 26.4(a). Plastic bottles are made by blowing instead: heated tube is clamped in a split mold and expanded with compressed air to take up its shape (Figure 26.4(b)). Both methods are cheap and quick and can be fairly accurate.

Compression molding

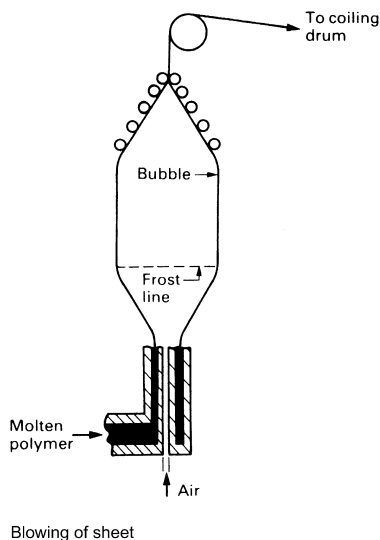
Both thermoplastics and thermosets can be formed by *compression molding* (Figure 26.5). The polymer, or resin, is heated and compressed between dies. The method is well suited to the forming of thermosets (casings for appliances, for instance) and of composites with a thermosetting matrix (car bumpers, for example). Since a thermoset can be removed while it is still hot, the cycle time is as short as 10 s for small components, 10 min for large thick-walled moldings. Pressures are lower than for injection moldings, so the capital cost of the equipment is less.

Films and fibers

Thin sheet and fine fibers of polymers are extruded, using a narrow slit, or a die with many small holes in it (a *spinnerete*). The molten polymer cools so fast when it is extruded that it solidifies in the amorphous state. A great

**FIGURE 26.5**

Compression molding: the thermoset is squeezed to shape and cured (by heating) at the same time. Once it has cured it can be taken from the mold while still hot.

**FIGURE 26.6**

Production of plastic sheet by blowing. The bubble is flattened and rolled onto a drum.

increase in strength is possible if the film or fibers are drawn off through a tensioning device which stretches them, unraveling the tangled molecules and aligning them in the plane of the sheet or along the axis of the fiber. Film has to be stretched in two directions at once: one way of doing so is to blow an enormous thin-walled bag (Figure 26.6) which is then cut, opened out flat, and rolled onto a drum.

26.5 JOINING POLYMERS

Polymers are joined by cementing, by welding, and by various sorts of fasteners, many themselves molded from polymers. Joining, of course, can sometimes be avoided by integral design, in which coupled components are molded into a single unit.

A polymer can be joined to itself by *cementing* with a solution of the same polymer in a volatile solvent. The solvent softens the surfaces, and the dissolved polymer molecules bond them together. Components can be joined by *monomer cementing*: the surfaces are coated with monomer which polymerizes onto the preexisting polymer chains, creating a bond.

Polymers can be stuck to other materials with *adhesives*. They can be attached by a variety of *fasteners*, which must be designed to distribute the fastening load uniformly over a larger area than is usual for metals, to avoid fracture. Ingenious splined or split fasteners can be molded onto polymer components, allowing the parts to be snapped together; and threads can be molded onto parts to allow them to be screwed together. Finally, polymers can be *welded* by heating the joint surfaces and then pressing them together until they have cooled.

WORKED EXAMPLE

The four photographs show uses of polymers in a petrol-engine rotary lawn mower. The polymers are all either thermoplastics or rubbers (apart from the spark plug cover, which is a thermoset). The table summarizes the parts made from plastics, and the processing routes used to make them.

Parts	Processing Route
Chassis, wheels, tires, height adjuster knob, engine cowling/fuel tank, fuel tank cap, air filter housing/gasket, fuel tap, oil filler tube, dipstick, spark plug cover, handle assembly knobs, cable clips, starter cord knob, throttle lever/housing, throttle cable ferrule, handle tube end plugs, grass box guard stop	Injection molding
Fuel line, crankcase breather tube, coating on throttle/brake cable sheaths, ignition lead insulation, grass box sealing strips, grass box floor panel, grass box guard sealing strip	Extrusion
Air filter element (open cell foam)	CO ₂ foamed molding
Starter cord, grass box	Fiber spinning, weaving

This is a graphic illustration of how polymer parts gradually replaced metals from the 1960s onward. A lawn mower from an earlier period would have



had almost no plastic parts. Uses of metals in the lawn mower are now restricted to parts which must not break or deflect significantly under large stresses or must have high fatigue and wear resistance (often under very hot conditions). These include the engine itself, the handle tubes, wheel axles/height adjusters, control cables, and numerous nuts, bolts, screws, springs, clips, and brackets. Every such part will be scrutinized by a large volume manufacturer to see if replacement by a polymer would do the job and save money. Of course, “you get what you pay for,” so excessive replacement of metals (or natural materials like wood) by polymers can result in products with an imprecise “soggy” feel to them, which does the image of plastics no favors! (No skilled artisan would ever use hammers or wood chisels with rubber-coated handles, of the kind popular with DIY superstores.)

EXAMPLES

26.1 Describe in a few words (using examples or sketches if you want to) what is meant by the following:

- (a) An addition reaction.
- (b) A condensation reaction.

- 26.2** Describe in a few words (using examples or sketches if you want to) what is meant by the following:
- (a) A copolymer.
 - (b) A block copolymer.
- 26.3** Describe in a few words (using examples or sketches if you want to) what is meant by the following:
- (a) A plasticizer.
 - (b) A toughened polymer.
 - (c) A filler.
- 26.4** What forming process would you use to manufacture each of the following items:
- (a) A continuous rod of PTFE.
 - (b) Thin polyethylene film.
 - (c) A PMMA protractor.
 - (d) A ureaformaldehyde electrical switch cover.
 - (e) A fiber for a nylon rope.
- 26.5** Low-density polyethylene is being extruded at 200 °C under a pressure of 60 MN m⁻². What increase in temperature would be needed to decrease the extrusion pressure to 40 MN m⁻²? The shear rate is the same in both cases. (Hint: use Equations (25.13) and (25.14) with $C_1 = 17.5$, $C_2 = 52$ K, and $T_0 = T_G = 270$ K.)

Answer

32 °C.

- 26.6** Discuss the problems involved in replacing the metal parts of an ordinary bicycle with components made from polymers. Illustrate your answer by specific reference to the frame, wheels, transmission, and bearings.
- 26.7** The elastic stress–strain relations for an isotropic material are

$$\begin{aligned}\varepsilon_1 &= \frac{\sigma_1}{E} - \nu \frac{\sigma_2}{E} - \nu \frac{\sigma_3}{E} \\ \varepsilon_2 &= \frac{\sigma_2}{E} - \nu \frac{\sigma_1}{E} - \nu \frac{\sigma_3}{E} \\ \varepsilon_3 &= \frac{\sigma_3}{E} - \nu \frac{\sigma_1}{E} - \nu \frac{\sigma_2}{E}\end{aligned}$$

1, 2, 3 represent the three principal axes (the x , y , z axes). ε_1 , ε_2 , ε_3 are the strains along the 1, 2, 3 axes, σ_1 , σ_2 , σ_3 are the stresses along the 1, 2, 3 axes, E is Young's modulus, and ν is Poisson's ratio. (See EM1Ed4, Chapter 3, A Note on Stresses and Strains in 3 Dimensions.) An elastic material is loaded in tension along direction 3, but the Poisson's ratio contraction that would normally occur along directions 1 and 2 is prevented by applying sufficiently large balancing tensile stresses along the 1 and 2 directions. In this case, by

definition, $\varepsilon_1 = 0$, $\varepsilon_2 = 0$; and $\sigma_1 = \sigma_2$ by symmetry. Calculate the value of the tensile elastic modulus in direction 3 in terms of E and ν . This highly constrained modulus is called the axial modulus and is given by $E_{\text{ax}} = \sigma_3/\varepsilon_3$.

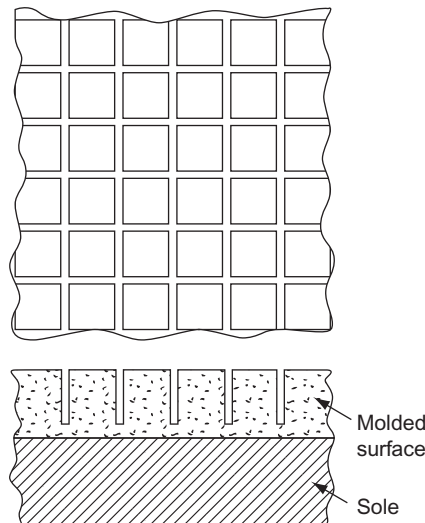
Answer

$$E_{\text{ax}} = \frac{E(1 - \nu)}{(1 - 2\nu)(1 + \nu)}.$$

- 26.8** The diagram shows the sole of a shoe which is surfaced with a soft rubber layer. The rubber has a Poisson's ratio of 0.49. The diagram shows treads molded in the surface layer, but in the interests of reducing manufacturing costs, *solid* rubber sheet (with no treads) is to be stuck on to the sole instead. The sole is hard rubber and has a much larger Young's modulus than the soft rubber used for the surface layer. The sole constrains the surface layer, so when the layer is compressed normal to the surface and wants to expand sideways (owing to the Poisson's ratio expansion) it cannot do so. Calculate the ratio of the axial modulus (normal to the surface) to Young's modulus for the surface layer. If the surface layer is molded as shown in the diagram, what modulus should be used to describe its stiffness normal to the surface? Comment on how the "softness" of the shoe is affected by having treads.

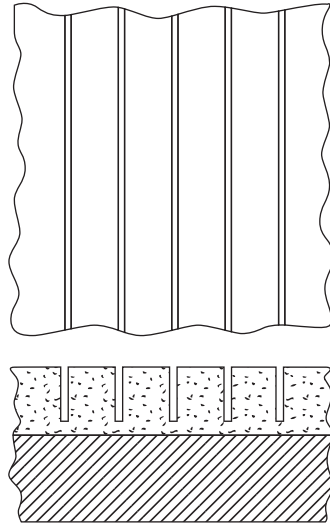
Answer

17.1.



- 26.9** Having been convinced by your calculations that treads are worth the extra cost, a colleague suggests that a surface layer which is almost as soft can be

produced at lower cost by molding a surface layer as shown in the following diagram.



The sole now only constrains the surface layer along the length of the treads. Using the elastic stress–strain relations given in Example 26.7, obtain an expression for the value of the elastic modulus normal to the surface in terms of E and ν (this modulus is the plane-strain modulus, E_{ps}). Hence calculate the ratio of the plane-strain modulus to Young’s modulus for the surface layer. Was your colleague’s intuition correct?

Answers

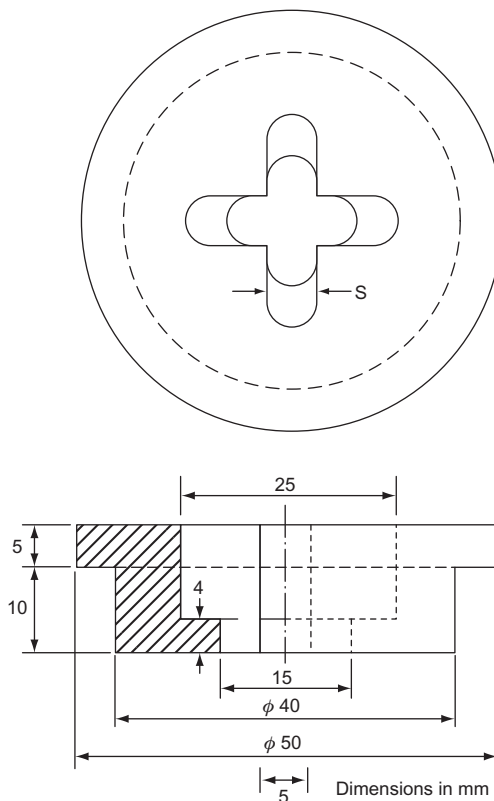
$$E_{ps} = \frac{E}{(1 - \nu^2)}; \quad 1.32.$$

26.10 Referring to Examples 26.8 and 26.9, an objective way of comparing the performance of the three different types of rubber surface layer is to apply a compressive stress normal to the surface and increase the stress until a fixed amount of elastic strain energy U_{el} has been put into the rubber. The peak stress for each surface layer is then compared. Using this method, calculate the ratio of (a) (peak stress no-tread layer)/(peak stress two-way tread layer), (b) (peak stress one-way tread layer)/(peak stress two-way tread layer), (c) (peak stress no-tread layer)/(peak stress one-way tread layer). Comment on your answers. Assume as a first approximation that $U_{el} = \sigma^2/2E$, where U_{el} is a constant and E is any one of the three moduli under consideration.

Answers

(a) 4.14; (b) 1.15; (c) 3.61.

- 26.11** Assuming that the long-chain molecules of the rubber in both the surface layer and the sole have the same composition and average degree of polymerization, how would you process the rubber so the sole has a much higher Young's modulus than the surface layer?
- 26.12** List the main methods by which the component shown in the following diagram could be made from aluminum alloy, alumina, or high-density polyethylene. For each method, state briefly any advantages and disadvantages and say whether it is more suitable economically for the production of (a) a single component, (b) a small batch, or (c) large scale production.



- 26.13** A plastic gear rack was made by hot-pressing small beads (≈ 0.2 mm diameter) of thermoplastic in a split mold. Owing to incomplete densification, pores ≈ 1 mm in diameter were left in the product. These led to cases of gear teeth breaking off in service. When the fracture surfaces were examined, pores could be seen intersecting them. Because of the incomplete fusion of the polymer beads, the edges of the pores were quite "sharp" (the neck between adjacent beads had not grown very much). Treating the pore as a sharp crack with an effective crack length a equal to the pore radius, estimate the fracture stress caused by the pores. Use Equation (25.15). Assume that

$K_c = 1 \text{ MN m}^{-3/2}$ and $Y = 1$. Compare your answer to the tensile strength of the solid polymer ($\approx 50 \text{ MN m}^{-2}$) and comment on the implications for quality control in polymer processing.

Answer

25 MN m^{-2} .

- 26.14** Even when the temperature is $\leq T_G$, the modulus of unreinforced plastics is still much less than those of metals or ceramics. Explain, giving examples, why this is an advantage when assembling plastic parts either to other plastic parts, or to parts made from metals or ceramics.
- 26.15** A long horizontal plastic trim is to be fitted to the side of an automobile at a position $\approx 200 \text{ mm}$ above the level of the door sills. The trim is an extruded section measuring 30 mm wide by 10 mm thick. The face of the trim in contact with the thin ($\approx 1 \text{ mm}$) steel skin of the doors and body can be recessed by the extrusion die to give any reasonable cross section required. Design plastic fittings which are suitable for fixing the trim to the skin by means of 5 mm holes drilled through the skin every 200 mm along the centerline of the trim. You may assume that it is not necessary to remove the trim once it has been fitted.
- 26.16** Electrical wires made from copper are often covered with a tubular layer of polymer (e.g., PVC) to insulate them. Design a die which can be connected to the output end of an extruder and used to coat wire with polymer insulation on a continuous basis.
- 26.17** When polymer tubes are extruded, it is usual practice to attach a quite long metal tube to the end of the extruder and to pass the extruded tube through the metal tube. The bore of the metal tube is the same as the outer diameter of the extrusion die. The metal tube is externally cooled by a cold water jacket. Explain why this is done.

Case Studies in Polymers

27.1 FATAL BUNGEE JUMPING ACCIDENT

Bungee jumping is a very popular sport worldwide, and the spectacular vertical movements of its practitioners are made possible only by the enormous elastic extensions (up to 800%) of the rubber filaments used to make the ropes.

http://en.wikipedia.org/wiki/Bungee_jumping; http://www.youtube.com/watch?v=Ve_MADvATyQ (17 55 42.60 S 25 51 26.25 E)

It is said that a million successful jumps have been made to date, so on a purely statistical basis it is not surprising that there have been a few serious accidents on the way, as we illustrate in this case study.

Figure 27.1 shows the general set-up for the bungee jump. The jumper (height 1.83 m and weight 132 kg) jumped from a crane-mounted cage, which had its floor approximately 53 m above ground level. The inboard end of the bungee rope was secured to a pair of snap hooks mounted on the vertical centerline of the cage and positioned approximately 1.35 m above the cage floor. The rope passed vertically down through a large circular hole in the floor of the cage. Before the jump commenced, the rope would have turned back up again so that the outboard end would have entered the cage through the access gateway and sat on the cage floor.

The jumper was attached to the outboard end of the rope by means of a pair of cuffs pulled tight around the lower legs. Each cuff was attached to the end of the rope by a webbing strap. As a safety measure, the jumper was independently attached to the end of the rope by a length of webbing tape (woven from polymer fibers), knotted to his body harness. The nominal strength of the tape was 12,500 N, but in practice the breaking strength would have been less because of the weakening effect of the knot.

The jumper jumped off the edge of the cage through the open gateway, taking the outboard end of the rope with him in the normal way. During the

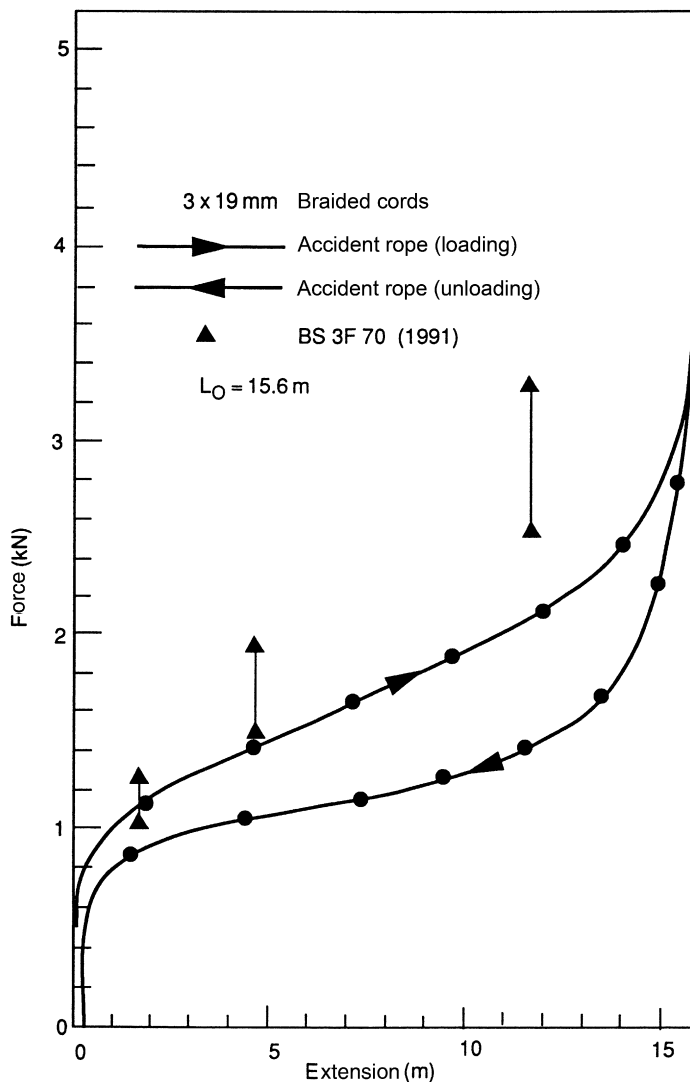
side by side and taped together with insulating tape at regular intervals. Each cord had a braided sheath (19 mm OD) woven from polymer fibers, containing a large number of fine, parallel rubber filaments.

The tapes were removed, and the three cords separated. One of the cords was tested to an extension of 16.0 m (100% strain). At this extension, the measured force was 135 kg (1324 N). The force/extension curve for the complete assembly of three cords was obtained by multiplying the forces measured in the single cord by a factor of 3. As shown in [Figure 27.2](#), the curve has a highly nonlinear shape, which is primarily determined by the complex extensional behavior of the braided sheath. Note, that at the extension of 16.0 m, the force rises almost vertically with extension. The breaking strength of the rope was not determined on safety grounds but is likely to be much higher than the maximum force of 3972 N obtained from the test. Nevertheless, the rope had become a very stiff structural element at an extension of 16.0 m, and a small additional extension would probably have caused failure of the braid. The extension of 16.0 m can therefore be considered as being the “limit of extension” in practical terms. The area under the force/extension curve represents the stored strain energy in the complete rope assembly. The fact that the unloading curve falls well below the loading curve means that only a proportion of the stored strain energy is released on unloading. This *hysteresis* energy loss explains why in a normal bungee jump, the jumper rebounds to a height significantly less than the height of the cage.

A tensile test to fracture was carried out on a webbing assembly identical to that which failed in the accident. The graph of the force/extension curve is shown in [Figure 27.3](#); the sling broke at 5000 N near a knot.

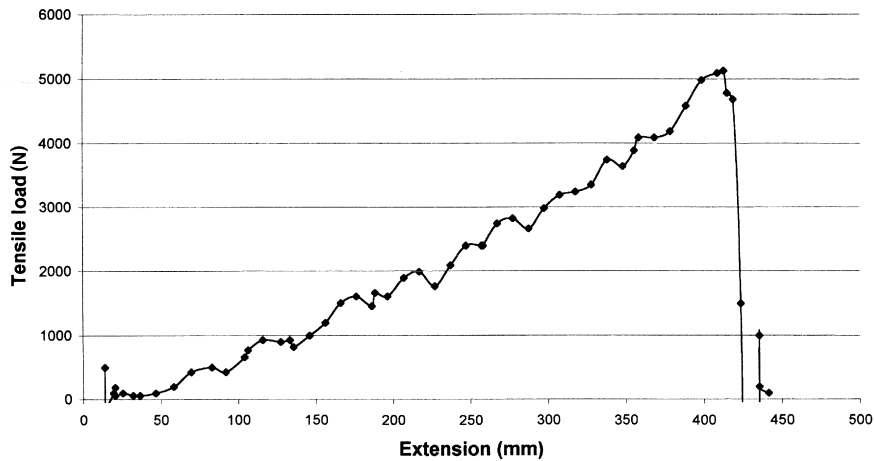
The mechanics of the jump were analyzed using an energy-based approach, as shown in [Figure 27.4](#). In the first stage of the descent, the jumper is in freefall. He progressively loses potential energy, which goes into progressively increasing his kinetic energy (and hence his speed). However, once the rope becomes taut and then stretches, it absorbs strain energy. In this second stage of the descent, the loss in the potential energy of the jumper is converted into strain energy as well as kinetic energy. This has the effect of slowing the jumper down. However, the jumper will only be arrested safely if all his potential energy can be absorbed as strain energy in the rope.

The calculations show that the maximum strain energy which the bungee rope can absorb before it reaches the limit of extension (the area under the loading curve in [Figure 27.2](#)) is 28,660 J. However, the potential energy released by the jumper as he falls to the limit of extension is 42,344 J. This leaves a surplus of 13,684 J as kinetic energy, so he continues to travel downward (at a speed of 14.4 m s^{-1}) rather than being arrested by the rope.

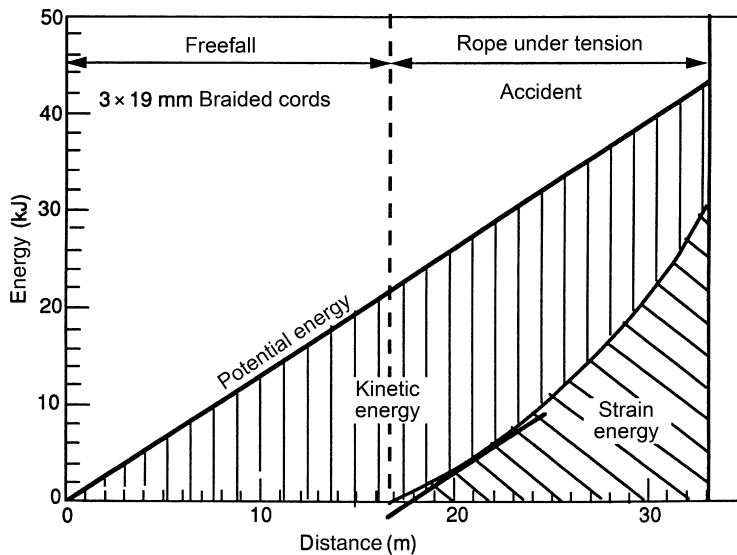
**FIGURE 27.2**

Force/extension curve for the bungee rope, showing both loading and unloading curves. The force/extension characteristics for a new rope consisting of three 19 mm cords, as specified by BS 3F 70, are shown as triangular data points.

The shape of the force/extension curve in Figure 27.2 indicates that the force in the rope at the moment of release could have been anywhere between 3972 N (405 kg) and the breaking strength of the rope. In this context, it is hardly surprising that the cuffs were pulled off the jumper's legs. Once the legs have pulled out of the cuffs, the remaining kinetic energy of the falling

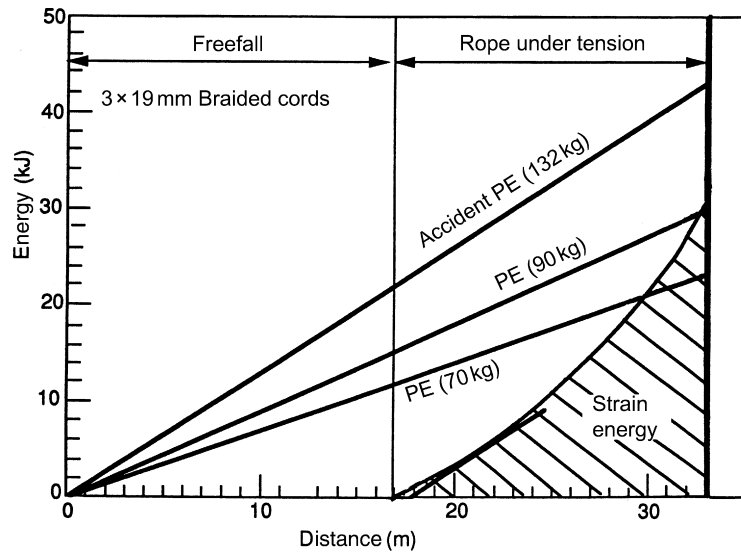
**FIGURE 27.3**

Force/extension curve for the webbing tape.

**FIGURE 27.4**

Energy diagram for the bungee jumping process (accident case).

jumper (13,684 J) must be absorbed by the safety webbing if arrest is to occur. The energy absorbed by the safety webbing was calculated from the area under the force/extension curve (see Figure 27.3) and was found to be 940 J—only 7% of the 13 684 J required for arrest. In other words,

**FIGURE 27.5**

Energy diagram for the bungee jumping process (accident case, plus variants for reduced body mass of 90 and 70 kg).

the webbing was totally inadequate in terms of static strength and, most crucially, energy-absorbing capacity. A dedicated energy-absorbing device should have been used instead, capable of absorbing the kinetic energy of the falling jumper without applying excessive force to his body.

In spite of the defects of the cuffs and the safety webbing, the root cause of the accident was the use of a bungee rope with an unsuitable force/extension curve. As shown in Figure 27.5, to bring the falling jumper to rest at the limit of extension, the weight of the jumper should have been no more than 90 kg.

To have a *safe* arrest, the rope must absorb all the potential energy of the falling jumper well *before* the limit of extension of the rope is reached. This will also limit the maximum force in the load-bearing system to calculable levels, reducing the risk of cuff release. If the cuffs do release, a well-designed safety webbing should not break in these circumstances. As an example, Figure 27.5 shows the energy balance for a body weight of 70 kg. In this case, it is clear that there is significant spare energy-absorbing capacity in the rope. The rope is only extended by 13 m, 3 m short of the limit of extension. This produces a force of 2250 N (229 kg) (see Figure 27.2). However, even this force is 3.27 times body weight, and a g-force of 3.27 may well cause physical damage to the jumper.

Cords should be tested on a periodic basis to ensure that there is no drift in the force/extension curve with time and usage. The force/extension characteristics specified in BS 3F 70 for new 19 mm cord are as follows. For 10% extension (1.56 m in the case study), the force must be at least 340 N (1020 N for three cords in parallel). For 30% extension (4.68 m), the force must be between 500 and 650 N (1500 and 1950 N for three cords). For 70% extension (11.70 m), the force must be between 850 and 1100 N (2550 and 3300 N for three cords). The minimum total extension must be 105% (16.38 m). These data points are plotted in [Figure 27.2](#). Comparison of the specified and actual data shows that the bungee rope has suffered significant degradation of energy-absorbing capacity as the result of repeated use.

In conclusion, the technical cause of the accident was the use of a bungee rope with an unsuitable force/extension curve, only able to absorb 68% of the potential energy of the falling jumper at the limit of extension. This was partly due to degradation of the cords, presumably as the result of repeated use. As a result, the rope did not arrest the falling jumper, who was consequently subjected to a large force, sufficient to pull the cuffs off his legs. Subsequent to cuff release, the safety webbing took the full force of the rope. Because of its low strength and inadequate energy-absorbing capacity, the webbing broke and the jumper fell to the ground with a speed of impact equivalent to a freefall from a height of 31 m. However, had the relevant authorities imposed a mandatory code derived from a quantitative mechanics-based analysis (such as that done here), the accident could not have occurred.

On a final note, braided ropes of the type encountered in this case study are generally used when it is important to impose a well-defined limit on the distance fallen (essentially so that jumpers falling from low platforms do not bang their heads on the ground). Although the rubber filaments themselves are capable of very large extensions, the much stiffer braided sheath imposes a limit of extension on the assembly of only 105% (or a little more). On the other hand, unbraided ropes are generally used when much greater percentage elongations are required, as in the more extreme sporting situations. Although the analysis described here can in principle be applied to unbraided ropes, they have a very much “softer” force/extension curve than braided ropes. Then, the critical parameter is not the maximum force, but the maximum extension. One of the authors (DRHJ) has witnessed jumpers descending head first from the deck of the Victoria Falls railway bridge (on the border between Zambia and Zimbabwe) to within a few feet of the Zambesi river, some 360 ft below. In such situations, minor changes in the force/extension characteristics of the rope can have tragic results (not because the jumper breaks away from the rope, but because the jumper smashes their head on a rock in the river bed).

27.2 POLYETHYLENE GAS PIPES

Gray cast iron was first used for underground pipes for the distribution of water and gas over 150 years ago, and pipes installed 80–100 years ago are still in service today. They are cast to tubular shape, and connected end to end by spigot-and-socket joints (Figure 27.6). The joint gap is packed with hemp fibers (a natural fiber) and molten lead poured into the joint. The lead solidifies and seals the ends of the pipes together. The pipes have two main disadvantages: the material is inherently brittle (because of the weakening effect of the graphite flakes), and it corrodes (damp soil can be very corrosive). The elongation to failure and fracture toughness are typically only 0.4% and $10 \text{ MN m}^{-3/2}$. A secondary disadvantage is the tedious process of making the joints, and (for water mains in soft water areas) the undesirability of having lead in contact with drinking water.

Old water mains often develop leaks because the gray iron pipes have fractured or corroded. This is a major problem to water utilities because of the proportion of the water supply lost as leaks, the disruption to supplies, and the expense of replacing degraded lengths of main. However, such failures rarely endanger life and limb. On the other hand, leaks from broken or corroded gas mains are potentially lethal. Between 1972 and 1984 in the UK, leaks from cast iron gas mains led to an average of 18 explosions per year (there were 19 fatalities as a result). A particularly bad (and therefore well documented) incident occurred in 1985 in Putney, South-West London, UK, in a block of apartments called Newnham House (part of a development called Manor Fields, built in 1934)—51° 27' 14.70" N 0° 13' 15.00" W.

Early in the morning of 10 January 1985, a resident of one of the top floor apartments noticed a slight smell of gas. He opened his front door and found that the smell of gas on the landing outside was much stronger. A few minutes later, a huge explosion occurred which demolished the six apartments in the center of the block and broke windows in buildings over a

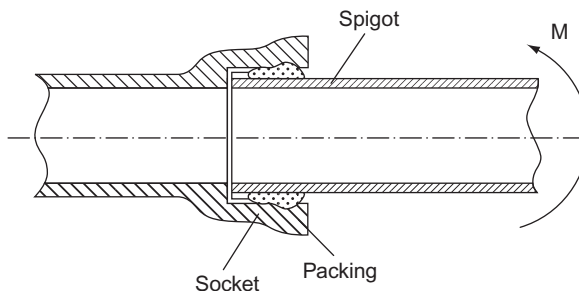


FIGURE 27.6

Longitudinal section through spigot-and-socket joint.

quarter mile radius. Of the nine people in the apartments at the time, only one survived. This major incident really set alarm bells ringing, as the following links show:

<http://www.guardian.co.uk/fromthearchive/story/0,,1378751,00.html>

<http://hansard.millbanksystems.com/commons/1985/jan/10/putney-explosion>

http://hansard.millbanksystems.com/written_answers/1984/jan/17/gas-explosion-putney

http://hansard.millbanksystems.com/written_answers/1985/jul/25/putney-gas-explosion

Origin of gas leak

Figures 27.7 and 27.8 show the location of the gas leak. A narrow access road runs along the back of Newnham House. Buried about 0.8 m beneath the surface of the road was a gas supply main made up from lengths of gray cast iron pipe joined together by spigot-and-socket joints. The pipe had a nominal bore of 150 mm and wall thickness of 11 mm.

The road had originally been laid as reinforced concrete panels of various lengths. The concrete was 100–150 mm thick and had a central layer of reinforcing mesh. The road had been dug up on previous occasions and when the surface had been reinstated, the concrete had not been reinforced. Because of this there were a number of transverse breaks in the road surface.

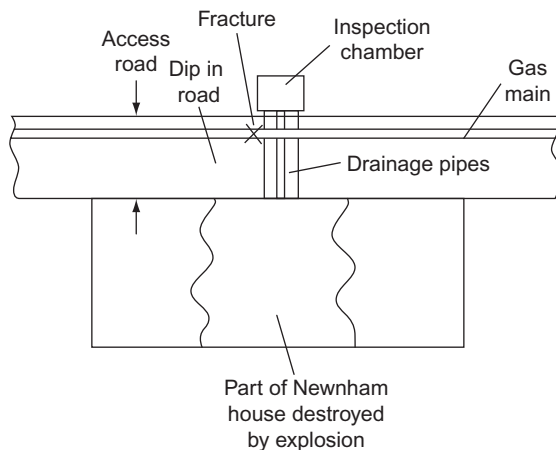
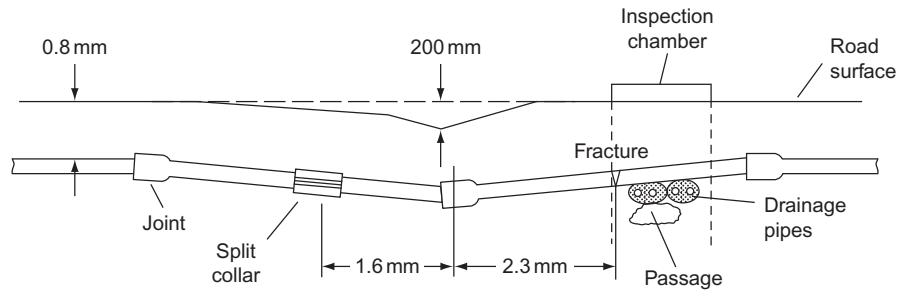


FIGURE 27.7

Plan view showing location of leaking gas main.

**FIGURE 27.8**

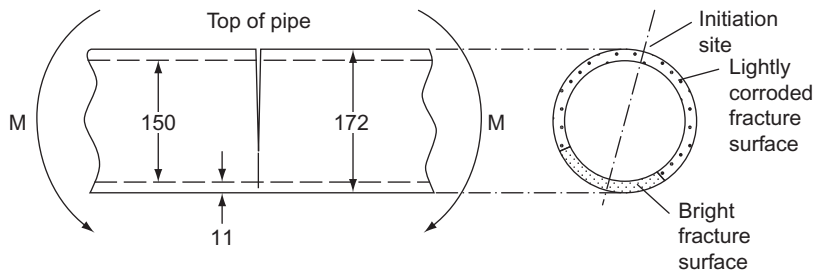
Elevation of gas main in region of leak.

As shown in Figure 27.8, the surface of the road had settled by 200 mm in one place. The settlement was first noticed in 1983, and by 1984 the residents were complaining about the pool of water which gathered in the depression when it rained.

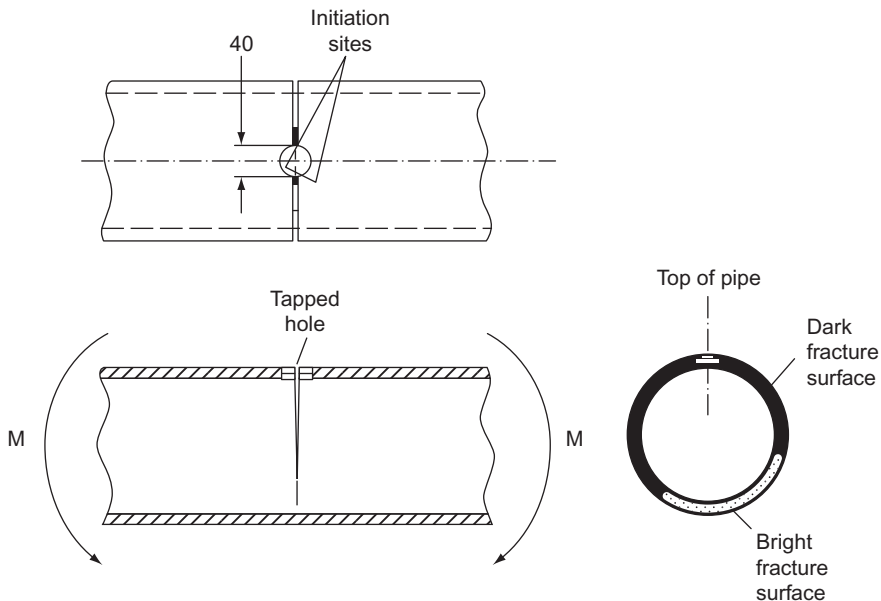
The ground beneath the gas main was found to be poorly consolidated. Presumably, when the footings were dug for Newnham House the ground under the access road was filled with loose subsoil and rubble which was not adequately compacted. As shown in Figure 27.8, the gas main had settled where it ran below the dip in the road. The ground had obviously given way below the pipes and this meant that they had to support the weight of the soil and concrete that lay immediately above.

On the opposite side of the road from Newnham House was a brick-built inspection chamber which took the outflow from two pairs of drainage pipes. Each drainage pipe was made from earthenware sections and the two pipes in each pair were cased in concrete. The underside of the gas main was in firm load-bearing contact with the top of the concrete casings. The pipe was not able to settle in this place and differential settlement had set up a bending stress in the pipe. The pipe had fractured close to the point of support and this had allowed gas to escape from the main.

Settlement beneath the drainage pipes had opened up a horizontal passage about 75 mm deep and 300 mm wide which allowed the leaking gas to pass from the break in the pipe to the outside wall of Newnham House. The gas then seeped through gaps in the brickwork below road level into the open void which lay beneath the ground floor of the building. Once in the void, the gas was able to spread around the building through the service ducts and the gaps between the wooden floorboards. Eventually an explosive mixture formed and it only needed someone to light a gas ring for the mixture to explode.

**FIGURE 27.9**

Details of the 1985 failure. Dimensions in millimeters.

**FIGURE 27.10**

Details of the 1982 fracture. Dimensions in millimeters.

Details of fractures

Figure 27.9 shows details of the 1985 fracture. There had also been an earlier crack in 1982 (Figure 27.10), which started at a threaded hole for a branch pipe (generating a stress concentration of ≈ 2.4). The 1982 crack had been repaired with a gas-tight “split collar” (see Figure 27.8). One would think this earlier fracture should have flagged up that the pipe was subjected to bending stresses. Analyzing the stresses involved is not simple, partly because

Table 27.1 Bending Moments (kN m) at the Two Failure Locations

Failure Location	Moment to Break Pipe	Applied Moment at Failure Location (Joint Assumed Solid)	Applied Moment at Failure Location (Joint Assumed Flexible)
1982	12 (SCF ≈ 2.4)	19	31
1985	29	19	23 (30 with garbage truck)

of the uncertain nature of the loading and support conditions, but also because it is not clear to what extent the lead-filled joint could have deformed by creep. Table 27.1 gives best estimates, which demonstrate that the 1982 failure should certainly have occurred; and the 1985 failure was plausible (when account is taken of the extra load imposed by the weekly appearance of the garbage truck!)

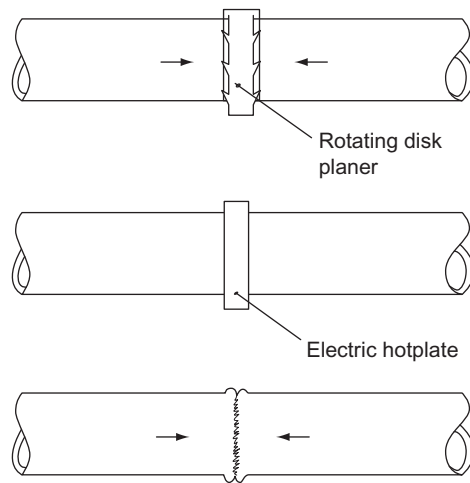
Polymers to the rescue

The Putney gas explosion was a real wake-up call, and accelerated the replacement of old gray cast iron pipes by polymers such as medium-density polyethylene (MDPE), high-density polyethylene (HDPE), and unplasticized polyvinylchloride (UPVC). HDPE has a tensile strength of $\approx 20\text{--}37\text{ MN m}^{-2}$ (which is more than adequate for typical internal pressures). Most importantly, though, it has a *Young's modulus* which is $\approx 150\text{--}300$ times less than cast iron. This means that HDPE pipes can *deflect* under misalignments of the kind experienced in the Putney explosion *without reaching the fracture stress*. Even better, over a long time the polymer also *creeps*, which further dissipates the stresses caused by misalignment. Polymers are also very resistant to corrosion, so should last indefinitely in the ground.

But how are lengths of polymer pipe joined together? The following clip shows how:

<http://www.youtube.com/watch?v=83PTUoFBq9s&feature=related>

The steps in the process are shown in Figure 27.11. First, the ends of the pipe to be joined are machined flat and parallel using a double-sided rotating disk planer. Then the ends are heated with an electric hotplate. Finally, the hot faces are pushed together using a hydraulic ram. The softened thermoplastics fuse together, making a high-strength leak-proof joint. This is a quick, reproducible method, which requires little skill on the part of the operator—in marked contrast to the lead-filled spigot-and-socket joints of the old cast iron system. Figures 27.12 and 27.13 show an alternative joining method, where one end of the pipe has an enlarged bore into which

**FIGURE 27.11**

Welding plastic pipe ends together.

**FIGURE 27.12**

A stack of plastic pipes ready to go in the ground. Harbour Street, Mosman, NSW, Australia (33 49 33.60 S 151 14 21.20 E).

the mating pipe can be inserted. This overlapping joint can then be fixed and sealed with polymer adhesive. It would be hard to envisage any replacement materials so well adapted to this challenging environment than thermoplastics.

**FIGURE 27.13**

Pipe ends, showing enlarged diameters for sleeve-type joints.

We leave you with an amusing story (well, not if you have to pay the bill), which shows how things can occasionally go wrong even with polymer pipes—and continue to go wrong with cast iron pipes.

<http://www.scotcourts.gov.uk/opinions/A53009.html>

This also gives a taste of the sorts of complications engineers can get into if they have to appear in a courtroom!

27.3 ULTRA-STRONG FIBERS FOR YACHT RIGGING

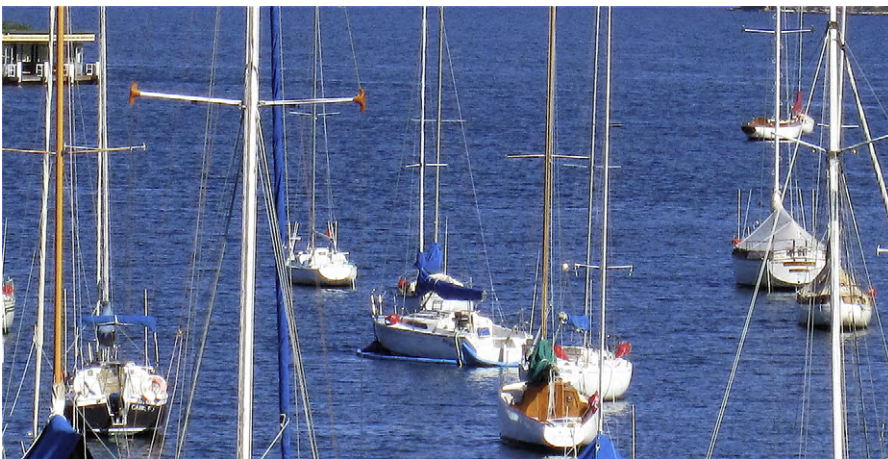
In our final case study, we turn from the highly extendable rubber filaments used in bungee ropes, through polymer pipes strong enough to resist internal pressure but able to bend when the ground subsides, to the very strongest and stiffest of polymer fibers, used for lightweight tension members in structures like yacht rigging, buildings, bridges (and for many other things, too). Typical data for fibers are given in Table 27.2.

Figure 27.14 shows a typical scene in yachting territory. You can see masts held up by *standing rigging*—the *shrouds* (which stop the mast going sideways), the *forestay* (which stops the mast going backward), and the *backstays* (which stop the mast going forward). The boats shown are quite old and conventional, with rigging made from hard drawn stainless steel wires (because of salt water corrosion). As Table 27.2 shows, steel wire has a low value of σ_{TS}/ρ , and the weight of the rigging could be reduced by a factor of $3700/250 = 15$, if PBO polymer fiber bundles were used instead. Of course, strength is not the only criterion here, because rigging must also be *stiff*—the

Table 27.2 Typical Data for Strong, Stiff Polymer Fibers, Ceramic Fibers, and Steel Wire

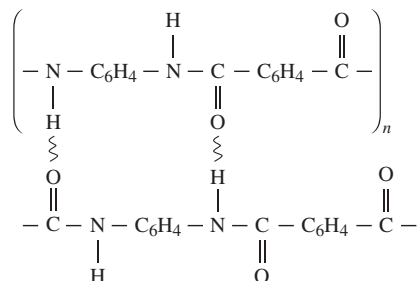
Fiber/Wire	E (GN m ⁻²)	σ_{TS} (MN m ⁻²)	ρ (Mg m ⁻³)	σ_{TS}/ρ	ϵ_f (%)
Steel wire (hard drawn)	200	2000	7.85	250	≥1
Carbon fiber (Polyacrylonitrile, PAN)	390	4000	1.90	2100	1
Aramid fiber (Kevlar, high modulus)	126	3600	1.44	2500	2.9
PBO (Polybenzoxazole, Zylon)	270	5800	1.56	3700	2.2
UHMWPE (ultrahigh-molecular-weight polyethylene, Dyneema)		2400	0.97	2500	
Glass fiber (S-Glass)	69	4000	2.48	1600	5

Note—the mechanical properties of fibers vary greatly depending on the processing parameters. <http://en.wikipedia.org/wiki/Kevlar>; <http://en.wikipedia.org/wiki/Zylon>; http://en.wikipedia.org/wiki/Ultra-high-molecular-weight_polyethylene

**FIGURE 27.14**

Yacht rigging. Mosman Bay, NSW, Australia (33 50 19.20 S 151 13 49.30 E).

stays must not *extend* much when they come under load, otherwise the mast will not be supported properly. High-strength steel wire extends by little more than 1% when it reaches the tensile limit, so it works well as a stay material; so does carbon, for the same reason. PBO extends by more—2.2%—but this is small enough in many situations. It is therefore not surprising that in recent years polymer fibers such as PBO, and other strong, stiff fibers like Kevlar, UHMWPE, and carbon are now standard in the huge ocean racing yachts like the “Maxis.” In fact, the properties of the four best materials in Table 27.2 are sufficiently close that other properties may determine which to choose for a specific use. For example, some fibers degrade in

**FIGURE 27.15**

Aligned molecular structure of Kevlar fibers.

UV, visible light, or seawater (although this is usually prevented by coating the aligned fiber bundle with a skin of an “ordinary” polymer like polyethylene, which also protects the fibers from mechanical damage).

<http://www.futurefibres.com/Rigging.html>

These strong, stiff polymer fibers are also much used in specialized civil engineering applications (for the same reasons that they are in yacht rigging). An interesting example is the Kevlar cable stays on the Aberfeldy Foot Bridge, Scotland, UK: 56 37 30.00 N 3 52 13.35 W. Built in 1992, this was the World’s first all-plastic footbridge: <http://linearcomposites.net/?pageid=Parafil.xml>. Another example (which generations of Cambridge engineering students will have seen without ever thinking about it) are the Kevlar snow-loading stays on the roof of the Cambridge Bus Station, UK (built 1991): 52 12 19.40 N 0 07 26.60 E.

Why are these polymer fibers so strong and stiff? As an example, [Figure 27.15](#) shows the aligned molecular structure of Kevlar fibers. As well as the carbon–carbon bonds being aligned parallel to the loading direction, adjacent long-chain molecules are bonded together very tightly by the frequent hydrogen bonds between the oxygen and hydrogen side groups. This is an excellent example of using polymer chemistry to tailor-make the properties you want by manipulating the molecular structure and bonding.

EXAMPLES

- 27.1** Give examples of applications of polymer fibers which require (a) a high stiffness, (b) a low stiffness. Explain why your examples *do* require the specified fiber stiffness.
- 27.2** Why is it important that strong, stiff fibers do not creep appreciably in use? What features of the molecular structure of aligned Kevlar fibers are likely to minimize creep?

- 27.3** Explain what is meant by hysteresis. How does it affect the shape of the force–extension curve for a bungee rope? Why is it important that bungee ropes show hysteresis? How does the behavior of the long-chain molecules cause hysteresis?
- 27.4** The fracture toughness of high-density polyethylene at room temperature is about 1/3 that of gray cast iron. However, although buried cast iron pipes will usually snap if the ground subsides, HDPE pipes will not. Explain this apparent paradox.
- 27.5** The tensile strength of a particular grade of PBO is 2700 MN m^{-2} . However, a 40 mm diameter cable made from parallel PBO fibers has a tensile strength of only 1800 MN m^{-2} , calculated as (breaking load of cable)/(gross cross-sectional area of cable). Explain this difference.
- 27.6** A large cylindrical storage tank (axis vertical) was made from polypropylene sheet 12 mm thick. The tank was 3.6 m high and 2.7 m diameter. The tank wall was made from three rectangles of sheet, each 1.2 m wide by $\pi 2.7$ m long. These were bent at room temperature into the required radius, and the ends brought together, before the (vertical) joint was heat welded. The three cylindrical pieces were then welded end to end to make up the complete tank wall. In service, the tank contained dense chemical liquid, which imposed a uniform hoop stress on the vertical welds. However, only 5 months after installation, the vertical weld in the lowest section of the tank ruptured due to the growth of a creep crack, which had started at the outside surface of the tank. Why did the rupture occur near the bottom of the vessel? Why did the creep crack start at the outside surface?

Properties of Composites and Foams

28.1 INTRODUCTION

The word “composites” has a modern ring. But using the high strength of fibers to stiffen and strengthen a cheap matrix material is probably older than the wheel. The Processional Way in ancient Babylon, one of the lesser wonders of the ancient world, was made of bitumen reinforced with plaited straw. Straw and horse hair have been used to reinforce mud bricks (improving their fracture toughness) for at least 5000 years. Paper is a composite; so is concrete: both were known to the Romans. And almost all natural materials which must bear load—wood, bone, muscle—are composites.

The composite industry, however, is much more recent. It has grown rapidly in the past 60 years with the development of *fiber composites* starting with *glass-fiber reinforced polymers* (GFRP or fiberglass) and followed by *carbon-fiber reinforced polymers* (CFRP) and Kevlar-fiber reinforced polymers (KFRP). Their use in boats, and their increasing replacement of metals in aircraft and ground transport systems, is a revolution in material usage which is still accelerating.

Composites need not be made of fibers. Plywood is a *lamellar composite*, giving a material with uniform properties in the plane of the sheet (unlike the wood from which it is made). Sheets of GFRP or of CFRP are laminated together, for the same reason. And sandwich panels—composites made of stiff skins with a low-density core—achieve special properties by combining, in a sheet, the best features of two very different components.

Cheapest of all are the *particulate composites*. Aggregate plus cement gives concrete, and the composite is cheaper (per unit volume) than the cement itself. Polymers can be filled with sand, silica flour, or glass particles, increasing the stiffness and wear resistance, and often reducing the price. And one particulate composite, tungsten carbide particles in cobalt (known as “cemented carbide” or “hard metal”), is the basis of the cutting tool industry.

But high stiffness is not always what you want. Cushions, packaging, and crash padding require materials with moduli that are lower than those of any solid. This can be done with *foams*—composites of a solid and a gas—which have properties that can be tailored, with great precision, to match the engineering need.

We now examine the properties of fiber composites and foams in a little more detail. With these materials, more than any other, properties can be designed-in; the characteristics of the material itself can be engineered.

28.2 FIBER COMPOSITES

Polymers have a low stiffness and (in the right range of temperature) are ductile. Ceramics are stiff and strong but are brittle. In *fiber composites*, we exploit the great strength of ceramic while avoiding catastrophe: brittle failure of fibers leads to a progressive, not a sudden, failure.

If the fibers of a composite are aligned along the loading direction, then the stiffness and the strength are, roughly speaking, an average of those of the matrix and fibers, weighted by their volume fractions. But not all composite properties are just a linear combination of those of the components. Their great attraction lies in the fact that, frequently, something extra is gained.

The toughness is an example. If a crack simply ran through a GFRP composite, one might expect the toughness to be a simple weighted average of glass and epoxy; and both are low. But that is not what happens. The strong fibers pull out of the epoxy. In pulling out, work is done and this work contributes to the toughness of the composite. The toughness is greater—often much greater—than the linear combination.

Polymer–matrix composites for aerospace and transport are made by laying up glass, carbon, or Kevlar fibers (Table 28.1) in an uncured thermoset resin. The resin is then cured, taking up the shape of the mold and bonding to the fibers. Many composites are based on epoxies, though there is now a trend to using the cheaper polyesters.

Laying-up is a slow, labor-intensive job. It can be by-passed by using thermoplastics containing chopped fibers which can be injection molded. The random chopped fibers are not as effective as laid-up continuous fibers, which can be oriented to maximize their contribution to the strength.

But the flow pattern in injection molding helps to line the fibers up, so that clever mold design can give a stiff, strong product.

Making good fiber composites is not easy; large companies have been bankrupted by their failure to do so. But suppose you can make them, you still have to know how to use them. That needs an understanding of their

Table 28.1 Properties of Some Fibers and Matrices

Material	Density ρ (Mg m ⁻³)	Modulus E (GN m ⁻²)	Strength σ_f (GN m ⁻²)
Fibers			
Carbon, Type 1	1.95	390	2200
Carbon, Type 2	1.75	250	2700
Cellulose fibers	1.61	60	1200
Glass (E-glass)	2.56	76	1400–2500
Kevlar	1.45	125	2760
Matrices			
Epoxies	1.2–1.4	2.1–5.5	40–85
Polyesters	1.1–1.4	1.3–4.5	45–85

Table 28.2 Properties of Composites

Material	Density ρ (Mg m ⁻³)	Youngs Modulus E (GN m ⁻²)	Strength σ_y (MN m ⁻²)	Fracture Toughness K_{Ic} (MN m ^{-3/2})
Composites				
CFRP, 58% uniaxial C in epoxy	1.5	189	1050	32–45
GFRP, 50% uniaxial glass in polyester	2.0	48	1240	42–60
Kevlar epoxy (KFRP), 60% uniaxial	1.4	76	1240	—
Kevlar in epoxy				
Metals				
High-strength steel	7.8	207	1000	100
Aluminum alloy	2.8	71	500	28

properties, which we examine next. The important properties of three common composites are listed in Table 28.2, where they are compared with a high-strength steel and a high-strength aluminum alloy of the sort used for aircraft structures.

28.3 MODULUS

When two linear elastic materials (with different moduli) are mixed, the mixture is also linear elastic. The modulus of a fiber composite when loaded *along* the fiber direction (Figure 28.1(a)) is a linear combination of that of the fibers, E_f , and the matrix, E_m

$$E_{c||} = V_f E_f + (1 - V_f) E_m \quad (28.1)$$

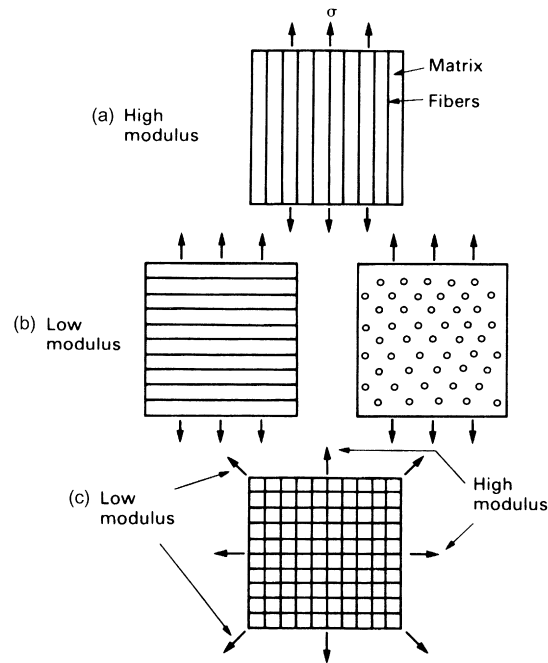


FIGURE 28.1

(a) When loaded along the fiber direction the fibers and matrix of a continuous fiber composite suffer equal strains. (b) When loaded across the fiber direction, the fibers and matrix see roughly equal stress. (c) $0-90^\circ$ laminate has high and low modulus directions; $0-45-90-135^\circ$ laminate is nearly isotropic.

where V_f is the volume fraction of fibers (see EMIEd4, Chapter 6). The modulus of the same material, loaded across the fibers (Figure 28.1(b)) is much less—it is only

$$E_{c\perp} = \left\{ \frac{V_f}{E_f} + \frac{1-V_f}{E_m} \right\}^{-1} \quad (28.2)$$

(see EMIEd4, Chapter 6 again).

Table 28.1 gives E_f and E_m for common composites. The moduli $E_{||}$ and E_{\perp} for a composite with, say, 50% of fibers, differ greatly: a uniaxial composite (one in which all the fibers are aligned in one direction) is exceedingly anisotropic. By using a cross-weave of fibers (Figure 28.1(c)), the moduli in the 0° and 90° directions can be made equal, but those at 45° are still very low. Approximate isotropy can be restored by laminating sheets, rotated through 45° , to give a plywood-like *fiber laminate*.

28.4 TENSILE STRENGTH

Many fiber composites are made of strong, brittle fibers in a more ductile polymer matrix. Then the stress–strain curve looks like the heavy line in Figure 28.2. The figure largely explains itself. The stress–strain curve is linear, with slope E (Equation (28.1)) until the matrix yields. From there on, most of the extra load is carried by the fibers which continue to stretch elastically until they fracture. When they do, the stress drops to the yield strength of the matrix (though not as sharply as the figure shows because the fibers do not all break at once). When the matrix fractures, the composite fails completely.

In any structural application it is the peak stress which matters. At the peak, the fibers are just on the point of breaking and the matrix has yielded, so the stress is given by the *yield* strength of the matrix, σ_y^m , and the *fracture* strength of the fibers, σ_f^f , combined using a rule of mixtures

$$\sigma_{TS} = V_f \sigma_f^f + (1 - V_f) \sigma_y^m. \quad (28.3)$$

This is shown as the line rising to the right in Figure 28.3. Once the fibers have fractured, the strength rises to a second maximum determined by the fracture strength of the matrix

$$\sigma_{TS} = (1 - V_f) \sigma_f^m \quad (28.4)$$

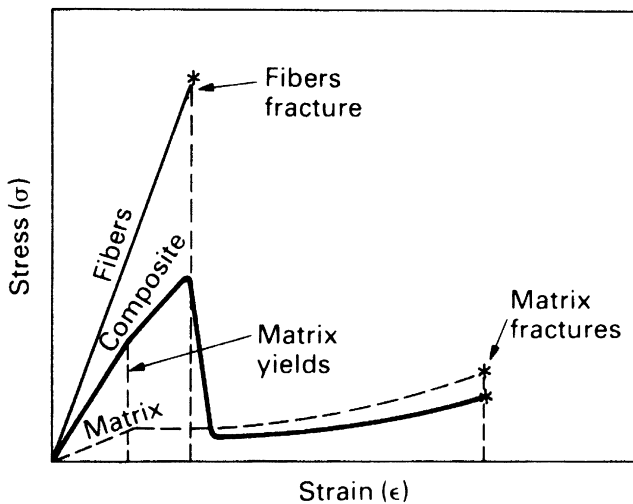
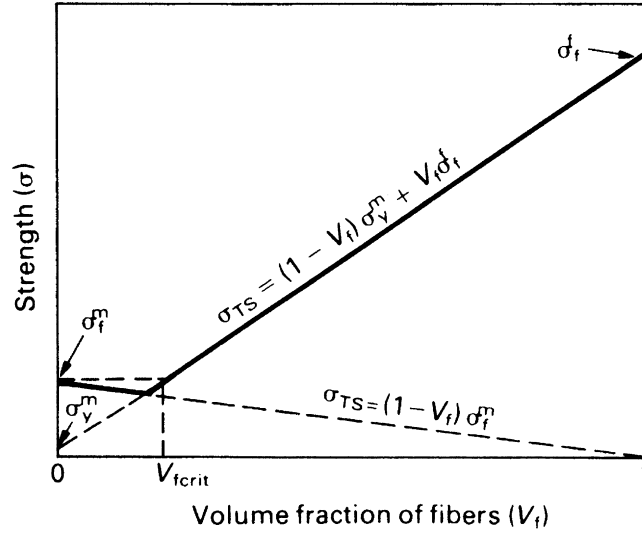


FIGURE 28.2

The stress–strain curve of a continuous fiber composite (heavy line), showing how it relates to those of the fibers and the matrix. At the peak the fibers are on the point of failing.

**FIGURE 28.3**

The variation of peak stress with volume fraction of fibers. A minimum volume fraction ($V_{f,crit}$) is needed to give any strengthening.

where σ_f^m is the fracture strength of the matrix; it is shown as the line falling to the right on Figure 28.3. The figure shows that adding too few fibers does more harm than good: a critical volume fraction $V_{f,crit}$ of fibers must be exceeded to give an increase in strength. If there are too few, they fracture before the peak is reached and the ultimate strength of the material is reduced.

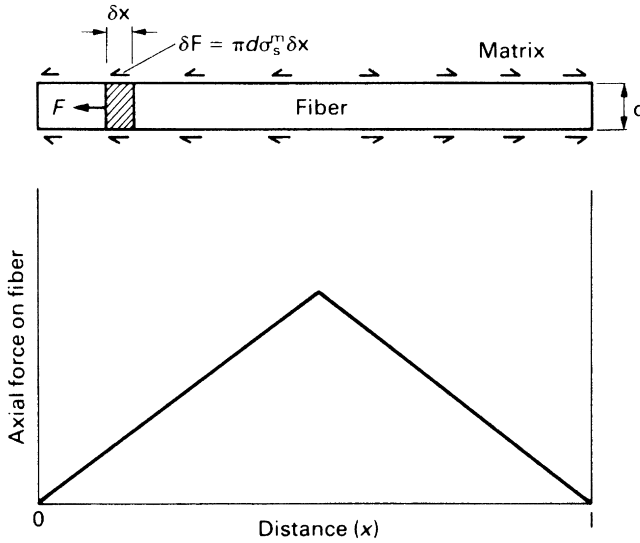
For many applications (e.g., body pressings), it is inconvenient to use continuous fibers. It is a remarkable feature of these materials that chopped fiber composites (convenient for molding operations) are nearly as strong as those with continuous fibers, provided the fiber length exceeds a critical value.

Consider the peak stress that can be carried by a chopped-fiber composite which has a matrix with a yield strength in shear of σ_s^m ($\sigma_s^m \approx -0.5 \sigma_y^m$). Figure 28.4 shows that the axial force transmitted to a fiber of diameter d over a little segment δx of its length is

$$\delta F = \pi d \sigma_s^m \delta x. \quad (28.5)$$

The force on the fiber thus increases from zero at its end to the value

$$F = \int_0^x \pi d \sigma_s^m dx = \pi d \sigma_s^m x \quad (28.6)$$

**FIGURE 28.4**

Load transfer from matrix to fiber causes the tensile stress in the fiber to rise to a peak in the middle. If the peak exceeds the fracture strength of the fiber, it breaks.

at a distance x from the end. The force which will just break the fiber is

$$F_c = \frac{\pi d^2}{4} \sigma_f^f. \quad (28.7)$$

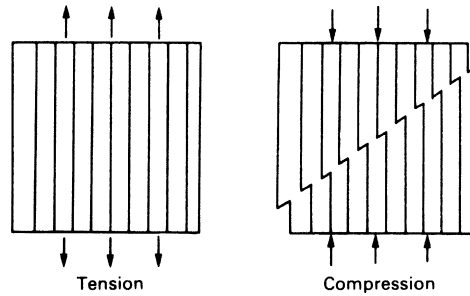
Equating these two forces, we find that the fiber will break at a distance

$$x_c = \frac{d}{4} \frac{\sigma_f^f}{\sigma_s^m} \quad (28.8)$$

from its end. If the fiber length is less than $2x_c$, the fibers do not break—but nor do they carry as much load as they could. If they are much longer than $2x_c$, then nothing is gained by the extra length. The optimum strength (and the most effective use of the fibers) is obtained by chopping them to the length $2x_c$ in the first place. The average stress carried by a fiber is then simply $\sigma_f^f/2$ and the peak strength is

$$\sigma_{TS} = \frac{V_f \sigma_f^f}{2} + (1 - V_f) \sigma_y^m. \quad (28.9)$$

This is more than one-half of the strength of the continuous-fiber material (Equation (28.3)). Or it is if all the fibers are aligned along the loading direction. That, of course, will not be true in a chopped-fiber composite. In

**FIGURE 28.5**

Composites fail in compression by kinking, at a load which is lower than that for failure in tension.

a car body, for instance, the fibers are randomly oriented in the plane of the panel. Then only a fraction of them—about $1/4$ —are aligned so that much tensile force is transferred to them, and the contributions of the fibers to the stiffness and strength are correspondingly reduced.

The compressive strength of composites is less than that in tension. This is because the fibers buckle or, more precisely, they *kink*—a sort of cooperative buckling, shown in Figure 28.5. So while brittle ceramics are best in compression, composites are best in tension.

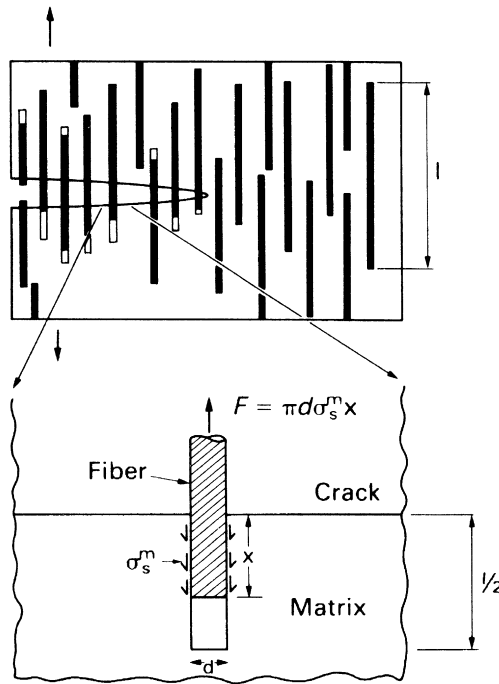
28.5 TOUGHNESS

The *toughness* G_c of a composite (like that of any other material) is a measure of the energy absorbed per unit crack area. If the crack simply propagated straight through the matrix (toughness G_c^m) and fibers (toughness G_c^f), we might expect a simple rule-of-mixtures

$$G_c = V_f G_c^f + (1 - V_f) G_c^m. \quad (28.10)$$

But it does not usually do this. We have already seen that, if the length of the fibers is less than $2x_c$, they will not fracture. And if they do not fracture, they must instead pull out as the crack opens (Figure 28.6). This gives a major new contribution to the toughness. If the matrix shear strength is σ_s^m (as before), then the work done in pulling a fiber out of the fracture surface is given approximately by

$$\int_0^{1/2} F \, dx = \int_0^{1/2} \pi d \sigma_s^m x \, dx = \pi d \sigma_s^m \frac{l^2}{8} \quad (28.11)$$

**FIGURE 28.6**

Fibers toughen by pulling out of the fracture surface, absorbing energy as the crack opens.

The number of fibers per unit crack area is $4V_f/\pi d^2$ (because the volume fraction is the same as the *area* fraction on a plane perpendicular to the fibers). So the total work done per unit crack area is

$$G_c = \pi d \sigma_s^m \frac{l^2}{8} \times \frac{4V_f}{\pi d^2} = \frac{V_f}{2d} \sigma_s^m l^2. \quad (28.12)$$

This assumes that l is less than the critical length $2x_c$. If l is greater than $2x_c$ the fibers will *not* pull out but will break instead. Thus, optimum toughness is given by setting $l = 2x_c$ in Equation (28.12) to give

$$G_c = \frac{2V_f}{d} \sigma_s^m x_c^2 = \frac{2V_f}{d} \sigma_s^m \left(\frac{d \sigma_f^f}{4 \sigma_s^m} \right)^2 = \frac{V_f d (\sigma_f^f)^2}{8 \sigma_s^m}. \quad (28.13)$$

The equation says that, to get a high toughness, you should use strong fibers in a weak matrix (though of course a weak matrix gives a low strength). This mechanism gives CFRP and GFRP a toughness (50 kJ m^{-2}) far higher than

that of either the matrix (5 kJ m^{-2}) or the fibers (0.1 kJ m^{-2}); without it neither would be useful as an engineering material.

28.6 FOAMS AND CELLULAR SOLIDS

Many natural materials are cellular: wood and bone, cork and coral, for instance. There are good reasons for this: cellular materials permit an optimization of stiffness, or strength, or of energy absorption, for a given weight of material. These natural foams are widely used by people (wood for structures, cork for thermal insulation), and synthetic foams are common too: cushions, padding, packaging, insulation, are all functions filled by cellular polymers. Foams give a way of making solids which are very light and, if combined with stiff skins to make sandwich panels, they give structures which are exceptionally stiff and light. The engineering potential of foams is considerable.

Most polymers can be foamed easily. It can be done by simple mechanical stirring or by blowing a gas under pressure into the molten polymer. But by far the most useful method is to mix a chemical blowing agent with the granules of polymer before processing: it releases CO_2 during the heating cycle, generating gas bubbles in the final molding. Similar agents can be blended into thermosets so that gas is released during curing, expanding the polymer into a foam; if it is contained in a closed mold, it takes up the mold shape accurately with a smooth, dense, surface.

The properties of a foam are determined by the properties of the polymer, and by the *relative density*, ρ/ρ_s : the density of the foam ρ divided by that of the solid ρ_s of which it is made. This plays the role of the volume fraction V_f of fibers in a composite, and all the equations for foam properties contain ρ/ρ_s . It can vary widely, from 0.5 for a dense foam to 0.005 for a particularly light one.

The cells in foams are polyhedral, like grains in a metal (Figure 28.7). The cell walls, where the solid is concentrated, can be open (like a sponge) or

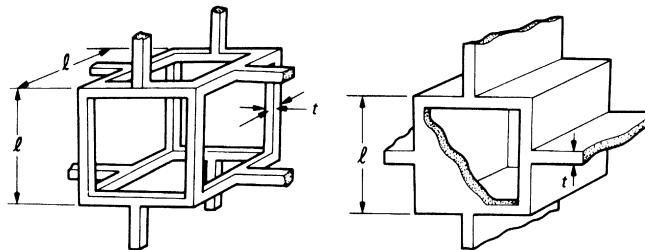


FIGURE 28.7

Polymer foams, showing the polyhedral cells. Some foams have closed cells, others have open cells.

closed (like a flotation foam), and they can be equiaxed (like the polymer foam in the figure) or elongated (like cells in wood). But the aspect of structures which is most important in determining properties is none of these; it is the relative density. We now examine how foam properties depend on ρ/ρ_s and on the properties of the polymer of which it is made.

28.7 PROPERTIES OF FOAMS

When a foam is compressed, the stress–strain curve shows three regions (Figure 28.8). At small strains, the foam deforms in a *linear elastic* way: there is then a *plateau* of deformation at almost constant stress; and finally there is a region of *densification* as the cell walls crush together.

At small strains the cell walls at first *bend*, like little beams of modulus E_s , built in at both ends. Figure 28.9 shows how a hexagonal array of cells is distorted by this bending. The deflection can be calculated from simple beam theory. From this, we obtain the stiffness of a unit cell, and thus the modulus E of the foam, in terms of the length l and thickness t of the cell walls. But these are directly related to the relative density: $\rho/\rho_s = (t/l)^2$ for open-cell foams, the commonest kind. Using this gives the foam modulus as

$$E = E_s \left(\frac{\rho}{\rho_s} \right)^2. \quad (28.14)$$

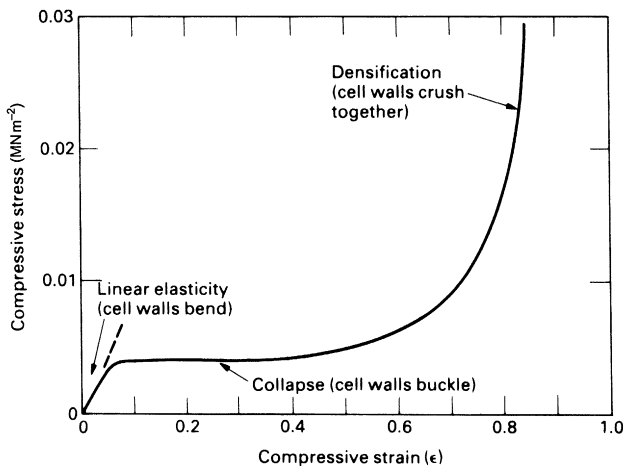
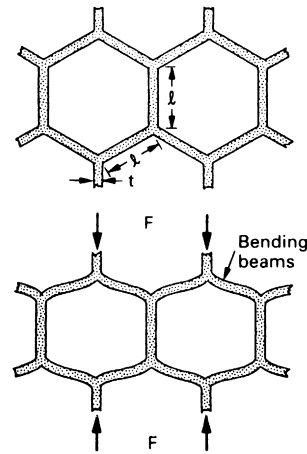
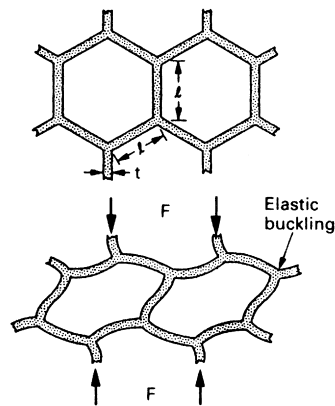


FIGURE 28.8

The compressive stress–strain curve for a polymer foam. Very large compressive strains are possible, so the foam absorbs a lot of energy when it is crushed.

**FIGURE 28.9**

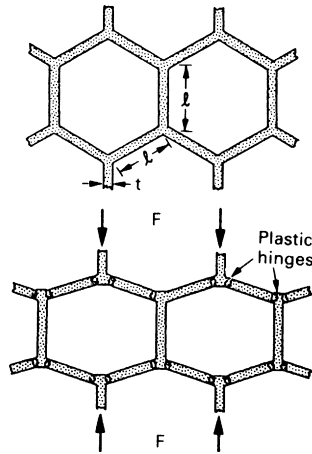
Cell wall bending gives the linear elastic portion of the stress—strain curve.

**FIGURE 28.10**

When an elastomer foam is compressed beyond the linear region, the cell walls buckle elastically, giving the long plateau shown in [Figure 28.8](#).

Real foams are well described by this formula. Note that foaming offers a vast range of modulus: ρ/ρ_s can be varied from 0.5 to 0.005, a factor of 10^2 , by processing, allowing E to be varied over a factor of 10^4 .

Linear elasticity, of course, is limited to small strains (5% or less). Elastomeric foams can be compressed far more than this. The deformation is still recoverable (and thus elastic) but is nonlinear, giving the plateau on [Figure 28.8](#). It is caused by the *elastic buckling* of the columns or plates which make up the cell edges or walls, as shown in [Figure 28.10](#). Again using

**FIGURE 28.11**

When a plastic foam is compressed beyond the linear region, the cell walls bend plastically, giving a long plateau like that of [Figure 28.8](#).

standard results of beam theory, the *elastic collapse stress* σ_{el}^* can be calculated in terms of the density ρ . The result is

$$\sigma_{el}^* = 0.05 E_s \left(\frac{\rho}{\rho_s} \right)^2. \quad (28.15)$$

As before, the strength of the foam is controlled by the density and can be varied at will through a wide range. Low-density ($\rho/\rho_s = 0.01$) elastomeric foams collapse under tiny stresses; they are used to package small, delicate instruments. Denser foams ($\rho/\rho_s = 0.05$) are used for seating and beds: their moduli and collapse strengths are 25 times larger. Still denser foams are used for packing heavier equipment: appliances or small machine tools, for instance.

Cellular materials can collapse by another mechanism. If the cell wall material is *plastic* (as many polymers are), then the foam as a whole shows plastic behavior. The stress–strain curve still looks like [Figure 28.8](#), but now the plateau is caused by plastic collapse. Plastic collapse occurs when the moment exerted on the cell walls exceeds its fully plastic moment, creating plastic hinges as shown in [Figure 28.11](#). Then the collapse stress σ_{pl}^* of the foam is related to the yield strength σ_y of the wall by

$$\sigma_{pl}^* = 0.3 \sigma_y \left(\frac{\rho}{\rho_s} \right)^{3/2}. \quad (28.16)$$

Plastic foams are good for the kind of packaging which is meant to absorb the energy of a single impact: polyurethane automobile crash padding, polystyrene foam to protect a television set if it is accidentally dropped during delivery. The long plateau of the stress–strain curve absorbs energy but the foam is damaged in the process.

28.8 MATERIALS THAT ARE ENGINEERED

The materials described in this chapter differ from most others available to the designer in that their properties can be engineered to suit, as nearly as possible, the application. The stiffness, strength, and toughness of a composite are, of course, controlled by the type and volume fraction of fibers. But the materials engineering can go further than this, by orienting or laminating the fiber weave to give directional properties, or to reinforce holes or fixing points, or to give a stiffness which varies in a controlled way across a component. Foaming, too, allows new degrees of freedom to the designer. Not only can the stiffness and strength be controlled over a vast range (10^4 or more) by proper choice of matrix polymer and foam density but gradients of foam density and thus of properties can be designed-in. Because of this direct control over properties, both sorts of composites offer special opportunities for designing *weight-optimal structures*, particularly attractive in aerospace and transport. Examples of this sort of design can be found in the books listed in the References.

EXAMPLES

28.1 A unidirectional fiber composite consists of 60% by volume of Kevlar fibers in a matrix of epoxy. Find the moduli $E_{c||}$ and $E_{c\perp}$. Comment on the accuracy of your value for $E_{c\perp}$. Use the moduli given in Table 28.1, and use an average value where a range of moduli is given.

Answers

77 GN m⁻² and 9 GN m⁻².

28.2 A unidirectional fiber composite consists of 60% by volume of continuous type-1 carbon fibers in a matrix of epoxy. Find the maximum tensile strength of the composite. You may assume that the matrix yields in tension at a stress of 40 MN m⁻².

Answer

1336 MN m⁻².

28.3 A composite material for a car-repair kit consists of a random mixture of short glass fibers in a polyester matrix. Estimate the maximum toughness G_c of the composite. You may assume that the volume fraction of glass is 30%, the fiber diameter is 15 μm, the fracture strength of the fibers is 1400 MN m⁻², and the shear strength of the matrix is 30 MN m⁻².

Answer

37 kJ m⁻².

28.4 Calculate the critical length $2x_c$ of the fibers in Example 28.3. How would you expect G_c to change if the fibers were substantially longer than $2x_c$?

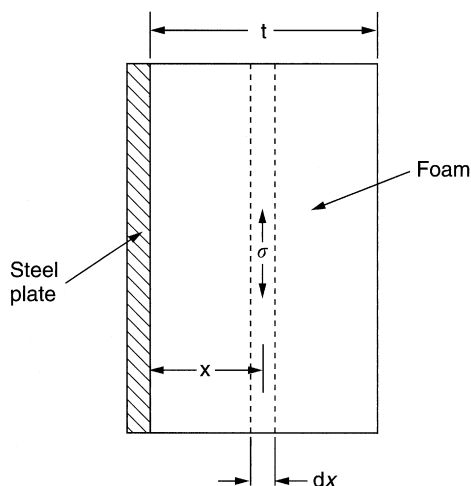
Answer

0.35 mm.

28.5 The diagram shows a layer of brittle polyurethane foam which is stuck to a steel plate. The foam is part of the thermal insulation system surrounding a liquid methane tank. In service, the temperature distribution in the foam is linear, with

$$T(^{\circ}\text{C}) = -100\left(\frac{x}{t}\right).$$

If the steel plate is considered to be infinitely stiff, find an expression for the tensile stress σ in the foam as a function of x . If the Young's modulus and coefficient of thermal expansion of the foam are 34 MN m^{-2} and $10^{-4} ^{\circ}\text{C}^{-1}$, find the maximum value of the tensile stress. Where is this maximum stress located?

**Answers**

$\sigma = E\alpha 100(x/t)$; 0.34 MN m^{-2} ; at $x = t$.

28.6 In Example 28.5, the tensile thermal stress in the foam makes it crack. The cracks form at the free surface ($x = t$) and then run inward through the thickness of the layer. It is important to prevent cracking in order to have a liquid-proof safety barrier next to the methane tank. How would you modify the material to prevent it cracking?

28.7 What are the requirements for a polymer foam used in (a) a seat cushion, (b) a safety helmet for climbers. How do the deformation mechanisms in the two foams differ? Why can a seat cushion last indefinitely, when a climbing helmet must be thrown away if it has been involved in a fall?

- 28.8** A bookshelf is essentially a beam of constant cross section simply supported at each end, and carrying a uniformly distributed load (which makes it deflect by amount δ at mid-span). Explain why δ for a bookshelf made from plywood will be approximately twice that for one made from sawn timber of the same cross section.
- 28.9** Explain why it is impossible to split a small square of plywood (measuring say $75 \times 75 \times 10$ mm) by driving a large nail through its thickness, whereas it is all too easy to do this with a square of wood of the same dimensions.
- 28.10** Explain why aligned fiber composites are generally stronger in tension than in compression.
- 28.11** Take a look around your home. Write a representative list of the things you see which are made from foams and cellular solids (both natural and human-made). List specialized applications (where only one or a very limited range of foams or cellular solids will perform adequately in the service environment).
- 28.12** Refer to [Figure 28.11](#). Imagine that the drawing shows a cross section through a foam which consists of cells that are very long compared to their width. How would you modify the cross section of the cells to produce a *negative* Poisson's ratio in response to the loading geometry shown?

Wood Structure and Properties

29.1 INTRODUCTION

Wood is one of the most widely used structural materials. Its documented use in buildings and ships spans more than 5000 years. In the sixteenth century, the demand for stout oaks for ship building was so great that the population of suitable trees was seriously depleted, and in the seventeenth and eighteenth centuries much of Europe was deforested by the exponential growth in consumption of wood. Today the world production is about the same as that of iron and steel: roughly 10^9 ton year⁻¹. Much of this is used structurally: for beams, joists, flooring, or supports which will bear load. Then the properties which interest the designer are the *moduli*, the *yield* or *crushing strength*, and the *toughness*. These properties, summarized in Table 29.1, vary considerably: oak is about 5 times stiffer, stronger, and tougher than balsa, for instance. In this chapter, we examine the structure of wood and the way the mechanical properties depend on it, using many of the ideas developed in the preceding chapters.

29.2 STRUCTURE OF WOOD

It is necessary to examine the structure of wood at three levels. At the macroscopic (unmagnified) level the important features are shown in Figure 29.1. The main cells (“fibers” or “tracheids”) of the wood run axially up and down the tree: this is the direction in which the strength is greatest. The wood is divided radially by the growth rings: differences in density and cell size caused by rapid growth in the spring and summer, and sluggish growth in the autumn and winter. Most of the growing processes of the tree take place in the *cambium*, which is a thin layer just below the bark. The rest of the wood is more or less dead; its function is mechanical: to hold the tree up. With 10^8 years in which to optimize its structure, it is perhaps not surprising that wood performs this function with remarkable efficiency.

Table 29.1 Mechanical Properties of Woods

Wood	Density ¹ (Mg m ⁻³)	Youngs Modulus ^{1,2} (GN m ⁻²)		Strength ^{1,3} (MN m ⁻²) to grain		Fracture Toughness ¹ (MN m ^{-3/2})	
		to grain	⊥ to grain	Tension	Compression	to grain	⊥ to grain
Balsa	0.1–0.3	4	0.2	23	12	0.05	1.2
Mahogany	0.53	13.5	0.8	90	46	0.25	6.3
Douglas fir	0.55	16.4	1.1	70	42	0.34	6.2
Scots pine	0.55	16.3	0.8	89	47	0.35	6.1
Birch	0.62	16.3	0.9	—	—	0.56	—
Ash	0.67	15.8	1.1	116	53	0.61	9.0
Oak	0.69	16.6	1.0	97	52	0.51	4.0
Beech	0.75	16.7	1.5	—	—	0.95	8.9

¹Densities and properties of wood vary considerably; allow $\pm 20\%$ on the data shown here. All properties vary with moisture content and temperature; see text.

²Dynamic moduli; moduli in static tests are about two-thirds of these.

³Anisotropy increases as the density decreases. The transverse strength is usually between 10% and 20% of the longitudinal.

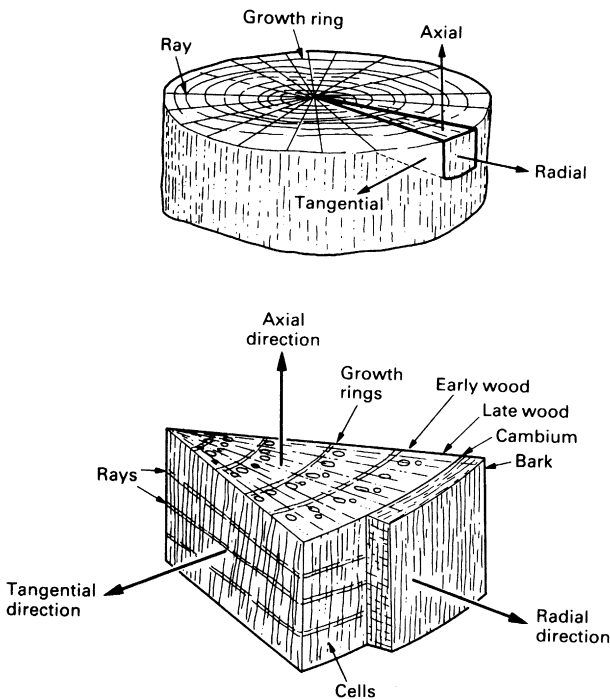


FIGURE 29.1

The macrostructure of wood. Note the coordinate system (axial, radial, tangential).

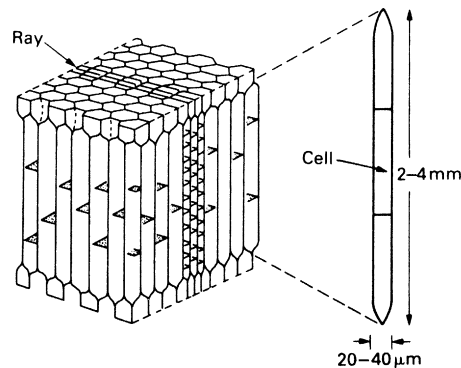


FIGURE 29.2

The microstructure of wood. Woods are foams of relative densities between 0.07 and 0.5, with cell walls which are fiber reinforced. The properties are very anisotropic, partly because of the cell shape and partly because the cell wall fibers are aligned near the axial direction.

To see how it does so, one has to examine the structure at the microscopic (light microscope or scanning electron microscope) level. [Figure 29.2](#) shows how the wood is made up of long hollow cells, squeezed together like straws, most of them parallel to the axis of the tree. The *axial* section shows roughly hexagonal cross sections of the cells: the *radial* and the *tangential* sections show their long, thin shape. The structure appears complicated because of the fat tubular *sap channels* which run up the axis of the tree carrying fluids from the roots to the branches, and the strings of smaller cells called *rays* which run radially outward from the center of the tree to the bark. But neither is of much importance mechanically; it is the fibers or tracheids which give wood its stiffness, strength, and toughness.

The walls of these tracheid cells have a structure at a molecular level, which (but for the scale) is like a composite—like fiberglass, for example ([Figure 29.3](#)). The role of the strong glass fibers is taken by fibers of crystalline *cellulose*, a high polymer $(C_6H_{10}O_5)_n$, made by the tree from glucose, $C_6H_{12}O_6$, by means of a condensation reaction, and with a \overline{DP} of about 10^4 . Cellulose is a linear polymer with no cumbersome side groups, so it crystallizes easily into *microfibrils* of great strength (these are the fibers you can sometimes see in coarse paper). Cellulose microfibrils account for about 45% of the cell wall. The role of the epoxy matrix is taken by the *lignin*, an amorphous polymer (like epoxy), and by *hemicellulose*, a partly crystalline polymer of glucose with a smaller \overline{DP} than cellulose; between them they account for a further 40% of the weight of the wood. The remaining 10–15% is water and *extractives*: oils and salts which give wood its color, its smell, and (in some instances) its resistance to beetles, bugs, and bacteria. The chemistry of wood is summarized in [Table 29.2](#).

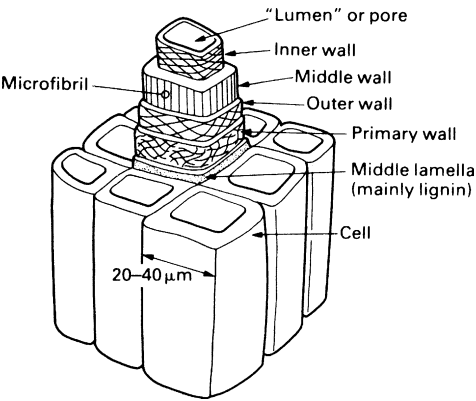


FIGURE 29.3

The molecular structure of a cell wall. It is a fiber-reinforced composite (cellulose fibers in a matrix of hemicellulose and lignin).

Table 29.2 Composition of Cell Wall of Wood		
Material	Structure	Approximate wt%
Fibers		
Cellulose ($C_6H_{10}O_5$) _n	Crystalline	45
Matrix		
Lignin	Amorphous	20
Hemicellulose	Semicrystalline	20
Water	Dissolved in the matrix	10
Extractives	Dispersed in the matrix	5

It is a remarkable fact that, although woods differ enormously in appearance, the composition and structure of their cell walls do not. Woods as different as balsa and beech have cell walls with a density ρ_s of 1.5 Mg m^{-3} with the chemical makeup given in Table 29.2 and with almost the same elaborate lay-up of cellulose fibers (Figure 29.3). The lay-up is important because it accounts, in part, for the enormous anisotropy of wood—the difference in strength along and across the grain. The cell walls are helically wound, like the handle of a CFRP golf club, with the fiber direction nearer the cell axis rather than across it. This gives the cell wall a modulus and strength which are large parallel to the axis of the cell and smaller (by a factor of about 3) across it. The properties of the cell wall are summarized in Table 29.3; it is a little less stiff, but nearly as strong as an aluminum alloy.

Wood, then, is a foamed fibrous composite. Both the foam cells and the cellulose fibers in the cell wall are aligned predominantly along the grain of the

Table 29.3 Properties of Cell Wall

Property	Axial		Transverse
Density, ρ_s (Mg m^{-3})		1.5	
Modulus, E_s (GN m^{-2})	35		10
Yield strength, σ_y (MN m^{-2})	150		50

wood (i.e., parallel to the axis of the trunk). Not surprisingly, wood is mechanically very anisotropic: the properties along the grain are quite different from those across it. But if all woods are made of the same stuff, why do the properties range so widely from one sort of wood to another? The differences between woods are primarily due to the differences in their relative densities (see Table 29.1).

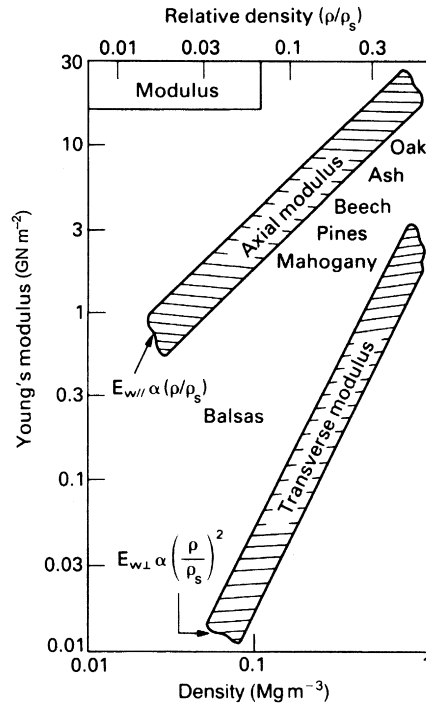
29.3 MECHANICAL PROPERTIES OF WOOD

All the properties of wood depend to some extent on the amount of water it contains. Green wood can contain up to 50% water. Seasoning (for 2–10 years) or kiln drying (for a few days) reduces this to around 14%. The wood shrinks, and its modulus and strength increase (because the cellulose fibrils pack more closely). To prevent *movement*, wood should be dried to the value which is in equilibrium with the humidity where it will be used. In a centrally heated house (20°C , 65% humidity), for example, the equilibrium moisture content is 12%. Wood shows ordinary thermal expansion, of course, but its magnitude ($\alpha = 5 \text{ MK}^{-1}$ along the grain, 50 MK^{-1} across the grain) is small compared to dimensional changes caused by drying.

29.4 ELASTICITY

Woods are viscoelastic solids: on loading they show an immediate elastic deformation followed by a further slow creep or “delayed” elasticity. In design with wood it is usually adequate to treat the material as elastic, taking a rather lower modulus for long-term loading than for short loading times (a factor of 3 is realistic) to allow for the creep. The modulus of a wood, for a given water content, then depends principally on its density, and on the angle between the loading direction and the grain.

Figure 29.4 shows how Young’s modulus along the grain (“axial” loading) and across the grain (“radial” or “tangential” loading) varies with density. The axial modulus varies linearly with density and the others vary roughly as its square. This means that the anisotropy of the wood (the ratio of the

**FIGURE 29.4**

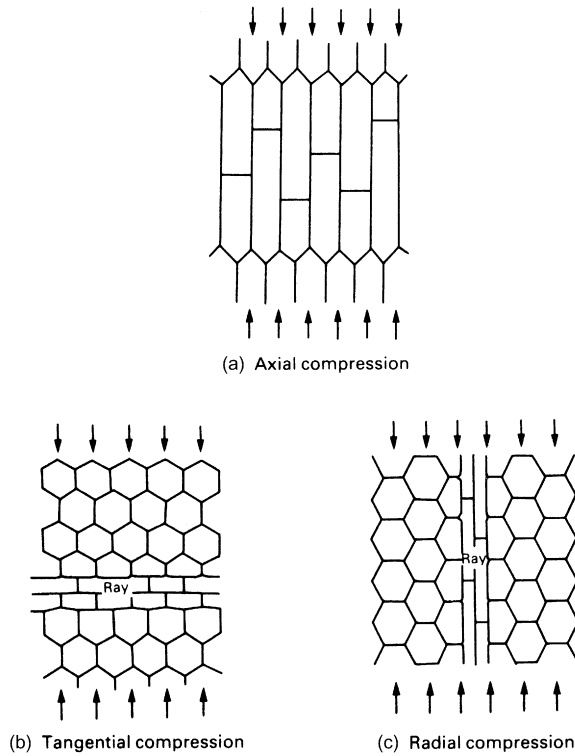
Young's modulus for wood depends mainly on the relative density ρ/ρ_s . That along the grain varies as ρ/ρ_s ; that across the grain varies roughly as $(\rho/\rho_s)^2$, like polymer foams.

modulus along the grain to that across the grain) increases as the density decreases: balsa woods are very anisotropic; oak or beech are less so. In structural applications, wood is usually loaded along the grain: then only the axial modulus is important. Occasionally, it is loaded across the grain, and then it is important to know that the stiffness can be a factor of 10 or more smaller (Table 29.1).

The moduli of wood can be understood in terms of the structure. When loaded along the grain, the cell walls are extended or compressed (Figure 29.5(a)). The modulus $E_{w||}$ of the wood is that of the cell wall, E_s , scaled down by the fraction of the section occupied by cell wall. Doubling the density obviously doubles this section, and therefore doubles the modulus. It follows immediately that

$$E_{w||} = E_s \left(\frac{\rho}{\rho_s} \right) \quad (29.1)$$

where ρ_s is the density of the solid cell wall (Table 29.3).

**FIGURE 29.5**

(a) When wood is loaded along the grain most of the cell walls are compressed axially; (b) when loaded across the grain, the cell walls bend like those in the foams described in Chapter 28.

The transverse modulus $E_{w\perp}$ is lower partly because the cell wall is less stiff in this direction, but partly because the foam structure is intrinsically anisotropic because of the cell shape. When wood is loaded across the grain, the cell walls bend (Figure 29.5(b,c)). It behaves like a foam (Chapter 28) for which

$$E_{w\perp} = E_s \left(\frac{\rho}{\rho_s} \right)^2. \quad (29.2)$$

The elastic anisotropy

$$E_{w\parallel} / E_{w\perp} = (\rho_s / \rho). \quad (29.3)$$

Clearly, the lower the density the greater is the elastic anisotropy.

29.5 TENSILE AND COMPRESSIVE STRENGTH

The axial tensile strength of many woods is around 100 MN m^{-2} —about the same as that of strong polymers like the epoxies. The ductility is low—typically 1% strain to failure.

Compression along the grain causes the kinking of cell walls, in much the same way that composites fail in compression (Chapter 28, Figure 28.5). The kink usually initiates at points where the cells bend to make room for a ray, and the kink band forms at an angle of $45\text{--}60^\circ$. Because of this kinking, the compressive strength is less (by a factor of about 2—see Table 29.1) than the tensile strength, a characteristic of composites.

Like the modulus, the tensile and compressive strengths depend mainly on the density (Figure 29.6). The strength parallel to the grain varies linearly with density, for the same reason that the axial modulus does: it measures

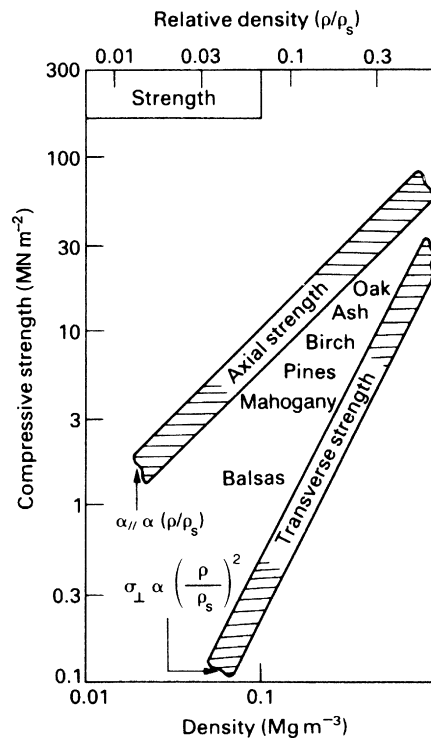


FIGURE 29.6

The compressive strength of wood depends, like the modulus, mainly on the relative density ρ/ρ_s . That along the grain varies as ρ/ρ_s ; that across the grain varies as $(\rho/\rho_s)^2$.

the strength of the cell wall, scaled by the fraction of the section it occupies, giving

$$\sigma_{\parallel} = \sigma_s \left(\frac{\rho}{\rho_s} \right), \quad (29.4)$$

where σ_s is the yield strength of the solid cell wall.

Figure 29.6 shows that the transverse crushing strength σ_{\perp} varies roughly as

$$\sigma_{\perp} = \sigma_s \left(\frac{\rho}{\rho_s} \right)^2. \quad (29.5)$$

The explanation is almost the same as that for the transverse modulus: the cell walls bend like beams and collapse occurs when these beams reach their plastic collapse load. As with the moduli, moisture and temperature influence the crushing strength.

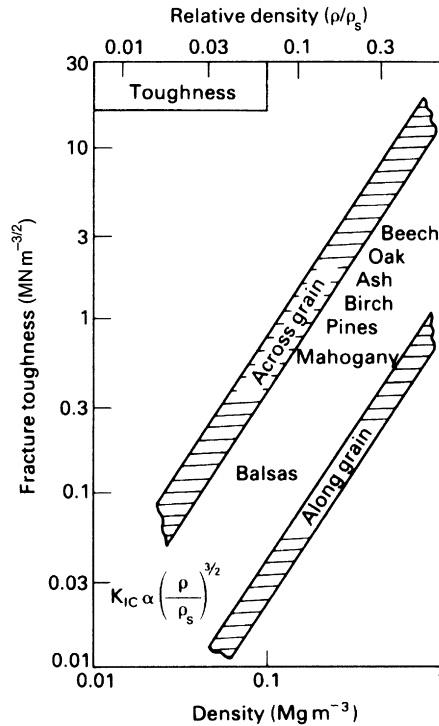
29.6 TOUGHNESS

The toughness of wood is important in design for exactly the same reasons that of steel is: it determines whether a structure (a frame building, a pit prop, the mast of a yacht) will fail suddenly and unexpectedly by the propagation of a fast crack. In a steel structure, the initial crack is that of a defective weld or is formed by corrosion or fatigue; in a wooden structure, the initial defect may be a knot, or a saw cut, or cell damage caused by severe mishandling.

Recognizing its importance, various tests have been devised to measure wood toughness. A typical static test involves loading square section beams in three-point bending until they fail; the “toughness” is measured by the area under the load–deflection curve. A typical dynamic test involves dropping, from an increasingly great height, a weight of 1.5 kg; the height which breaks the beam is a “toughness”—of a sort. Such tests (still universally used) are good for ranking different batches or species of wood; but they do not measure a property which can be used sensibly in design.

The obvious parameter to use is the fracture toughness, K_{Ic} . Not unexpectedly, it depends on density (Figure 29.7), varying as $(\rho/\rho_s)^{3/2}$. It is a familiar observation that wood splits easily along the grain, but with difficulty across the grain. Figure 29.7 shows why: the fracture toughness is more than a factor of 10 smaller along the grain than across it.

Loaded along the grain, timber is remarkably tough: much tougher than any simple polymer, and comparable in toughness with fiber-reinforced composites. There appear to be two contributions to the toughness. One is the very

**FIGURE 29.7**

The fracture toughness of wood, like its other properties, depends primarily on relative density. That across the grain is roughly 10 times larger than that along the grain. Both vary as $(\rho/\rho_s)^{3/2}$.

large fracture area due to cracks spreading, at right angles to the break, along the cell interfaces, giving a ragged fracture surface. The other is more important, and it is exactly what you would expect in a composite: fiber pull-out (Chapter 28, Figure 28.6). As a crack passes across a cell, the cellulose fibers in the cell wall are unraveled, like pulling thread off the end of a bobbin. In doing so, the fibers must be pulled out of the hemicellulose matrix, and a lot of work is done in separating them. It is this work which makes the wood tough.

For some uses, the anisotropy of timber and its variability due to knots and other defects are particularly undesirable. Greater uniformity is possible by converting the timber into board such as laminated plywood, chipboard, and fiber-building board.

29.7 WOOD COMPARED TO OTHER MATERIALS

The mechanical properties of wood (a structural material of first importance because of the enormous scale on which it is used) relate directly to the

Table 29.4 Specific Strength of Structural Materials

Material	E/ρ	σ_y/ρ	K_c/ρ
Woods	20–30	120–170	1–12
Al-alloy	25	179	8–16
Mild steel	26	30	18
Concrete	15	3	0.08

shape and size of its cells, and to the properties of the composite-like cell walls. Loaded along the grain, the cell walls are loaded in simple tension or compression, and the properties scale as the density. But loaded across the grain, the cell walls bend, and then the properties depend on a power (3/2 or 2) of the density. That, plus the considerable anisotropy of the cell wall material (which is a directional composite of cellulose fibers in a hemicellulose/lignin matrix), explain the enormous difference between the modulus, strength, and toughness along the grain and across it.

The properties of wood are generally inferior to those of metals. But the properties per unit weight are a different matter. Table 29.4 shows that the specific properties of wood are better than mild steel, and as good as many aluminum alloys (that is why, for years, aircraft were made of wood). And, of course, it is much cheaper.

WORKED EXAMPLE

The following photographs give a few examples of the huge range of things that wood and related products are used for, and why wood is such a valuable material. The first shows a typical North American home which, apart from the foundations and fireplaces/chimneys (which are made from concrete, cement block, and brick) is made largely from wood, plywood, and chipboard. This includes all the structural framing, external weatherboarding, floor joists, floor boards, internal walls, roof timbers, doors, deck, veranda, kitchen units, and so on. Wood is relatively cheap in North America, and construction is quicker with wood than brick. Construction can also be carried out in subzero temperatures (which would make it impossible to lay bricks because the cement mix would freeze). Wood is an excellent thermal insulator, so when the cavities between the inner and outer skins are filled with glass fiber wool insulation, the house will be warm even in the depths of the Connecticut winter. Disadvantages of wood construction are the fire risk (moderated by treating the wood with fire-retarding chemicals), potential damage from wet or dry rot (it is important to keep the

wood dry and well ventilated), relatively poor sound insulation properties, the need to regularly repaint large exterior areas, and damage by insect pests (termites are a real problem in northern parts of Australia, for example, and structures must be separated from the foundations by galvanized steel sheet which termites cannot eat through).

The second photograph shows a public bench on Columbus Avenue, Manhattan. The seat and back are made from substantial slats of high-quality hardwood. These look very nice and will last a long time even when exposed to the extremes of the New York climate. The slats are easy to make, transport, and assemble. Most importantly, because wood has a very low thermal conductivity and thermal mass, when you sit down on a wooden bench, it quickly warms up, and then it stays warm. Contrast this with the bench you can see in central Cambridge, UK on Street View at 52 12 20.50 N 0 07 15.33 E (Sydney Street). The seat is made from tubes of (probably) steel, placed side by side. These have large thermal conductivity and thermal mass, and if you sit on them in the winter they are freezing cold and stay that way. This is a great way to get a chill. Outdoor metal seats are simply not fit for purpose. Metal seats (made from perforated steel sheet) are also common in railroad stations across the UK (see Cambridge Station, UK, on Street View at 52 11 39.00 N 0 08 14.20 E). Some seats are even made from aluminum alloy—which is a better conductor of heat again. There are very good reasons why a traditional material like wood is often best and to replace it with a radically different material having grossly inappropriate properties for its prime function (of making people feel comfortable) displays either ignorance or indifference on the part of modern “designers” that makes proper engineers like us want to cry!

Our third photograph brings us indoors, with an example of the use of wood in furniture. This shows a dining chair made from oak. For this application, wood is stiff, strong, and relatively light (a very good restaurant in Wales has dining room chairs made from steel rods welded together—you can hardly get your feet under the table, because it is so hard to move the chairs). Wood can easily be shaped into elegant, economical, and pleasing geometrical forms, and it *looks* good. The chair in the photograph is a replica of one designed by one of the foremost designers of the early twentieth century, Charles Rennie Mackintosh. A look at the web sites show some of his furniture designs, which were ground breaking for their time, and are now revered for their elegance and innovation. It would be hard to make such items from anything other than wood. In fact, wood is huge in the furniture industry—just think of the volume of wood or wood products shipped by manufacturers like Ikea, and try to imagine life without this material.

Our final two photographs show a fence made from Australian brushwood. This is included as an example of the use of wood-like products direct from the plant without any processing at all other than separating branches and cutting to length. Tree branches, bamboo, and reeds have been used like this since the dawn of the human race and continue to be used in large quantities. Other examples are the use of Norfolk Reed for renewing the thatched roofs on old houses in England, <http://www.norfolkreed.co.uk/pages/thatch.htm>; <http://en.wikipedia.org/wiki/Thatching>

Street View 52 05 08.00 N 0 01 25.03 E, the use of coppiced branches for making woven fence panels or “wattles,” <http://www.challengefencing.com/products/panels/hazel+wattle+hurdles>, and the use of bamboo in many Asian countries for construction and scaffolding, <http://en.wikipedia.org/wiki/Bamboo>.

It is now being recognized again that plants can provide a highly sustainable source of natural fibre composites if used unprocessed in this way (a lesson which had never been forgotten in many parts of the world).



A typical North American home, built largely from wood (apart from the foundations and fireplaces/chimneys). Region of Greenwich, CT, USA (41 02 20.00 N 73 36 48.90 W).



A public bench, with wooden slats for the seat and back. Manhattan, Columbus Avenue at W 80th Street—behind the American Museum of Natural History. Also note cast metal supports (aluminum alloy?) and base of stone blocks (granite sets?) (40 46 57.30 N 73 58 29.30 W).



A dining table chair made from European oak (stained to give it the desired color). An accurate reproduction of one of the “high back” chairs designed by the famous Scottish architect and interior designer Charles Rennie Mackintosh. <http://www.crmsociety.com/>



A fence made from brushwood. Mosman, NSW, Australia (33 49 16.70 S 151 14 09.50 E). The long fine branches are harvested from commercial plantations of the evergreen shrub *Melaleuca Uncinata*, which is native to Australia. This grows to a bush 2 m high. It is well suited to dry climates such as those of inland California.



Close-up of the brushwood fence showing individual wooden stems.

EXAMPLES

- 29.1** Explain how the complex structure of wood results in large differences between the along-grain and across-grain values of Young's modulus, tensile strength, and fracture toughness.
- 29.2** What functions do the polymers cellulose, lignin, and hemicellulose play in the construction of the cells in wood?

- 29.3** Discuss, giving specific examples, how the anisotropic properties of wood are exploited in the design applications of this material.
- 29.4** Discuss, giving specific examples, how the anisotropic properties of wood are exploited in processes for manufacturing items from wood.
- 29.5** Chipboard and fiberboard are manufactured by gluing small chips or fibers of wood together. Why is the Young's modulus of these materials in the plane of the board (a) isotropic, (b) approximately mid-way between the along-grain and across-grain moduli of the source wood?
- 29.6** Plywood is made from alternate layers of wood (each some 2 mm thick) with the grain direction in successive layers arranged to produce a 0–90 laminate. Why is the Young's modulus in the 0 and 90 directions approximately 50% of the along-grain modulus of the source wood? How would you expect the splitting resistance of plywood to differ from that of the source wood?
- 29.7** I (DRHJ) have a curtain pole at home which is made from a solid rod of wood (beech) 1½" diameter; the span of the pole is unusually large at 5' 8" (some English units to keep non-USA readers on their toes—often much easier to use for construction than the over-fine mm). It carries a heavy curtain which reaches down to the floor. Every month or so, I feel compelled to rotate the pole about its long axis through an angle of 180° (this is an affliction of the kind well understood by other engineers). What is the engineering reason that makes me rotate the pole?
- 29.8** In what way is bamboo a much more optimized structure than wood? How does this optimization influence the uses of bamboo?
- 29.9** Why do the axial moduli and axial strengths of different woods scale as the density of the wood?
- 29.10** Why do the transverse moduli and transverse crushing strengths of different woods scale as the density of the wood squared?
- 29.11** Why does the elastic anisotropy of different woods scale *inversely* as the density of the wood?

Case Studies in Composites

30.1 MATERIALS FOR VIOLIN BODIES

The violin (Figure 30.1) is a member of the family of musical instruments which we call “string” instruments. Table 30.1 shows just how many different types of string instruments there are of European origin alone—not to mention the fascinating range that we can find in African, Asian, or Oriental cultures.

String instruments all work on the same basic principle. A thin string, of gut or metal, is stretched tightly between two rigid supports. If the string is plucked, or hit, or bowed, it will go into sideways vibrations of precisely defined frequency which can be used as musical notes. But a string vibrating on its own can hardly be heard—the sideways moving string cuts through the air as a cheesewire cuts through cheese and the pressure wave that reaches our eardrums has scarcely any amplitude at all. For this reason, all string instruments have a *soundboard*. This is forced into vibration by the strings and radiates strong pressure waves which can be heard easily.

But soundboards are much more than just radiating surfaces. They have their own natural frequencies of vibration and will respond much better to notes that fall within the resonance peaks than notes which fall outside. The soundboard acts rather like a selective amplifier, taking in the signal from the string and radiating a highly modified output; and, as such, it has a profound effect on the tone quality of the instrument.

Soundboards are traditionally made from wood. The leading violin makers can work wonders with this material. By taking a thin plate of wood and hollowing it out here and there they can obtain a reasonably even response over a frequency range from 200 to 5000 Hz. But the process of adjusting a soundboard is so delicate that a trained listener can tell that 0.1 mm has been removed from an area of the soundboard measuring only 20 mm × 20 mm.

Such skills are rare, and most students today can only afford rather indifferent mass-produced instruments. But the music trade is big business and there is a powerful incentive for improving the quality of the mass-market product.

One obvious way of making better violins would be to dismantle a fine instrument, make accurate thickness measurements over the whole of the soundboard, and mass-produce soundboards to this pattern using computer-controlled machine tools. But there is a problem with this approach: because



FIGURE 30.1
A young violinist.

Table 30.1 Some European String Instruments				
Violin Family	Viol Family	Guitar Family	Harp Family	Keyboard Family
Violin	Treble	Guitar	Modern harp	Piano
Viola	Tenor	Lute	Folk harps	Harpsichord
Cello	Bass	Zither		Clavichord
Double bass		Balalaika		

wood is a natural material, soundboard blanks will differ from one another to begin with, and this variability will be carried through to the finished product. But we might be able to make a good violin every time if we could replace wood by a synthetic material having reproducible properties. This case study, then, looks at how we might design an artificial material that will reproduce the acoustically important properties of wood as closely as possible.

Soundboard vibrations

In order to design a replacement for wood, we need to look at the vibrational behavior of soundboards in more detail. As Figure 30.1 shows, the soundboard of a violin has quite an ornate shape and it is extremely difficult to analyze its behavior mathematically. But an adequate approximation for our purposes is to regard the soundboard as a rectangular panel simply supported along two opposing edges and vibrating from side to side as shown in Figure 30.2.

The natural frequencies are then given by

$$f_n = n^2 \left(\frac{\pi}{2l^2} \right) \left(\frac{EI}{\rho b d} \right)^{1/2} \quad (30.1)$$

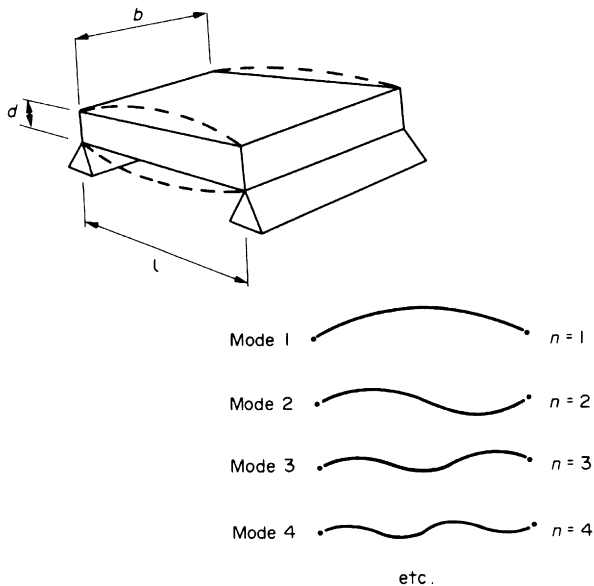


FIGURE 30.2

Idealized vibration modes of a soundboard. The natural frequencies of the modes are proportional to n^2 .

where E is Young's modulus, $I(=bd^3/12)$ is the second moment of area of the section, and ρ is the density of the soundboard material. We get the lowest natural frequency when the panel vibrates in the simplest possible way (see Figure 30.2 with $n = 1$). For more complex vibrations, with mode numbers of 2, 3, 4, and so on, f scales as the square of the mode number.

Making the soundboard out of wood introduces a complication. As we saw in Chapter 29, wood has a much bigger modulus along the grain than across the grain. A wooden soundboard therefore has both along-grain and across-grain vibrations (Figure 30.3).

The frequencies of these vibrations are then

$$f_{\parallel} = n^2 \left(\frac{\pi}{2l_{\parallel}^2} \right) \left(\frac{E_{w\parallel} I_w}{\rho_w b_{\parallel} d_w} \right)^{1/2} \quad (30.2)$$

and

$$f_{\perp} = n^2 \left(\frac{\pi}{2l_{\perp}^2} \right) \left(\frac{E_{w\perp} I_w}{\rho_w b_{\perp} d_w} \right)^{1/2} \quad (30.3)$$

where $E_{w\parallel}$ is the axial modulus and $E_{w\perp}$ is the radial modulus.

In order to estimate the soundboard frequencies, we set $d_w = 3$ mm, $l_{\parallel} = 356$ mm, and $l_{\perp} = 93$ or 123 mm (Figure 30.4). Violin soundboards are usually made from spruce, which typically has $E_{w\parallel} = 11.6$ GN m⁻²,

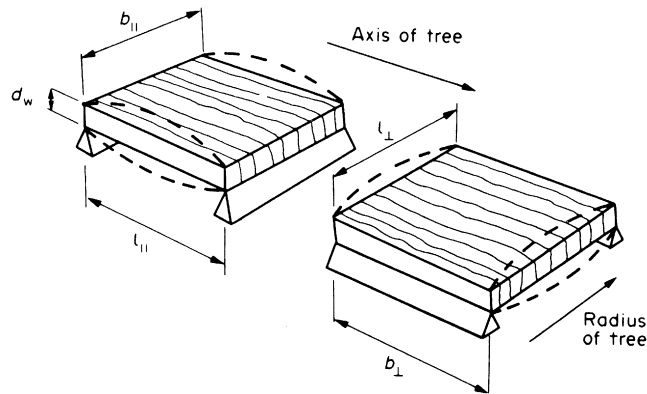
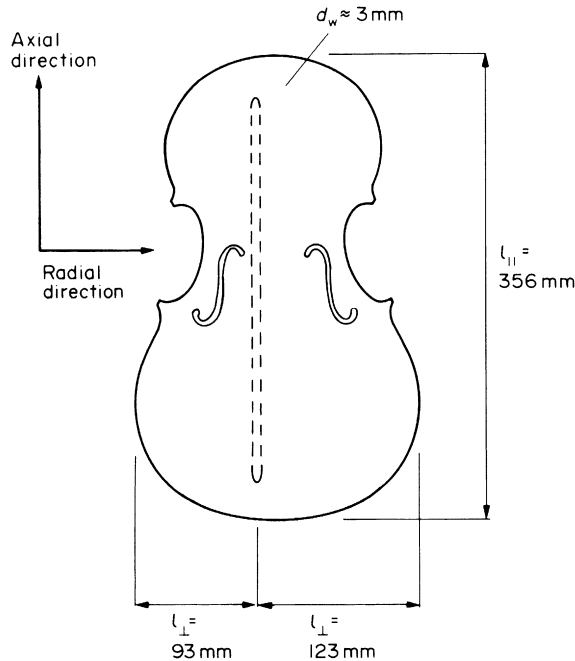


FIGURE 30.3

A wooden soundboard has both along-grain and across-grain vibrations. Although not shown here, both types of vibration have a full set of modes, with $n = 1, 2, 3, \dots$

**FIGURE 30.4**

Dimensions of a violin soundboard. The dashed outline marks the position of the bass bar—a wooden “girder” stuck underneath the soundboard in an off-center position. This effectively divides the soundboard into two different across-grain regions.

$E_{w\perp} = 0.71 \text{ GN m}^{-2}$ and $\rho_w = 0.39 \text{ Mg m}^{-3}$. Equations (30.2) and (30.3) then give us the following data.

$$f_{\parallel}(\text{s}^{-1}) \approx 59 \quad 236 \quad 531 \quad 944 \quad 1475 \quad 2124 \quad 2891 \quad \text{etc.}$$

$$f_{\perp}(\text{s}^{-1}) \approx \begin{cases} 217 & 868 & 1953 & 3472 & \text{etc.} \\ 124 & 496 & 1116 & 1984 & 3100 & \text{etc.} \end{cases}$$

For all the crudity of our calculations, these results show clearly that wooden violin soundboards have an impressive number of natural frequencies.

Replacement materials

Spruce soundboards have a Young’s modulus anisotropy of about $(11.6 \text{ GN m}^{-2}/0.71 \text{ GN m}^{-2}) = 16$. A replacement material must therefore have a similar anisotropy. This requirement immediately narrows the choice down to composites (isotropic materials like metals or polymers will probably sound awful).

Because it is fairly cheap, we should begin by looking at GFRP. The moduli of glass fibers and resin matrices are 72 and 3 GN m^{-2} , respectively, giving us

$$E_{c\parallel} = 72 V_f + 3(1 - V_f) \quad (30.4)$$

and

$$E_{c\perp} = \left(\frac{V_f}{72} + \frac{1-V_f}{3} \right)^{-1}. \quad (30.5)$$

Now, as Figure 30.5 shows, $E_{c\parallel}/E_{c\perp}$ can never be greater than 6.6 for GFRP; and this is far too small to give a useful soundboard.

We must therefore hope that CFRP can give us the required anisotropy. The modulus of type-1 carbon fibers is 390 GN m^{-2} along the fiber axis (although it is only 12 GN m^{-2} at right angles to this). So

$$E_{c\parallel} = 390 V_f + 3(1 - V_f) \quad (30.6)$$

and

$$E_{c\perp} = \left(\frac{V_f}{12} + \frac{1-V_f}{3} \right)^{-1}. \quad (30.7)$$

This gives a maximum ratio of 43, which is more than enough. In fact, to bring the anisotropy down to the target figure of 16 we need to reduce the volume fraction of fibers to only 0.13!

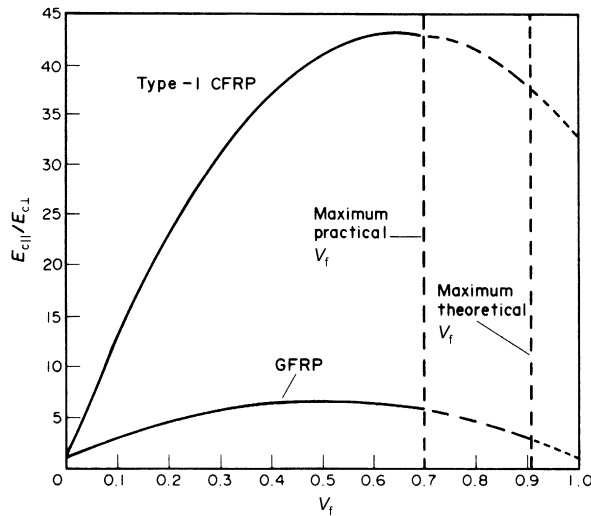


FIGURE 30.5

Modulus anisotropies $E_{c\parallel}/E_{c\perp}$ for aligned GFRP and CFRP composites.

Having matched f_{\parallel}/f_{\perp} in this way we must now go on to match the frequencies themselves. We can see from Equation (30.2) that this requires

$$n^2 \left(\frac{\pi}{2l_{\parallel}^3} \right) \left(\frac{E_{w\parallel} b_{\parallel} d_w^2}{\rho_w b_{\parallel} d_w 12} \right)^{1/2} = n^2 \left(\frac{\pi}{2l_{\parallel}^2} \right) \left(\frac{E_{c\parallel} b_{\parallel} d_c^3}{\rho_c b_{\parallel} d_c 12} \right)^{1/2} \quad (30.8)$$

which tells us that the composite plate must have a thickness of

$$d_c = d_w \left(\frac{E_{w\parallel} \rho_c}{E_{c\parallel} \rho_w} \right)^{1/2}. \quad (30.9)$$

Now we already know three of the terms in this equation: d_w is 3 mm, $E_{w\parallel}$ is 11.6 GN m^{-2} and ρ_w is 0.39 Mg m^{-3} . The last two unknowns, $E_{c\parallel}$ and ρ_c , can be calculated very easily. When $V_f = 0.13$ Equation (30.4) tells us that $E_{c\parallel} = 53 \text{ GN m}^{-2}$. ρ_c can be found from the simple rule of mixtures for density, with

$$\begin{aligned} \rho_c &= (0.13 \times 1.9 + 0.87 \times 1.15) \text{ Mg m}^{-3} \\ &= 1.25 \text{ Mg m}^{-3} \end{aligned} \quad (30.10)$$

Equation (30.9) then tells us that $d_c = 2.52 \text{ mm}$.

This value for the thickness of the substitute CFRP soundboard sets us a difficult problem. For the *mass* of the CFRP plate is greater than that of the spruce plate by the factor

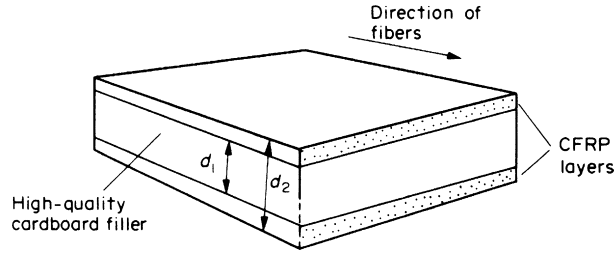
$$\frac{2.52 \text{ mm} \times 1.25 \text{ Mg m}^{-3}}{3 \text{ mm} \times 0.39 \text{ Mg m}^{-3}} = 2.69. \quad (30.11)$$

This excessive mass is quite unacceptable—the CFRP plate will need far too much energy to get it vibrating. But how can we reduce the mass without shifting the vibration frequency?

Sectional composites

One solution that has been adopted by makers of composite soundboards is to fabricate a sandwich structure where a layer of high-quality cardboard is glued between two identical layers of CFRP (Figure 30.6). The philosophy of this design modification is to replace some CFRP by a much lighter material in those regions that contribute least to the overall stiffness of the section.

The density of the cardboard layer is around 0.2 Mg m^{-3} . To match the mass of the sandwich to that of the spruce soundboard we must then have

**FIGURE 30.6**

Sandwich-type sectional composites give a much-improved stiffness-to-mass ratio.

$$0.39d_w = 1.25(d_2 - d_1) + 0.2d_1 \quad (30.12)$$

or

$$d_w = 3.21d_2 - 2.69d_1. \quad (30.13)$$

In order to formulate the criterion for frequency matching we can make the very reasonable assumption that the CFRP dominates the stiffness of the sandwich section. We also simplify Equation (30.2) to

$$f_{\parallel} = n^2 \left(\frac{\pi}{2l_{\parallel}^{3/2}} \right) \left(\frac{E_{w\parallel} I_w}{m_w} \right)^{1/2} \quad (30.14)$$

where $m_w = \rho_w b_{\parallel} l_{\parallel} d_w$ is the total mass of the wooden soundboard. Then, because we want $m_w = m_{\text{sandwich}}$, frequency matching requires

$$E_{w\parallel} I_w = E_{c\parallel} I_c \quad (30.15)$$

or

$$E_{w\parallel} \frac{b_{\parallel} d_w^3}{12} = E_{c\parallel} b_{\parallel} \frac{(d_2^3 - d_1^3)}{12}. \quad (30.16)$$

We know that $E_{c\parallel}/E_{w\parallel} = 53/11.6 = 4.6$ so that Equation (30.16) reduces to

$$d_w^3 = 4.6(d_2^3 - d_1^3). \quad (30.17)$$

Finally, combining Equations (30.13) and (30.17) gives us

$$(3.21d_2 - 2.69d_1)^3 = 4.6(d_2^3 - d_1^3). \quad (30.18)$$

This result can be solved numerically to give $d_1 = 0.63d_2$; and, using Equation (30.13), we can then show that $d_2 = 0.66d_w$.

This design study has shown that it is possible to design a sectional composite that will reproduce both the vibrational frequencies and the mass of a traditional wooden soundboard. For a soundboard made out of spruce the equivalent composite is a sandwich of cardboard glued between two identical layers of aligned CFRP with a fiber volume fraction of 0.13. If the wooden soundboard is 3 mm thick, the replacement composite must be 1.98 mm thick with a cardboard core of 1.25 mm.

30.2 FAILURE OF A GFRP SURGICAL INSTRUMENT

Figure 30.7 shows the cross section of a tubular surgical instrument used in minimally invasive surgery. The main length of tube is made from stainless steel, but a short bush of composite (GFRP) tube is attached to the end with a screw thread (prevented from unscrewing by Loctite adhesive). When the instrument is in position, a small loop of electrical resistance wire is passed down the tube and out through the GFRP bush. The wire loop is heated by current from a low voltage d.c. source, and is used to burn away tissue, using

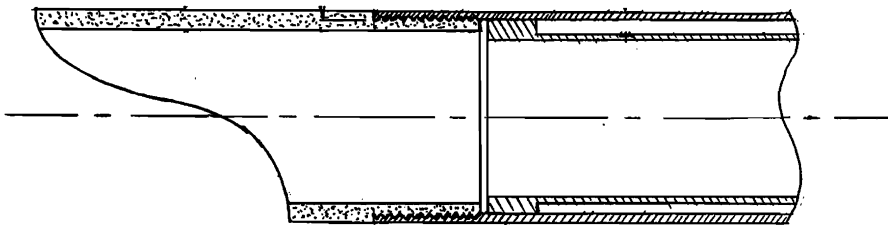


FIGURE 30.7

Cross section through surgical instrument (to scale). The outer diameter of the tube is 8 mm.

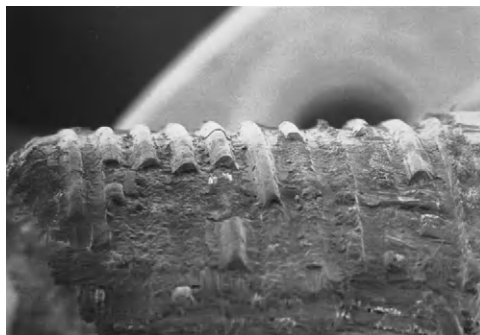


FIGURE 30.8

Screw thread on the outer circumference of the GFRP tube.

a repeated gouging action. The end of the instrument has to be fitted with an electrically insulating bush so the main length of the instrument does not become electrically live.

During use, the GFRP bush became detached from the end of the steel tube and had to be retrieved from the patient (with some difficulty and collateral damage). As part of the subsequent investigation, the GFRP bush and the mating steel screw threads were examined using the light microscope and



FIGURE 30.9

"Over and under" woven structure of glass fiber bundles as seen on the outer circumference of the GFRP tube (unthreaded portion).

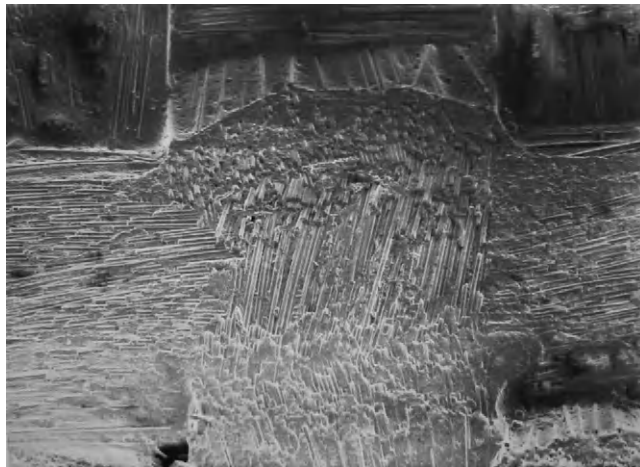


FIGURE 30.10

Close-up from [Figure 30.9](#). Note how the crests of the woven structure have been abraded in the surface finishing process.

scanning electron microscope. The screw thread was very fine (pitch 0.29 mm, depth 0.17 mm) and when the thread on the outer circumference of the bush was examined (Figure 30.8), it was found that much of the thread profile was missing. When a new instrument was sectioned and dismantled, it was also found that much of the thread profile on the bush was missing—and this was not due to disassembly, because very little GFRP was left adhering to the mating steel threads. This indicated that thread loss was not caused by the GFRP bush detaching but by thread cutting during manufacture.

It was decided to look at the structure of the GFRP. As shown in Figures 30.9 and 30.10, the composite was fabricated from an “over and under” weave of glass fiber bundles, impregnated with resin (probably epoxy). The bundles were 0.4 mm wide, so the pitch of the weave is $\approx 40\%$ greater than that of the thread. The thread pitch is less than a major characteristic dimension of the composite microstructure. The strength and toughness which define the bulk composite material cannot be used to characterize the strength and toughness of a small sample of material on the scale of the thread pitch. The photographs also show that there was incomplete penetration and wetting of the GF bundles by the resin, with gaps and voids. The thread cutting die would have cut through fiber bundles, removing their strengthening effect, and plucking material out of the surface. You cannot simply transfer a forming operation (in this case thread cutting) from the class of material it was designed for metals to a radically different class of material (a fiber composite) without thinking through the consequences.

30.3 CORK—A UNIQUE NATURAL FOAM

You landed in Lisbon (Portugal) airport a couple of hours ago and are now driving east in your hire car toward the Spanish border, ready for your overnight stop at the historic walled town of Elvas. You decided to use the new toll road, the A6, and are glad that you did, for you are now driving along one of the stretches built alongside the old two-way road—which is choked with traffic, especially heavy trucks who do not want to pay the toll. You have just passed the second off-ramp to the ancient town of Évora, with its Roman temple, and soon the dramatic hilltop fortress of Évoramonte will come into view dead ahead. But as you cruise along the almost empty road, your eye turns to the rolling landscape. The long, lush grass is already turning brown as the baking heat of the summer takes hold, and the herds of grazing sheep find shade beneath the leafy canopies of the many evergreen cork oak trees, *Quercus Suber*. Zoom in on 38 44 21.20 N 7 45 48.90 W and you will see them clearly. The trees are as much as 200 years old and are the key element in an ancient and fragile ecosystem which supports grazing



FIGURE 30.11

Cork drawn from a bottle of red wine from Navarrete, La Rioja, Spain (42 25 46.05 N 2 33 41.00 W). Note the small holes where the lenticels intersect the surface.

animals, a rich bird and insect life, and helps stabilize soils and vegetation through the hot, arid summers.

http://en.wikipedia.org/wiki/Quercus_suber

<http://www.azenhadoramalho.com/montados-alentejo-portugal>

Even the trees themselves are specially adapted. To keep them cool (and stop the sap evaporating), they grow a very thick layer of *cork* bark. Left alone, the cork grows to many centimeters in thickness, but every 10 years or so, when the bark is around 3 cm thick, it is peeled right off. This does not harm the tree, which is simply rested for another 10 years to grow a new bark layer. So the cork oak is not only an entirely renewable resource of a special material, but it is also host to a whole range of other species as well. Engineers with an environmental conscience need to think about this—would they rather buy a bottle of wine with a plastic stopper made from oil won by deep-sea drilling and processed in a whole series of carbon-generating industrial operations, or just peel it off a tree (which supports much other life too)?

We will look at cork's special properties shortly, and see why cork is such a valuable material for a whole range of applications. But first, we mention some examples of the uses of cork. Cork was (and still is) used for bottle stoppers (wine, champagne, and general storage—see [Figure 30.11](#)); gasket linings in metal screw tops; floats for fishing nets, lifejackets, and yachtsmen's keys; shoe soles (especially high-heeled—see [Figure 30.12](#)); flooring material; shelf lining for machine tool cabinets; vibration isolators; low-temperature/pressure gaskets in car engines and domestic appliances; tone-hole pads and airtight joints in woodwind instruments ([Figure 30.13](#)); table mats;



FIGURE 30.12

A high-heeled sandal with a sole made largely from cork—close-up showing layers containing lenticels.

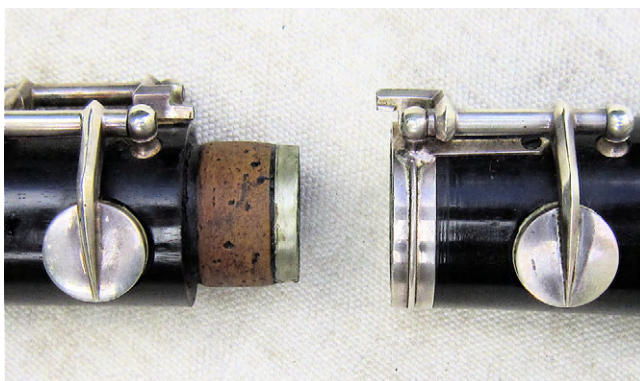


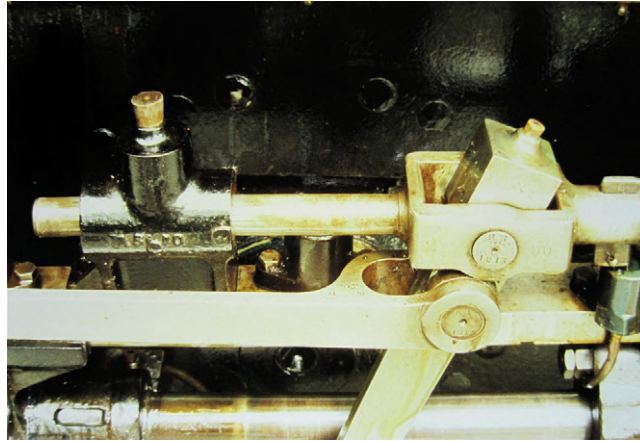
FIGURE 30.13

A tenon/socket joint in a modern oboe.

corks for test tubes and chemical apparatus; bulletin boards; fishing rod handles; cores of baseballs and cricket balls; thermal insulation in buildings and refrigerators; soundproofing; oil box plugs in steam locomotive bearings (Figure 30.14); fruit packing; space vehicle heat shields (yes, really!) — http://marsrover.nasa.gov/mission/spacecraft_edl_aeroshell.html.

In fact, cork oaks are able to survive grassland fires quite well because of the fire-retarding properties of their cork skin.

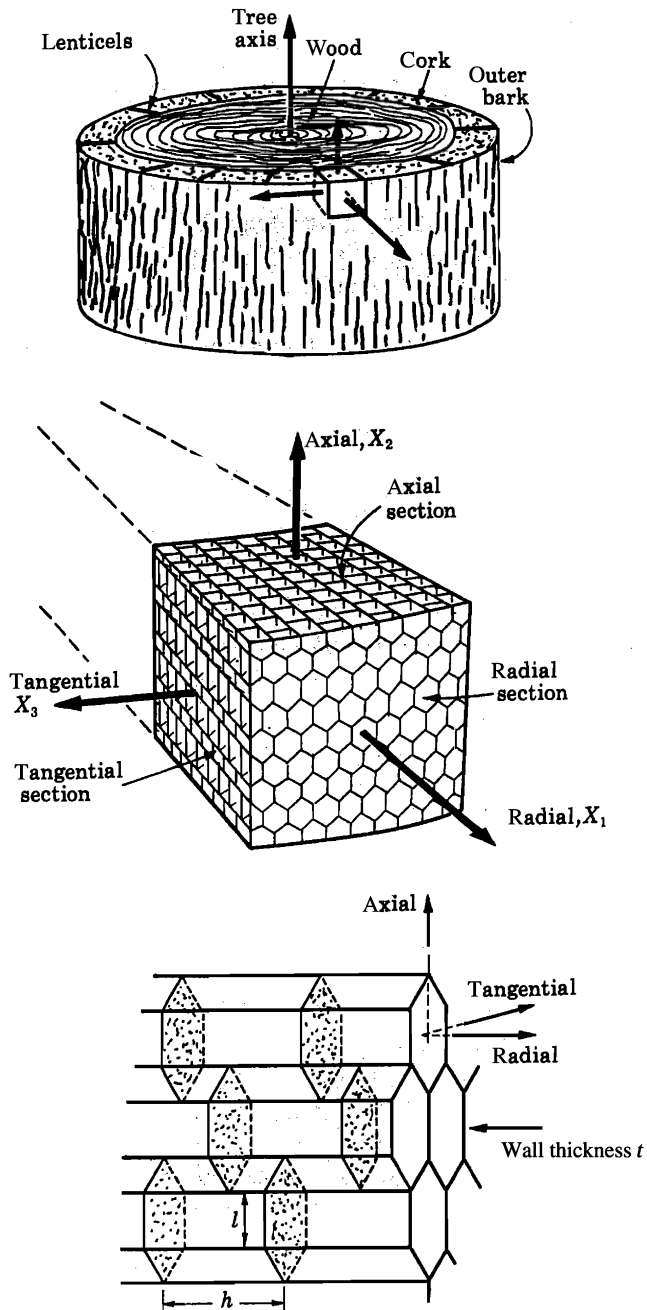
Figure 30.15 shows the cell structure of cork, and its relationship to the three principal directions—radial, axial, and tangential. The foam is a closed-cell foam, because the hexagonal prisms are blocked by cell walls spaced a

**FIGURE 30.14**

Valve gear on the steam loco No 9, Prince of Wales on the Vale of Rheidol narrow gauge railway in Wales, UK (1' 11 $\frac{1}{2}$ " gauge). Note the corks in the oilers for the valve spindle extension guide (top left) and combination lever top bearing (top right). <http://www.rheidolrailway.co.uk/> (52 23 56.75 N 3 59 14.60 W).

distance h apart along the prism axis. The cork is therefore waterproof, apart from the occasional radial passages called *lenticels*. Typical dimensions (in μm) are $t = 1 \pm 0.5$, $l = 20 \pm 5$, $h = 40 \pm 5$. The cell wall density and Young's modulus are $\approx 1.150 \text{ Mg m}^{-3}$ and 9 GN m^{-2} (the density of a *piece* of cork is $\approx 0.170 \text{ Mg m}^{-3}$, roughly 1/6th the density of water, which is why cork floats so well). The stiffest component in the cell walls is cellulose (12%, $E \approx 25 \text{ GN m}^{-2}$), followed by various oils and fatty acids (60%, average $E \approx 8 \text{ GN m}^{-2}$) then lignin (27%, $E \approx 2 \text{ GN m}^{-2}$). The oils and fatty acids make the cell walls waterproof—a perfect example of natural selection for optimum function.

The hexagonal prisms have periodic corrugations along their length (like a concertina), and when cork is compressed in the *radial* direction these corrugation grow (it is like squeezing a concertina) and the cells get shorter (like the concertina again). Up to a strain of about 7%, the behavior is linear elastic ($E \approx 20 \pm 7 \text{ MN m}^{-2}$ for a piece of cork), but at about 10% strain the prisms collapse *irreversibly* (*not* like the concertina!). There is no net lateral expansion of the prisms (there isn't for the concertina either—the corrugations grow equally inward and outward), so Poisson's ratio is zero for axial compression. In axial *tension*, the corrugations straighten out (like pulling a concertina right out). This takes a strain of about 5%, after which the cell walls extend (much more stiffly) like a straight tube in tension; if the load is increased sufficiently, they fracture after a small additional strain (the concertina would if you pulled it hard enough).

**FIGURE 30.15**

The cell structure of cork. In reality, the cell walls are not flat as drawn here but have periodic corrugations along the length of the cell.

When cork is compressed in either the *axial* or *tangential* directions the walls of the prisms *bend*, in the way that polymer foams do (see Figures 28.9 and 28.10). Up to a strain of about 7% the behavior is linear elastic ($E \approx 13 \pm 5 \text{ MN m}^{-2}$ for a piece of cork), but after about 10% strain the loading curve flattens out, and large *reversible* deformation occurs up to a strain of roughly 100%. This stress–strain curve is just like the one for polymer foams (see Figure 28.8). Axial compression results in tangential expansion ($\nu = 0.5$) but no radial expansion. Tangential compression results in axial expansion ($\nu = 0.5$) but no radial expansion. This behavior is what we would expect from the geometry of the cell structure (see Figure 28.10).

How do these properties affect the ways in which cork is used?

(a) Shoe soles (see Figure 30.12). The heel is built up from layers $\approx 10 \text{ mm}$ thick glued together. The lenticels can clearly be seen on the side of the heel; they show that the radial direction is normal to the plane of the layers. This is what we would expect, because it is the only way to cut a single extended piece (up to $115 \times 65 \text{ mm}^2$) from 10 years growth of bark. The compressive service loads applied normal to the layer do not cause any lateral expansion—they might progressively weaken the glue layers if they did. Finally, the heel is waterproof (so no shoe polish or other sealant is needed) and is very light, so the shoe is not tiring to wear. (Climbers are fond of saying that every pound of weight in a pair of boots is equivalent to carrying 7 pounds in a rucksack.)

(b) Airtight tenon/socket joints in musical instruments (see Figure 30.13). These are made from thin ($\approx 2 \text{ mm}$) cork sheet, cut with the plane of the sheet normal to the radial direction. A strip of sheet is rolled around the tenon and glued in position. The lenticels can be seen as randomly positioned holes (up to $\approx 0.5 \text{ mm}$ diameter) going through the sheet. These holes do not matter, because air-tightness is required along the sheet not through it. When the joint is assembled, the sheet is compressed slightly. But because radial compression does not increase the area of the sheet, there is no tendency to lift the cork off the tenon. In use, the cork must always be lubricated with “cork grease,” or friction between the cork of the tenon and the german silver of the socket would make it hard to assemble the instrument without causing damage (even a greased joint must be rotated back and forth during assembly). This is because the coefficient of friction of dry cork against metal is $\approx 0.2\text{--}0.4$, depending on the load. (However, this is much less than the friction coefficient between rubber and metal, typically $1\text{--}1.5$.)

(c) Corks for wine bottles (see Figure 30.11). The axis of the cork is perpendicular to the radial direction, so the axes of the hexagonal prisms point across, not up and down, the neck of the wine bottle. Again, this orientation is necessary if a sufficiently long cork is to be cut from a bark layer only 2 or

3 cm thick. It also has the advantage that the lenticels do not provide a leak path between the contents of the bottle and the atmosphere. One would think the mechanical optimum is to have the cork axis oriented in the radial direction, because otherwise the force needed to push the cork into the neck against friction would dilate the cork, making it even harder to push it in. However, the bulk modulus of cork—which measures the resistance to volume change during fully constrained loading—is very small, so the cork can be pushed into the bottle easily, without jamming. (Rubber has an extremely large bulk modulus and this, together with its large coefficient of friction, makes it virtually useless for corks—and not much better for bungs in chemistry apparatus either.) Natural corks are essential for the proper aging of bold red wines, because they are just sufficiently permeable to oxygen from the atmosphere; the totally gas-proof screw tops and plastic “corks” cannot achieve this.

(d) Oil box plugs in steam locomotives (see [Figure 30.14](#)). The mechanical aspects are similar to corks for wine bottles, but the very low mass of cork is important because the centrifugal loading from rapidly moving parts like big-end bearings could easily throw out a heavier plug (at best losing oil and overheating the bearing, at worst injuring someone).

(e) Flooring material. Cork has a very low thermal conductivity—no convection can occur within the cells (because they are so small), and only a small fraction of the cross section consists of the solid cell wall material needed for heat conduction. The low density of cork means it also has a very low thermal mass. In bathroom floors, for example, a cork floor does not feel cold underfoot. (One alternative material, ceramic tiles, certainly does feel cold; hence, the modern vogue for under-floor electric heating in bathrooms). Cork “tiles” with a large surface area are made by hot-pressing chips of cork together (the oils and fatty acids in the cell walls provide the necessary “adhesive”).

WORKED EXAMPLE

One of the most demanding applications for composites is in the reentry heat shields of space vehicles. One such famous example is the nose cone and wing leading edges of the space shuttle, which were built up from thin profiled panels of reinforced carbon–carbon (RCC) composite 0.25–0.5 in. thick (density 2.0 Mg m^{-3}). These withstood maximum temperatures of 1500–1650 °C every time the shuttle reentered earth’s atmosphere. RCC is also used for brake disks and pads in Formula 1 cars. A later development of RCC is C/SiC (carbon reinforced silicon carbide), used for brake disks and pads in aircraft and high-performance road cars (e.g., Bugatti, Ferrari, Lamborghini, Porsche, etc.).

RCC parts are made from layers of rayon fabric, which have been graphitized and impregnated with phenolic resin. These are laid up in a mold and cured at high temperature and pressure. The part is then packed in calcined coke (clean elemental carbon) and fired in a furnace to convert all the materials in the composite to carbon. This is followed by three more cycles where the part is infiltrated with furfuryl alcohol and furnace fired. Of course, during reentry, as the oxygen content of the atmosphere increases, the carbon has a tendency to oxidize. To prevent this, a surface layer 20–40 thou deep is converted to SiC by packing the part in a powder mixture of Al_2O_3 , Si, and SiC and heating it to 1650 °C in an argon atmosphere (the Si diffuses into the RCC surface and reacts with the carbon). When the parts cool down after being removed from the furnace, the SiC layer contracts more than the RCC core and develops hairline cracks. These are filled with tetraethyl orthosilicate to prevent oxidation of RCC exposed at the crack tips.

http://science.ksc.nasa.gov/shuttle/technology/sts-newsref/sts_sys.html#sts-rcc

RCC became prominent after the loss of the space shuttle Columbia during reentry on 1 February 2003 (17 years after the Challenger was lost just during launch).

<http://caib.nasa.gov/news/report/volume1/default.html>

During launch, a piece of polymer foam (estimated dimensions $19 \times 12 \times 5$ ", estimated weight 1.7 lb) detached from the external tank and was hit by the left wing leading edge at an estimated relative speed of 416–573 mph. This punched a hole through RCC panel number 8 (there were 22 RCC panels on each wing leading edge), and the ingress of hot gases weakened the wing structure to the extent that it failed under aerodynamic forces. This highlighted the fact that, although RCC is tough as ceramic composites go, it is still not a tough material when compared with metals or polymers. It also highlighted continuing and systemic cultural issues at NASA, which had not been overcome in spite of the findings of the Challenger enquiry. Shedding of foam from the external tank insulation had been observed from the earliest launches (of 79 missions for which recorded images are available, foam was shed in 65). And on six previous missions, a chunk of foam had been shed from exactly the same area on the tank as featured in the Columbia disaster. Yet—as in the Challenger disaster (when indications of O-ring seal blow-by became the accepted norm)—foam shedding became an accepted part of shuttle launches, without a rational risk assessment of the potential consequences. This acceptance of events which are not supposed to happen has been termed "The normalization of deviance" by sociologists. A choice finding of the Columbia enquiry was that "Organizational barriers prevented effective communication of critical safety information and stifled professional differences of opinion." A management

would not authorize a take-over bid without taking expert legal advice, so it should not have authorized shuttle launches without taking—and listening to—expert engineering advice.

EXAMPLES

- 30.1** The photograph is a close-up of a cork-heeled sandal. What are the (approximately parallel) wavy lines? They are spaced about 4 mm apart. Use this information to estimate what thickness the cork layer would grow to 10 years after the previous cork-harvesting operation.



- 30.2** Why is it easy to screw a corkscrew through a wine bottle cork, but impossible to do that with a rubber bung.
- 30.3** A cork borer is a very thin-walled tube with a sharpened end. It is pushed into corks by hand (and rotated at the same time) in order to make holes for glass tubes when assembling chemistry apparatus. Why is it easy to bore a hole through a cork using a cork borer, but impossible to do that with a rubber bung?
- 30.4** One way of making a clean hole in a rubber bung is to cool it in liquid nitrogen, then put it straight into a lathe chuck (with plastic jaws to minimize heat transfer) and drill the hole using a twist drill in the tailstock chuck. Why does this work? Can you think of any other way of making a clean hole through a rubber bung?
- 30.5** Why is cork an excellent thermal insulator?
- 30.6** The photograph shows a champagne cork after drawing from the bottle. Examine the surface features carefully. The cork consists of three quite distinct regions. What are the characteristics of these regions? State how the cork was manufactured. What can you say about the orientations of the hexagonal prisms in the three regions? Champagne contains a high pressure of carbon dioxide gas. What special features of the cork are intended to make it as impermeable to CO_2 as possible?



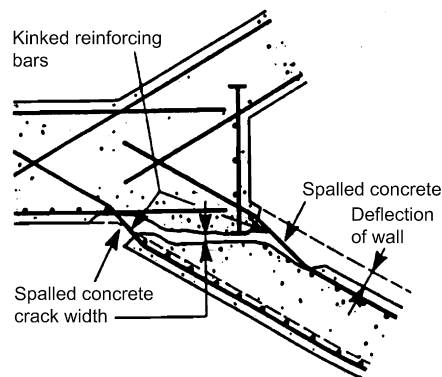
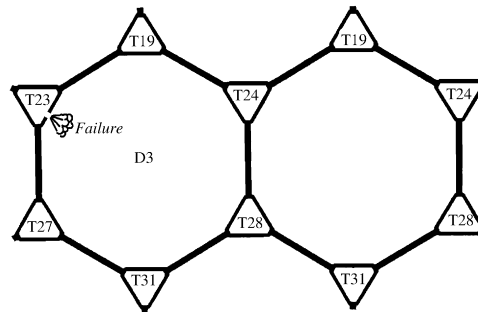
- 30.7** Assume that the champagne cork has returned to the dimensions it had before it was inserted into the neck of the bottle. The neck has a bore of 18 mm. The diameter of the lower end of the cork is 30 mm, and the diameter just beneath the bulbous top is 24 mm. Estimate the nominal strains at these two positions required to insert the cork into the bottle.

Answer

40%; 25%.

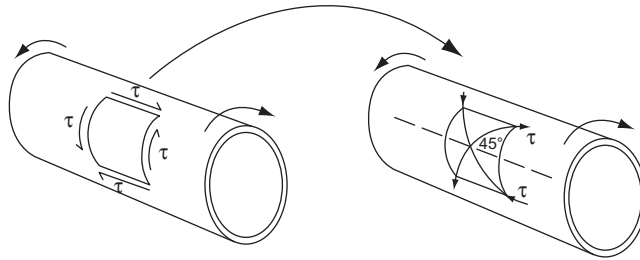
- 30.8** Explain why the lower end of the champagne cork is able to withstand a reversible compressive strain of 40%. Why does the cork not split the neck of the glass bottle when it is inserted? Why is it possible to extract the cork from the bottle without breaking off the bulbous top? How would you design a jig for inserting corks into champagne bottles? Why does the structure of the cork minimize its cost?
- 30.9** Take a look around your home. Write a representative list of the things you see which are made from cork. In each case, state what properties of cork are particularly relevant to choosing cork.
- 30.10** Why is cork excellent for packaging fragile items?
- 30.11** What properties of wood make it ideal for the bodies of string instruments like violins?
- 30.12** Sleipner A is a gas drilling platform which taps into the Sleipner natural gas field, located in the North Sea midway between Scotland and Norway—58°16'19.24" N 1°55'31.28" E. The depth of water at this location is 83 m. The base of the rig sits on the seabed. The platform itself is supported by four towers which rise up from the base, and pass through and above the sea surface. The base consists of a raft of 24 vertical cylinders each 12 m diameter (placed side by side in a close-packed array) made from reinforced concrete, and the towers are extensions of four of these cylinders. The rig was built inshore, floated out to the site (with water ballast in the cylinders), and then put down on the seabed by admitting more water into the cylinders. The present Sleipner A rig is not the

original. The original sank under test in a 220 m deep fjord near the construction yard. The top diagram shows a cross section through two of the base cylinders. The cylinders are joined by hollow triangular structures called “tricells.” The tricell spaces were subjected to an internal pressure of 67 m head of water during the test—less than the design pressure of 73 m—but the wall of one space broke, flooded a cylinder, and sank the rig. (When the rig hit the bottom of the fjord, it smashed itself to pieces, and registered a Richter 3 scale on the seismographs!) The total loss was estimated as US\$ 700 million. The bottom diagram shows how the tricell wall fractured. *Explain why the failure occurred. How would you have altered the design of the steel reinforcement to prevent the failure?* The failure was caused by an incorrect finite element stress analysis at the design stage. Investigators commented as follows: “Probably the biggest lesson is the need never to treat computer analysis as a black box process. Computer analysis is only as good as the user who inputs the model and interprets the results. Proper modeling and interpretation requires a strong understanding of the theoretical and practical workings of the programs and a thorough understanding of what the results mean. Rational methods of checking results should always be employed and QA processes should allow the time for proper attention to such details.”



(Powerful stuff—readers note this as an important life lesson!)

- 30.13** The drive shafts for a Formula 1 car are made from thin-walled tubes of epoxy resin reinforced with continuous carbon fibers. The main loading on the prop shaft is torsion (both clockwise and anticlockwise). Along which directions would you place the carbon fibers in order to optimize the resistance to fracture under torsion? You may refer to the following diagram, which shows how the stress state of pure shear in the tube wall may be transformed into two principal stresses (you may already know how to do this using Mohr's circle in two dimensions).
- 30.14** The prop shafts also have to resist lateral deflection, otherwise they could suffer from whirling instability at high speed (see EM1Ed4, Example 7.6). How would you position carbon fibers in order to resist lateral deflection?
- 30.15** A 300 mm length of wood (with the grain running along its length) has a square section 20 mm × 20 mm. The wood is twisted about its long axis. Describe the geometry of the fracture. Why is wood weak in torsion?



$$\sigma_{ij} = \begin{pmatrix} 0 & \tau & 0 \\ \tau & 0 & 0 \\ 0 & 0 & 0 \end{pmatrix} \quad \sigma_p = \begin{pmatrix} \tau & 0 & 0 \\ 0 & -\tau & 0 \\ 0 & 0 & 0 \end{pmatrix}$$

- 30.16** A large hot water tank (90 °C) comprises a cylinder with a vertical axis, closed at the bottom by a flat disk resting on a level foundation slab. The tank liner is fabricated by bending and welding polypropylene sheets. An external reinforcing skin is then added by wrapping a glass fiber “prepreg” mat around the tank, and applying polyester resin by hand using a roller. This process is repeated until a GFRP skin 7 mm thick has been built up. The mat contains chopped glass fibers ≈ 25 mm long, arranged randomly in the plane of the mat. Owing to creep in the matrix phase at the high temperature, the skin near the bottom of the tank developed a crack, and the tank suffered catastrophic failure. What is the dominant stress state in the skin? Why did failure occur near the bottom? How could you prevent a creep failure of this type by changing the length and orientation of the glass fibers?

Symbols and Formulae

LIST OF PRINCIPAL SYMBOLS

Symbol	Meaning (units)
Note:	Multiples or submultiples of basic units indicate the unit suffixes normally used in materials data.
a	lattice parameter (nm)
a	crack length (mm)
A	availability (J)
A_1	eutectoid temperature ($^{\circ}\text{C}$)
A_3	first ferrite temperature ($^{\circ}\text{C}$)
A_{cm}	first Fe_3C temperature ($^{\circ}\text{C}$)
b	Burgers vector (nm)
c	height of c.p.h. unit cell (nm)
C	concentration (m^{-3})
CCR	critical cooling rate ($^{\circ}\text{C s}^{-1}$)
DP	degree of polymerization (dimensionless)
E	Young's modulus of elasticity (GN m^{-2})
f	force (N)
F	force (N)
g	acceleration due to gravity on the Earth's surface (m s^{-2})
G	shear modulus (GN m^{-2})
G	Gibbs function (J)
G_c	toughness (kJ m^{-2})
H	hardness (GN m^{-2})
ΔH	latent heat of transformation (J)
I	second moment of area of structural section (mm^4)
k	ratio of $C_{\text{solid}}/C_{\text{liquid}}$ on phase diagram (dimensionless)
k	Boltzmann's constant (J K^{-1})

k	shear yield strength (MN m^{-2})
K_{c}	fracture toughness ($\text{MN m}^{-3/2}$)
L	liquid phase
m	mass (kg)
m	Weibull modulus (dimensionless)
M	bending moment (N m)
M_{F}	martensite finish temperature ($^{\circ}\text{C}$)
M_{S}	martensite start temperature ($^{\circ}\text{C}$)
n	time exponent for slow crack growth (dimensionless)
p	pressure (N m^{-2})
P_{f}	failure probability (dimensionless)
P_{S}	survival probability (dimensionless)
q	activation energy per atom (J)
Q	activation energy per mole (kJ mol^{-1})
r^*	critical radius for nucleation (nm)
R	universal gas constant ($\text{J K}^{-1} \text{mol}^{-1}$)
S	solid phase
T	absolute temperature (K)
T_{e}	equilibrium temperature (K)
T_{G}	glass temperature (K)
T_{M}	melting temperature (K)
ΔT	thermal shock resistance (K), undercooling (K)
v	velocity (m s^{-1})
V	volume (m^3)
V	volume fraction (dimensionless)
W_{A}	weight % (dimensionless)
W_{f}	free work (J)
X_{A}	mol % (dimensionless)
α	linear coefficient of thermal expansion (MK^{-1})
γ	energy of interface (J m^{-2}) or tension of interface (N m^{-1})
δ	elastic deflection (mm)
ε	true (logarithmic) strain (dimensionless)
ε_{f}	(nominal) strain after fracture; tensile ductility (dimensionless)
$\dot{\varepsilon}_{\text{ss}}$	steady-state tensile strain rate in creep (s^{-1})
η	viscosity (P, poise)
ν	Poisson's ratio (dimensionless)
ρ	density (Mg m^{-3})
σ	true stress (MN m^{-2})
σ_{c}	(nominal) compressive strength (MN m^{-2})
σ_{r}	modulus of rupture (MN m^{-2})
σ_{TS}	(nominal) tensile strength (MN m^{-2})
σ_{y}	(nominal) yield strength (MN m^{-2})
	Greek letters are used to label the phases on phase diagrams.

SUMMARY OF PRINCIPAL FORMULAE

Chapters 3 and 4: Phase diagrams

Composition is given by

$$W_A = \frac{\text{weight of A}}{\text{weight of A} + \text{weight of B}} \times 100$$

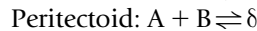
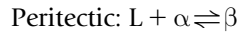
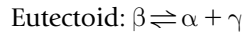
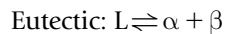
in weight %, and by

$$X_A = \frac{\text{atoms (mols) of A}}{\text{atoms (mols) of A} + \text{atoms (mols) of B}} \times 100$$

in atom (mol) %.

$$W_A + W_B = 100\%; \quad X_A + X_B = 100\%.$$

Three-phase reactions



Chapter 5: Zone refining

$$C_S = C_0 \left\{ 1 - (1 - k) \exp\left(-\frac{kx}{l}\right) \right\}.$$

C_S = concentration of impurities in refined solid; C_0 = average impurity concentration; $k = C_{\text{solid}}/C_{\text{liquid}}$; x = distance from start of bar; l = zone length.

Chapter 6: Driving forces

Driving force for solidification

$$W_f = -\Delta G = -\frac{\Delta H}{T_M}(T_M - T) \equiv -\frac{\Delta H \Delta T}{T_M}.$$

ΔH = latent heat of solidification; T_M = absolute melting temperature; T = actual temperature (absolute).

Driving force for solid-state phase change

$$W_f = -\Delta G = -\frac{\Delta H}{T_e}(T_e - T) \equiv -\frac{\Delta H \Delta T}{T_e}.$$

ΔH = latent heat of transformation; T_e = equilibrium temperature (absolute).

Chapter 7: Kinetics of diffusive transformations

Speed of interface

$$v \propto e^{-q/kT} \Delta T.$$

q = activation energy per atom; k = Boltzmann's constant; T = absolute temperature; ΔT = difference between interface temperature and melting or equilibrium temperature.

Chapter 8: Nucleation

Nucleation of solids from liquids: critical radius for homogeneous *and* heterogeneous nucleation

$$r^* = \frac{2\gamma_{SL}T_M}{|\Delta H|(T_M - T)}.$$

γ_{SL} = solid–liquid interfacial energy; T_M = absolute melting temperature; ΔH = latent heat of solidification; T = actual temperature (absolute).

Chapter 9: Displacive transformations

Overall rate of *diffusive* transformation

$$\text{Rate (volume s}^{-1}\text{)} = \text{interface area} \times \text{interface speed}$$

Chapter 10: Constitutional undercooling

$$\frac{G}{v} > \frac{mC_0}{D} \left(\frac{1-k}{k} \right).$$

G = temperature gradient in liquid; v = interface speed; m = slope of liquidus line; C_0 = average impurity concentration; D = diffusion coefficient in liquid; $k = C_{\text{solid}}/C_{\text{liquid}}$.

Chapter 11: Light alloys

Solid solution hardening

$$\sigma_y \propto \varepsilon_s^{3/2} C^{1/2}.$$

C = solute concentration; ε_s = mismatch parameter.

Work hardening

$$\sigma_y \propto \varepsilon^n.$$

ε = true strain; n = constant.

Chapter 13: Phases in stainless steels

Nickel equivalent = $\text{Ni} + 30\text{C} + 0.5\text{Mn} + 25\text{N}$

Chromium equivalent = $\text{Cr} + \text{Mo} + 1.5\text{Si} + 0.5\text{Nb}$

The chemical symbols represent the concentrations in weight % of the element concerned.

Chapter 14: Carbon equivalent

$$\text{CE} = \text{C} + \frac{\text{Mn}}{6} + \frac{\text{Cr} + \text{Mo} + \text{V}}{5} + \frac{\text{Ni} + \text{Cu}}{15}.$$

The chemical symbols represent the concentrations in weight% of the element concerned.

Chapter 15: Deformation processing

Forming pressure

No friction

$$P_f = \sigma_y.$$

Sticking friction

$$P_f = \sigma_y \left\{ 1 + \frac{(w/2) - x}{d} \right\}.$$

σ_y = yield strength; w = width of forging die; x = distance from center of die face; d = distance between dies.

Chapter 19: Ceramic strengths

Sample subjected to uniform tensile stress

Tensile strength

$$\sigma_{\text{TS}} \approx \frac{K_c}{\sqrt{\pi a_m}}.$$

K_c = fracture toughness; a_m = size of largest microcrack (crack depth for surface crack; crack half-width for buried crack).

Modulus of rupture

$$\sigma_r = \frac{3Fl}{2bd^2}$$

F = central load to cause rupture; l = span of beam; b = width of beam; d = depth of beam.

Tensile strength from modulus of rupture

$$\sigma_{TS} = \frac{\sigma_r}{\{2(m+1)^2\}^{1/m}}.$$

σ_r = modulus of rupture; m = Weibull modulus.

Probability of survival in individual test

$$P_s = 1 - \frac{j - 0.375}{n + 0.25}.$$

j = rank of individual test in order of increasing strength; n = number of tests.

Weibull equations

General stress state

$$P_s(V) = \exp \left\{ -\frac{1}{\sigma_0^m V_0} \int_V \sigma^m dV \right\}.$$

Uniform stress

$$P_s(V) = \exp \left\{ -\frac{V}{V_0} \left(\frac{\sigma}{\sigma_0} \right)^m \right\}.$$

Plotting test data

$$\ln \left\{ \ln \left(\frac{1}{P_s(V_0)} \right) \right\} = m \ln \sigma_r - m \ln \sigma_0.$$

P_s = survival probability of component; V = volume of component; σ_0 = stress for $P_s = 1/e = 0.37$; m = Weibull modulus; V_0 = volume of test sample; σ = tensile stress on volume element dV of component; σ_r = modulus of rupture.

Compressive strength

$$\sigma_c \approx 15\sigma_{TS},$$

$$\sigma_c \approx \frac{CK_c}{\sqrt{\pi\bar{a}}}.$$

C = constant (≈ 15); \bar{a} = average crack size.

Thermal shock resistance

$$\Delta T = \sigma_{TS}/E\alpha.$$

σ_{TS} = tensile strength; E = Young's modulus; α = linear coefficient of thermal expansion.

Slow crack growth

$$\left(\frac{\sigma}{\sigma_{TS}}\right)^n = \frac{t(\text{test})}{t}.$$

σ = strength of component after time t ; σ_{TS} = strength of component measured over time $t(\text{test})$; n = slow crack growth exponent.

Creep

$$\dot{\epsilon}_{ss} = A\sigma^n \exp(-Q/RT).$$

$\dot{\epsilon}_{ss}$ = steady-state tensile strain rate; A , n = constants; σ = tensile stress; Q = activation energy for creep; R = universal gas constant; T = absolute temperature.

Viscosity of glass

$$\eta = \frac{\sigma_s}{10\dot{\gamma}} \propto \exp(Q/RT).$$

σ_s = shear stress; $\dot{\gamma}$ = shear strain rate; Q = activation energy for viscous flow; R = universal gas constant; T = absolute temperature.

Chapter 20: Ceramics processing

Sintering

$$\frac{d\rho}{dt} = \frac{C}{a^n} \exp(-Q/RT).$$

ρ = density; t = time; C , n = constants; a = particle size; Q = activation energy for sintering; R = universal gas constant; T = absolute temperature.

Chapter 21: Cement and concrete

Hardening rate $\propto \exp(-Q/RT)$.

Q = activation energy for hardening reaction; R = universal gas constant; T = absolute temperature.

Young's modulus of concrete

$$E_{\text{concrete}} = \left\{ \frac{V_a}{E_a} + \frac{V_p}{E_p} \right\}^{-1}.$$

V_a , V_p = volume fractions of aggregate, cement paste; E_a , E_p = moduli of aggregate, cement paste.

Chapter 25: Mechanical properties of polymers

Modulus: WLF shift factor

$$\log(a_T) = \frac{C_1(T_1 - T_0)}{C_2 + T_1 - T_0}.$$

C_1 , C_2 = constants; T_1 , T_0 = absolute temperatures. Polymer viscosity

$$\eta_1 = \eta_0 \exp \left\{ \frac{-C_1(T_1 - T_0)}{C_2 + T_1 - T_0} \right\}.$$

C_1 , C_2 = constants; T_1 , T_0 = absolute temperatures; η_1 , η_0 = viscosities at T_1 , T_0 .

Chapter 28: Composites

Unidirectional fiber composites

$$\begin{aligned} E_{c\parallel} &= V_f E_f + (1 - V_f) E_m, \\ E_{c\perp} &= \left\{ \frac{V_f}{E_f} + \frac{1 - V_f}{E_m} \right\}^{-1}. \end{aligned}$$

$E_{c\parallel}$ = composite modulus parallel to fibers; $E_{c\perp}$ = composite modulus perpendicular to fibers; V_f = volume fraction of fibers; E_f = Young's modulus of fibers; E_m = Young's modulus of matrix.

$$\sigma_{TS} = V_f \sigma_f^f + (1 - V_f) \sigma_y^m.$$

σ_{TS} = tensile strength parallel to fibers; V_f = volume fraction of fibers; σ_f^f = fracture strength of fibers; σ_y^m = yield strength of matrix.

Optimum toughness

$$G_c = V_f \frac{d (\sigma_f^f)^2}{8 \sigma_s^m}.$$

V_f = volume fraction of fibers; d = fiber diameter; σ_f^f = fracture strength of fibers; σ_s^m = shear strength of matrix.

Modulus of foams

$$E = E_s \left(\frac{\rho}{\rho_s} \right)^2.$$

E_s = modulus of solid cell wall; ρ = density of foam; ρ_s = density of solid cell wall.

Chapter 29: Wood

Along-grain modulus

$$E_{w\parallel} = E_s \left(\frac{\rho}{\rho_s} \right).$$

Across-grain modulus

$$E_{w\perp} = E_s \left(\frac{\rho}{\rho_s} \right)^2.$$

Elastic anisotropy

$$E_{w\parallel} / E_{w\perp} = (\rho_s / \rho).$$

E_s = modulus of solid; ρ = density of wood; ρ_s = density of solid cell wall.

Along-grain compressive strength

$$\sigma_{\parallel} = \sigma_s (\rho / \rho_s) \approx \sigma_{TS} / 2.$$

Across-grain compressive strength

$$\sigma_{\perp} = \sigma_s (\rho / \rho_s)^2.$$

σ_s = yield strength of solid cell wall; ρ = density of wood; ρ_s = density of solid cell wall; σ_{TS} = tensile strength.

Fracture toughness

$$K_{c\parallel} \approx \frac{K_{c\perp}}{10} \propto \left(\frac{\rho}{\rho_s}\right)^{3/2}.$$

$K_{c\parallel}$ = fracture toughness along grain; $K_{c\perp}$ = fracture toughness across grain;
 ρ = density of wood; ρ_s = density of solid cell wall.

Magnitudes of properties: The listed properties for most structural materials are in the ranges shown in this table.

Property		Metals	Ceramics	Polymers (unfoamed)	Composites (polymer matrix)
Density	(Mg m ⁻³)	2 to 10	1 to 5	1 to 2	1.5 to 2.0
Young's modulus	(GN m ⁻²)	50 to 200	10 to 1000	0.01 to 10	10 to 200
Yield strength	(MN m ⁻²)	25 to 1500	3000 to 50,000	—	—
Tensile strength	(MN m ⁻²)	50 to 2000	1 to 800	5 to 100	100 to 1000
Fracture toughness	(MN m ^{-3/2})	5 to 200	0.1 to 10	0.5 to 5	20 to 50
Creep temperature	(°C)	50 to 1000	−20 to 2000	0 to 200	0 to 200

References

- Angus, H.T., 1976. Cast Iron: Physical and Engineering Properties. second ed. Butterworth.
- Ashby, M.F., Jones, D.R.H., 2012. Engineering Materials I - An Introduction to Properties, Applications and Design. fourth ed. Elsevier.
- ASM, 1999. Metals Handbook. second desktop ed. ASM.
- Atkins, M., 1980. Atlas of Continuous Cooling Transformation Diagrams for Engineering Steels. British Steel Corporation.
- British Standards Institution, 1991. BS 3F 70: Specification for Heavy Duty Braided Rubber Cord.
- Brydson, J.A., 1999. Plastics Materials. seventh ed. Butterworth-Heinemann.
- Calladine, C.R., 1985. Plasticity for Engineers. Ellis Horwood.
- Campbell, J., 2003. Castings. second ed. Butterworth-Heinemann.
- Charles, J.A., Crane, F.A.A., Furness, J.A.G., 1997. Selection and Use of Engineering Materials. third ed. Butterworth-Heinemann.
- Cottrell, A.H., 1975. An Introduction to Metallurgy. second ed. Arnold.
- Crawford, R.J., 1998. Plastics Engineering. third ed. Butterworth-Heinemann.
- Desch, H.E., 1985. Timber, its Structure, Properties and Utilization. sixth ed. Macmillan.
- Easterling, K.E., 1992. Introduction to the Physical Metallurgy of Welding. Butterworth-Heinemann.
- Gale, W., Totemeier, T., 2003. Smithells Reference Book. eighth ed. Elsevier.
- Gibson, L.J., Ashby, M.F., 1997. Cellular Solids. second ed. Butterworth-Heinemann.
- Gordon, J.E., 1988. The New Science of Strong Materials, Or Why you Don't Fall Through the Floor. second ed. Princeton University Press.
- Gordon, J.E., 2003. Structures—Or Why Things Don't Fall Down. Da Capo Press.
- Hertzberg, R.W., 1996. Deformation and Fracture of Engineering Materials. fourth ed. Wiley.
- Honeycombe, R.W.K., Bhadeshia, H.K.D.H., 1995. Steels: Microstructure and Properties. second ed. Arnold.
- Hull, D., Clyne, T.W., 1996. An Introduction to Composite Materials. second ed. Cambridge University Press.
- Jones, D.R.H., 2004. Analysis of a fatal bungee-jumping accident. Eng. Fail. Anal. 11, 857–872.
- Kalpakjian, S., Schmid, S.R., 2002. Manufacturing Processes for Engineering Materials. fourth ed. Addison-Wesley.
- Kingery, W.D., Bowen, H.F., Uhlmann, D.R., 1976. Introduction to Ceramics. second ed. Wiley.
- Lawn, B.R., 1993. Fracture of Brittle Solids. second ed. Cambridge University Press.
- Lewis, P.R., Gagg, C., 2010. Forensic Polymer Engineering. CRC Press.

- Lewis, P.R., Reynolds, K., Gagg, C., 2004. *Forensic Materials Engineering—Case Studies*. CRC Press.
- Llewellyn, D.T., Hudd, R.C., 1998. *Steels—Metallurgy and Applications*. third ed. Butterworth-Heinemann.
- McEvily, A.J., 2002. *Metal Failures*. Wiley.
- Polmear, I.J., 2005. *Light Alloys*. fourth ed. Elsevier.
- Porter, D.A., Easterling, K.E., 1992. *Phase Transformations in Metals and Alloys*. second ed. Chapman and Hall.
- Powell, P.C., Ingen Housz, A.J., 1998. *Engineering with Polymers*. second ed. Stanley Thornes.
- Reed-Hill, R.E., 1964. *Physical Metallurgy Principles*. Van Nostrand Reinhold.
- Seymour, R.B., 1987. *Polymers for Engineering Applications*. ASM International.
- Shewmon, P.G., 1989. *Diffusion in Solids*. second ed. TMS Publishers.
- Ward, I.M., Sweeney, J., 2004. *An Introduction to the Mechanical Properties of Solid Polymers*. Wiley.
- Waterman, N.A., Ashby, M.F., 1991. *Elsevier Materials Selector*. Elsevier.
- Young, W.C., Budynas, R.G., 2001. *Roark's Formulas for Stress and Strain*. seventh ed. McGraw-Hill.

Index

Note: Page numbers followed by “*f*” and “*t*” refer to figures and tables, respectively.

A

Adhesives

- aircraft structures, 417
- anaerobic, 281–282
- Araldite, 281–282, 415–416
- autoclave, 417
- curing, 415–416
- epoxy resin, 416
- honeycombe cores, 416
- joint thickness, 465
- Loctite, 281–282, 517–518
- one-part, 417
- phenolic resin, 417
- scrim, 417
- Superglue, 281–282
- thermoset, 416
- two-part, 417

Aero engine fan blades, 289*f*

Age hardening, 193–199

Alloys, 34

- crystal structure of, 21*f*

Alumina, 315–316

Alumina powder, 345–346

Aluminum, 9*f*, 10, 10*t*

Aluminum alloys, 265–266

Amorphous metals, 179–182

- C-curve, 180*f*

- melt spinning, 181–182, 181*f*

Amorphous polymers, 413–415

Amorphous solid, *see* Glassy solid

Annealing, 272, 273*f*

Aramid (Kevlar) fiber, 471*t*

Arrest points, 46

Austenite, 288–289

B

Bicycle chain links and pins, 219–220

“Big-bang” nucleation, 175–177

Binary alloy, defined, 34

Binary system, defined, 41, 48–49

Block copolymer, 443

Blow molding, 350, 351*f*, 447*f*

Body-centered cubic (b.c.c.) crystals, 15, 17*t*

Brass, 7–8

Brazing

- brazed joint, 280–281

- brazing alloy, 27–28

Bubble-free ice, making, 98–101

- clear ice machine, 100*f*

- eutectic reaction, 99–100

- stages in freezing, 99*f*

Bungee jumping accident

- case study in polymers, 457–463, 458*f*, 460*f*

C

Carbon equivalent, 243–244

Carbon fibers, 307

Carbon steels

- changes during the tempering of martensite, 214*f*

- mechanical properties of normalized carbon steel, 211

- changes with carbon content, 210*f*

- microstructures produced by normalizing

- cooling of eutectoid steel, 208*f*, 209*f*

- cooling of pure iron, 207*f*

- iron–carbon phase diagram, 206*f*

- phases in Fe–Fe₃C system, 206*t*

- quenched and tempered carbon steels, 211–212

- mechanical properties, 215*f*

- TTT diagrams, 213*f*

- Carbon-carbon composite (RCC), 304, 525
- Case carburizing, 285*t*
- Cast iron, 6–7, 264–265
- Casting alloys, 263–264
- Casting defects, 257
- Castings
 - die, 122
 - fine grained, 173–177
 - investment, 261–263
 - permanent mold, 260
 - sand, 258–260
 - shaped, 258
- C-curve, *see* TTT diagram
- Cells, 493–497
 - composition, 497*t*
 - molecular structure of a cell wall, 496*f*
 - properties, 497*t*
- Cellular solids and foams, 486–487
 - mechanical properties, 487–490
 - cell wall bending, 488*f*
 - compressive stress–strain curve, 487*f*
 - elastomeric foam compression, 488*f*
 - plastic foam compression, 489*f*
 - polymeric foams, 486*f*
- Cement, 361
 - chemistry of, 361–366
 - and concrete, 304, 306, 306*t*, 368–369
 - compressive crushing of, 371*f*
 - reinforcing, 373–375
 - strength of, 370–372
 - stress–strain curve, 372*f*
- hardening, 364
- high-alumina cement, 365–366
- high-strength, 372–373
- Portland cement structure, 366–368
- pozzolana cement, 362*f*
- Ceramic alloys, 320
- Ceramic composites, 307, 307*t*
- Ceramics
 - case studies in, 379
 - glass roof beams, 384–388
 - flint, 379–380
 - slate, 380–384
- Ceramics and glass, 297
 - cement and concrete, 306, 306*t*
- ceramic composites, 307, 307*t*
- ceramics production, forming and joining, 345
- data for ceramics, 307–312, 309*t*
- engineering ceramics, 304, 309*t*
- forming of engineering ceramics, 346–350
 - hot pressing powder, 348*f*
 - liquid phase sintering, 349*f*
 - rate of densification, 347
 - sintering, 346*f*, 347*f*
- glasses, 299, 304–305, 305*t*
- improving ceramics, 352–354
 - cermet, 354*f*
 - fiber strengthening, 354
 - high performance ceramics, 355*t*
 - increasing fracture toughness, 353
- joining ceramics, 355, 356*f*, 357*t*
- mechanical properties of ceramics, 327
 - compression test, 333–334
 - creep of ceramics, 337–344
 - elastic moduli, 327–328
 - fracture strength of ceramics, 330–332
 - modulus of rupture, 332–333
 - strength, hardness and lattice resistance, 328–330
 - thermal shock resistance, 335
 - time dependence of strength, 335–336
- natural ceramics, 306, 307*t*
- pottery, porcelain and brick, 352
- production and forming of glass, 350–351
- production of engineering ceramics, 345–346
- toughened glass, 351
- structure of ceramics, 313
 - ceramic alloys, 320
 - ceramic phase diagram, 321*f*
 - ceramic composites, 323
 - covalent ceramics, 316–317, 316*f*
 - ionic ceramics, 313–314
 - structures, 314*f*, 315*f*
 - microstructure of ceramics, 321, 322*f*
 - silica and silicates, 316*f*, 317–319
 - silicate glasses, 319–320, 319*f*
 - stone or rock, 323
 - vitreous ceramics, 304–305, 305*t*, 322
- Cermet, 354*f*
- CFRP, 393, 477
- Chalk, 361
- Chemical vapor deposition (CVD) processes, 285*t*, 350
- Chill crystals, 173–174, 175*f*
- Chromium equivalent, 230, 232–233

Chvorinov's rule (solidification time), 259
 Clays, 352
 Close-packed hexagonal (c.p.h.) crystals, 15, 17*t*
 Columbia space shuttle, 526
 Comet aircraft, 416
 Components, defined, 34
 Composites, 475
 applications, 482
 cellular solids and foams, 486–487
 mechanical properties, 487–490
 cell wall bending, 488*f*
 compressive stress–strain curve, 487*f*
 elastomeric foam
 compression, 488*f*
 plastic foam compression, 489*f*
 polymeric foams, 486*f*
 failure in compression, 484*f*
 fibrous composites, 478–479
 properties, 479*t*
 materials that can be engineered, 490–492
 modulus, 479–480
 particulate composites, 477
 tensile strength, 480*f*, 481–484
 stress–strain curve, 481*f*
 tensile stress in the fiber, 483*f*
 variation of peak stress, 482*f*
 toughness, 484–486, 485*f*
 types of composite, 477
 Compression molding, 447, 448*f*
 Compression test, 333–334
 Concorde aircraft, 202
 Concentration, defined, 35

Concrete, 368–369, 368*f*
 reinforcing, 373–375
 strength of, 370–372
 Constitution
 of an alloy, defined, 37
 variables, defined, 39
 Constitution point, 41–43
 Constitutional undercooling (CU), 184
 Continuous casting, 257
 Continuous cooling transformation (CCT), 282
 Copper alloys, 7–9
 generic copper-based metals, 7*t*
 Cork, 519–525, 520*f*
 applications of, 520–521
 cell structure of, 523*f*
 champagne corks, 527–528
 wine corks, 520*f*, 524–525, 527
 Covalent ceramics, 316–317, 316*f*
 Creep of ceramics, 337–344
 Critical cooling rate (CCR), 221–222

D

Darwin sculpture, 262*f*
 Data for ceramics, 307–312
 Deformation processing, 266–272
 drawing, 269
 extrusion, 268–269
 forces in forging and rolling, 270–272
 forging, 267–268
 rolling, 266–267
 Dendrites, 70, 70*f*, 71*f*, 135, 135*f*

Dense random packing (d.r.p), 16
 Densification, rate of, 347
 “Detwinning,” 288–289
 Diameter of the equivalent bar, 284
 Die casting, 122
 Die pressing, 348*f*
 Differential thermal analysis (DTA), 46–47
 Diffusion bonding, 355
 Diffusion-controlled kinetics, 132–134
 Displacive transformations, 155
 Distribution of strength, 331–332
 Drawing, 269
 Drinks cans, metals for, 9–10
 Ductile iron, 264–265

E

Elastic anisotropy, 498*f*, 499
 Elastic moduli, of ceramics, 327–328
 Elasticity, 497–499
 Elastomers, 397, 398*t*, 410
 Electroplating, 285*t*
 Engineering ceramics, 309*t*
 Equilibrium constitution, defined, 39
 Equilibrium constitution diagram, *see* Phase diagrams
 Equivalent bar diameter, 284
 Error function, 293
 Eutectic point, defined, 64
 Eutectic reactions, 68, 89–91, 99–100, 133–134, 165
 Eutectics, 63–65
 structure, 69*f*
 Eutectoid point, 73

Eutectoid reaction, 73
 for steel, 133
 Eutectoids, 72–74, 75*f*
 structure, 74–75
 Extrusion, 445–446, 446*f*

F

Face-centered cubic (f.c.c.)
 crystals, 15, 17*t*
 Face-centered tetragonal unit
 cell, 167*f*
 Failure in compression, 484*f*
 Fasteners, 281, 449
 Ferrous metals, 3–4, 7
 cast iron, 6–7
 generic iron-based metals, 5*t*
 high-carbon steels, 4–6
 stainless steel, 6, 6*f*
 Fibrous composites, 478–479
 properties, 479*t*
 Films and fibers, 447–448
 Fire grate, 6*f*
 Flame hardening, 285*t*
 Flint
 case study, 379–380, 381*f*
 knapping, 380, 388
 tools, 379
 Float molding, 350, 351*f*
 Forging, 267–268, 270–272
 Forging forces, 270–272
 Forsterite, 320
 Fracture strength of ceramics,
 330–332
 Friction stir welding, 287, 287*f*
 Friction welding, 286–288, 286*f*
 Fusion welding, 280

G

Generic metals, properties
 of, 13*t*
 Generic polymers, 395–398

elastomers, 397, 398*t*
 natural polymers, 398, 399*t*
 properties, 398, 400*t*
 thermoplastics, 395, 396*t*
 thermosets and resins,
 395–397, 397*t*
 GFRP, 393, 477
 GFRP surgical instrument,
 517–519
 Gibbs phase rule, 54–55, 117
 Glass, 345
 forming methods for, 351*f*
 production of engineering
 ceramics, 345–346
 toughened, 351
 Glass fibers, 471*t*, 490–491,
 503–504, 530
 Glass-metal seals, 27
 Glass roof beams
 case study, 384–388
 Glassy solids, 16, 132
 grain and phase boundaries,
 19–22
 interphase boundaries,
 21–22, 23*f*
 semicoherent and incoherent
 boundaries, 21–22
 structure of grain boundary, 21*f*
 Glaze bonding, 355
 Glazes, 356
 Gold leaf manufacture, 274–275
 Growth facets, 136
 Grain and phase boundaries,
 19–22
 Grain-boundary diffusion,
 346–347
 Grains and phases, shapes of,
 22–25

H

Hardenability, 221–224
 shape factors for quenching,
 221–222

Heat-treatable alloys, 282–284
 Heat shields, 189, 525
 Heterogeneous nucleation,
 143–147
 effect of temperature, 146,
 147*f*
 solid catalyst surface, 144–146,
 144*f*
 High-alumina cement,
 365–366
 High-impact polystyrene, 444
 High-performance
 engineering ceramics,
 304–306
 Hip joints, metals for, 10–12
 Homogeneous nucleation,
 142, 143*f*
 Hot isostatic pressing, 348*f*
 Hot pressing powder, 348*f*

I

“Ice-minus” mutant, 172
 Impression forging, 267–268
 Induction hardening, 285*t*
 Ingot casting, 277
 Injection molding, 446, 446*f*
 Inoculants, 177
 Interphase boundaries, 21–22,
 23*f*
 Interstitial solid solutions,
 18–19, 18*f*
 Investment casting, 261–263,
 262*f*
 Ionic ceramics, 313–314
 Iron-based metals, generic, 5*t*

J

Joining metals, 280–282
 Jominy end-quench test for
 hardenability, 223,
 224*f*, 229*f*

K

Kaolin, 322
 Kevlar cable, 471*f*, 472, 472*f*
 Kinetics of structural change,
 125, 141, 155
 diffusive transformations, 125
 diffusion-controlled kinetics,
 132–134
 eutectoid reaction for steel,
 133, 133*f*
 heat flow effects, 131–132
 heat-flow control of
 solidification, 131*f*
 shapes of grains and phases,
 131*f*
 metals with dendritic
 structure, 135*f*
 solidification, 125–131
 equation for solidification
 rate, 130–131
 Gibbs free energy
 equation, 126
 measuring speed of
 solidification, 128*f*
 solid and liquid in
 equilibrium, 128*f*
 solid–liquid interface,
 130*f*
 solid-state phase changes,
 132
 displacive transformations, 155
 characteristics, 161–162,
 163*t*
 displacive f.c.c. → b.c.c.
 transformation,
 161–162, 161*f*, 162*f*
 martensite, 163–164
 coherent with the parent
 lattice, 161–162, 163*f*
 eutectoid, 165, 166*f*
 structure, 167*f*
 transformation in steel,
 165–166, 165*f*

unit cells in iron, 164*f*,
 165–166
 time–temperature–
 transformation (TTT)
 diagram, 160–161, 160*f*
 nucleation in liquids,
 141–143
 heterogeneous nucleation,
 143–147
 effect of temperature,
 146, 147*f*
 solid catalyst surface,
 144–146, 144*f*
 homogeneous nucleation,
 142, 143*f*
 work needed to form
 a crystal, 141, 142*f*
 nucleation in solids, 147
 heterogeneous nucleation,
 148*f*
 King's Bridge, Australia,
 247–248
 Kovar low-expansion alloy,
 27–28

L

Laser hardening, 285*t*
 Lattice resistance, 328–330
 Lawn mower, use of polymers,
 449–455
 Light alloys, 189, *see also* Metal;
 Steel; Structural
 changes in metals
 age hardening, 193–199
 Al–Cu phase diagram, 193*f*
 coherency stress hardening,
 195
 microstructure, 194*f*
 precipitation hardening, 195
 dislocations, 198*f*
 particle spacing with time,
 199*f*
 TTT diagram, 199*f*

yield strength, 198*f*, 200*t*
 precipitation stages, 197*f*
 solid solution hardening,
 195
 TTT diagram, 195*f*
 mechanical properties of metals
 and alloys, 190*t*
 solid solution hardening,
 190–192
 Al–Mg phase diagrams, 191*f*,
 192*f*
 heat treatment, 191
 yield strength, 190–191,
 192*t*
 thermal stability, 202
 work hardening, 200
 Lime cement render, 363*f*
 Lime mortar, 361, 363*f*
 Linear polyethylene, 407*f*, 409*f*
 Linear polymers, 395
 Liquid phase sintering, 349,
 349*f*
 Liquidus line, defined, 63
 “Lost wax” process, 261
 Low-grade ceramics, 345

M

Machining, 279, 280*f*
 Magnesia, 315
 Martensite, 163–164
 Martensite transformation, 179
 Material data, 398–401
 Melt spinning, 256
 Metal *see also* Light alloys; Steel;
 Structural changes in
 metals
 aluminum, 9*f*, 10, 10*t*
 generic aluminum-based
 metals, 10*t*
 brass, 7–8
 copper alloys, 7–9
 generic copper-based
 metals, 7*t*

Metal (*Continued*)

- data for metals, 12–13
- for drinks cans, 9–10
- ferrous metals, 3–4, 7
 - cast iron, 6–7
 - generic iron-based metals, 5*t*
 - high-carbon steels, 4–6
 - stainless steel, 6, 6*f*
- for hip joints, 10–12
- for model steam engine, 3–9, 4*f*, 92–93, 93*f*
- nickel metals, 8–9
 - generic nickel-based metals, 8*t*
- properties of the generic metals, 13*t*
- structures, 15
 - crystal structures of pure metals, 15, 17*t*
 - body-centered cubic (b.c.c.), 15, 17*t*
 - close-packed hexagonal (c.p.h.), 15, 17*t*
 - face-centered cubic (f.c.c.), 15, 17*t*
- glassy solids, 16
 - grain and phase boundaries, 19–22
 - interphase boundaries, 21–22, 23*f*
 - semicoherent and incoherent boundaries, 21–22
 - structure of grain boundary, 21*f*
- phases, defined, 19
- polymorphism, 15, 18*f*
- range over which a material has structure, 16*t*
- shapes of grains and phases, 22–25

- example of soap bubbles, 24*f*
- grain boundary angle, 23–24
- two-phase structure, 23–24, 25*f*
- structures of solutions and compounds, 16–19
- crystal structure of alloys, 21*f*
- solid solutions, 16–19
- solid solutions, interstitial or substitutional, 18–19, 18*f*
- titanium, 11–12, 11*f*, 12*t*
 - generic titanium-based metals, 12*t*

Metallic alloy, defined, 34

Metals, processing, 255–256

- casting, 256–266
 - aluminum alloys, 265–266
 - cast irons, 264–265
 - casting alloys, 263–264
 - investment casting, 261–263, 262*f*
 - permanent mold casting, 260
 - sand casting, 258–260
 - shaped castings, 258
- deformation processing, 266–272
 - drawing, 269
 - extrusion, 268–269
 - forces in forging and rolling, 270–272
 - forging, 267–268
 - rolling, 266–267
- friction stir welding, 287, 287*f*
- friction welding, 286–288, 286*f*
- heat treating, 282–284
- joining, 280–282
- machining, 279, 280*f*

- processing routes for metals, 255*f*
- recrystallization, 272–274
- shape memory alloys (SMAs), 288–290
- superplastic forming (SPF), 288
- surface engineering, 285–286

Microstructure of alloys, 36

Model steam engine, metals for, 3–9

Modulus, 479–480

Modulus of rupture, 332–333

Molecular architecture of polymers, 408–410

Mullite, 320

Mushy freezers, 263–264

N

Natural ceramics, 306, 307*t*

Natural polymers, 398, 399*t*

Nickel equivalent, 230, 232–233

Nickel metals, 8–9

- generic nickel-based metals, 8*t*

Nitriding, 285*t*

Nucleation

- heterogeneous, 143–147
 - effect of temperature, 146, 147*f*
 - solid catalyst surface, 144–146, 144*f*
- homogeneous, 142, 143*f*
- in liquids, 141–143
- in solids, 147

P

Partially stabilized zirconia (PSZ), 353–354

Particulate composites, 477

- Pearlite, 133–134
- Peritectics, 76–77, 76f
- Peritectoids, defined, 77
- Permanent mold casting, 260
- Phase, defined, 37
- Phase diagrams, 33, 63
 - case studies, 89
 - bubble-free ice, 98–101
 - clear ice machine, 100f
 - eutectic reaction, 99–100
 - stages in freezing, 99f
 - silicon for microchips, 93–98
 - multiheater, 98f
 - repeat refining, 98f
 - stages in zone refining, 94f, 95–96
 - soft solders, 89–93
 - eutectic, 89–91
 - lead–tin phase diagram, 90f
 - plumbers' solder, 91f
 - properties, 90t
- defined, 40
- teaching yourself phase
 - diagrams, 33, 63
 - binary systems, 48–49
 - composition of the phases, 49–50
 - constitution, 37
 - cooling curves, 45–46
 - dendrites, 70, 70f, 71f
 - differential thermal analysis (DTA), 46–47
 - equilibrium constitution, 39
 - eutectic reaction, 67–68
 - eutectic structure, 69f
 - eutectics, 63–65
 - eutectoids, 72–74, 75f
 - Gibbs' phase rule, 54–55
 - one-component systems, 43–45
 - peritectics, 76–77, 76f
 - peritectoids, 77
 - phase diagrams, 40–41
 - phase reactions, 65–67
 - proportions of the phases in two-phase alloys, 51
 - segregation, 71–72, 71f
 - structure, 36
- Phase reaction, defined, 65–67
- Phase transformations, 171
 - amorphous metals, 179–182
 - C-curve, 180f
 - martensite transformation, 179
 - melt spinning, 181–182, 181f
 - fine-grained castings, 173–177
 - casting in the laboratory, 174f
 - chill crystals, 173–174, 175f
 - grain structure with
 - columnar crystals, 173–174, 175f
 - segregation and grain size, 174–175
 - use of inoculants, 177
- making rain, 171–173
 - heterogeneous nucleation, 172
 - Pseudomonas syringae* as catalyst, 172
 - silver iodide as nucleating agent, 172, 173f
- single crystals for
 - semiconductors, 178
 - growing single crystals, 179f
 - integrated circuits, 178, 178f
- Phases, defined, 19
- Physical vapor deposition (PVD), 285t
- Plastic shear, 279
- Poisson's ratio, 451–452, 522
- Polycrystalline metal, 19–20
- Polyethylene gas pipes
 - case study, 464–470
- Polymer crystals, 411–413
- Polymers, 391
 - case studies, 457
 - fatal bungee jumping accident, 457–463, 458f
 - polyethylene gas pipes, 464–470
 - details of fractures, 467–468
 - origin of gas leak, 465–466
 - polymers to the rescue, 468–470
 - ultrastrong fibers for yacht rigging, 470–473
- classes of polymers, 394
- generic polymers, 395–398
- elastomers, 397, 398t
- natural polymers, 398, 399t
- properties, 398, 400t
- thermoplastics, 395, 396t
- thermosets and resins, 395–397, 397t
- joining of polymers, 449
- mechanical behavior, 419
- stiffness, 419
 - decomposition, 428
 - glass or viscoelastic transition, 423–426
 - glassy regime, 421–423
 - modulus diagrams, 428–429
 - rubbery behavior and elastomers, 426–427
 - time and temperature dependant modulus, 420f
 - viscous flow, 427–428
- strength, 430–440
 - brittle fracture, 431, 431f
 - cold drawing, 432–433, 432f
 - crazing, 433, 433f
 - shear banding, 434f

Polymers (*Continued*)
 strength diagrams,
 434–440, 435*f*
 viscous flow, 433
 processing, 441
 forming of polymers,
 445–448
 compression molding, 447,
 448*f*
 extrusion, 445–446, 446*f*
 films and fibers, 447–448
 injection molding, 446,
 446*f*
 vacuum and blow forming,
 446–447, 447*f*, 448*f*
 polymer alloys, 443–445
 copolymers, 443, 443*f*
 solid solutions and
 plasticizers, 443
 stabilization and
 vulcanization, 444–445
 two-phase alloys and
 toughened polymers,
 444, 444*f*
 synthesis of polymers,
 442–443
 addition and condensation
 reactions, 442
 structure, 405
 amorphous polymers,
 413–415
 molecular architecture,
 408–410
 elastomers, 410
 linear polyethylene, 407*f*,
 409*f*
 vinylidene, 409
 molecular length, 406–408
 ethylene molecule, 406*f*
 linear polymers, 407*f*
 packing of polymer
 molecules, 410–415
 chain-folded, 412*f*
 polymer crystals, 411–413

 spherulite, 413*f*
 volume change on
 crystallization, 414*f*
 WLF equation, 425–426
 Polymorphism, 15, 18*f*
 Portland cement, 362–364
 hardening of, 365*f*, 366, 367*f*
 versus high-alumina cement,
 365–366
 structure of, 366–368
 Pottery, porcelain and
 brick, 352
 Pozzolana cement, 361–362,
 362*f*
 Precipitation hardening, *see* Age
 hardening
 Pressure die-casting, 260
 Primary solid, 68
 Pure metals, 189
 Putney gas explosion, 464, 468

R

Rain making, 171–173
 Reaction bonding, 349–350
 Recovery, 272–273
 Recrystallization, 272–274
 Reinforcing cement and concrete
 asbestos cement, 373
 bridge girder, 281
 Christ's College Lasdun
 building, UK, 363*f*,
 369*f*, 387*f*
 Hoover dam, USA, 364
 cooling during hardening
 reactions, 364–365
 modernist home, 303–304
 pressurized water pipe,
 375–376
 Sleipner drilling platform
 sinking, 528–530
 Sydney Opera House,
 Australia, 303
 Residual tensile stresses, 351

Rheocasting, 175–177
 Rocks and minerals, 304
 Rolling, 22–23, 266–267,
 270–272, 350
 Rolling forces, 270–272
 Roman aqueduct at
 Segovia, Spain, 300,
 300*f*, 301*f*
 Rotation viscometer, 338*f*
 Rubber, 394, 397–398,
 401–402, 415,
 426–427

S

Salol, 126
 Sand casting, 258–260
 Schaeffler diagram, 229,
 232–233
 Sectional composites, 515–517
 sandwich-type, 516*f*
 Segovia aqueduct, Spain, 300,
 300*f*, 301*f*
 Segregation, 256–257
 Segregation in alloys, 71–72,
 71*f*, 72*f*
 Semiconductors, 178
 Shape memory alloys (SMAs),
 288–290
 Shaped castings, 258
 Silica and silicates, 316*f*,
 317–319
 Silicon ceramics, 349*f*, 350
 Silicon for microchips,
 93–98
 multiheater, 98*f*
 repeat refining, 98*f*
 stages in zone refining,
 94*f*, 96
 Sintering, 346*f*, 347*f*
 Site saturation, 157–160
 Skin freezers, 263–264
 Slate
 case study, 380–384

- modern house roofed with, 381*f*, 382*f*
- splitting, 383*f*
- Slow crack growth, 335, 385–386
- Sodium modification of Al-Si casting alloys, 265
- Soft solders
 - eutectic, 89–91
 - lead–tin phase diagram, 90*f*
 - plumbers' solder, 91*f*
 - properties, 90*t*
- Soldering, 89–91, 280–281
- Solid solutions, 16–19, 20*f*
 - hardening, 190–192
 - interstitial/substitutional, 18–19, 18*f*
- Solidification, 125–131
 - equation for solidification rate, 130–131
 - Gibbs free energy
 - equation, 126
 - heat-flow control of solidification, 131*f*
 - measuring speed of solidification, 128*f*
 - solid and liquid in equilibrium, 128*f*
 - solid–liquid interface, 130*f*
- Solid-state phase changes, 132
- Solidus line, defined, 63
- Space shuttle, 525
- Sphalerite, 317
- Spherulite, 413*f*
- Spot welding, 280
- Stainless steel, 6, 6*f*, 226–229
 - Fe–Cr phase diagram, 227*f*
 - Fe–Ni phase diagram, 228*f*
 - improving, 230
 - phases in, 229–230
- State variables, defined, 39
- Steel, 205, 221, 237
 - alloy steels, 221
 - corrosion resistance, 226
 - hardenability, 221–224
 - alloying elements, 223*f*
 - Jominy end-quench test, 224*f*, 229*f*
 - precipitation hardening, 225–226
 - tool steels, 225
 - solution hardening, 225
 - stainless steel, 226–229
 - Fe–Cr phase diagram, 227*f*
 - Fe–Ni phase diagram, 228*f*
 - improving, 230
 - phases in, 229–230
- carbon steels, 205
 - changes during the tempering of martensite, 214*f*
 - mechanical properties
 - of normalized carbon steel, 211
 - changes with carbon content, 210*f*
 - microstructures produced
 - by normalizing, 205–210
 - composite structures, 207*t*
 - cooling of eutectoid steel, 208*f*, 209*f*
 - cooling of pure iron, 207*f*
 - iron–carbon phase diagram, 206*f*
 - phases in Fe–Fe₃C system, 206*t*
 - quenched and tempered
 - carbon steels, 211–212
 - mechanical properties, 215*f*
 - TTT diagrams, 213*f*
- case studies, 237
 - boiler explosion, 237–241
 - failure of tube, 238–239, 238*f*
 - temperature distribution, 240*f*
 - tube hardness, 238–239, 239*f*
 - broken hammer, 244–253
 - austenitizing, 246*f*
 - hardness, 244–246
 - welding steel safely, 241–244
 - pressure vessel steel, 244
 - structural steel, 243–244
 - welding temperatures, 242*f*
- high-carbon, 4–6
- Stiffness
 - decomposition, 428
 - glass or viscoelastic transition, 423–426
 - glassy regime, 421–423
 - modulus diagrams, 428–429
 - rubbery behavior and elastomers, 426–427
 - time and temperature dependant modulus, 420*f*
 - viscous flow, 427–428
- Stone or rock structure, 323
- Strength, 430–440
 - brittle fracture, 431, 431*f*
 - cold drawing, 432–433, 432*f*
 - crazing, 433, 433*f*
 - shear banding, 434*f*
 - strength diagrams, 434–440, 435*f*
 - viscous flow, 433
- Strength, hardness and lattice resistance, 328–330
- Structural changes in
 - metals, 109, *see also* Light alloys; Metal; Steel
 - driving forces, 109–112, 120*t*

Structural changes in
 metals (*Continued*)
 energy changes, 110–111
 sizes of, 120
 grain growth, 119–120
 precipitate coarsening,
 118–119
 energy equation, 118–119
 solid state diffusion, 119*f*
 recrystallization, 120
 reversibility, 113–114
 second law of
 thermodynamics, 113
 solid state phase
 changes, 117
 solidification, 115–117
 energy changes, 116
 Gibbs function for ice–water,
 117*f*
 stages in the freezing of ice,
 116*f*
 stability, 114*f*
 Structure of alloys, 36
 Structure-insensitive
 properties, 12
 Structure-sensitive
 properties, 12
 Submerged arc welding, 280
 Substitutional solid solutions,
 18–19, 18*f*
 Superplastic forming (SPF),
 288
 Surface engineering, 285–286
 Surface growth steps, 137–140
 Sydney Opera House, Australia,
 302*f*, 303

T

Tensile and compressive
 strengths, 499*f*,
 500–501
 Tensile strength, 480*f*, 481–484
 stress–strain curve, 481*f*

tensile stress in the
 fiber, 483*f*
 variation of peak stress, 482*f*
 Ternary system, defined, 41
 Thermal shock resistance, 335
 Thermal spraying, 285*t*
 Thermal stresses, 307,
 342–344, 353
 Thermodynamics, 111, 113
 Thermoplastics, 395, 396*t*
 Thermosets and resins,
 395–397, 397*t*
 Tie line, 49–50
 Tiles
 Almagro, Spain, 323
 ceramic, 323–325
 glazing, 323–325
 Sydney Opera House,
 Australia, 300, 311
 Time dependence of strength,
 335–336
 Time–temperature–
 transformation diagram,
 see TTT diagram
 Titanium, 11–12, 11*f*, 12*t*
 generic titanium-based
 metals, 12*t*
 Tool steels, 225
 Toughened glass, 351,
 385–386, 385*f*
 Toughness, 484–486, 485*f*,
 501–502, 502*f*
 TTT diagram, 160–161, 192*f*,
 195*f*, 212–220
 Tube sinking, 269
 Turbochargers, 201
 Twinning, 288–289

U

Ultrastrong fibers for yacht
 rigging
 case study, 470–473
 Underground pipes, 464

V

Vacuum and blow forming,
 446–447, 447*f*, 448*f*
 Vinylidene, 409
 Violin bodies, 509–517
 replacement materials,
 513–515
 glass fiber resins, 514
 modulus anisotropies, 514*f*
 sectional composites,
 515–517
 thickness calculation, 515
 soundboard vibrations,
 511–513
 dimensions, 513*f*
 frequencies, 511–512
 idealized vibration modes,
 511*f*
 wooden soundboard, 512*f*
 Vitreous ceramics, 304–305,
 305*t*, 345
 Vitreous enamel, 356

W

Water-tube boiler, 237–238
 Weld deposition, 285*t*
 Weibull distribution, 331–332,
 372
 Weibull modulus, 388–389
 Welding
 electron beam, 292–295
 friction, 286–288
 friction stir, 287
 fusion, 280–281
 gas welding, 280
 laser beam, 280
 railroad rails, 266–267,
 290–291
 spot welding, 280
 submerged arc, 280
 thermit, 290–291
 Wire drawing, 269

Wood, 493
brushwood, 505, 507*b*
cells, 493–497
composition, 497*t*
molecular structure of a cell
wall, 496*f*
properties, 497*t*
chipboard, 503–504, 508
comparison with other
materials, 502–503
fiberboard, 508
mechanical properties, 493,
494*t*, 497

elastic anisotropy, 498*f*, 499
elasticity, 497–499
tensile and compressive
strengths, 499*f*,
500–501
toughness, 501–503, 502*f*
Young's Modulus, 498*f*
plywood, 477, 503–504, 508
splitting, 508
structure, 493
macrostructure, 494*f*
Work hardening, 200

Y

Yacht rigging, ultrastrong
fibers for
case study, 470–473
Young's Modulus,
498*f*

Z

Zirconia, 346